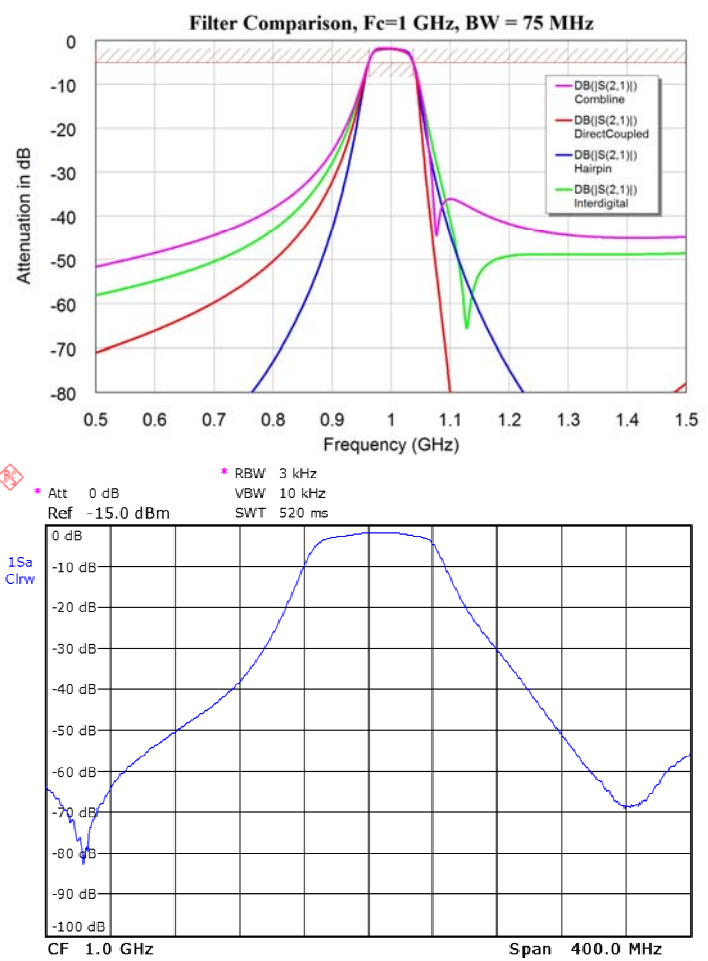
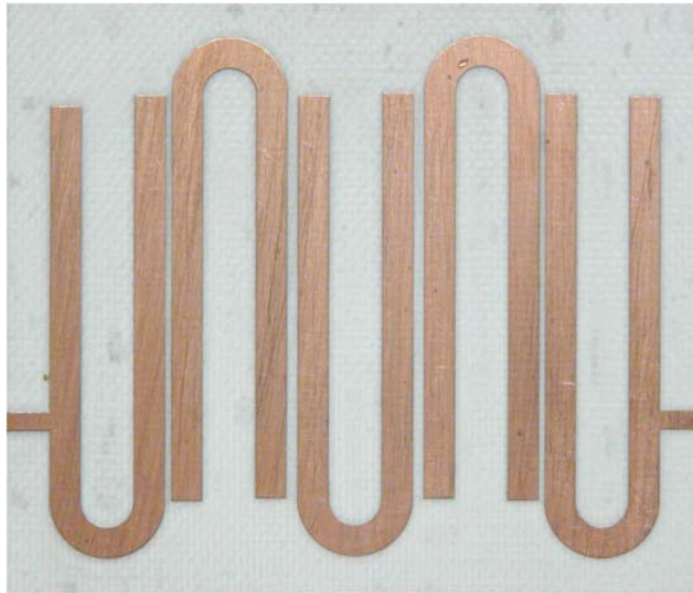
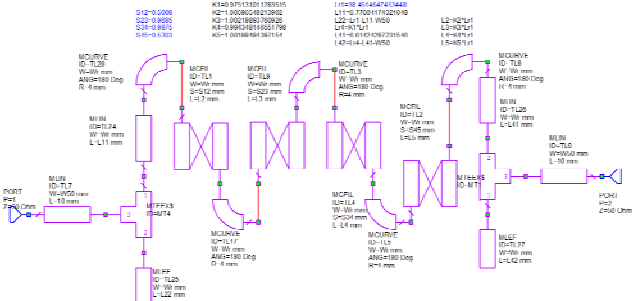


RF Electronics: Design and Simulation



Cornelis J. Kikkert

James Cook University
Townsville, Queensland, Australia
3rd Edition, 2018

RF Electronics Design and Simulation

Publisher: James Cook University, Townsville, Queensland, Australia, 4811. <http://www.jcu.edu.au>

2018 Edition, Copyright © 2018 C. J. Kikkert, ISBN 978-0-9954470-8-0

This is an update on the 2015 and 2013 Editions, Copyright © 2015 C. J. Kikkert, ISBN 978-0-9942333-0-1 and © 2013 C. J. Kikkert, ISBN 978-0-9873109-3-4.

All rights reserved. No part of this publication may be reproduced or distributed, in any form or by any means, without the prior permission of Cornelis J. Kikkert.

All web pages linked from the references were accessed and checked to be correct in May 2018.

The accompanying project files are also Copyright © 2018 C. J. Kikkert, ISBN 978-0-9954470-8-0. C. J. Kikkert grants readers of this book permission to use these project files and to modify them, in order to gain an understanding of the material presented in this publication. The text contained in the “Design Notes” of the project files may not be altered.

AWR Corporation has been given a licence to distribute this publication and the accompanying project files through the University Program of AWR. For details, please see their web site <http://www.awrcorp.com/support-resources/university-support/professors-partnership/professor-keith-kikkert>.

A catalogue record for this book is available from the James Cook Library.

RF Electronics

Design and Simulation

Cornelis J. Kikkert

James Cook University
Townsville, Queensland, Australia

Contents

	Page
Preface	VIII
Acknowledgement	IX
About the Author	IX
Chapter 1: Introduction	1
RF Electronics Design	1
Computer Simulation	3
References	4
Chapter 2: Computer Simulation	5
Introduction	5
Basic Operation	6
Example 2.1: Low Pass Filter	6
Equations in AWRDE	10
Optimisation	11
Example 2.2: Diplexer	11
Example 2.3: Amplifier	16
Transistor Models	18
Determination of Line Parameters	22
Nonlinear Simulation	24
Time Domain Transient Circuit Simulation	25
Example 2.4: Buck DC-DC Converter	25
Harmonic Balance Circuit Simulation	30
Black Box Matching of Circuits to Measurements	32
Example 2.5: Bandpass T Matching Network	32
S Parameter Measurements	34
Impedance Measurements	37
Summary	44
References	44
Chapter 3: Transformers and Hybrids	46
Introduction	46
Wideband Transformers	47
Example 3.1: RF Transformer Design	48
Bifilar and Trifilar Windings	49
Transmission line transformers with ferrite cores	50
Transformer Hybrids	52
Power Combiner / Splitter	53
Wilkinson Transformer Hybrid	53
Example 3.2 Wilkinson Transformer Hybrid Design	55
Transmission Line Hybrid with Ferrite Cores	56
Many Way Hybrids	57
References	58

	Page
Chapter 4: Transmission Line Transformers and Hybrids	59
Introduction	59
Example 4.1: Bandwidth Calculation	60
Wilkinson Transmission Line Hybrid	61
Compensated Wilkinson Hybrid	66
Unequal Split Wilkinson Hybrid	67
Wideband Wilkinson Hybrid	68
Example 4.2: 90 to 270 MHz Wilkinson Hybrid	69
Quarter Wave Hybrid or 1.5λ Rat-race hybrid	72
Branchline Coupler	75
Backward Travelling Wave Hybrid	82
Edge Coupled Lines	83
Example 4.3: 20 dB Coupler	83
Lange Coupler	87
Broadside Coupled Lines	88
Example 4.4: 100 Watt 3 dB Broadside Coupler	89
References	92
Chapter 5: Frequency Mixers	93
Introduction	93
Definition of Terms	94
Conversion Loss	94
Isolation	95
Compression Point	95
Dynamic Range	96
Two-tone Third Order Intermodulation Distortion	96
Third Order Intercept Point	97
LO Level	98
Example 5.1: Mixer LO Level Calculation	99
Single Diode Mixer	99
Computer Simulation of Mixers	101
Balanced Mixer	107
Double Balanced Mixer	111
Microwave Mixers	119
Microwave Mixer using a Branchline Coupler	121
Active Single Transistor Mixer	125
Gilbert Cell Active Mixer	125
Quadrature Mixers	130
Active IQ Mixers	131
Image Reject Mixers	131
Examples of Commercial Active Mixers	135
LTCC Mixers	136
Other Mixers	137
Additional Resources	137
References	137

	Page
Chapter 6: Oscillators	139
Principles of Oscillators	139
Requirements	139
Oscillator Types	139
Positive Feedback Oscillators	139
Oscillator Design Process	140
Frequency Selective Networks	141
Oscillator Design Procedure	142
Step 1: Select an amplifier type	142
Step 2: Design an amplifier	143
Step 3: Design a resonator	144
Step 4: Linear Oscillator Analysis	145
Step 5: Nonlinear Oscillator Analysis	145
Example 6.1: Low Phase Noise Design	148
Crystal Oscillators	151
Quartz Crystals	151
Example 6.2: Crystal Oscillator Design	151
RF and Microwave Oscillators	155
Example 6.3: 1 GHz Microstrip Oscillator Design	155
Dual Resonator Oscillator	160
Design Improvements	164
References	166
Chapter 7: RF Filters	167
Introduction	167
Electrical Filters	167
Acoustic Filters	167
Filter Design Revision	167
Filter Tables	168
Butterworth Filters	169
Bessel Filter	171
Chebyshev Filter	172
Cauer-Chebyshev Filter	172
Reflectionless Filters	174
RF Lowpass Filter Design	178
Bandpass Filter Design	183
LC Bandpass Filters	183
Low-Pass to Band-Pass Transformation	183
LC Coupled Resonator Filter	184
HF Filters	191
Cauer-Chebyshev Bandpass Filters	192
Parallel Coupled-Line Filter	192
Example 7.1: 1 GHz, 70 MHz Bandwidth Filter	192
Hairpin Filter	195
Helical Filters	199
Example 7.2: 100 MHz, 1 MHz Bandwidth Filter	200
Interdigital Filters	203

	Page
Round Rod Interdigital Filters	204
PCB Interdigital Filters	205
Example 7.3: 1GHz, 70 MHz Bandwidth Filter	206
Direct Coupled Resonator Filters	211
Example 7.4: 1 GHz, 500 MHz Bandwidth Filter	212
Fine Tuning the Filter	214
Microstrip Filter Comparison	216
EM Simulation	221
Coaxial Filters	228
Ceramic Filters	231
SAW Filters	232
References	232
Chapter 8: Amplifiers: Stability, Noise and Gain	234
Introduction	234
MMIC	234
Requirement for Stability	235
Smith Chart Revision	236
Scattering Parameter Revision	237
Stability	239
Stability Circles	239
Unconditional Stability	241
Conditional Stability	241
Stability Factors: Measures of Stability	241
Design for Maximum Gain	242
Amplifier Noise Figure	242
Improving the Noise Figure	247
Improving Amplifier Stability	250
Coupers at Input and Output	250
Bandwidth Limiting using Reflectionless Filters	252
Resistors at Output	254
References	256
Chapter 9: Impedance Matching of Power Amplifiers	257
Introduction	257
Large Signal Parameters	257
Types of Matching	257
Choice of Components and Q value	257
LC Matching	258
PI Network	259
Low Pass T Network	260
Bandpass L Network	261
Bandpass T Network	261
Capacitive Impedance Transformer	262
Example 9.1: 150 MHz, 35W Amplifier	263
PI Network	266
Low Pass T Network	266
Bandpass L Network	267

	Page
Bandpass T Network	267
Capacitive Impedance Transformer	268
Transformer Matching	269
Transmission Line Matching	271
Broadband Matching	272
Example 9.2: Broadband Amplifier	277
References	285
Chapter 10: Operational Amplifiers	286
Introduction	286
Voltage Feedback Theory	286
Current Feedback Theory	287
Current and Voltage Feedback Amplifier Comparison	288
Example 10.1: High Impedance 10kHz-20MHz Amplifier	289
High Impedance Input Stage	290
Other OpAmp Stages	294
Low Noise Designs using Operational Amplifiers	295
Example 10.2: Amplifier Design for Noise Performance	297
Oscillators using Operational Amplifiers	302
Limitation of Simulations	306
References	307
Chapter 11: Circuit Manufacture	308
Introduction	308
Subtractive Process: Conductive Track Removal	308
Additive Process: Depositing Tracks and Vias	308
Printed Circuit Board Materials	309
Conventional PCB Substrates	309
Paper and Resin Substrates; FR2 and FR3	309
Fibreglass and Epoxy Substrates; FR4, FR408, IS400	310
Microwave and RF Printed Circuit Board Materials	311
RT/duroid 58X0	311
RT/duroid 6000	312
RO3000 and RO3200	312
RO4000	312
Other Laminates	313
Multilayer Boards	313
Non-Clad Substrates	314
Alumina Substrates	314
Other Substrates	315
Manufacturing	315
Manufacturing using a PCB Milling Machine	315
Manufacturing using Laser Ablation	315
Layout Hints	316
Thin Film	316
Thick Film	318
Printing Screens	318
Pastes (Inks)	319

	Page
RF Applications of Thick Film Circuits	319
Manufacturing using 3D printing	320
Low Temperature Cofired Ceramic (LTCC)	321
References	322
Appendix: Importing Local Vendor and XML Libraries	324
Local Vendor Libraries	324
Importing Spice Device Models	324
References	326

Preface

The material presented in this book evolved from teaching analogue electronics courses at James Cook University (JCU) over many years. When I started teaching, electronics design, computer simulation tools were non-existent and most of the design optimisation was done by replacing components in hardware. It was a big step forward when EESOF became available in the mid 1980's. The computer simulation tools have progressed enormously since then. Early in my career, I was given the following advice for designing electronic circuits. "Get the circuit to work and then start taking components out. Put back the one that stops the circuit from working." This is a silly statement, since in a proper design removing any component will stop it from working, but it does illustrate the goal of any designer: *Design a circuit that will work first time, according to specification. It must do so reliably and at as low a cost as possible.* Since labour is expensive, the circuits also should not require any adjustments after manufacture in order that they meet the specifications.

Using the computer simulation used in this book, we can now design our analogue electronic circuits such that they satisfy all these conditions. We can change active device parameters in the simulation, to ensure that variations in performance during manufacturing do not cause the circuit to fail to meet the specifications. We can check that the circuit will meet specifications under any permitted temperature, power supply and input signal variations. For RF circuits, we can, by simulation, change microwave PCB substrates for lower cost FR4 type substrates and ensure that the circuit still performs correctly. For consumer or space critical applications, the computer simulation tools used in this book will allow Low Temperature Cofired Ceramic (LTCC) circuits to be designed. With those circuits, one cannot open them up to change components. They must be correct right from the start.

During the last 20 years, much of the analogue electronics in radio and TV receivers has been replaced with digital electronics, causing a change in the operating frequency of analogue electronic designs. There has been a rapid growth in the number of radio transmitters and receivers used. Many developed countries now have more mobile phones than people and most smart-phones and computers use WLAN/WiFi to access the internet. WLAN/WiFi, Bluetooth, Wireless Gigabit, WiMax, Zigbee, W-CDMA, LTE and 5G are all relatively new communication systems using microwave (above 1 GHz) frequency bands. Because of this demand for radio spectrum, the operating frequencies are getting higher and the spectrum is becoming more crowded.

This explosion in microwave system applications requires a matching RF and microwave electronic design capability from our engineers. More stringent filtering is required and less intermodulation distortion is permitted from amplifiers, to ensure systems do not interfere with each other. 20 years ago, most electronic designs using microwave frequencies were for military, instrumentation, or high-end communication applications, such as microwave radio links operated by Telcos. Now most microwave designs are for consumer applications. As a result, the emphasis on reducing the cost of both the circuit and the design has become more important. RF and microwave circuit simulation play a significant part in this cost reduction.

It is important for Universities to realise however, that computer simulation of an electronic design is not the end-point, but only a step in the realisation of the production of hardware that operates as required. That is why in this book, firstly computer simulation has been used to enhance the understanding by students and designers of the properties and

limitations of their designs, and secondly many photographs and measured performance of the hardware realisation of these designs presented have been included. I hope that the material presented in this book will increase the RF and microwave design skills of many students and practicing designers.

This whole book is suitable for teaching RF and microwave electronic design in the final year of an undergraduate Bachelor Degree program or as a course in a postgraduate program. Chapter 2 can be used at earlier years of a Bachelor Degree program to teach the principles of computer simulation, the design of analogue electronic circuits and passive circuit analysis. These computer simulation techniques are not limited to RF and Microwave frequencies. For that reason, chapter 2 includes examples operating below 100 kHz. The modelling of mains (50/60 Hz) power distribution transformers, described in chapter 2, could not have been done without the optimisation capability of AWRDE.

Unless otherwise indicated, any of the hardware shown in photographs, have been designed by the author and produced by him with assistance from JCU and technical staff. There are some photos of hardware from unknown manufacturers (UM). Those have been labelled with (UM).

This third edition includes a new chapter on RF Operational Amplifiers (OpAmps). With OpAmps now available with bandwidths >1 GHz, they offer exciting new opportunities. This edition also includes new material on reflectionless filters and 3D printing of PCB's, as well as many other minor updates.

This third edition initially included NI AWR DE V13 project files. This minor update on the third edition has the same text, but includes NI AWR DE V14 project files, as a result, some figures have been updated to reflect the colour changes and slight simulation differences in V14.

Acknowledgment

I thank my wife Maxine for her patience and tolerance of my absences over many years, as I fulfil my desire to teach students the art of electronic design, being absorbed in research in the design of instrumentation and communication equipment. I thank her for being able to spend a lot of time in writing and updating this book and the accompanying project files, even in my “retirement”.

I also thank my past and present colleagues at James Cook University, for their encouragement and feedback on the course that resulted in this book. I thank NI-AWR for making their software available for teaching at James Cook University at a reasonable cost. Without that, this book could not have been written. I thank Dane Collins and Sherry Hess from NI AWRCorp, for the novel step that we took in distributing this book on their web site. That allows this book to be used by many more students. I thank Prof Mike Heimlich, from Macquarie University, who peer reviewed the first edition of this book and made many very valuable comments, which resulted in this book being much better than the draft version. I thank David Niven from NI AWRCorp Support, for helping me when I could not get some of the project files to work correctly. Finally, I thank Prof. Mohan Jacob from James Cook University, who peer reviewed the new material included in this third edition.

About the Author

Cornelis Jan Kikkert obtained his BE and PhD from Adelaide University in 1968 and 1972 respectively. He is a Fellow of Engineers Australia and a Life Senior Member of IEEE. He was a lecturer at Adelaide University for 3 years and was at James Cook University in

Townsville for 37 years, as a Lecturer, Senior Lecturer, Associate Professor and 7 years as Head of Electrical and Computer Engineering.

He "retired" in 2010 to have more time for research. Since 2010, he is an Adjunct Associate Professor at both James Cook University and The University of Adelaide.

He has more than 50-year experience in the design of electronics for communication equipment, broadcast transmitters, satellite beacon receivers, weather satellite receivers and many other applications, as well as the design of electronic instrumentation for measuring RF and microwave signals.

In addition to this book, he is the author of more than 100 peer-reviewed papers, 4 book chapters and an inventor on 8 patents.

Email Keith.Kikkert@jcu.edu.au, Keith.Kikkert@adelaide.edu.au.

November 2018

Chapter 1

Introduction

RF Electronics Design

RF electronic designs require different techniques than electronic designs at lower frequency since:

- 1 The resistors, capacitors and inductors used do not necessarily behave like ideal components. In particular, leads on resistors and capacitors have an inductance associated with them, which can easily dominate.
- 2 The wavelength of the signals is comparable to the size of components used. This presents some challenges and some opportunities.
- 3 The track lengths may be a significant fraction of a wavelength, allowing Microstrip-lines or Striplines, to be used as elements for filters, couplers, impedance matching circuits etc.
- 4 The tracks on the circuit boards should be seen as transmission lines with a characteristic impedance, chosen such that the transmission line and the devices connected to it, satisfy the circuit specifications at all the required frequencies. Conventional printed circuit boards are lossy at high frequencies. Circuit boards for RF and Microwave frequencies normally use low loss materials and have carefully controlled thicknesses, to provide constant impedances for transmission lines.

At lower frequencies, many of the analogue circuits are being replaced with digital circuits. Analogue circuit design techniques are used for much of the circuitry in any transmitter and receiver circuit used in Radio, TV, Microwave, Mobile Phone, Wireless LAN etc. Digital techniques, such as software-defined radio, digital predistortion and digital signal processing techniques are increasingly being used to enhance the performance, reduce the cost and make the transmitters and receivers more flexible.

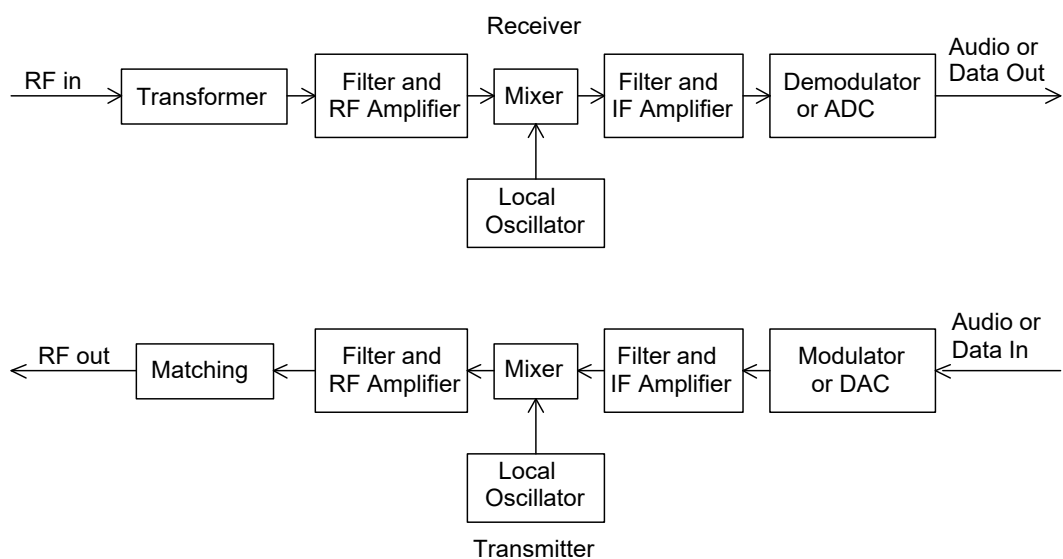


Figure 1.1. Typical Transmitter and Receiver Block Diagram.

A traditional block diagram of a receiver and a transmitter is shown in figure 1.1. The basic building blocks in this diagram are RF Transformer, Mixer, RF and IF amplifier, Local Oscillator and a demodulator or detector. In this course, we will look at many of these elements in detail.

For consumer devices with large production runs, such as mobile phones and USB dongles for Digital TV, Bluetooth or WLAN, many of the blocks in figure 1.1, are combined in one package, which contains one or more ICs. A typical example of this is a Bluetooth dongle, shown in figure 1.2. All the RF functions, including the 2.5 GHz transmitter and receiver, all the protocol handling and the USB interface are contained in the two IC's on figure 1.2. The antenna is included as an element on the PCB.

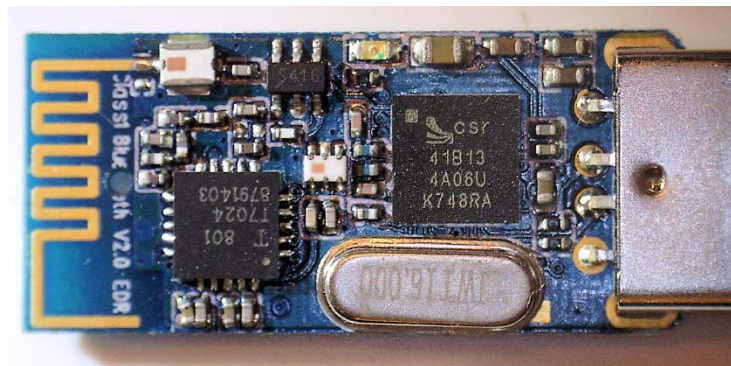


Figure 1.2. Typical Consumer RF Module. (Unbranded Bluetooth USB Adapter)

For many applications, such IC's may be too expensive for the small number of circuits to be produced, or the performance that can be obtained from an IC cannot meet the required specifications, such as output power or adjacent carrier rejection. For high power applications such as transmitters, IC's alone cannot meet the impedance matching and power demands. As a result, a discrete implementation is often required. This book deals with the design of such RF circuits.

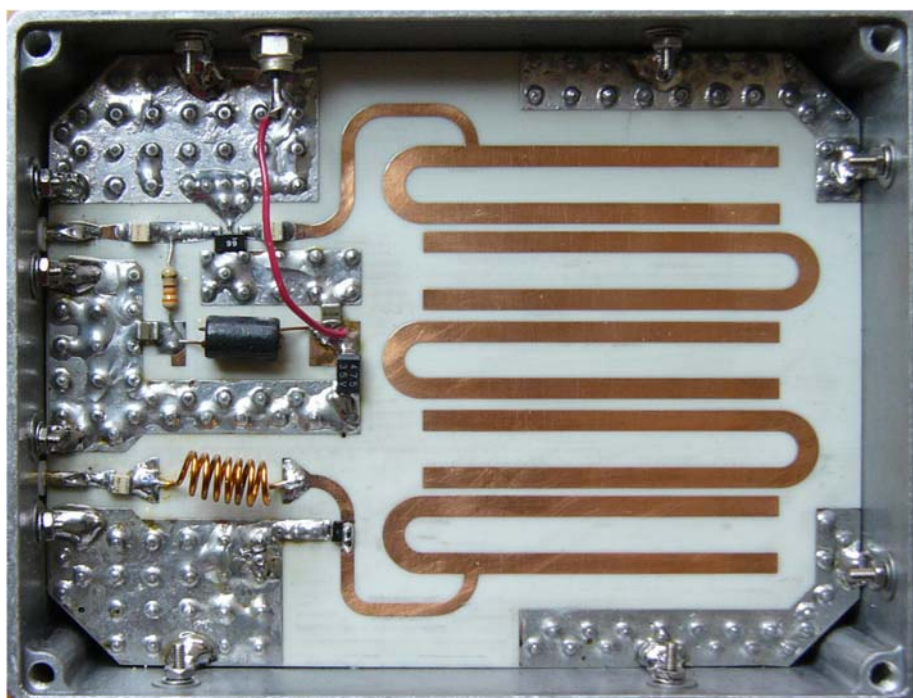


Figure 1.3. Harmonic Multiplier, to produce 810 MHz from 162 MHz.[1]

Figure 3 is a typical example and shows a harmonic multiplier for a Satellite Beacon Receiver built at James Cook University. The input is a 162 MHz signal and the output is the 5th harmonic at 810 MHz. The active device is a Microwave Monolithic IC (MMIC) amplifier. Currently wireless services operate at frequencies of 1.8 GHz for mobile phones, 2.5 GHz for Bluetooth and WLAN and 5 GHz for WLAN. In many cases, IC's specially designed for these applications can be used at other frequencies. The designer should keep this in mind as can reduce the cost of specialised circuits.

This book does not specifically deal with the design of RF IC's. The techniques described here are directly applicable to the design of RF IC's and have even been used through microwave and up to millimetre-wave [2, 3], since those need to allow for the IC to be comparable with the wavelength for GHz frequency designs. In addition, the chapters on amplifiers and oscillators allow for the design of circuits, which can be directly implemented in RF IC's.

Computer Simulation

For any commercial design, it is important to produce a properly functioning design as quickly as possible. Ideally, there should be just one design iteration, it should be correct and reliable with the first realisation, since any further design-iterations will cost more money and will delay the time before product comes to market, thus reducing any competitive advantage.

Computer simulation allows most aspects of the design to be investigated and optimised quickly before any hardware is produced. The modern computer simulation tools are very good and generally allow a correctly functioning design to be produced first time. The main commercial computer simulation systems are 1) EEsof, which was purchased by Hewlett-Packard, then spun off as Agilent and now Keysight EEsof EDA [2] comprising Advanced System Design (ADS), **GoldenGate RFIC Simulator (EMDS)**, **EMPro 3D and other packages**. 2) NI AWR Design Environment (NI AWR DE) software [3] comprising Microwave Office (MWO), Visual Systems Simulator (VSS), Analogue Office, AXIEM, Analyst and other packages. Both perform well, and both allow linear and non-linear circuit analysis, using steady state and time-domain circuit simulation, as well as the more detailed electromagnetic simulation of circuits. The author has used both EEsof EDA and NI AWR DE for many years. In the author's experience, NI AWR DE is easier for the students to learn and as a result, NI AWR DE has been used in the RF electronics course and entry-level electronics and circuit simulation courses at James Cook University. The authors lecture notes for the RF electronics course form the basis of this book. Chapter 2 has deliberately been written allow it to be used for both advanced RF electronics courses and entry-level courses.

Both the Agilent and NI AWR software allow the design and simulation of RF IC's. Depending on quantities and manufacturing technology, it can be expensive to manufacture an RF IC. The author encourages the RF designs by the students to be manufactured, to allow the students hardware experience in measurement and faultfinding of RF circuits, as well as providing feedback on their designs. As a result, this book concentrates on using commercial PCB substrates for components like couplers, combiners and filters and using commercial transistors and IC's in active RF designs.

The NI AWR DE project files for each figure in this book are included with this book and are available for download from the NI AWR web site [5]. For the 2015 edition of this book, NI AWR DE version V11 has been used for all the simulations.

References

1. Kikkert, C. J. "The design of a Ka band satellite beacon receiver". Sixth International Conference on Information, Communications and Signal Processing (ICICS 2007), Singapore, 10-13 Dec, Publisher IEEE.
2. Macquarie University, Wireless Communications and Networking Laboratory, <http://research.science.mq.edu.au/wireless/>
3. WiFi Alliance, <http://www.wi-fi.org/>
4. Keysight Technologies EEs of Electronic Design Automation (EDA) software, <http://www.keysight.com/find/eesof>
5. NI AWR Corp: NI AWR Design Environment <http://www.awrcorp.com/>

Chapter 2

Computer Simulation

Introduction

There are many circuit-simulation programmes available. Most of these use SPICE models, which include all relevant parameters. At lower frequencies, programmes like the commercial “Multisim” program are useful, but for RF circuits, frequency-domain computer simulation tools are much more computationally efficient for steady state analysis than SPICE based programmes. Frequency-domain computer simulation tools also allow transmission lines to be used as elements and are able to evaluate Intermodulation (IM) distortion caused by two closely spaced tones. Typical examples of RF circuit simulation software are EEsof EDA by Keysight Technologies [1] and NI AWR Design Environment (NI AWR DE) [2].

NI AWR DE contains five very different simulation programs: Microwave Office (MWO), which is used for circuit simulation. This chapter describes its use for circuit simulation. The second part is Visual System Simulation (VSS), which is used to simulate whole systems. VSS is typically used to simulate communication systems to determine the performance of different modulation techniques. The third part is Analog Office, which is used for RF-IC design. The fourth part is AXIEM, which is used for 3D planar electromagnetic (EM) simulation, and the fifth part is Analyst, which is a full 3D EM simulation software. This is a very powerful computer simulation suite. During operation of the NI AWR DE software, all the different components MWO, VSS, Analog Office, AXIEM and APLAC that have valid licences, are all available. In some instances, more than one of these NI AWR DE components are used at the same time, the generic name NI AWR DE is used in this book, unless a specific components is mentioned. For the 2015 edition of this book, NI AWR DE version V11 [3] is used for all the simulations.

NI AWR DE is very good for both RF and lower frequency simulations. Many RF transistors and diodes devices models are available for both linear models and non-linear (Transient or Harmonic Balance) models. In addition, the required model parameters can often be downloaded from the device manufacturer’s web site. The device models used and the modern communication simulation programmes are very accurate, resulting in a good agreement between the computer simulations and the resulting hardware.

The linear models treat any passive and active devices as “linear” devices and use conventional circuit analysis techniques to solve the equations for the circuit to be simulated. As a result, the simulation is fast, but it will not deal with non-linear effects such as those that occur in a mixer, oscillator or amplifier. Applying optimisation techniques to the linear simulation of the circuit allows the best performance to be obtained quickly. Simulation of non-linear circuits can be done in two ways: Firstly, Harmonic Balance is a frequency-based, steady state analysis that uses non-linear differential equations to model the devices and then uses a linear combination of excitation tones to balance currents and voltages to satisfy Kirchhoff’s law. Examples of this are the simulation of the harmonics produced by an oscillator. Secondly, transient time domain simulation using SPICE models can be used to analyse the non-linear behaviour of a circuit. Examples of this are the simulation of an oscillator starting up. Nonlinear circuit simulation is described in detail later in this chapter, using example 2.4: Buck DC-DC Converter.

Computer simulation is a powerful tool for ensuring that a circuit has been designed to perform correctly. It is best practice for commercial designs to firstly check the circuit under the ideal design conditions and then check that the circuit still performs correctly for all realistic component tolerances variations. Since the production of a PCB, containing an RF circuit is quite expensive it is always good practice to first fully simulate the circuit. Inadequate circuit modelling and computer simulation may result in a design fault being discovered in the hardware after it is built. Even though modern computer simulation tools are very good, they are no substitute for good design by an experienced designer. Even then, one will often find something that was not known and was not considered in the simulation, especially at RF and microwave frequencies, that can seriously affect the circuit's performance.

The computer simulation process is illustrated by some examples.

Basic Operation

Example 2.1: Low-Pass Filter

Design a 4th order low-pass filter and a high-pass filter to have a cut off frequency of 250 MHz and an impedance level of 75Ω , and in the second example combine these filters to form a VHF-UHF TV antenna diplexer. The Coaxial cables used for TV antennae are 75Ω impedance. Hence, 75Ω is used for the impedance of this diplexer.

For Butterworth filters [4] the design equations for L and C are well known and obtained using the Cauer topology realisation for Butterworth polynomials and are used for the filter tables of [5] for these filters. The components are [4]:

$$C_i = \frac{1}{\pi F_c R} \sin\left(\frac{(2i-1)\pi}{2n}\right) \quad i = 1, 3, 5, \dots \quad \text{Eqn. 2.1}$$

$$L_i = \frac{R}{\pi F_c} \sin\left(\frac{(2i-1)\pi}{2n}\right) \quad i = 2, 4, 6, \dots \quad \text{Eqn. 2.2}$$

Where R is the desired load impedance and F_c is the cut off frequency. Later in this chapter, it is shown how these equations can be used directly in NI AWR DE. The high-pass filter is obtained using the standard low-pass to high-pass transformation described in most filter textbooks, such as section 5.4 of Zverev [5] and section 2.6 of Huelsman [6]. The low-pass to high-pass transformation simply results in the normalised L and C values being swapped and replacing L with C and C with L in the circuit. As can be seen by comparing figures 2.3 or 2.7 with figure 2.8.

These equations can easily be entered into a spreadsheet, to give the results for the 250 MHz filter shown in table 2.1. This spreadsheet is also included in the zip file containing all the NI AWR DE project files used in this chapter.

We now enter these values into MWO. To do this we must create the required project as follows:

Open NI AWR DE. This will then open up a blank project as shown in figure 2.1.

Select *Project* \Rightarrow *Add Schematic* \Rightarrow *New Schematic* and name the Schematic "LowPass". Then type CNTL+L or select the Element window at the bottom left of the Design Environment window and select *Lumped Elements* \Rightarrow *Capacitor* and drag the CAP symbol into the circuit schematic as shown in figure 2.2.

Impedance	75	
Freq MHz	250	
Order	4	
Element		
Normalised	Low-pass	High-pass
Rs, Rn	R 75	R 75
1 0.765367	C 6.497E-12	L 6.23838E-08
2 1.847759	L 8.822E-08	C 4.59382E-12
3 1.847759	C 1.568E-11	L 2.58402E-08
4 0.765367	L 3.654E-08	C 1.10905E-11

Table 2.1. Butterworth filter element values.

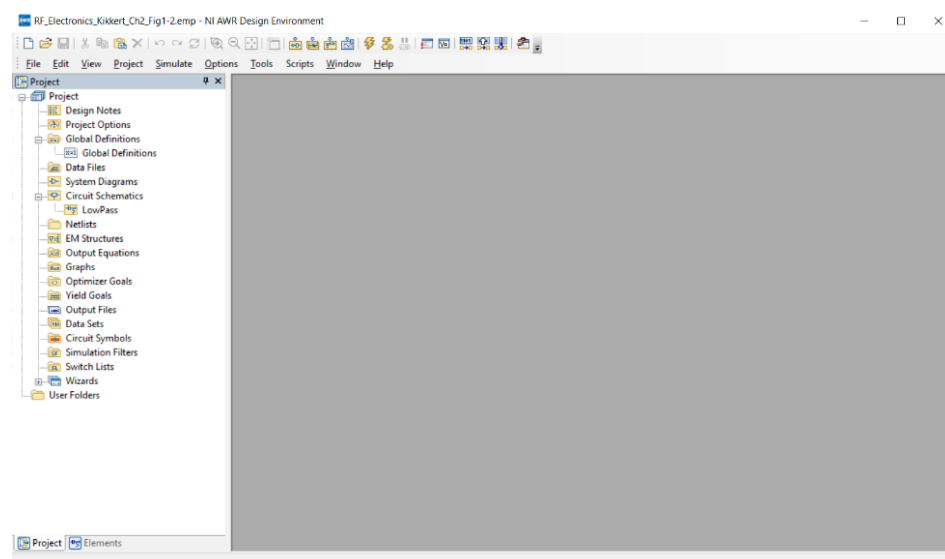


Figure 2.1. MWO blank project screen.

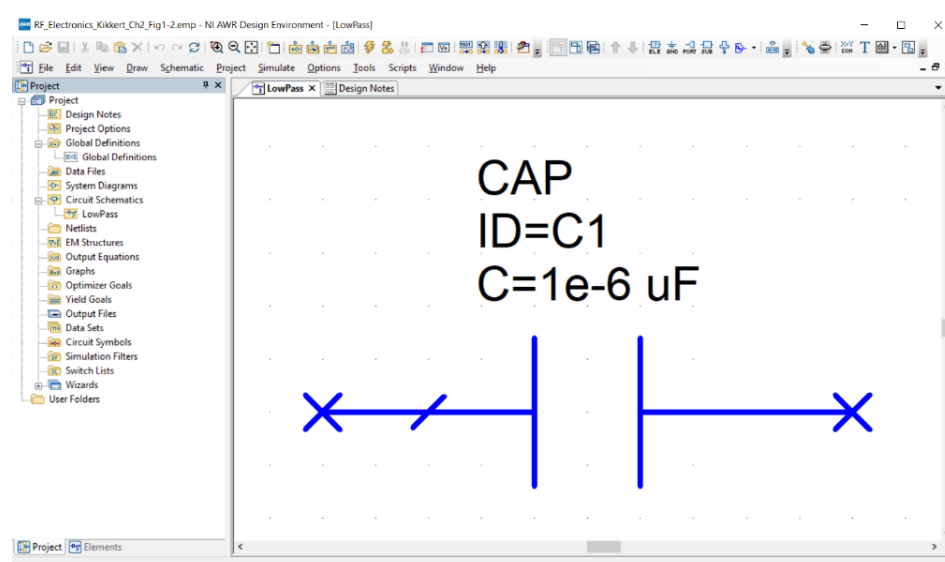


Figure 2.2. Capacitor placed.

Now place all the other capacitors and inductors in the correct location. When placing the component, a right mouse click rotates the component. Selecting the port symbol from the mini toolbar, or selecting *Draw* \Rightarrow *Add Port* allows the input and output ports to be added to the circuit. *Draw* \Rightarrow *Add Ground* allows a ground connection to be added. Double Left Click on a component or on the property's text in the schematic, allows the required value for that component to be entered. Repeat this for all the other components to give the final circuit as shown in figure 2.3.

Note that normally filters are designed with the smallest number of inductors, so that odd order filters with the end elements being capacitors are far more common.

Practical Note: The filters are to be used as part of a diplexer, consisting of a high-pass and a low-pass filter in parallel. The high-pass filter must not short out the low-pass filter at low frequencies and the low-pass filter must not short out the high-pass filter at high frequencies, so that an open circuit input impedance is required in the stopband of these filters. This is achieved with the first (series) element being an inductor for the low-pass filter, and the first element being a capacitor for the high-pass filter.

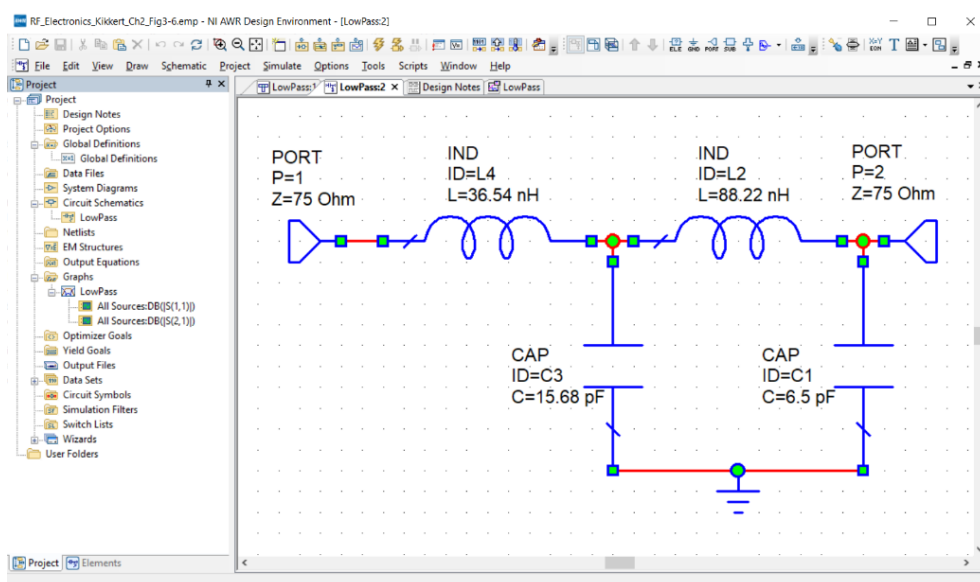


Figure 2.3. Low-pass filter circuit.

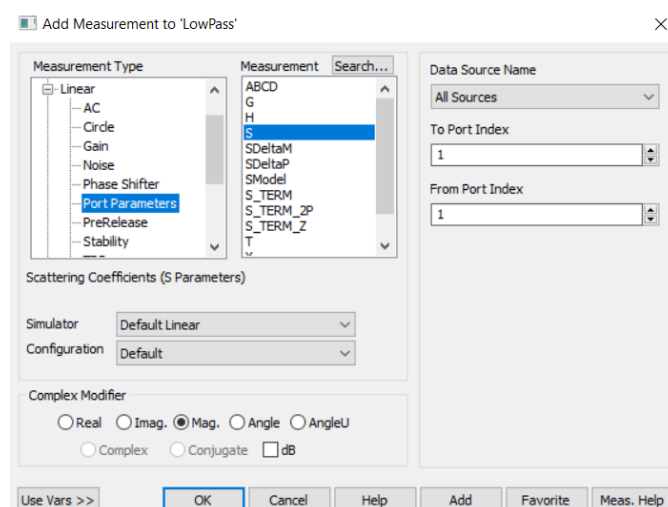


Figure 2.4. "Add Measurement" window.

Select the project window again and select Graph and right mouse click and select add measurement. This opens the window shown in figure 2.4. RF devices are normally specified by the Scattering (S) parameters. These are described in more detail in chapter 8 and equations 8.3 to 8.12. Pozar [7] in section 4.3 gives a detailed description of S parameters. They give a simple performance measurement of the circuit. S_{11} and S_{22} are the input and output return loss, indicating how well the device is matched. S_{21} and S_{12} are the forward and reverse gains. Select *Linear Measurement type* \Rightarrow *Port Parameter* and *S parameter* to obtain S parameter measurements of the filter, as shown in figure 2.4. Save the project as “LowPassFilter” to keep these values. Since this circuit is to be connected using TV Coaxial cable, ensure that the impedance of the ports is changed from the default value of 50Ω to 75Ω .

Now set the operating frequency range using the *Project options* entry in the left bar. Set the *Global Units frequency* to MHz and then set the operating frequency range in the *Frequencies* window as shown in figure 2.5.

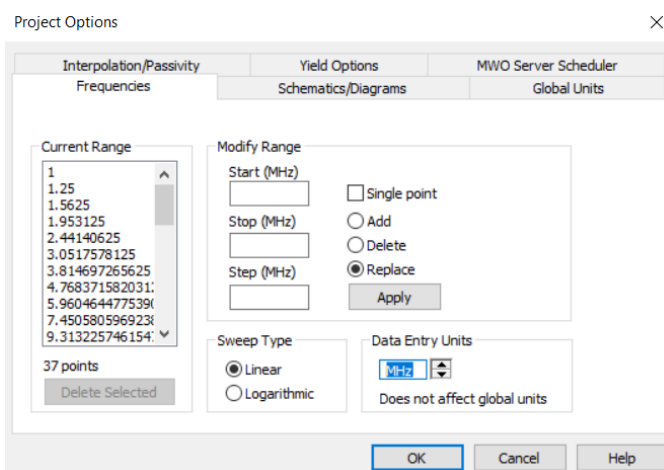


Figure 2.5. Project frequencies.

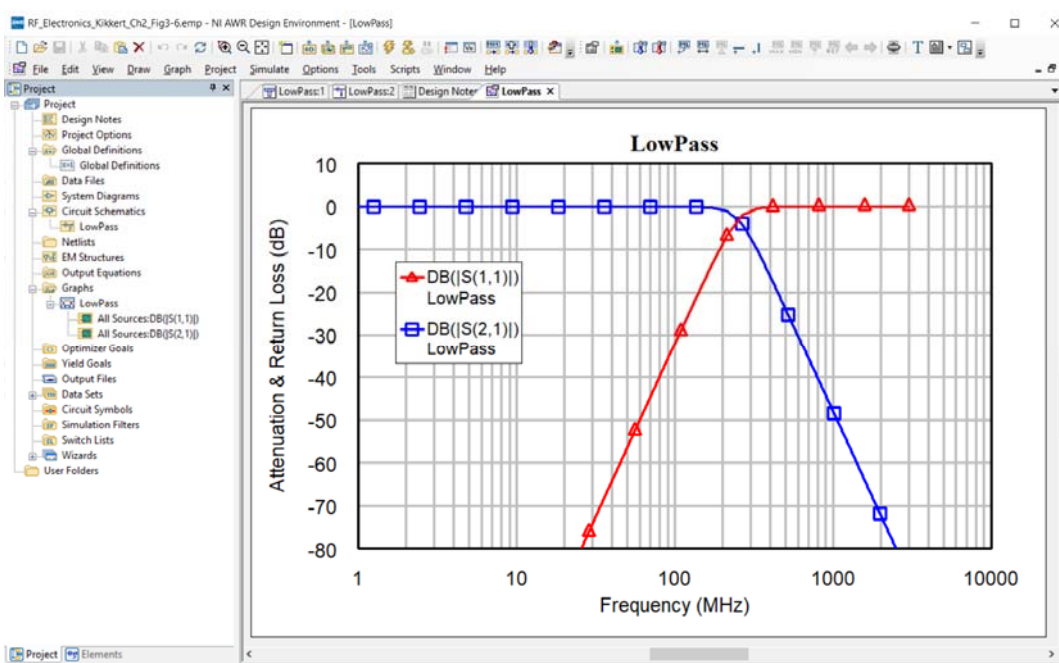


Figure 2.6. Frequency response of the low-pass filter.

Select *Simulate* \Rightarrow *Analyse* to give the required frequency response as shown in figure 2.6. The scales, line thickness and other parameters of the graph can be set from inside the Graph Property toolbar, (the left element of the right toolbar shown the blue top area in figure 2.6), or the properties can be accessed by right clicking inside the Low Pass graph and selecting *Properties*.

In figure 2.6, the blue graph is the transfer function S_{21} and the magenta one is the input reflection coefficient S_{11} .

Equations in NI AWR DE

It is possible to use variables and equations as part of the circuit diagram. This allows greater control over the filter parameters and avoids having to use a spreadsheet to calculate the filter element values. For instance by making the cut off frequency a variable, the filter can easily be tuned to achieve a required cut off frequency. The cut off frequency can be tuned or optimised to meet required specifications. The resulting circuit diagram is shown in figure 2.7. The variables can be placed in any order, but any variable specification must be above the use of that variable. The resistance R and frequency variable F_c must thus be on top, since those are used by C_1 , L_2 , C_3 and L_4 . The equations are added to the circuit diagram using: *Draw* \Rightarrow *Add Equation*, and then placing the equation location on the circuit diagram. Variables, which NI AWR DE cannot find, either globally or in the current schematic, are shown in red. Any corrective action may simply be the moving around of a variable to satisfy this top to bottom flow requirements. The full list of built in functions is shown in section 8.5.3 of the 2010 NI AWR DE users-guide, available by selecting Help on the pull down menu. Variables can be tuned manually or be changed automatically as part of optimisation by selecting Properties and then enabling the Tune and/or Optimize check boxes. If needed the range of values can be constrained to specified upper and lower values. It is desirable to constrain R , L and C from becoming negative.

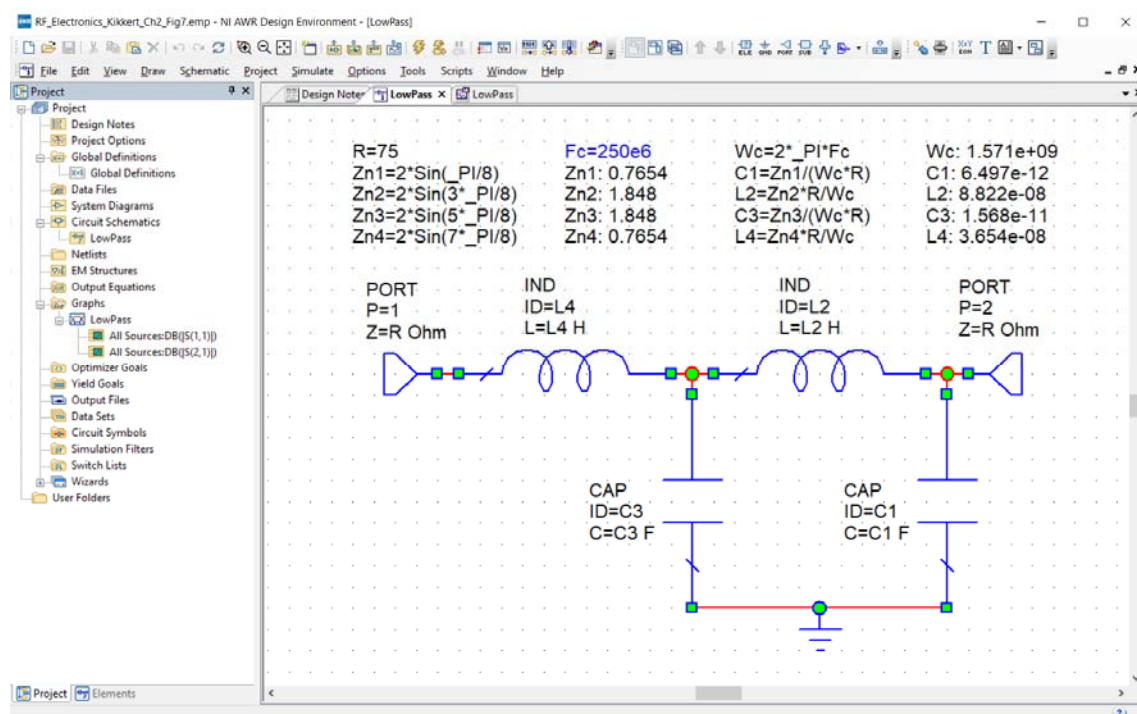


Figure 2.7. Tuneable filter.

Any variables or equations whose variables can be tuned are displayed in a blue font as shown in figure 2.7. Circuit values can either be shown as base values, such as H, F or Hz or as convenient values, such as nH, nF or MHz. If the base values are used, then equations such as equations 2.1 and 2.2 can be used. If convenient units are used, then the appropriate multipliers need to be included in the equations to result in say nF for the capacitance, when a frequency in MHz is entered. When convenient units are used, all the graphs will have the x-axis in the convenient (MHz) units. If the same equations or the same variables are shared in more than one circuit, it is better to locate the equations in the Global Definitions window shown in the left pane of figure 2.7. Those equations are then available to all circuits.

In figure 2.7, the thickness of the lines can be changed by selecting Environment Options \Rightarrow Schematics/Diagrams and setting Symbol Thickness to 10. It is also possible to have equations using the output parameters of a circuit. This is demonstrated in example 5, Bandpass T Matching Network, of this chapter.

Optimisation

Example 2.2: Diplexer

It is required to design a Diplexer to permit VHF and UHF TV signals to be received by separate antennae and then combined, for use by a TV. In Australia the VHF TV frequencies range from 46 MHz to 230 MHz and the UHF TV frequencies range from 527 MHz to 820 MHz. Similar frequency ranges are used in other countries. For this example, 250 MHz is used as the boundary between VHF and UHF. As a result S_{21} (low-pass transfer function) is to be greater than -3 dB for frequencies below 250 MHz and S_{31} (high-pass transfer function) is to be greater than -3 dB for frequencies above 250 MHz. A low pass filter with a cut off frequency of 250 MHz, as shown in figure 2.6 is used thus for the VHF signals and a high-pass filter with a cut off frequency of 250 MHz, is used for the UHF signals. These two filters are then connected as shown in figure 2.9. The same circuit can be used as a splitter, to separate FM radio and UHF TV signals. A diplexer consists of a low-pass filer selecting the low frequency components and a high-pass filter selecting the high frequency components.

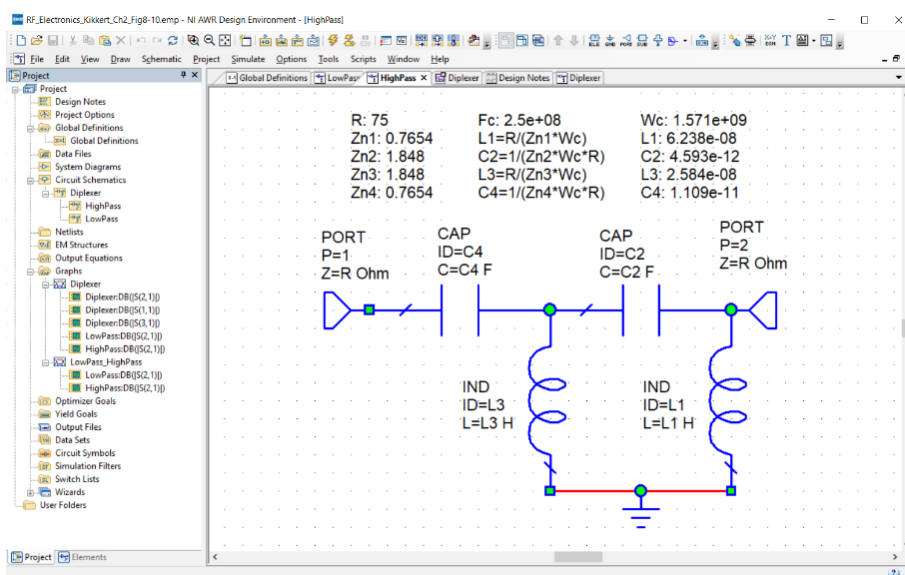


Figure 2.8. High-pass filter.

The easiest way to produce the diplexer is to produce a separate high-pass filter and then use that and the low-pass filter as sub-circuits to produce the diplexer. The low-pass filter can be the Butterworth low-pass filter of figure 2.7. The high-pass filter shown in figure 2.8, uses the component values from table 2.1. The full diplexer is shown in figure 2.9, and the resulting S parameters are shown in figure 2.10.

Practical Note: Since the high-pass and low-pass filter are in parallel, the low-pass filter must have an open-circuit input impedance at high frequencies and the high-pass filter must have an open circuit input impedance at low frequencies. This is achieved by using filters that have the first element as a series element for the input.

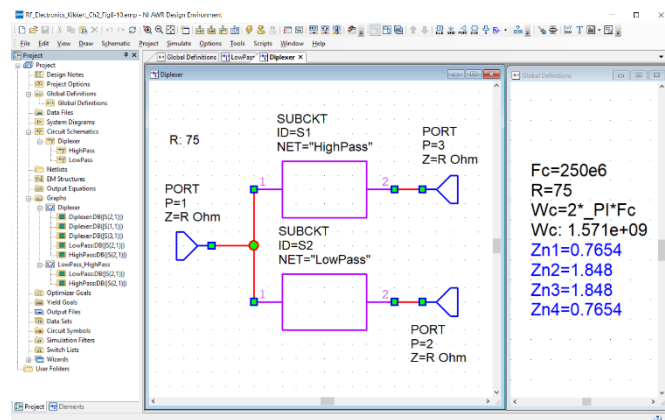


Figure 2.9. Diplexer using low-pass and high-pass sub-circuits.

In this example, one could optimise each of the 8 individual components of the high-pass and low-pass filters. To facilitate the optimisation, it is desirable to keep the number of parameters to be optimised as small as possible, and optimise the 4 values $Zn1$ to $Zn4$, shown in figure 2.9. These are located in the Global Definitions and are used to calculate the element values for both the high-pass and low-pass filters, using the equations in figures 2.7 and 2.9. The corner frequency Fc and Impedance R , are also located in the Global Definitions to allow those to be changed without affecting the optimisation.

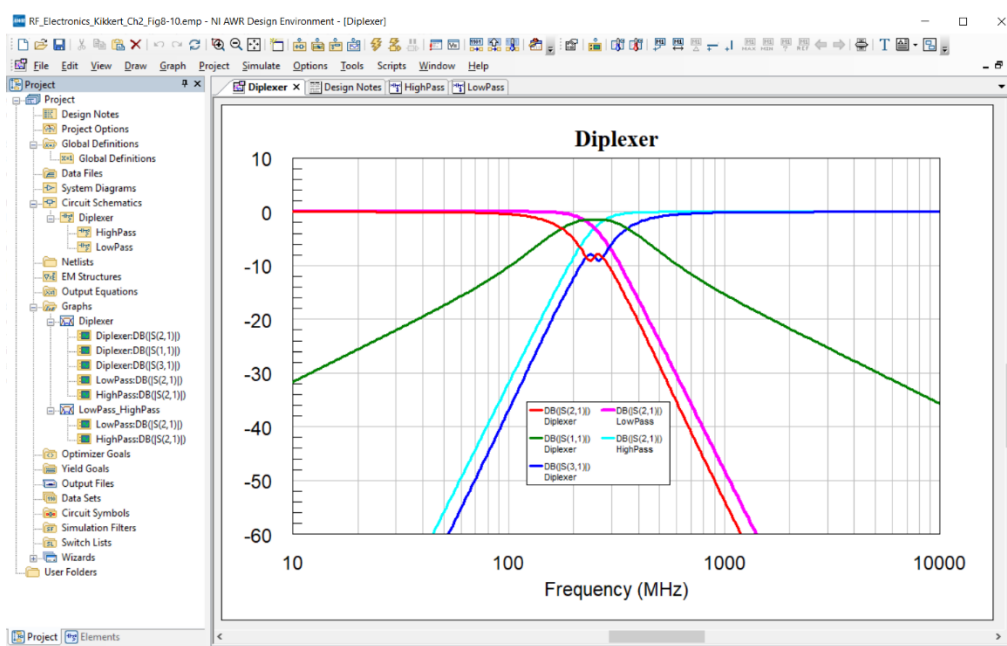


Figure 2.10. Frequency response of the diplexer.

As can be seen from figure 2.10, return loss (S_{11}) is only -1.4 dB near the cut off frequency of the filters so that the input is poorly matched. By comparing the blue curve of the low-pass filter by itself, with the cyan curve of the low-pass filter as part of the diplexer, it can be seen that there is a significant interaction between the low-pass and high-pass filters. There is a similar degradation in performance of the high-pass filter, as shown by the red and magenta traces. One can use the optimisation capability to improve the performance of the diplexer at the crossover frequency range. The first task is to specify the optimisation goals. For this design, the requirements are that S_{11} is less than -20 dB over the entire VHF and UHF TV frequency range.

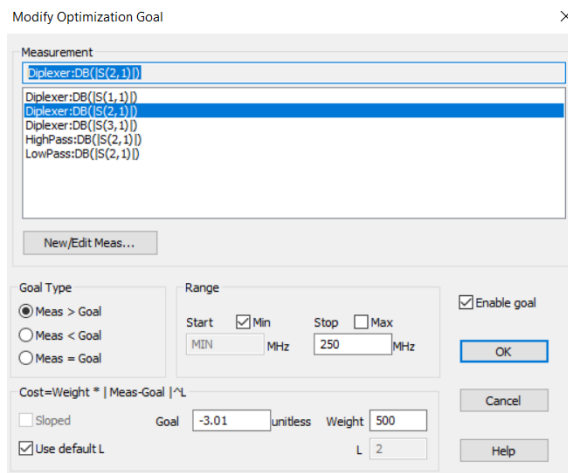


Figure 2.11. Specification of optimisation goals.

These optimisation goals are entered in the optimisation goal function as shown in figure 2.11. Double click on the elements to be optimised and select the “optimize” checkbox in the element options window, for the component or the variable linked to a component as shown in figures 2.7 and 2.8, to ensure that the element can be optimised. In addition, some attenuation limits at 100 MHz and -35 dB and 625 MHz and -35 dB, for S_{21} and S_{31} can be added, to prevent the components being changed so that all frequencies are passed by both the high-pass and low-pass networks. Finally, the S_{11} limit is set to -45 dB to ensure a near perfect match over the entire frequency band. Often the optimisation limits are changed during the optimisation process, to ensure the best performance to be obtained for the final network. For most circuits a higher return loss is normally acceptable, however this network will optimise in one-step to meet these limits. The weighting of the pass-band optimisation limits for S_{21} and S_{31} are made 1000 since the typical errors are much smaller than the error in S_{11} , which is given a weighting of 1 to give comparable errors at the start, thus ensuring that all limits receive sufficient optimisation effort.

Select *Simulate* \Rightarrow *Optimise* to start the optimisation. For this optimisation, "Simplex Optimisation" is a good optimisation method to use and the optimisation will reach its goal in one-step. Figure 2.12 shows the optimisation starting performance with the optimisation goals and the Optimizer panel. A logarithmic frequency scale is used since that will clearly show the straight lines of the 80dB/decade stopband attenuation. Figure 2.13 shows the optimisation criteria and the performance after the optimisation has been completed. It can be seen that the diplexer meets all the required specifications and that it is even possible to meet a -45 dB return loss on S_{11} . Less than 300 iterations of the "Simplex Optimisation" are required to obtain the final values. Changing the S_{11} optimisation limit to -60 dB, allows S_{11} to be reduced even further.

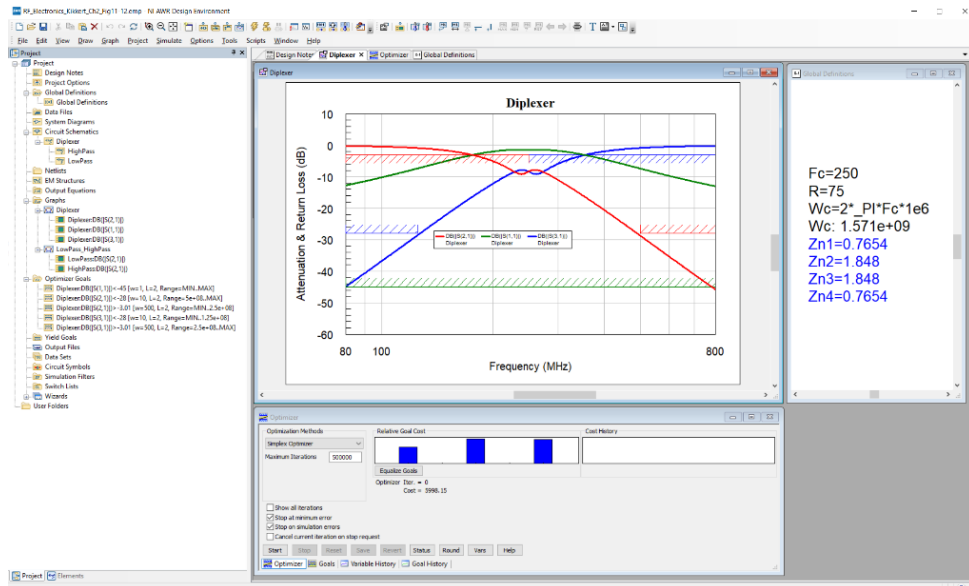


Figure 2.12. Optimisation criteria and the diplexer performance before optimisation.

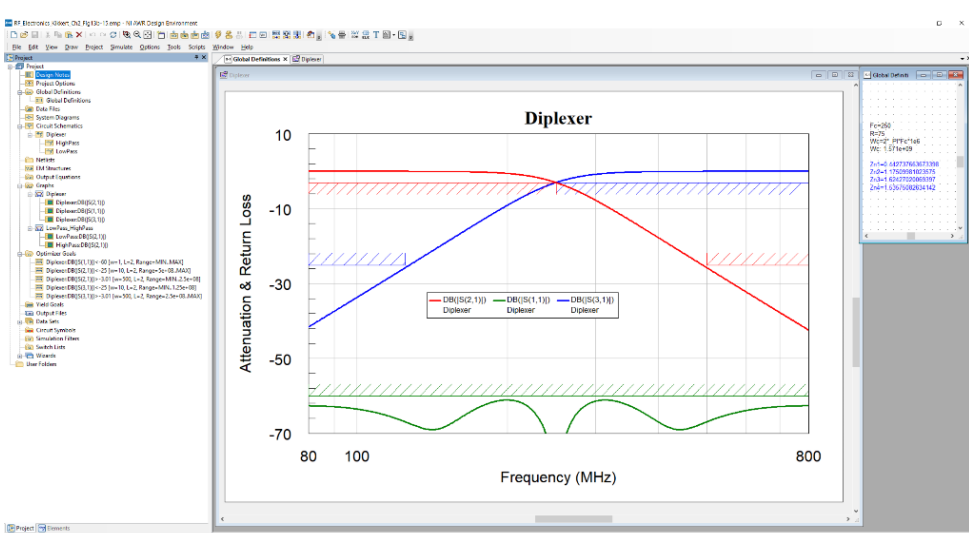
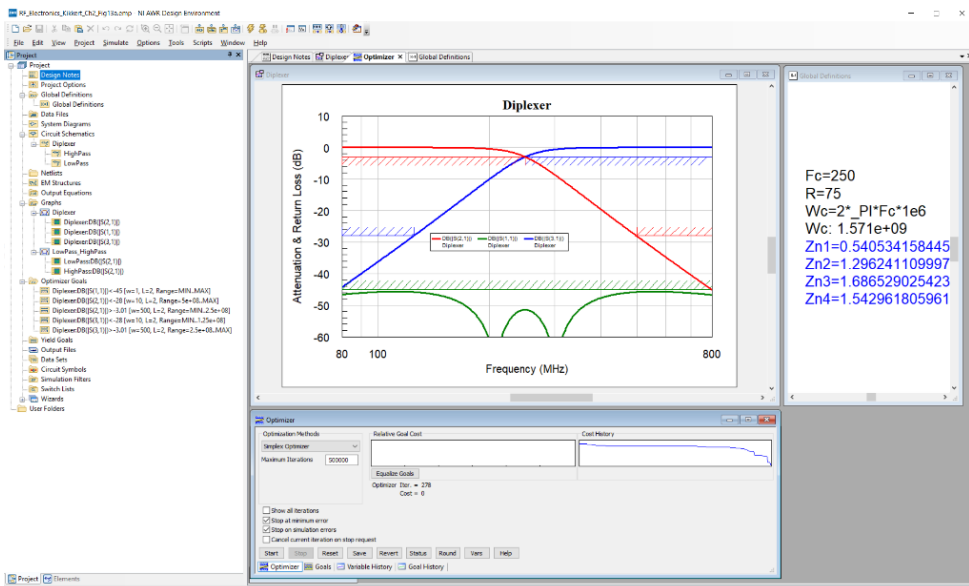


Figure 2.13. Diplexer performance after optimisation. Top 45dB, bottom 60dB for S11.

For the -60dB optimisation of S11, the stopband attenuation limits need to be reduced slightly from -28 dB to -25 dB. It then becomes a choice whether a better S11 or a higher stopband attenuation is more important. Zn1 reduces more but Zn4 does not change much when going from -45 dB for S11 to -60dB.

When the cost function does not decrease, it is worthwhile to change some conditions since the optimisation may be stuck in a local minimum rather than the global minimum for the cost function. Changing the weight for one or more of the goals or changing the optimisation function may get the optimisation out of the local minimum. The “random local” optimiser is good for a complex optimisation function that will exist close to the global optimum condition. Other optimisation methods, such as Simulated Local Annealing or Discrete Local Search can also be tried to ensure the optimisation is not stuck in a local minimum. It may even be necessary to alternate between several optimisation strategies and change optimisation limits and weights in order to ensure that a good performance is obtained. For this example, a Discrete Local Search will not produce a good optimisation, however for complex problems [20] it gives better results than the Simplex Optimisation. It is thus important to try different optimisation techniques to obtain the best results. A good overview of each optimisation method can be found in section 2.6.8 of the NI AWR DE Simulation and Analysis Guide.

The component values of the filter after optimisation with a -60 dB S₁₁ return loss for the low-pass sub-circuit are shown in figure 2.14 and those for the high-pass sub-circuit are shown in figure 2.15. Note that the component values are significantly different from the starting values using the Butterworth filter table values. The component values are very practical, so that the diplexer can easily be made.

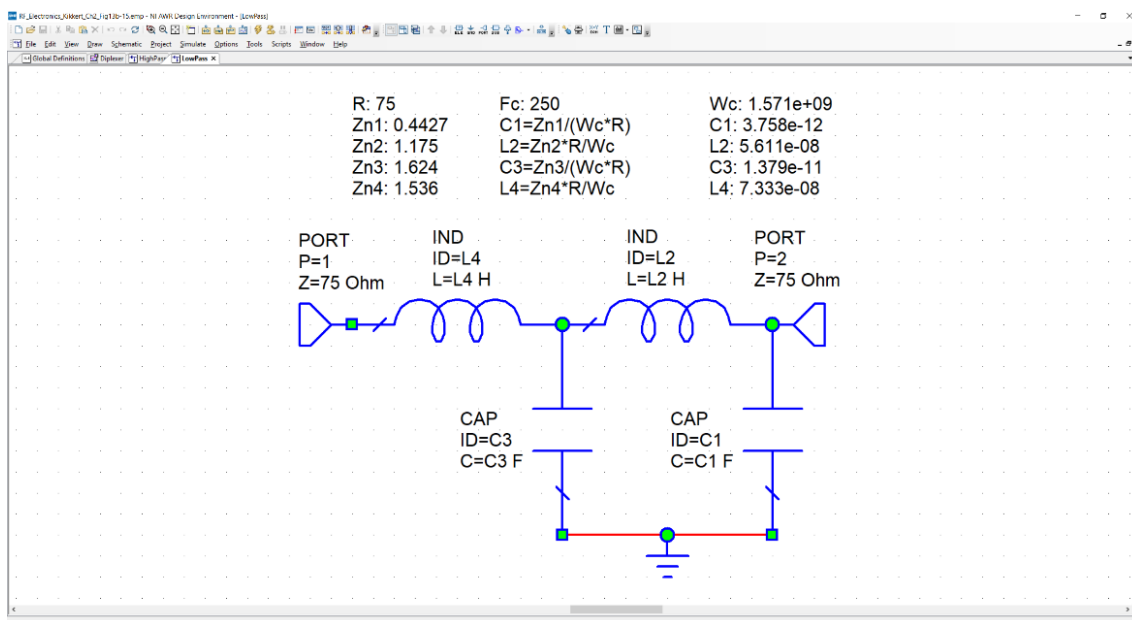


Figure 2.14. Final low-pass filter for diplexer.

It is possible to replace the inductors using Microstrip lines as shown in figures 7.10 and 7.11 of Chapter 7. Using Microstrip lines allows this diplexer to be made on a low cost FR3 or FR4 PCB using only capacitors and Microstrip lines. If this is done then the length and impedances of the Microstrip lines must be further optimised to meet the same specifications as this diplexer, since figures 7.10 and 7.11 show that Microstrip lines behave different from inductors when their line length becomes comparable to a quarter wavelength.

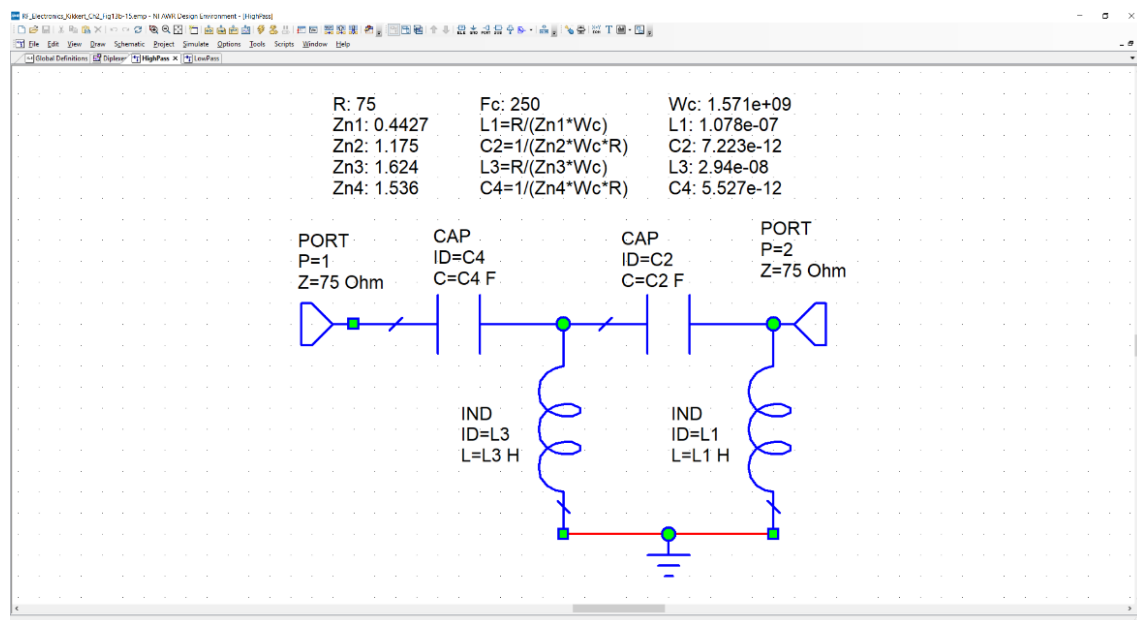


Figure 2.15. Final high-pass filter for diplexer.

Example 2.3: Amplifier

For the third example, an amplifier is designed and its performance is determined. The design is to use a BRF340F transistor. The full transistor model can be obtained from the AWR Vendor Library from *Parts By Type* \Rightarrow *Nonlinear* \Rightarrow *Infineon* \Rightarrow *GBJT* \Rightarrow *BRF340F*. If desired, the Vendor Library Parts can be installed locally, using the procedure outlined in Appendix 1. Using this nonlinear model, the quiescent voltages can be determined by MWO using the DC solver in the harmonic balance simulator. This is very useful to ensure that the biasing is correct. For a load resistor at port 2 = 1 k Ω and R1 = 1 k Ω , a 500 Ω effective load resistor results. For a gain of 5, a 100 Ω emitter resistor is required, since the gain is approximately (Load Resistance)/R4. For a 12 V supply, a collector voltage of close to 7V will result in close to the maximum output swing from the amplifier. Figure 2.16 shows the circuit of a simple amplifier using the BRF340F transistor and the vendor library data. This transistor is available from several manufacturers and many have SPICE-compatible transistor models on their web sites [8-13].

The first and very critical step of any transistor design is the biasing. By right clicking on the “Transamp” circuit-schematic and selecting “Add Annotation” and then selecting “DCVA_N” will provide voltages at all the nodes in the circuit, to enable the biasing voltages to be checked and compared with the design values. The node voltage annotation is shown in figure 2.16. Similarly, currents in and out of all the nodes can also be shown. The resistors R1 and R4 can be adjusted to ensure that the correct gain and quiescent collector current are obtained and the biasing resistors R2 and R3 can be adjusted to ensure that the maximum output swing is obtained. For most transistors, the effect of supply voltage, temperature, and component variations can be investigated, to ensure that the design works properly for all expected component tolerances. However not all device models include a temperature model.

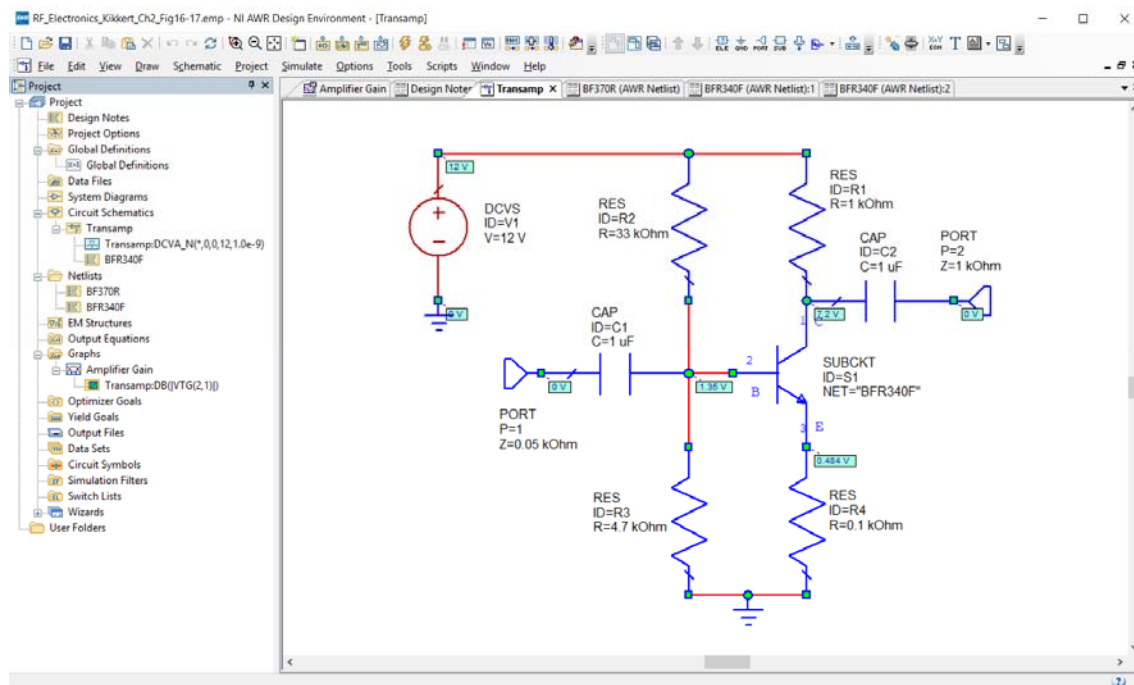


Figure 2.16. Transistor amplifier circuit diagram.

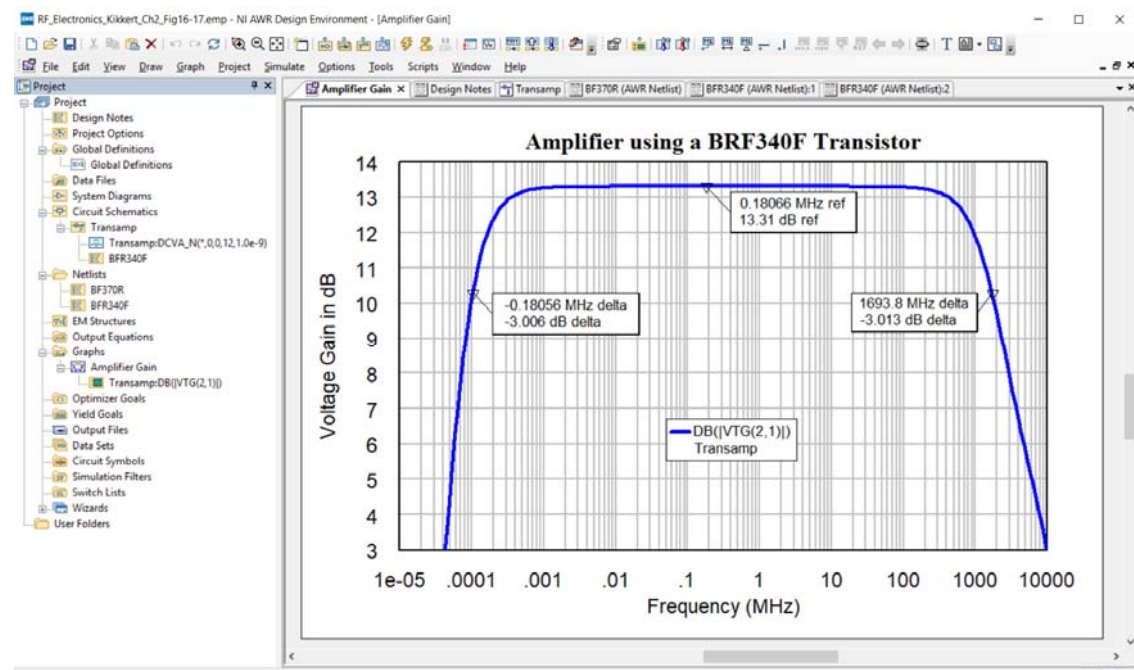


Figure 2.17. Frequency response of the amplifier of figure 2.16.

The resulting frequency response of the amplifier is obtained by selecting *Graph* \Rightarrow *New Graph* \Rightarrow *Rectangular*. Then right clicking in on that graph label in the *Project Browser* and selecting *Add Measurement* \Rightarrow *Linear* \Rightarrow *Gain* to add the measurement required. In this case, a linear Voltage gain from input to output terminal (VGT), with a magnitude response in dB is selected. It is also possible to perform a non-linear, steady state, voltage gain analysis using Harmonic Balance, where for instance the variation of gain of this amplifier can be determined as the input signal is varied. Harmonic Balance simulations are essential to determine the performance of power amplifiers.

The frequency range over which the measurements are made are set by double clicking on “Project Options” in the Project Browser and then specifying the frequency range. In this case, the data entry units are set to *MHz*, the start frequency is set to 1e-5 MHz and the stop frequency is set to 1e4 MHz. The sweep type is set to *Logarithmic* and the number of points per decade is set to 25. The resulting frequency response from the amplifier is shown in figure 2.17. Selecting *Graph* \Rightarrow *Marker* \Rightarrow *Add Marker*, allows markers to be added to the graph. These markers can search for the maximum value of the voltage, or for specific attenuation values or frequencies. Using these markers, the amplifier has a gain of 13.3 dB and an upper 3 dB frequency of 1.69 GHz. A gain of 5 corresponds to 14 dB. The actual amplifier gain is thus just 0.7 dB less than the ratio of the load resistor to the emitter resistor.

Transistor Models

Several different types of transistor models can be used. The simplest ones are linear analytical models, such as the Hybrid, Pi or T models used in basic electronic design subjects. For these models, MWO treats the transistor as a linear device and only an AC analysis can be performed. A linear measurement based model of a device can be an N port subcircuit containing an S-parameter data file. For example placing the uPC8181TB MMIC amplifier from Renesas in a circuit, by selecting *Element* \Rightarrow *Libraries* \Rightarrow *AWR Web site* \Rightarrow *Parts by Type* \Rightarrow *Data* \Rightarrow *Renesas* \Rightarrow *IC* \Rightarrow *1_Wide_Band_Amp* \Rightarrow *uPC8181TB* $V_{cc}=3V$ $I_{cc}=23mA$. Inserts a 2-port subcircuit in the circuit schematic that contains an S parameter file for the model. The BIP linear model of a transistor used by MWO is shown in figures 2.18. This model includes lead inductances, are normally ignored for lower frequency models.

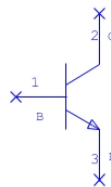
The second type are non-linear analytical models. MWO includes a large range of non-linear analytical device models. These include Angelov, Gummel-Poon, Parker-Skellern, SPICE, Statz and Volterra based transistor models. These non-linear models result in a more accurate analysis of the transistor circuit. Non-linear measurement based models include the Cardiff Model and Keysight’s X-Parameter model. A good description of different non-linear device models is given in [14]. The model for the BRF340F transistor used in figure 2.16 and 2.17 is a text based spice model. That netlist can be opened and observed, from the project browser of the project file for figure 2.16.

The Gummel-Poon Transistor model [15] included in NI AWR DE has the circuit diagram shown in figure 2.19. The model includes some device non-linearity but significantly more complex than the BIP model shown in figure 2.18.

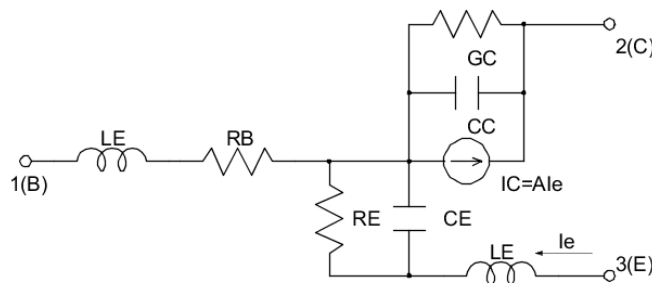
Details of the Gummel-Poon model for a BC337 transistor can be seen by selecting *Circuit Elements* \Rightarrow *Libraries* \Rightarrow *AWR web site* \Rightarrow *Parts by Type* \Rightarrow *Nonlinear* \Rightarrow *Zetex* \Rightarrow *GBT* \Rightarrow *NPN* \Rightarrow *BC337*, and placing that transistor in a transistor amplifier, like the one of figure 2.16. Simply changing the transistor in figure 2.16 results in a slight change of gain in the passband, but results in an upper -3dB frequency of 50 MHz due to the reduced frequency response of the transistor. Right clicking on the transistor symbol in the schematic and selecting *Properties* \Rightarrow *Show Secondary*, opens up the parameters list, shown in figure 2.20.

Bipolar Transistor (Closed Form): BIP

Symbol



Equivalent Circuit



Parameters

Name	Description	Unit Type	Default
ID	Element ID	Text	B1
A	Magnitude of DC current gain (alpha)		0.8
T	Current gain time delay	Time	0 ns
F	-3dB frequency for current gain	Frequency	0 GHz
CC	Collector capacitance	Capacitance	0 pF
GC	Collector conductance	Conductance	0 S
RB	Base resistance	Resistance	1 Ohm
LB	Base inductance	Inductance	0 nH
CE	Emitter capacitance	Capacitance	0 pF
RE	Emitter resistance	Resistance	1 Ohm
LE	Emitter inductance	Inductance	0 nH

Figure 2.18. BIP circuit of the closed form transistor model from NI AWR DE [16].

Equivalent Circuit (Vertical)

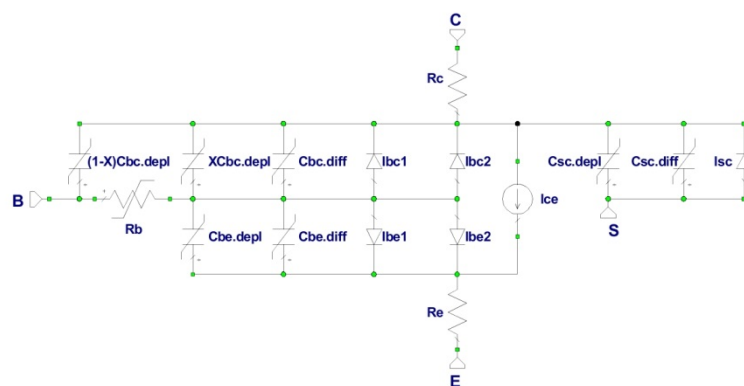


Figure 2.19. Circuit diagram of the Gummel-Poon Transistor model From NI AWR DE.

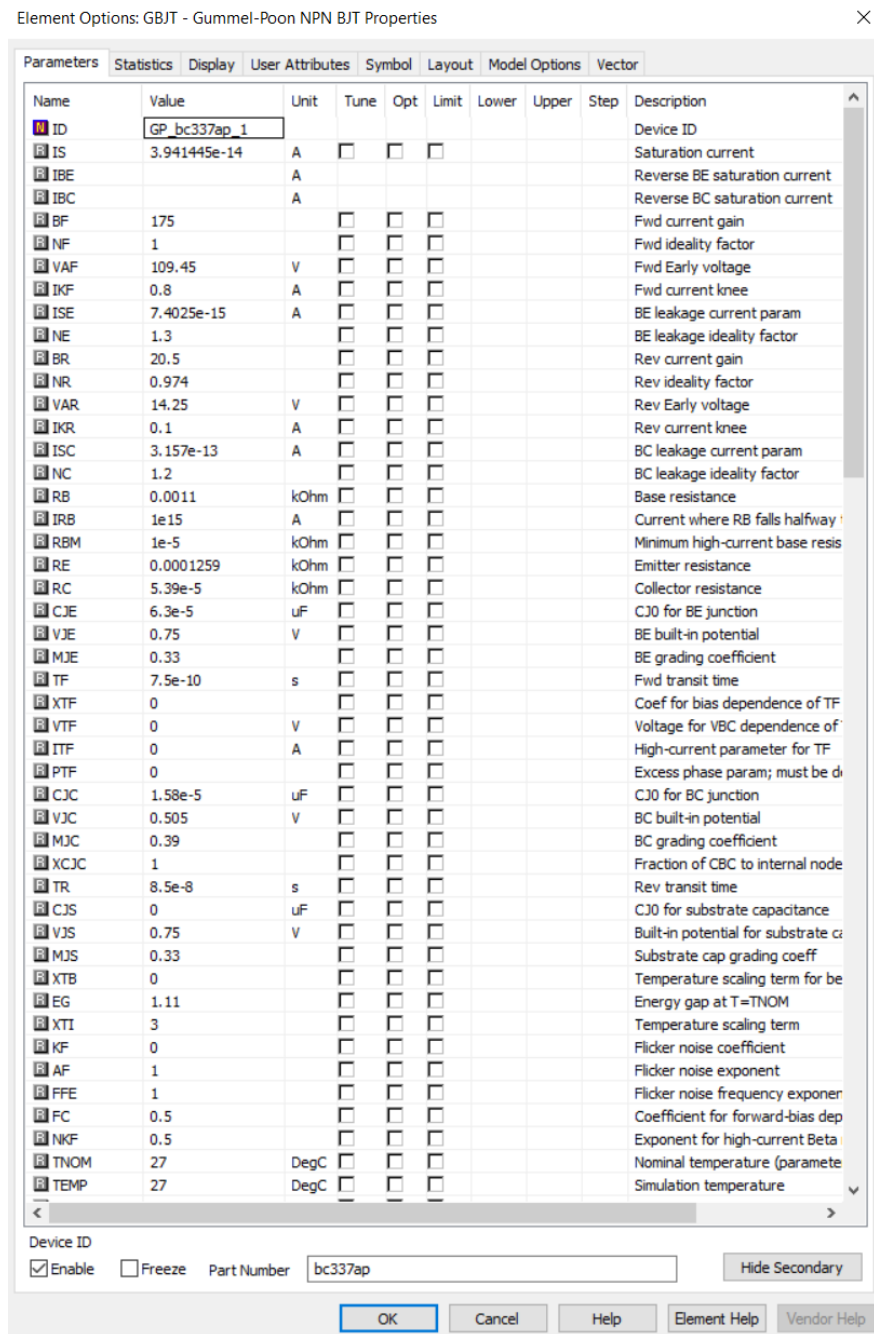


Figure 2.20. Parameters of a BC337 Gummel-Poon transistor model.

Using an existing transistor as a starting point or the Gummel-Poon model available at *Circuit Elements* \Rightarrow *Nonlinear* \Rightarrow *BJT* \Rightarrow *GBJT*, the model for another transistor can be produced by editing the secondary parameters and then saving that with a new part number.

For some transistors, instead of the device parameters of figure 2.20, a SPICE netlist, imported as a data file, is included in the NI AWR device libraries from the web site. As an example a BFR340 transistor SPICE file can be used can be used by selecting *Elements* \Rightarrow *Libraries* \Rightarrow **AWR web site* \Rightarrow *Parts by Type* \Rightarrow *Nonlinear* \Rightarrow *Infineon* \Rightarrow *RF Bipolar Transistors* \Rightarrow *Low Noise Si Transistors up to 2.5 GHz*. That transistor is used in figure 2.16 and right clicking on its symbol shows it is linked to the shows the following Gummel-Poon SPICE data:

```

! ****
! Infineon Technologies AG
! GUMMEL-POON MODEL IN SPICE 2G6 SYNTAX
! VALID UP TO 10 GHZ
! >>> BFR340F <<<
! (C) 2008 Infineon Technologies AG
! Version 0.1 August 2008
! ****
! .OPTION TNOM=25, GMIN= 1.00e-12
! BFR340F B C E
DIM
  TEMP C
  FREQ HZ
  RES OH
  COND /OH
  IND H
  CAP F
  LNG M
  TIME SEC
  ANG DEG
  VOL V
  CUR A
  PWR DBM

CKT
CAP 22 33 ID="CBEPAR" C=4.4e-014
CAP 22 11 ID="CBCPAR" C=6.5e-014
CAP 11 33 ID="CCEPAR" C=3.885e-014
IND 22 2 ID="LB" L=5.70986e-010
IND 33 3 ID="LE" L=5.56805e-010
IND 11 1 ID="LC" L=4.17072e-010
CAP 2 3 ID="CBEPCK" C=4.182e-015
CAP 2 1 ID="CBCPCK" C=6.05287e-014
CAP 1 3 ID="CCEPCK" C=9.15498e-014
GBJT 22 11 33 4 ID="Q1" IS=2.588e-017 BF=208.3 NF=1 &
  VAF=80.12 IKF=0.1012 ISE=1.921e-015 NE=2 BR=8.99 &
  NR=0.95 VAR=2.277 IKR=0.1924 ISC=3.85e-015 NC=1.5 &
  RB=9.93 IRB=0 RBM=4.697 RE=1.016 RC=5.655 XTB=1.3 &
  EG=1.11 XTI=6.55 CJE=9.724e-014 VJE=0.693 MJE=0.2059 &
  TF=6.468e-012 XTF=12.98 VTF=1.928 ITF=0.04152 &
  PTF=0.1 CJC=1.25e-013 VJC=0.5602 MJC=0.09189 &
  XCJC=0.7499 TR=8.853e-005 CJS=1.249e-013 MJS=0.3243 &
  VJS=0.5013 FC=0.5 KF=0 AF=1
! ****
DEF3P 2 1 3 "BFR340F"

```

Alternately, SPICE models for a wide variety of transistors can be obtained from several websites. As an example, the model for the BD136 transistor obtained from the ONsemi [12, 13] web site is as follows:

```

*****
* Model Generated by MODPEX *
*Copyright(c) Symmetry Design Systems*
* All Rights Reserved *
* UNPUBLISHED LICENSED SOFTWARE *
* Contains Proprietary Information *

```

```

* Which is The Property of      *
* SYMMETRY OR ITS LICENSORS    *
* Modeling services provided by *
* Interface Technologies www.i-t.com *
*****
.MODEL Qbd136 pnp
+IS=1e-09 BF=681.414 NF=0.85 VAF=10
+IKF=0.196957 ISE=1e-08 NE=1.57381 BR=56.5761
+NR=1.5 VAR=0.975138 IKR=0.952908 ISC=1e-08
+NC=3.58666 RB=40.4245 IRB=0.1 RBM=0.106663
+RE=0.00034585 RC=1.31191 XTB=22.4074 XTI=1
+EG=1.05 CJE=1e-11 VJE=0.75 MJE=0.33
+TF=1e-09 XTF=1 VTF=10 ITF=0.01
+CJC=1e-11 VJC=0.75 MJC=0.33 XCJC=0.9
+FC=0.5 CJS=0 VJS=0.75 MJS=0.5
+TR=1e-07 PTF=0 KF=0 AF=1
* Model generated on Feb 22, 2004
* Model format: PSpice

```

The functionality of both these methods is identical and the technique for importing SPICE files into NI AWR DE, is shown in appendix 2. Alternately, one can simply change the format by entering the BRF340F parameter values shown on the previous page into the parameter window shown in figure 2.20 for the BC337 and then renaming and saving the device. If needed circuit symbols can also be changed.

Determination of Transmission Line Parameters

In many applications, a printed circuit layout using microwave printed circuit board materials needs to be made. The widths and lengths required can be determined from a program TXLine, which is part of NI AWR DE. This program does not cover all the different coupled lines or strip lines available. In many cases, it is more convenient to use the schematic circuit realisation of the transmission line models to determine the required line parameters, rather than using TXLine. This technique is illustrated by the following example of a quarter-wavelength long Microstrip line with a 50Ω impedance at 1 GHz.

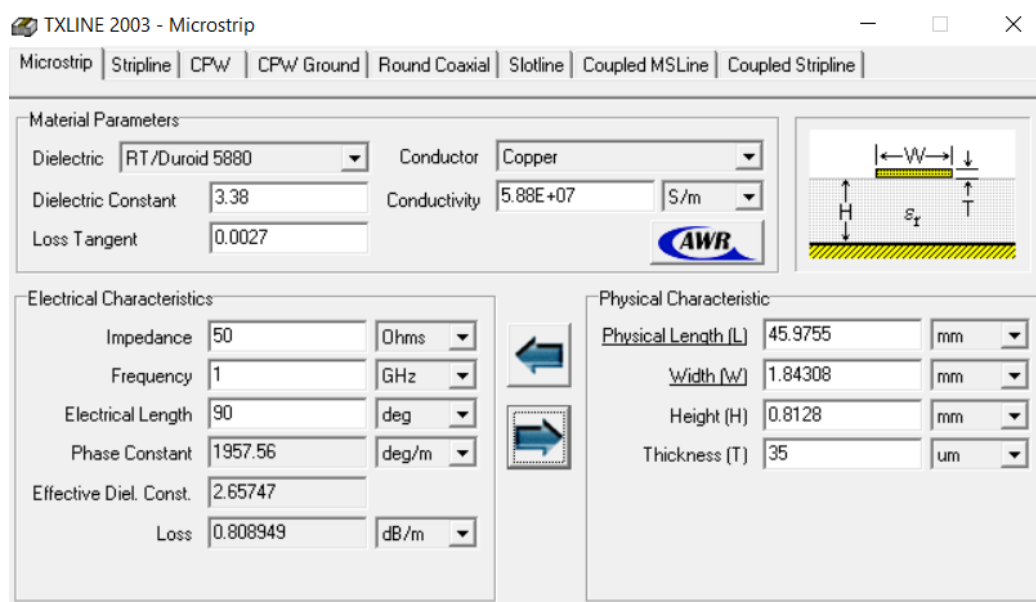


Figure 2.21. TXLine program for calculating line parameters.

The calculations for the width of a 50Ω Microstrip line using TXLine for a Rogers RO4003 substrate, with a dielectric constant of 3.38, a loss tangent of 0.0027, a substrate thickness of 0.8128 mm and 35 micron (1 oz.) copper cladding, is shown in figure 2.21. This shows that: a quarter-wavelength long Microstrip line with a 50Ω impedance at 1 GHz requires a track width of 1.84308 mm and length of 45.9755 mm.

The same line width determination can be done by making some very simple test circuits and optimising the relevant parameters. Figure 2.22 shows a schematic for determining the correct line width for a 50Ω track on a RO4003 substrate. The same PCB parameters that are used in TXLine are used for the substrate element in the circuit schematic of figure 2.22. When the line is exactly 50Ω , then the return loss (S_{11}) is very small regardless of frequency, as described in Chapter 4 "Transmission Line Transformers and Hybrids" of this book. Tuning or optimising the line width to give the lowest return loss S_{11} results in a -60 dB return loss for a 1.851mm line width. That width is close to the result from TXLine.

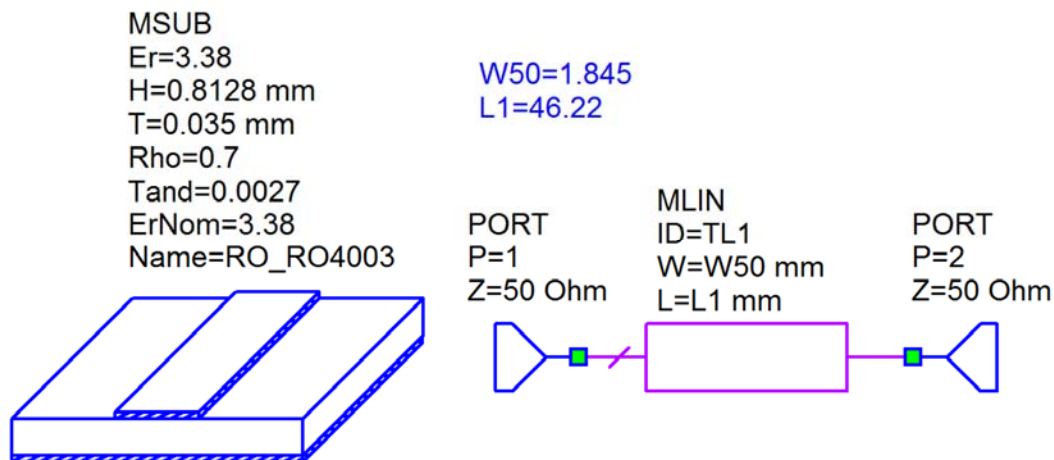


Figure 2.22. Circuit for determining microstrip line widths.

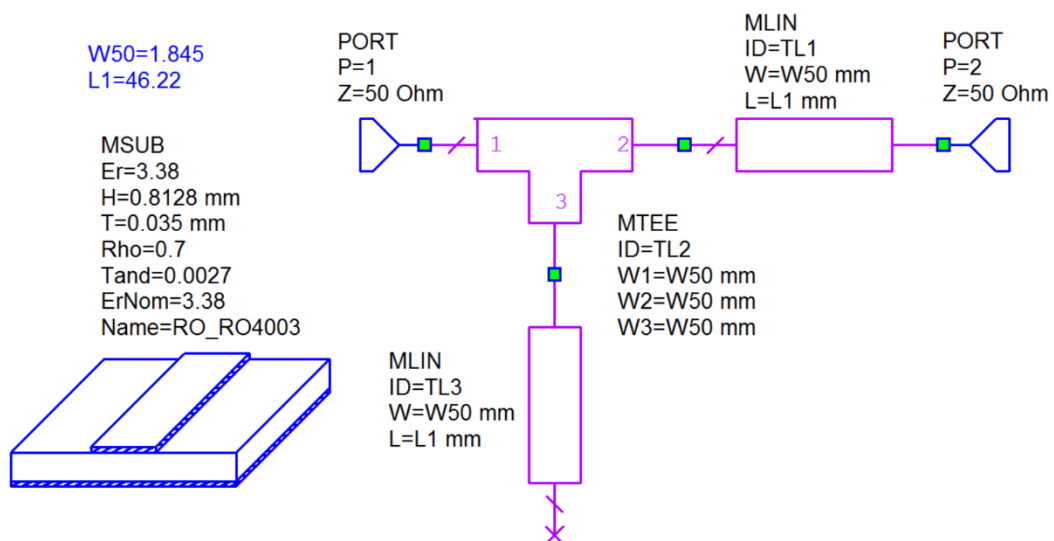


Figure 2.23. Circuit for determining the length of one-quarter wavelength.

When the length of a quarter wavelength long line needs to be determined, then the circuit of figure 2.23 can be used. The open circuited stub will reflect as a short-circuit, when

the length of the stub is one quarter wavelength. Using the width as determined in figures 2.21 or 2.22, the length is now tuned or optimised to produce a notch at the required frequency, as shown in figure 2.24. The T junction can be included to ensure that the actual layout, including the required junctions, performs exactly as required.

For many circuits, simple test circuits like those of figures 2.22 and 2.23 can be used to determine the basic parameters of Stripline or Microstrip lines that can then be used as part of a more complex circuit. This is used in several places throughout this book.

This technique is very useful for obtaining the correct length when the stub has bends in it, as is the case for the design of a Branchline coupler with folded lines to reduce the size, as described in Chapter 4 "Transmission Line Transformers and Hybrids" of this book.

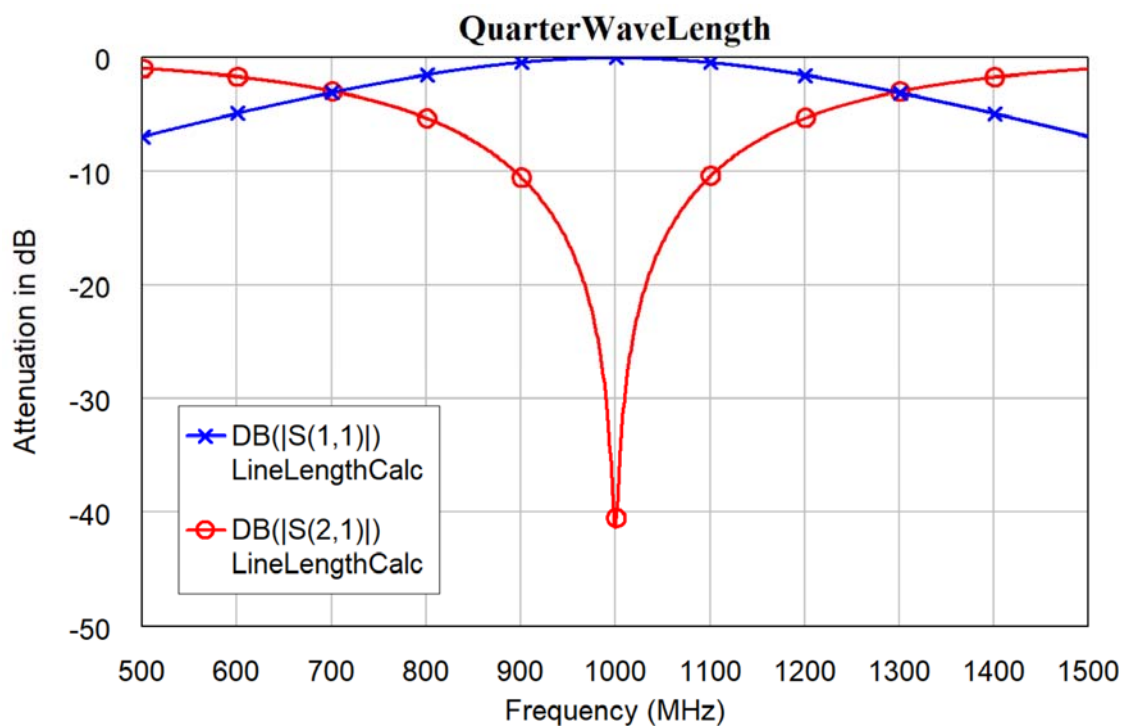


Figure 2.24. Frequency response of the circuit in figure 2.23.

Nonlinear Simulation

Many electronic circuits are nonlinear. For example, frequency mixers described in chapter 5 use nonlinear properties of diodes to produce the frequency shifting of RF signals used in most radio and TV receivers. The output amplitude of oscillators described in chapter 6, is determined by the saturation of the active devices. Power amplifiers, described on chapter 9, are normally operated at power levels where the active devices are operating close to saturation and are thus operating in nonlinear regions. The ability to analyse the effect of the nonlinear operation of circuits is thus an important part of any design.

There are two types of nonlinear simulation. The first type is time domain based **transient** simulation, like the classical Laplace transform based circuit analysis for linear circuits. The time waveforms produced by computer simulation programs such as Multisim, Microcap and LTSPICE use SPICE time based simulation. NI AWR DE includes transient time based simulation using APLAC® or the optional HSPICE® and Spectre® software. Transient analysis, begins at time $t = 0$ and assumes that only DC sources are

connected to the circuit to be analysed, before that time. At time $t=0$ a stimulus is applied and the resulting current and voltage waveforms are determined at ports or test points. The transient simulators start with the largest possible time increment and reduce that time increment automatically if the results are not accurate enough. If needed the automatic time increment selection can be overridden. See *Basic_Transient.emp* project in the MWO/AO /Examples [17] for an example included with the NI AWR DE software. It is desirable to read the help file NI AWR DE Simulation and *Analysis Guide* > *Transient Analysis* > *Transient Analysis Basics* (Section 7.1) [18], included with NI AWR DE software for additional information if needed. These help files contain much more detail than what is needed for this book. Transient analysis is useful for determining the transient time and voltage waveforms of a circuit.

The second type is Harmonic Balance (HB). This is a frequency based, **steady state** analysis that uses non-linear differential equations to model the devices and then uses a linear combination of excitation tones to balance currents and voltages to satisfy Kirchhoff's law. The inputs applied to the circuit are one or two tone signals, whose amplitudes or frequency can be swept if needed. The amplitude, phase and frequency at the ports or test points in the circuit, as determined by HB can be used to calculate the corresponding time waveforms.

HB has a lower noise floor than transient time simulation and is thus better for determining harmonics. Examples of harmonic balance simulations are shown in Chapter 5 "Mixers" and Chapter 6 "Oscillators" of this book. Harmonic Balance provides a fast simulation of the most common RF circuit analysis; the steady state operation of non-linear circuits, and it able to easily display the corresponding time waveforms and spectra. Harmonic Balance is thus used more often than transient time domain simulation.

NI AWR DE comes with a built-in HB analyser and more recently with the APLAC™ simulator, which includes both HB and transient analysis simulation.

Time Domain Transient Circuit Simulation

The time domain transient analysis is illustrated with the simulation of a Buck DC-DC converter, used in many power supplies. For this circuit the maximum voltages and currents in the start-up transients are important as well as the steady state operations. This example is used to show both transient and harmonic balance analysis operation.

Example 2.4: Buck DC-DC Converter

The specifications are for the buck converter to change 24 Volt DC to 6 Volt DC. An output current of 0.5 Amp is required and the switching frequency of the converter is to be 20 kHz, to place it outside the audible range. For a 0.5 A output current, the load resistor must be $6/0.5 = 12$ ohm.

The first step is to set the frequency of operation by setting the Frequencies in the project options as a single frequency of 20 kHz as shown in figure 2.25. Setting this frequency automatically controls the time steps used in the simulation in order to obtain an accurate solution. It is possible to do simulations for multiple operating frequencies of the Buck converter. However this would tend to confuse the output plots, so single frequencies are best.

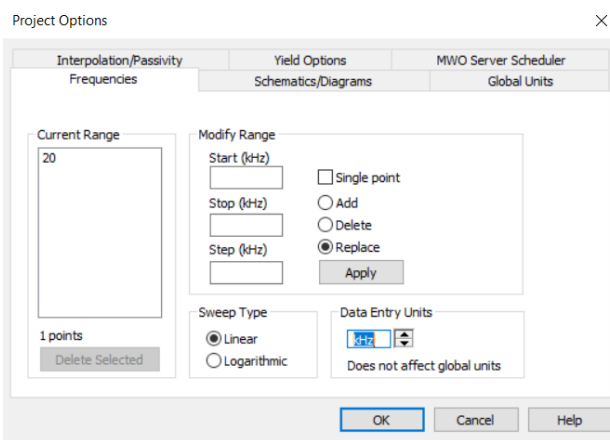


Figure 2.25. Frequency setting for transient simulation.

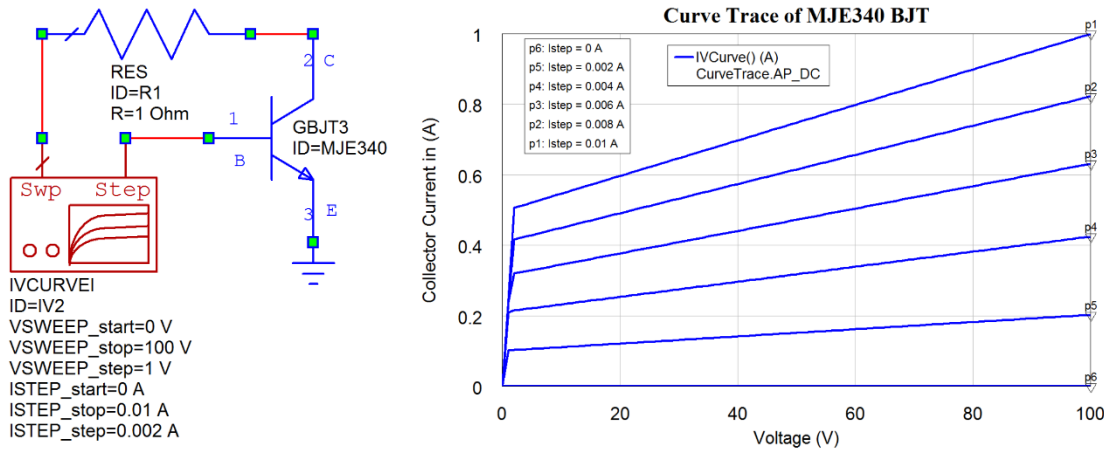


Figure 2.26. Curve tracer use and output for MJE340 BJT.

NI AWR DE allows the transistor's IV curves versus bias current to be plotted using the IVCURVEEI measuring device. Figure 2.26 shows that for a 0.5 Amp collector current, and 24 V, a 10mA base current is required. For a 10 V control source, a 1 kΩ base resistor is thus the largest value that can be used. To provide some overdrive and allow for transistor gain variations, a 470 Ω base resistor is used. For a 1% output ripple, F_c , the corner frequency of the LC network is 1 kHz. When the load resistor and capacitor form a network with a Q of 0.7, then the transient response of the output voltage has minimal overshoot and this corresponds to a C of 9 μF and an inductor of 2.6 mH.

The circuit of the buck converter is shown in figure 2.27. Ideally, for a 24 Volt input and a 6 Volt output, the transistor switch needs to be ON for 6/24 i.e. one quarter of the period. 20 kHz is a 50 μs period, so that the switch needs to be ON for 12.5 μs. In figure 2.27, Voltage probes have been used for the measurement points. They are not really needed since VP1 is the same as the voltage at node 1 of the inductor, IND.L2@1 and VP2 is the same as IND.L2@2. The use of voltage probes makes it easier to identify the measurement locations.

In this example, we want to analyse the transient response and settling of the output voltage. This requires 5ms or 100 periods of the 20 kHz pulse generator V_{PLS} to be observed. This is set by setting *Options* ⇒ *Default Circuit options* and selecting *APLAC Sim* and then setting the number of periods to 100, as shown on the left of in figure 2.28, to provide accurate waveforms.

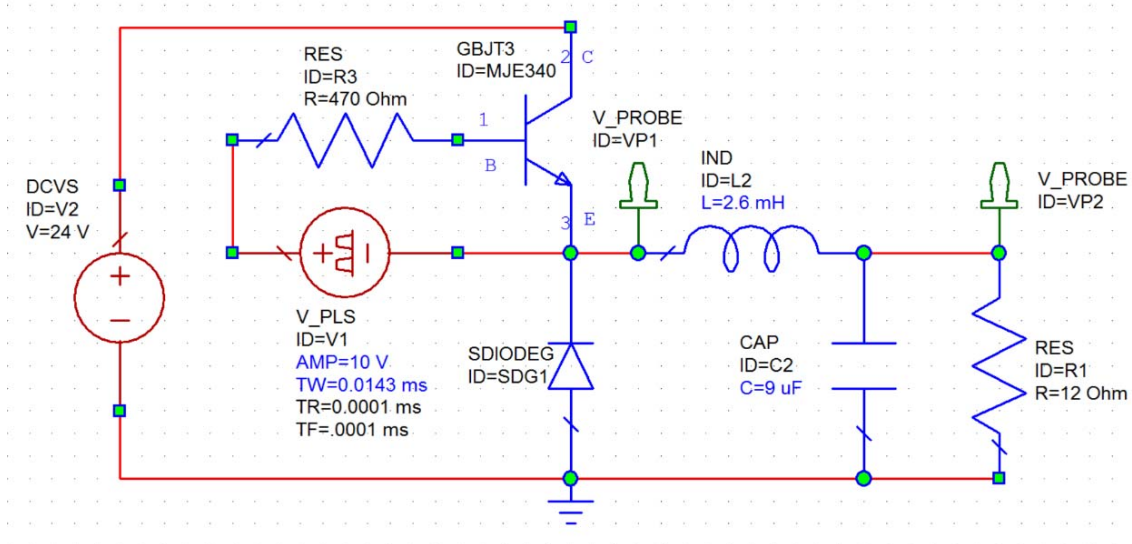


Figure 2.27. Buck DC-DC converter circuit.

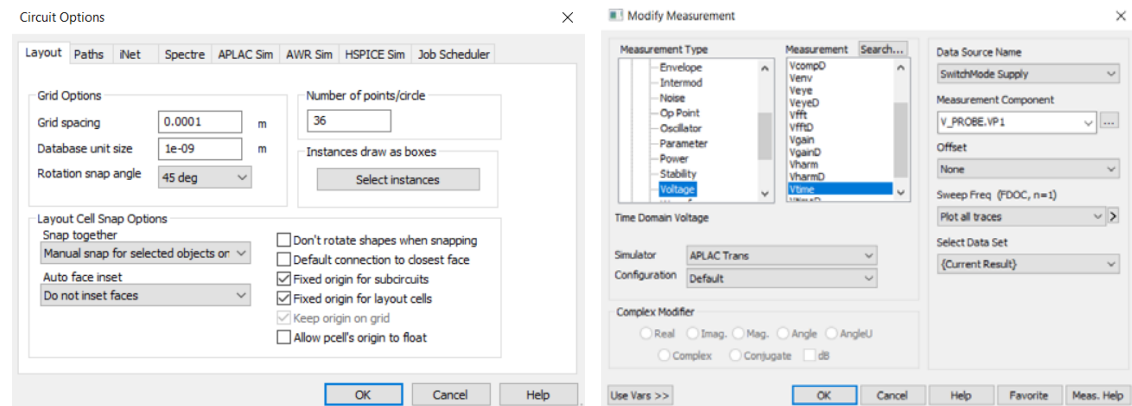


Figure 2.28. Option settings (L) and measurement type window (R) for transient analysis.

To specify the measurement points, select *Nonlinear* and *Current* and *Itime* for current measurements versus time and *Voltage* and *Vtime* for voltage measurements versus time. Ensure that the simulator selected is *ApLAC Trans* for the transient analysis required, as shown on the right in figure 2.28. This then turns on the APLAC transient analysis and turns off any HB analysis for that measurement. Then select the location of the voltage or current to be measured, by double clicking on the small window showing "..." next to "Measurement Component" in figure 2.28. This then shows the circuit diagram of figure 2.27 and allows the selection of the component or lead where the current or voltage is to be measured and plotted. With AWRDE V13, the initial conditions for the simulation correspond to the first sample and are slightly different from V12. Setting the rise (TR) and fall (TF) times to a small value say 0.0001 ms, (i.e. 2% of the 0.05 ms period) provides the correct initial condition of 0V at VP2.

Selecting *simulate* will then perform the transient simulation. By making variables or elements tuneable, the effect of their variation can easily be investigated. For the calculated ON time of 12.5 μ s, the switching delays result in a steady state output voltage for the converter of 5.25 V. Changing the ON time of the pulse generator to 14.3 μ s results in a close to 6V output with little overshoot and ripple as shown in figure 2.29.

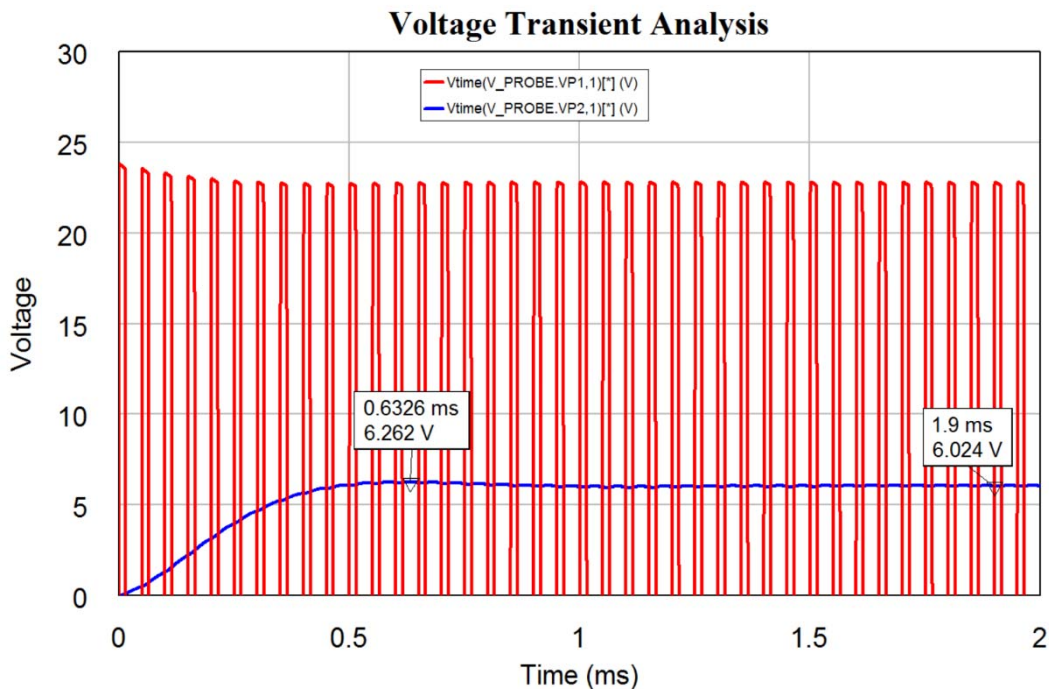


Figure 2.29. Buck Converter voltage waveforms at probes and pulse generator.

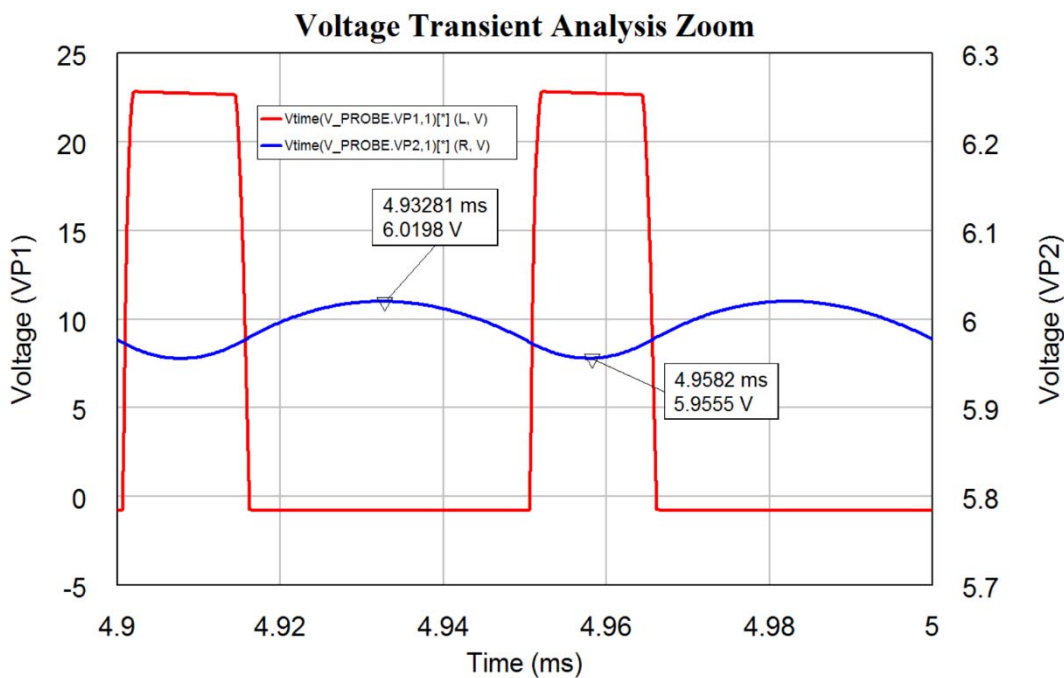
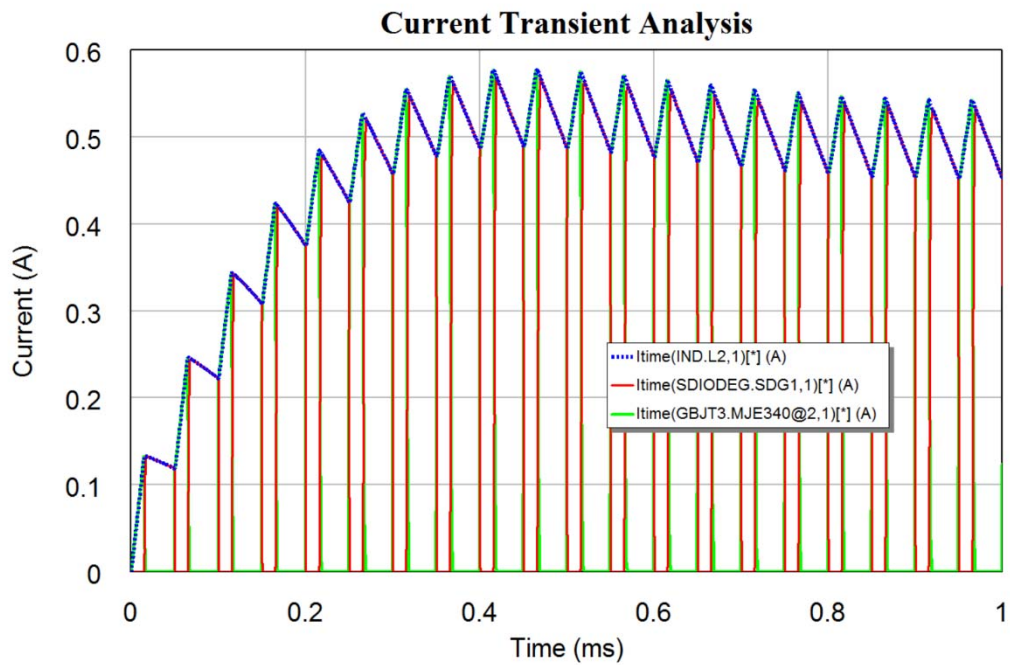
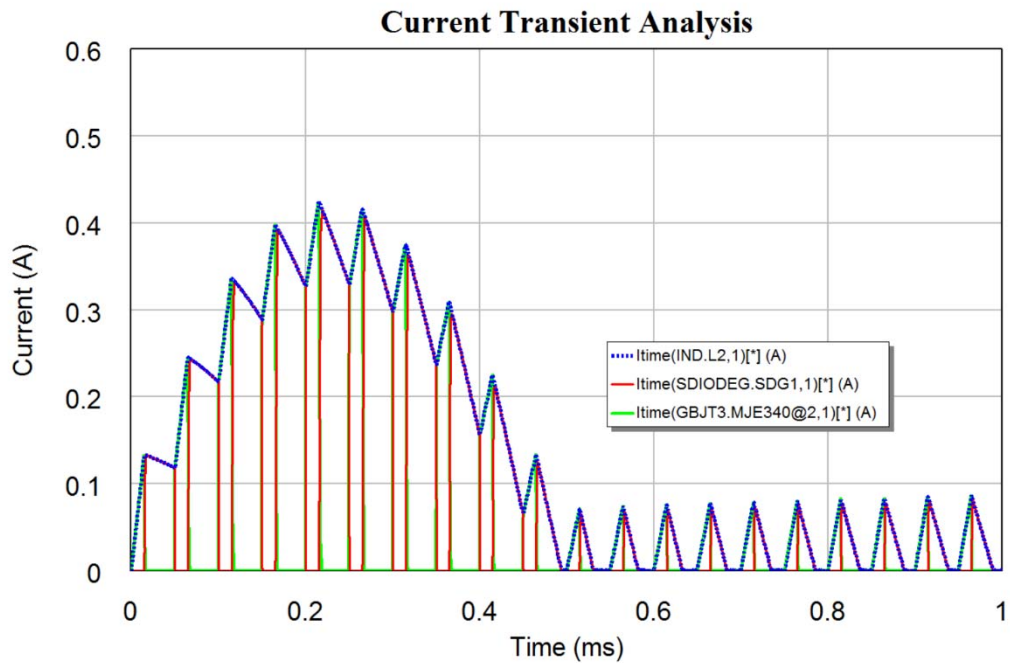


Figure 2.30. Close-up of steady state voltage of figure 2.29.

The output voltage has a small steady state ripple, which can be seen plotting the time waveforms from 4.9 to 5 ms. Plotting the output voltage (VP2) on the right axis allows the voltage scale to be magnified. The steady state output voltage as obtained by the transient analysis is close to 6 V as shown in figure 2.30. The corresponding current waveforms are shown in figure 2.31.

Figure 2.31. Buck Converter current waveforms with $R_L=12 \Omega$.Figure 2.32. Buck Converter current waveforms with $R_L=120 \Omega$.

Changing the load resistor from 12Ω to 120Ω causes a larger transient output voltage overshoot and results in the converter operating in a discontinuous conduction mode as shown in figure 2.32. The plot of voltage waveforms similar to figure 2.29, show some damped high frequency oscillations, when the transistor switches OFF, as shown in figure 2.33, from 0.5 ms to 1.5 ms. This figure also shows that the output voltage has an overshoot to 10.8V, which may be too high for safe operation of any hardware connected to the DC-DC converter. This simulation is done with the time and step settings of figure 2.28 (L). Using the Use HB settings produces slightly different results and may not clearly show the oscillations.

Observing the steady state transient output similar to figure 2.30, shows that the output voltage has a peak of 11.2V and a steady state voltage of about 6.52 V. The slight voltage increase is due to the reduced current causing smaller losses in the transistor, diode and inductor of figure 2.27.

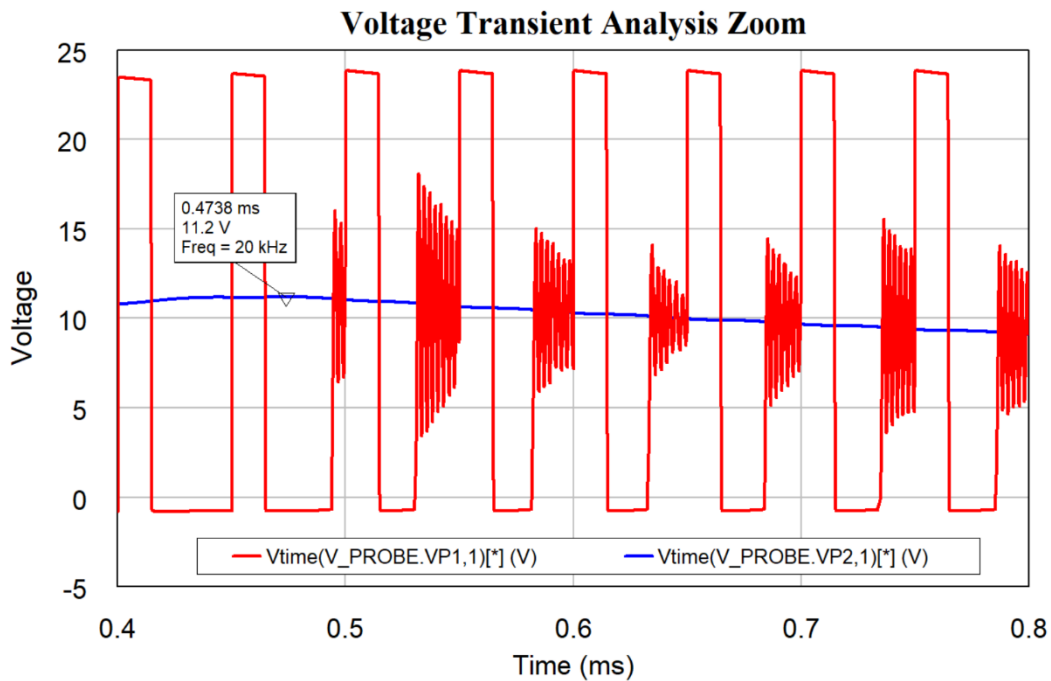


Figure 2.33. Buck Converter voltage waveforms with $R_L=120 \Omega$.

Harmonic Balance Circuit Simulation

Harmonic balance (HB) is used in chapter 5, to determine the conversion loss and waveforms of mixers, it allows the variations of gain with signal amplitude in an amplifier to be calculated and it allows all the harmonics produced by the oscillator to be determined. Using the appropriate non-linear amplifier models, HB allows the inter-modulation distortion of an amplifier to be determined as a function of output power. Because HB simulation is takes significantly longer to complete, most designs are initially done using linear simulation models and then the final design is optimised using the harmonic balance models. HB simulation produces steady state results only.

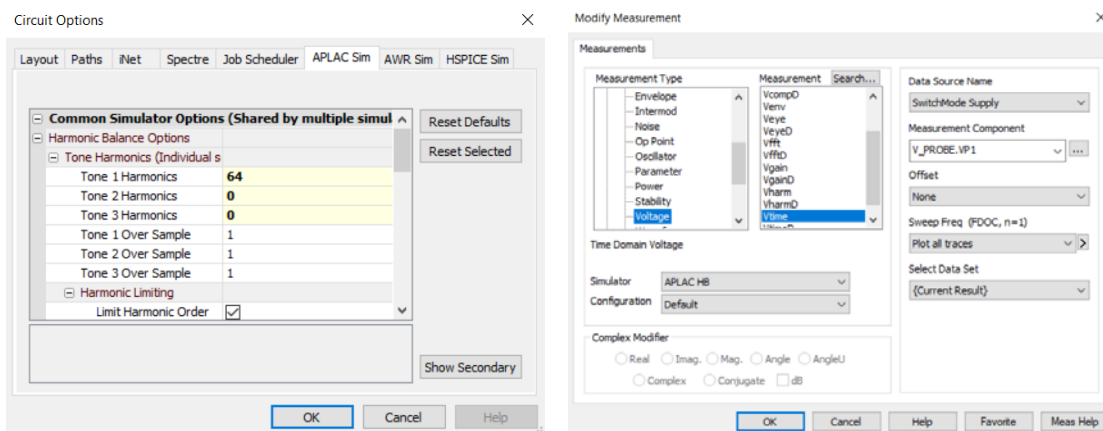


Figure 2.34. Harmonic Balance option windows. (compare with figure 2.28)

Harmonic balance simulation can be carried out by simply duplicating the voltage transient analysis graph and then changing the properties of the measurements from APLAC Trans to APLAC HB. Since the input waveform is a square wave, the number of tone harmonics to be used needs to increase. Select *Options* \Rightarrow *Default Circuit Options* \Rightarrow *Harmonic Balance*, and then increase the number of harmonics to 64. In addition, the simulator must be selected as APLAC HB as shown in figure 2.34.

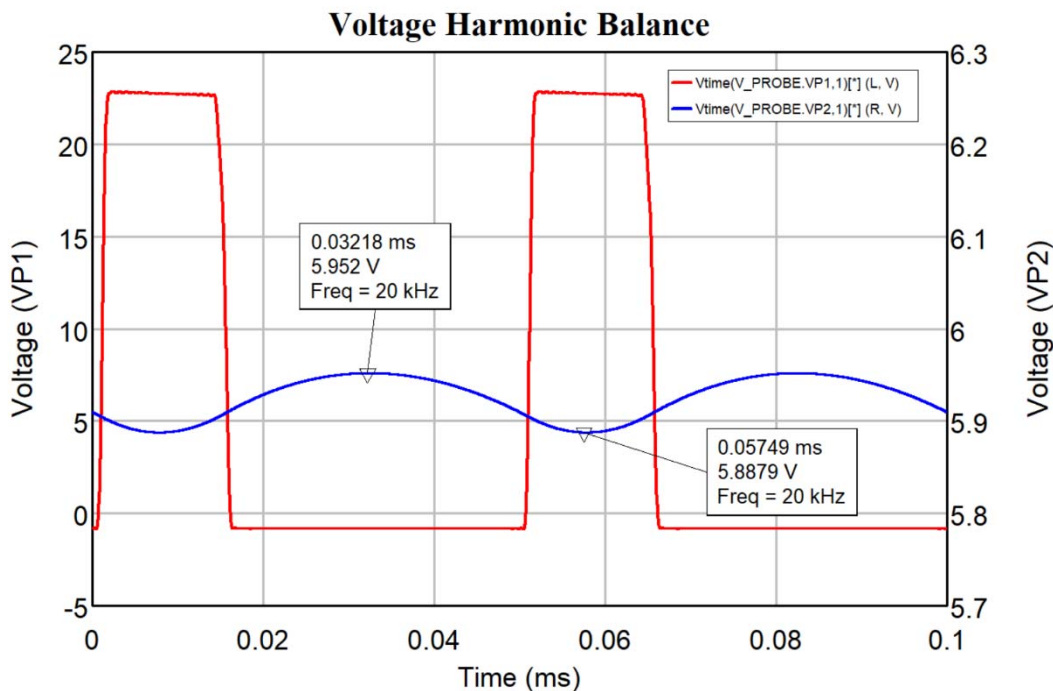


Figure 2.35. Waveforms for the circuit of figure 2.27 using Harmonic Balance.

Figure 2.35 shows the voltage waveform resulting from the Harmonic Balance simulation, using 64 harmonics. The time scale corresponds to 2 steady state cycles of the input waveform. The output voltage level is slightly different from the one obtained using the time domain simulation, as shown in figure 2.30. Having a lower number of harmonics results in a more distorted square waveform and a higher output voltage. Changing the number of harmonics to 128 will produce similar looking waveforms to figure 2.35, but with an average output of 5.961 V, compared with 5.920 V for figure 2.35. Changing the number of harmonics to 256 changes the output to 5.988 V and changing it to 1024 reduces the output slightly to 5.973 V. The output voltage is slightly different to that shown in figure 2.30 for the APLAC transient time domain, simulation. For most RF circuits, square waves are not used, so that a high number of harmonics is not required.

When $R_L = 120 \Omega$, high frequency oscillations occur in the transient response as shown in figure 2.33. For AWRDE V13, APLAC HB converges, but is slow and for 1024 harmonics, only part of an input cycle is displayed.

The transient analysis fully includes all nonlinearities specified in the device parameters and accurately incorporates unexpected conditions like the oscillations shown in figure 2.33. Accurate nonlinear analysis as described here is thus essential in ensuring a design operates fully as required over all expected input and load conditions. The Transient and Harmonic Balance simulations give very similar steady state results, but for <64 harmonics, APLAC HB simulation is normally quicker.

Black Box Matching of Circuits to Measurements

Sometimes one needs to model an existing device, without having direct access to all the elements making up that circuit. An example [19,20] is the development of a model can be used to model a mains power distribution transformer, at frequencies up to 5 MHz, so that one knows the impedances the transformer presents at Power Line Carrier frequencies (up to 150 kHz), which are used for Smart Grid applications or determining the effects of lightning through power networks. A single-phase power distribution transformer has 2 terminals for its low voltage (LV) winding, 2 terminals for its medium voltage (MV) winding and a terminal for the metal case of the transformer, a total of 5 terminals. A 3-phase power distribution transformer has 3 LV phase terminals, 3 MV terminals, a Neutral terminal and a case, a total of 8 terminals. To simplify the model, each LV phase winding and each MV winding is assumed to be identical. So that a similar model to the single phase transformer results, as shown in [20].

One can measure the impedances seen between any 2 of the 5 terminals of a single phase transformer. As shown in [19], a sufficiently accurate model can be developed using 5 measurements, rather than the 10 possible measurements that can be made between the 5 terminals. The problem now becomes how to match the components in the model to those impedance measurements. One could write down equations for the impedances that can be seen in each of the 5 measurement points and solve the resulting complex equations to obtain the component values. Since the impedances of the inductances and capacitances change with frequency, solving these equations is an exceedingly difficult task.

It is possible to guess a circuit configuration and use MWO and optimisation tools, to "solve" the simultaneous equations by optimisation and match the circuit elements to the measurements. To illustrate this technique, the process is performed on a relatively simple network.

Example 2.5: Bandpass T Matching Network

A simple Bandpass T matching network described in Chapter 9 "Impedance Matching of Power Amplifiers" of this book is used to illustrate the impedance matching process. These networks are used to match power transistors to $50\ \Omega$ loads. For this example, an input matching network is chosen to match a device with an input impedance of $X_D = 5 + j 0.9\ \Omega$ to a source with $X_L = 50\ \Omega$ at 150 MHz with a Q of 3.5. The equations in Chapter 9 are entered into the Global Definitions window, as shown in figure 2.36. Two versions of the circuit are shown in figures 2.37 and 2.38 respectively. Lbt, Cbt1 and Cbt2 are the component value variables evaluated from the equations in the Global Definitions window.

Band Pass T		
$RI=50$	$Q=3.5$	$TwoPi=2*\pi$
$Rd=5$	$Xd=0.9$	$Fm=150$
$Wm=TwoPi*Fm*1e6$	$Ld=Xd/Wm$	
$A2=((Rd*(1+Q*Q)/RI) - 1)$	$A=Sqrt(A2)$	
$B=Rd*(1+Q*Q)$	$Qmin=sqrt(RI/Rd-1)$	
$Xlbt= (Rd*Q - Xd)$	$Lbt=Xlbt/Wm$	
$Xcbt2=RI*A$	$Cbt2= 1/(Wm*Xcbt2)$	
$Xcbt1=B/(Q-A)$	$Cbt1= 1/(Wm*Xcbt1)$	

Figure 2.36. Bandpass T equations in *Global Definitions* window.

Figure 2.37 uses a voltage controlled voltage source to implement the impedance of the source and is only included to show the complex source impedance of transistor can be realised. The Voltage Controlled Voltage Source, resistor R_1 and inductor L_1 , provide the same impedance as the transistor. Figure 2.38 implements that complex impedance as part of port 1. The component values are calculated to be $L_{bt} = 17.61 \text{ nH}$, $C_{bt1} = 46.92 \text{ pF}$ and $C_{bt2} = 37.22 \text{ pF}$. In addition, the components were assigned typical Q values of 100 for the inductor and 300 for the capacitors. Figure 2.39 shows the resulting frequency response of the network of figure 2.38. The impedance match is very good at 150 MHz and is better if ideal elements are used.

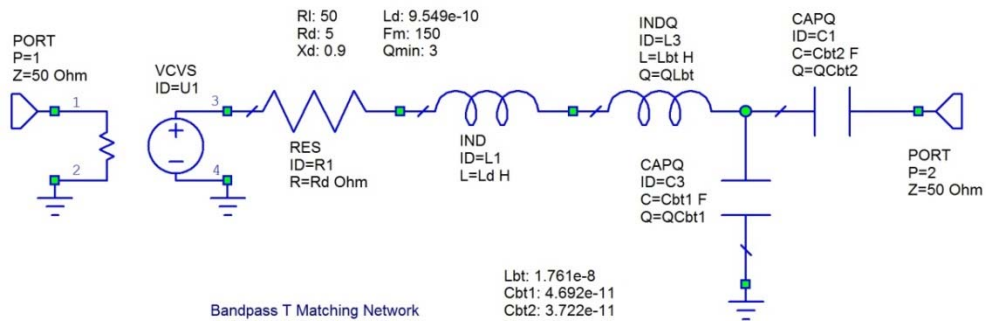
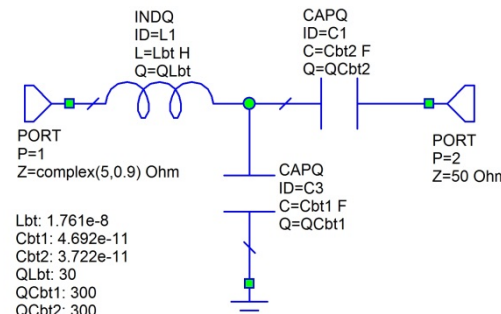


Figure 2.37. Calculated Bandpass T matching network.



Bandpass T Matching Network

Figure 2.38. Calculated Bandpass T matching network.

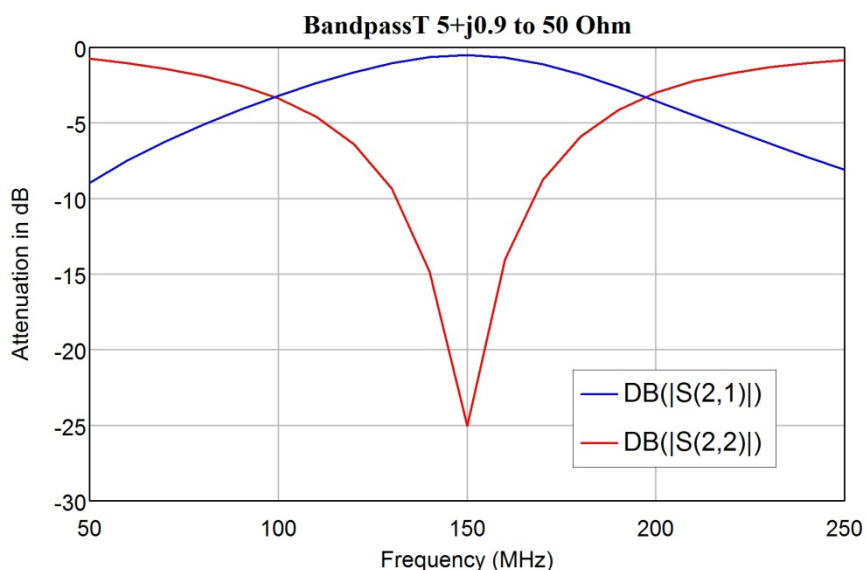


Figure 2.39. Frequency response of calculated Bandpass T matching network.

S Parameter Measurements

The network of figure 2.38 is used to generate an S parameter file. Such a data file is similar to S parameter data obtained from a network analyser. This file is obtained by exporting the trace data of a table-graph containing the complex S parameters of the circuit in figure 2.38. This can be saved as a text file. Change the .txt extension to .S2p to denote a 2-port S parameter file. This file can then be imported as a Touchstone file, by right clicking on *Data Files* and selecting *Import Data File* or by using the *Project* \Rightarrow *Add Data File* \Rightarrow *Import Data File* dropdown menu. This data file can be named “Measurements”. The Touchstone heading “#MHz S RI” needs to be added, to denote that the frequency is in MHz, it is an S parameter file and the data are Real and Imaginary values.

The Touchstone file format for a 2-port S parameter network typically is as follows:

```
# GHZ S RI R 50
f1 ReS11 ImS11 ReS21 ImS21 ReS12 ImS12 ReS22 ImS22
f2 ReS11 ImS11 ReS21 ImS21 ReS12 ImS12 ReS22 ImS22
f3 ReS11 ImS11 ReS21 ImS21 ReS12 ImS12 ReS22 ImS22
```

In addition the heading lines of text need to be denoted as comments by inserting a “!” at the beginning of the line. The resulting Touchstone file is as shown in table 2.2. To keep the number of lines in this table small a 10 MHz frequency increment is chosen in the project options, resulting in 21 frequencies being used. In practice, many more frequencies would be used.

!1	2	3	4	5	6	7	8	9
#MHz S RI								
!Freq	S(1,1) (Real) (Imag)	S(2,1) (Real) (Imag)	S(1,2) (Real) (Imag)	S(2,2) (Real) (Imag)				
50	-0.243196 -0.731472	0.59059 0.130582	0.59059 0.130582	0.550605 -0.561518				
60	-0.375925 -0.65411	0.624213 0.0449708	0.624213 0.0449708	0.484718 -0.598862				
70	-0.47541 -0.575551	0.634624 -0.0349784	0.634624 -0.0349784	0.425575 -0.633207				
80	-0.552339 -0.499376	0.628902 -0.10684	0.628902 -0.10684	0.370205 -0.66539				
90	-0.613449 -0.426228	0.61193 -0.170042	0.61193 -0.170042	0.316886 -0.695395				
100	-0.662903 -0.355774	0.587119 -0.224755	0.587119 -0.224755	0.264712 -0.722954				
110	-0.703262 -0.287473	0.556924 -0.271444	0.556924 -0.271444	0.213273 -0.747795				
120	-0.736122 -0.220851	0.523162 -0.310684	0.523162 -0.310684	0.162454 -0.769717				
130	-0.762495 -0.155588	0.487214 -0.343089	0.487214 -0.343089	0.112306 -0.788613				
140	-0.783052 -0.0915112	0.450145 -0.369279	0.450145 -0.369279	0.0629657 -0.804466				
150	-0.79827 -0.0285797	0.412785 -0.38986	0.412785 -0.38986	0.0146048 -0.817331				
160	-0.808518 0.0331546	0.375778 -0.405423	0.375778 -0.405423	0.0325988 -0.827327				
170	-0.814116 0.0935747	0.339618 -0.416533	0.339618 -0.416533	0.0784796 -0.834611				
180	-0.81536 0.152526	0.30468 -0.423723	0.30468 -0.423723	0.122895 -0.839373				
190	-0.812541 0.209837	0.271237 -0.427495	0.271237 -0.427495	0.16573 -0.84182				
200	-0.805953 0.265335	0.239481 -0.428314	0.239481 -0.428314	0.206899 -0.842168				
210	-0.795895 0.31886	0.209536 -0.426606	0.209536 -0.426606	0.246341 -0.840633				
220	-0.782667 0.37027	0.181472 -0.422762	0.181472 -0.422762	0.284025 -0.837429				
230	-0.766573 0.419448	0.155312 -0.417133	0.155312 -0.417133	0.319939 -0.832757				
240	-0.747909 0.466301	0.131047 -0.410032	0.131047 -0.410032	0.354093 -0.826812				
250	-0.726969 0.510764	0.108637 -0.40174	0.108637 -0.40174	0.386513 -0.81977				

Table 2.2. Bandpass T, S parameters figure 2.38.

The data in table 2.2 is used in a new circuit, by right clicking on *Circuit Schematics* and selecting *New Schematic* and giving that a suitable name like “Measured_Ckt”. Select *Draw* \Rightarrow *Add Subcircuit* and for the Subcircuit select the Measurement Touchstone file. Add ports to result in the circuit shown in figure 2.40.

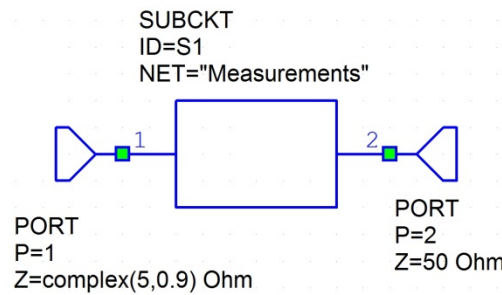
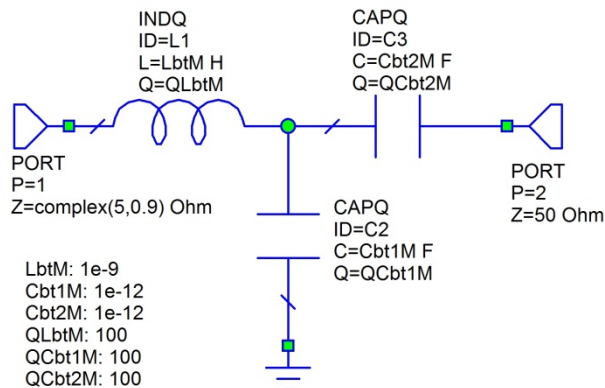


Figure 2.40. Circuit containing the measurements Touchstone file.

Sometimes one needs to develop a circuit model corresponding to measured data. In most cases, one has to develop a circuit schematic based on physical properties of frequency behaviour. To develop a Bandpass T matching network model of the measured data of table 2.2, the circuit is known, but component values are not known. To develop a model of the network, a suitable circuit diagram is developed, with trial guesses for the component values. As shown in figure 2.41, the components are guessed to be 1 pF for the capacitors and 1 nH for the inductor. A value of 100 is used for the initial Q values.



Bandpass T Matching Network Model

Figure 2.41. Model of Bandpass T matching network.

The model needs to be tuned or optimised to ensure its S parameters match the measurements for all S parameters and all frequencies. To achieve this error equations are produced, like the equations 2.3 shown below for S_{11} .

$$\begin{aligned}
 \text{MoS11Re} &= \text{Bandpass T Model:Re}(S(1,1)) \\
 \text{MoS11Im} &= \text{Bandpass T Model:Im}(S(1,1)) \\
 \text{MeS11Re} &= \text{Measured_Ckt:Re}(S(1,1)) \\
 \text{MeS11Im} &= \text{Measured_Ckt:Im}(S(1,1)) \\
 \text{MeS11} &= \text{Complex}(\text{MeS11Re}, \text{MeS11Im}) \\
 \text{MoS11} &= \text{Complex}(\text{MoS11Re}, \text{MoS11Im}) \\
 \text{ES11C} &= (\text{MeS11} - \text{MoS11}) / (\text{MeS11} + \text{MoS11})
 \end{aligned} \tag{Eqn. 2.3}$$

MoS11Re is the real part of S_{11} of the Bandpass T model. The format on the right hand side of the = sign is exactly like the format of measurements used in graphs. ES11C is the normalised Error of the S_{11} parameters in Complex form. Similar equations are produced for S_{21} , S_{12} , and S_{22} .

Since the impedance measurements only exist at the frequencies shown in table 2.2, the project frequencies must be set to the same values, so that the error equations can be evaluated. Section 13: Scripts of the AWRDE users Guide has details on scripts and how to write new ones. Fortunately, the required Match_Proj_Freq_to_Datafile_Freq script is one, which is already included in NI AWR DE. That script is accessed from *Scripts* \Rightarrow *Simulation* menu. This script requires a Touchstone data file containing the relevant frequency values. Since that Touchstone file is already included in the project, the project frequencies are immediately set to the values in table 2.2, so that the optimisation can be done.

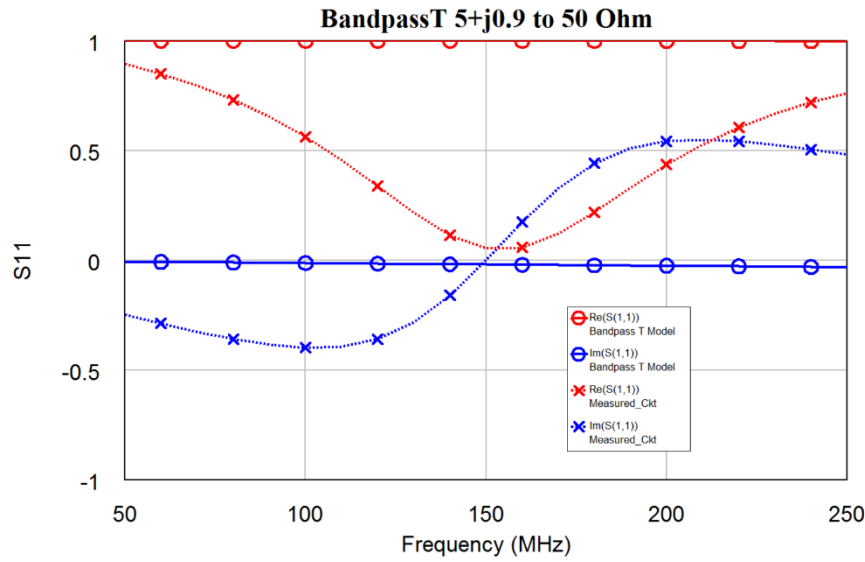


Figure 2.42. S_{11} for Bandpass T model and measurements before optimisation.

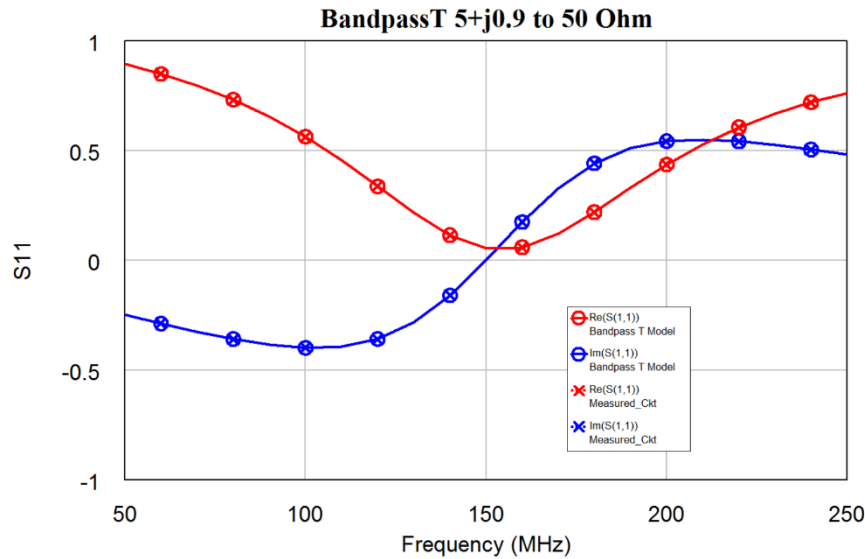


Figure 2.43. S_{11} for Bandpass T model and measurements after optimisation.

Figure 2.42 shows S_{11} from both the model of figure 2.41 and the measurements of table 2.2 as a function of frequency. As expected, our initial are not correct and there is a significant difference between the guessed and required values. The 3 element values in figure 2.41 and the three Q values are allowed to change under optimisation. The real and imaginary parts of S_{11} and the corresponding error equations for S_{21} , S_{12} , and S_{22} with

desired values of zero are set as optimiser goals. Running the optimiser quickly reduces the errors to very close to zero and results in both the model and the measurement having the same S parameters as shown for S_{11} in figure 2.43. The component values of the Bandpass T network model shown in figure 2.41, have changed to perfectly match the values shown in figure 3.38.

Touchstone files as data files have the advantage that NI AWR DE knows what the frequency units, i.e. MHz or GHz are. The frequencies in the Touchstone file can also be used to set the frequencies for the project, using the Match_Proj_Freq_to_Datafile_Freq script.

Impedance Measurements

For Touchstone files and multiport networks, all the relevant parameters S_{11} , S_{21} , S_{12} , and S_{22} for all the ports must be contained in the Touchstone file. It is possible to develop suitable models for many port networks using less than all the required measurements. The three phase mains distribution transformer model developed by [20] and described at the end of this chapter is one example.

To illustrate this, the Bandpass T transformer model described above is also developed using impedance measurements, made by measuring impedances between each of the 3 terminals of the network of figure 2.38. Similarly, to the S parameter measurements described above, the impedances are calculated by NI AWR DE and saved as a data file.

The Bandpass T network has 3 terminals and the impedances between each of those terminals can be measured using Mixed Mode Converter (MMCONV) elements in NI AWR DE, as shown in figure 2.44. The differential (Diff) port (1) on the MMCONV, measures the difference in the voltages and currents between terminals 3 and 4 of the MMCONV. To prevent the impedances connected to the Common mode (Comm) terminals (2) of the MMCONV to affect the measured impedances, the Common mode terminals on the MMCONV must be left an open circuit. The MMCONV element provides an isolation, so that the impedance at ports 1 to 3, do not affect the measured impedances. For the analysis to be performed without errors, one point in the circuit needs to be earthed, as shown in figure 2.44.

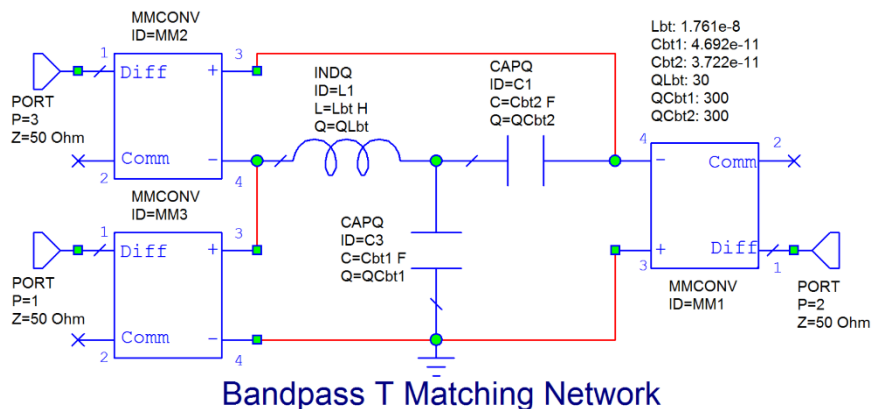


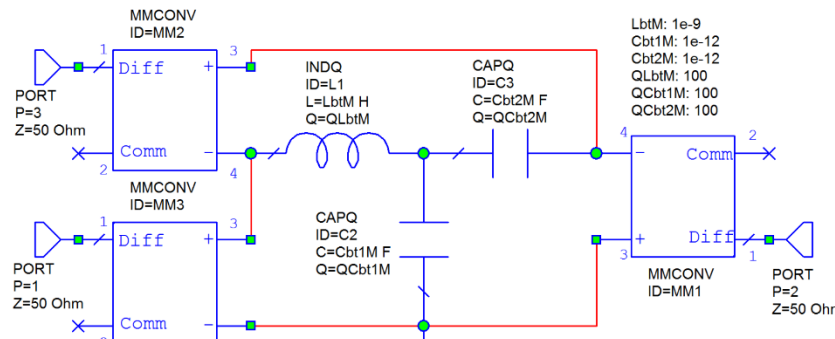
Figure 2.44. Measuring Impedances of Bandpass T matching network.

The resulting impedances can be plotted in NI AWR DE, and exported to a text file. This text file with "!" added to the first few lines is shown in Table 2.3. This table is in a format that allows it to be directly imported into NI AWR DE as a data file for use and plotting. Any line starting with "!" denotes a comment and is useful for showing what values are

being imported into the project. To keep the number of lines in this table small a 10 MHz frequency increment is chosen in the project options, resulting in 21 frequencies being used. In practice, many more frequencies would be used.

!	Port1		Port12		Port2	
!1	2	3	4	5	6	7
!(Hz)	Ohm	Rad	Ohm	Rad	Ohm	Rad
!Freq	Z(1,1)	Ang	Z(1,1)	Ang	Z(1,1)	Ang
5e+007	62.3068	-1.55103	79.9836	-1.55319	153.34	-1.5608
6e+007	49.8955	-1.55026	64.6261	-1.55305	127.785	-1.56246
7e+007	40.7142	-1.5487	53.3402	-1.55224	109.531	-1.56365
8e+007	33.5517	-1.5464	44.5991	-1.5509	95.8405	-1.56455
9e+007	27.7353	-1.54329	37.5547	-1.54903	85.1919	-1.56524
1e+008	22.8613	-1.53917	31.6981	-1.54659	76.673	-1.5658
1.1e+008	18.6729	-1.53365	26.7054	-1.54346	69.7028	-1.56625
1.2e+008	14.999	-1.52604	22.3608	-1.53941	63.8944	-1.56663
1.3e+008	11.7215	-1.515	18.515	-1.53407	58.9795	-1.56695
1.4e+008	8.75645	-1.49766	15.0612	-1.5268	54.7667	-1.56722
1.5e+008	6.0441	-1.46659	11.9217	-1.51639	51.1157	-1.56746
1.6e+008	3.54601	-1.39517	9.03836	-1.50028	47.921	-1.56767
1.7e+008	1.29202	-1.07732	6.36831	-1.47213	45.1021	-1.56786
1.8e+008	1.23578	1.05858	3.88314	-1.41062	42.5965	-1.56802
1.9e+008	3.2318	1.38396	1.59862	-1.17756	40.3546	-1.56816
2e+008	5.20895	1.45618	0.968778	0.893954	38.3368	-1.5683
2.1e+008	7.11364	1.48751	2.94209	1.36479	36.5113	-1.56842
2.2e+008	8.94914	1.505	4.9482	1.44975	34.8517	-1.56852
2.3e+008	10.7227	1.51618	6.88928	1.48451	33.3364	-1.56862
2.4e+008	12.4415	1.52394	8.76478	1.50338	31.9474	-1.56871
2.5e+008	14.1117	1.52965	10.5805	1.51524	30.6695	-1.5688

Table 2.3. Bandpass T impedances of figure 2.44



Bandpass T Matching Network Model

Figure 2.45. Initial Bandpass T matching network model.

When one needs to develop a model of an unknown network, impedance measurements will need to be made between all terminals of that network and a table similar to the one shown in table 2.3 is then produced using those measurements. To develop a model of the network, the same trial guesses for the component values as shown in figure 2.41 are used, as shown in figure 2.45. As before these initial guessed values, will change during the network optimisation.

To import measured data, a spreadsheet containing the measurements is normally imported as a data file. As NI AWR DE does not easily recognise frequency units other

than Hz, when.txt data files are used, it is easiest to use Base Units (Hz, Henry and Farad) for the error calculations. As a result, the measurements that are imported as data files may need to be changed to contain Base Units values. A Txt Data file is imported in the same way as Touchstone files, by right clicking on *Data Files* and selecting *Import Data File* or by using the *Project* \Rightarrow *Add Data File* \Rightarrow *Import Data File* dropdown menu. Again, it is worthwhile to add some comments and headings with each line starting with a “!”. In this example, the impedance data produced as table 2.3 is used as the measurement file.

It is slightly more difficult to use the data text data file in NI AWR DE than it is to use Touchstone files. This data can be imported into the project, using the following equations 2.4 in the global definitions:

```
MeFreq = Col(datafile("Measurements"),1)
MeP1Z11M = Col(datafile("Measurements"),2)
MeP1Z11Ph = Col(datafile("Measurements"),3)
MeP12Z11M = Col(datafile("Measurements"),4)
MeP12Z11Ph = Col(datafile("Measurements"),5)
MeP2Z11M = Col(datafile("Measurements"),6)
MeP2Z11Ph = Col(datafile("Measurements"),7) Eqn. 2.4
```

MeFreq, are the measurement frequencies, *MeP1Z11M* is the measured Port 1 impedance magnitude, *MeP1Z11Ph* is the measured Port 1 impedance phase and so on. These variables can now be used, to set up the error equations shown in figure 2.46, which correspond to a normalised difference between the measured impedances and those obtained from the impedance seen at ports 1 to 3.

LC Matching Networks

Rl: 50		
Rd: 5	Fm: 150	A: 0.5701
Xd: 0.9	Qmin: 3	B: 66.25
Ld: 9.549e-10		

Band Pass T

Lbt: 1.761e-8	LbtM: 1e-9
Cbt2: 3.722e-11	Cbt1M: 1e-12
Cbt1: 4.692e-11	Cbt2M: 1e-12

```
MoP1Z11M = BandpassTModel:|Z(1,1)|
MoP1Z11Ph = BandpassTModel:Ang(Z(1,1))
EP1Z11M = (MeP1Z11M-MoP1Z11M)/(MeP1Z11M+MoP1Z11M)
EP1Z11Ph = (MeP1Z11Ph-MoP1Z11Ph)
```

```
MoP2Z11M = BandpassTModel:|Z(2,2)|
MoP2Z11Ph = BandpassTModel:Ang(Z(2,2))
EP2Z11M = (MeP2Z11M-MoP2Z11M)/(MeP2Z11M+MoP2Z11M)
EP2Z11Ph = (MeP2Z11Ph-MoP2Z11Ph)
```

```
MoP12Z11M = BandpassTModel:|Z(3,3)|
MoP12Z11Ph = BandpassTModel:Ang(Z(3,3))
EP12Z11M = (MeP12Z11M-MoP12Z11M)/(MeP12Z11M+MoP12Z11M)
EP12Z11Ph = (MeP12Z11Ph-MoP12Z11Ph)
```

Figure 2.46. Error equations in *Output Equations Window* of NI AWR DE project.

In figure 2.46 EP1Z11M is the error for the magnitude of Z11 for Port 1, MeP11Z11M is the measured value of the magnitude of Z11 for Port 1 and MoP11Z11M is the magnitude of Z11 for Port 1 of the model. EP1Z11P is the error for the phase of Z11 for Port 1, MeP11Z11P is the measured value of the phase of Z11 of Port 1 and MoP11Z11P is the phase of Z11 for Port 1 of the model.

Similar equations are used for ports 2 and 3 of the networks in figures 2.44 and 2.45. These error equations are used as part of the optimisation process, where the component values of the black box model are optimised to minimise the values of these error equations.

Since the impedance measurements only exist at the frequencies shown in table 2.3, the project frequencies must again be set, as described above, to the same values, using the *Match_Proj_Freq_to_Datafile_Freq* script. That script is accessed from *Scripts* \Rightarrow *Simulation* menu. This script requires a Touchstone data file containing the relevant frequency values. For the S parameter data, the Touchstone file was part of the project. That is not the case now, so that a simple dummy Touchstone file containing the frequency values must now be produced from the measurements in table 2.3.

Import the data from table 2.3 into a spreadsheet program. In many cases, the relevant data already exists in a spreadsheet. Make a new sheet in the spreadsheet program and paste the measurement frequency data into the first column, corresponding to the frequencies at which the equations are to be evaluated. Then add 8 columns containing a zero, to represent the 4 complex S-parameter values (one entry for magnitude and one for angle) required by Touchstone files. Create a new Touchstone file in the NI AWR DE project by right clicking on Data Files and select Touchstone File option. The Touchstone like spreadsheet data is then pasted in that Touchstone data file and the text “#Hz S MA R 50” is added as the first line to produce the Touchstone data file shown in table 2.4.

	#Hz S MA R 50							
5e+007	0	0	0	0	0	0	0	0
6e+007	0	0	0	0	0	0	0	0
7e+007	0	0	0	0	0	0	0	0
8e+007	0	0	0	0	0	0	0	0
9e+007	0	0	0	0	0	0	0	0
1e+008	0	0	0	0	0	0	0	0
1.1e+008	0	0	0	0	0	0	0	0
1.2e+008	0	0	0	0	0	0	0	0
1.3e+008	0	0	0	0	0	0	0	0
1.4e+008	0	0	0	0	0	0	0	0
1.5e+008	0	0	0	0	0	0	0	0
1.6e+008	0	0	0	0	0	0	0	0
1.7e+008	0	0	0	0	0	0	0	0
1.8e+008	0	0	0	0	0	0	0	0
1.9e+008	0	0	0	0	0	0	0	0
2e+008	0	0	0	0	0	0	0	0
2.1e+008	0	0	0	0	0	0	0	0
2.2e+008	0	0	0	0	0	0	0	0
2.3e+008	0	0	0	0	0	0	0	0
2.4e+008	0	0	0	0	0	0	0	0
2.5e+008	0	0	0	0	0	0	0	0

Table 2.4. Touchstone file for setting the project frequencies.

The line beginning with # is a header, specifying the parameters to be used. # MHz, denotes that the frequencies are in MHz, Hz denotes the frequencies are in Hz. S denotes that this is an S parameter file,

MA indicates that the complex data is in polar form (magnitude, angle), the angle of which is always in units of degrees;

Selecting *Select Scripts* \Rightarrow *Simulation* \Rightarrow *Match_Proj_Freq_to_Datafile_Freq* will set the project frequencies to the ones in the Touchstone file of table 2.4. In many cases automatic measurements are made on the network to be determined so that more than one thousand measurements result. The frequency setting script described above is then the only practical way to match the project frequencies to the measurements. Once the project frequencies have been set to correspond to the measured frequencies, the Touchstone file can be deleted from the project if desired.

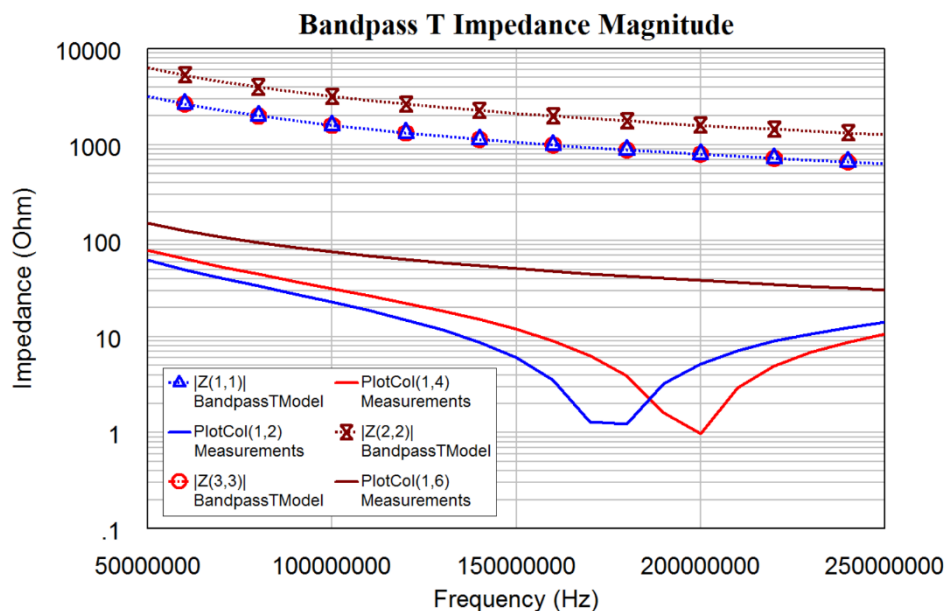


Figure 2.47. Starting impedance magnitude comparison of circuits of figures 2.44 and 2.45.

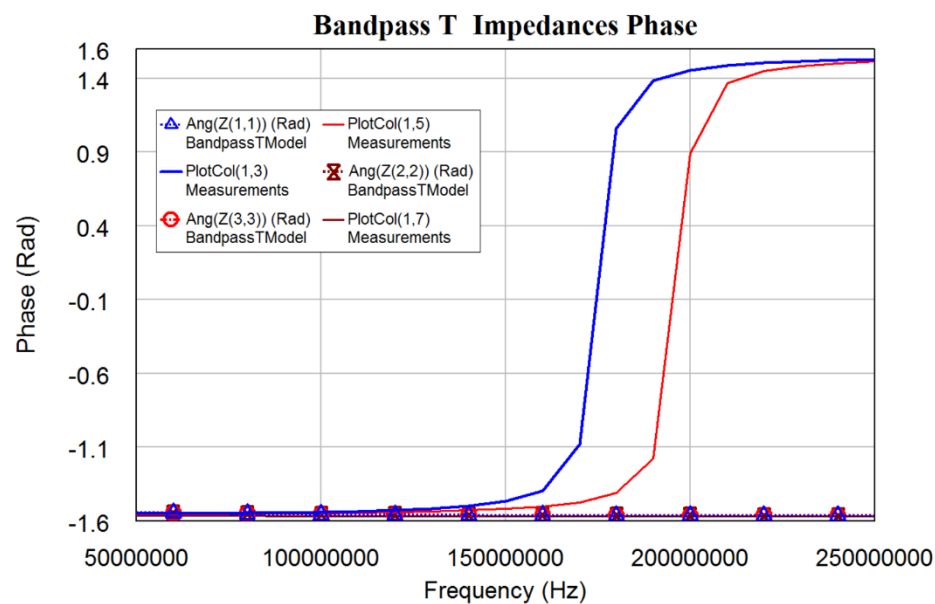


Figure 2.48. Starting impedance phase comparison of circuits of figures 2.44 and 2.45.

Figures 2.47 and 2.48 compare the impedance measurements of the calculated Bandpass T circuit of figure 2.44 and those of the model using the starting values in figure 2.45. The curves with the markers, i.e. the top two curves in figure 2.47 and the bottom two curves in figure 2.48, are the starting impedances of the model. The curves without the markers are the impedances of the Bandpass T circuit. There are thus significant differences between the circuit and the model at the start of the optimisation.

Optimisation goals are set to reduce the phase and magnitude errors to zero. The circuit simulator is then set to optimise the guessed component values to minimise the error equations shown in figure 2.46.

In this application, the simplex optimiser results in a fast optimisation, to produce the results, in figures 2.49 and 2.50. These figures compare the impedance measurements of the calculated Bandpass T circuit of figure 2.44 with that of the model of figure 2.45 and show that after optimisation, the impedances for the calculated Bandpass T matching network are exactly the same values, as those of the modelled network.

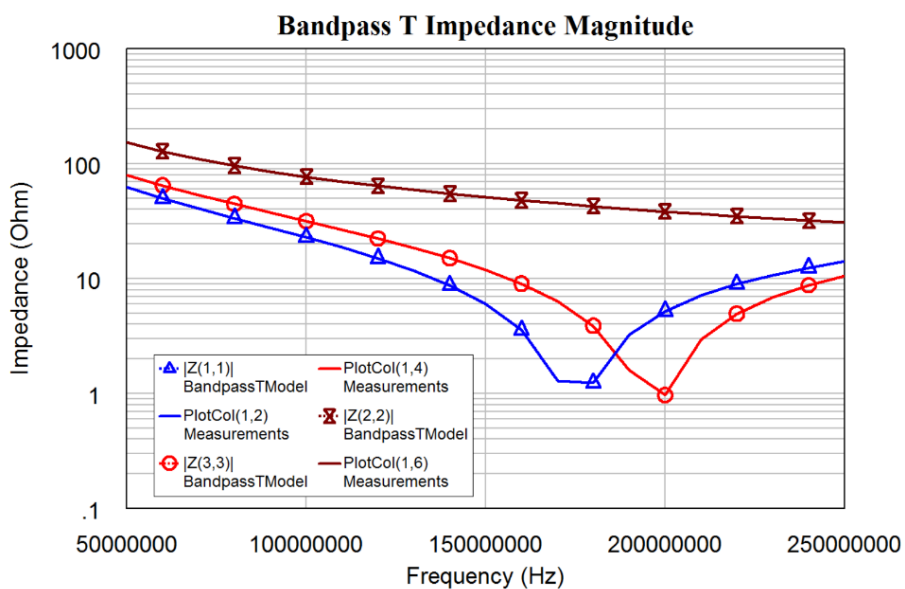


Figure 2.49. Impedance magnitude comparison after optimisation.

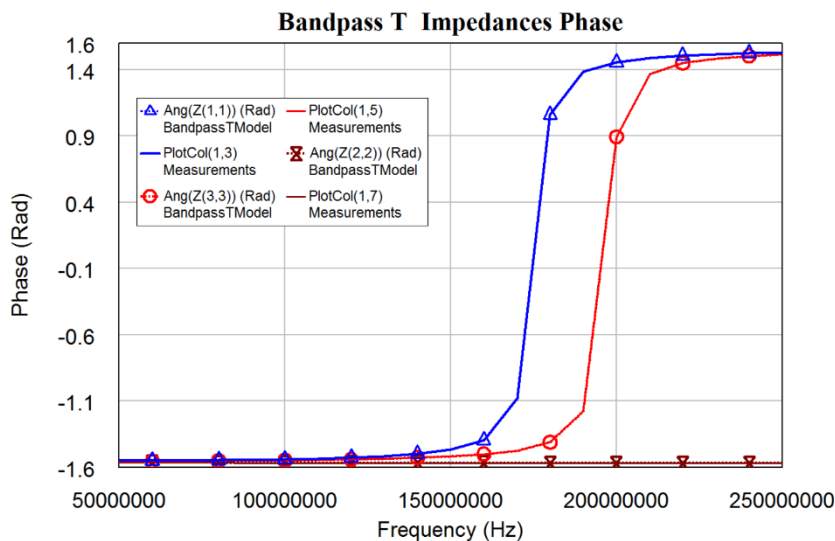
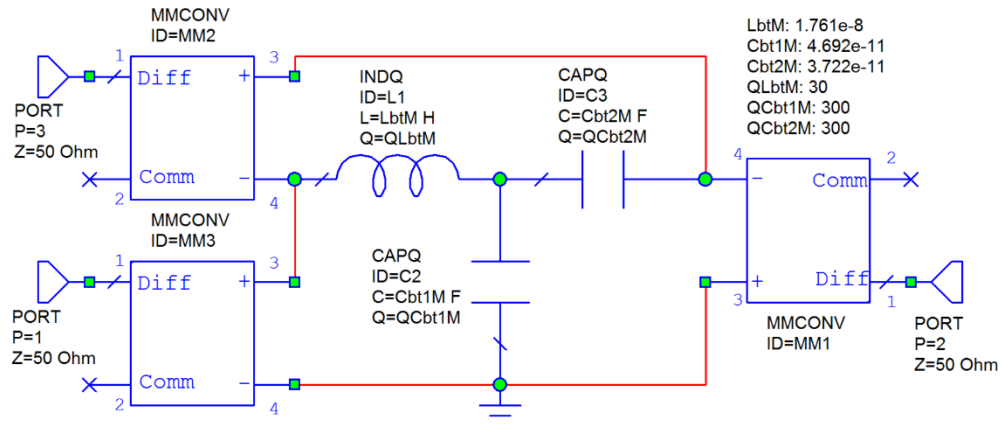


Figure 2.50. Impedance phase comparison after optimisation.



Bandpass T Matching Network Model

Figure 2.51. Bandpass T Matching network model after optimisation.

Both the magnitude and the phase response of the calculated circuit and the model match exactly. The components and their Q values of the circuit model, after optimisation are shown in figure 2.51 and exactly match the component values of the Bandpass T network of figure 2.38, showing that we have perfectly modelled the circuit from impedance measurements only.

One application of this technique is the modelling of mains power transformers for use at 50 kHz to 150 kHz Power Line Carrier (PLC) frequencies. This technique was successfully applied to single-phase transformers and three phase transformers to allow low cost coupling networks, to couple the PLC signals onto the High Voltage power lines to be designed. These coupling networks rely on the transformer circuit model developed using this technique for part of the coupling network [19, 20].

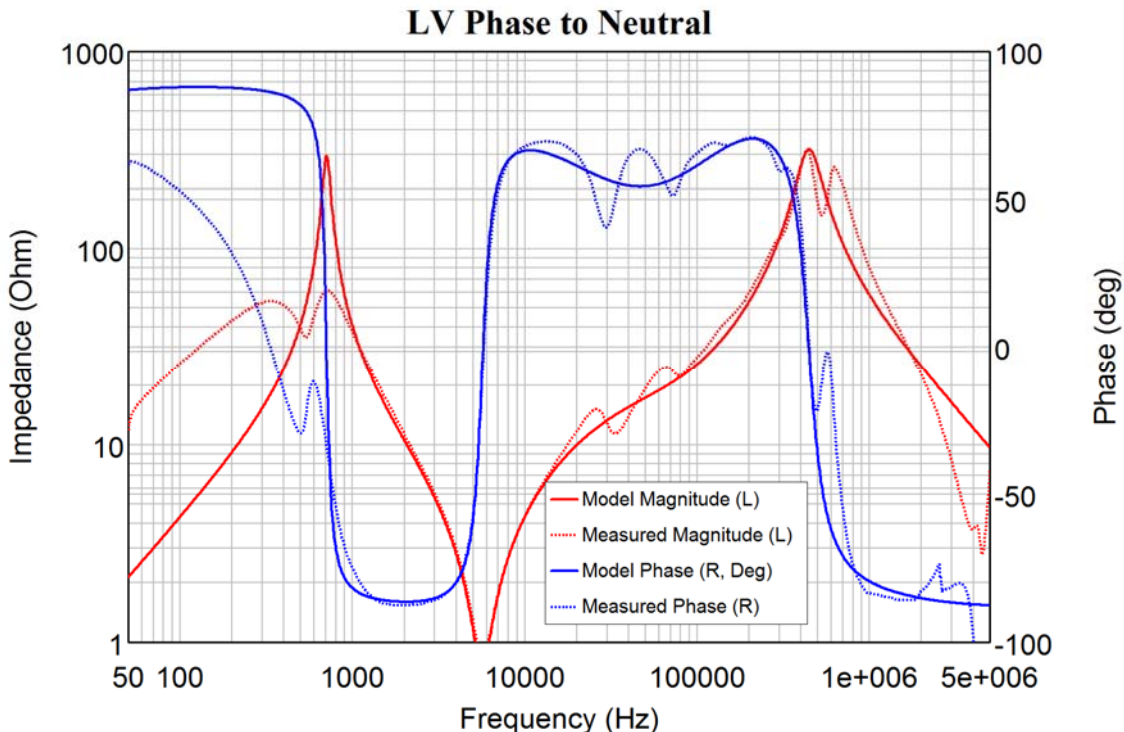


Figure 2.52. Comparison of measured and modelled low voltage winding impedances of a 200 kVA mains power distribution transformer. (Fig 7 of ref [12])

Figures 2.52 and 2.53 show the results from this technique being applied to the modelling of a power distribution transformer at power line carrier (PLC) frequencies, for Smart Grid applications [20]. One thousand impedance measurements are made on each of the 23 selected combinations of 10 terminals, using frequencies from 50 Hz to 5 MHz. A 3-phase model is developed and the circuit values are then matched, to provide the best match to the measurements. The actual circuit model required is far more complex than the model used and as a result, a good match is obtained for 10 kHz to 400 kHz frequencies used for PLC, but a poorer match is obtained at 50 Hz to 500 Hz. Without using this black box impedance matching technique, a suitable transformer model could not be developed.

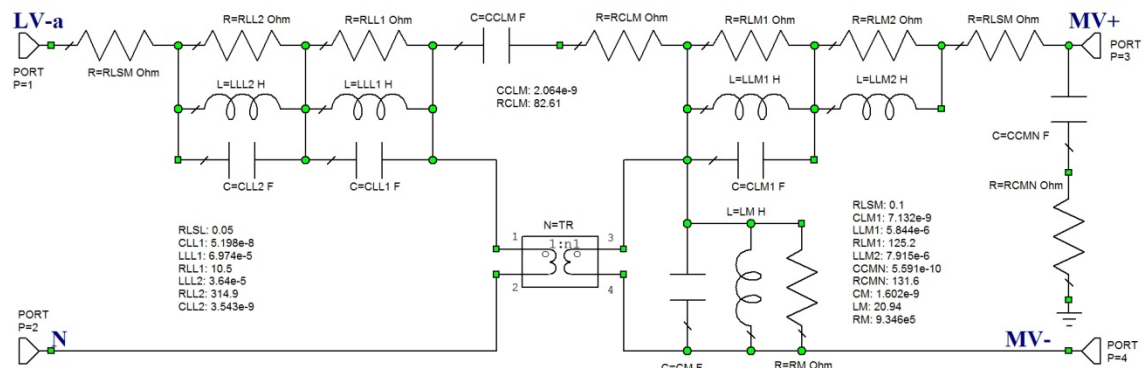


Figure 2.53. One phase of the 3-phase transformer circuit model. (Fig 6 of ref [12])

Figure 2.53 shows one phase of this three-phase transformer model. In addition coupling between each of the windings to the transformer case are included in the full model. These circuits are much more complex than the circuits of figures 2.44 and 2.45, but the same optimisation techniques are used.

Summary

This chapter has introduced some basic aspects of computer simulation using the NI AWR DE and APLAC components of the NI AWR Design Environment. In the rest of this book, the computer simulation will be expanded with both linear and non-linear applications and examples.

NI AWR DE has a good interactive help capability, with specific information available for every circuit element or measurement. The interactive element help can be accessed by right clicking on the element and selecting “Element Help”. In addition, the examples included with the NI AWR DE software will assist in understanding the operation of computer simulation software for electronic circuits at all frequencies.

References

1. Keysight Technologies EEsof Electronic Design Automation (EDA) software, <http://www.keysight.com/find/eesof>
2. NI AWR Corp: MWO, VSS Design Software <http://www.awrcorp.com/products/ni-awr-design-environment/visual-system-simulator>
3. Microwave Office <http://www.awrcorp.com/products/ni-awr-design-environment/microwave-office>
4. Butterworth Filters; http://en.wikipedia.org/wiki/Butterworth_filter

5. Zverev, A. I. "Handbook of filter Synthesis", Book Publisher John Wiley & sons 1967.
6. L. P. Huelsman, "Active and Passive Analog Filter Design", McGraw-Hill, 1993.
7. D. M. Pozar, "Microwave Engineering" 3rd Edition, Wiley, 2005, Section 4.3.
8. 5SPICE: web site has links to many SPICE model web sites.
<http://www.5spice.com/links-tutorials.htm>
9. Microchip AN1297 "Microchip's Op Amp Spice Macro Models",
<http://ww1.microchip.com/downloads/en/AppNotes/01297a.pdf>
10. Fairchild Discrete PSPICE Models:
<http://www.fairchildsemi.com/models/modelDetails?modelType=PSPICE>
11. Infineon: <http://www.infineon.com/cms/en/tools/>
12. ONSemiconductor <http://www.onsemi.com/PowerSolutions/supportResources.do>
13. BD136 SPICE file http://www.onsemi.com/pub_link/Collateral/BD136.LIB
14. M. Edwards, AWR Nonlinear Modeling White Paper " AWR's support of polyharmonic distortion and nonlinear behavioural models", Available from:
<http://www.awrcorp.com/sites/default/files/content/attachments/AWR-Nonlinear-Modeling-White-Paper.pdf>.
15. NI AWR Corp. "Element Help files: MWO/AO Element Catalog>Nonlinear>Gummel-Poon BJT:GBJT".
16. NI AWR Corp. "Element Help files: MWO/AO Element Catalog > Linear Devices >Bipolar Transistor (Closed Form): BIP".
17. NI AWR Corp, MWO/AO /Examples "Basic_Transient.emp project"
18. NI AWR Corp, NI AWR DE Help files Section 7.1 "Transient Analysis Basics".
19. Kikkert C. J. "Modelling Power Transformers for the Design of SWER line Coupling Networks.", 1st IEEE International Conference on Smart Grid Communications (SMARTGRIDCOMM 2010), October 4-6, Maryland USA.
20. Kikkert C. J. "A PLC Frequency Model of 3 Phase Power Distribution Transformers", SmartGridComm2012, 5-8 November 2012, Tainan City, Taiwan.

Chapter 3

Transformers and Hybrids

Introduction

At RF frequencies, Transformers are used to:

- 1 Invert signals by producing a 180-degree phase shift.
- 2 Change Impedances, to ensure that devices are matched correctly, thus ensuring that most of the power is transferred into or out of the devices.
- 3 Change balanced signals from a TV antenna to unbalanced signals for transmission using coaxial cables and connecting to a TV set.
- 4 Change unbalanced signals to balanced ones for use in mixers.
- 5 Provide DC isolation and permit DC and RF signals to be carried on the same coaxial cable for masthead amplifiers and other remote powered applications.

RF Transformers differ from audio and 50 Hz mains transformers in that:

- 1 Ferrites are normally used for the magnetic material.
- 2 The windings may be an appreciable fraction of the wavelength.
- 3 Capacitive coupling between the primary and secondary windings and the self-capacitance of the windings must be taken into account. The capacitance between the windings, extends the frequency response, but at a 1:1 turns ratio. The self-capacitance of the windings causes resonances.
- 4 The transformers may need to operate over several decades of frequency.
- 5 At VHF frequencies and above, transmission lines may be used as transformers, without the use of ferrites. Such transformers operate over a relatively small frequency range.

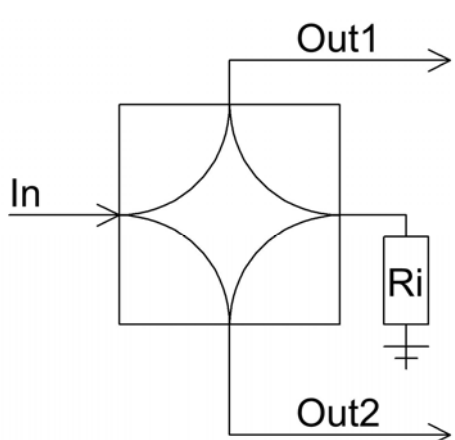


Figure 3.1. Hybrid symbol.

Hybrids are used to split or combine signals, while providing isolation between those signals.

Figure 3.1 shows the commonly used symbol for a hybrid. The input signal is divided equally between Out1 and Out2. Out1 and Out2 are isolated from each other. This allows us to drive two amplifiers, thereby improving amplifier stability and increasing the output power handling capability.

The power-handling capability of RF transistors operating up to 1 GHz can be as high as 100 Watt. Figure 3.2 shows how two such 100 Watt amplifiers, together with two hybrids can be used to produce a 200 Watt amplifier. This also gives some redundancy against failure of an amplifier.

For an ideal hybrid, if one amplifier fails, the output will drop by 6 dB, with the power from the remaining amplifier being split between the antenna and the resistive load at the output hybrid, but the system still operates. For higher

power output requirements, many of these modules can be combined in a similar manner. As a result, solid-state amplifier modules with output powers of several kW can be made.

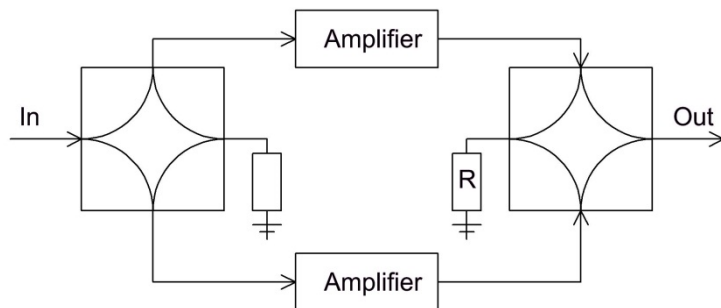


Figure 3.2. Parallel operation of amplifiers.

At VHF frequencies the hybrids are normally made using transmission lines. At lower frequencies, the hybrids can be made using transformers. Most telephone handsets, operating at audio frequencies, have either a transformer hybrid or an active hybrid using an Application Specific Integrated Circuit, (ASIC).

Wideband Transformers

For a conventional ferrite transformer, the upper length of the winding is limited to approximately 10% of the wavelength. At 1 GHz the wavelength is 300 mm and the maximum winding length is thus 30 mm. If the windings are like a transmission line, as used in TV baluns shown in figures 3.7 and 3.8, this limit does not apply. The corresponding lower limit [1] is:

$$l_{min} = \frac{R_l}{2(1+\mu_r)f_{min}} \quad \text{Eqn. 3.1}$$

Where R_l is load impedance in Ohm, f_{min} is the lowest operating frequency of the transformer in MHz and l_{min} is the length of the winding in metres. For a Neosid F14 material with a μ_r of 220, operating at 1 MHz in a 50Ω system, the minimum winding length is thus 113 mm. This minimum winding length should be allowed for in transformers made using ferrites.

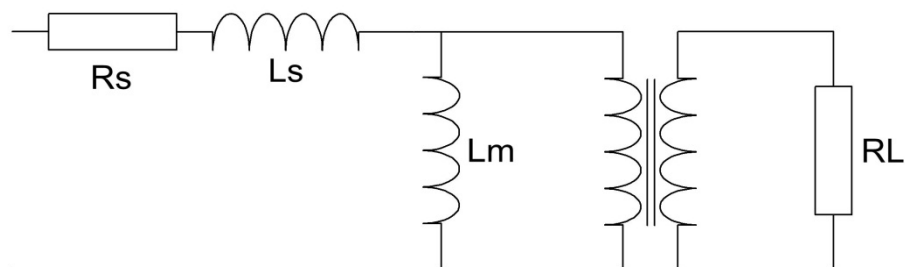


Figure 3.3. Simplified RF transformer model.

Transformers can be designed using the above equations, however by considering the simple conventional transformer model [2] shown in Figure 3.3, containing a Leakage inductance L_s and a Magnetising inductance L_m , the optimum number of turns required for RF transformers can be easily determined. To simplify the calculations assume that the transformer has a 1:1 turns-ratio, so that the load R_L is also the load reflected into the primary. For other turns ratios, the load impedance reflected into the primary, is the impedance used for calculations.

At low frequency, the Magnetising inductance L_m shunts the output load. The lower cut off frequency is thus when $j\omega L_m = R_L$. At high frequencies, the Leakage inductance is in series with the output. The upper cut off frequency is thus when $j\omega L_s = R_L$.

For the model of figure 3.3, the leakage inductance can most easily be measured by short-circuiting the secondary winding of the transformer. Under those conditions the input impedance of the transformer is $R_s + j\omega L_s$. When the transformer is open circuited, the input impedance is $R_s + j\omega L_s + j\omega L_m$. Since L_m is typically 1000 times larger than L_s , the leakage inductance can be ignored as part of the lower frequency calculation. This simple model does not include inter-winding and self-capacitances, but for many applications, it is accurate enough as R_s often governs the upper cut-off frequency (F_{high}).

If one normally wants to operate the transformer at a frequency F_c then it is desirable to make this $F_c = \sqrt{F_{low} F_{high}}$ where F_{low} and F_{high} are the upper and lower cut off frequencies of the transformer. As described above, the upper and lower cut off frequencies are determined by the leakage and magnetising inductance respectively.

The input impedance of the transformer at the centre frequency is thus:

$$Z_c = \sqrt{Z_{Ls} Z_{Lm}} = \sqrt{\omega L_s \omega L_m} \quad \text{Eqn. 3.2}$$

For a 50Ω system, one wants this Z_c to be 50Ω . Under those conditions $R_s + j\omega L_s$ is much smaller than R_L and $j\omega L_m$ is much larger than R_L , so that virtually all the input power is transferred to the output.

Since the inductance is proportional to the number of turns squared, the characteristic impedance of the transformer is also proportional to the number of turns squared. The number of turns chosen for the transformer winding is such that the characteristic impedance of the transformer matches the system impedance. Since in many cases the detailed properties of the ferrite may not be known, the characteristic impedance is most easily determined by winding a trial-winding on the transformer and using the measured open and short circuited impedances to then calculate the correct number of turns required.

In practice, the magnetising inductance has some losses associated with it and the resistive losses of the windings are in series with the leakage inductance. The resistive losses are normally very small. Since the inductance is proportional to the frequency, at the upper and lower frequency limits the inductance dominates, so that in the calculation for the upper and lower frequency limits, the resistive part of the measured input impedance can be ignored.

Example 3.1: RF Transformer Design

A ferrite coil has an 11 turn bifilar trial winding on it. At 1 MHz, input impedance with the secondary winding short-circuited is $Z_{Ls} = j0.4 \Omega$, corresponding to a leakage inductance of 64 nH. The input impedance measured with the secondary open-circuited is $Z_{Lm} = j400 \Omega$, corresponding to a magnetising inductance of 64 μ H. From equation 3.2, the characteristic impedance is thus $Z_c = \sqrt{(400 \times 0.4)} = 12.65 \Omega$.

The inductance is proportional to the square of the number of turns. Thus, for a 50Ω transformer we need $11 \times \sqrt{(50/12.65)} = 22$ turns. For the 22 turn winding one will thus have a leakage inductance of 256 nH and a magnetising inductance of 256 μ H.

The ratio of the open circuit to the short circuit impedance is 1000:1. The ratio of the upper and lower cut off frequency is thus also 1000:1, with the centre frequency being at the geometric mean of the upper and lower cut off frequencies. The upper cut off frequency is thus $1 * \sqrt{1000}$ MHz = 32 MHz. The lower cut off is $1 / \sqrt{1000}$ MHz = 32 KHz.

The measured performance normally agrees closely with the calculated one. The actual upper corner frequency is often a little lower than the calculated one, since the losses in the ferrite increase non-linearly with frequency and are thus proportionally lower at the centre frequency, where the measurements of the leakage and magnetising inductance are made. RF transformers using bifilar and trifilar windings operate well at frequencies up to several GHz.

Bifilar and Trifilar Windings

For a bifilar winding, two wires are twisted together to form a primary and secondary winding of a transformer, with close capacitive coupling between the windings, which result in a wide frequency response. Bifilar windings are used for inverting transformers. Trifilar windings use three wires twisted together as shown in figures 3.4 and 3.5. Trifilar windings are used for Baluns (Balanced-Unbalanced transformers) [3] and for transformers with a 4:1 impedance transformation ratio, as shown in figure 3.4. For most TV antennae, the output from the antenna is a balanced signal, on two active wires carrying signals of opposite polarity. For low loss transmission without interference, a coaxial cable is normally used to transmit this signal between the antenna and the TV set. A Balun is used to convert the balanced signals from the antenna to the match the unbalanced signal for the coaxial cable.

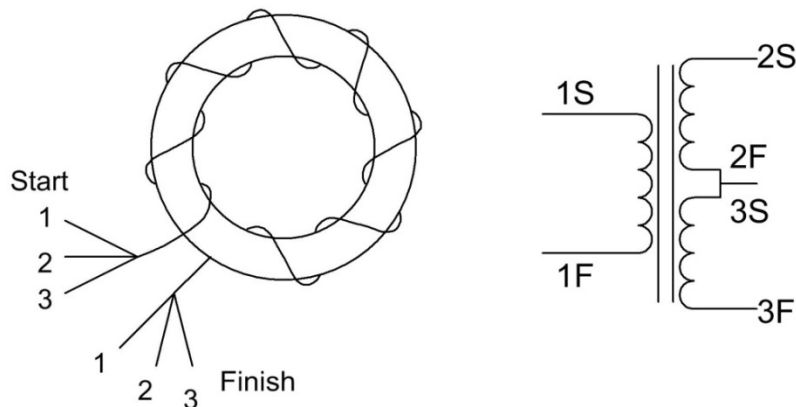


Figure 3.4. Trifilar winding diagram.

If port 2F-3S is earthed in figure 3.4, then the transformer is a balanced to unbalanced transformer, called Balun. For a 75Ω input impedance, a 300Ω output-impedance is obtained. Such a Balun is often used in TV antenna systems.

To construct a bifilar or trifilar winding, take the required number of wires, in parallel, put one end in a vice and the other in the chuck of a hand drill and turn the operate the drill until the required amount of twisting has been done. The inter-winding capacitance can be controlled by selecting the insulation thickness on the wires. Winding self-capacitance can be minimised by using a single layer winding. Figure 3.5 shows a typical bifilar and pentafilar transformer using single layer windings. Such transformers typically have a 3 decade frequency bandwidth.



Figure 3.5. A trifilar wound RF Transformer (left) and a pentaфilar transformer (right).

For instrumentation grade double balanced mixers a very good balance in the output signals is required, then an additional core, as shown in figure 3.6, can be added [3]. This provides winding 1 with a balanced input, thus causing the impedances at 2S to be exactly the same as those at 3F. Often the cost of the additional core is not justified.

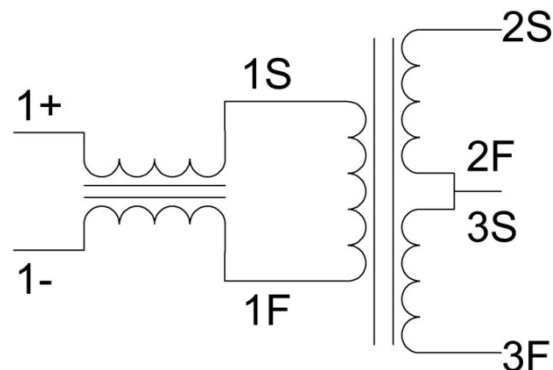


Figure 3.6. Balun with improved output balance.

Transmission Line Transformers with Ferrite Cores

At high frequencies, the primary and secondary windings are sometimes wound using transmission lines, as shown in Figures 3.7. This then uses inter-winding capacitances to use capacitive coupling at high frequency and magnetic coupling at lower frequency thus extending the bandwidth, significantly above what can be obtained using the construction technique of figure 3.5.

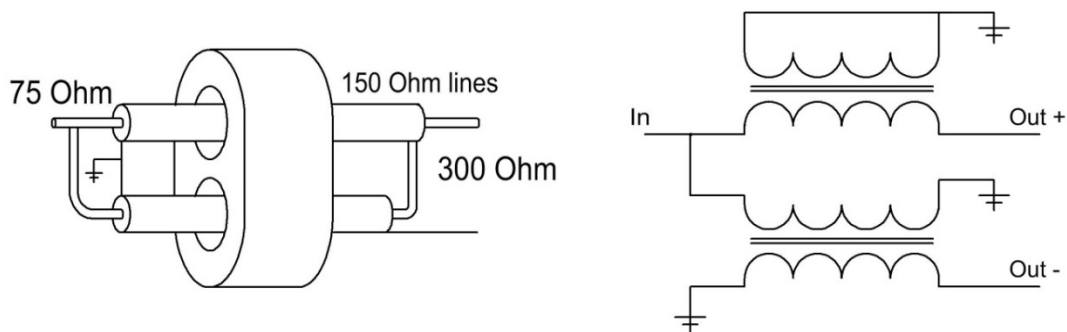


Figure 3.7. Diagram of transformers with ferrites and transmission lines.

For a $50\ \Omega$ system, the characteristic impedance for the transmission lines used for the windings are $100\ \Omega$. There is thus no reflection at the junction, where the two lines are connected in parallel. The two transmission lines are in series at the right hand side and the balanced output then form a $200\ \Omega$ system. Since the same propagation delay occurs through both the top and bottom transmission lines, the + and - signals are perfectly balanced at all frequencies.

The determination of the number of turns required for this transformer is the same as that for the bifilar or trifilar winding outlined above. The lower corner frequency is determined by the magnetising inductance. The upper corner frequency is determined by the losses in the ferrite. For the transmission-line transformer the winding length is no longer limited to be less than 10% of the wavelength, as both outputs have the same propagation delay through the transmission line. Typically, these cores are wound on low loss ferrites, giving them very high upper cut-off frequencies.

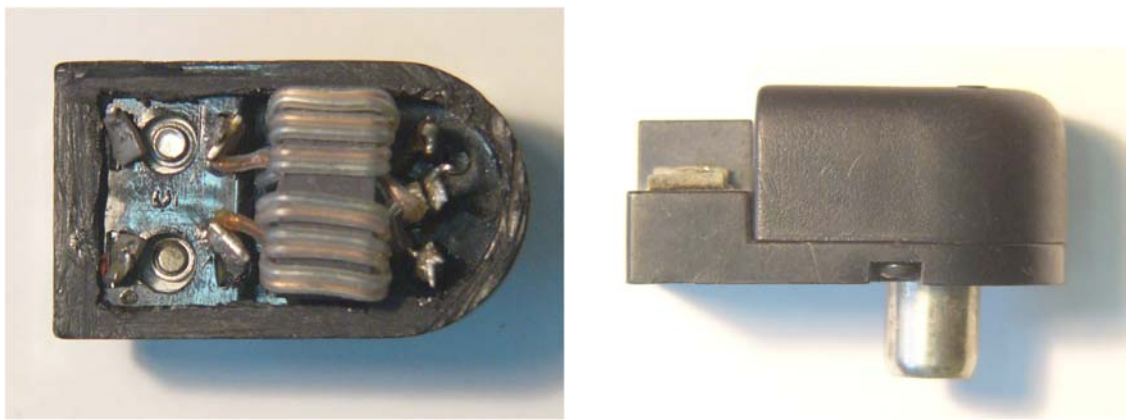


Figure 3.8. TV Balun using Ferrite RF transformer and transmission line windings.

Figure 3.8 shows a TV balun (*Balanced to Unbalanced*) transformer, corresponding to the circuit diagram in figure 3.7. This allows a typical dipole antenna, which has a balanced output of $300\ \Omega$ impedance to be connected to a $75\ \Omega$ coaxial cable, for a low loss connection to a TV. The transmission line balun is an ideal match at high frequencies and the ferrite provides the isolation at low frequency.

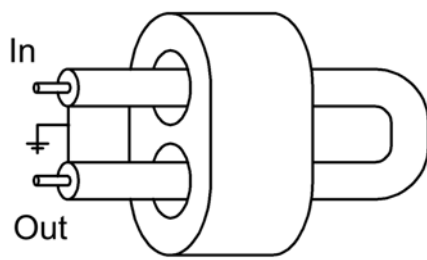


Figure 3.9. Non-inverting transformer.

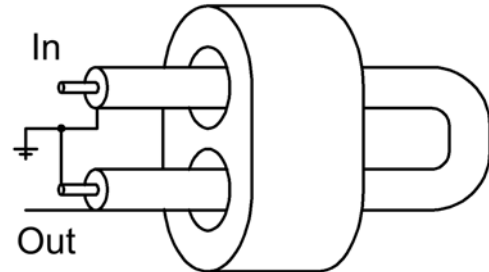


Figure 3.10. Inverting transformer.

By simply wrapping a coaxial lead around a ferrite or steel former, a non-inverting transformer, like figure 3.9, is obtained. This will provide isolation between both ends of the coaxial cable. Such a lead is useful in preventing earth loops for μV measurements.

A transformer, using transmission lines for the windings, can be used as an isolating transformer, by connecting opposite sides of the transmission line to ground as indicated in figure 3.10. The lower frequency of this transformer is determined by the magnetising

inductance of the former. This can be increased by simply adding more cores or having the transmission line go through the hole in the core many times.

Transformer Hybrids

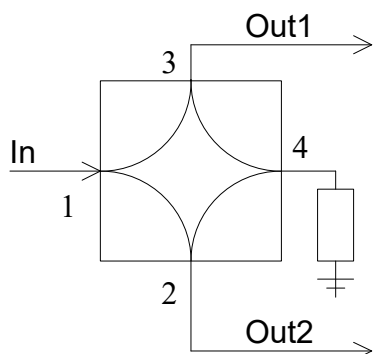


Figure 3.11. Hybrid.

In a hybrid, the input power at port 1 is split two ways to adjacent ports 2 and 3. Port 4, opposite the input port is isolated from the input port, and should have no energy going to it. A hybrid can thus be used as a power splitter.

Hybrids are normally symmetrical and bi-directional. Port 2 can thus also be used as an input, and under those conditions, half the power appears at port 1 and the other half appears at port 4. Under these conditions, port 3 is isolated. If we now apply another input signal at port 3, that will also split two ways with half appearing at port 1 and the other half at port 4. For most hybrids, the phase angle at port 4 is 180 degrees out of phase

for inputs at either port 2 or port 3, so that if equal signals are applied to ports 2 and 3, the sum of the signals will appear at port 1 and the difference will appear at port 4. If the signals applied to port 2 and port 3 are the same, the powers are combined at port 1. A hybrid can thus be used as a power combiner as well.

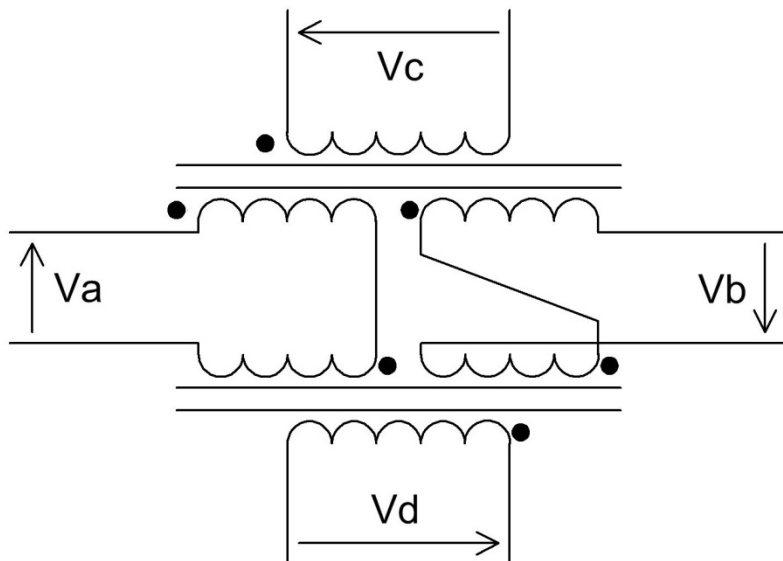


Figure 3.12. Audio transformer hybrid.

Transformer hybrids like the ones in figure 3.12 are used in telephony networks, where the signals to and from the normal telephone are sent in both directions on two wires.

Assume that all the windings on the transformers have the same number of turns. For the Audio transformer hybrid in figure 3.12, the voltages at each of the ports are related as:

$$\begin{aligned}
 V_a &= V_c + V_d \\
 V_b &= V_c - V_d \\
 2V_c &= V_a + V_b \\
 2V_d &= V_a - V_b
 \end{aligned} \tag{Eqn. 3.3}$$

By changing the turns ratio to 0.707, the same equations are obtained for all the ports:

$$\begin{aligned}
 V_a &= 0.707V_c + 0.707V_d \\
 V_b &= 0.707V_c - 0.707V_d \\
 V_c &= 0.707V_a + 0.707V_b \\
 V_d &= 0.707V_a - 0.707V_b
 \end{aligned} \tag{Eqn. 3.4}$$

This ensures that the impedance levels in each port are the same. Note that V_a does not couple into V_b and V_c does not couple into V_d and vice versa. A 40 dB isolation is typical under properly matched conditions.

Figure 3.13 shows how this audio hybrid can be wired up for use with amplifiers to produce a bi-directional amplifier, to amplify signals travelling in both directions along a wire. If the 2-wire circuit is not terminated properly, then part of the energy travelling out of this amplifier will be reflected and come back as input to the amplifier and be amplified again. If the gain of the amplifier is A dB and the isolation is B dB, then the singing margin is $2 \times (B - A)$. The singing margin is the gain around the amplifier/hybrid loop. If the gain around the loop is more than 0 dB, then oscillations will occur. In practice, the singing margin should be better than 6 dB. We should thus have more than 6 dB loss around the loop, even in the worst conditions.

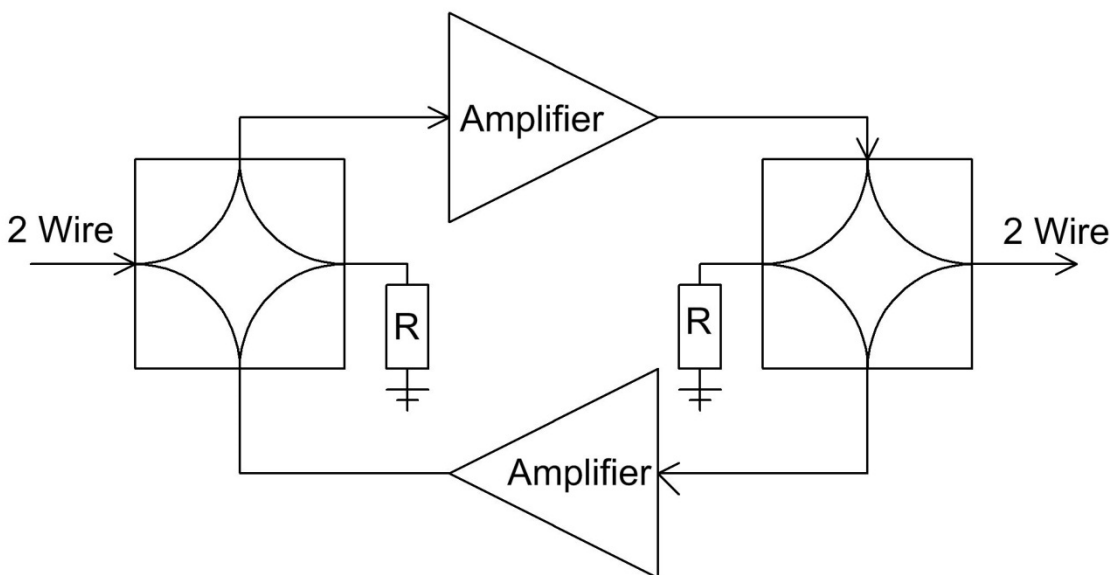


Figure 3.13. Bi-directional amplifier.

Power Combiner / Splitter

In a power combiner or power splitter, the terminating port is not brought out. The power combiner or power splitter is thus a 3-port device. Since linear passive devices are bi-directional, the same device can be used as both a power splitter and a power combiner. Often these devices are still called a hybrid. A common transformer based power splitter is a Wilkinson Hybrid. The two-way power splitters sold by department stores to permit two TVs to be operated from one antenna are Wilkinson Hybrids.

Wilkinson Transformer Hybrid

Figure 3.14 shows the circuit diagram of a Wilkinson Transformer Hybrid. If the same voltage input is applied to both ports A and B, then there is no voltage drop across the

terminating resistor or transformer and port C is at same voltage as ports A and B. If the impedance levels for ports A and B are Z_0 , then for power conservation, the impedance level at port C must be $\frac{1}{2} Z_0$. For those situations where the output impedance should be Z_0 then a 3:2 turns ratio transformer will change the impedance level by 2.25, which is close enough to 2:1.

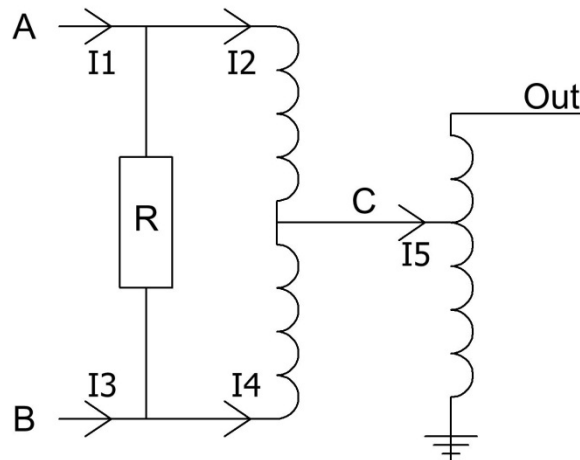


Figure 3.14. Wilkinson Transformer Hybrid.

If a voltage is applied to port A and 0 Volt is applied to port B, then the voltage at port C is $\frac{1}{2}$ of that at port A. If the input current at port A entering the transformer is I_2 then through transformer action an equal and opposite current is flowing through the bottom part of the transformer, so that $I_2 = I_4$, under all conditions. If the load impedance at port C is $\frac{1}{2} Z_0$ as before then the input impedance seen at port A at the input of the transformer is $2 Z_0$ since the transformer has a 2:1 turns ratio and a 4:1 impedance transformation ratio, since at port C one has half the voltage and twice the current.

Consider figure 3.14. For complete isolation between ports A and B, if a signal is applied at port A then the voltage at port B is zero, so that $I_3 = 0$. The current I_4 must thus flow through the resistor. The value of R required for complete isolation between ports A and B can now be calculated. The voltage across the resistor is:

$$V_a = \frac{I_4}{R} = \frac{I_2}{2Z_0} \quad \text{Eqn. 3.5}$$

Since $I_2 = I_4$, we must have $R = 2Z_0$ to achieve isolation between both input ports. Under those conditions the impedance seen at the input port A is Z_0 , being the transformer input impedance of $2Z_0$ in parallel with the terminating resistor of $2Z_0$.

If this hybrid is used as a power splitter and the loads on ports A and B are matched, then no current will flow through the terminating resistor. Under those conditions that can be removed, at the expense of a poor isolation if unequal loads are present. For a power combiner in an antenna systems, where the output from two identical antenna elements are combined, a hybrid can be used that does not contain any isolating resistor, since the signals arriving at each of the antennae is identical and as a result no power is dissipated in the isolating resistor.

The Wilkinson transformer hybrids are commercially available as wideband power-splitters and power-combiners manufactured by companies such as Minicircuits.

The conventional TV splitter is a cut down version of the Wilkinson hybrid. Since the cable losses will mask any unequal loads, the terminating resistor is not normally present

and since impedance variations can be tolerated, no output transformer is used. The omission of those components reduces the cost for this consumer-oriented circuit.

If a Wilkinson Transformer hybrid is used to combine the output from two transmitters, any unbalance will be dissipated in the resistor R. For two 100 Watt transmitters, 50 Watt will be dissipated in the resistor and 50 Watt will be radiated if one of the amplifiers fails. The resistor must thus be selected with this power requirement in mind.

Example 3.2: Wilkinson Transformer Hybrid Design

The method of determining the required number of turns for a transformer operating at a specified centre frequency and impedance level described in example 3.1 can also be used to determine the number of turns of the windings for a Wilkinson transformer hybrid. In this example, the same transformer as used in the example 3.1 is used for the design of a Wilkinson hybrid to operate at 1 MHz as before. If the basic hybrid is unbalanced (an input is applied to port 2 but no input is applied to port 3), it behaves like a $25\ \Omega$ to $100\ \Omega$ transformer. The transformer of the previous example had an 11 turn winding with a characteristic impedance of $12.65\ \Omega$. For the $25\ \Omega$ side $11\sqrt{(25/12.65)}\ \text{turns} = 15.5$ turns is required. Since this has to be an integer number, 16 turns are used. The leakage inductance will then be $64(16/11)^2 = 135\ \text{nH}$ and the magnetising inductance will be $135\ \mu\text{H}$. The $25\ \Omega$ to $50\ \Omega$ impedance transformation transformer will have a 2:3 turns ratio auto-transformer, with an 8 turns trifilar winding, so that the $25\ \Omega$ winding will consist of two 8 turn windings in series, resulting in the required 16 turns. The $50\ \Omega$ port 1 will thus see 24 turns, corresponding to a leakage inductance of $270\ \text{nH}$ and the magnetising inductance will be $270\ \mu\text{H}$.

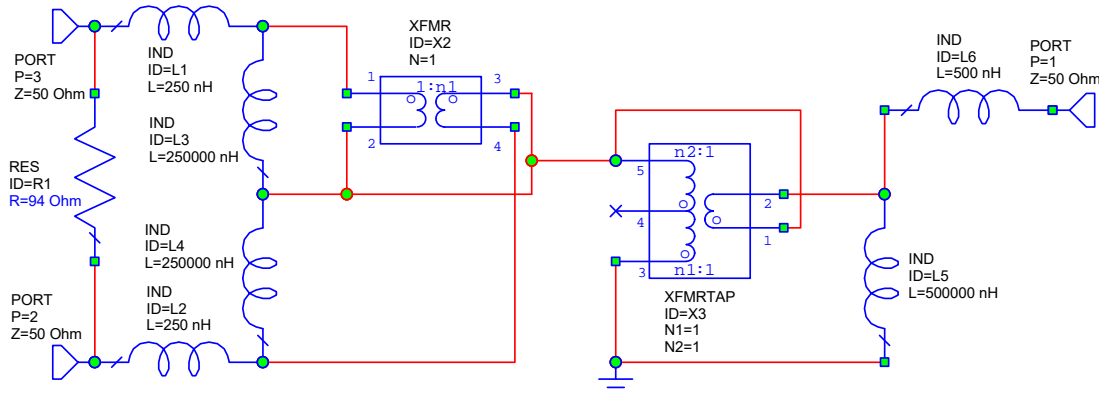


Figure 3.15. Wilkinson Hybrid model for computer simulation.

The performance of the Wilkinson Hybrid can be determined from computer simulation using NI AWR DE as shown in figures 3.15 and 3.16. It can be seen that a good isolation and return loss on all ports is obtained at the design frequency of 1 MHz. Constructing this hybrid normally results in a close agreement with the simulation and typically result in a three decade frequency bandwidth.

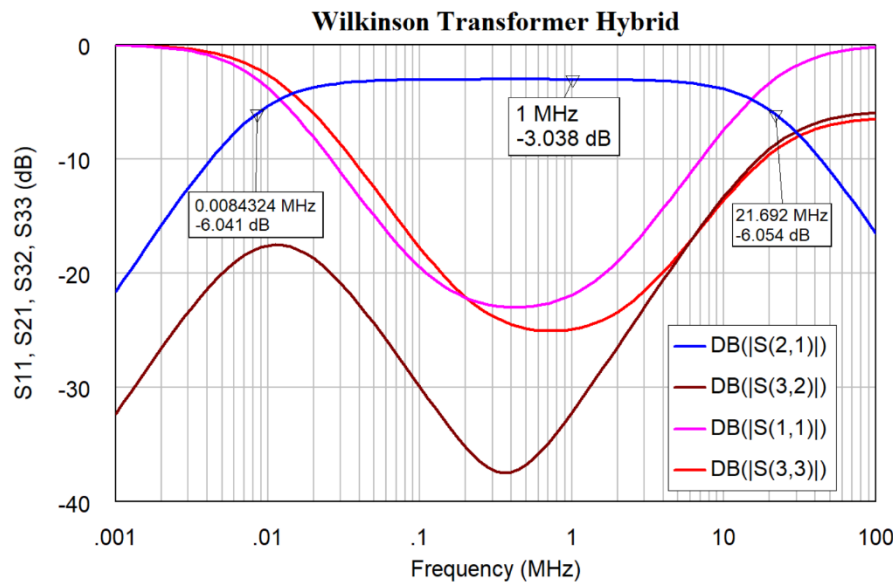


Figure 3.16. Simulated performance of Wilkinson Hybrid.

Transmission Line Hybrid with Ferrite Cores

A simple hybrid made using standard 50Ω transmission line hybrid and ferrite cores is shown in figure 3.17. If the impedance at A and B is Z_0 then at C the impedance is $\frac{1}{2}Z_0$. The impedance seen when B=0 is $2 \times (\frac{1}{2}Z_0) = Z_0$. The power dissipated in the load resistor is the power associated with the difference in the input signals. For high power operation, the rating of that resistor must be carefully considered. If the input at A and B are the same then no power will be dissipated in the load resistor.

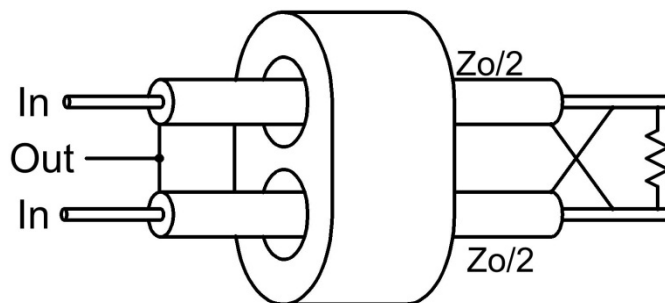


Figure 3.17. Hybrid with ferrite cores.



Figure 3.18. Circuit of hybrid in figure 3.17

The realisation of the hybrid is shown in figure 3.18 and the circuit can be analysed using the circuit representation in figure 3.19. In figure 3.18, the $25\ \Omega$ transmission lines are obtained by having two $50\ \Omega$ transmission lines in parallel.

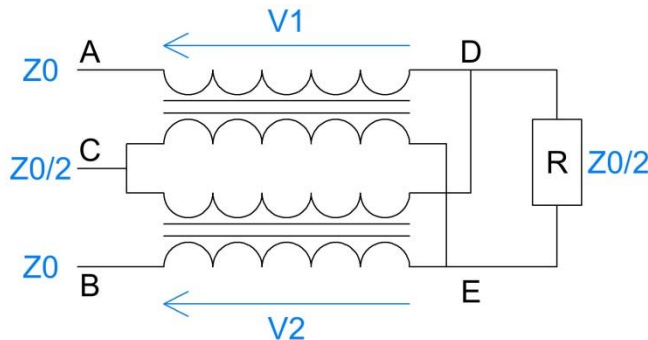


Figure 3.19. Circuit of hybrid in figure 3.17.

The equations for this hybrid are:

$$\begin{aligned} V_a - V_d &= V_1 \\ V_c - V_e &= V_1 \\ V_c - V_d &= V_2 \\ V_b - V_e &= V_2 \end{aligned} \quad \text{Eqn. 3.6}$$

Subtracting the first two equations and the last two equations and adding the resulting equations gives:

$$V_c = \frac{V_a + V_b}{2} \quad \text{Eqn. 3.7}$$

Now consider the conditions required for isolation. If $V_b=0$. For isolation between ports A and B, the current through the bottom transformer is zero, since with a load connected to B the voltage must be zero. That means $V_2=0$ and thus $V_e=0$ and $V_d=\frac{1}{2}V_a$.

For the input impedance at A to be Z_0 then the load resistor must be $\frac{1}{2}Z_0$. Under those conditions, the current into A goes through the load and out of C. The voltages are thus:

$$\text{At input A} \quad V_a = Z_0 \bullet I \quad \text{Eqn. 3.8}$$

$$\text{Across the Load} \quad \frac{1}{2}V_a = \frac{1}{2}Z_0 \bullet I \quad \text{Eqn. 3.9}$$

$$\text{At the output C} \quad \frac{1}{2}V_a = \frac{1}{2}Z_0 \bullet I \quad \text{Eqn. 3.10}$$

The equations are thus consistent and the assumption that $V_b=0$ is justified and we have full isolation when $R=\frac{1}{2}Z_0$. The circuit works thus as a proper hybrid.

Note: Like the Wilkinson transformer, the impedance at the summing port C has an impedance of $\frac{1}{2}Z_0$ and a transformer needs to be used to change that to Z_0 if required, similar to that for the Wilkinson transformer of figure 3.14.

Many Way Hybrids

In some instances, many signals need to be combined or a signal needs to be split many ways. The hybrids described above can be cascaded to provide a many way splitter/combiner. However, each of those hybrids will include a $25\ \Omega$ to $50\ \Omega$ impedance transformation transformer. Some savings can be made by using a 4 way hybrid as shown

in figure 3.20, where three of two way hybrids are used together to combine 4 input signals and then have a 12.5Ω output, which can be transformed to 50Ω by using a 2:1 transformer, as shown in figure 3.20. This saves two transformers, each of which will have some losses associated with it. In addition, the 4:1 impedance transformation is exact, while the 2:1 impedance transformation is actually a 2.25:1 impedance transformation with the 3:2 turns ratio of the transformer. Two of the hybrids below operate at a 50Ω impedance and one operates at a 25Ω impedance. The number of turns on the transformer coils needs to be adjusted to allow for this.

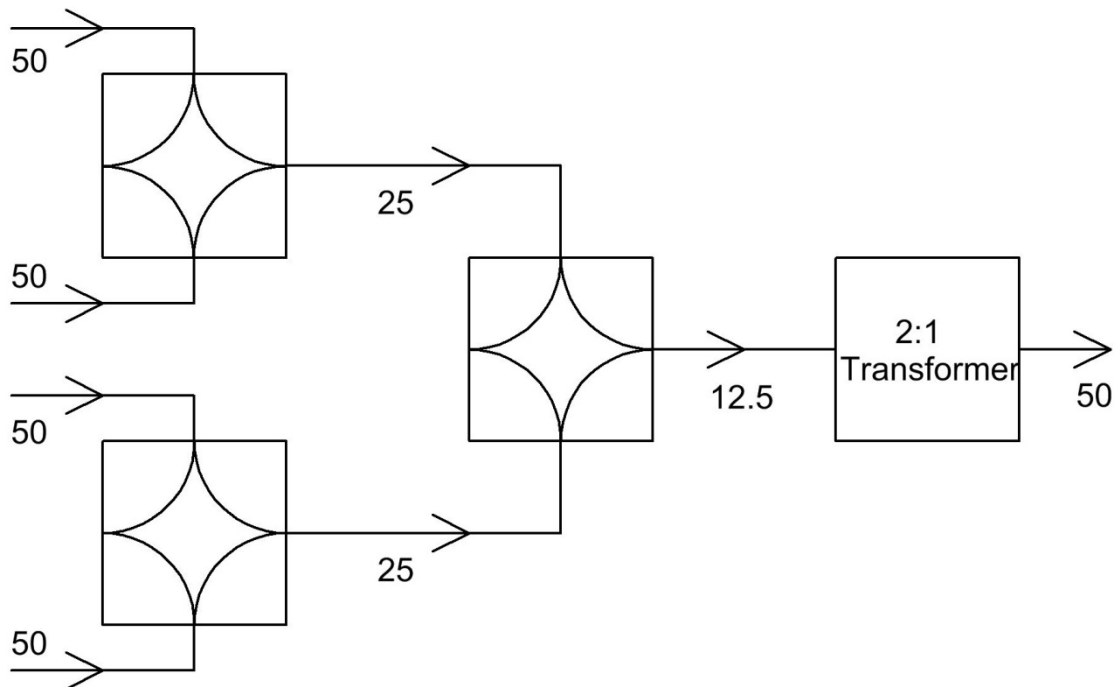


Figure 3.20. A four-way combiner.

References

1. H. Granberg, "Broadband transformers and power combining techniques for RF", Motorola Application note AN749, Motorola RF Circuits Engineering, 1993.
2. Minicircuits Application note AN20-001 "How RF Transformers work"
<http://www.minicircuits.com/app/AN20-001.pdf>
3. Minicircuits Application note AN20-002 "Application Note on Transformers"
<http://www.minicircuits.com/app/AN20-002.pdf>

Chapter 4

Transmission Line Transformers and Hybrids

Introduction

At RF and microwave frequencies, lines connecting devices can be an appreciable fraction of a wavelength. As a result, transmission lines models should be used, to connect all devices. Those transmission lines can also be used to change impedances, just like the transformers in chapter 3. In addition, by connecting transmission lines in special ways, circuits like hybrids, power splitters, power combiners and couplers can be made. Their design is described in this chapter.

Since this chapter deals with transmission lines and their use in transformers, hybrids and couplers, a brief review of properties of transmission lines will be given.

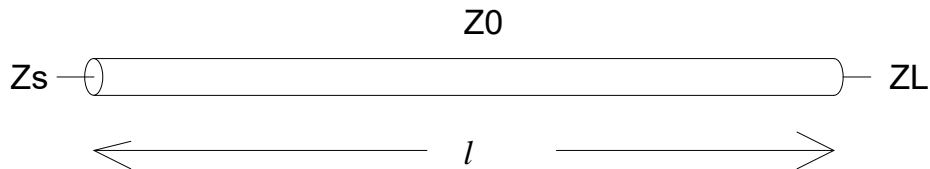


Figure 4.1. Transmission line parameters.

For a transmission line of characteristic impedance Z_0 and length l , the sending end impedance is given by [1 - 3]:

$$Z_s = Z_0 \frac{Z_L + jZ_0 \tan(\beta l)}{Z_0 + jZ_L \tan(\beta l)} \quad \text{Eqn. 4.1}$$

If the transmission line is close to one quarter wavelength long then $\tan(\beta l) \gg 1$ so that:

$$Z_s = Z_0 \frac{jZ_0 \tan(\beta l)}{jZ_L \tan(\beta l)} = \frac{Z_0^2}{Z_L} \quad \text{Eqn. 4.2}$$

so that: $Z_s Z_L = Z_0^2$ or $Z_s = Z_0^2 / Z_L$ Eqn. 4.3

The impedance transformation ratio R is given by:

$$R = \frac{Z_0}{Z_s} = \frac{Z_L}{Z_0} \quad \text{or} \quad Z_s = \frac{Z_0}{R} \quad \text{and} \quad Z_L = RZ_0 \quad \text{Eqn. 4.4}$$

If the allowable Voltage Standing Wave Ratio (VSWR) is W , so that the limiting value of the sending end impedance is WZ_s , substituting equation 4.4 into equation 4.1 gives:

$$WZ_s = W \frac{Z_0}{R} = Z_0 \frac{\{RZ_0 + jZ_0 \tan(\beta l)\}}{\{Z_0 + jRZ_0 \tan(\beta l)\}} \quad \text{Eqn. 4.5}$$

Solving for $\tan(\beta l)$ and using the fact that normally $W^2 \ll R^4$ gives:

$$\tan(\beta l) = \sqrt{\frac{R^4 - W^2}{R^2(W^2 - 1)}} \cong R \sqrt{\frac{1}{W^2 - 1}} \quad \text{Eqn. 4.6}$$

The higher R , the higher $\tan(\beta l)$ must be and thus the narrower the bandwidth for a given VSWR. This can easily be illustrated with an example.

Example 4.1: Bandwidth Calculation

If the allowable VSWR is 1.2, that is for a 50Ω system the impedance should be between 60Ω and 41.6Ω , and if $R = 2$ (i.e. a 4:1 impedance transformation) then $\beta l = 70.8^\circ$ i.e. $l = 0.197\lambda$. The bandwidth is thus $2(90-70.8)/90 = 43\%$

If R is changed to $R = \sqrt{2}$ (i.e. a 2:1 impedance transformation) then the same total impedance transformation can be achieved by having two transmission line sections in cascade. If the load impedance is Z_L then the impedance at the end of the first section is $2Z_L$ and the impedance at the end of the second section is $4Z_L$. The total length of the transformer is thus half a wavelength. Solving for βl gives $\beta l = 59.6^\circ$ i.e. $l = 0.166\lambda$. The bandwidth is thus $2(90-59.6)/90 = 67.5\%$

For very high frequencies, many sections can be cascaded and the line will have an exponential change of impedance for each of the quarter wavelength sections. This can readily be produced using RF PCB technology.

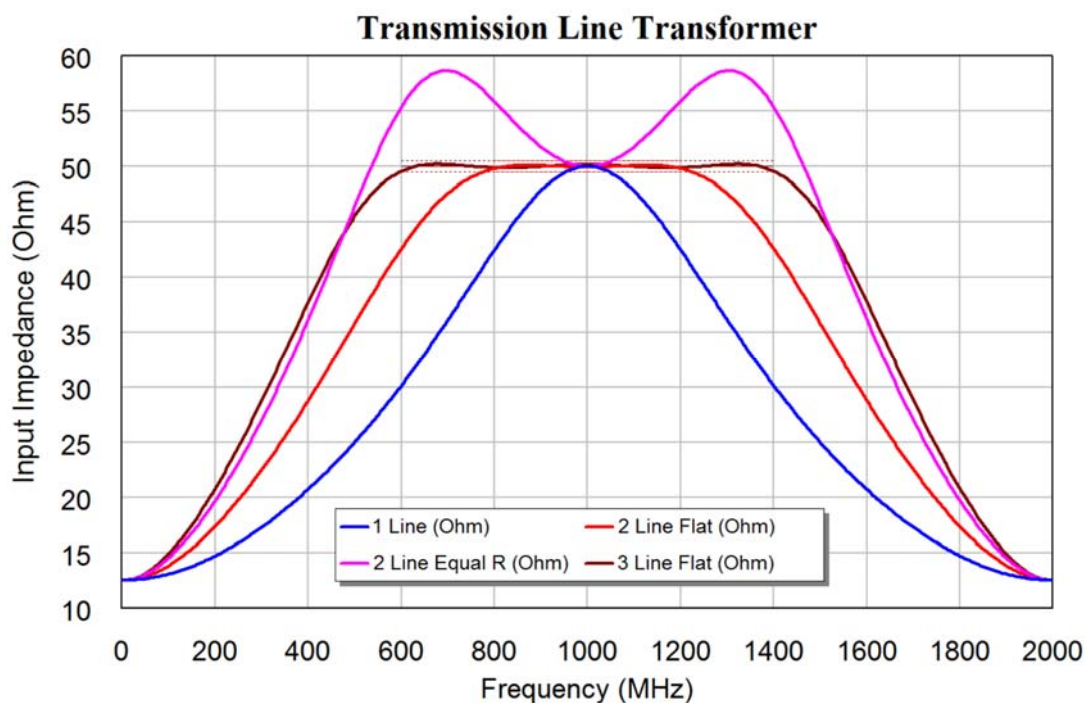


Figure 4.2. Plot of impedance variation versus frequency.

Figure 4.2 shows a plot of the input impedance variation of a transmission line transformer, transforming a 12.5Ω load into a 50Ω load. For the one line transformation, the impedance transformation is done in one transmission line section with a characteristic impedance of 25Ω . The Magenta curve is for a 2-line transformation, with the impedance transformation ratio $R = \sqrt{2}$ for each line.

If the impedance transformation ratio of the two lines in a two line impedance transformer is changed from the $R = \sqrt{2}$ for each of the lines, such that the total impedance transformation is still a 4:1 impedance transformation, but that each line has a slightly different transformation ratio, then a very good match can be obtained over a specified

bandwidth. For this design, the transformation ratio is made a variable constant, which is optimised to provide the minimum deviation from $50\ \Omega$, over the required frequency range.

For a two-line matching network, a good match can be obtained over the 800 MHz to 1200 MHz frequency range. The result of this optimisation is shown by the red curve in figure 4.2. The first line has $R = Z_{in}/Z_{d1} = 1.638$, where Z_{d1} is the impedance of line 1, corresponding to a characteristic impedance of $30.53\ \Omega$ and the second line has $R = Z_{d2}/Z_{out} = 1.222$ corresponding to a characteristic impedance of $15.28\ \Omega$, instead of the $R = \sqrt{2}$ for the un-optimised transmission line transformer. (Note: The numerical results obtained from NI AWR DE project files are normally presented in this book with the default 4 digit display accuracy of NI AWR DE. Results that are more accurate can be obtained by running the corresponding NI AWR DE project files.)

Applying similar principles to a 3-line section gives an even wider bandwidth. The brown curve in figure 4.2 shows the optimisation result of matching $50\ \Omega$ to $12.5\ \Omega$, using 3 quarter-wavelength long lines over a 600 MHz to 1400 MHz bandwidth. Instead of all the three transformer ratios being $\sqrt[3]{2} = 1.260$, the ratios are 1.450, 1.357, 1.087 and this corresponds to transmission line impedances are $34.48\ \Omega$, $18.71\ \Omega$ and $13.58\ \Omega$.

Instead of being as close to $50\ \Omega$ as possible over the specified frequency range, it is possible to specify optimisation limits to be say $>45\ \Omega$ and $<55\ \Omega$, and then making the bandwidth wider. This then allows very wide bandwidth impedance transformers, with tightly specified VSWR's to be designed.

Wilkinson Transmission Line Hybrid

The Wilkinson transmission line hybrid [4] consists of two quarter-wavelength long transmission lines forming a combiner, together with a load resistor to provide isolation. The circuit is shown in figure 4.3 and the performance is shown in figure 4.4.

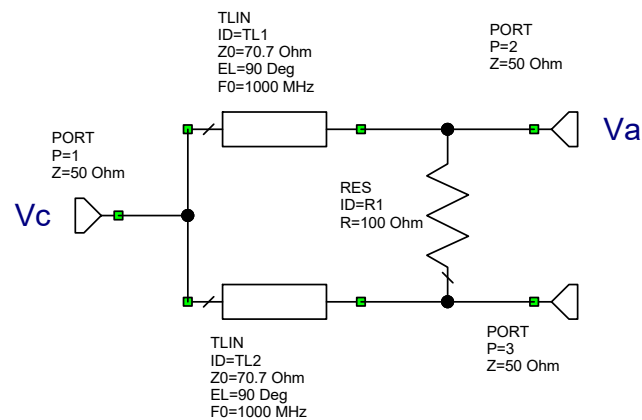


Figure 4.3. Ideal Wilkinson hybrid.

For the analysis, an input is applied to port 2 in figure 4.3. For proper hybrid operation, no voltage should appear at Port 3. Transmission line TL2 has a standing wave on it with 0 Volt at the Port 3 side. Since the line is one-quarter wave long, there will be no current flowing into the line at the Port 1 side, as shown in figure 4.5. For the analysis of the voltage on port 1, we can thus remove TL2, since it is an open circuit at the port 1 end. The voltage at port 1 will thus simply be what we would have if one had the transmission line only, as shown in figure 4.6.

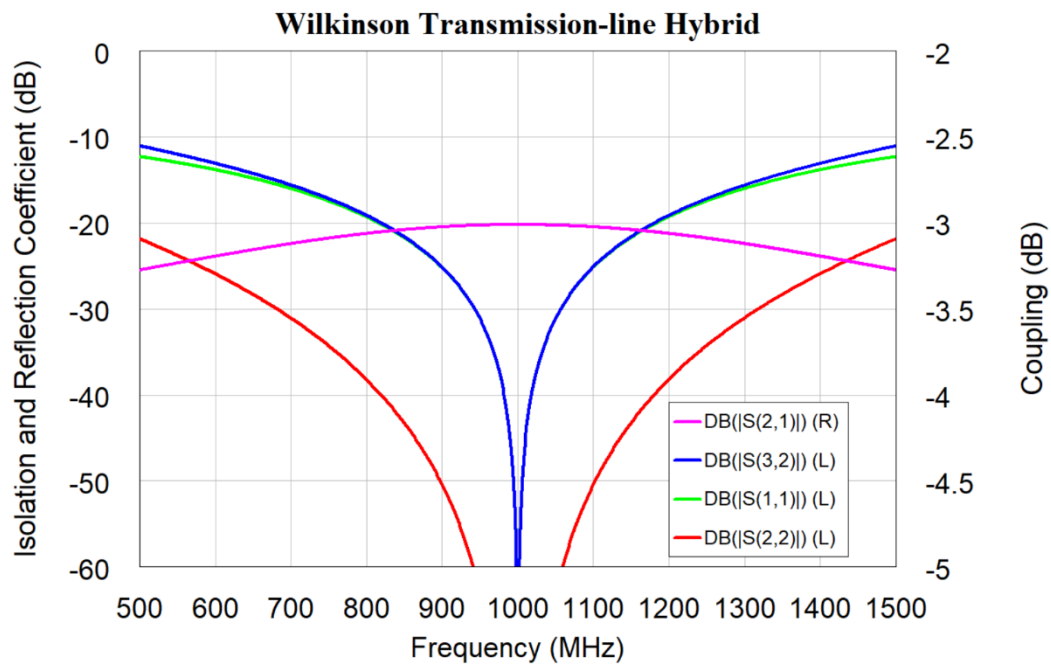


Figure 4.4. Ideal Wilkinson hybrid.

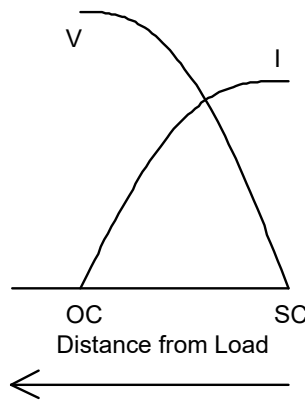


Figure 4.5. Standing wave along TL2.

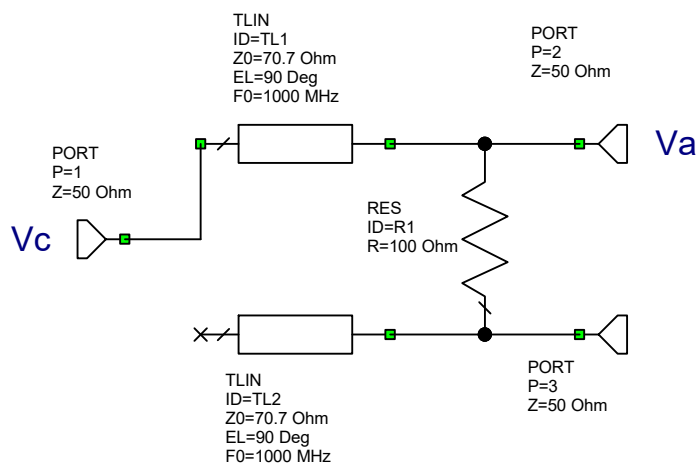


Figure 4.6. Circuit for analysis purposes.

Since the input power is the same as the output power, the voltage V_c at port 1 and the voltage V_a at port 2 relate as $V_a = \sqrt{2} V_c$.

The maximum current and maximum voltage on a transmission line relate as:

$$V_{\max} = Z_0 I_{\max} \quad \text{Eqn. 4.7}$$

In figure 4.3, the current at the port 3 side of TL2 will thus be:

$$I_{\max} = \frac{V_c}{\sqrt{2}Z_0} = \frac{V_a}{\sqrt{2}\sqrt{2}Z_0} = \frac{V_a}{2Z_0} \quad \text{Eqn. 4.8}$$

Since this current must come through the load resistor R then

$$I_{\max} = \frac{V_a}{R} = \frac{V_a}{2Z_0} \quad \text{Eqn. 4.9}$$

So that $R = 2Z_0$ for best isolation.

The circuit can be realised using a Microstrip PCB layout. A Rogers 4003 laminate with 1 oz. copper and 0.8128mm thickness are to be used. To calculate the required track widths and lengths, the properties of the PCB to be used are to be selected first. The parameters of the Rogers RO4003 substrate can be obtained by using the *Libraries* \Rightarrow *AWR Web Site \Rightarrow Rogers \Rightarrow RO \Rightarrow RO4003 and select 32 mil, 1 oz. and place that as a component in a circuit. Until recently Rogers only specified an $\text{Er} = 3.38$ for the RO4003 laminate. The latest data sheet from Rogers for RO4003C [5] indicates Er (Process specification) = 3.38 and Er (Design specification) = 3.55. Suggesting that for simulation the value of $\text{Er} = 3.55$ gives better results. Those values are used here. The values indicated in MSUB for RO4003 on the NI AWR Web site are $\text{ErNom} = 3.48$ and $\text{Er} = 3.55$. The value of ErNom is ignored by NI AWR DE and $\text{Er} = 3.55$ is used in the simulation. Note some of the earlier designs in this book using the RO4003 substrate still use the 3.38 value.

Determining the required track width and length, as shown in figures 2.21 to 2.23, results in a track width of 1.788 mm for the 50Ω lines and 0.9519 mm for the 70.71Ω lines. The layout must allow the isolation resistor to be soldered to the PCB. This requires that a resistor, with a PCB footprint is used. Firstly, determine the size of the surface mount resistor to be used. In our layout, an AVX 1206 resistor was used. AVX resistors are no longer included in the NI AWR web site libraries in NI AWR DE V10 or later, but Panasonic resistors are. Selecting *Libraries* \Rightarrow *AWR web site \Rightarrow *Parts by type* \Rightarrow *Lumped element* \Rightarrow *Resistor* \Rightarrow *Panasonic* \Rightarrow *Resistor* \Rightarrow *For General Equipment* \Rightarrow *S parameter*, allows different size footprint resistors to be selected (0603, 1005, 1608). Simply place the resistor with the required size footprint in the schematic, this will then automatically include the footprint in the layout. If another size footprint, say 1206 is required, then the footprint can be imported by simply placing a suitable size component like a capacitor or inductor. For our circuit, a Coilcraft inductor is used to provide the 1206 footprint. Select *Libraries* \Rightarrow *AWR web site \Rightarrow *Parts by type* \Rightarrow *Lumped element* \Rightarrow *Inductor* \Rightarrow *Coilcraft* \Rightarrow *RF Inductors* \Rightarrow *Data* \Rightarrow *1206CS series*. Then place any inductor in list in the circuit. Right clicking and selecting the inductor's properties, then selecting *Layout*, shows all the available Coilcraft Footprints, as shown in figure 4.7. The layout properties of the isolation resistor in the Wilkinson Hybrid can now be selected. The library name will be blank. Selecting the Coilcraft Library and the 1206 footprint will then link that footprint to the resistor. The inductor can then be removed from the circuit, as the footprint will remain linked to the resistor.

If internet speeds to the NI AWR DE website are too slow, local vendor libraries need to be installed and used. The Appendix shows how these can be installed. Then simply select the Library parts and footprints from the local libraries instead of the web site.

The rest of the PCB schematic can now be made. The $70.71\ \Omega$ Microstrip lines are made using MLIN elements. The two $70.71\ \Omega$ lines need to be joined to the $50\ \Omega$ line, using a MTEE. There are different versions of this. The most basic one is MTEE, where every connecting line width needs to be specified. MTEEX\$ is an intelligent version, which automatically uses the line widths of the connecting lines. MTEEX\$ is an EM based model of the junction and is more accurate. MTEEX\$ is the corresponding intelligent version of this and this element is used in the circuit. To get the most accurate results, EM based models should be used whenever possible.

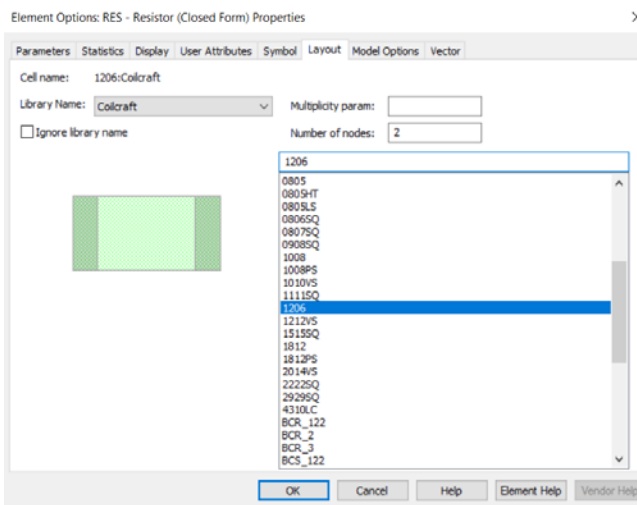


Figure 4.7. Selecting a footprint for resistor R1.

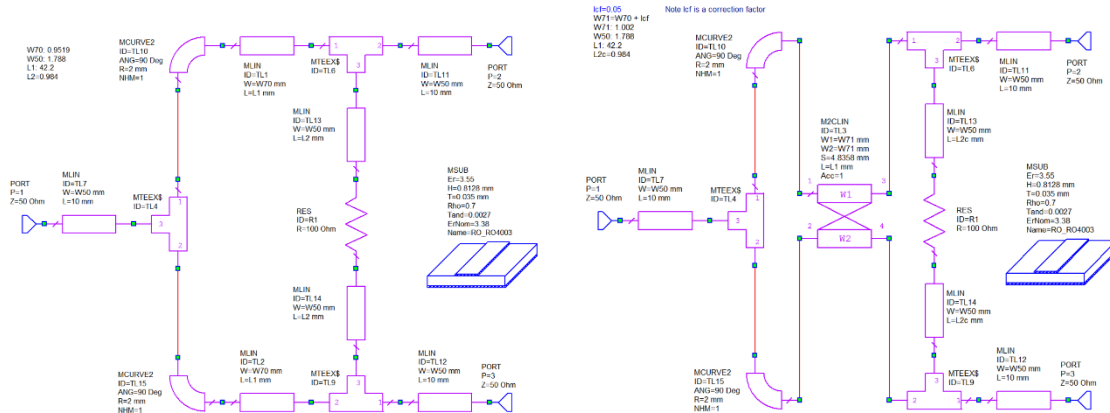


Figure 4.8. Schematics for Wilkinson hybrid PCB layout, using TLIN (Left) and MCLin (Right).

To keep the coupling between the two $70.71\ \Omega$ lines small, they are separated by more than 4 mm. This is achieved by using the two 90 degree bends with 2 mm radius each. Again, there are 4 different versions of bends. Since an intelligent MTEEX\$ is used, the width of the curved track should be specified. The MCURVE2 element uses EM mode matching and is the most accurate, but will take longer to be evaluated. The length of the $70.71\ \Omega$ lines, TL1 and TL2, is made variable, to allow the hybrid to be tuned to the correct centre frequency. Two more MTEEX\$ elements are used to allow the resistor to be connected correctly. Two small lines, TL13 and TL14, with a suitable width to allow

the isolation resistor R1 to be soldered to it are connected to the MTEEX\$ elements. Three 10mm long tracks, TL7, TL11 and TL12 are used, to allow connections to be made to the circuit. The left part of figure 4.8 shows the corresponding circuit.

The PCB layout of the circuit can be seen by selecting *View* \Rightarrow *View Layout*. To connect all the lines together, select *Edit* \Rightarrow *Select All* (or *Ctrl A*) and then select *Edit* \Rightarrow *Snap Together*. That will snap all the elements together. Check that there are no red crosses on the layout, which indicate that the elements are not properly connected together. If that is the case, change line lengths such as L2 for TL13 and TL14 to ensure that the layout fits exactly. These short lines will have some effect on the performance as shown in figure 4.10, where the notch of S_{22} is shifted in frequency as a result. The performance is however still satisfactory, since a 20 dB isolation or return loss is normally sufficient.



Figure 4.9. PCB layout of a Wilkinson hybrid.

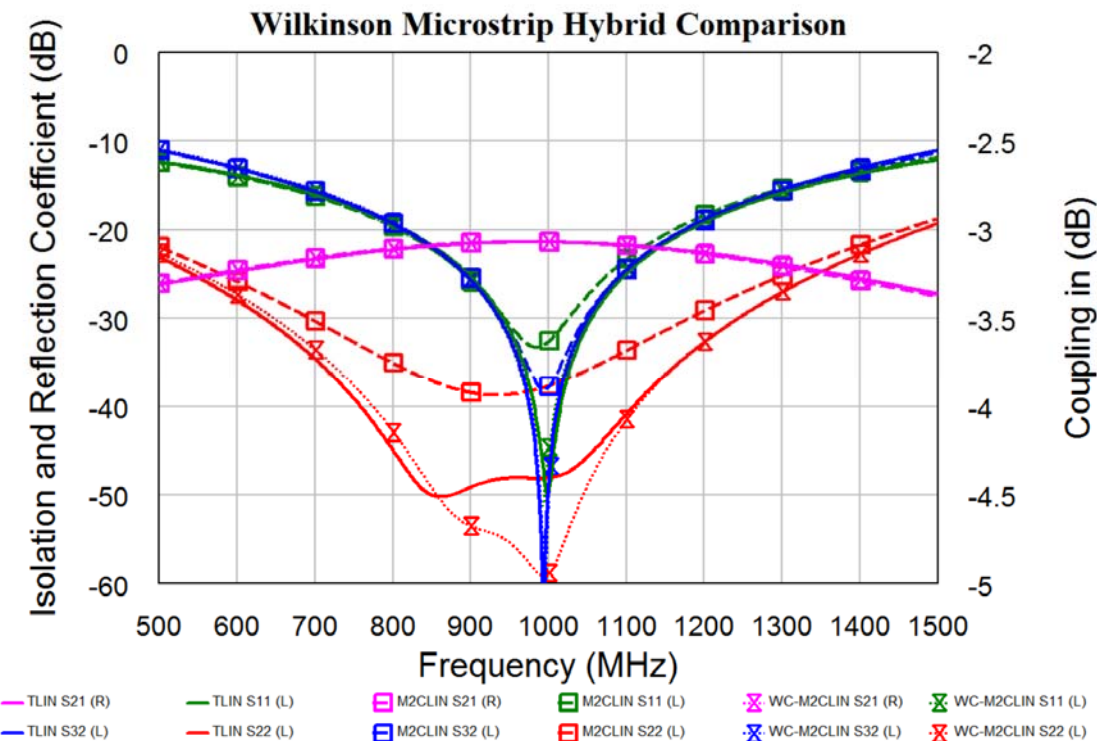


Figure 4.10. Performance of stripline Wilkinson hybrids of figure 4.7.

The line length L1 of TL1 and TL2 can be tuned to ensure that the best isolation occurs at 1.0 GHz. There will be some coupling between TL1 and TL2, since they are in close proximity. The effect of this coupling can be investigated using an EM simulator like AXIEM, which is included with NI AWR DE. In chapter 7, the section on *EM Simulation*, shows how AXIEM can be used to analyse circuits. A good indication of the coupling between lines TL1 and TL2 can simply be obtained by replacing them with a coupled line element M2CLIN as shown in the right part of figure 4.8. The length of the coupled line is the same as TL1 or TL2. The line width is 0.9519 mm like TL1 or TL2. The spacing is

set to 4.836 mm, corresponding to the spacing between TL1 and TL2. The layout is the same as figure 4.9, but now the effect of the coupling between TL1 and TL2 is included.

Figure 4.10 shows a comparison between the performance of the layout of figure 4.9, when TLIN elements are used for TL1 and TL2 and then these are replaced with a coupled line M2CLIN, initially with a width correction factor $lcf=0$. The coupling does not change but the isolation (S_{32}) and the return loss of S_{11} and S_{22} are reduced. If needed, the line widths used for M2CLIN can be changed slightly, by varying lcf , to improve these values. Optimising the width of the 70.71Ω lines, results in a width correction factor, $lcf = 0.05$ mm, and results in $S_{22} = -59$ dB at 1 GHz, as shown in the width-corrected WC-M2CLIN curves in figure 10. A similar improvement in S_{22} can be made by slightly tuning the width of the lines for the circuit in the left of figure 4.9.

Figure 4.10 does show that unintended coupling between lines can seriously degrade the performance of a circuit, but that steps can easily be taken to overcome any performance degradation.

Compensated Wilkinson Hybrid

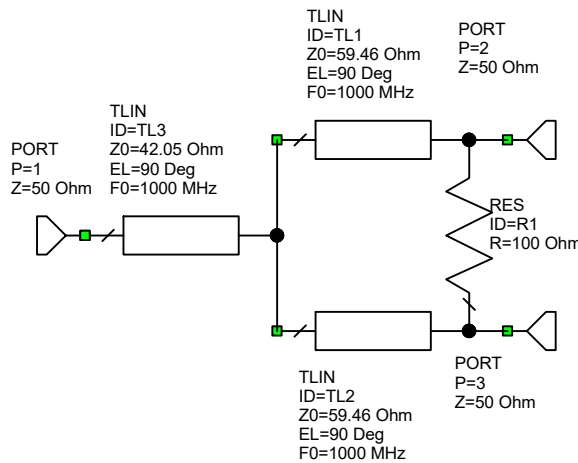


Figure 4.11. Compensated Wilkinson hybrid.

In a compensated Wilkinson hybrid, a two-step impedance transformation is used, like the two line impedance transformation of figures 4.1 and 4.2. The resulting circuit is shown in figure 4.11. The impedance transformation from line TL3 is from 50Ω at port 1 to 35.36Ω at the right of TL3. Lines TL1 and TL2 do an impedance transformation from 50Ω at port 2 and port 3 to 70.71Ω at the left hand side of transmission lines TL1 and TL2. Those in parallel give a 35.36Ω , which matches that at the right hand side of line TL3. Each of the three transmission lines will thus have the same impedance transformation ratio of $\sqrt{2}$.

Figure 4.12 shows a comparison between the conventional, shown in red, and the compensated (blue) Wilkinson hybrid. The compensated Wilkinson hybrid shown in blue has a wider frequency response for both the isolation and coupling. In addition, the compensated Wilkinson hybrid uses lower impedance transmission lines, resulting in wider track widths for the Microstrip layout, thus lowering the resistive losses in the circuit.

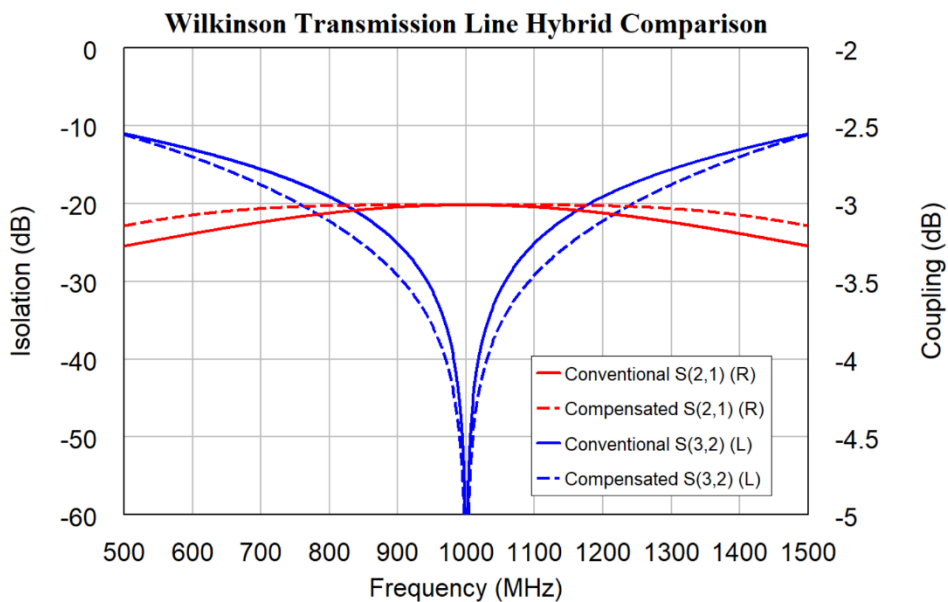


Figure 4.12. Comparison of conventional and compensated Wilkinson hybrid performance.

Unequal Split Wilkinson Hybrid

Sometimes an unequal power split is required. If a power ratio of P:1 is required, then the impedances seen at the source end of each of the transmission lines must also have a ratio of P:1. Since the total impedance must be $Z_0 = 50 \Omega$, then the impedances are:

$$\frac{1}{Z_0} = \frac{1}{Z_1} + \frac{1}{Z_2} = \frac{1}{Z_1} + \frac{1}{P * Z_1} = \frac{P+1}{P * Z_1} \quad \text{Eqn. 4.10}$$

The line impedances are thus:

$$Z_1 = \sqrt{\frac{P+1}{P}} Z_0 \quad \text{Eqn. 4.11}$$

$$Z_2 = \sqrt{P+1} * Z_0 \quad \text{Eqn. 4.12}$$

where Z_1 and Z_2 are the transmission line impedances of the hybrid. As a check when an equal split is used, $P=1$, so that $Z_1=Z_2=\sqrt{2}Z_0$.

Thus for a 10:1 power split in a 50Ω system, the transmission line impedances are:

$Z_1=\sqrt{1.1} Z_0$ and $Z_2=\sqrt{11} Z_0$. For a 50Ω system, $Z_2 = 165 \Omega$. For an RF circuit board substrate, RO4003, which is 0.818 mm thick, at 1 GHz a 50Ω track is 1.855 mm wide and a 165Ω track is 0.063 mm wide. As shown in chapter 10, the thinnest recommended track width for PBC manufacture is 0.2 mm. Using laser ablation 0.1 mm tracks are possible. The 165Ω track is too thin to make accurately, even using laser ablation. In addition, the resistance due to the copper losses of the 165Ω track is 29 times that of the 50Ω track. The ability to manufacture and copper losses will thus limit the ratio of the power split. Lowering the impedances of the split lines by reducing the impedance at the junction point just like the compensated Wilkinson hybrid, will reduce the impedances of the transmission lines of the hybrid and may permit it to be constructed. Increasing the substrate thickness will also increase the track width and thus reduce losses as well as easing manufacturing difficulties.

Large differences in power ratios are typically required for sampling signals such as transmitter outputs. Edge coupled lines as described in example 4.2 are very suitable for this, so that the limitation on power ratios for Wilkinson hybrids is not a serious limitation.

Wideband Wilkinson Hybrid

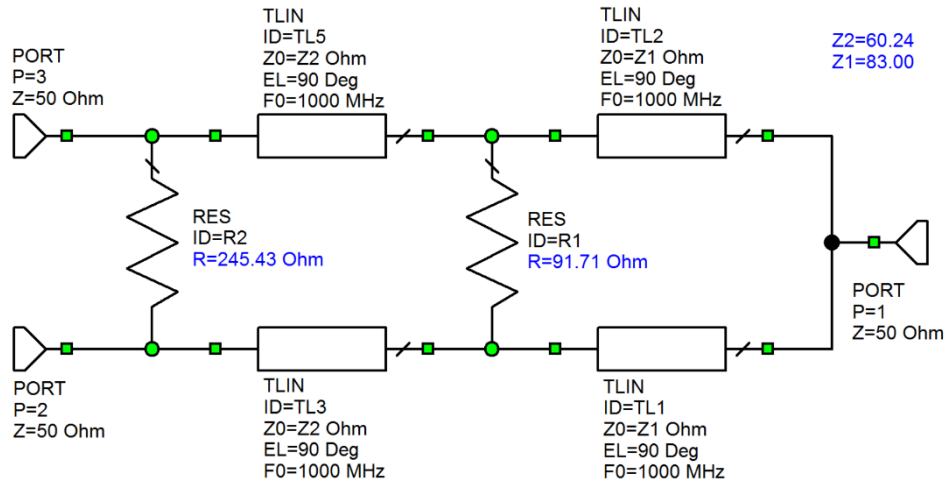


Figure 4.13. Two-stage wideband Wilkinson hybrid.

The bandwidth of the Wilkinson hybrid can be increased by cascading two resistor linked transmission lines as shown in figure 4.13. The characteristic impedances of the lines and the resistor values can be optimised to give the required isolation over the specified bandwidth. There is a compromise between bandwidth and isolation. A wide bandwidth will result in a low isolation and a smaller bandwidth can result in a better isolation. For the hybrid shown in figure 4.13, the isolation was specified as -30 dB.

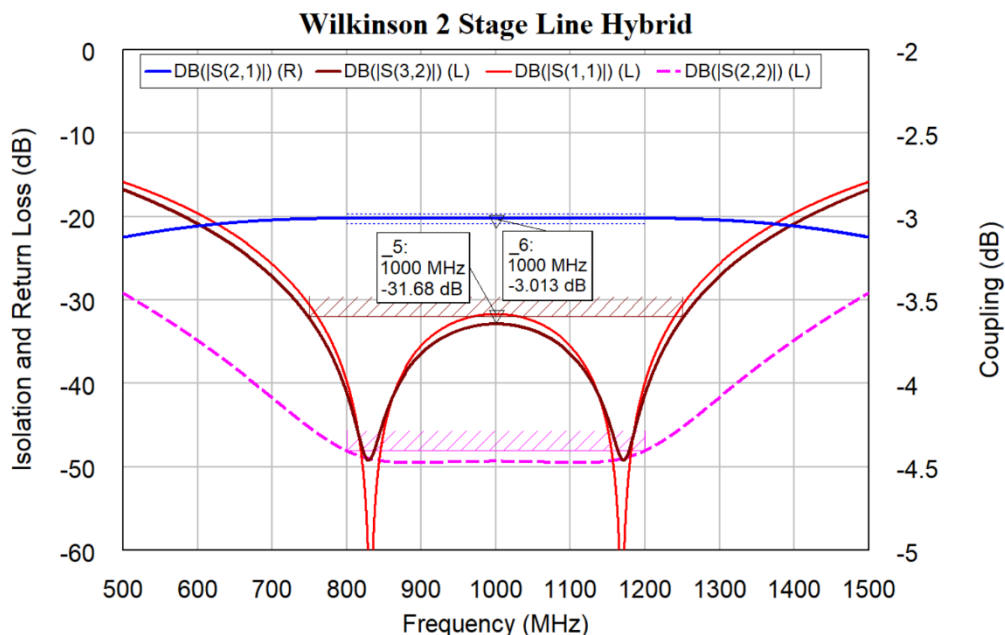


Figure 4.14. Performance of a 2-stage wideband Wilkinson hybrid.

From figure 4.14, it can be seen that a wide bandwidth hybrid results. The impedance for the first section has increased to 83Ω compared with 70.71Ω for the conventional hybrid. The higher impedance will result in an increased insertion loss of the hybrid, due to

thinner PCB tracks being required. A compensated hybrid configuration will reduce the impedance values and thus reduce the insertion loss of the hybrid as well as having a wider bandwidth still.

Example 4.2: 90 MHz to 270 MHz Wilkinson Hybrid

This process can be extended to produce Wilkinson hybrids with good isolation and return loss on all ports over a 2:1 or even 3:1 frequency range. As an example, a Wilkinson hybrid covering the frequency range from 90 MHz to 270 MHz is to be designed. The target specification is a better than 30 dB isolation over the 90 to 270 MHz frequency range and better than 30 dB return loss for all the ports from 95 MHz to 260 MHz.

The design process requires two steps. 1) The circuit is designed and optimised, using ideal transmission lines for the hybrid. 2) Once the specifications are achieved for this ideal circuit, then the ideal transmission lines are replaced with Microstrip lines, with the same electrical line length and impedance.

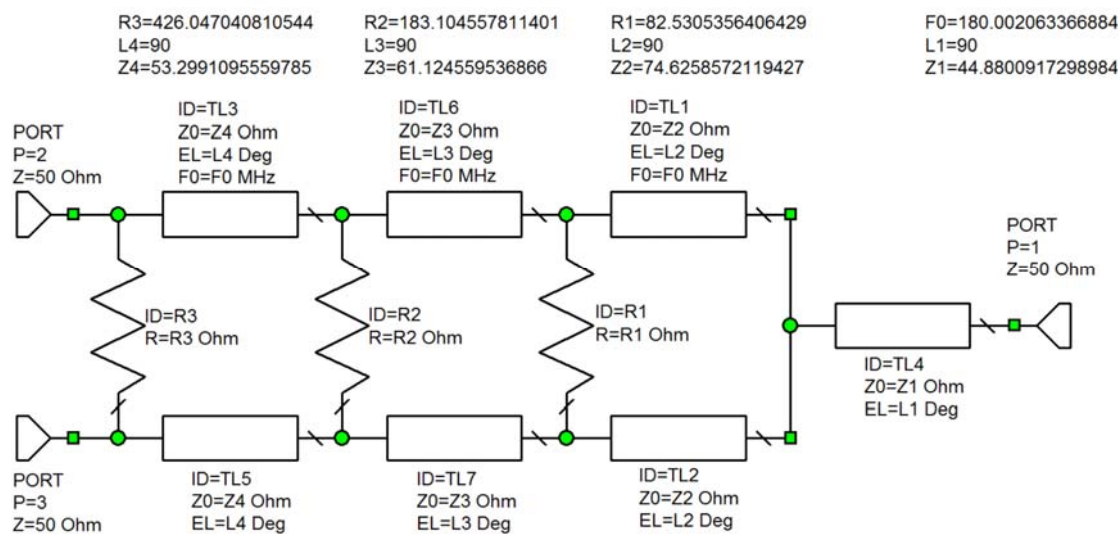


Figure 4.15. Circuit for a 90 MHz to 270 MHz Wilkinson hybrid.

Figure 4.15 shows the schematic for a suitable design. The variables for the centre frequency F_0 , the transmission line impedances Z_1 to Z_4 and the isolation resistors R_1 to R_3 are all enabled for optimisation. The initial values for Z_1 and Z_2 are chosen to be $42\ \Omega$ and $60\ \Omega$ respectively, similar to the values of the compensated Wilkinson hybrid shown in figure 4.11. The initial value for Z_4 is chosen to be $50\ \Omega$ as that should be a close match to the impedance at port 1 and Z_3 is chosen to be $55\ \Omega$, being in between the values of Z_2 and Z_4 . The initial value of R_1 is chosen to be $100\ \Omega$, being the value of the isolating resistor in figure 4.11. R_2 is chosen to be $200\ \Omega$, similar to R_2 in figure 4.13 and R_3 is chosen as $400\ \Omega$. The initial value of F_0 is chosen to be $156\ \text{MHz}$, the geometric mean of $90\ \text{MHz}$ and $270\ \text{MHz}$. The optimisation goals are set up to match the specifications. To achieve a better return loss and isolation, the goals are for $S_{11} < -32\ \text{dB}$, $S_{22} < -32\ \text{dB}$ and $S_{32} < -33\ \text{dB}$. Setting the circuit to optimise using the Simplex optimiser then yields the circuit values shown in figure 4.15. This circuit achieves the specifications as shown in figure 4.16. Notice that no optimisation goals are set for the through coupling, S_{21} , since if the circuit is matched then the coupling loss will be as small as possible.

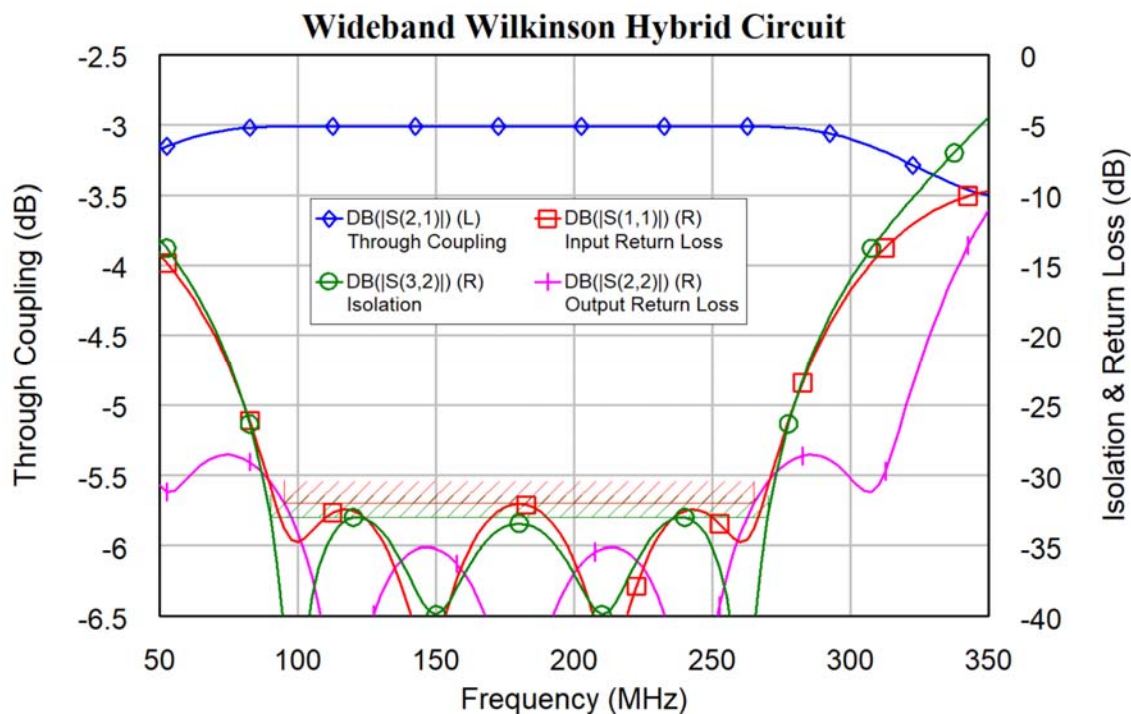


Figure 4.16. Simulated performance of the hybrid of figure 4.15.

Figure 4.15 can now be used as the basis for a PCB layout. Often it is necessary to bend the Microstrip lines to fit the circuit in the available space, as shown in figure 4.16. Each of the transmission lines are a quarter wavelength long. If in figure 4.15 lines TL2 and TL5 are disabled, resistors R1 and R3 are disabled and resistor R2 is made a short circuit ($0\ \Omega$), then the circuit becomes a transmission line of various impedances connecting port 1 to port 2 with an open circuited quarter wavelength stub consisting of TL7 connected to it. This line will thus present itself as a short circuit at R2 at the centre frequency. A similar circuit is shown on the right of figure 4.29. The transfer function from ports 1 to 2 will thus have a notch exactly at the centre frequency of the hybrid, where TL7 is a quarter wavelength. The length of the folded sections making up TL7 in figure 4.15, can be adjusted to be exactly a quarter wavelength by changing the lengths of the sections to ensure that the notch in the transfer function from ports 1 to 2 occurs exactly at the centre frequency of the hybrid. This process is repeated for the other three different transmission lines in the hybrid. Variables are used to ensure that the folded transmission lines corresponding to the sets of lines TL1 and TL2, lines TL3 and TL5 and lines TL6 and TL7 are exactly the same length and impedances.

Finally, the line lengths and widths are optimised to provide the final layout and meet the required specifications. Figure 4.17 shows the hardware for this layout and figure 4.18 shows the simulated frequency response for the hybrid. The details of the PCB layout are included in the NI AWR DE project file for figures 4.17 and 4.18. The measured performance is shown in figure 4.19. This agrees closely with the calculated values. The hardware has an isolation that is better than 26.9 dB over the entire 90 to 270 MHz frequency range and the return loss is better than 22.0 dB. Figures 4.8 and 4.9 show that just a 50 μm change in track width results in significant changes in the return loss. Manufacturing tolerances on the dielectric constant of the laminate and track width imperfections as part of the PCB milling process resulted in the return loss and isolation not being as good as simulated. The insertion loss of the coupled path is also 0.24 dB more than obtained by the simulation. Part of this loss could be due to the thin protective

coating used to prevent the copper tracks from oxidising. This hybrid has a very satisfactory performance over a 3:1 frequency range and could not have been realised without the computer simulation and optimisation described in this book.

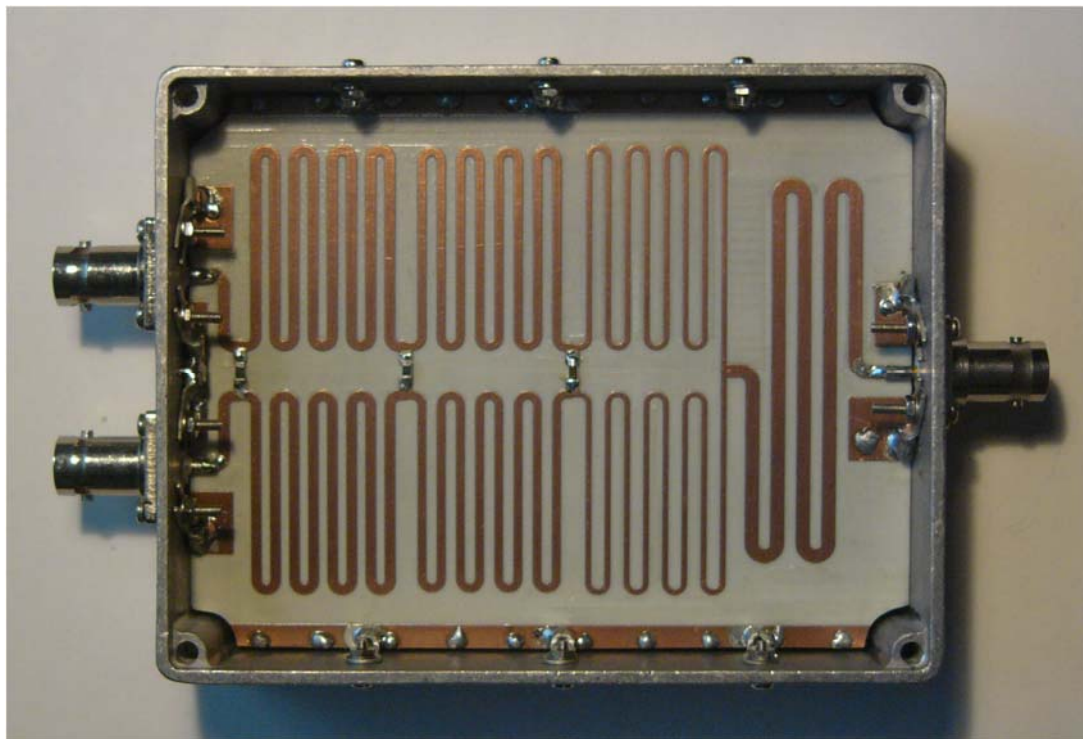


Figure 4.17. Hardware for 90 MHz to 270 MHz Wilkinson Transmission-line hybrid.

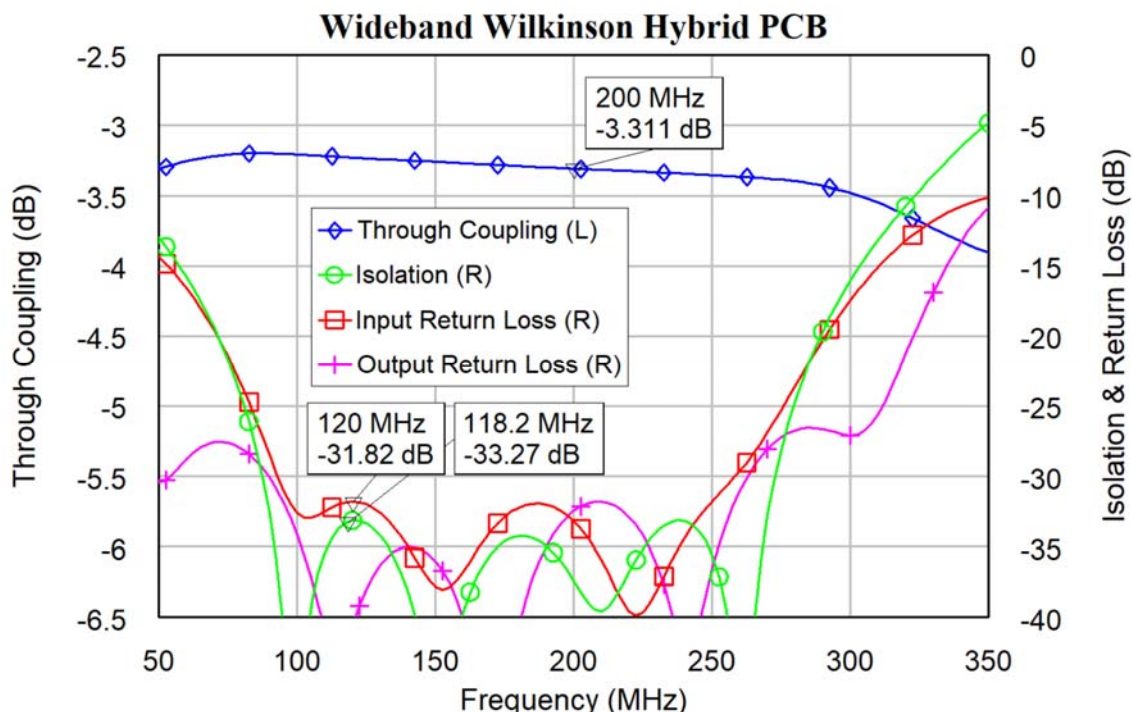


Figure 4.18. Simulated performance of the hybrid of figure 4.17.

The losses in the circuit due to the resistance of the tracks, dielectric losses of the substrate and radiation losses of the Microstrip lines, vary with frequency, as can be seen in figures 4.18 and 4.19. Since the difference is only 0.25 dB over a 3:1 frequency range, this is

often ignored in practice. Due to this frequency dependence of the losses, it is better to optimise for input reflection coefficient rather than transfer function since a low input reflection coefficient ensures all the energy passes through the hybrid, thus giving the highest S_{21} possible. Optimising for a value of S_{21} may result in a poor return loss at lower frequencies.

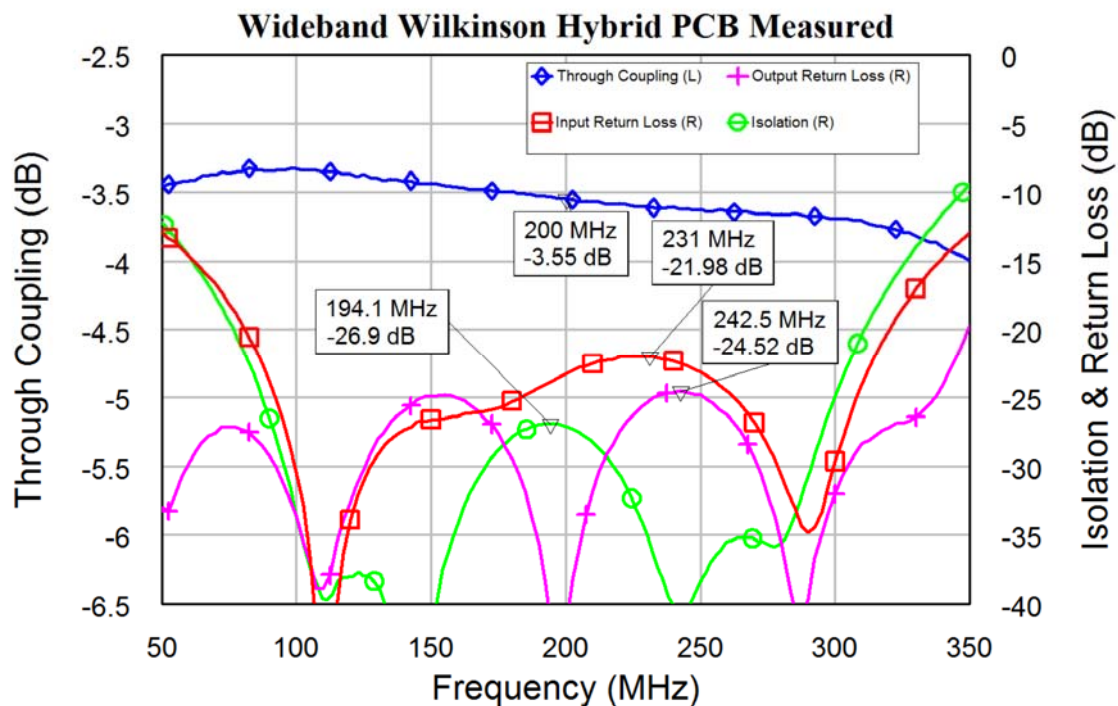


Figure 4.19. Measured performance of the hybrid of figure 4.17.

Quarter Wave Hybrid or 1.5λ Rat-Race Hybrid

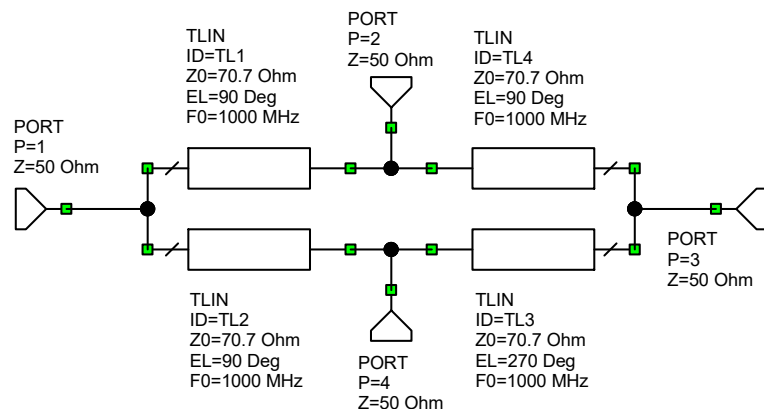


Figure 4.20. 1.5λ Rat-Race hybrid.

The circuit diagram of this hybrid is shown in figure 4.20 and its performance is shown in figure 4.21. For the analysis, consider the function of the hybrid. If an input is applied to port 1, then no signal should appear at port 3, resulting at 0 Volt at port 3. Under these conditions, the circuit is similar the Wilkinson hybrid of figures 4.5 and 4.6, and no current flows into TL3 of figure 4.20 at port 2 and into TL4 at port 4. The transmission

line TL3 can thus be disconnected at port 4 and line TL4 can be disconnected at port 2, without any effect, as shown in figure 4.22.

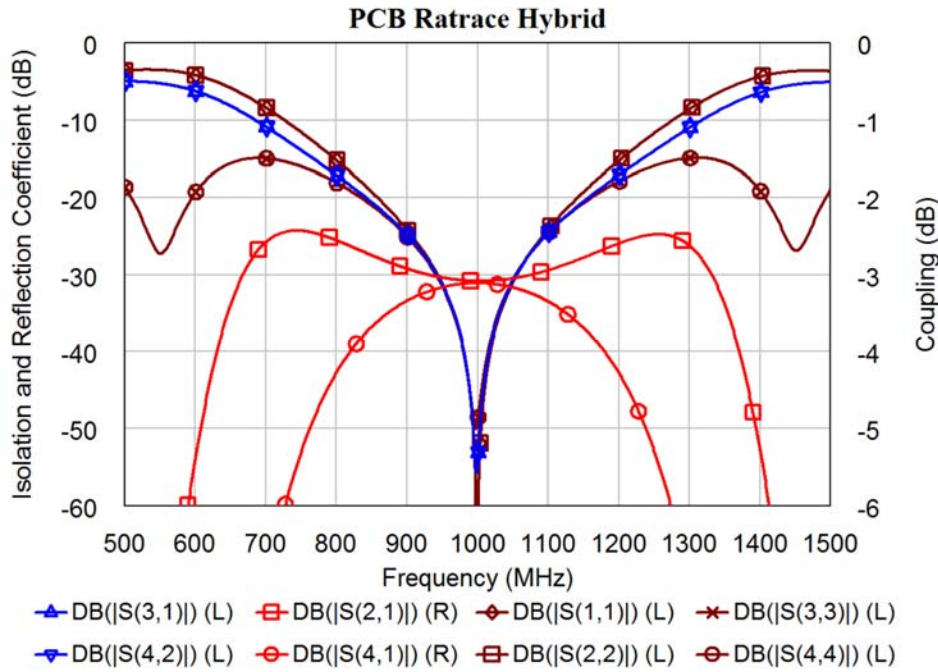


Figure 4.21. Performance of 1.5λ Rat-Race hybrid.

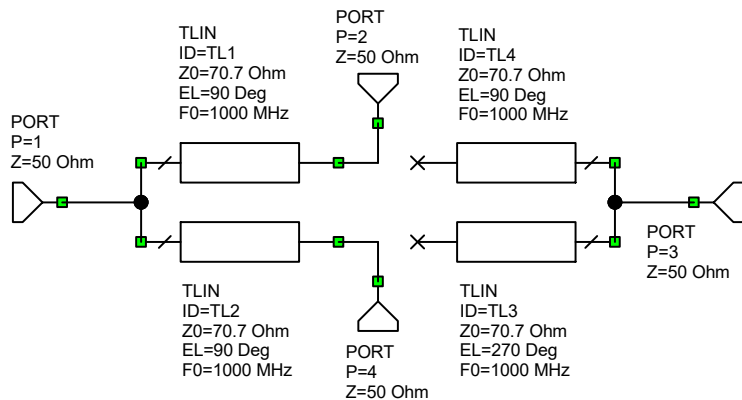


Figure 4.22. 1.5λ Rat-Race hybrid for analysis.

The resulting circuit is thus just like a Wilkinson hybrid, without the terminating resistor. The line impedances should thus be 70.71Ω , just like the Wilkinson hybrid. The same analysis can be repeated by looking into each port in turn. A three-quarter wavelength transmission line has exactly the same impedance transformation ratio as a quarter-wavelength line. All the line impedances will thus be $\sqrt{2}Z_0$.

The 1.5λ Rat-Race hybrid is commonly used in high power transmitters, and has an advantage over the Wilkinson hybrid that for a 50Ω system, a 50Ω load resistor to ground is required for the termination, rather than a 100Ω load resistor between two active inputs. High power 50Ω loads are readily available from several manufacturers. 100Ω floating loads are however more difficult to obtain.

For the 1.5λ Rat-Race hybrid, a three-quarter wavelength and three one-quarter wavelength transmission lines are required. At microwave frequencies, it is very convenient to arrange these transmission lines in the shape of a circle, as shown in figure 4.23, with the three quarter wavelength line on top and the three quarter wavelength lines at the bottom. One-quarter wavelength will thus occupy a 60-degree arc. The layout can then be made conveniently using six 60-degree arcs, 4 T-junctions and 2 short transmission lines with the same length as the T-junctions are wide, as spacers.

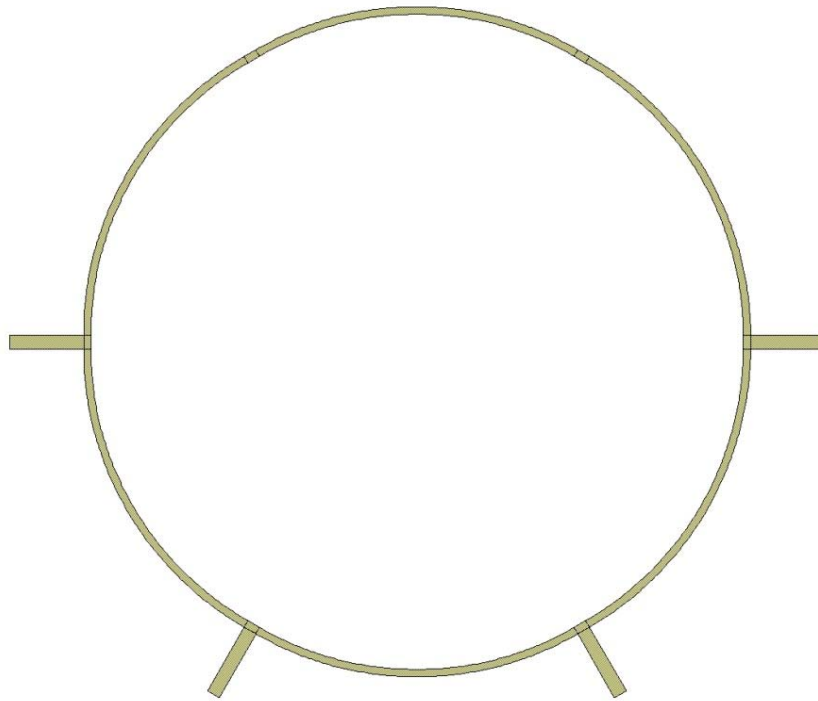


Figure 4.23. PCB layout of a 1.5λ Rat-race hybrid.

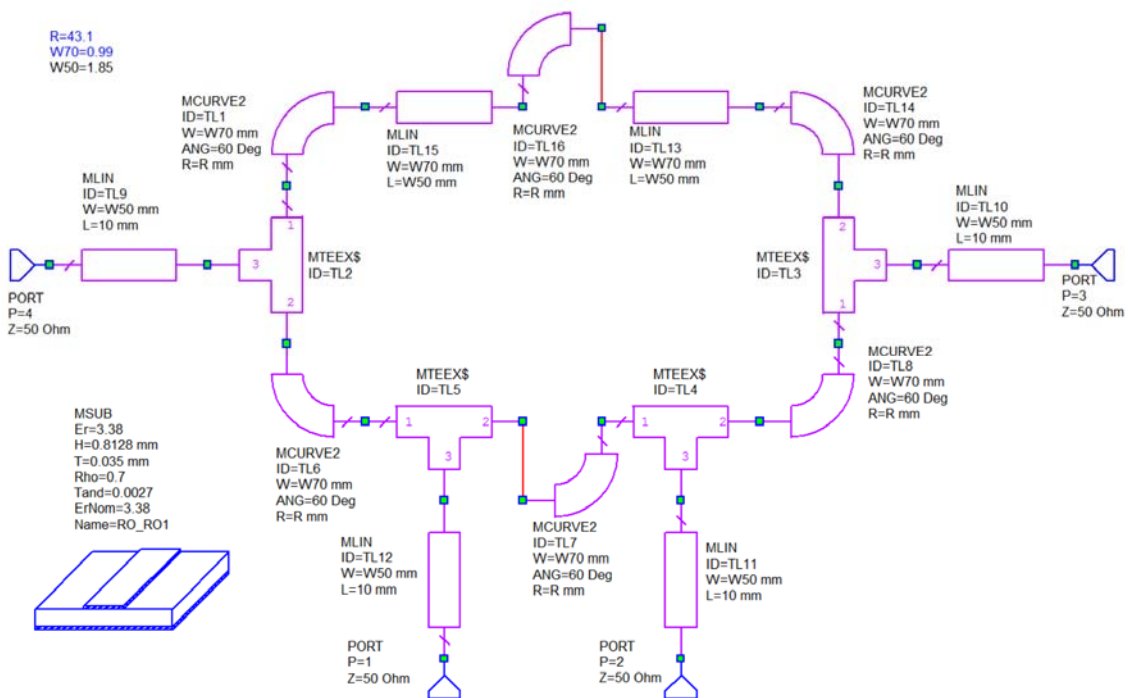


Figure 4.24. 1.5λ Rat-Race hybrid circuit for PCB layout.

Figure 4.24 shows the circuit schematic, which results in the PCB layout of figure 4.23. The radii of the arcs can be tuned, to obtain the correct centre frequency, without causing any track connection errors. In figure 4.24, MCURVE2 tracks are used to include EM mode matching in the simulation. Intelligent EM based T-junctions, MTEEX\$, are used to ensure that the simulation is as accurate as possible, without doing a full EM simulation using AXIEM.

The simulation of the PCB circuit of figures 4.23 and 4.24 shows a near identical performance to the one shown in figure 4.21. The main difference is a 0.07 dB increase in insertion loss of the coupled ports due to the resistive losses in the Microstrip tracks.

Lower line impedances can be obtained with a compensated 1.5λ Rat-race hybrid, by having 44.5Ω , quarter wavelength transmission lines at the 4 inputs to the hybrid, for a 50Ω system. The line impedances of the hybrid then become 56.119Ω instead of 70.71Ω . Computer simulation shows that this does not increase the bandwidth of the isolation and it does not reduce the losses for a typical PCB layout, so that compensated 1.5λ Rat-race hybrids are not used in practice.

Branchline Coupler

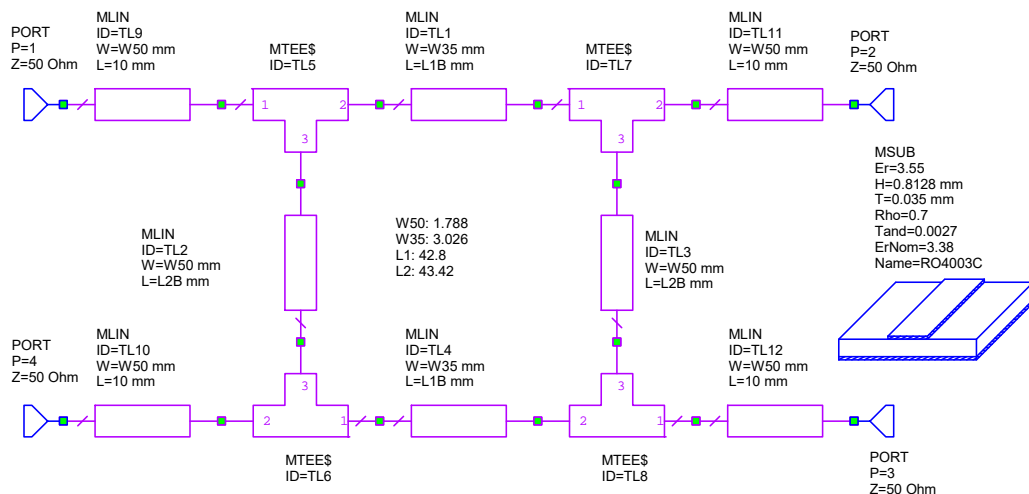


Figure 4.25. Branchline coupler circuit.

The Branchline coupler consists of 4 transmission lines in a ring, as shown in figures 4.25 and 4.26. If an input is applied at the top left port 1, then part of the output appears the coupled port, the bottom right port 3. The remainder appears at the main output port 2 and no power appears at the isolated port 4. For a 3 dB coupler in a 50Ω system, lines TL1 and TL4 have an impedance of $50/\sqrt{2}\Omega$ and lines TL2 and TL3 have an impedance of 50Ω . A Microstrip PCB layout is shown in figure 4.26. The resistive losses of a Branchlike coupler are less than that of a 1.5λ Rat-race hybrid.

For the analysis, consider figures 4.25 and 4.27. When an input is applied at port 1, port 4 is isolated and has no voltage at that port. Since lines TL3 and TL4 are quarter wavelength long, no current flows in line TL4 at port 3, so that TL4 can be disconnected from the circuit without any effect. Similarly, no current flows in TL3 at port 1, so that TL3 can also be disconnected, resulting in figure 4.27.

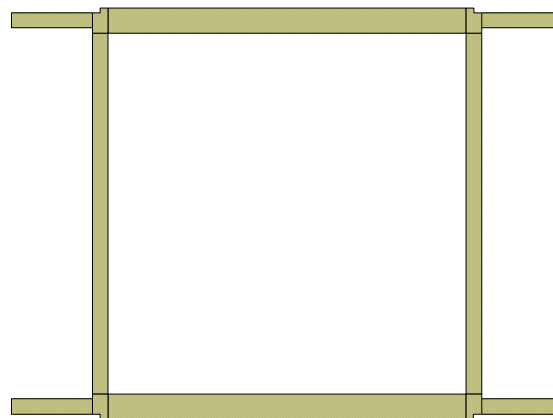


Figure 4.26. Branchline coupler PCB layout.

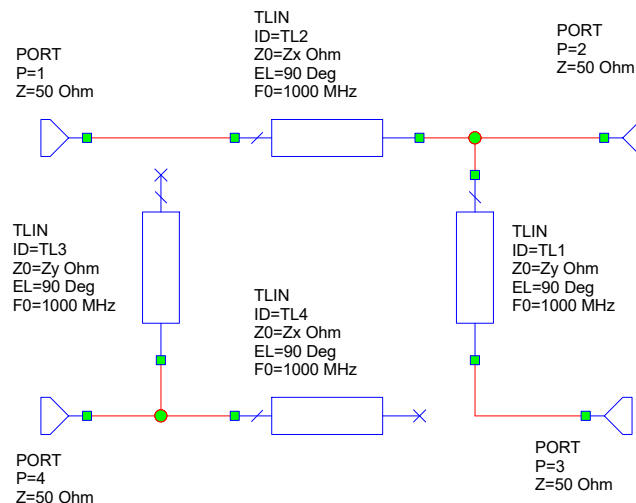


Figure 4.27. Branchline Coupler analysis.

If a normalised input power of \mathbf{I} is applied at port 1 and we want an output power of \mathbf{P} to occur at port 3, then a power of $(\mathbf{I}-\mathbf{P})$ will be available at port 2.

At port 2, the load impedance is Z_0 , which typically is 50Ω . If the voltage at port 2 is V_2 , then the power split at port 2 is given by:

$$V_2^2 = PZ_p = (1 - P)Z_0 \quad \text{so that:} \quad Z_p = \frac{(1 - P)Z_0}{P} \quad \text{Eqn. 4.13}$$

Where Z_p is the impedance of port 3 transformed through TL1 and seen at port 2 looking into TL1. Since this is obtained by impedance transformation through the quarter wave long transmission line TL1, the impedance required for TL1 is given by:

$$Z_y = \sqrt{Z_p Z_0} = Z_0 \sqrt{\frac{(1 - P)}{P}} \quad \text{Eqn. 4.14}$$

The impedance Z_2 seen at the end of TL2 is Z_0 in parallel with Z_p and is thus:

$$\frac{1}{Z_2} = \frac{1}{Z_p} + \frac{1}{Z_0} = \frac{P}{(1 - P)Z_0} + \frac{1}{Z_0} = \frac{1}{(1 - P)Z_0} \quad \text{Eqn. 4.15}$$

The line impedance Z_x to transform this to Z_0 is thus:

$$Z_x = Z_0 \sqrt{1 - P} \quad \text{Eqn. 4.16}$$

In many cases an equal power split is required, so that $P=0.5$. Typically $Z_0 = 50 \Omega$. Substituting this in equations 14 and 16 results in $Z_Y = Z_0 = 50 \Omega$ and $Z_X = 0.707*Z_0 = 35.36 \Omega$. For a 10 dB coupler $P = 0.1$, so that $Z_Y = 3Z_0 = 150 \Omega$ and $Z_X = 0.949*Z_0 = 47.43 \Omega$. These can just be made using Microstrip circuits, however any lower amount of coupling is extremely difficult to make.

Figure 4.28 shows the performance of the Branchline coupler. This coupler is a convenient structure with low impedance values (50Ω and 35.36Ω) thus allowing low loss hybrids to be made using Microstrip-line circuits.

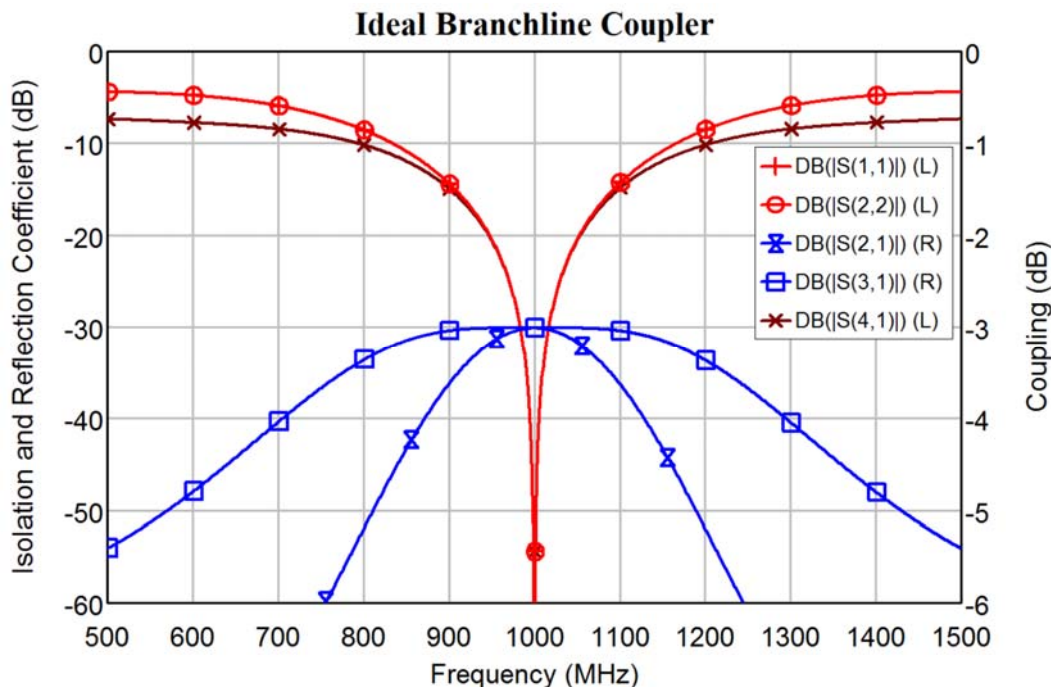


Figure 4.28. Ideal Branchline coupler performance.

To realise the design as a printed circuit board, the required track widths and lengths need to be calculated. The Roger's RO4003 substrate [5] that was used for the circuits in figures 4.8 and 4.9 is also used in this example. The parameters can be obtained by using the *Libraries* \Rightarrow *AWR Web Site \Rightarrow Rogers \Rightarrow RO \Rightarrow RO4003 and select 32 mil, 1 oz. and place that as a component in a circuit. Remember to set $\epsilon_r = 3.55$ and $\epsilon_r^{\text{Nom}} = 3.38$ to match ϵ_r with the substrate data sheet [5] as described earlier.

To determine the length and width required, TX line from the Tools menu in NI AWR DE can be used or measurements on some simple test circuits can be made. Figure 4.24 shows the resulting test circuit. W50, the width of a 50Ω track and W35, the width of a 35.36Ω track are made as variables, so that those values can be used in the rest of the design. The line between port 1 and 2 is very long. W50 is determined by observing S_{11} and tuning S50 to be less than -60 dB over the required frequency band. Similarly, W35 is obtained by tuning it and minimising S_{33} . To determine the length of the quarter wavelength long lines, the circuit between ports 5 and 6 is used. The circuit uses a 50Ω line between ports 5 and 6 and a 35.36Ω line as a stub. Thus, TL4 and TL6 in figure 4.29 correspond to TL1 and TL2 in figure 4.27 respectively. (For a 3 dB coupler $Z_Y=50 \Omega$ and $Z_X=35.36 \Omega$). To

obtain accurate results, elements incorporating EM models, such as MTEEX and MLEFX are used in this circuit. The MLEFX element, with the length of half a $50\ \Omega$ track-width is used to place the end of the quarter wavelength stub on the middle of the $50\ \Omega$ track that is to join as shown in figure 4.29, to produce the complete coupler shown in figures 4.31 and 4.32. The length of the stub (L_2) is tuned to place the notch at 1 GHz. A similar circuit is made to determine the required length of the $50\ \Omega$ quarter-wavelength lines.

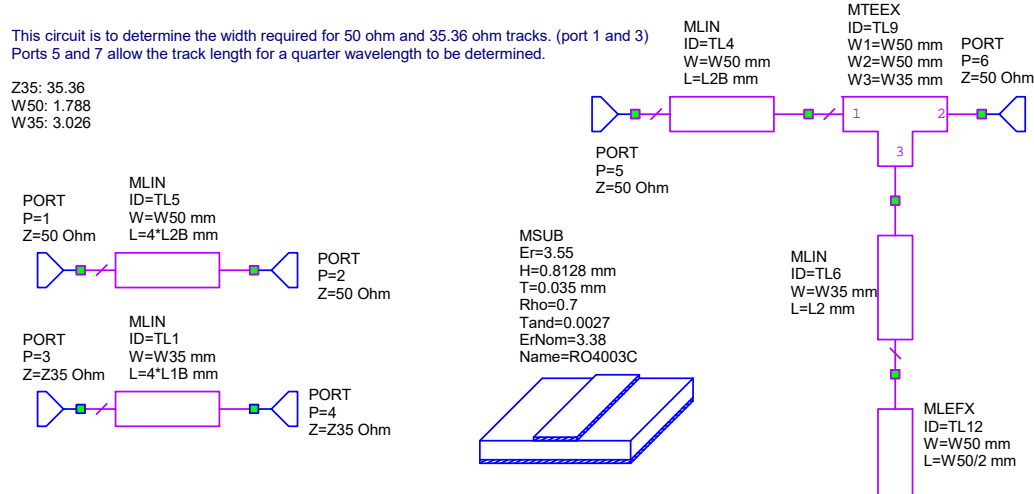


Figure 4.29. Microstrip test circuits for determining length and width of lines.

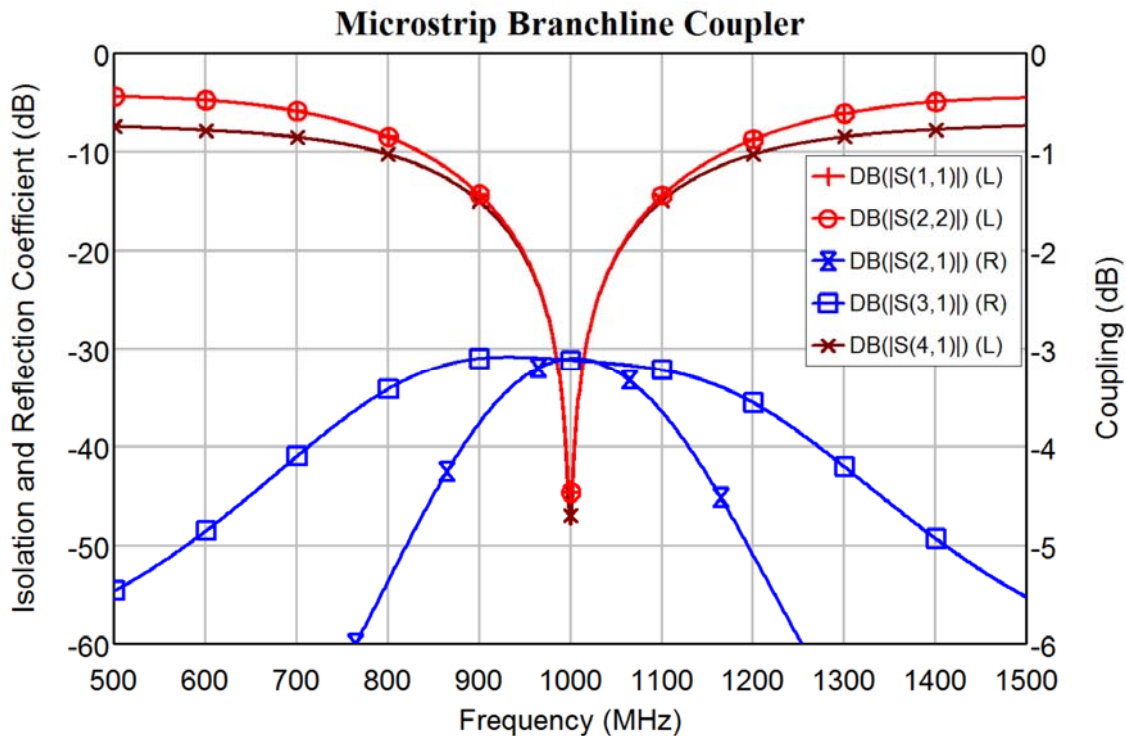


Figure 4.30. Microstrip Branchline coupler performance.

When the line lengths obtained from figure 4.29 are used in the circuit of figure 4.25, the centre frequency is slightly offset. Fine-tuning is achieved by using the line lengths $L_{1B} = L_1 * K$ and $L_{2B} = L_2 * K$ in figure 4.31, where K is a constant used to fine-tune the both

lengths at the same time. $K=1.004$ places the isolation notch exactly at 1 GHz as shown in figure 4.30. The design procedure will thus result in a design that requires an adjustment of less than 0.4%. Comparing figure 4.28 and 4.30, the frequency dependent losses of the Microstrip lines, resulting in the slight skewing of the coupling output can clearly be seen. This also causes the isolation to be slightly worse.

In many cases, the transmission lines are folded in order to reduce the printed circuit board area, as shown in figures 4.31 and 4.32. Like figure 4.8, a M2CLIN coupled line is used, to include the EM coupling between the folded lines. The length of the coupled lines is tuned to place the centre frequency at 1 GHz.

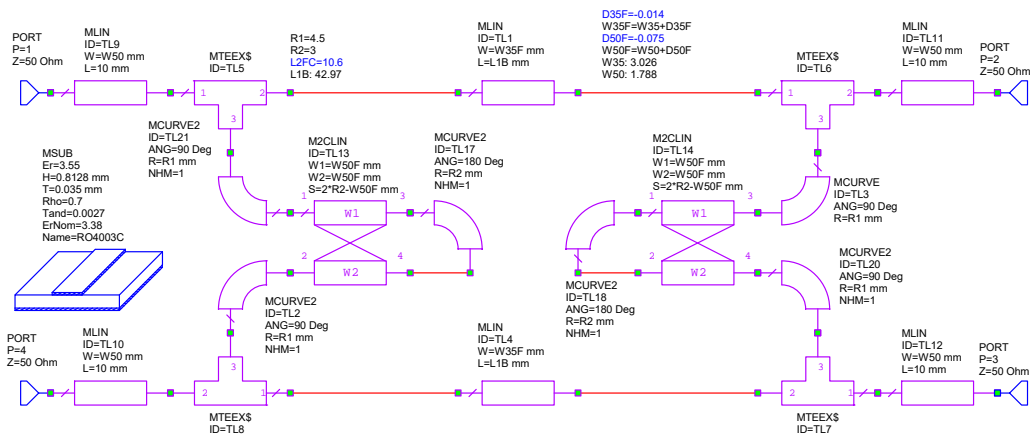


Figure 4.31. Folded Microstrip Branchline coupler schematic.

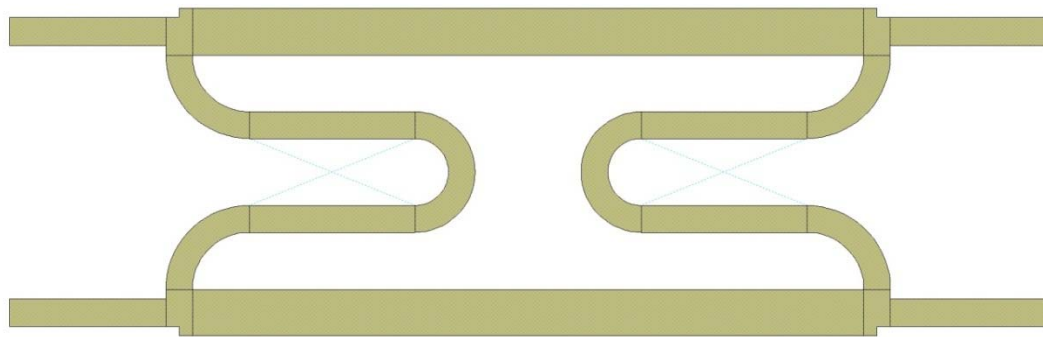


Figure 4.32. Folded Microstrip Branchline coupler PCB layout.

The power split between port 2 and port 3, is determined by the impedance of this folded line. Ideally, it should be a 50Ω transmission-line. For an input at port 1, an equal power split at TL6 results in a slightly smaller output at port 3, due to resistive losses in TL3, TL14, TL18, TL20 and TL7. A slight fine-tuning is included by making the line-width of $W_{50F} = W_{50} + D_{50F}$, where D_{50F} is a small correction factor. D_{50F} is then tuned to change the power split to allow for these losses and make the outputs at ports 2 and 3 identical at the centre frequency.

This changes power split causes a change in the impedance seen at terminal 1 of TL6 and will require a slight change in the impedance transformation produced by TL1 and TL4, to present a 50Ω impedance (S_{11}) at port 1. This is achieved by making $W_{35F} = W_{35} +$

D35F, where D35F is a small correction factor. D35F is tuned to make S_{11} as small as possible at the centre frequency.

Figure 4.33 shows the frequency response of the resulting folded Branchline coupler. There is virtually no difference between figure 4.30 and 4.33. However, the circuit with the bent lines occupies a much smaller area. Constructing the hybrid of figure 4.32 results in a measured performance, that is very close to the calculated performance shown in figure 4.33.

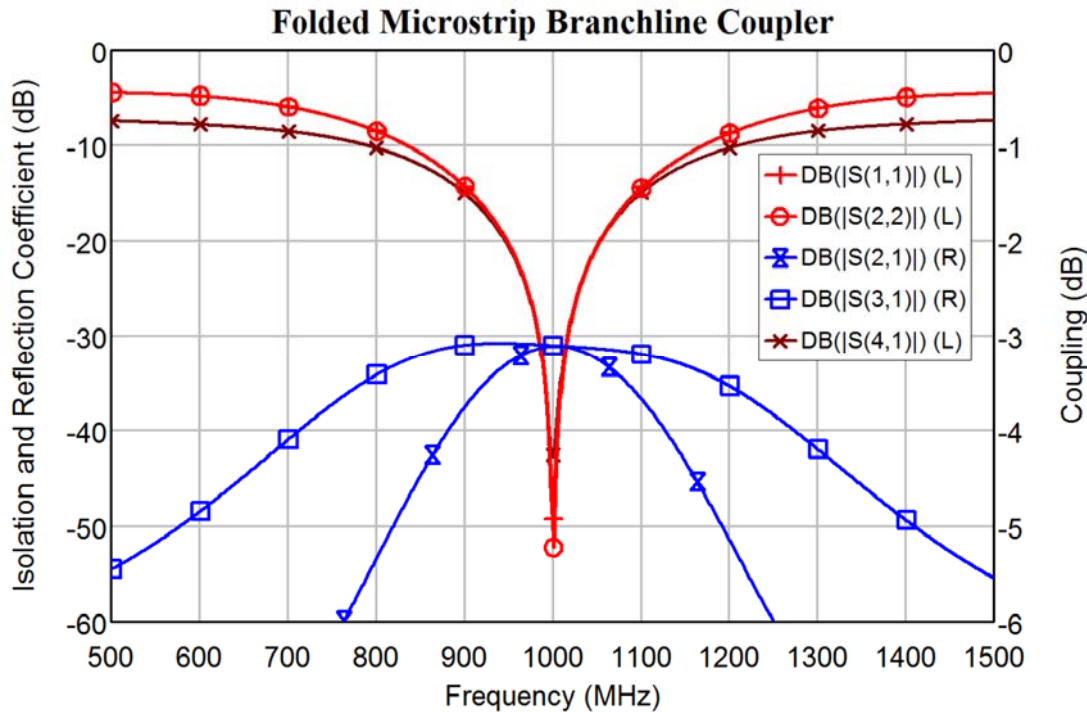


Figure 4.33. Folded Microstrip Branchline coupler performance.

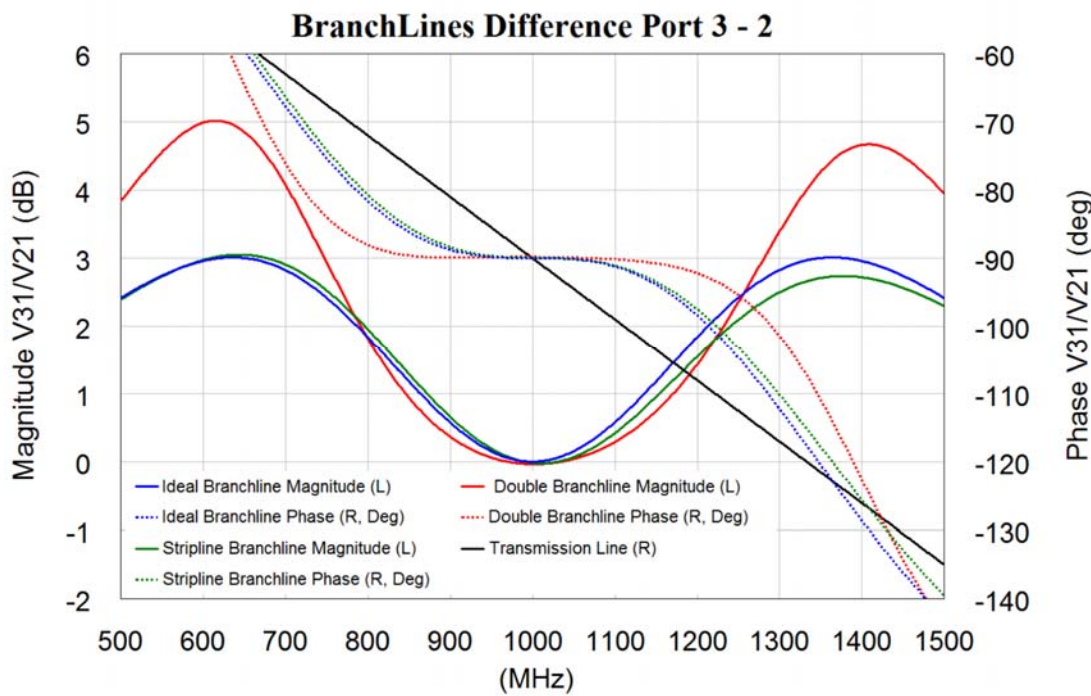


Figure 4.34. Branchline coupler phase difference between coupler ports (2-3).

The output at the coupled port has a 90° phase shift compared with the output at the direct port and that is useful for many applications. Figure 4.34 shows the phase difference of signals at port 2 and 3 due to an input at port 1 for the different Branchline couplers and compares this with the phase shift in a simple transmission line. It can be seen that from 900 MHz to 1100 MHz, the ideal Branchline coupler has less than $\pm 1.3^\circ$ variation in phase, the Double Branchline coupler has less than $\pm 0.2^\circ$ variation in phase and there is $\pm 9^\circ$ variation in phase for a single transmission line. Over that bandwidth, the magnitude varies by less than 0.58 dB for the ideal Branchline coupler and less than 0.37 dB for the Double Branchline coupler. Branchline couplers can thus be used to provide the I and Q signals, required for image suppressing mixers, with good phase and amplitude accuracy over a 20% bandwidth.

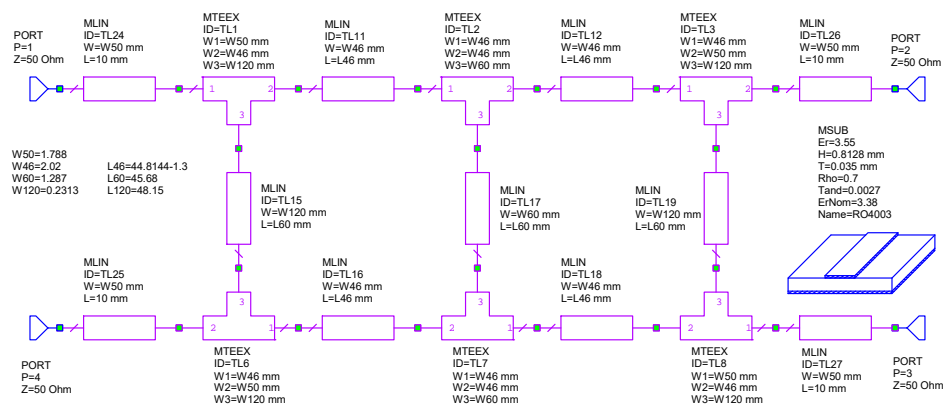


Figure 4.35. Wideband Branchline coupler schematic and PCB layout.

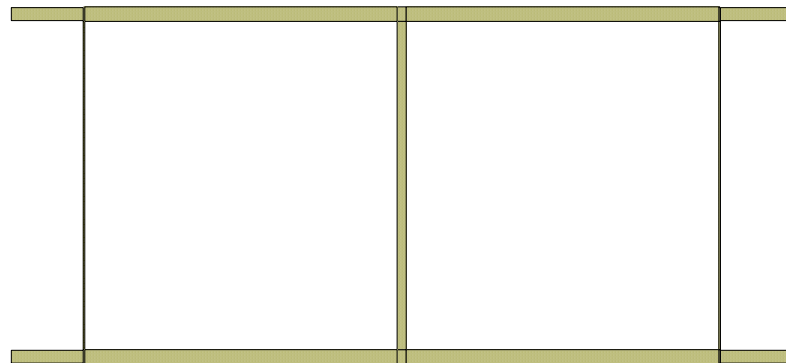


Figure 4.36. Wideband Quadrature hybrid Schematic and the corresponding PCB layout.

It is possible to produce a wider bandwidth Branchline coupler, by having two loops together as shown in figure 4.35. For a 3 dB coupler the characteristic impedances of the lines can be shown to be 120.7Ω for the outer vertical lines, 60.35Ω for the centre line and 46.2Ω , for the horizontal lines. Figure 4.36 shows the corresponding PCB layout of the circuit. Using TXLine, for a RO4003 RF PCB substrate with $\epsilon_r=3.55$, and a 0.818 mm thickness at 1 GHz, the 120.7Ω transmission lines require $231.3 \mu\text{m}$ wide tracks, which is close to the smallest track width that can be realised. These track-widths are thus very difficult to achieve in practice. In addition, the track width are so small that warnings are generated for the MTEEX sections connecting to them, as $W3/W2$ being too small for

the model. The quarter wavelength long track for the 60.35Ω impedance is 45.68 mm long, while the corresponding length for the 120.7Ω track is 48.15 mm long. For straight lines, all three vertical lines should be the same length, so that a compromise is required.

It is possible to increase the bandwidth further by using three loops for the coupler. The outer track impedances are then 175Ω . For this RO4003 substrate, this corresponds to a 0.04 mm wide track, which is not possible to realise. Doubling the substrate thickness doubles the track width for the same impedance. Using thicker substrates may make some of these configurations realisable.

Figure 4.31 shows a comparison of the single, double and triple loop Branchline coupler. The green curves are the single line coupler, the blue curves are the double line coupler and the red curves are the triple line coupler. The most significant difference is the isolation (between port 1 and 4). The bandwidth over which a good isolation is obtained is increased significantly by using multiple loops.

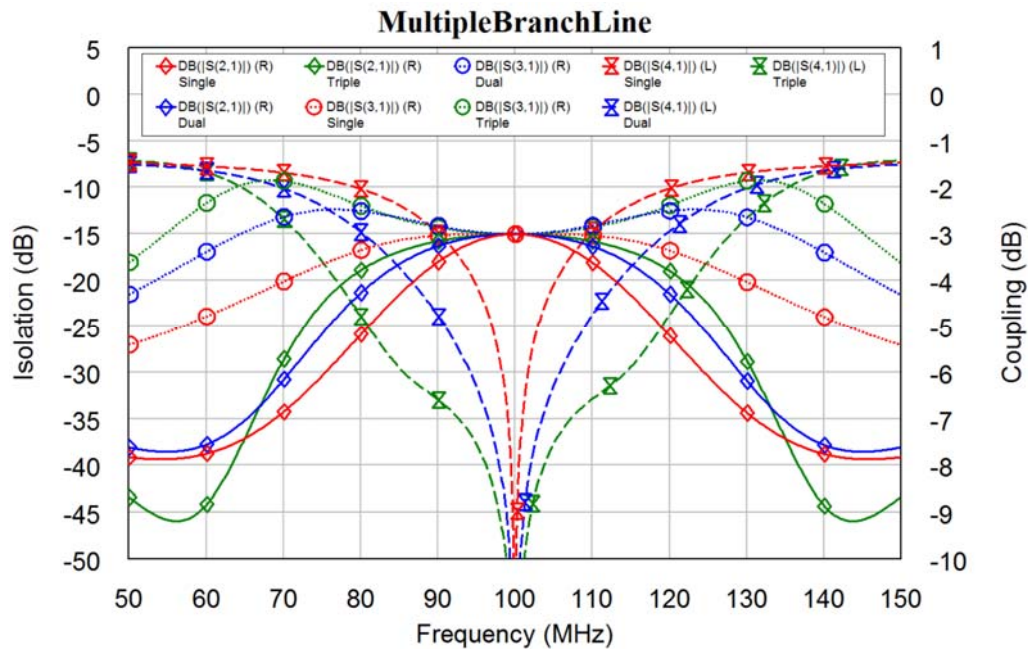


Figure 4.37. Multi-loop Quadrature hybrid performance.

Backward Travelling Wave Hybrid

If two lines are in close proximity, then there is coupling between the lines. The amount of coupling depends on the spacing between the lines. Consider the two Microstrip coupled lines as shown in figures 4.39 and 4.40. The maximum coupling will occur when the coupled lines are a quarter wavelength long. The resulting coupling is related to the even and odd mode impedances by:

$$Z_{OE} = Z_0 \sqrt{\frac{1+C}{1-C}} \quad \text{Even mode impedance.} \quad \text{Eqn. 4.17}$$

$$Z_{OO} = Z_0 \sqrt{\frac{1-C}{1+C}} \quad \text{Odd mode impedance.} \quad \text{Eqn. 4.18}$$

Where C is the voltage at the coupled output relative to the input, Z_{OO} is the odd mode impedance, where the two lines of the transmission line are of opposite polarity, so that

most of the field is between the conductors. Z_{OE} is the even mode impedance, where both the lines are at the same potential, so that most of the field is between the conductors and the ground-plane.

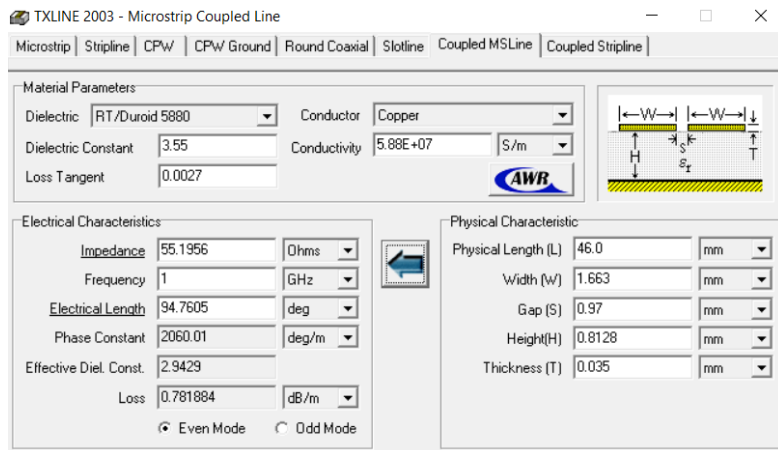


Figure 4.38. Calculated geometry for a $\lambda/4$ 20 dB coupler.

Edge-Coupled Lines

Edge-coupled lines correspond to the geometry shown in the top right hand side of figure 4.38. The coupled lines are made using conventional Microstrip lines using double sided PCB with the bottom side a ground-plane. This is easy to manufacture, but places restrictions on the amount of coupling that can be obtained. Typically, the spacing between the lines is very small and this spacing must be accurately controlled along the entire line length to obtain the correct amount of coupling. Edge coupled lines are very suitable for sampling the forward and reverse power from transmitters and for filters. The design process of a backward-coupled hybrid using edge-coupled lines is illustrated as follows:

Example 4.3: 20 dB Coupler

A 20 dB coupler at 900 MHz is required. The coupled output is thus 20 dB below the input. The coupled voltage is one tenth of the input voltage, i.e. $C = 0.1$. From the above equations one obtains $Z_{OO} = 45.23 \Omega$ and $Z_{OE} = 55.28 \Omega$. The required physical spacing can now be determined iteratively using the TXLine program. The results from the TXLine calculations are shown in figure 4.38. Note that for the same line length, the electrical length is different for the even and odd mode, since the propagation velocity of these modes is different. The length chosen is such that the average is correct, but it is likely that the length needs to be fine-tuned to obtain the desired performance.

These calculated values are substituted in the coupled-line circuit diagram shown in figure 4.39. Figure 4.40 shows the corresponding PCB layout including 50Ω lines needed to connect the input and output ports to the coupler. Figure 4.41 shows the simulated performance. The coupling is 20 dB as expected. Note that the coupled port is in a different location compared with the Branchline coupler.

The coupler was designed for a centre frequency of 1 GHz. Coupled lines have a null in coupling at multiples of a half wavelength length. This was used to tune the length of the coupled line to give a null at 2 GHz, thereby giving maximum coupling at the required 1 GHz. Note that the bandwidth of the coupling and the isolation is very wide compared

with the other hybrids described before in these notes. At 1 GHz, the isolation (S_{31}) is only 5 dB less than the coupled output (S_{41}), so that further design changes are required to improve its performance.

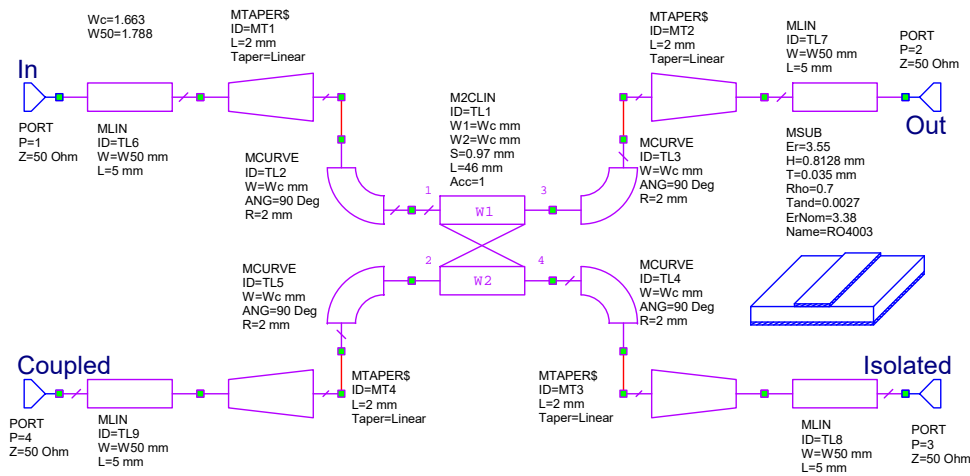


Figure 4.39. $\lambda/4$ 20 dB coupler schematic and corresponding Microstrip layout.

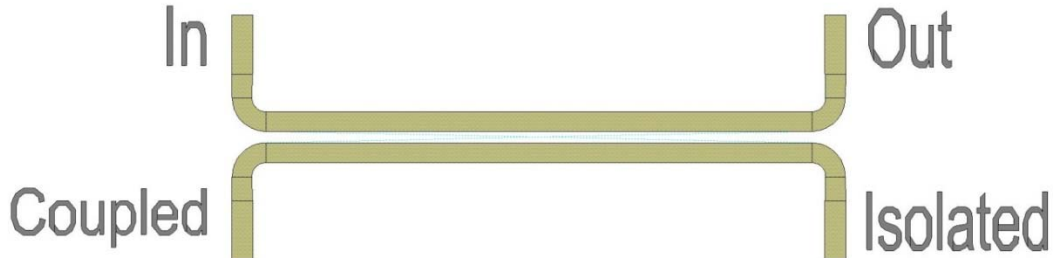


Figure 4.40. $\lambda/4$ 20 dB coupler schematic and corresponding Microstrip layout.

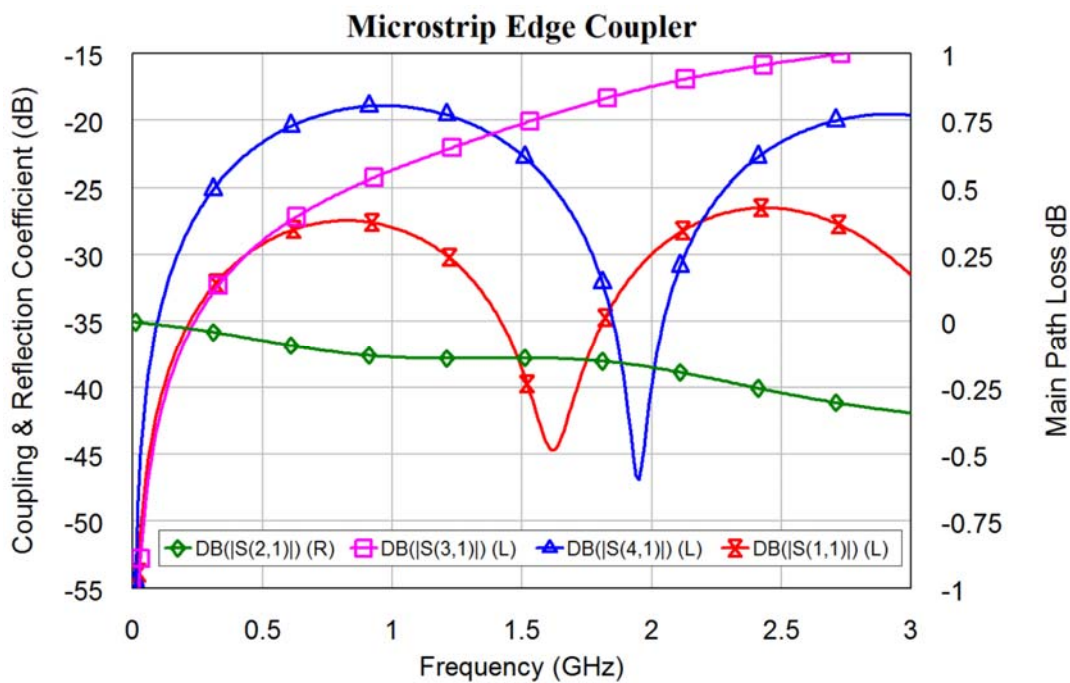


Figure 4.41. $\lambda/4$ Microstrip 20 dB coupler performance.

Alternately, the coupling can be obtained directly from figure 4.41. The same coupler can be designed, without using the TXLine program. The first step involves changing the length of the coupled lines, such that a coupling null is obtained at twice the frequency for maximum coupling, (2 GHz for figure 4.39). The spacing of the coupled lines is then changed to obtain the correct coupling factor and finally the width of coupled line with is changed to obtain a low return loss (S_{11}). Since there is an interaction between these values, these steps should be repeated until no further changes occur. These values can also be determined using the optimisation routines included in MWO.

Note that in figure 4.41, the difference between the coupled port S_{41} and the isolated port S_{31} is less than 10 dB at the centre frequency of 1 GHz. By including some very small, sub-pF, capacitors across the terminals 1 and 4 and terminals 2 and 3 the phase velocity is more equalised over a wide frequency range and a lower input return loss (S_{11}) and flatter isolation (S_{31}) is obtained. These capacitors can be obtained as pads on the output transmission lines, or they can be realised using small gaps, using the MGAP2 element.

One application of the backward travelling wave coupler is in the measurement of power at the output of a device, such as a signal generator or a transmitter. Typically, a coupled signal -20 dB below the forward or reverse power is required. The forward power is the transmitter output power and the reverse power is the reflected signal that occurs if the load for the transmitter is mismatched. At least a 20 dB front to back isolation is required, to accurately measure forward and reflected power. The hybrid will thus require a coupled output of -20 dB and an isolated signal <-40 dB.

As can be seen from figure 4.41, the signal at the isolated port (S_{31}) is too large when a quarter wavelength long coupler is used. A suitable coupler with a good forward to reverse ratio can be obtained by making the length of the coupler much smaller than a quarter wavelength and using capacitors shunting the forward and reverse coupled outputs to produce a constant frequency response over the required frequency band.

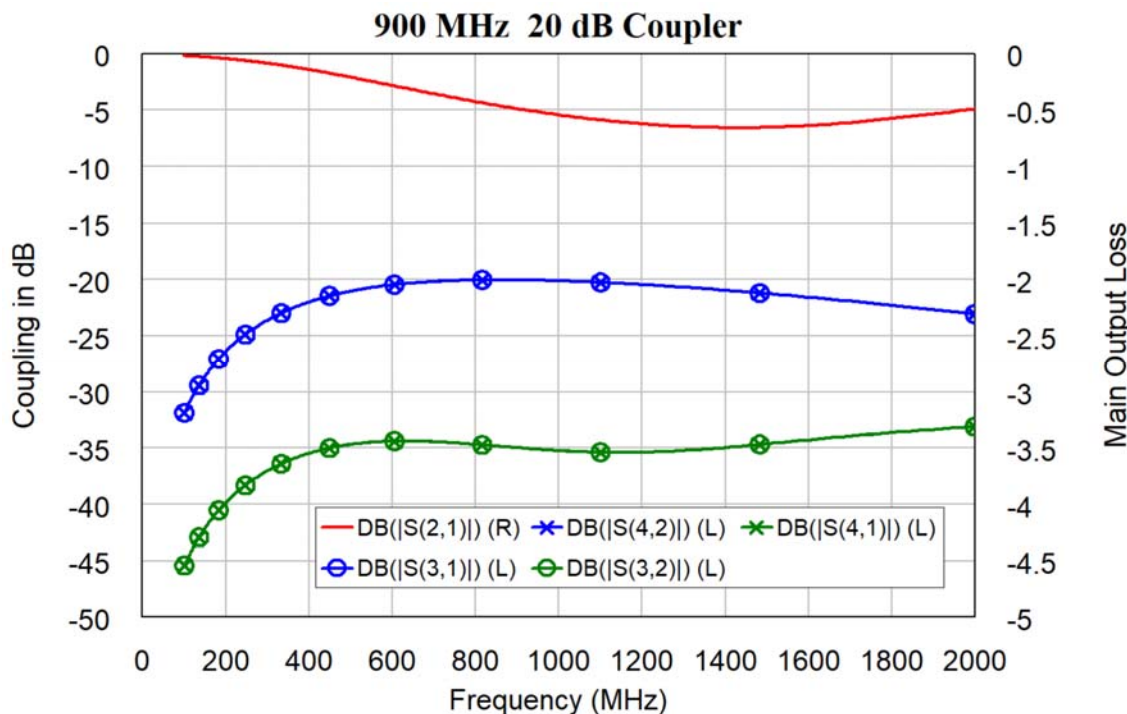


Figure 4.42. Simulated performance of the Microstrip coupler.

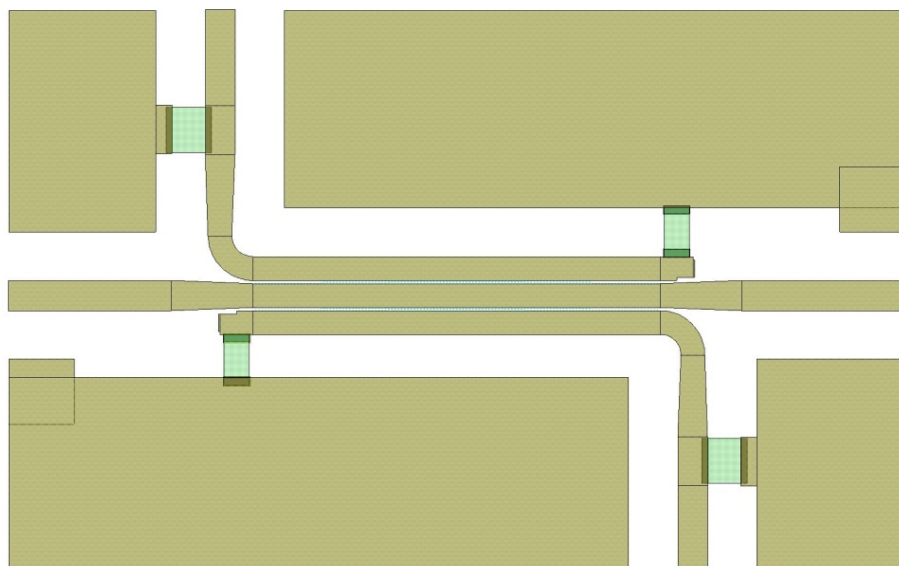


Figure 4.43. Layout of the Microstrip coupler.

Figure 4.42 shows the simulated performance of such a 20 dB coupler. Comparing this with figure 4.41 shows that the isolated port has a much better isolation and the coupled port has a flatter and wider frequency response. This performance is obtained by using the optimiser in NI AWR DE to vary the coupling gap, line widths, lengths and capacitance values until a suitable performance is obtained. The resulting PCB layout is shown in figure 4.43. For a $\lambda/4$ long coupler and -20 dB coupling, a 0.95 mm gap is required. For the shorter length coupler of figure 4.43, the coupling gap is 0.2 mm, which is easy to achieve using current technology.

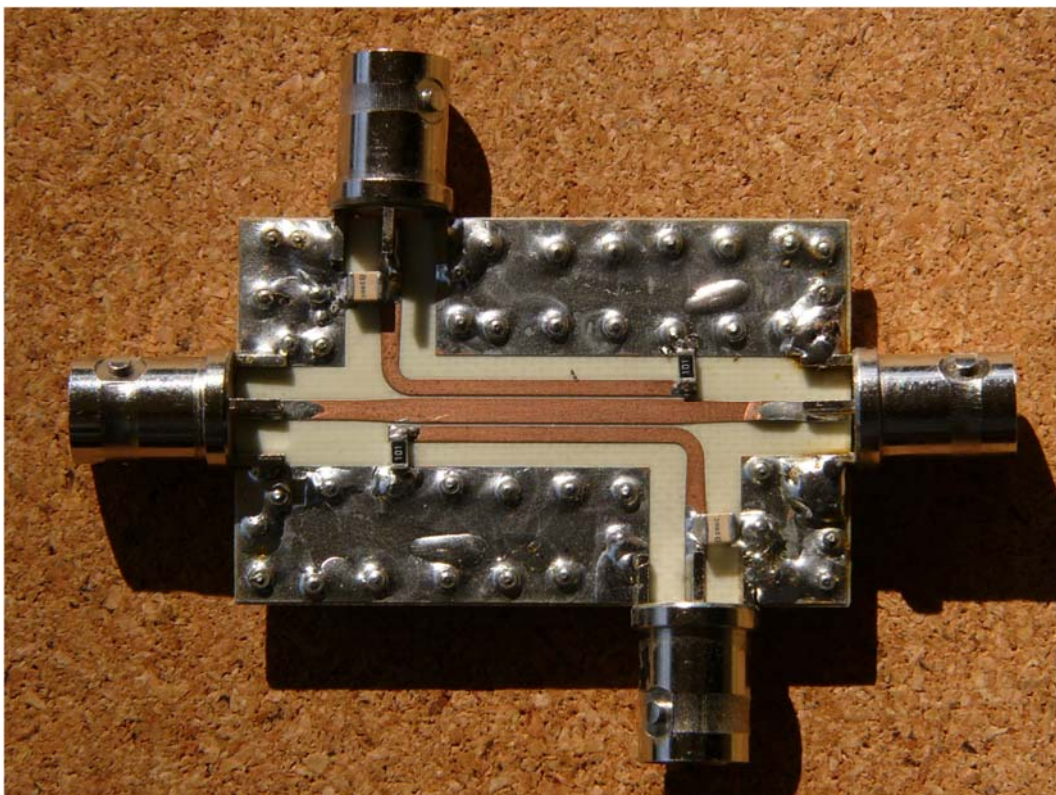


Figure 4.44. Photograph of the Microstrip coupler.

Figure 4.44 shows a photograph of the Microstrip coupler. To provide suitable shielding and allow for the resistors, capacitors and BNC connectors to be soldered to the PCB, large earth pads are incorporated. Such an earth-plane also allows the circuit to be mounted in a metal box, without affecting the performance. That top ground-plane needs to be solidly connected to the bottom ground-plane, using lots of vias or pins. This is commonly done in commercial designs and figure 7.59 shows a commercial design from Codan [6], using many vias, connecting the top and bottom ground planes. The measured performance closely matches the simulated performance. The spacing between the vias or pins needs to be a small fraction of a quarter wavelength at the highest operating frequency of the circuit. Figure 4.45 shows the corresponding circuit diagram. The blue variables for widths, length, coupling gap and capacitor values are the parameters that are optimised to obtain the specified performance.

Edge-coupled Backward travelling wave hybrids as shown in figure 4.42, are the best choice if a wide bandwidth and low coupled outputs (-20 dB) and good front to back ratios are required.

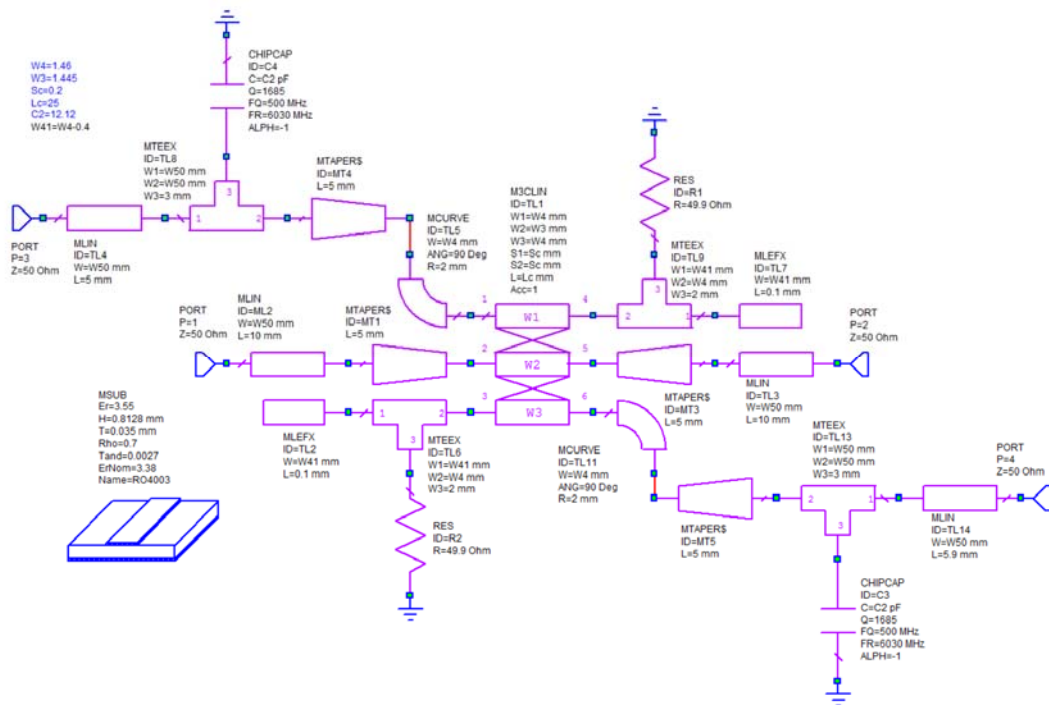


Figure 4.45. Circuit diagram of Microstrip coupler.

Lange Coupler

For a 3 dB coupler, $C=0.707$ and $Z_{OE}=120.7 \Omega$ and $Z_{OO}=20.7 \Omega$. For edge coupled Microstrip lines, this requires a coupling gap far smaller than 0.1 mm, which is impossible to make. To increase the coupling, many lines can be used in parallel. This is called a Lange Coupler. Figure 4.46 shows a layout of a Lange coupler. At the middle, a bonding-wire is used to connect the upper track end to the middle track and the lower other track end, thus keeping those transmission lines in parallel. Similarly, the track ends at the edges of the coupler are connected to the other appropriate lines. One will thus have the top left port connected by a set of parallel lines to the bottom right port. The top right port is connected by a set of parallel lines to the bottom left port. Typically, the spacing between the tracks and the track widths are of the order of 0.25 mm, which is close to the smallest widths that can conveniently be made using conventional processes.

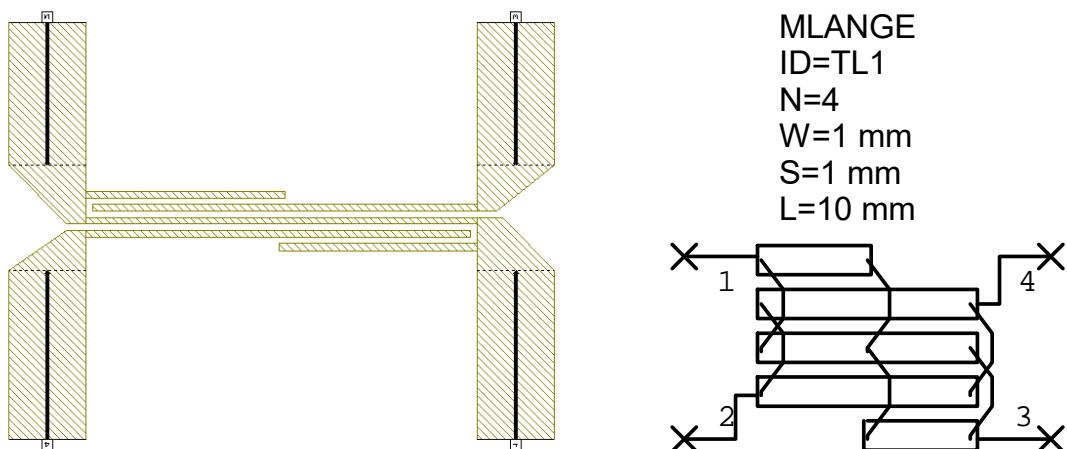


Figure 4.46. Lange coupler layout from MLANGE and schematic.

Even having these parallel lines result in very fine track widths and coupling gaps, making the Lange Coupler expensive to make. The Lange coupler [7] is however, the only planar hybrid that offers better than an octave (2:1) of useable bandwidth. With the high cost of manufacturing the Lange Coupler, due to the small track and gap widths and the high cost of attaching the bond wires, Lange Couplers are not often used. The required coupling can be obtained at a lower cost and can be better controlled, using broadside coupled lines and multilayer RF printed Circuit Boards. They can also be implemented using Low Temperature Co-fired Ceramic (LTCC) substrates, which are discussed in chapter 10. Since NI AWR DE V10, the Lange coupler circuit element MLANGE and the associated layout as shown in the left of figure 4.46 is no longer available since it was not accurate enough. The replacement circuit elements MLANG and the more accurate M2LANGE, which includes an EM model, only shows the thin coupled lines of the schematic in the layout.

Broadside Coupled Lines

It is possible to have multilayer printed circuit boards with RF substrates. These can be used to design coupling structures with higher coupling and 3 dB couplers are quite practical. The typical configuration is shown in figure 4.47.

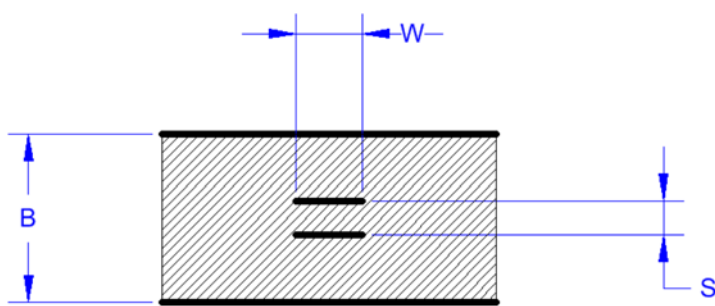
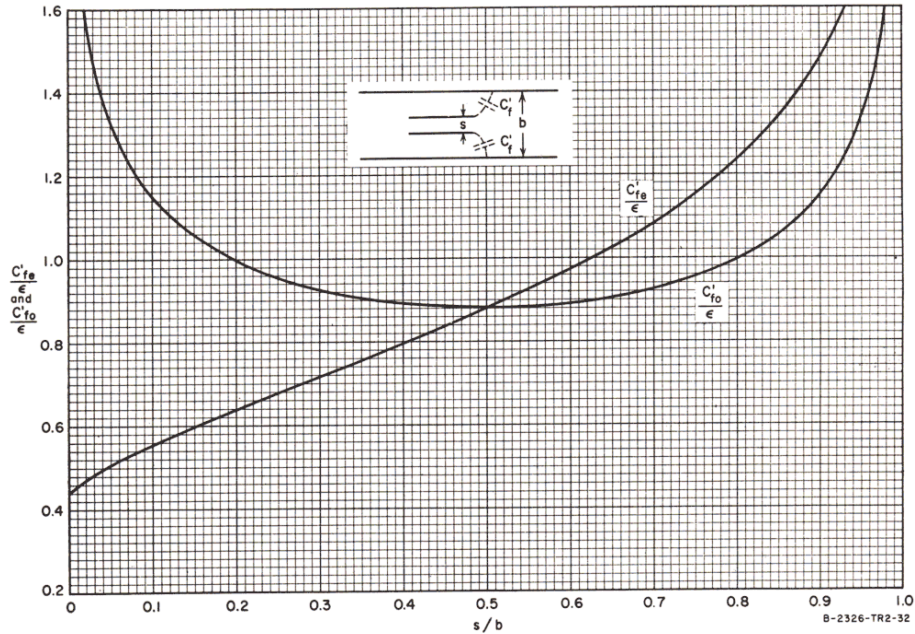


Figure 4.47. Stripline broadside coupled lines

The advantages of this structure are firstly that bigger coupling between the transmission-lines can be obtained with a good control over impedance values. Secondly, the Stripline structure has no radiation losses. The disadvantage is that a non-planar structure is required.

TXLine is not capable of calculating the broadside-coupled transmission-line coupling gap (s) and line width (W), shown in figure 4.47. Books like Matthei, Young and Jones [8]. *Microwave Filters, Impedance Matching Networks and Coupling Structures*. Artech House 1980. (McGraw Hill 1964) pages 180 and 181 give empirical equations for Z_{oe} and Z_{oo} are given in equations 4.19 and 4.20. The capacitance C_{fe} and C_{fo} are fringing capacitances between the coupled lines and the ground plane and these can be determined from figure 4.48.



SOURCE: Final Report, Contract DA-36-039 SC-74862, SRI; reprinted in *IRE Trans., PGMTT* (see Ref. 5, by S. B. Cohn).

Figure 4.48. Table for C_{fe} and C_{fo} from Matthei, Young and Jones, pp181.

$$Z_{oe} = \frac{188.3/\sqrt{\epsilon_r}}{\frac{w/b}{1-(s/b)} + \frac{C_{fe}}{\epsilon}} \quad \text{Eqn. 4.19}$$

$$Z_{oo} = \frac{188.3/\sqrt{\epsilon_r}}{\frac{w/b}{1-(s/b)} + \frac{w}{s} + \frac{C_{fo}}{\epsilon}} \quad \text{Eqn. 4.20}$$

Using the two-line broadside coupled line element, SBCPL, and the schematic circuit simulation, allows an easier and more accurate determination of the broadside coupler parameters, than using equations 4.19, 4.20 and figure 4.48. The SBCPL element is a two-line broadside-coupled line element. The cross-section is similar to that of figure 4.47.

In addition, the width of each of the lines can be specified independently, the lines can be offset and the dielectric constants between the lines can be different from that above and below the line. None of these advanced features can be determined using the alternative techniques. The use of the SBCPL element to determine the required coupling gap and line width for a coupler is illustrated in the following example.

Example 4.4: 100 Watt 3 dB Broadside Coupler

A 3 dB coupler was required to operate at a power level of about 100 Watt at a frequency of 100 MHz. At the time of the design, MWO did not yet exist and the equations 4.19 and 4.20 and Figure 4.48 were required to complete the design.

Two 12.6 mm thick pieces of Polyethylene, which has a dielectric constant of $\epsilon_r = 2.26$, were used for the top and bottom dielectric sheets for this coupler. Polyethylene sheets of this thickness can conveniently be purchased as a cutting board for bread from most local supermarkets. For a 3dB coupler, $C = 0.707$ and $Z_{OE} = 120.7 \Omega$ and $Z_{OO} = 20.7 \Omega$. Since these impedances must be evaluated iteratively, it is the easiest to enter the above equations for Z_{OE} and Z_{OO} into an Excel or other spreadsheet. Using the values $B = 29$ mm, $s = 2.9$ mm, $w = 12.7$ mm, gives $\frac{s}{B} = 0.1$ and thus from the table gives $\frac{C_{fe}}{\epsilon} = 0.56$

and $\frac{C_{fo}}{\epsilon} = 1.15$. This then results in $Z_{OE} = 119.7 \Omega$ and $Z_{OO} = 20.8 \Omega$, which is close enough. At 100 MHz the length of a quarter wavelength line is given by: $\frac{\lambda}{4} = \frac{c}{\sqrt{\epsilon}F} = 50\text{cm}$. As shown in figure 4.49, the width of 50 Ω terminating lines can be

calculated using TXLine or equivalent programmes as 23.2 mm. A 2.9 mm thickness of Polyethylene is not readily available. However, a 3.17 mm thickness of Perspex, with a dielectric constant of approximately 3.42 was available and was used. The effect of this substitution cannot readily be calculated using the above techniques. This coupler was constructed and performed as expected, even though the line spacing was not ideal.

The use of SBCPL in NI AWR DE gives much more flexibility and allows a more accurate determination of the performance. The actual cutting boards used are 12.6 mm (0.5 inch) thick, pieces of Polyethylene. They are used for the top and bottom dielectric and a 3.17 mm (0.125 inch) thick Perspex sheet is used to separate the tracks. Entering these values in the SBCPL element and then fine-tuning the track width, track length and offset, allows the required performance to be obtained. Polyethylene has a dielectric constant of $\epsilon_r = 2.26$ and Perspex has a dielectric constant of 3.42 ± 0.3 .

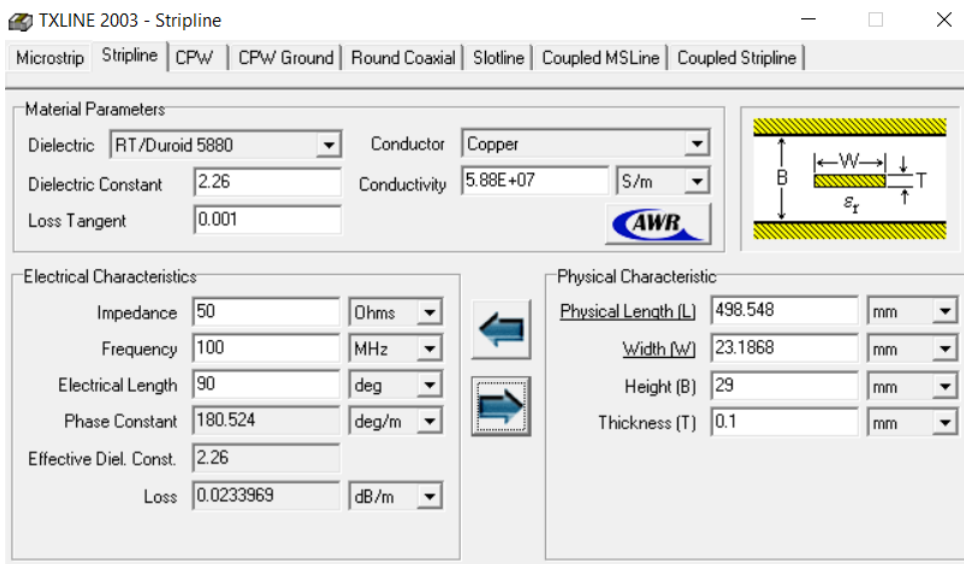


Figure 4.49. Terminating line-width calculation.

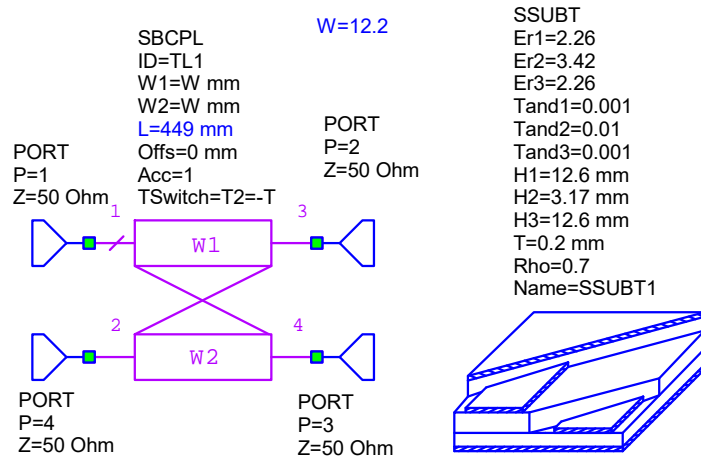


Figure 4.50. MWO broadside coupled-line circuit using SBCPL.

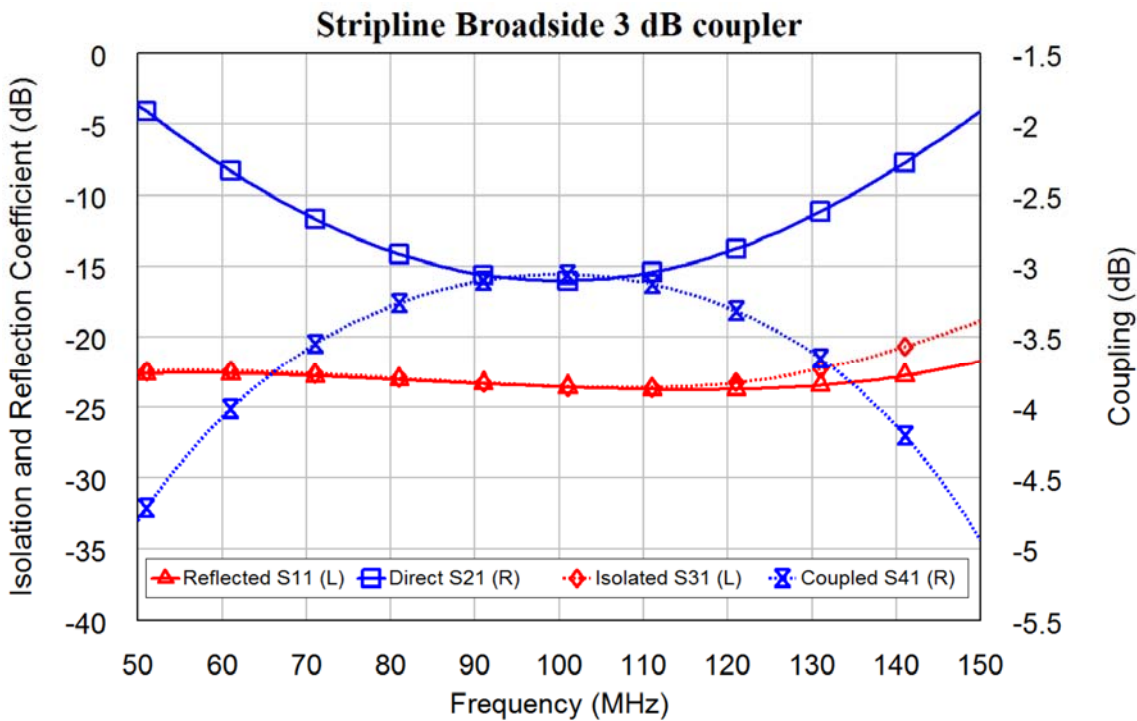


Figure 4.51. Performance of broadside coupled-line circuit using SBCPL element.

Tuning the coupler length ($L = 449$) sets the centre frequency of the coupler to 100 MHz and tuning the line width ($W = 12.2$) adjusts the coupling to have close to 3 dB coupling over the 85 MHz to 115 MHz frequency range and achieve a return loss on the ports of less than -20 dB. The resulting MWO circuit diagram is shown in figure 4.50 and its performance is shown in figure 4.51. The track width of 12.2 mm and length of 440 mm obtained from MWO agrees closely with the 12.7 mm and 500 mm obtained for the earlier design, which used equations 4.19 and 4.20 together with figure 4.48. The MWO design is far more accurate since it allows for losses in the dielectric and the Perspex sheet for separating the tracks, having a different dielectric constant and loss tangents compared with the Polyethylene. The constructed coupler has a measured isolation and coupling very similar to the performance shown in figure 4.51 and is able to handle 100W of output power.

Prepreg sheets are available [9], which can be used to convert single layer PCB's to multilayer PCB's, so that broadside couplers can be constructed. The Roger's RO4403 Prepreg sheets have a dielectric constant of 3.17 and are 0.1 mm thick and can be used to bond two single layer PCB's to form a multilayer PCB. The sandwich is pressed together with a pressure of 2.8 MPa (400 psi) and a temperature controlled profile up to 180 °C (350 °F) for a cycle time of 2 hours to form the correct bond. For further details, see the RO4403/4450 data sheet. Other manufacturers have similar materials.

References

1. W. C. Johnson, *Transmission Lines and Networks*, Mc Graw Hill June 1950.
2. Wikipedia Transmission lines: http://en.wikipedia.org/wiki/Transmission_line
3. D. M. Pozar, "*Microwave Engineering*", 3rd Ed, Wiley, 2005.
4. E Wilkinson, "*An N way Hybrid Power Divider*," IRE Trans. Trans Microwave Theory and Techniques, vol. MTT-8, pp. 116-118, Jan. 1960.
5. Rogers R04000 Series High Frequency Circuit materials Datasheet. <http://www.rogerscorp.com/documents/726/acm/RO4000-Laminates---Data-sheet.pdf>
6. Codan, <http://www.codan.com.au/>
7. J. Lange, "*Interdigitated stripline Quadrature Hybrid*", IEEE Trans Microwave Theory and Techniques, vol. MTT-17, pp1150-1151, Dec 1969.
8. Matthaei, George L.; Young, Leo and Jones, E. M. T. "*Microwave Filters, Impedance-Matching Networks, and Coupling Structures*", McGraw-Hill, 1964.
9. Rogers Corporation, "RO4400 Series Prepreg Data Sheet", www.rogerscorp.com.

Chapter 5

Frequency Mixers

Introduction

Figure 5.1 shows the typical block diagram of a transmitter and a receiver. It can be seen that in both cases frequency translation is achieved by the use of a frequency mixer. A frequency mixer can be a passive mixer using diodes or it can be an active mixer using transistors or FETs. In many receivers and transmitters, a succession of frequency mixing and filtering stages are used, to ensure that the filtering requirements can be satisfied.

A frequency mixer is used as an up-converter when the output frequency is higher than the input frequency. This is typical in a transmitter. A frequency mixer is used as a down-converter when the output frequency is lower than the input frequency. This is typical for a receiver. In this chapter, the term *mixer* denotes a frequency mixer.

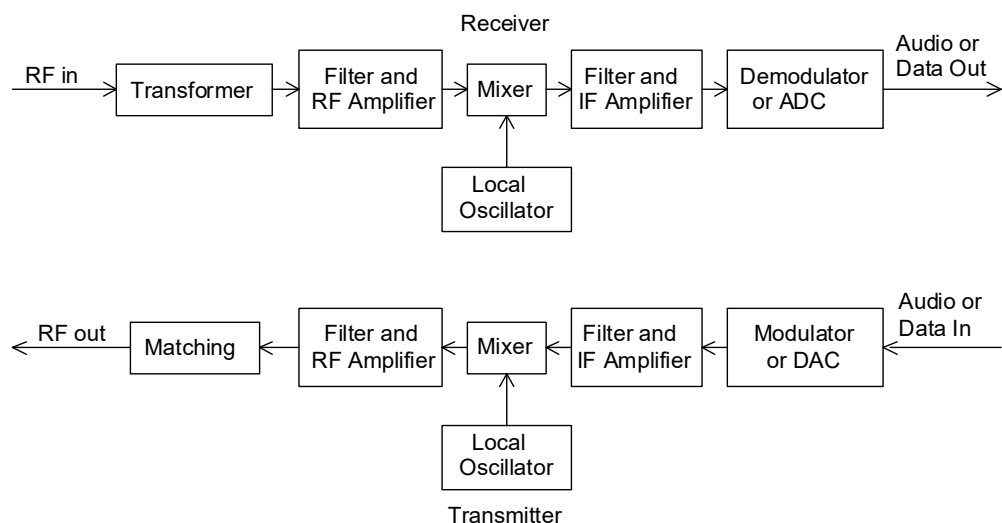


Figure 5.1. Typical transmitter and receiver block diagram.

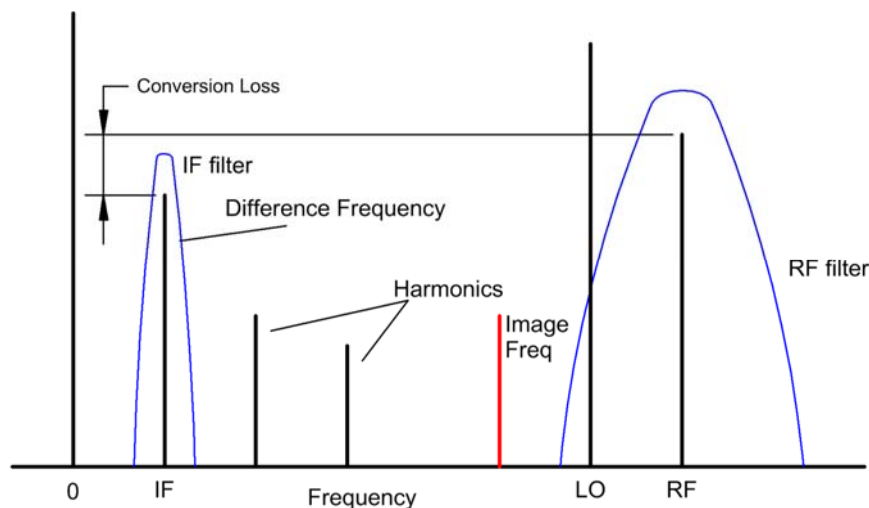


Figure 5.2. Frequencies of a mixer.

A mixer produces sum and difference frequencies. An ideal multiplier is a perfect mixer since mathematically it produces sum and difference frequencies. The aim in frequency mixer design is thus to make the frequency mixer behave as close to an ideal multiplier as possible. This chapter describes different circuits to achieve this.

For a receiver the RF signal is down converted. A receiver has a Local Oscillator (LO), the frequency of which is determined by the radio frequency (RF) or TV signal that is to be received. Figure 5.2 shows the frequencies for a receiver or down-converter. F_{LO} is the frequency of the LO and F_{RF} is the frequency of the RF signal. The RF signal is mixed with a LO signal to produce sum and difference frequencies. The sum frequency $F_{LO} + F_{RF}$ is outside the operating frequency range of the system and the difference frequency $F_{LO} - F_{RF}$ is the required Intermediate Frequency (IF) signal, which is filtered and amplified using an IF filter and its associated amplifiers. The IF frequency is $F_{IF} = F_{LO} - F_{RF}$. It should be noted that a signal at the image frequency results in a signal at the same IF frequency since for the image frequency $F_{IF} = F_{IM} - F_{LO}$, where F_{IM} is the image frequency. The RF filter should be sufficiently narrow so that the image frequency, shown in figure 5.2, is not passed through the RF filter, since the difference frequency of the image frequency and the local oscillator is at exactly the same frequency as the required IF signal.

For an up-converter, the LO signal is multiplied by an IF signal and a double sideband suppressed carrier RF signal results. The resulting RF frequencies are $F_{RF} = F_{LO} \pm F_{IF}$. Generally only one of these RF signals are required, so that an RF filter, like the one shown in figure 5.2 is required to remove the unwanted signal.

There are two types of frequency mixers: 1) Passive mixers, using diodes, FETs or other nonlinear devices. In passive mixers the power in the LO signal provides the power for producing the sum and difference frequencies. 2) Active mixers, where transistors or FETs supplied with DC power provide the frequency mixing action.

Definition of Terms

Conversion Loss

For a down-converter, the conversion loss [1] is the ratio of the RF input signal to the wanted IF output signal. Most frequency mixers are used in receivers, for which this definition is applicable. For up-conversion, the conversion loss is the ratio of one of the wanted RF output signal spectral components to the IF input signal. For an ideal frequency mixer, half the input power is frequency shifted to the difference frequency and half the power is shifted to the sum frequency. The conversion loss is the ratio of the input signal to either the sum or the difference component. An ideal passive mixer will thus have a conversion loss of 3 dB. Practical balanced or double balanced mixers typically have a conversion loss of less than 6 dB. The conversion loss does depend on the amount of LO signal power applied to the LO port as can be seen in figures 5.12, 5.21 and 5.31. The frequency mixer is normally operated at a LO power close to that giving the lowest conversion loss. Active mixers can have a conversion gain.

The conversion loss must be taken into account in noise figure calculations of a receiver. A frequency mixer with a 6 dB conversion loss typically has a 6.5 dB noise figure. For high quality receivers, an amplifier with a gain much greater than the conversion loss is normally used before the mixer, to ensure that the mixer does not dominate the noise performance of the receiver.

Note NI AWR DE calculates the conversion gain. As a result, it is more appropriate to use a consistent term conversion gain in the plots and have negative dB values to indicate the loss. The term conversion loss is however used more frequently in literature. To use “*Conversion Loss*” would require the minus signs to be removed from the NI AWR DE generated plots, which is not easy to do. Similarly the term Insertion Gain and Return Gain are used in plots, with negative dB values indicating when the plotted variables have a loss.

Isolation

In practice it is desirable to have isolation between the LO, RF and IF ports of the mixer. Typical double balanced mixers have more than 30 dB isolation [1, 2] between all ports. Single diode mixers have virtually no isolation between ports. Since single diode mixers are used in TV receivers, the LO signal is coupled to the antenna, which radiates the LO signal. In countries where TV licences are required, the “detector vans” look for the LO radiation and match the radiation coming from a house with any licence fee payment. One can also do a good survey to find out what TV channel people are watching by simply driving around a street with a spectrum analyser and noting the LO frequencies. For a balanced mixer, the isolation is directly related to the match between the diodes used. As a result, many manufacturers sell matched sets of diodes, especially for use in mixers. In many cases two or 4 diodes come as one package.

Compression Point

For an ideal down-conversion mixer the IF output produced should be directly proportional to the RF input signal. However as the RF input approaches about 10 dB below the LO power. The IF output starts to saturate and the conversion loss starts to increase, as is shown in figure 5.3. Most manufacturers of frequency mixers specify the 1 dB compression point for their mixers [1, 2]. The 1 dB compression point is typically 6 dB below the LO level for mixers up to +23 dBm LO power.

Since the 1 dB compression point is related to the LO drive, a higher LO level results in a higher 1 dB compression point and as a result a bigger dynamic range of the mixer.

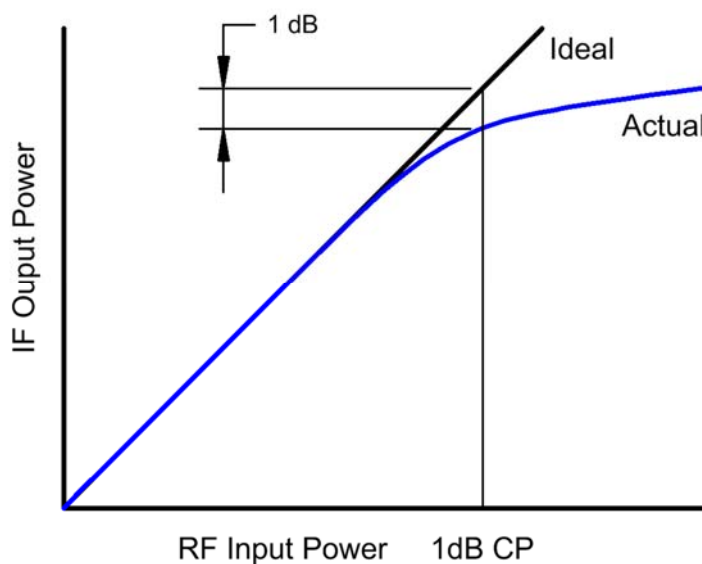


Figure 5.3. 1 dB Compression Point of a mixer.

Dynamic Range

Dynamic range is the range over which a frequency mixer provides useful operation. The 1 dB compression point determines the upper limit of the dynamic range. The noise figure of the mixer determines the lower limit of the dynamic range. Since the mixer noise figure is only about 0.5 dB higher than its conversion loss, the lowest conversion loss is desirable to obtain the largest dynamic range. High and Extra High level mixers have a higher 1 dB compression point and thus a bigger dynamic range. Higher-level mixers are significantly more expensive and require more LO power, so that a compromise between cost, power consumption and dynamic range exists.

Two-tone Third Order Intermodulation Distortion

In this section one considers the frequency mixer as a “linear” device, since for a down-converter, the IF mixer output amplitude is directly related to the RF input amplitude. The output $Y(t)$ of a frequency mixer or amplifier will depend on the input $X(t)$. The gain of the device, relating the output to the input is a_1 . In addition, a DC component and harmonics of the input may be created due to the distortion of the device. The output is thus:

$$Y(t) = a_0 + a_1 X(t) + a_2 X(t)^2 + a_3 X(t)^3 + a_4 X(t)^4 + a_5 X(t)^5 + \dots \quad \text{Eqn. 1}$$

For the devices we are considering, the terms above the 5th harmonic are so small they can be ignored.

When two signals X_1 and X_2 are used as input. The output will then be:

$$Y(t) = a_0 + a_1 [X_1(t) + X_2(t)] + a_2 [X_1(t) + X_2(t)]^2 + a_3 [X_1(t) + X_2(t)]^3 + a_4 [X_1(t) + X_2(t)]^4 + a_5 [X_1(t) + X_2(t)]^5 + \dots \quad \text{Eqn. 2}$$

When $X_1(t)$ is a sine wave of frequency F_1 and $X_2(t)$ is a sine wave of frequency F_2 , ($F_2 > F_1$) the frequency components at the fundamental and different intermodulation frequencies can be collected as follows:

The fundamental frequency component, i.e. at F_1 due to $X_1(t)$ and at F_2 due to $X_2(t)$ is:

$$Y_F = a_1 + \left(\frac{3}{4} + 3\frac{1}{2}\right)a_3 + \left(\frac{5}{8} + 10\frac{3}{8} + 5\frac{3}{8}\right)a_5 = a_1 + \frac{9}{4}a_3 + \frac{25}{4}a_5 \quad \text{Eqn. 3}$$

The Third Order Intermodulation (3IM) frequencies are 3IM(upper) due to $\pm F_1 \pm 2F_2$ and 3IM(lower) due to $\pm 2F_1 \pm F_2$, and are given by:

$$Y_{3IM} = \frac{3}{4}a_3 + \frac{1}{2}(5\frac{1}{2} + 10\frac{3}{8})a_5 = \frac{3}{4}a_3 + \frac{25}{8}a_5 \quad \text{Eqn. 4}$$

The Fifth Order Intermodulation (5 IM) frequencies are 5IM(upper) due to $\pm 2F_1 \pm 3F_2$ and 5IM(lower) due to $\pm 3F_1 \pm 2F_2$, and are given by:

$$Y_{5IM} = \frac{1}{2}10\frac{1}{8}a_5 = \frac{5}{8}a_5 \quad \text{Eqn. 5}$$

The frequencies of these spectral components are shown in figure 5.4. The second order intermodulation (2IM) and the fourth order intermodulation (4IM) distortion produced by the amplifier or mixer do not create any components near the desired frequency components. As a result the 2IM and 4IM performance is less important for an amplifier.

The second order intermodulation produces the required mixing action in a mixer and is thus of utmost importance.

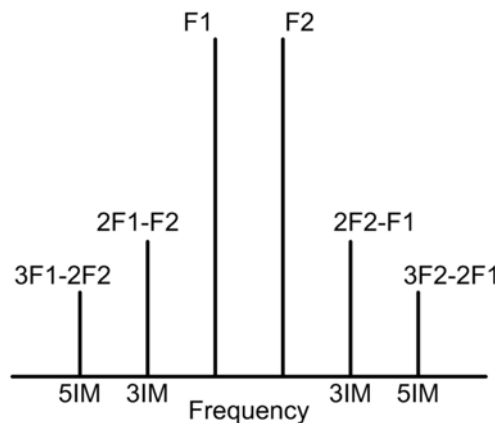


Figure 5.4. IM distortion of an amplifier or frequency mixer.

The third order IM (3IM) and fifth order IM performance is very important in linear amplifiers since when two tones are used as an input to the amplifier, the 3IM and 5IM distortion results in additional frequency components, which again cannot be filtered out, as can be seen in figure 5.4. The 5IM components are often too small to be observed in a spectrum like figure 5.4. For mobile phone base-stations, these IM signals are likely to create interference in adjacent mobile phone channels, as a result the IM performance of amplifiers and mixers are a critical part of their specification.

Third Order Intercept Point

In practice $a_1 \gg a_3 \gg a_5$, so that the fundamental frequency components are proportional to a_1 , the 3IM components are proportional to a_3 and the 5IM components are proportional to a_5 . If the input signals are increased by 1 dB, then the 3IM components will increase by 3 dB since they are caused by $a_3[X_1(t) + X_2(t)]^3$ in equation 2 and the 5IM components will increase by 5 dB since they are caused by $a_5[X_1(t) + X_2(t)]^5$ in equation 2.

A popular method of determining the "linearity" of a frequency mixer is the "third-order intercept" approach [1]. The Third-Order Intercept Point is a theoretical point on the RF input versus IF output curve where the desired input signal and third-order products become equal in amplitude as RF input is raised.

For a down converter, the RF power is the input and as the RF signal increases by 1 dB, the 3IM distortion component increases 3 dB. The Third Order Intercept Point is determined by increasing the RF level and noting both the desired and the 3IM levels. The third order intercept point is the point where the extension of the plotted desired output and 3IM output level versus RF input meet, as shown in figure 5.5. The corresponding level on the horizontal, input, axis (RF) is the third order input intercept point (IIP3) and the corresponding level on the vertical, output, axis (IF) is the third order output intercept point (OIP3). The difference is the conversion loss. It is not possible to drive the mixer to those RF levels. As a rule of thumb the third order intercept point is about 8 to 10 dB above the LO level for a typical diode based double balanced mixer and

up to 15 dB above the LO level for passive FET mixers. Passive FET mixers however have a much narrower bandwidth.

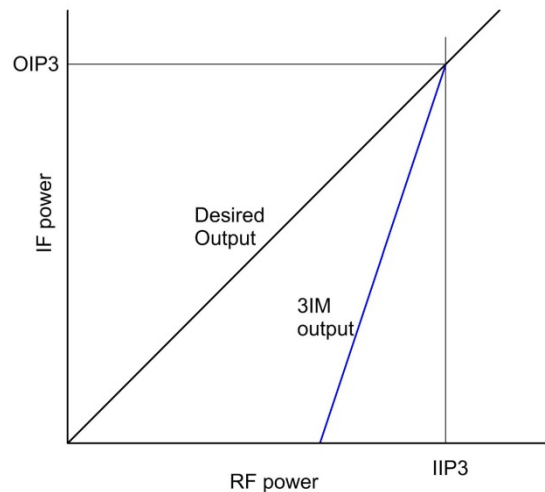


Figure 5.5. Third order input and output intercept points.

The third order intercept point is useful in determining the RF level required for a specified 3IM distortion performance. If for example, the 3IM signal is to be 40 dB below the required signal, then the RF level must be 20 dB below the Third Order Intercept Point, since then the desired signal will be 20 dB below the intercept point and the 3IM signals will be $3 \times 20 = 60$ dB below the intercept point.

LO Level

MIXER CLASS	CIRCUIT	LO POWER FOR DB MIXERS (dBm)
Class 1	—→	+7 to +13
Class 2, type 1	—→→	+13 to +24
Class 2, Type 2	—~—~→	+13 to -24
Class 3, Type 1	—~—~ →	-20 to +30
Class 3, Type 2	—~—~ →→	+20 to +30
Class 3, Type 3	—~—~ →→→	+20 to +30

Figure 5.6. Different diode configurations for different mixer levels [3].

Frequency mixer manufacturers make mixers to operate at different LO power levels. For standard level mixers, the LO power required is +7 dBm. Other mixer power levels are +10, +13, +17, +23, +27 dBm. Mini-Circuits [1, 2] denote their mixer according to the LO power required, so a Level 7 mixer requires a LO power of +7 dBm. For a good Double Balanced Mixer, the third order intercept point (IP3) is 10 dB above the LO level. By having a higher power level available, the manufacturers are able to control the diode

I-V characteristics more to ensure that the a_2 coefficient in the binomial expansion of the diode I-V characteristic shown as Equation 1, 2, 6 and 7 is maximized in relation to the other terms, thus minimizing the unwanted components. Figure 5.6 by Bert Henderson shows how diodes can be arranged in different diodes classes [3], to obtain these different mixer LO levels. These diode models can be implemented in AWDE to investigate the different mixer LO levels.

Example 5.1: Mixer LO Level Calculation

A maximum RF input signal of -10 dBm and a level of third order intermodulation products (3IM) of 60 dB below the desired signals is required for a specific application. For a typical 7 level mixer, the IP3 point is +17 dBm. The RF signal at -10 dBm is thus 27 dB below the IP3 point. This will result in the 3IM signals being $(3-1)*27 = 54$ dB below the wanted signal.

Similarly, a level 10 mixer will result in the 3IM signals being $(3-1)*30 = 60$ dB below the wanted signals, a level 13 mixer will result in the 3IM signals being $(3-1)*33 = 66$ dB below the wanted signals. A level 17 mixer will result in the 3IM signals being $(3-1)*37 = 74$ dB below the wanted signals. A level 23 mixer will result in the 3IM signals being $(3-1)*43 = 86$ dB below the wanted signals and a level 27 mixer will result in the 3IM signals being $(3-1)*47 = 94$ dB below the wanted signals. The higher the LO level, the higher the cost of the mixer. A level 10 mixer will thus be the lowest cost device, which will satisfy the specifications.

Single Diode Mixer

Single diode mixers use a single diode to produce the required frequency components.

Single diode mixers are often used in cost critical applications, such as Radio or TV receivers, where the low cost is more important than good performance. With the advent of low cost active mixer IC's, single diode mixers are progressively being used less. Single diode mixers are very suitable for microwave applications like speed guns and shopping centre door openers, where the transmitted signal is used as the LO for the received signal, and the receiver diode is simply mounted in the antenna horn. The resulting IF signal is the difference frequency, which is due to the speed of the car being detected or the speed of the person moving towards the door.

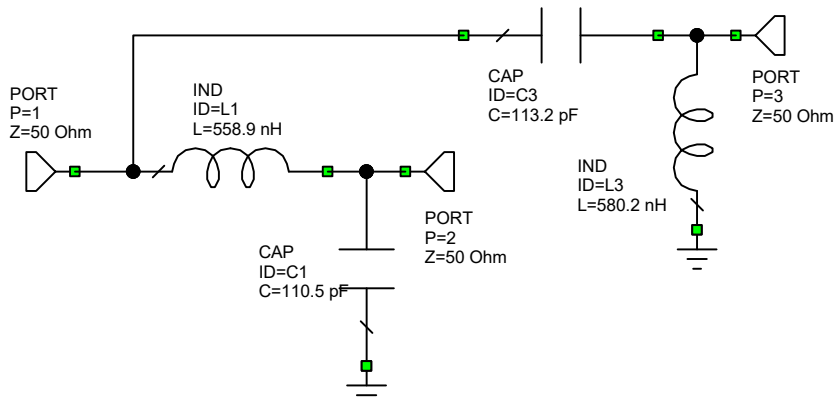


Figure 5.7. Diplexer circuit.

A single diode mixer requires a diplexer to separate the high frequency RF and LO signal from the low frequency IF signal. Since the single diode mixer is normally a lower cost consumer type application, the diplexer is normally kept simple with either a first or second order high pass and low pass filters.

Figure 5.7 shows a simple diplexer consisting of second order high pass and low pass filters. The crossover frequency is chosen to be 20 MHz, allowing baseband signals up to 15 MHz to be used. To obtain the best impedance looking into port 1, series elements are required to connect to port 1. A Butterworth high pass and low pass filter design is a good starting point and optimisation can be used to improve the impedance matches resulting in the diplexer performance as shown in figure 5.8.

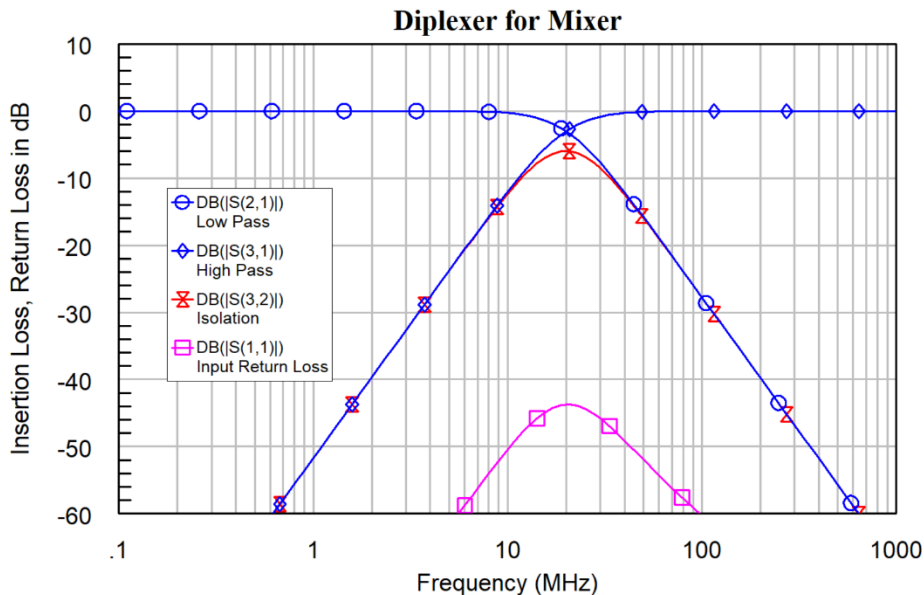


Figure 5.8. Frequency response of diplexer after optimisation.

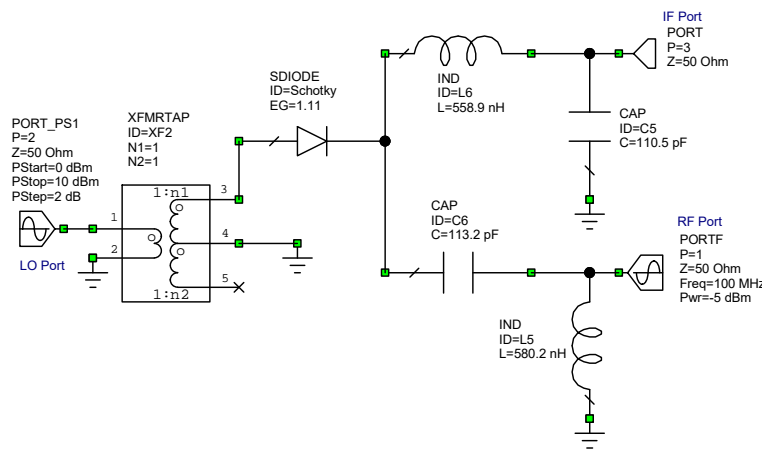


Figure 5.9. Circuit diagram of a single diode mixer as a down-converter.

Figure 5.9 shows the circuit diagram of a single diode mixer. The transformer is normally not included in the circuit, since in this case it is simply a non-inverting transformer. It is included here to illustrate the differences between the single diode mixer of figure 5.9 and the balanced mixer of figure 5.20.

The mixing behaviour of a single diode mixer can be demonstrated by considering the current flowing through the diode of figure 5.9. The current can be expressed as:

$$I_a = a_0 + a_1 V_a + a_2 V_a^2 + a_3 V_a^3 + a_4 V_a^4 + a_5 V_a^5 + \dots \quad \text{Eqn. 6}$$

If two voltages V_a and V_b are now applied to the diode, due to the LO and the RF signals, then the current will be

$$I_a = a_0 + a_1 (V_a + V_b) + a_2 (V_a + V_b)^2 + a_3 (V_a + V_b)^3 + a_4 (V_a + V_b)^4 + a_5 (V_a + V_b)^5 + \dots \quad \text{Eqn. 7}$$

The term $a_2 (V_a + V_b)^2 = a_2 (V_a^2 + 2V_a V_b + V_b^2)$ contains the required $2a_2 V_a V_b$, which results in the sum and difference frequencies. All the other terms cause unwanted frequency components. It is thus desirable to use diodes with an I-V characteristic where a_2 is large in comparison with the other terms in the binomial expansion of the I-V characteristic. Some of the additional frequency components due to the a_3 , a_4 and higher order diode nonlinearities, can fall close to the desired frequency thus causing an interference.

Computer Simulation of Mixers

The advanced RF Computer simulation programs like MWO and ADS allow frequency mixers to be simulated accurately. A frequency mixer requires two inputs, both at different frequencies and the output is normally at a frequency that is different from both the inputs to the mixer. The simulation is thus very different from that of a linear device, like a transformer, hybrid or filter.

The Project Options menu sets the frequencies used for the simulation. For the single diode mixer of figure 5.9, these frequencies are used by the PORT_PS1 port element, which is applied to the LO port (Port 2). The PORT_PS1 element allows the signal power to be varied as specified by the parameters for the PORT_PS1 element.

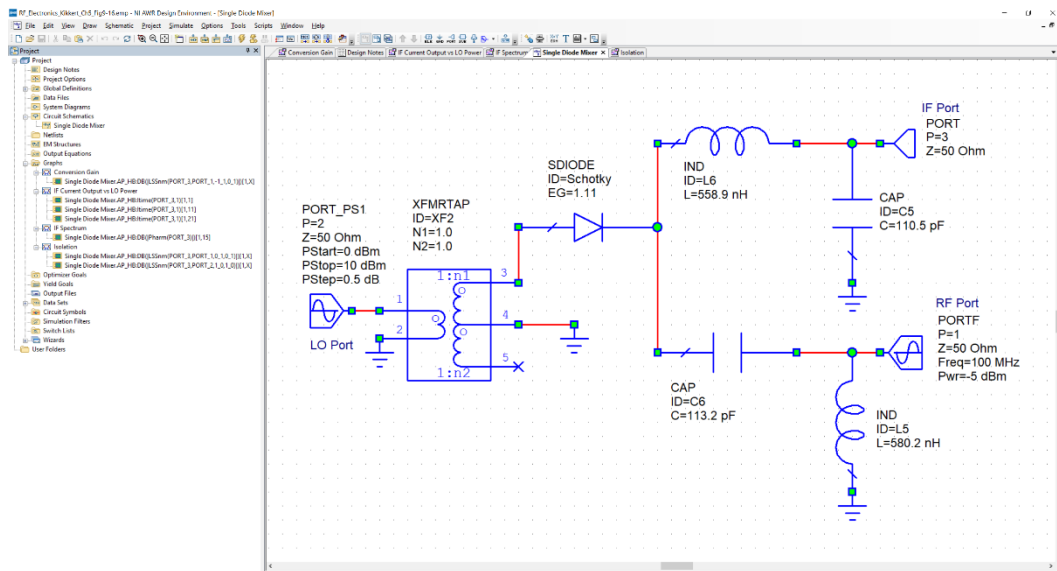


Figure 5.10. Typical Measurements for a mixer.

A PORTF element produces a single tone signal with frequency and power level set by the parameters for that element. For a down-conversion mixer, the PORTF element is applied to the RF port. The RF simulation will then use these frequency and power levels

to determine the time waveforms at the IF port, using a SPICE modelling of the diode and the circuit. Figure 5.10 shows the typical measurements that can be made on a mixer. The first one is the conversion loss.

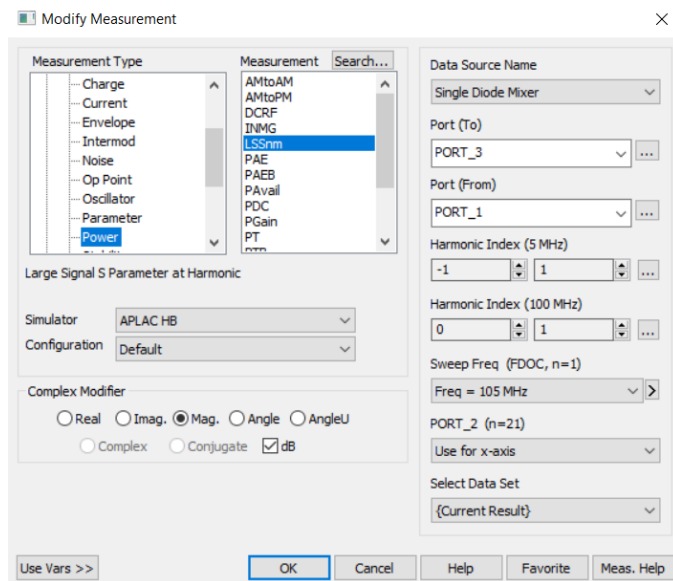


Figure 5.11. Parameters for conversion loss measurements.

When using Harmonic Balance (HB) for highly nonlinear circuits, such as a mixer, as shown in figure 5.11 for determining the conversion loss, it is important to include many harmonics and IM products, say up to the 7th or 9th order. Even though most of these IM products will fall outside the frequency range of interest, there will still be some falling inside the required bandwidth and will this affect the accuracy of the results produced by the simulation. If in doubt, simply increase the order of the harmonics and IM to be analysed and note any changes in the simulated results. As the speed of computers and the efficiency of the Harmonic Balance calculations increases, there is less cost in erring on the side of calculating an excess of harmonic and IM components. For the figures in this chapter, the Harmonic Balance settings use 9 harmonics for tone 1, tone 2 and tone 3 are used for the HB analysis. Different spectra result, when these values or the default values are used and when APLAC HB or Harmonic Balance (legacy) are used and when the harmonic order is limited to 9 orders or is not limited. Those changes are easily be observed and only effect small IM amplitudes. The 2015 edition of this book uses the APLAC HB simulator, since the Harmonic Balance simulator that was used in the 2013 edition is now a legacy product.

The conversion loss of the mixer can be determined as the LO power level is varied, by setting the relevant parameters of the PORT_PS1 element to provide a power level sweep at the LO port. The sum or difference frequency that is analysed for determining the conversion loss is set by the parameters for the Large Signal S parameter (LSSnm) measurement shown in figure 5.11. The conversion loss is determined as the ratio of the power levels at the specified frequencies of port 1 as input and port 3 as output.

For a realistic determination of performance of the frequency mixer, a LO frequency of 105 MHz and an RF frequency of 100 MHz with a level of -5 dBm is chosen. The project frequency is set as a single frequency at 105 MHz. If a range of frequencies is specified, then one or all of these can be used for the conversion loss calculations. It is thus possible to determine the conversion loss for a range of LO frequencies as well. For a LO input at

105 MHz and an RF input at 100 MHz, the desired IF output is at 5 MHz. The appropriate harmonic index combinations are selected such that the input is at 100 MHz and the output is at 5 MHz, as indicated in figure 5.11. MWO automatically calculates the relevant frequency as the harmonic indices are changed.

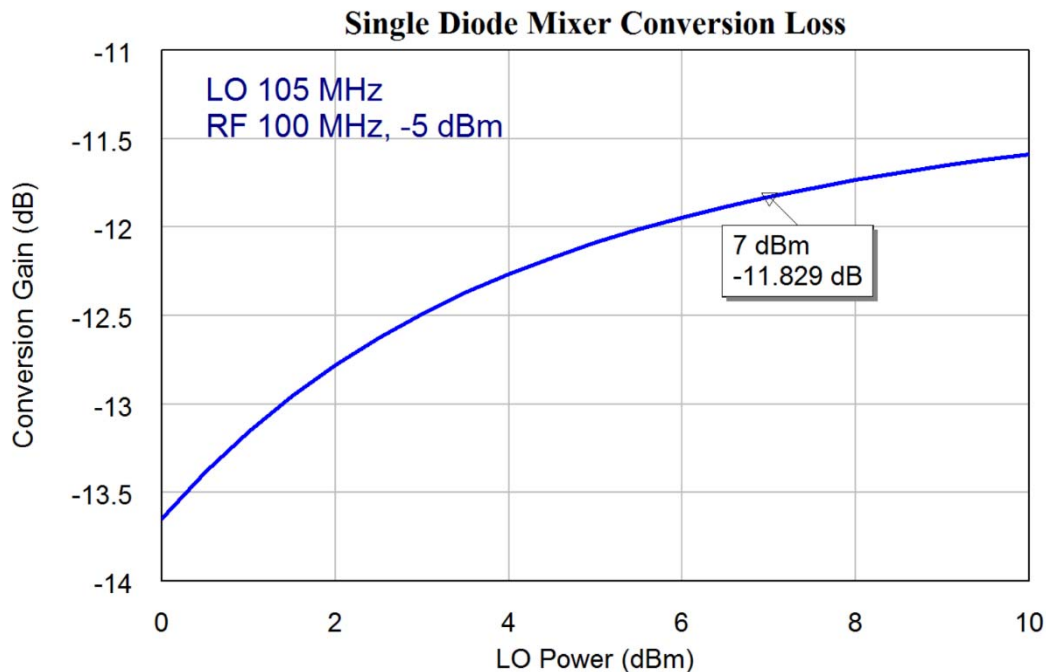


Figure 5.12. Conversion loss of a single diode down-conversion mixer.

Figure 5.12 shows the resulting conversion loss as a function of LO power level for the single diode mixer of figure 5.9. Note that the conversion loss decreases with an increasing LO drive level. A higher LO power level increases the power consumption of the mixer, requires a higher power LO source and dissipates more heat. By comparing figures 5.12 and 5.21, it can be seen that the conversion loss of the single diode mixer is very poor.

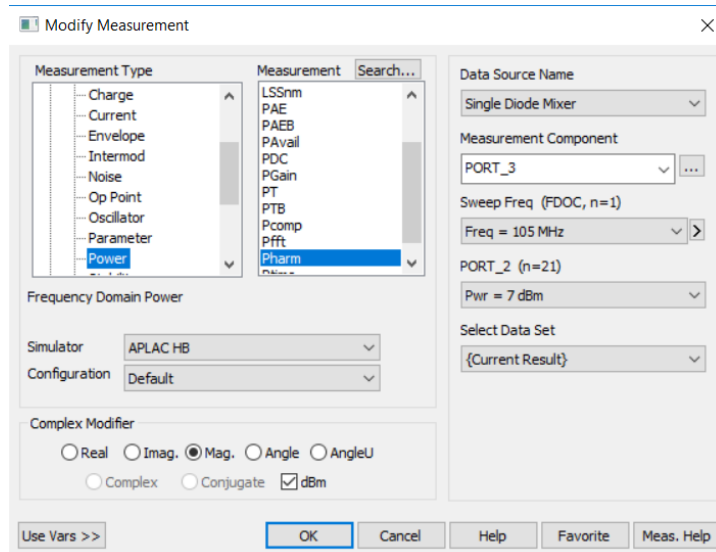


Figure 5.13. Frequency domain power measurement.

The IF spectrum can be determined using the Frequency Domain Power Measurement shown in figure 5.13. The waveform at the IF port is determined using the harmonic balance simulator. The spectral components are determined from that waveform. Figure 5.14 shows the resulting IF spectrum for an input power at the LO port of +6 dBm. It is possible to select other values or to plot the spectra for a sweep of power values.

In figure 5.13, the desired 5 MHz component is -16.6 dBm. Since the RF signal is -5 dBm, the conversion loss is 11.6 dB. The LO signal at 105 MHz is 7 dBm and the LO signal at the IF port is -30.26 dB. The LO to IF isolation is thus 37.26 dB. The RF signal at 100 MHz is -5 dBm and the RF signal appearing at the IF port is -28.66 dBm. The RF to IF isolation is thus 23.66 dB. Comparing this with the corresponding figure 5.22 for the balanced mixer, and figure 5.32 for the double balanced mixer, it can be seen that the conversion loss, the levels of the harmonics and the isolation produced by the single diode mixer are significantly worse than those of balanced mixers.

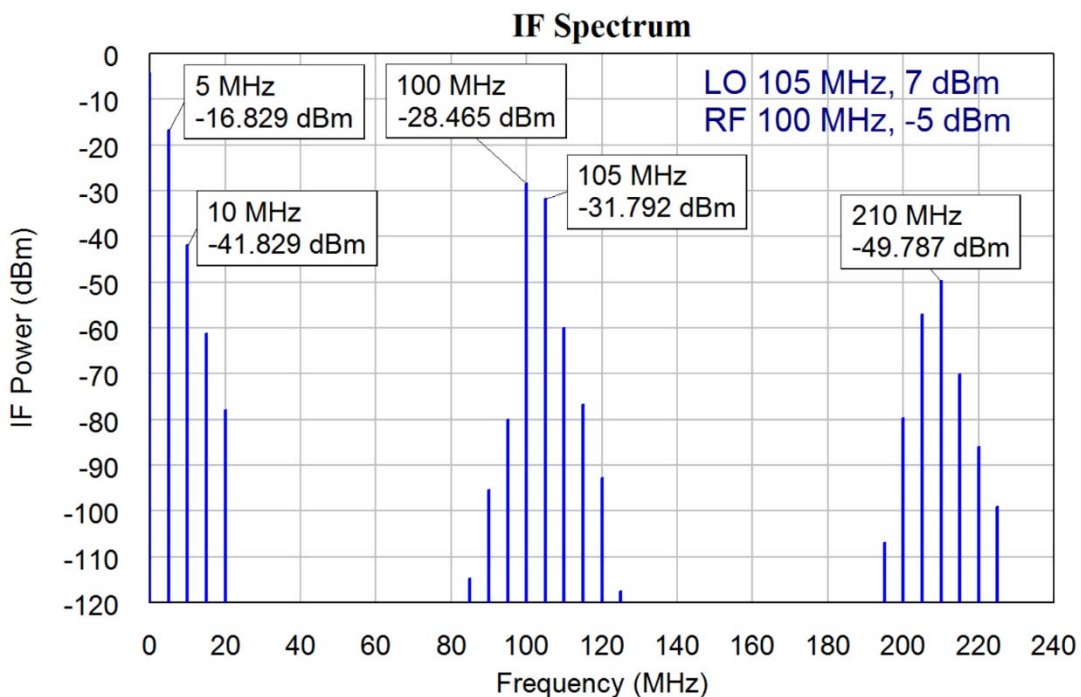


Figure 5.14. IF spectrum of a single diode mixer as a down-converter.

If a two-tone RF input signal is used, the single diode mixer has a high level of IM components. As a result, the single diode mixer requires more stringent RF filtering to avoid those IM signals being generated by the mixer and appearing in the IF output. The single diode mixer also requires more stringent IF filtering to remove those unwanted IF components from the IF signal, to prevent the unwanted signals from affecting the demodulated output from the receiver. Most AM radios use single diode mixers and this is one reason why their performance is poor compared to FM radios.

The voltage and current time waveforms can also be determined, using the Vtime and Itime measurements. The measurements can be done at a single LO power level or at a range of levels as is done by selecting plot all traces instead of the 0 dBm level in the Port_2 entry of the Itime measurement window shown in figure 5.15. Alternately, as has been done in this project, a limited power sweep can be obtained by performing multiple single level measurements as shown in figure 5.10.

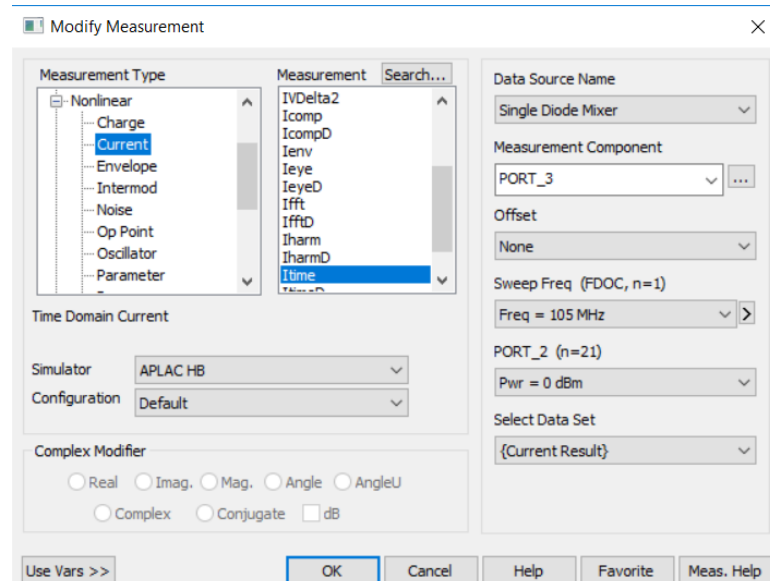


Figure 5.15. Itime measurement setting.

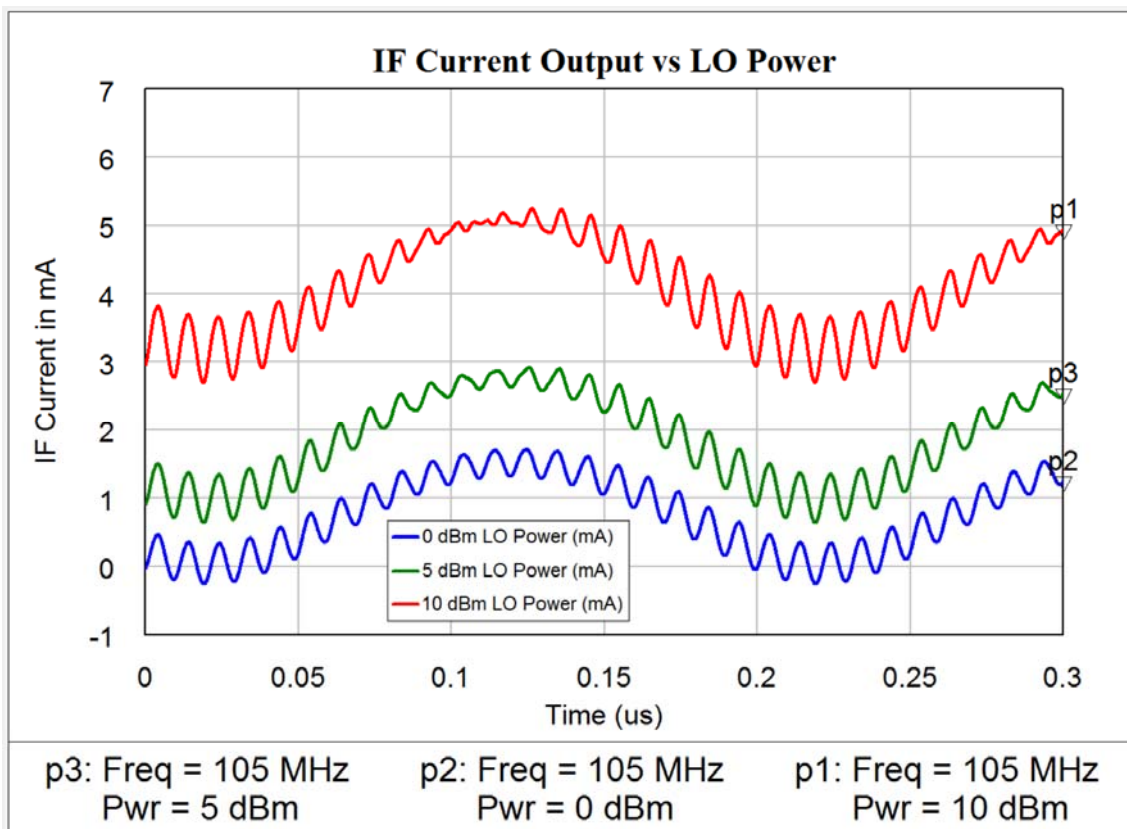


Figure 5.16. IF currents for a single diode mixer as a down-converter.

Figure 5.16 shows the resulting IF currents of a single diode mixer, notice with the 2nd order filters used in the diplexer, there is still significant RF current components present in the IF signal. A higher order filter will improve the isolation, but will not improve the performance sufficiently to justify the additional cost. For the frequencies used, the output spectra and conversion loss will be the same if higher order diplexer filters are used. As can be seen from figure 5.16, the single diode mixer has a significant DC current component, which changes with LO drive level.

To operate the frequency mixer as an up-converter, the PORTF element is applied to the IF port and the signal generated by that port is set to 5 MHz and a power of -5 dBm. The mixer output is then at the RF port. Figure 5.17 shows the resulting circuit diagram for the single diode mixer as an up-converter. The same measurements can be performed for the down-converter.

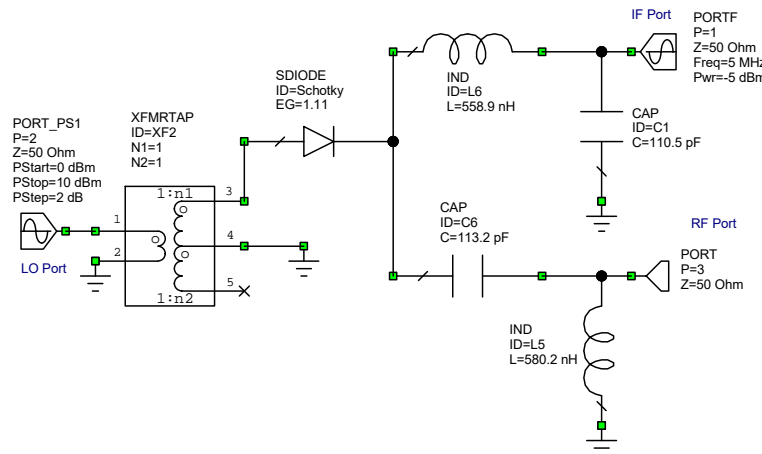


Figure 5.17. Circuit diagram of a single diode mixer as an up-converter.

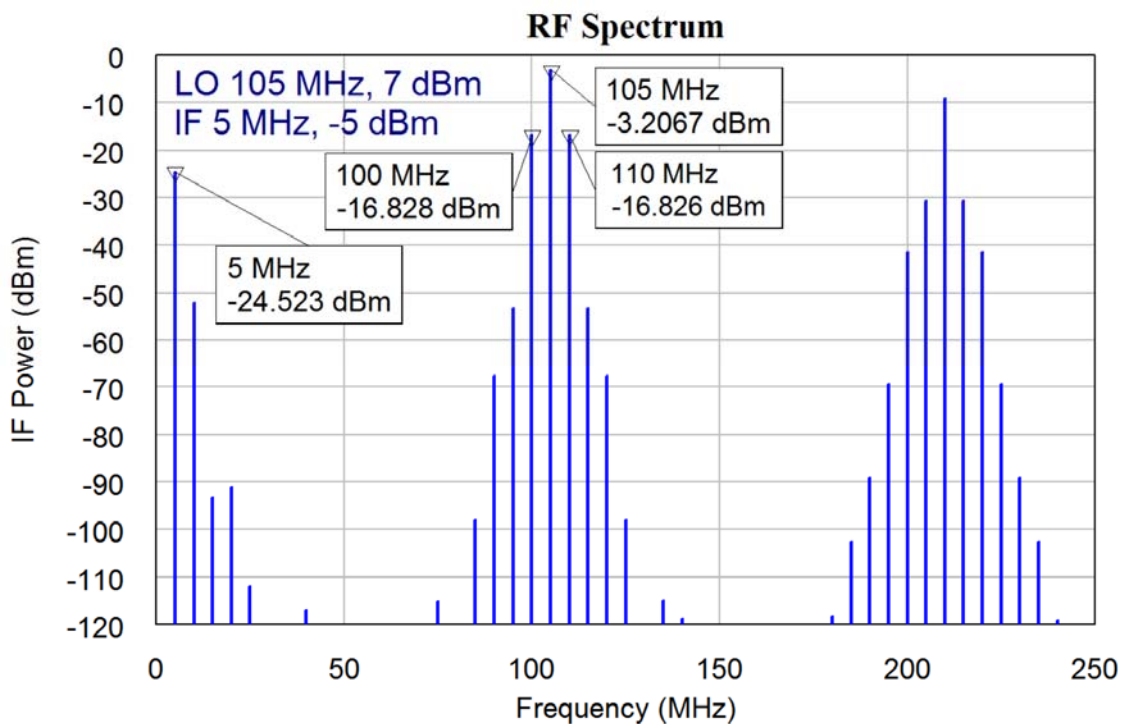


Figure 5.18. RF spectrum of a single diode mixer as an up-converter.

The RF output spectrum is shown in figure 5.18. From this spectrum, it can be seen that the conversion loss, being the amplitude of the 100 MHz RF component due to the 5 MHz IF signal is the same as for the down-converter. The components around 100 MHz show a large 105 MHz LO component in the RF output, indicating only an 8.6 dB LO-RF isolation. The LO spectral component at the RF port is larger than any of the wanted components. The second harmonic components at 90 MHz and 110 MHz are slightly

asymmetrical. There are significant components at harmonics of the LO frequency, which must be filtered out in most practical applications.

The RF current waveforms can be determined using the Itime measurement in a similar manner as for the down-converter shown in figure 5.16. The results for the up-converter are shown in figure 5.19 and are highly asymmetrical. The waveform is rich in harmonics as can be seen from the spectrum of figure 5.18.

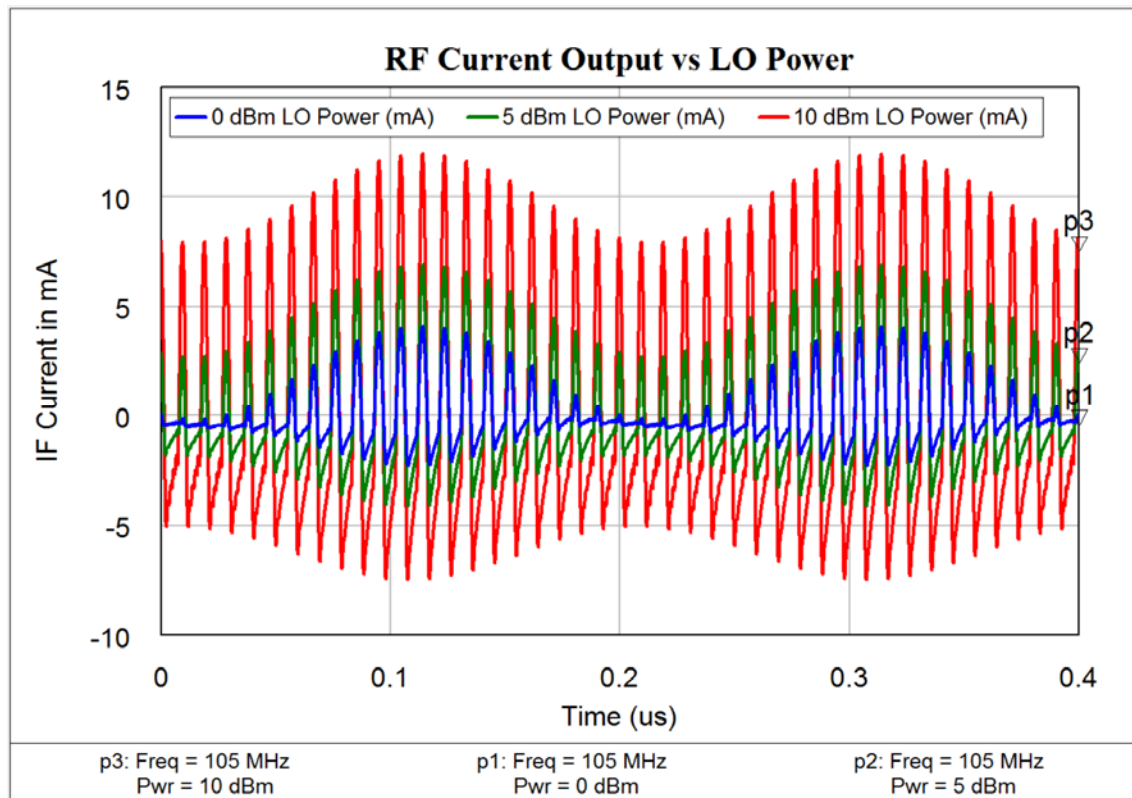


Figure 5.19. RF currents for a single diode mixer as an up-converter.

Advantages of single diode mixers:

1. They can be used at very high (microwave) frequencies.
2. They have a low cost, using only one diode.

Disadvantages of single diode mixers:

3. They have a high conversion loss.
4. A high level of unwanted components are generated. These must be filtered out using additional circuitry.
5. There is no RF to LO isolation, IF to LO and IF to RF isolation only due to diplexer.

Balanced Mixer

Adding a second diode to the circuit shown in figure 5.20 results in a balanced mixer. The first diode has $V_a + V_b$ across it and the second diode has $V_a - V_b$ where voltage V_a is the LO and V_b is the RF voltage. The currents through the diodes are thus:

$$I_{D1} = a_0 + a_1(V_a + V_b) + a_2(V_a + V_b)^2 + a_3(V_a + V_b)^3 + a_4(V_a + V_b)^4 + a_5(V_a + V_b)^5 + \dots \quad \text{Eqn. 8}$$

$$I_{D2} = a_0 + a_1(V_a - V_b) + a_2(V_a - V_b)^2 - a_3(V_a - V_b)^3 + a_4(V_a - V_b)^4 + a_5(V_a - V_b)^5 + \dots$$
Eqn. 9

The difference between the diode currents flows into the IF port and RF port, so that the current flowing through the IF and RF port is:

$$I_{IF-RF} = I_{D1} - I_{D2} = +2a_1V_b + 4a_2V_aV_b + 6a_3V_a^2V_b + 2V_b^3 + 8a_4(V_a^3V_b + V_aV_b^3) + 10a_5V_a^4V_b + 20a_5V_a^2V_b^3 + 2a_5V_b^5 + \dots$$
Eqn. 10

For a single diode mixer the current through the IF and RF port is the same as is shown in equation 8. Comparing equation 10 with equation 8, shows that most of the unwanted components cancel. The only components that are in the IF band are:

$$I_{IF} = 4a_2V_aV_b + 8a_4(V_a^3V_b + V_aV_b^3) + \dots$$
Eqn. 11

Which is close to ideal multiplication as the a_4 term is normally very small.

Since the LO voltage, $V_a \gg$ the RF voltage, V_b , the V_aV_b and the $V_a^3V_b$ terms dominate. The V_b and the $V_a^2V_b$ terms do not produce any frequency components in the region of interest. For an ideal frequency mixer one wants the a, c, d and e components to be as small as possible, the manufacturers of mixers ensure their diodes satisfy this as much as possible. The balanced mixer will thus have a much better performance than the single diode mixer.

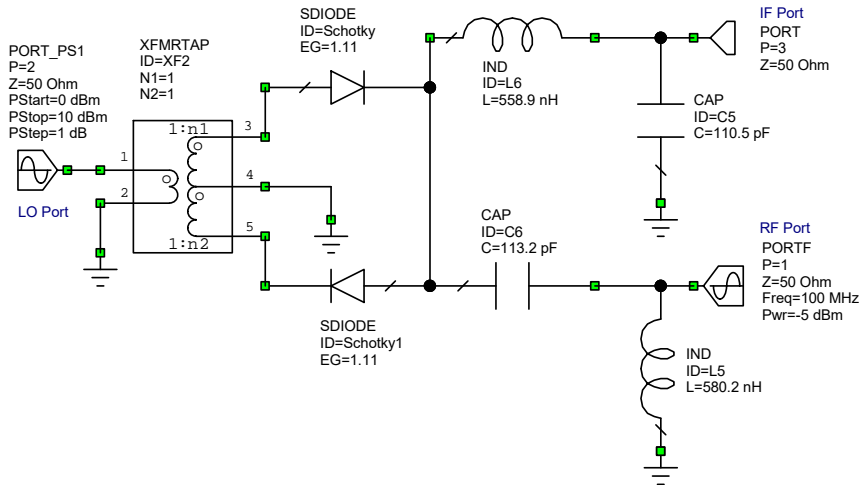


Figure 5.20. Circuit diagram of a balanced mixer.

The circuit diagram of the balanced mixer is shown in figure 5.20. The only difference between that and the circuit for the single diode mixer of figure 5.9 is the use of the second diode, but having the second diode results in a significant performance improvement.

The conversion loss of the frequency mixer is shown in figure 5.21. The conversion loss is far less than that of a single diode mixer. For LO levels of around 7 dBm, any variation in LO power does not cause any change in conversion loss, so that the mixer is then very insensitive to AM noise of the LO. This is an important advantage of the balanced mixer over the single diode mixer, or even the Gilbert Cell mixer shown in figure 5.50 later in this chapter.

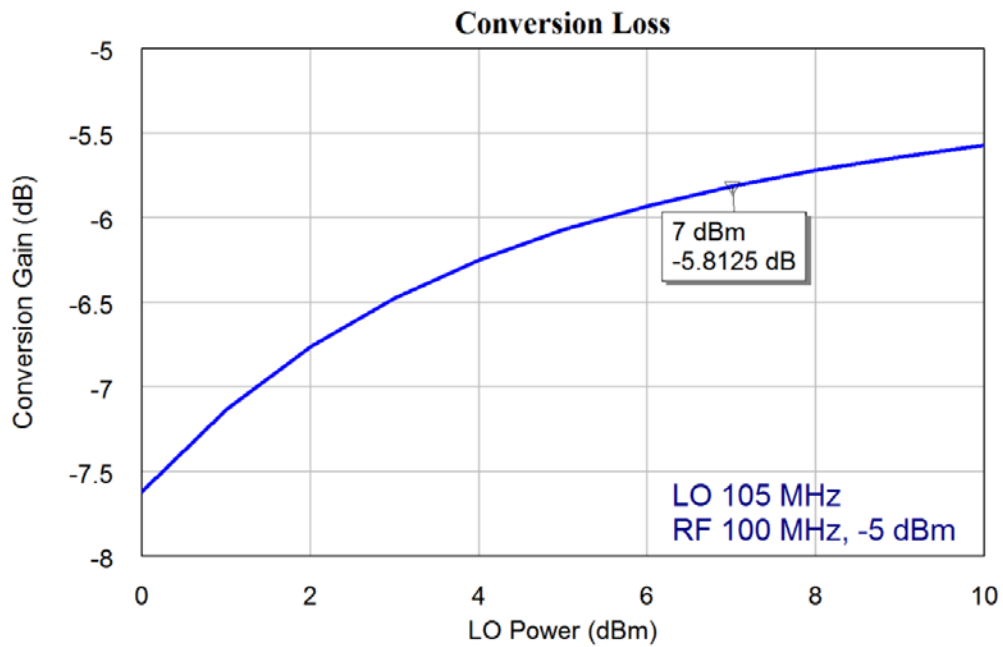


Figure 5.21. Conversion gain of a balanced diode mixer.

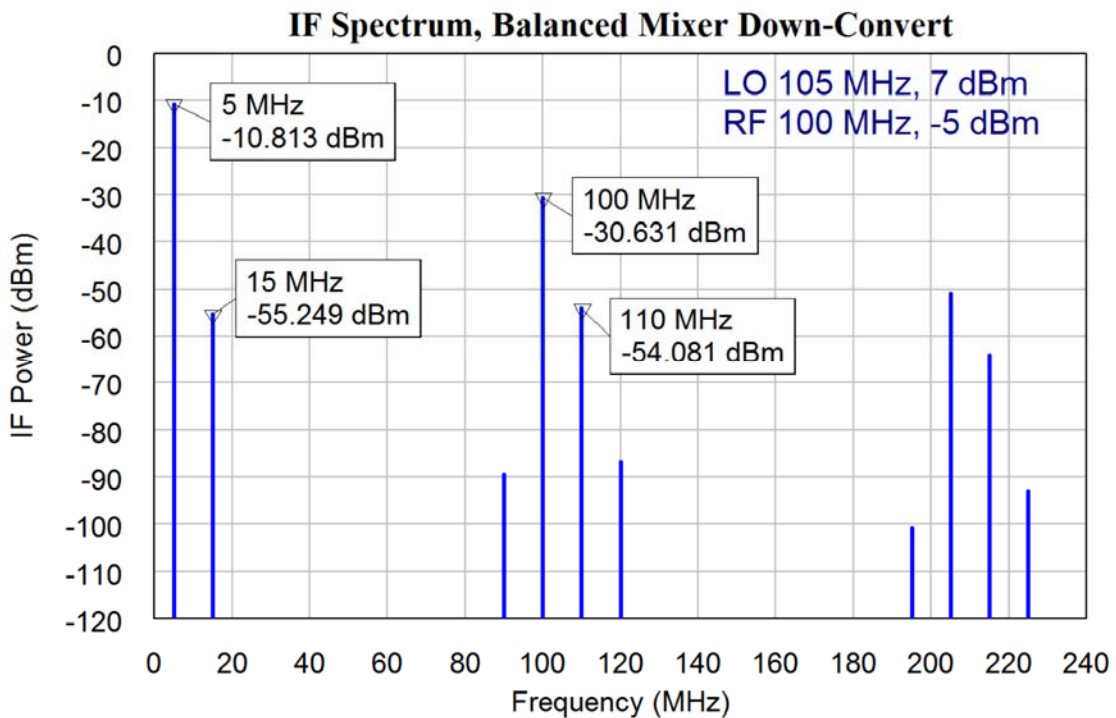


Figure 5.22. IF spectrum of a balanced diode mixer as a down-converter.

Figure 5.22 shows the IF spectrum of the balanced mixer. As expected from the equation 10, many of the unwanted spectral components have significantly reduced amplitudes compared with the single diode mixer. The second harmonic of the desired IF signal, at 10 MHz, is caused by the mixing process and is about 45 dB below the desired 5 MHz signal. The LO signal appearing in the IF spectrum is extremely small (-304.8 dB in the isolation plot). Bert Henderson shows that these harmonic levels depend on the diodes class [3], which determines the mixer LO level required. The isolation depends on how well the diodes are matched. In the computer simulation, the diodes are identical. In hardware, this is not the case.

The RF signal appearing at the IF port is -30.631 dBm. Since the RF signal is -5 dBm, The RF to IF is isolation is 25.6 dB. This can only be improved by using a higher order diplexer as part of the mixer, or by using another mixer configuration like the double balanced mixer.

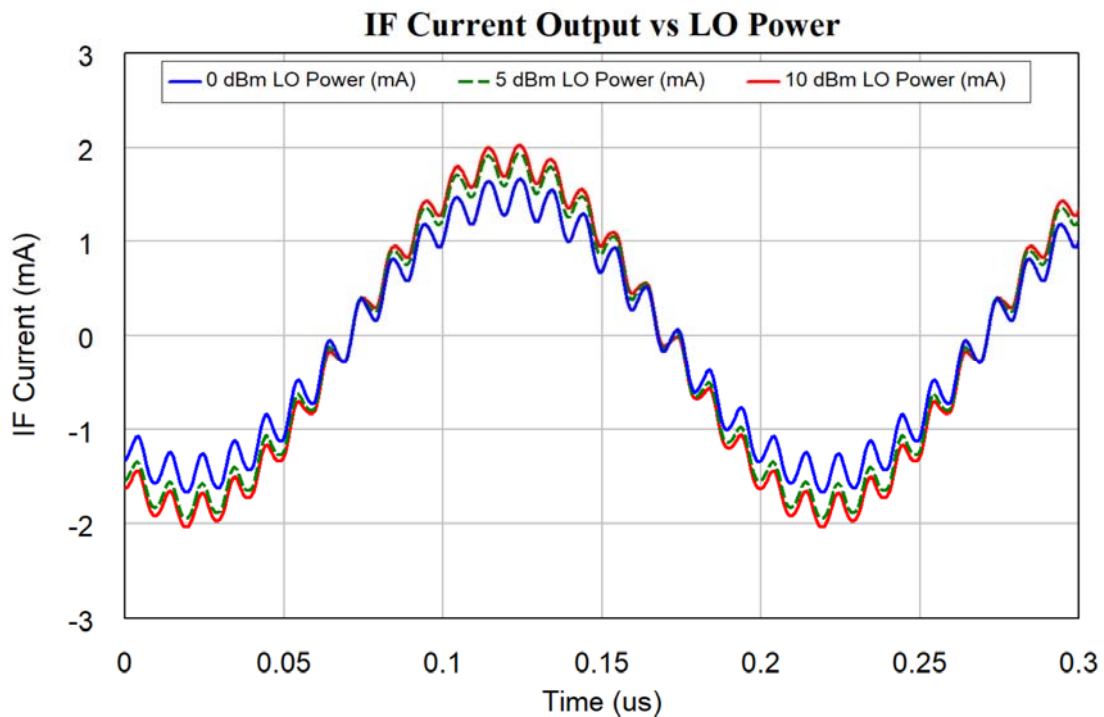


Figure 5.23. IF currents for a balanced diode mixer as a down-converter.

Figure 5.23 shows the IF currents for the balanced mixer and it can be seen that the waveforms are much more like a pure sine wave than the corresponding waveforms for the single diode mixer. With the second order filters used in the diplexer, there are still some RF signals present at the IF output but they are small enough not to cause any problems. As expected from equation 10, the balanced diodes mixer has no DC component produced at the IF port, in contrast to the single diode mixer.

Figure 5.24 shows the performance of the balanced mixer as an up-converter. It can be seen that a near ideal frequency mixer performance is obtained, with all the unwanted components more than 40 dB below the wanted components. This is good enough for practical applications. The 3IM components increase 3 dB for every 1 dB increase in the RF and IF levels. The RF level can thus be varied to obtain the specified 3IM performance, thereby maximising IF signal and the dynamic range. The LO feed-through at the RF port can be minimised by adding a very small DC signal to the IF port and adjusting that DC signal to cancel the LO signal at the RF port. This cancellation is temperature dependent, since the diode characteristics change slightly with temperature.

Figure 5.25 shows the RF currents for the balanced mixer. These waveforms closely resemble the ideal double balanced waveforms obtained by considering the frequency mixer as a multiplier. The results from the simulation closely agree with those obtained in practice. There are however still some IF components present, which are due to the limited RF-IF isolation caused by the diplexer. The Double Balanced mixer overcomes those limitations.

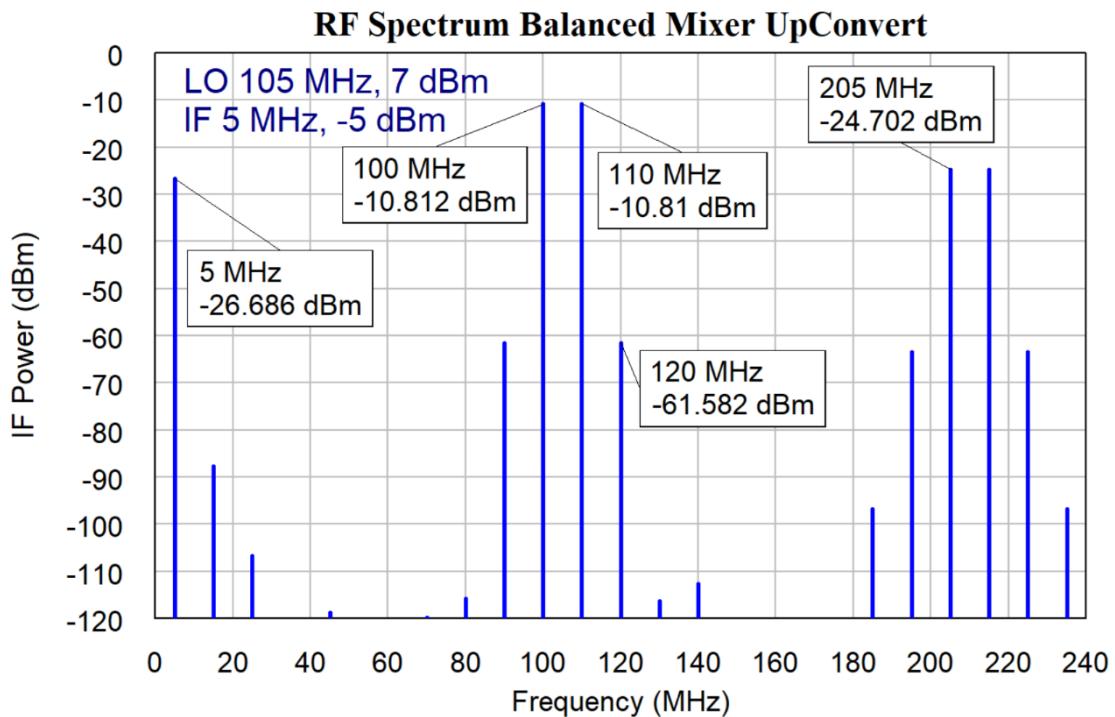


Figure 5.24. RF spectrum of a balanced diode mixer as an up-converter.

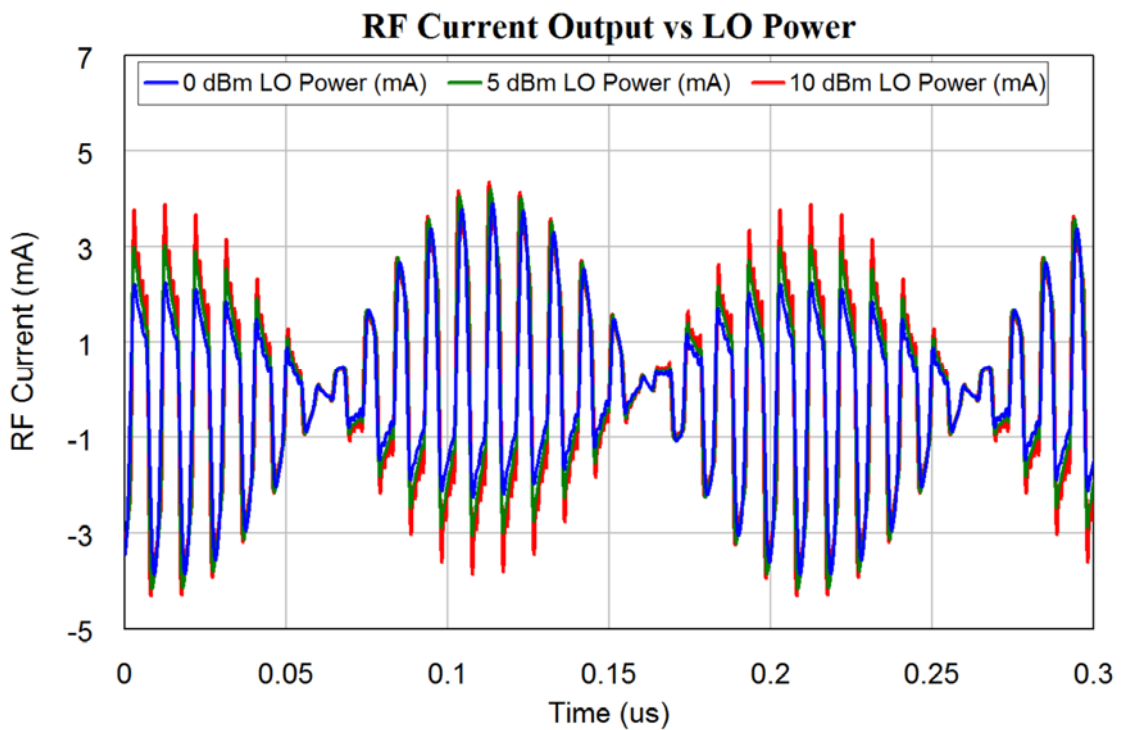


Figure 5.25. RF currents for a balanced diode mixer as an up-converter.

Double Balanced Mixer

Double balanced mixers, together with the active mixers are the dominant frequency mixers used in non-consumer oriented transmitters and receivers. There are several companies making double balanced mixers, Mini-Circuits is one of the largest of these. Part of the web pages of their mixer catalogue is shown in figures 5.26 and 5.27.

Frequency Mixers, Plug-In & Flatpack, Level 7, 500 Hz to 4.3 GHz

Model Number	Case Style	RF/LD Freq. Low (MHz)	RF/LD Freq. High (MHz)	IF Freq. Low (MHz)	IF Freq. High (MHz)	Conv. Loss (dB) Typ.	Conv. Loss (dB) Max.	Conv. Loss (dB) Min.	LO-RF Isolation (dB) Typ.	LO-IF Isolation (dB) Typ.
ASK-1+	W38	1.0	600.0	DC	600.0	5.58	0.06	8.5	35.0	30.0
ASK-1-KX81+	KX81	1.0	600.0	DC	600.0	5.58	0.06	8.5	35.0	30.0
ASK-1-X65+	X65	1.0	600.0	DC	600.0	5.58	0.06	8.5	35.0	30.0
SAM-1+	A03	1.0	600.0	DC	600.0	5.67	0.05	8.5	45.0	40.0
SBL-1+	A06	1.0	500.0	DC	500.0	5.6	0.09	8.0	45.0	40.0
SBL-11+	A06	0.1	400.0	DC	400.0	4.84	0.04	8.0	45.0	40.0
SBL-1X+	A06	10.0	1000.0	5.0	500.0	5.88	0.1	8.0	40.0	40.0
SBL-3+	A06	0.025	200.0	DC	200.0	4.81	0.05	8.5	45.0	40.0
SBL-11+	A06	5.0	2000.0	10.0	600.0	7.08	0.11	9.0	35.0	30.0
SRA-1+	A01	0.5	500.0	DC	500.0	5.11	0.09	8.5	45.0	40.0
SRA-1-1+	A01	0.1	500.0	DC	500.0	4.81	0.11	8.5	45.0	40.0
SRA-1W+	A01	1.0	750.0	DC	750.0	5.8	0.04	8.5	45.0	40.0
SRA-2+	A01	1.0	1000.0	0.5	500.0	5.66	0.07	8.5	35.0	30.0
SRA-3+	A01	0.025	200.0	DC	200.0	4.61	0.06	8.5	45.0	40.0
SRA-5+	A06	5.0	1500.0	10.0	600.0	6.69	0.07	8.5	35.0	30.0
SRA-6+	A01	0.003	100.0	DC	100.0	4.58	0.05	8.5	45.0	40.0
SRA-8+	A01	5.0E-4	18.0	DC	18.0	5.69	0.11	8.5	50.0	50.0
SRA-11+	A06	5.0	2000.0	10.0	600.0	6.72	0.07	9.0	35.0	30.0
SRA-12+	A06	800.0	1250.0	50.0	90.0	6.21	0.13	7.5	35.0	30.0
SRA-2000+	A06	100.0	2000.0	DC	600.0	8.6	0.13	9.5	37.0	30.0
SRA-2400+	A06	750.0	2400.0	DC	400.0	5.95	0.26	9.0	38.0	30.0
SRA-3500+	A06	500.0	3500.0	DC	1000.0	7.28	0.31	9.5	30.0	29.0
TAK-5+	A04	0.01	250.0	DC	250.0	4.65	0.02	8.5	50.0	45.0
TAK-6+	A04	0.5	600.0	DC	600.0	5.58	0.04	8.5	50.0	45.0
TFM-2+	B02	1.0	1000.0	DC	1000.0	5.74	0.07	8.5	40.0	35.0
TFM-3+	B02	0.04	400.0	DC	400.0	4.7	0.06	8.0	50.0	45.0
TFM-4+	B02	5.0	1250.0	DC	1250.0	6.47	0.05	8.5	40.0	35.0
TFM-11+	B13	1.0	2000.0	5.0	600.0	7.16	0.07	9.0	35.0	27.0
TFM-12+	B13	800.0	1250.0	50.0	90.0	6.86	0.14	7.5	35.0	30.0
TFM-2400+	B13	750.0	2400.0	DC	400.0	6.65	0.2	9.0	30.0	30.0
TFM-4300+	B13	300.0	4300.0	DC	800.0	5.87	0.13	10.5	30.0	15.0
TSM-3+	A11	0.1	500.0	DC	500.0	4.75	0.04	8.5	50.0	45.0
TUF-1+	B02	2.0	600.0	DC	600.0	5.85	0.04	8.0	42.0	47.0
TUF-2+	B02	50.0	1000.0	DC	1000.0	5.85	0.07	9.0	47.0	44.0

Figure 5.26. Mini-Circuit mixer catalogue, plugin [2].

Frequency Mixers, Surface Mount, Level 7, 50 kHz to 15 GHz

Model Number	Case Style	RF in @ 1 dB Comp. (dBm) Typ.	RF/LD Freq. Low (MHz)	RF/LD Freq. High (MHz)	IF Freq. Low (MHz)	IF Freq. High (MHz)	Conv. Loss (dB) Typ.	Conv. Loss (dB) Max.	Conv. Loss (dB) Min.	LO-RF Isolation (dB) Typ.	LO-IF Isolation (dB) Typ.	IP3 (dBm) Typ.	LTCC Construction	PCB Layout Dwg Pl.
SIM-153+	HY1195	1.0	3400.0	15000.0	DC	4000.0	8.0	0.4	13.2	36.0	30.0	10.0	LTCC	239
MCA1-12G+	DZ885	1.0	3800.0	12000.0	DC	1800.0	6.2	0.1	8.0	36.0	40.0	8.0	LTCC	045
MAC-12G+	DZ1650	1.0	3800.0	12000.0	DC	1800.0	6.3	0.25	8.8	26.0	15.0	9.0	LTCC	045
SIM-14+	HY1195	1.0	3700.0	10000.0	DC	4000.0	6.3	0.2	9.5	36.0	16.0	13.0	LTCC	239
MCA1-85+	DZ885	1.0	2800.0	8500.0	DC	1250.0	5.5	0.2	8.1	40.0	13.0	13.0	LTCC	045
MAC-85+	DZ1650	1.0	2800.0	8500.0	DC	1250.0	6.1	0.15	8.2	31.0	15.0	9.0	LTCC	045
SIM-63+	HY1195	1.0	2300.0	8000.0	DC	3000.0	6.0	0.2	9.8	32.0	28.0	15.0	LTCC	239
SKY-7G (+)	BU398	1.0	2000.0	7000.0	DC	1000.0	7.0	0.1	9.8	28.0	20.0	11.0	-	056
MBA-671 (+)	SM2	1.0	2400.0	6700.0	DC	1000.0	6.5	0.1	9.2	36.0	26.0	10.0	LTCC	067
SKY-6G+	BU398	1.0	2500.0	6000.0	DC	1500.0	6.2	0.2	9.7	28.0	14.0	11.0	-	056
MCA1-60+	DZ885	1.0	1600.0	6000.0	DC	2000.0	6.3	0.2	8.3	32.0	17.0	9.0	LTCC	045
MAC-60+	DZ1650	1.0	1600.0	6000.0	DC	2000.0	6.4	0.1	8.5	35.0	15.0	10.0	LTCC	045
MBA-591 (+)	SM2	1.0	2800.0	5900.0	DC	1000.0	6.5	0.1	9.0	36.0	26.0	10.0	LTCC	067
SIM-43+	HY1195	1.0	750.0	4200.0	DC	1500.0	6.3	0.2	8.6	37.0	24.0	12.0	LTCC	239
MCA1-42+	DZ885	1.0	1000.0	4200.0	DC	1500.0	6.1	0.1	8.9	35.0	20.0	10.0	LTCC	045
MAC-42+	DZ1650	1.0	1000.0	4200.0	DC	1500.0	6.1	0.1	8.9	35.0	20.0	10.0	LTCC	045
ADE-30W+	CD542	1.0	300.0	4000.0	DC	950.0	6.8	0.2	9.8	35.0	16.0	12.0	-	052
ADE-35+	CD542	1.0	1600.0	3500.0	DC	1500.0	6.3	0.5	9.8	25.0	22.0	11.0	-	051
ADE-18W+	CD542	1.0	1750.0	3500.0	DC	700.0	5.4	0.3	8.9	33.0	12.0	11.0	-	051
RMS-30+	TT240	1.0	200.0	3000.0	DC	1000.0	6.5	0.2	9.8	27.0	20.0	11.0	-	052
LRMS-30J (+)	QQQ569	1.0	200.0	3000.0	DC	1000.0	6.8	0.3	9.8	30.0	27.0	14.0	-	083
ADE-30 (+)	CD542	1.0	200.0	3000.0	DC	1000.0	4.5	0.2	9.8	35.0	20.0	14.0	-	052
ADE-30 (+)	CD542	1.0	2300.0	7700.0	DC	400.0	5.6	0.1	7.0	36.0	26.0	13.0	-	052
ADE-30JL+	CD541	1.0	2100.0	2600.0	DC	600.0	6.0	0.25	8.8	34.0	29.0	17.0	-	051
SYM-2500+	TTT167	1.0	2500.0	DC	500.0	6.5	0.1	9.8	50.0	30.0	12.0	-	079	
SIM-11+	TTT167	1.0	1.0	2500.0	10.0	600.0	7.0	0.3	10.5	40.0	35.0	10.0	-	079
SIM-2500+	YY109	1.0	500.0	2500.0	DC	500.0	5.88	0.08	10.0	35.0	18.0	13.0	-	130
MCA1-24+	DZ885	1.0	300.0	2400.0	DC	700.0	6.1	0.1	8.9	40.0	25.0	10.0	LTCC	045
MAC-24+	DZ1650	1.0	300.0	2400.0	DC	700.0	6.0	0.1	8.8	40.0	24.0	10.0	LTCC	045
RMS-11F+	TT240	1.0	350.0	2900.0	DC	400.0	5.5	0.2	9.2	36.0	29.0	12.0	-	052
ADE-20 (+)	CD542	1.0	1500.0	2900.0	DC	300.0	5.4	0.1	7.8	31.0	28.0	14.0	-	051
ADE-11X (+)	CD542	1.0	18.0	2000.0	5.0	1000.0	7.1	0.1	9.8	36.0	37.0	9.0	-	052
RMS-11X+	TT240	1.0	5.0	1900.0	5.0	1000.0	7.1	0.1	9.8	35.0	37.0	10.0	-	052

Figure 5.27. Mini-Circuit mixer catalogue, surface mount [2].

There are many different packages styles available as can be seen from figures 5.26 and 5.27. Surface mount packages are now a lot cheaper and thus more popular. The listing of surface mount mixers in figure 5.27 has been sorted for speed and shows that surface mount Double Balanced mixers to 15 GHz are available. It is interesting to see the change in price over time for different packaging styles. As an example, for many years the price for the SRA-1, a through hole or plugin mounted mixer shown in figure 5.26, was \$1.95, now it is \$17.95. A similar performance surface mount mixer, ADE-1, shown in figure 5.27, was more expensive initially and is now \$2.55. (All these prices are in \$USA and per mixer for 100 units). Because surface-mount packages are used in the vast majority of new designs, the cost of plugin packages is increasing and the cost of surface-mount packages is decreasing. Those costs should be considered in a design.

Double balanced mixers can be used as analogue multipliers in applications like a phase detector or a true RMS power meter. For phase detection, the IF port of a double balanced mixer provides the phase output. For mixer operation, the double balanced mixer operated in an unsaturated mode. For phase detection, the mixer is operated in a saturated mode, where large signals are applied to both the LO and RF ports. In addition the IF port must be DC coupled. Mini-Circuits make *Phase Detectors*, which are optimised for phase detection.

The circuit diagram of a Double Balanced Mixer is shown in figure 5.28. The two transformers provide isolation for all ports. Four diodes are now required.

For the analysis of the mixer consists of considering what happens if a +ve input signal is applied to the IF port. Under those conditions, the diodes shown in figure 5.29 conduct and the others are an open circuit. As a result a positive signal applied to the LO port, then a positive signal is obtained at the RF port.

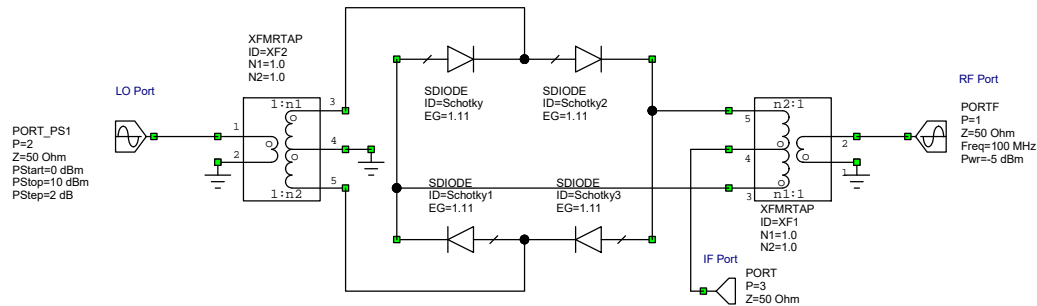


Figure 5.28. Circuit diagram of a double balanced mixer.

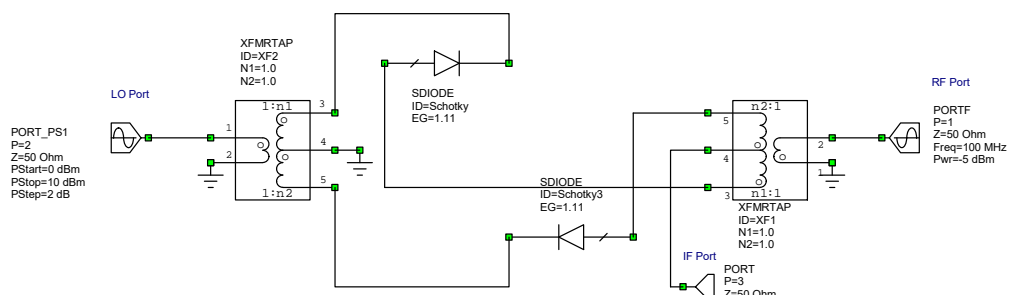


Figure 5.29 Mixer with +ve voltage applied at the IF port.

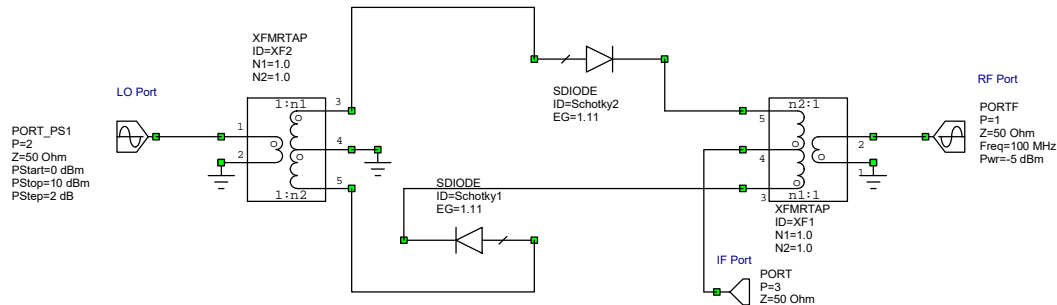


Figure 5.30. Mixer with -ve voltage applied at the IF port.

If a -ve input signal is applied to the IF port, the diodes shown in figure 5.30 conduct and the others are an open circuit. As a result if a positive signal is applied to the LO port, then a positive signal is obtained at the RF port. If a zero voltage signal is applied at the IF port all the diodes are equal resistances and the LO signal is cancelled at the RF port. In practice having a smaller IF, voltage results in a smaller RF voltage. The RF signal is thus the LO signal multiplied by the IF signal, resulting in a proper mixing action.

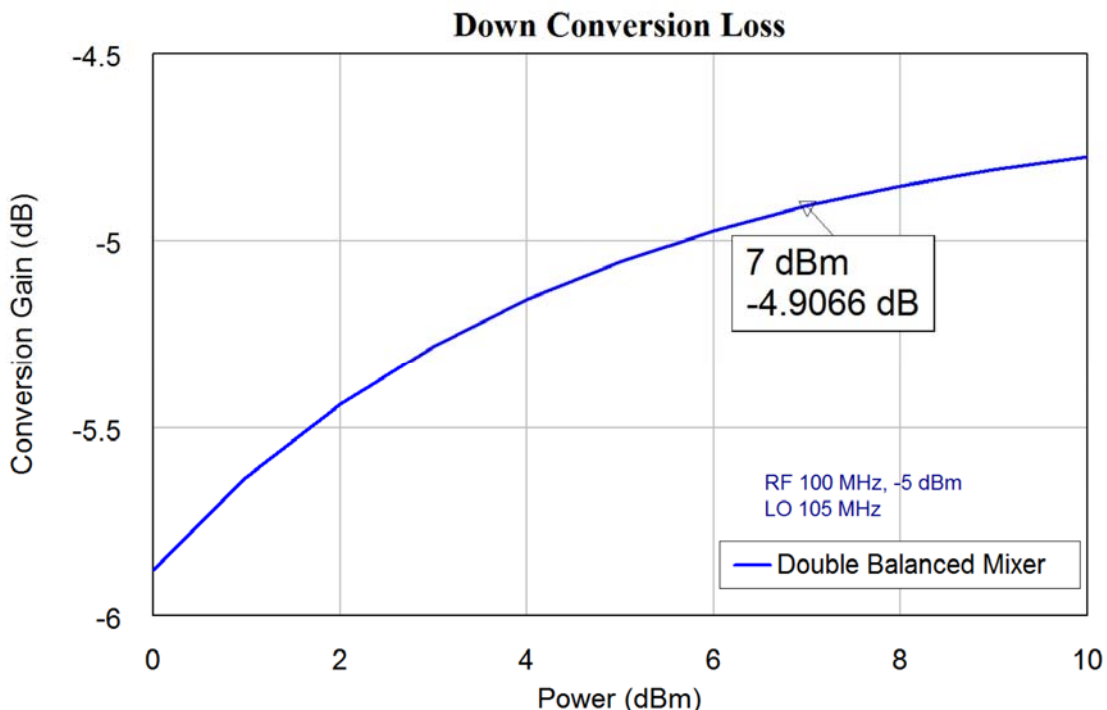


Figure 5.31. Conversion loss of a double balanced diode mixer.

Figure 5.31 shows that the conversion loss of a Double Balanced Mixer is approximately 0.5 dB less than that of a balanced mixer and more than 6 dB less than that of a single diode mixer. Comparing the IF spectrum of a down-converting Double Balanced Mixer as shown in figure 5.32 this with the corresponding figures 5.14 and 5.22 for single and balanced diode mixers, shows that only for this mixer there are no spectral components in the 80 to 120 MHz frequency range. The difference signal at 5 MHz and the sum signal at 205 MHz are the same amplitude. The signal at 215 MHz is due to the third harmonic of the input signal mixing with the local oscillator. In a receiver, these harmonic signals must be evaluated, to ensure that they do not cause signals in the IF frequency band.

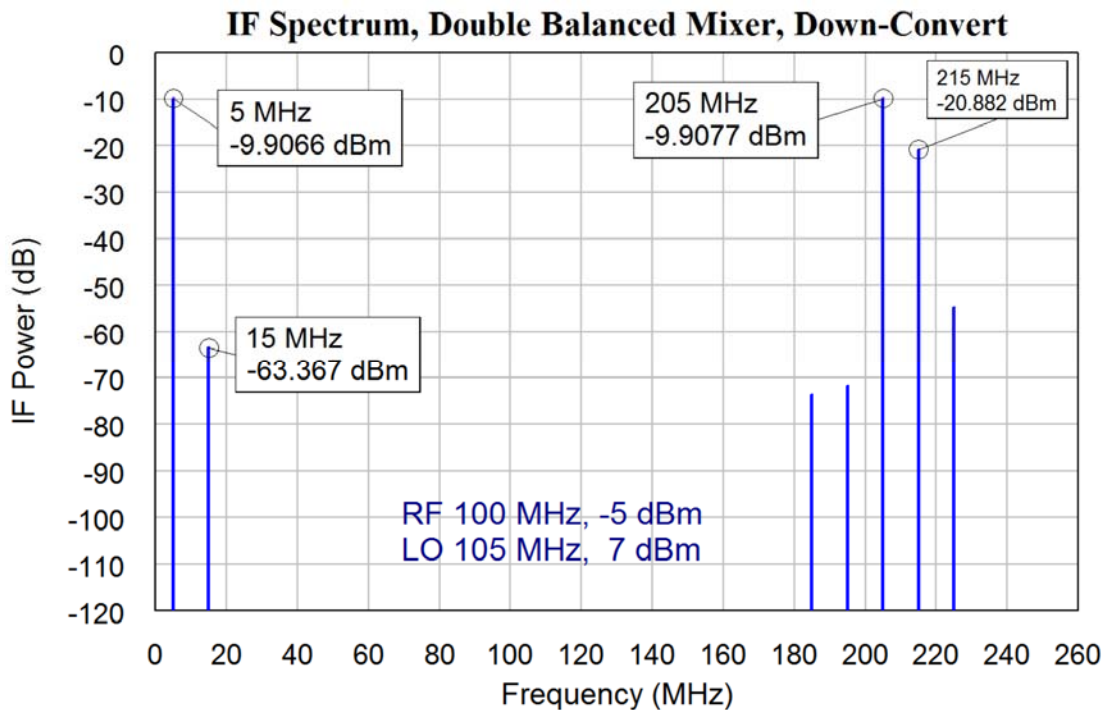


Figure 5.32. IF spectrum of a double balanced diode mixer as a down-converter.

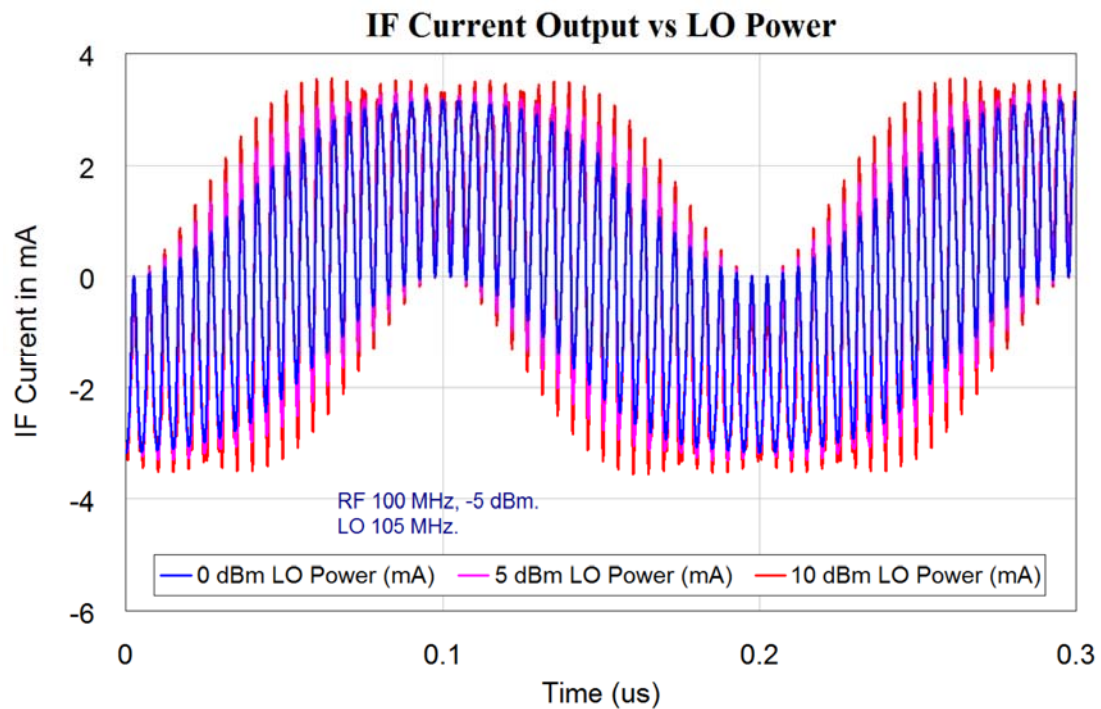


Figure 5.33. IF currents for a balanced diode mixer as a down-converter.

Figure 5.33 shows the IF currents. There is a significant high frequency content. Figure 5.34 shows the same IF currents with the IF signal passed through a 25 MHz low pass filter to remove the high frequency components. The waveform looks like an ideal Sine wave and there is little change in the output as the LO power is changed between 0 dBm and 10 dBm. The LO AM noise will thus have little effect on the IF output. Applying the low pass filter at the IF output reduces the conversion loss by 0.47 dB, due to a short circuit being presented at >25 MHz at the IF port of the mixer.

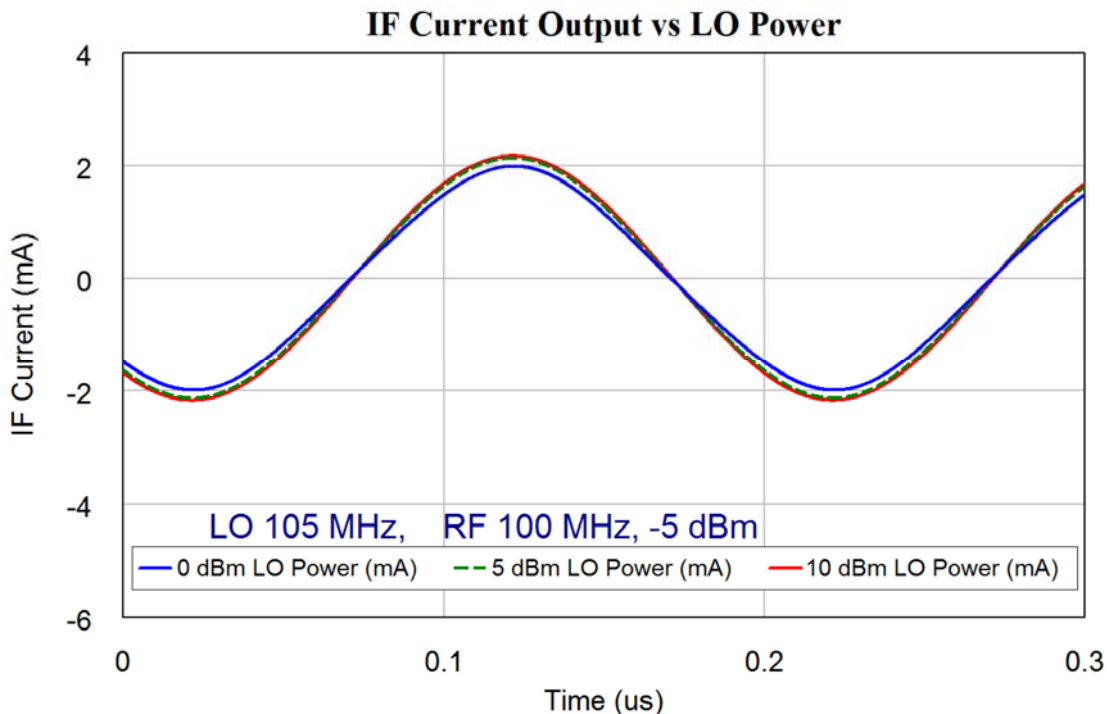


Figure 5.34. IF currents of figure 29 with frequency components >25 MHz removed.

Figure 5.35 shows the RF spectrum of a double balanced mixer as an up-converter. The desired spectrum around the 105 MHz LO is near ideal and shows no unwanted spectral components above -65 dBm. Figure 5.36 shows the corresponding RF currents. The spectrum and the waveform are very similar to that for an ideal multiplier. Note the 180° phase change in the waveforms at times $t=0.05$ and 0.15 μ s and the near constant amplitude of the RF current as the LO level is changed. This shows the mixer has a very low sensitivity to LO AM noise.

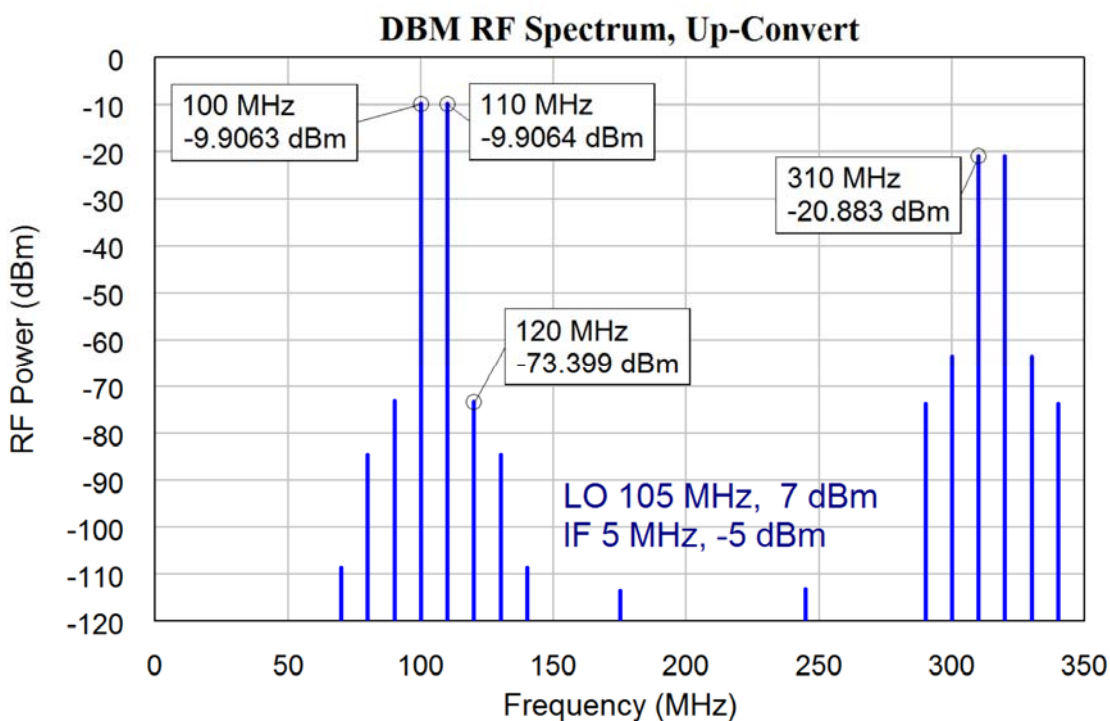


Figure 5.35. RF spectrum of a double balanced diode mixer as an up-converter.

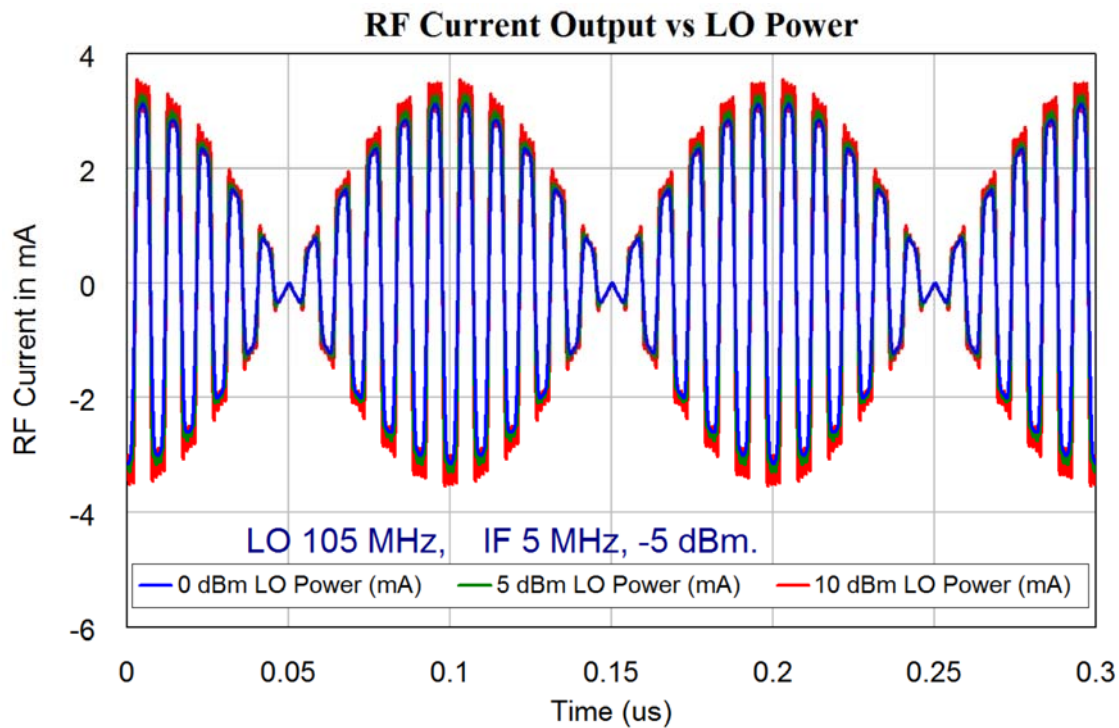


Figure 5.36. RF currents for a double Balanced Diode Mixer as an up-converter.

Figure 5.37 shows the construction of a simple home-made double balanced mixer, the transformers are held in-place with Silastic (Silicone Sealant). The diodes are conventional Shottky-Barrier diodes that have been matched for their V-I characteristic in order to obtain the best LO \Leftrightarrow RF isolation.

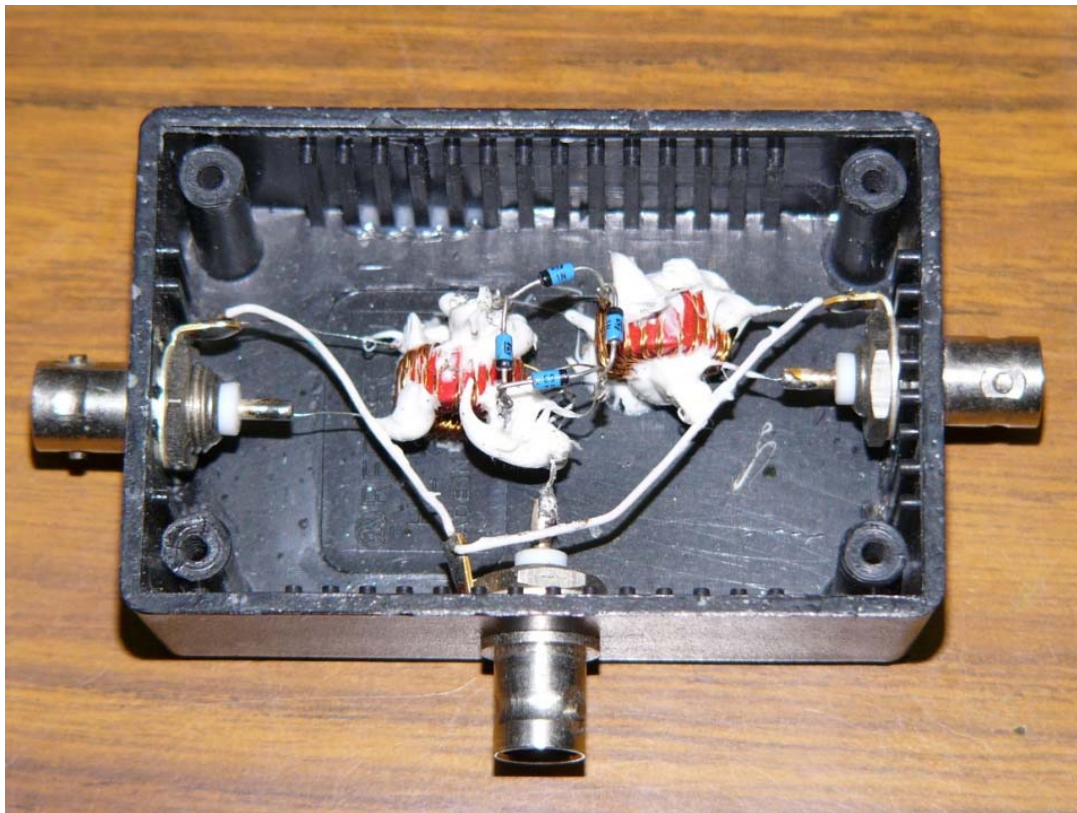


Figure 5.37. Construction of a Double Balanced Mixer for use in Practical Sessions.

The measured performance of this mixer is shown in Figure 5.38. The transformers for this mixer were designed for operation at 1 MHz. The mixer was found to perform well as a mixer for LO and RF frequencies between 20 kHz and 50 MHz. Above 50 MHz the mixer performance was good, but for up-conversion the LO carrier isolation became less. The mixer was still useful as a mixer to 100 MHz.

As a result an IF frequency of 250 kHz and an LO of 10 MHz was used for the spectrum in figure 5.38. For this figure, the LO signal had a level of +7 dBm. The IF signal was at a frequency of 250 kHz and a level of -10 dBm. The measured conversion loss is 6 dB and the LO \Rightarrow RF isolation is -60 dB. This mixer performs well for RF and LO signals in the range of 30 kHz to 30 MHz and IF signals up to 30 MHz.

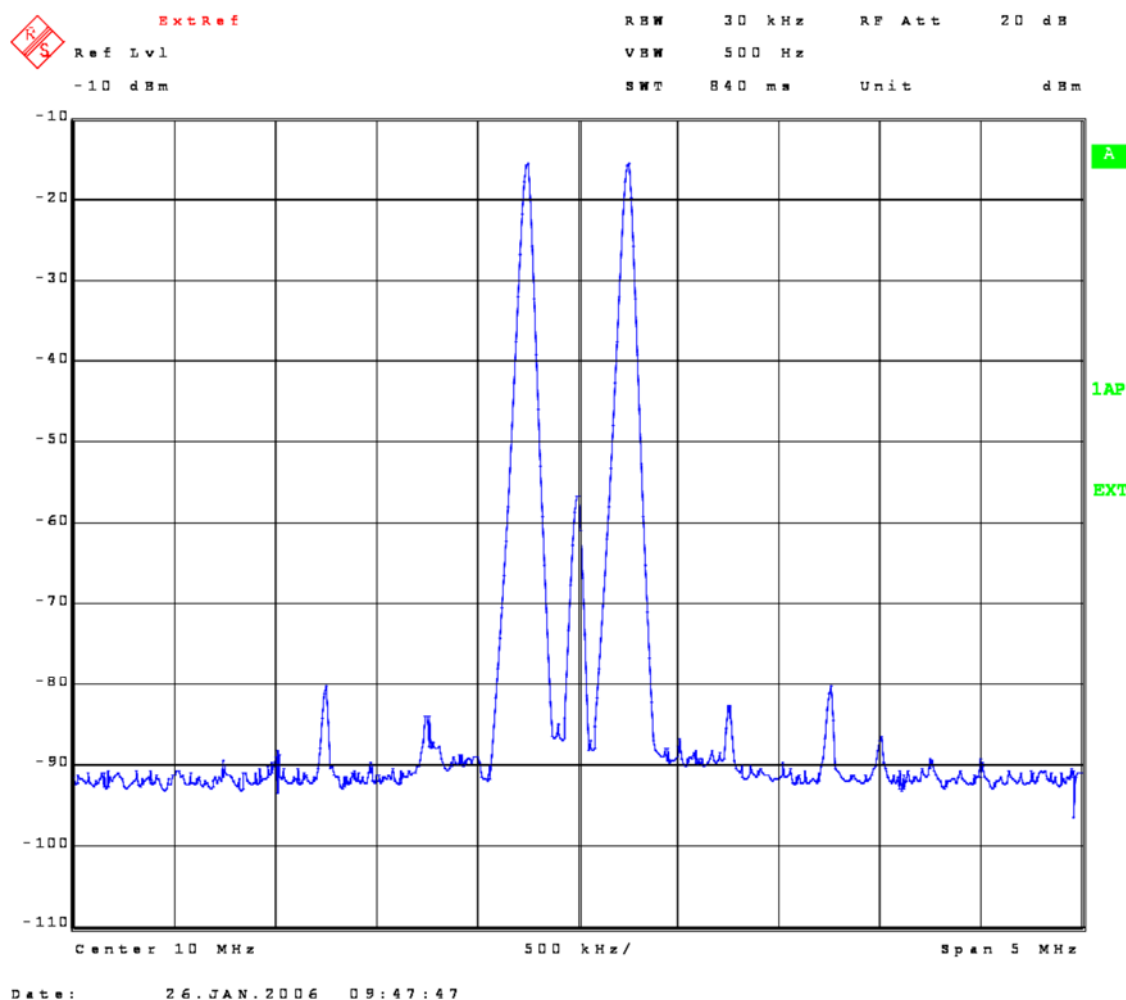


Figure 5.38. Measured performance of the mixer of figure 5.36. (Hor: Centre 10 MHz, 500 kHz/div, Vert: Max -10dBm, 10 dB/div.)

Comparing the spectrum around the LO in figure 5.38 with the corresponding spectrum around the LO in figure 5.35, shows that in practice there will be some LO \Rightarrow RF carrier feed-through due to a slight mismatch of the diodes or a slight mismatch in the signal path lengths. Such path lengths are particularly difficult to match exactly at microwave frequencies. Figure 5.38 shows that the 5IM distortion components, which are 1.250 MHz from the LO frequency at the centre of the plot, are bigger than the 3IM components, which are 750 kHz from the LO frequency.

Microwave Mixers

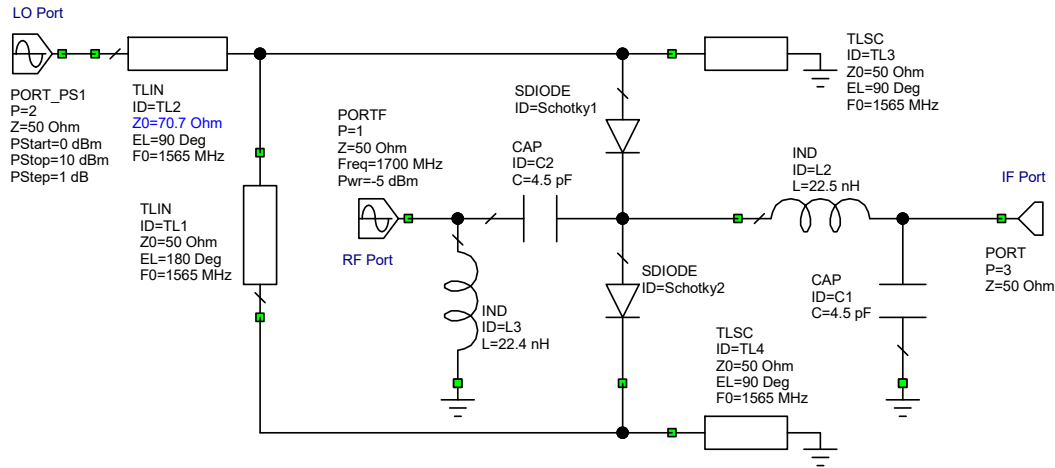


Figure 5.39. Circuit diagram of a Microwave Balanced mixer.

At microwave frequencies (>1 GHz) transformers become difficult to make. In addition, the capacitance associated with the diodes used in the mixer cause the diodes to become less efficient as a mixer. As a result, mixers at microwave frequencies have higher conversion losses than mixers used at lower frequencies. Conversion losses of 6 to 10 dB are typical. Microwave mixers have a higher insertion loss than RF mixers due to capacitances in the diodes and larger skin depth losses. The frequency dependence of the conversion loss on the RF frequency can easily be seen from [2], selecting surface mount and level 7 devices and then sorting the devices according to frequency. The ADE-6 mixer with a 250 MHz upper frequency has a conversion loss of 4.7 dB and the 15 GHz upper frequency SIM-153+ has a conversion loss of 8 db. Balanced based mixers are available for frequencies up to 90 GHz [4].

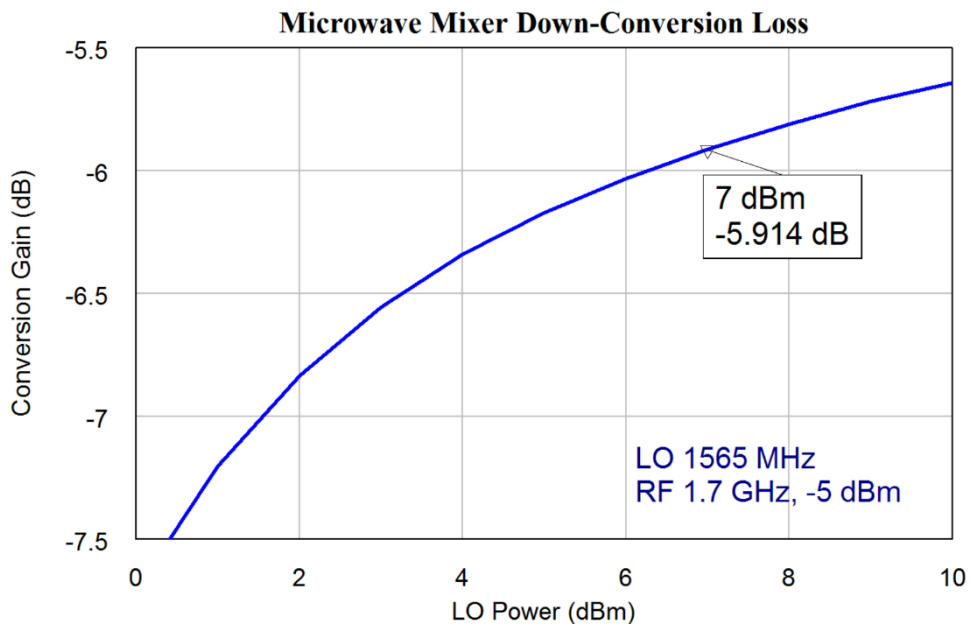


Figure 5.40. Conversion loss of a Microwave Balanced Diode mixer.

At microwave frequencies, transmission lines are often used to produce the two outputs with a 180° phase shift, to provide a replacement for the transformer in the balanced mixer shown in figure 5.20. The circuit for the corresponding microwave mixer is shown in figure 5.39. In this design, the mixer is used for a down-converter for a weather satellite receiver and uses a 1565 MHz Local Oscillator to shift a 1700 MHz RF signal to a 135 MHz IF frequency.

The conversion loss for this mixer is shown in figure 5.40, and is 0.3 dB less than the conversion loss for corresponding transformer-based mixer, shown in figure 5.21. Figure 5.41 shows the spectrum for the mixer as a down converter. The mixer performs well and the spectrum is similar to that of the transformer-based mixer in figure 5.22.

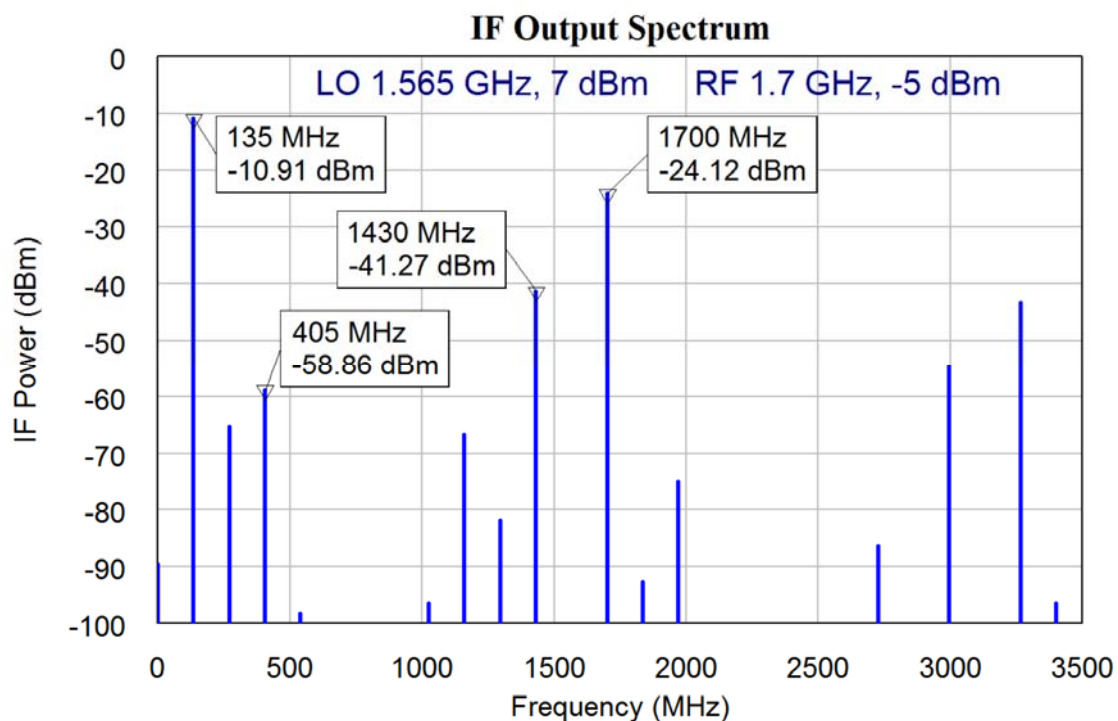


Figure 5.41. IF Spectrum of a Microwave Balanced Diode mixer as a down-converter.

Changing the transformer to a transmission line will thus not change the performance of the mixer very much apart from a reduction of the bandwidth, since the transmission line only produces a 180° phase shift at a single frequency. However, in many microwave applications the resulting bandwidth is sufficient. The mixer can also be used as an up-converter.

A transmission line, used to produce the 180° phase shift in figure 5.39 produces a linear phase shift with frequency. As shown in the lecture notes on Branchline couplers, the Branchline coupler has a nearly constant 90° phase shift over a 10% bandwidth.

The Branchline coupler can be used to produce the required phase shifts for efficient mixing as shown in figure 5.40. If the LO signal is applied at port 1 of the Branchline coupler in figure 5.42 and the RF signal is applied to port 2. The frequency of the Branchline coupler is chosen such that full isolation is obtained at the RF port for the LO signal, since the LO signal is much bigger in power than the RF signal. For a practical down-converting mixer, the LO and RF signals are within 10% of each other, so that reasonable isolation will be obtained for the RF signal at the LO port.

The signal at Port 3 will then be $LO\angle 90^\circ + RF\angle 180^\circ$ and the signal at Port 4 will be $LO\angle 180^\circ + RF\angle 90^\circ$. The phase angle between the LO and RF signals is $+90^\circ$ at Port 3 and -90° at Port 4. These are the correct conditions for obtaining balanced mixing in a down-converter.

Microwave Mixer using a Branchline Coupler

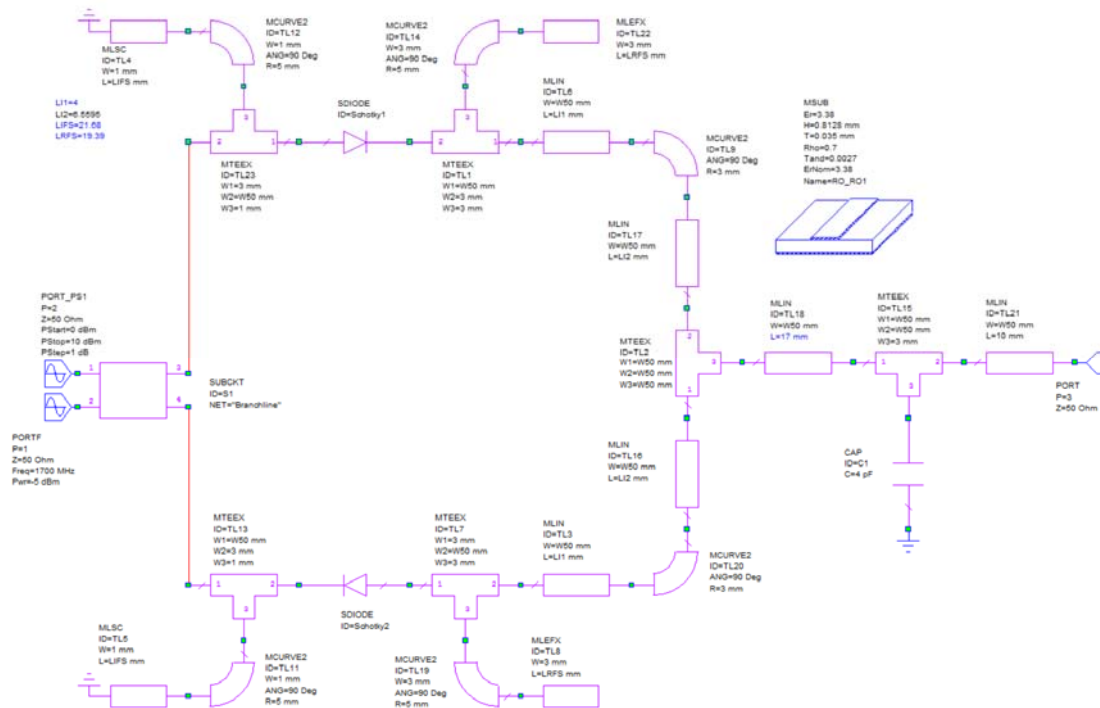


Figure 5.42. Circuit diagram of a balanced mixer with a Branchline coupler.

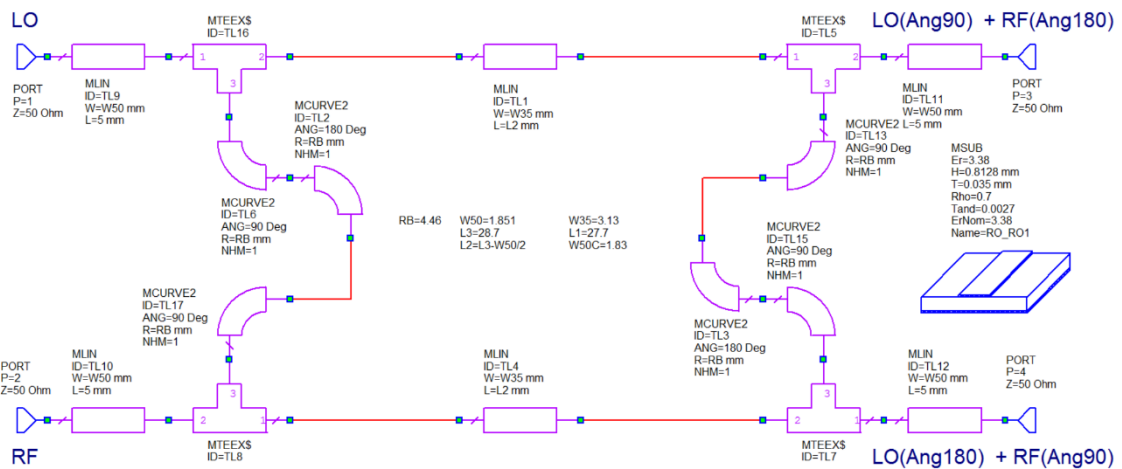


Figure 5.43. Circuit diagram of the Branchline coupler used as a subcircuit in figure 5.42.

Correct biasing for the diodes must be provided, such that all the RF and LO energy is dissipated in the diodes and all the resulting low frequency energy is passed to the IF port and is not reflected back into the RF or LO ports.

The transmission lines consisting of TL12 and TL8 and consisting of TL11 and TL14 are also one quarter wavelength long at the RF and LO frequencies and thus form a short

circuit at those frequencies and an open circuit at the IF frequency. All the RF and LO energy coming from the Branchline coupler is thus dissipated in the diodes.

The Short circuited transmission lines consisting of TL9 and TL4 and consisting of TL10 and TL5 are one quarter wavelength long at the LO and RF frequencies, so that they are an open circuit at the LO and RF frequencies and a short circuit at the IF frequency. All the frequency components at the IF signal band are thus passed unhindered to the IF port 3 of the mixer. To make the removal of the LO and RF signals at the IF port as effective as possible, the size of capacitor C1 is chosen to act as a short circuit to the RF and LO signals but have little effect at the IF frequency.

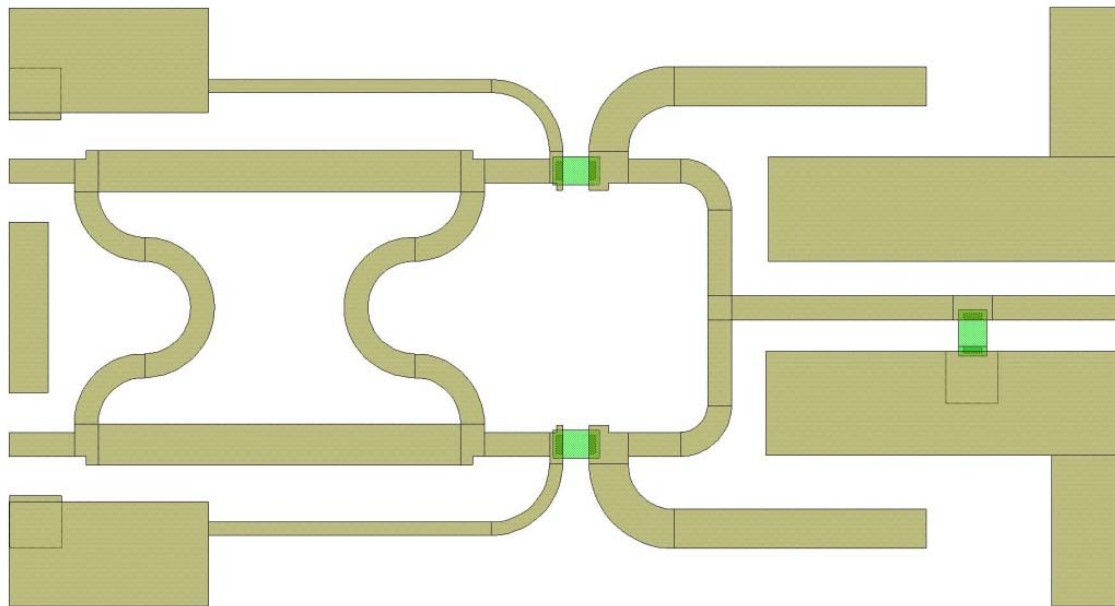


Figure 5.44. Branchline mixer layout.

Figure 5.44 shows the layout of the PCB layout corresponding to the circuit diagram of figures 5.42 and 5.43. The vertical transmission lines of the Branchline coupler are folded using bends, to reduce the size of the PCB. The green pads are the locations for the diodes and the capacitor. The short circuited quarter wave stubs are thin, corresponding to a high characteristic impedance to ensure as high an impedance over as wide a bandwidth around the LO and RF frequencies. The open circuited quarter wavelength stubs are wide transmission lines, providing a low shunt impedance for as wide a bandwidth as possible corresponding to as wide a bandwidth around the LO and RF frequencies, so that as much of the RF energy is converted to IF signals as possible. The distance between the capacitor and each of the diodes is half a wavelength at the LO frequency, to ensure that the low impedance of the capacitor reflects as a low impedance at the diodes. The length of the transmission line between the diodes is a half wavelength at the LO frequency to ensure each open-circuited stubs reflect as a short circuit at both diodes, thus enhancing the efficiency of the frequency conversion.

Figure 5.45 shows the conversion loss of the microwave mixer of figure 5.44. The conversion loss is 1.5 dB worse than that of the microwave mixer of figure 5.39. The conversion loss includes approximately 0.5 dB losses in the PCB tracks.

Figure 5.46 shows the IF spectrum of the mixer and it can be seen that the mixer performs well. The components above 1 GHz can easily be filtered out using a simple low pass filter at the IF output.

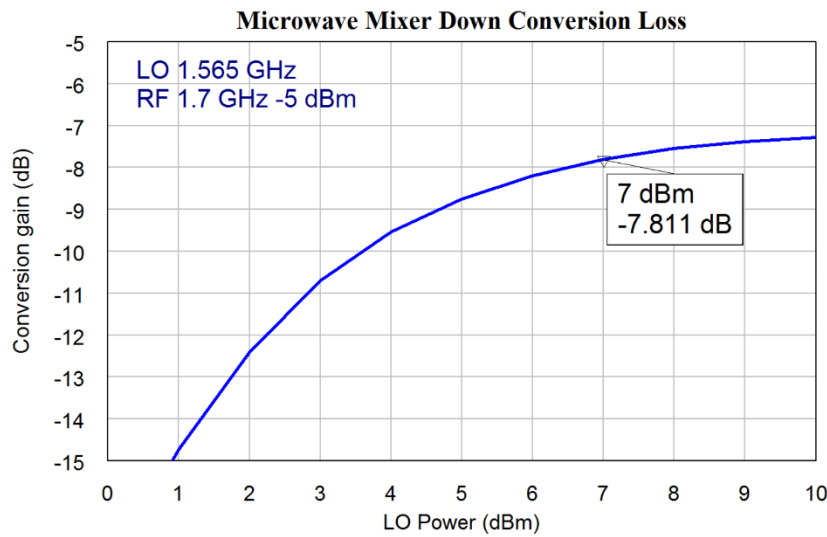


Figure 5.45. Conversion loss of a balanced mixer with a Branchline coupler.

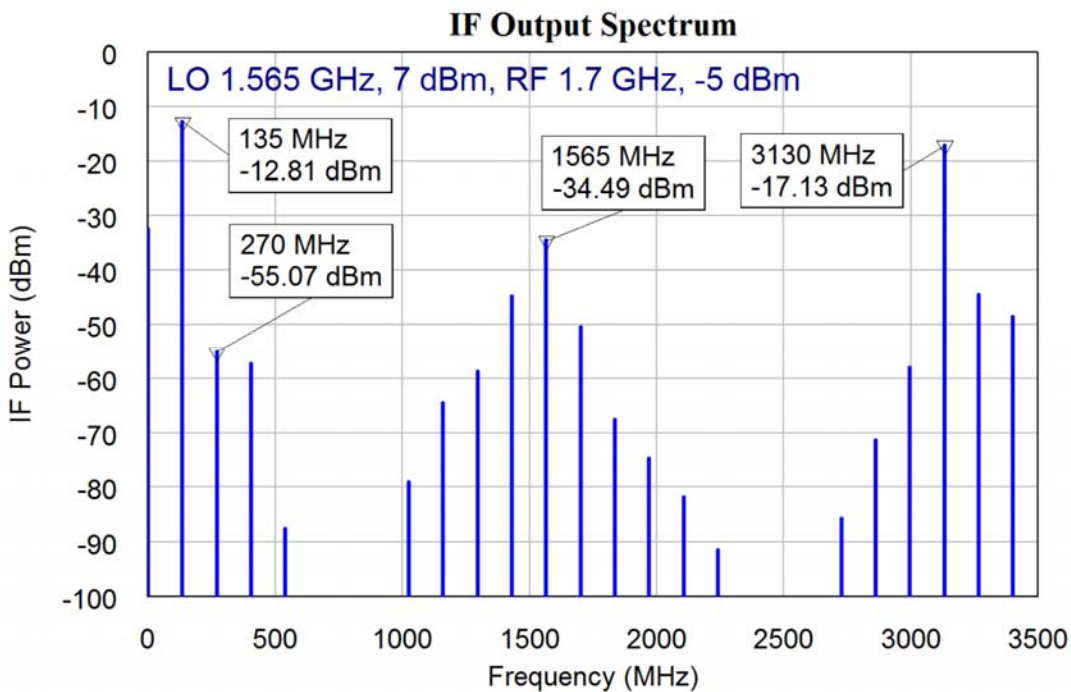


Figure 5.46. IF spectrum of a balanced mixer with a Branchline coupler.

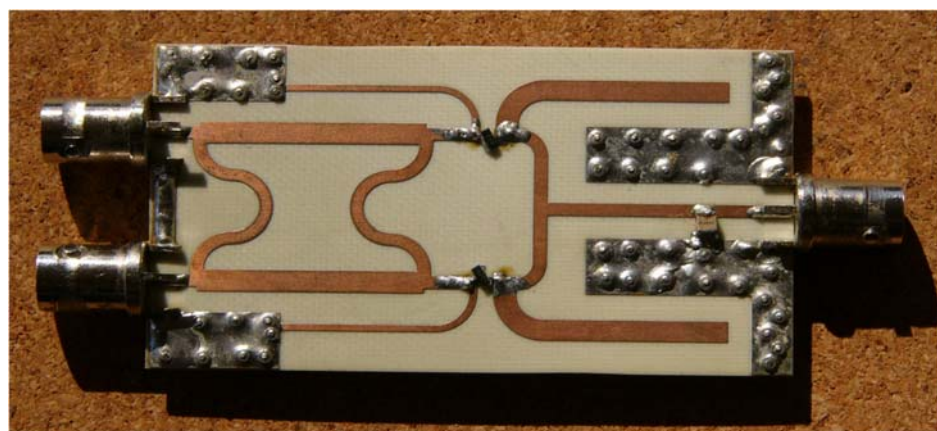


Figure 5.47. Hardware realisation of the balanced mixer using a Branchline coupler.

Figure 5.47 shows the hardware for the PCB layout of figure 5.44. Notice the many vias connecting the top ground-plane to the bottom ground-plane, to ensure that a good earth is obtained at the end of the quarter wavelength long lines TL4 and TL5 in figure 5.42, which are needed to provide a DC path for the diode currents.

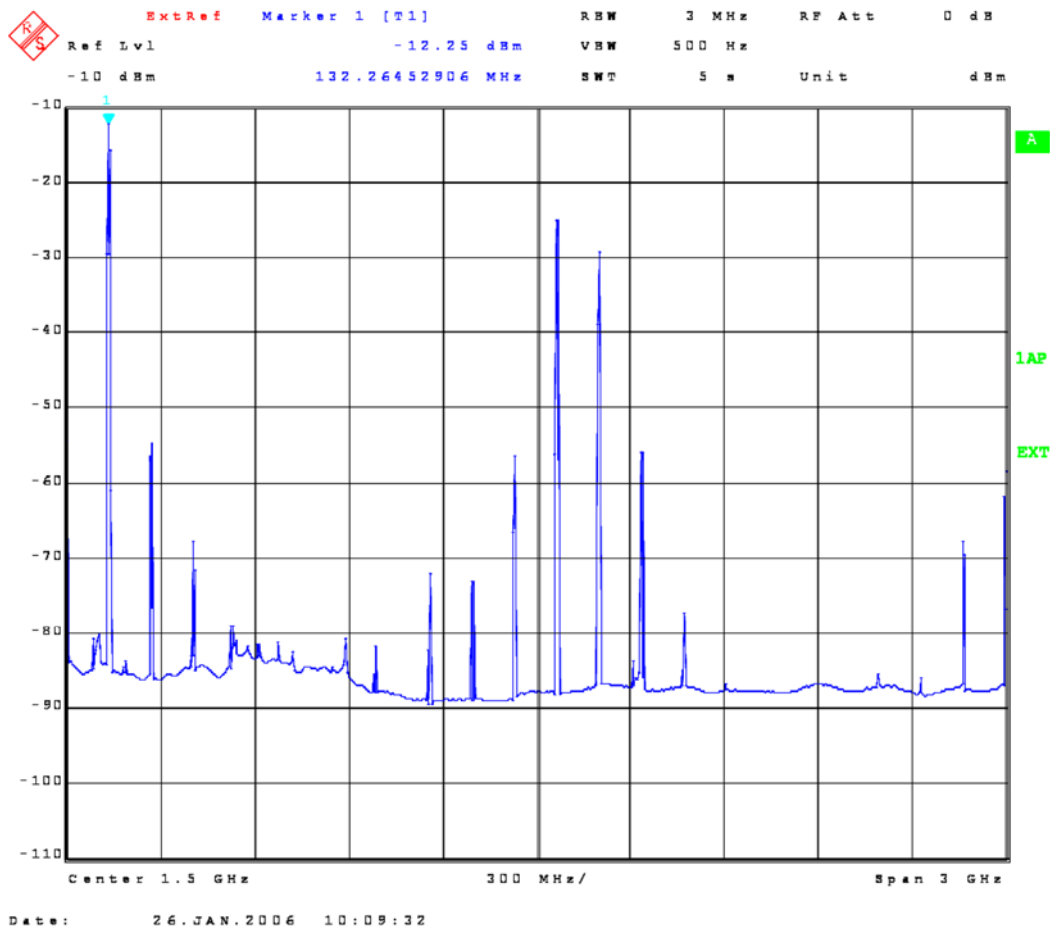


Figure. 5.48, Measured spectrum of Branchline coupler mixer of figure 5.47. (Hor: Centre Frequency 1.5 GHz, 300 MHz/div. Vert: Max -10 dBm, 10 dB/div.)

Figure 5.48 shows the measured performance of the hardware of figure 5.47. This IF spectrum closely resembles the simulation results shown in figure 5.46. The measured conversion loss for a LO level of 5 dBm at 1.565 GHz and an RF signal of -5 dBm at 1.7 GHz was 7.25 dB, being within 0.6 dB of the performance shown in figure 5.45. The second harmonic distortion at 270 MHz, at -55 dBm, is the same as the computer simulation. The LO feed-through is 10 dB larger, but two microwave diodes were selected for the mixer, without being matched. Third harmonic distortion is 10 dB larger in figure 5.46, than it is in figure 5.48. In figure 5.48, the signal components in the region 88 to 108 MHz at -80 dBm are the local 100 kW EIRP FM transmitters, located Mt. Stewart, 2.7 km from James Cook University. The 170 MHz TV transmitter and a block of five 200 kW DVB-T transmitters covering the spectrum from 545 to 625 MHz all located at Mt Stewart can also be seen on the spectrum.

At present companies like Mini-Circuits, produce commercial mixers for RF frequencies up to 20 GHz. For commercial designs, such mixers are smaller and cheaper than the design shown in figure 5.45. The design technique presented here can operate at frequencies above 20 GHz and demonstrates that as long as the RF, LO and IF signals are combined correctly, a good frequency mixer will result.

Active Single Transistor Mixer

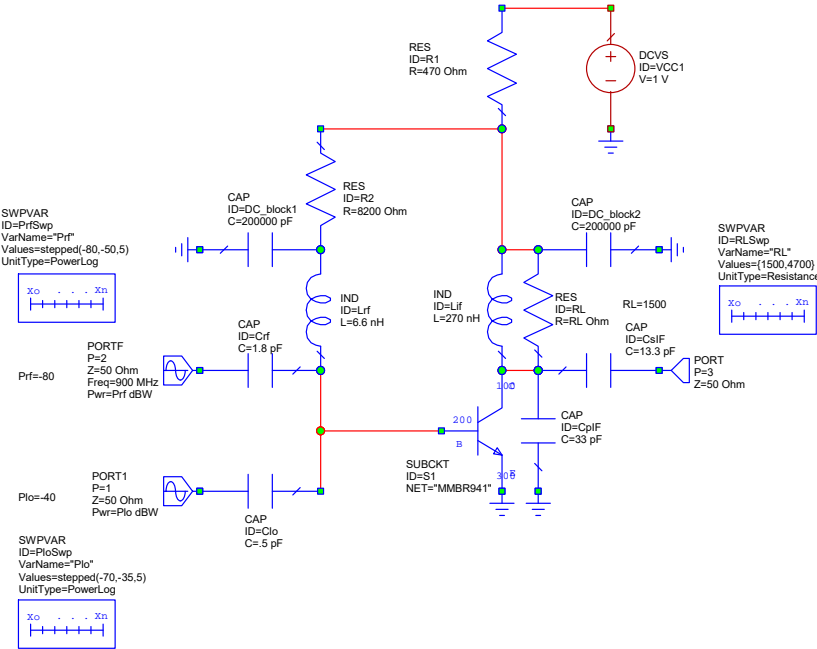


Figure 5.49. Active single diode mixer (NI AWR DE example, Low_Power_Mixer).

Figure 5.49 shows the *Low_Power_Mixer* [5], which is an active single diode mixer from the NI AWR DE mixer examples. This example also shows how Conversion Loss or Gain, Gain Compression and other mixer parameters can be determined using MWO. An active single transistor mixer has a similar spectral performance to a passive single diode mixer, but has a conversion gain. The mixer of figure 5.49 has a conversion gain of more than 10 dB. Active single transistor mixers are used in many consumer devices like radio and TV receivers.

Gilbert Cell Active Mixer

It is possible to use two transistors in a push-push amplifier configuration and thus produce an active balanced mixer. However, the long tail multiplier, first reported by Frater [6] and now more commonly known as the Gilbert Cell [7] is frequently used as an active mixer, as it provides close to ideal multiplier performance. The Gilbert cell mixer is used in many IC's. There is a *Gilbert-Cell* mixer in the examples provided by MWO. That Gilbert cell example has been simplified to illustrate its principle of operation as shown in figure 5.50. Gilbert Cell mixers with very good IM performances and a frequency range from DC to 5 GHz are available.

Normally all these components in figure 5.50 would be included in an IC. Figure 5.51 shows the resulting conversion gain. The LO and RF frequencies are chosen to be the same as that for the microwave mixers of figure 5.40 and 5.43. The circuit consists of 3 parts, the left part consisting of transistors TR1 to TR7 is the Gilbert Cell multiplier. Transistor TR1 is a constant current source for the long tail pair amplifiers making up the Gilbert Cell. The resistor chain R1 to R4 is a biasing chain, providing the biasing voltages. Transistors TR8 to TR11 form the output buffer amplifier, with transistors TR9 and TR11 being constant current sources and TR8 and TR10 being voltage followers.

A fully differential output circuit is required to obtain the best LO isolation, without having to tune the RL13 and RL24 for best LO \Rightarrow IF isolation. The differential IF output also minimises the IF harmonic output at 270 MHz. A simple transformer is used in figure 5.50 to convert this to a single ended output.

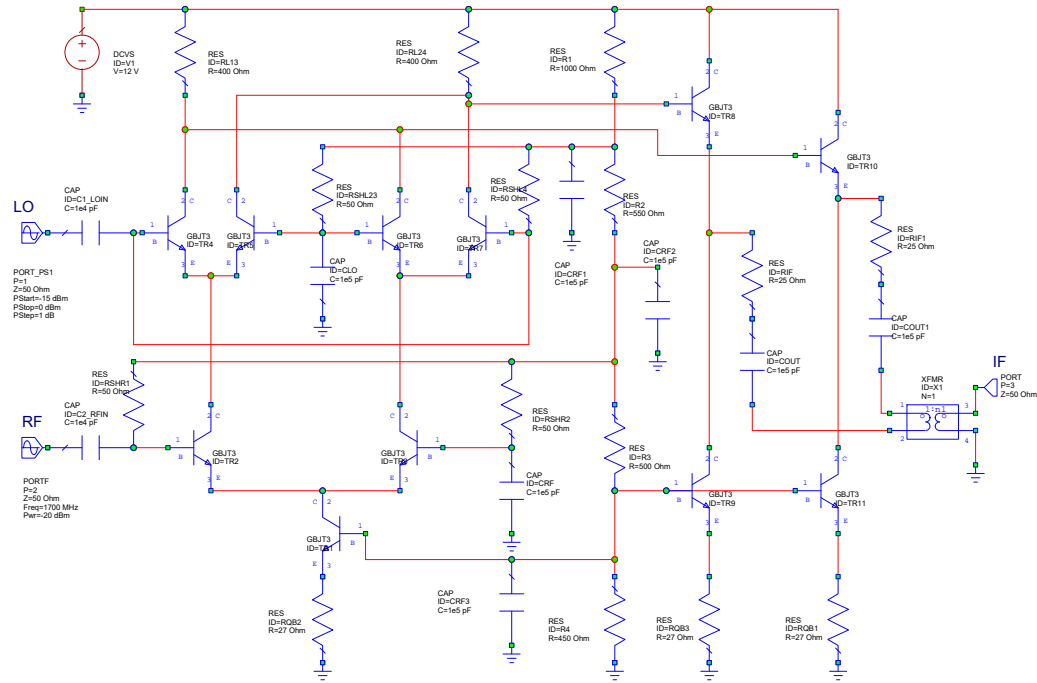


Figure 5.50. Basic Gilbert Cell active multiplier.

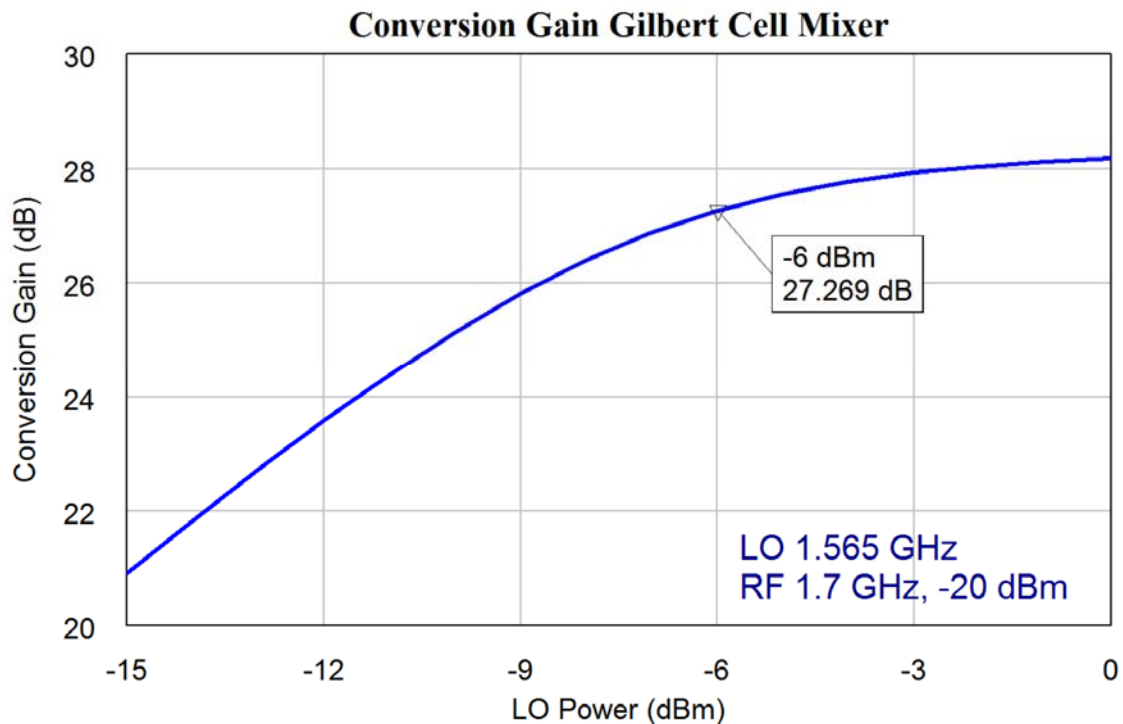


Figure 5.51. Conversion gain of the Gilbert Cell mixer of figure 5.48.

The Gilbert Cell mixer is different from the diode mixers in that the best performance is obtained when the LO signal does not cause saturation in the transistors of the Gilbert Cell. Comparing figure 5.51 with figure 5.21, shows that since the conversion gain keeps increasing in figure 5.51, variations in AM noise on the LO will cause this AM noise to appear on the IF signal. Figure 5.21 shows that the Double Balanced Mixer is much more immune to this AM noise. Figure 5.51 shows that the largest signal that can be used without the mixer saturating too much is about -6 dBm and that level of LO power has been used for the subsequent measurements. Using a lower LO power gives more ideal mixer action but reduces the conversion gain.

Figure 5.52 shows the IF output spectrum of the mixer as a down-converter. The LO power is -6 dBm and the RF level is -20 dBm. To enable a comparison to be made, the same frequencies are used as for figures 5.41 and 5.46. Using a lower RF power level gives a better performance with a better LO and RF isolation at the IF output. The RF signal is at 1.7 GHz and the LO signal is at 1.585 GHz resulting in a difference signal at 135 MHz and a sum signal at 3.265 GHz. Figure 5.52 shows that these nearly the same power level and are the largest signals. The Gilbert cell acts thus as a near ideal mixer.

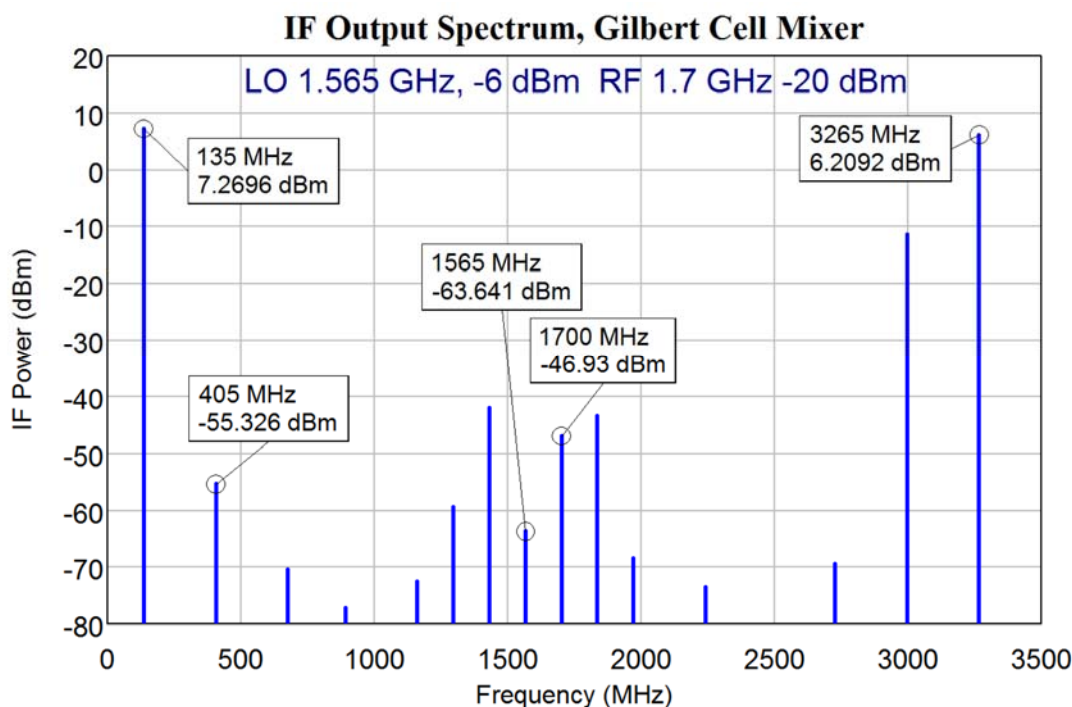


Figure 5.52. IF spectrum of the Gilbert Cell mixer of figure 5.50 as a down-converter.

Figure 5.53 shows a plot of the conversion gain for Gilbert Cell up-converter as the IF level is varied. To be able to trace the intermodulation levels as this IF level is changed, an LO frequency of 1.5 GHz and -6 dBm and with an IF frequency of 50 MHz, whose power level varies from -35 dBm to -15 dBm are used. The IF level of -18.13 dBm corresponds to a 1 dB reduction of the conversion gain of the mixer and thus corresponds to the 1 dB compression point.

Figures 5.54 to 5.58 show the RF spectra of the Gilbert Cell mixer used as an up-converter, when the IF signal level is varied. The LO signal is -8 dBm and IF signal level is -35 dBm, -30 dBm, -25 dBm and -20 dBm and -15 dBm. For an IF signal of -35 dBm, the unwanted components are more than 60 dB below the wanted components, so that the Gilbert Cell is near ideal mixer.

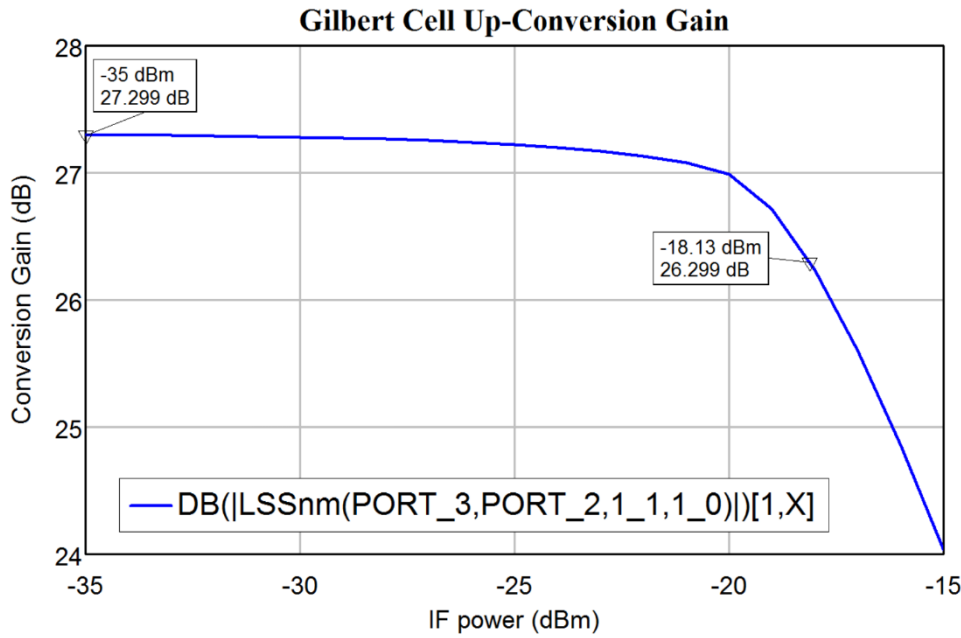


Figure 5.53. Up-conversion gain of the Gilbert Cell mixer of figure 5.50 versus IF power.

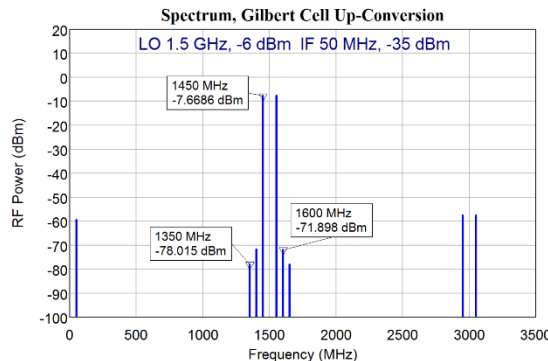


Figure 5.54. RF spectra for IF = -35 dBm

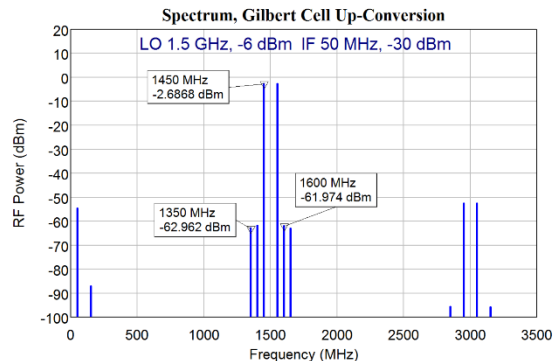


Figure 5.55. RF spectra for IF = -30 dBm

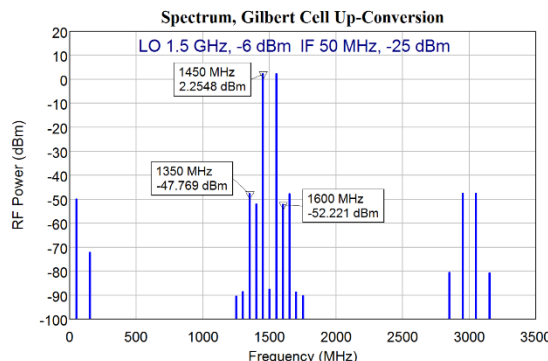


Figure 5.56. RF spectra for IF = -25 dBm

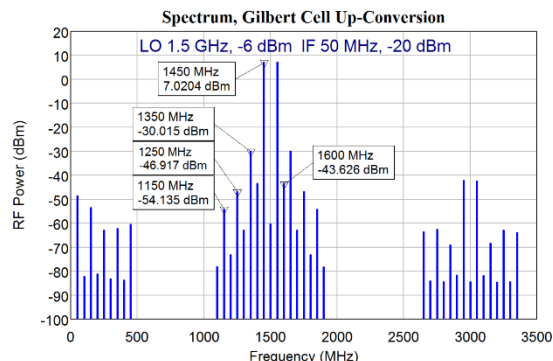


Figure 5.57. RF spectra for IF = -20 dBm

Changing the IF level by 10 dB, from -35 dBm to -25 dBm, causes a 10 dB change in level of the 1.45 GHz and 1.55 GHz components and a 30 dB change in the 3IM component at 1.35 GHz. The mixer is thus operating in a linear range and the expected third order output intercept point (OIIP3) from figure 5.54 is at $(0.5 * (-7.6688 - (-71.896)) - (-7.6688)) = 24.445$ dBm. Figure 5.53 shows that the conversion gain at IF = -35 dBm is 27.299 dB, the IIP3 point occurs at an IF input level of $24.445 - 27.299 = -2.854$ dBm. From figure 5.53, the 1 dB compression point is at an IF level of -18.13 dBm. These

computer simulations or similar measurements on the actual devices can thus easily determine the critical mixer parameters. Passive Double Balanced mixers, can operate at higher input levels, but produce lower output levels than Gilbert Cell mixers, because Gilbert Cell mixers have a conversion gain.

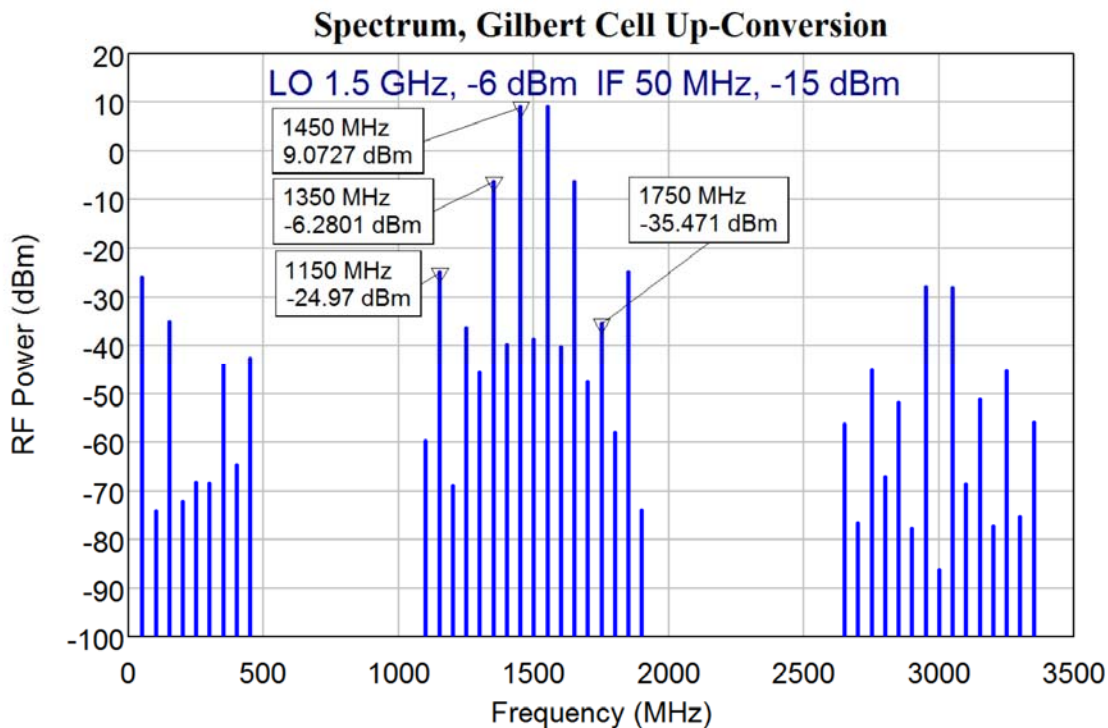


Figure 5.58. RF spectra for the mixer of figure 5.50 as an up-converter, IF = -15 dBm.

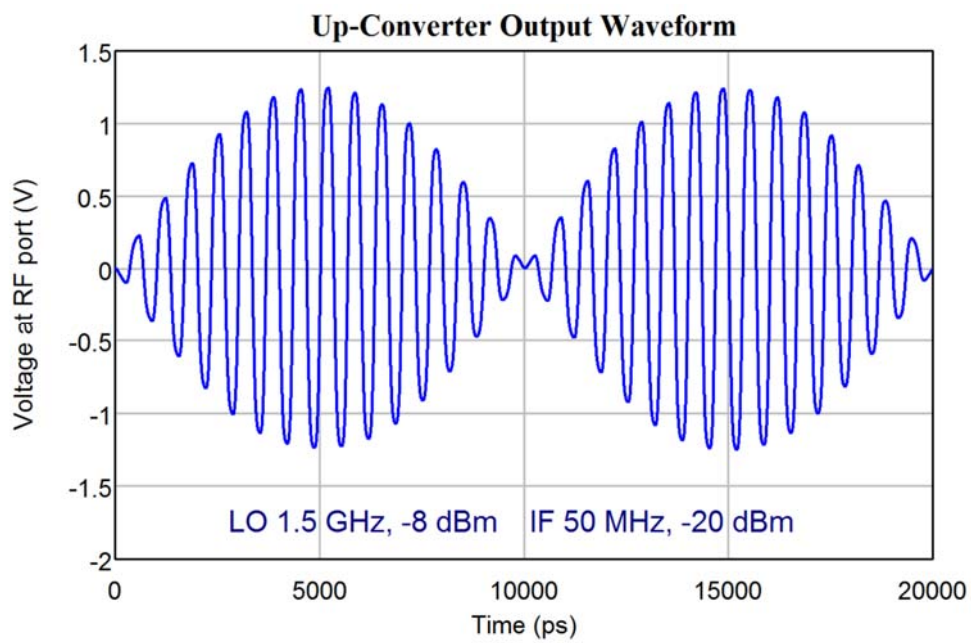


Figure 5.59. RF Waveform for the mixer of figure 5.50.

Figure 5.59 shows the corresponding RF waveform. The waveform corresponds to an ideal Double Sideband Suppressed Carrier waveform and any unwanted signals cannot be observed in the time waveform, but can be detected in the spectrum of figure 5.57.

Quadrature Mixers

In quadrature mixers a 90 degree hybrid, like a Branchline coupler is used to produce two LO signals, corresponding to Sine and Cosine of the LO frequency. In an Up-converter, the Cosine signal is then multiplied with the In-Phase (I) component of the baseband signal, and the Sine signal is multiplied with the Quadrature (Q) component of the baseband signal, as shown in figure 5.60. The resulting signals are then added, using a combiner like a Wilkinson hybrid to produce the RF signal. When the I and Q signals are the Hilbert transform of each other, then a Single Sideband RF signal results.

For a down-converter, when an RF signal that is passed through a 90° hybrid, such as a Branchline coupler, then I and Q signals are produced. When these are mixed in an IQ mixer, the ($RF = LO + IF$) frequency is shifted to the IF frequency by the mixer and the ($LO - IF$) or image frequency components are suppressed at the IF frequency. This allows a zero IF frequency to be used, thus allowing two low pass filters, one for the I baseband signal and one for the Q baseband signal, to be used. Those I and Q baseband signals are then digitised for signal processing and demodulation.

Most modern modulation methods, such as QAM, CDMA, OFDM and LTE all use vector modulation and require IQ modulators. Quadrature mixers are thus used in many modern communication systems.

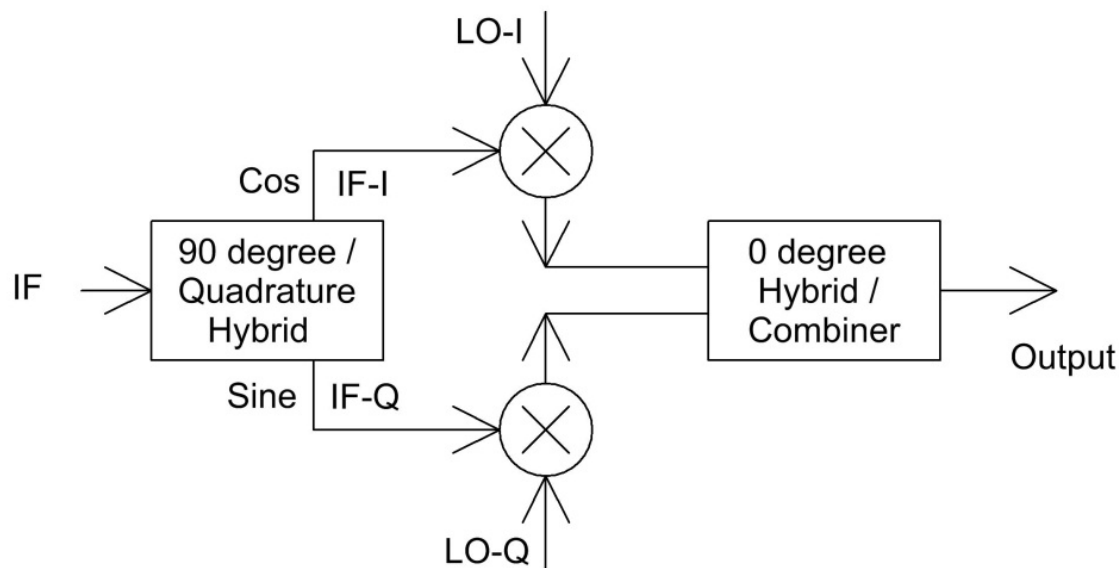


Figure 5.60. Block diagram of a quadrature mixer in Up-conversion.

The 90-degree hybrids required for quadrature mixers can also be produced using LC networks, so that quadrature hybrids at frequencies below 500 MHz are possible. As an example, Mini-Circuits make quadrature mixers, for IQ modulators and IQ demodulators, at a wide range of frequencies as shown in figure 5.61. Because of limitations in the bandwidth over which an accurate 90° phase shift can be produced, the bandwidth of these mixers is limited.

Local oscillators produced using phase locked loops or using Direct Digital Synthesis, can have two outputs, which have an exact 90° phase difference over a wide range of frequencies, as is required for the quadrature mixers. A simple twisted ring divide by 2 flip-flop circuit can produce two signals, which are exactly 90° apart. Some commercial IQ mixers include such divide by 2 circuits.

I & Q Modulators, Surface Mount, 52 MHz to 2000 MHz

Model Number	Case Style	RF/LO Freq. Low (MHz)	RF/LO Freq. Hi (MHz)	I&Q Freq. (MHz) Min., DC to ...	I&Q Freq. (MHz) Max., DC to ...	Conv. Loss (dB), Typ.	Conv. Loss (dB), (a)	Conv. Loss (dB), Max.	Carrier Rejection (dBc), Typ.	Carrier Rejection (dBc), Max.	Sideband Rejection (dBc) Typ.	Sideband Rejection (dBc) Min.	Harmonic Suppression (dBc), 3X/I/Q (dBc), 3X/I/Q (dBc), 5X/I/Q (dBc), 5X/I/Q (dBc)	Harmonic Suppression (dBc), 3X/I/Q (dBc), 3X/I/Q (dBc), 5X/I/Q (dBc), 5X/I/Q (dBc)	Harmonic Suppression (dBc), 3X/I/Q (dBc), 3X/I/Q (dBc), 5X/I/Q (dBc), 5X/I/Q (dBc)	Harmonic Suppression (dBc), 3X/I/Q (dBc), 3X/I/Q (dBc), 5X/I/Q (dBc), 5X/I/Q (dBc)	LTCC
IQBG-2000A+	SM20A	1800	2000	DC	10	7.5	-	9.0	30	20	34	28	50	45	70	50	LTCC
JCIQ-88M (+)	BG291	52	88	DC	5	5.6	0.10	7.0	40	32	35	30	45	35	65	50	-
JCIQ-176M (+)	BG291	104	176	DC	5	5.6	0.10	7.0	35	30	35	30	45	35	65	50	-
SYIQ-895M+	TTT1289	868	895	DC	5	6.4	0.10	7.5	38	30	39	30	45	35	64	50	-

I & Q Demodulators, Surface Mount, 104 MHz to 1880 MHz

Model Number	Case Style	RF/LO Freq. Low (MHz)	RF/LO Freq. Hi (MHz)	I&Q Freq. (MHz) Min., DC to ...	I&Q Freq. (MHz) Max., DC to ...	Conv. Loss (dB), Loss (dB), Typ.	Conv. Loss (dB), Loss (dB), (a)	Conv. Loss (dB), Max.	Unbalance (dB) Typ.	Unbalance (dB) Max.	Unbalance (dB) Typ.	Phase Unbalance (deg.)	Phase Unbalance (deg.) Max.	Harmonic Suppression (dBc), 3X/I/Q (dBc), 3X/I/Q (dBc), 5X/I/Q (dBc), 5X/I/Q (dBc)	Harmonic Suppression (dBc), 3X/I/Q (dBc), 3X/I/Q (dBc), 5X/I/Q (dBc), 5X/I/Q (dBc)	Harmonic Suppression (dBc), 3X/I/Q (dBc), 3X/I/Q (dBc), 5X/I/Q (dBc), 5X/I/Q (dBc)
JCIQ-176D (+)	BG291	104	176	DC	5	5.5	0.10	7.0	0.15	0.60	2	5	52	40	65	50
SYIQ-895D+	TTT1289	868	895	DC	5	6.4	0.10	7.5	0.15	0.40	1.5	4	45	35	64	50

Figure 5.61. Mini-Circuits IQ mixers. [8]

Active IQ Mixers

For cellular base stations, radio and TV transmitters, and their test equipment, IQ modulation is used to produce the complex modulated waveforms used in modern communication systems. The mixers used in such signal generators are often active (Gilbert cell) IQ mixers. Computer controlled DC bias (control and calibration) signals are used to ensure that the carrier feed-through, quadrature phase shifts and I and Q gains are correct. The design of such IC's can cost more than one million dollars. For large-scale applications, such as cellular base stations, commercial IQ modulator and demodulator IC's are available.

IQ demodulators allow a zero IF frequency to be used, by placing the LO is at the centre of the RF band, and producing I and Q baseband outputs, which are passed through simple low pass filters before being digitised. This avoids the need for bulky IF filters. The required filtering is then done digitally, allowing very frequency selective filtering to be achieved.

Image Reject Mixers

Figure 5.2 shows that a mixer operating as a down-converter will also shift an “image signal” into the required IF bandwidth. Normally a filter is used at the RF front end to filter out any signals inside this image frequency band. Any thermal noise inside this image frequency band will contribute to the noise at the IF frequency band. An image reject mixer will only shift the required signals to the IF frequency and will not shift the signals or noise of the image band to the IF frequency. Image reject mixers can thus provide an improved noise performance. IQ mixers can be used as image reject mixers, where by supplying the Q input to the mixer with a signal with a 90 degree phase shift, with respect to the I signal the RF signals at the image frequency are not produced for an up-converter and are not shifted in to the IF band for a down-converter.

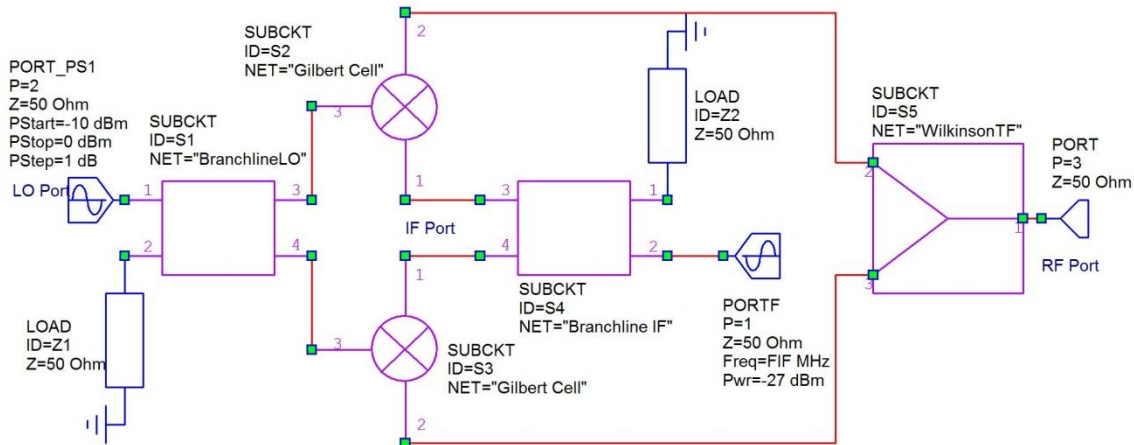


Figure 5.62. Image reject mixer (up converter).

This process is best illustrated, by using an up conversion mixer to produce a Single Sideband signal. For details of the mathematics involved, see articles on using the Hilbert Transform for generating Single Sideband [9]. In this design, Branchline couplers are used to produce the required 90-degree phase shifted signals. Figure 4.34 shows that Branchline couplers maintain a $90 \pm 1.22^\circ$ phase shift over a $\pm 10\%$ bandwidth, which is sufficient for many communication systems. To simplify the design, ideal transmission lines of 90° electrical length are used, without regard of the physical length of those lines. Figure 5.62 shows the schematic of the image reject mixer as an up converter. A Branchline coupler is used at the IF frequency of 50 MHz, clearly those lines would be too long to realise and normally LC networks or Digital Signal Processing (DSP) techniques are used to produce the required phase shifts at those frequencies. The block diagram is the same as that for the IQ mixer in figure 5.60, with the IF-Q signal being constrained to be the Hilbert transform (90-degree phase shift) of the IF-I signal. In figure 5.62, the in-phase combiner uses a transformer Wilkinson hybrid, however this can also be realised using a Wilkinson transmission line hybrid.

The Gilbert cell mixers in figure 5.62 are the same as the one shown in figure 5.50. For figure 5.55, a LO level of -6 dBm and an IF signal of -30 dBm were used. Since the LO signal is split to drive the 2 mixers, a LO of -3 dBm and an IF signal of -27 dBm is required. Figure 5.63 shows the resulting spectrum for the image reject mixer, when used as an upper sideband up-converter. Comparing this with figure 5.55, the signal at 1.55 GHz has increased due to the signals from both mixers being added. The signals at 1.4 GHz and 1.6 GHz are second harmonics of the LO and thus will have 180 degree phase shift at the output of the Branchline coupler, so that these signals do not have image rejection. The third harmonic of the LO signal has a 270 degree phase shift at the output of the Branchline coupler and that causes the signal to appear in the image frequency band.

Figure 5.64 shows the up-conversion gains for this mixer. Figure 5.51 shows the conversion gain of the same Gilbert Cell mixer when used as a down-converter operating at a similar LO frequency. The LO power of -3 dBm in figure 5.64 corresponds to LO power of -6 dBm in figure 5.51. The wanted sideband conversion gain in figure 5.66 is very similar to that in figure 5.51. Figures 5.63 and 5.64 show that the conversion gain for the unwanted image sideband is $-110.13 - (-27) \text{ dB} = -83.13 \text{ dB}$, so that this mixer works well as an image reject mixer. In practice a perfect match between the conversion gain and phase shifts produced by 2 separate mixers is unlikely to be achieved, in addition,

the hybrids used will not produce perfect 90 degree phase shifts, so that a 25 dB image rejection is more common [10, 11].

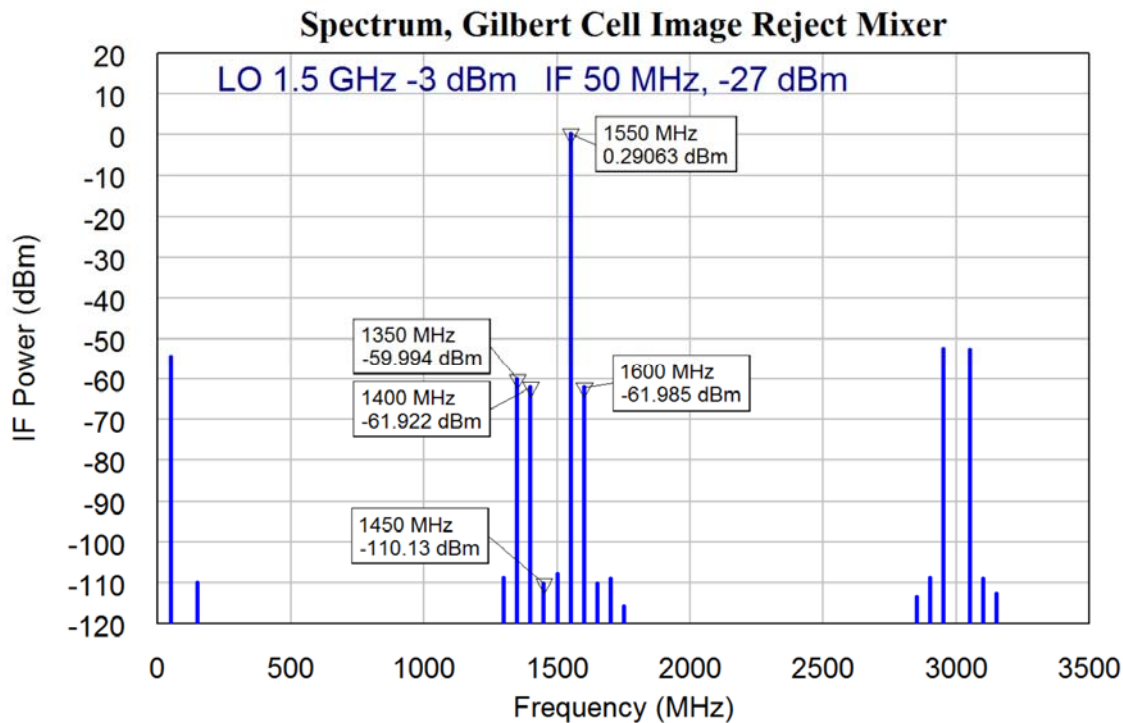


Figure 5.63. Image reject mixer spectrum for Gilbert Cell upper sideband up-converter.

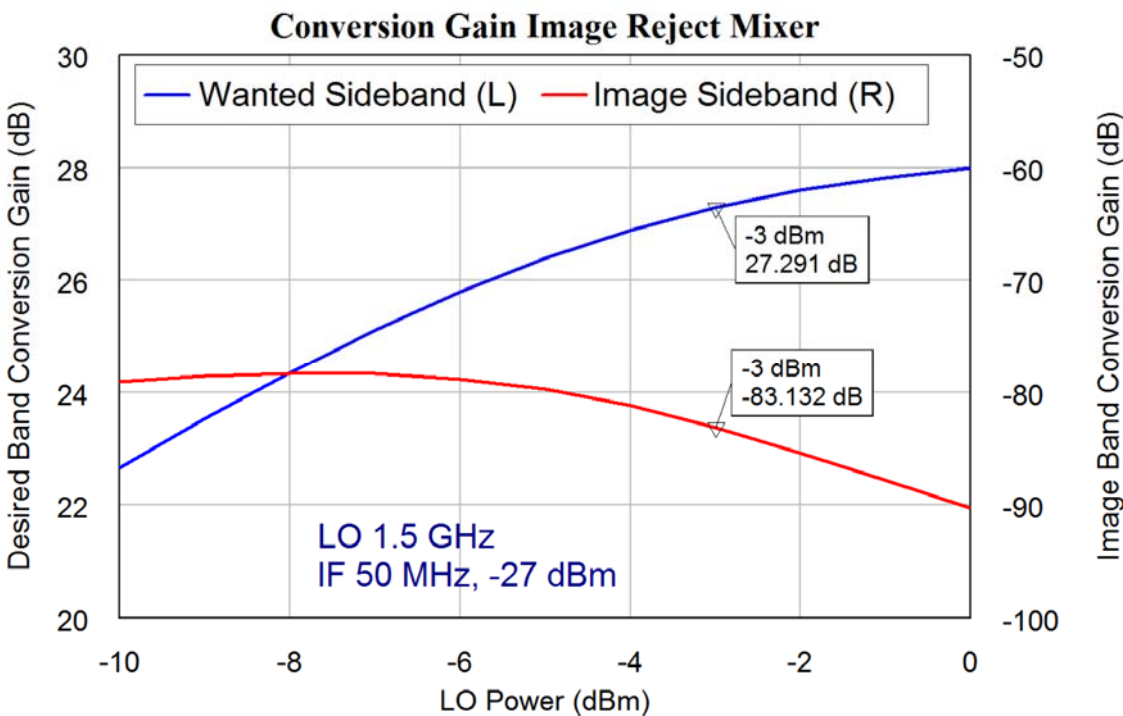


Figure 5.64. Conversion gains of image reject mixer.

Figure 5.65 shows the output current at the RF port of the mixer. For a -12 dBm LO, the output waveform is nearly a pure sine wave at 1.55 GHz. As the LO level is increased, the increase in the amplitude variation of the RF output can be seen.

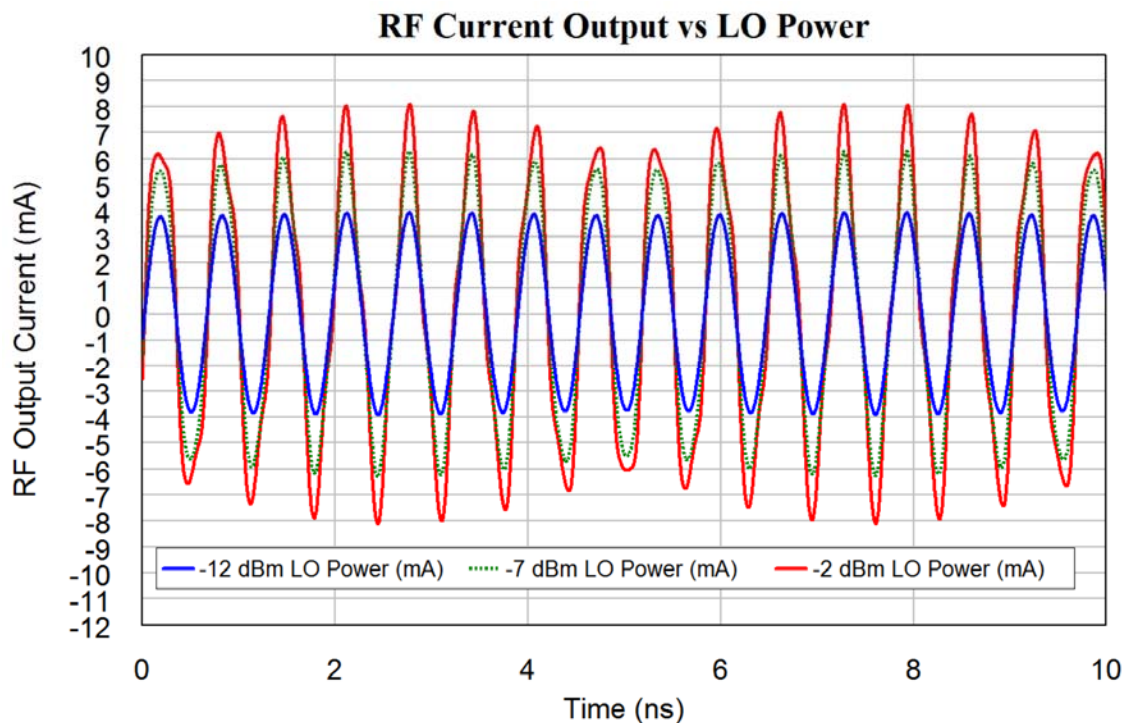


Figure 5.65. RF output current of image reject mixer.

The Gilbert Cell can be replaced by a double balanced mixer and the LO level and IF levels changed to match. Figure 5.66 shows the RF spectrum when the LO is +10 dBm and the IF level is -8 dBm. The conversion loss is -4.9 dB and the image rejection is more than 70 dB. In practice, the image rejection will be more like 25 dB [11] due to differences in diodes and the hybrids not producing perfect 90-degree phase shifts.

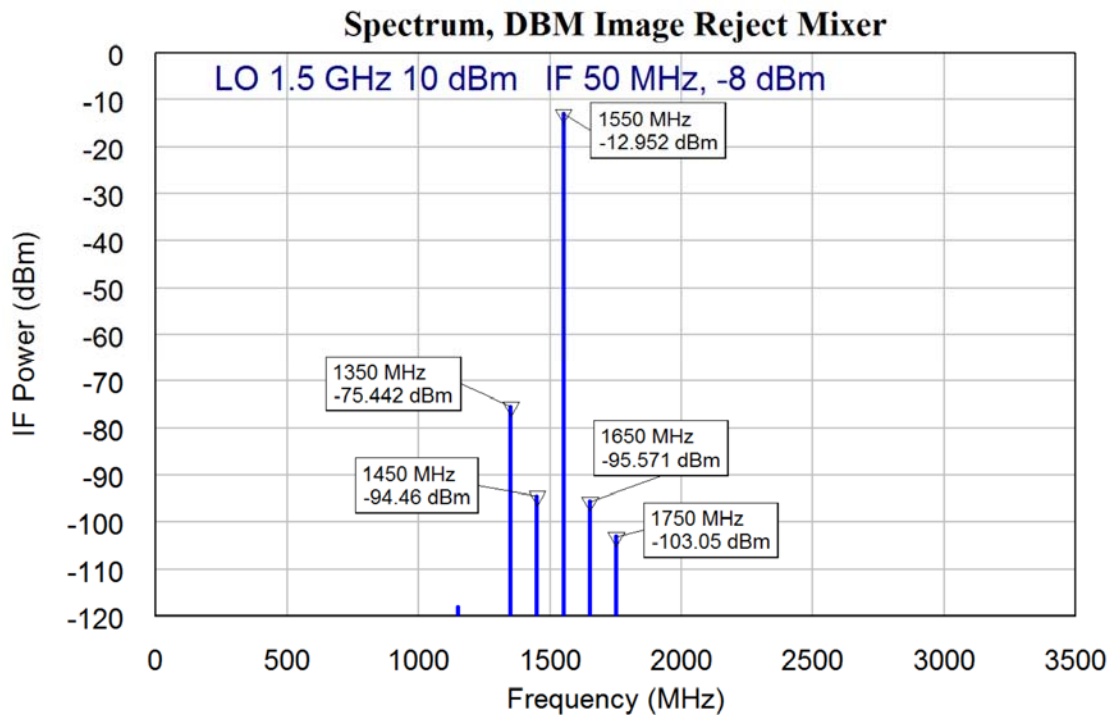


Figure 5.66. Spectrum for Double Balanced Mixer upper sideband up-converter.

For an image reject down-conversion mixer, the same block diagram of figure 5.64 is used, with the Branchline couplers on the RF and LO inputs and the in-phase combiner on the output. If a Double Balanced mixer is used, only the RF and IF ports need to be swapped. If Gilbert Cells are used then the mixer's input needs to be connected to the LO and RF 90 degree hybrids and the IF output of the Gilbert Cells need to be added using a transformer hybrid or operational amplifiers.

Examples of Commercial Active Mixers

Many manufacturers produce active mixers for use in commercial equipment. In particular, mixers for use in mobile and cordless phones, wireless LANs and similar consumer devices are readily available.

200MHz to 6000MHz Direct Conversion Transmitter Application

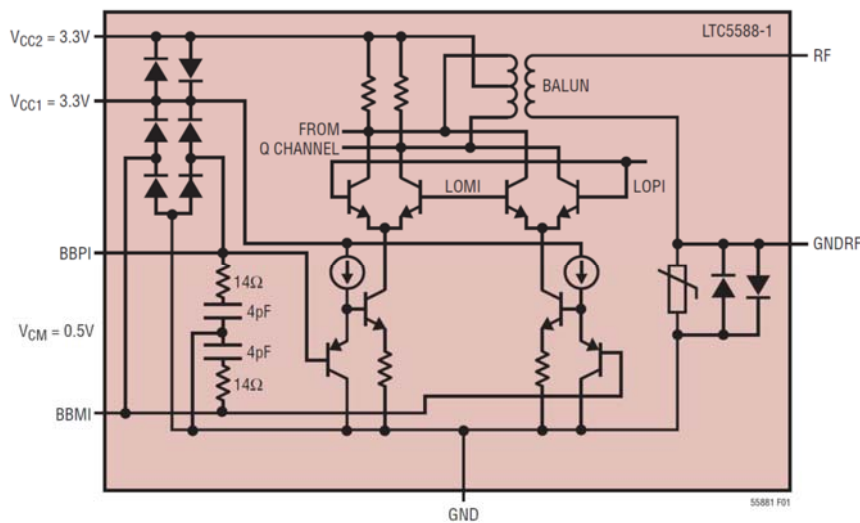
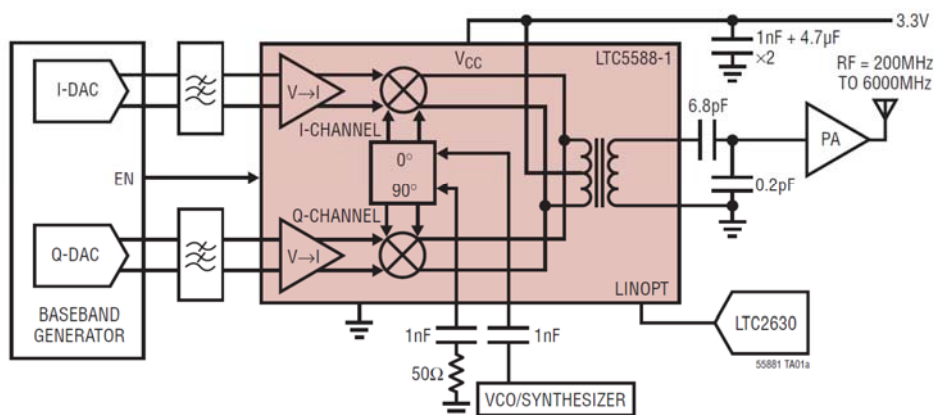


Figure 5.67. LTC5588-1 typical application (top) and simplified schematic for one channel [12]

The LTC5588-1 IQ mixer shown in figure 5.67 is used as an up-converter for mobile radio applications. This mixer uses Gilbert cells for the mixers. An IQ mixer allows the required RF output signal to be produced, without the need to filter out unwanted sidebands. The LTC5588-1 has a minimum image rejection of -27 dBc. An I and Q signal, up to 430 MHz can be used, to produce a quadrature modulated RF signal from 200MHz to 6GHz, with an output power up to -1.9 dBm. In the 900 MHz mobile/cellular phone

band, the typical image rejection is -45 dBc and in the 1.8 and 2.1 GHz bands, the typical image rejection is -55 dBc. The mixer performance satisfies all the G2 to G4 mobile radio standards. These devices are aimed at base-stations, point-to point microwave links, Digital TV and DAB modulators and military radios.

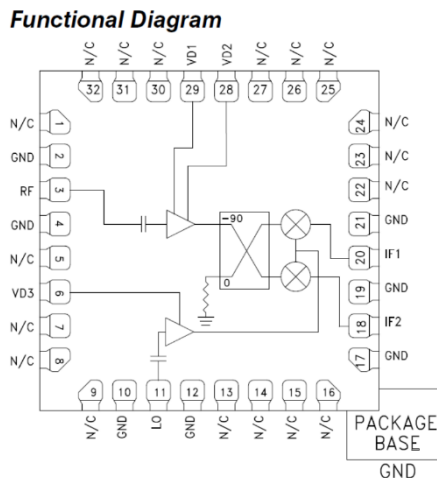


Figure 5.63. Analog Devices HMC1113LP5E [13].

GaAs Microwave Monolithic IC's (MMIC) are used for most commercial mixer applications. For Satellite receivers, a low noise amplifier (LNA) and an IQ active mixer are often combined in one IC [11, 12]. Figure 5.63 shows the block diagram of a HMC1113LP5E MMIC I/Q Mixer Downconverter [13]. It has a typical noise figure of 1.8 dB an image rejection of 25 dB and a conversion gain of 12 dB over the 10 to 16 GHz RF input frequency range. An external 90° hybrid is required to obtain upper or lower sideband suppression and to minimise the noise due to the image band. For higher RF frequencies, a frequency multiplier is included to ease the LO requirements. MMIC's are also available for up-converters [14].

LTCC Mixers

At higher frequencies, it becomes more difficult to wind the transformers required for the mixers. Low Temperature Cofired Ceramic (LTCC) thick film technology allows a circuit to be made up from multiple layers of ceramic materials. By depositing conductive or magnetic inks, a set of layers can form a strip-line transmission line, a ferrite loaded hybrid or it can contain semiconductor elements like diodes. Because high dielectric constant materials are used, the resulting package can be made small. Since the process can be automated, lower production costs result. Mini-Circuits use this technology for producing high frequency mixers. A typical example is their IQBG-2000A+ I&Q modulator [15]. The block diagram is the same as the IQ mixer in the top figure of 5.62. This device is designed for the 1.8 GHz to 2 GHz mobile phone market. The baseband I and Q inputs have a 10 MHz bandwidth, to produce a 20MHz wide RF signal. The mixer's package is shown in figure 5.69. This LTCC IQ mixer has a typical image rejection of 34 dB, and a typical carrier rejection of 30 dB. The carrier rejection is comparable to that of lower frequency transformer based mixers shown in figure 5.25, but this isolation could not be obtained using conventional transformers at 1.8 GHz. In the LTCC package, the transformers are made by printing conductors around a ferrite material.

For an IQ mixer Sine and Cosine LO signals are required. These are normally produced using a 90° hybrid, such as the Branchline coupler, described in chapter 4. LTCC allows a Branchline coupler to be incorporated in the same package as the transformers, thus reducing production costs, while maintaining a high consistency in performance.

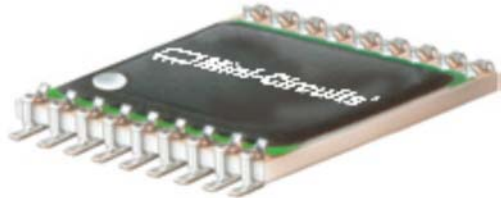


Figure 5.69. Mini-Circuits LTC IQ mixer, IQBG-2000A+ [15].

More details on LTCC circuits are given in chapter 10: Circuit Manufacture.

Other Mixers

Mixer manufacturers make other types of mixers, such as triple balanced mixers, which result in a better input impedance and double balanced mixers using FETs in a passive mode (no DC supplied to the FET) in order to obtain an improved IP3 performance. The description of such devices are beyond the scope of these notes, but some further details can be found at the Mini-Circuits web site (www.minicircuits.com).

Additional Resources

- 1 Mini-Circuits, Application notes on Frequency mixers AN00-001 to AN00-015 available from:
https://www.minicircuits.com/applications/application_notes.html
- 2 Mini-Circuits, “RF Frequency Mixers”, available from:
<https://www.minicircuits.com/WebStore/Mixers.html>
- 3 Stephen A Maas, “Microwave Mixers”, Artech House, 2nd Ed, 1993.

References

Note all web addresses were checked in June 2017.

- 1 Mini-Circuits, “Understanding Mixers- Terms Defined, and Measuring Performance”. Application note AN-00-009, available from:
<https://www.minicircuits.com/app/AN00-009.pdf>
- 2 Mini-Circuits “Frequency Mixer Selection Guide”, available from:
<https://www.minicircuits.com/WebStore/Mixers.html>
- 3 Bert Johnson, Watkins & Johnson Tech Note “Mixers in Microwave Systems (Part 1)” <https://www.scribd.com/document/231853839/Mixers-in-Microwave-Systems-WJ>
- 4 Analog Devices, HMC-MDB277 passive double balanced mixer,
<http://www.analog.com/media/en/technical-documentation/data-sheets/hmc-mdb277.pdf>
- 5 NI AWR DE V11, Examples: “*Low_Power_Mixer.emp*”. (Part of the NI AWR DE software installation).
- 6 R. H. Frater, “Accurate Wideband Multiplier-Square Law Detector,” Review of Scientific Instruments, Vol. 35, No 7, July 1964, pp 810-813

- 7 B. Gilbert, A precise four quadrant multiplier with subnanosecond response. IEEE Journal of Solid State Circuits Vol. 3 No 4. Dec. 1968, pp 365-373.
- 8 Mini-Circuits “I&Q Modulators, Surface Mount”, available from:
<https://www.minicircuits.com/WebStore/ModulatorsDemodulators.html>
- 9 Hilbert Transform for Single Sideband Modulation, Mathematical Formulation, Wikipedia, https://en.wikipedia.org/wiki/Hilbert_transform
- 10 Analog Devices, IQ and Image Reject Mixers <http://www.analog.com/en/products/rf-microwave/mixers/iq-and-image-reject-mixers.html>
- 11 Mini-Circuits , Application notes, I&Q and QPSK Modulators/ Demodulators MOD11-2 and Mod11-8.
https://www.minicircuits.com/applications/application_notes.html
- 12 Linear Technology Corporation, “LTC5588-1 data sheet”, available from:
<http://cds.linear.com/docs/en/datasheet/55881fb.pdf>
- 13 Analog Devices, HMC1113LP5E data sheet,
<http://www.analog.com/media/en/technical-documentation/data-sheets/HMC1113.pdf>
- 14 Analog Devices GaAs MMIC I/Q Upconverter HMC7912.
<http://www.analog.com/media/en/technical-documentation/data-sheets/HMC7912.pdf>
- 15 Mini-Circuits, IQBG-2000A Surface Mount I&Q Modulator data sheet,
<https://www.minicircuits.com/pdfs/IQBG-2000A+.pdf>

Chapter 6

Oscillators

Principles of Oscillators

Requirements

- 1 The LO must be able to supply required output power specified. For example +7 dBm to drive a level 7 mixer.
- 2 The LO must have a sufficient low Phase and amplitude noise for the application. For example, FM radio has a 75 kHz deviation. For 60 dB SNR at the receiver output, a LO with < 75 Hz phase noise when measured in the 50Hz to 15 KHz band is needed.
- 3 The harmonics of the LO must be sufficiently small not to cause interference to other users or other parts of the receiver. In particular, harmonic mixing products must be very small and not cause any unwanted spurious components (spurii).

Oscillator Types

There are two basic oscillator types:

Oscillator using positive feedback: This is the most common lower frequency oscillator design technique and can be used at any frequency with a variety of different topologies (see below).

Oscillator using negative Resistance: This relies on S_{11} of an amplifier in a circuit being >1 at some frequencies, resulting in oscillation. The amplifier is unstable at those frequencies where $S_{11} >1$, causing the amplifier to oscillate. This design technique is predominantly used for microwave operating frequencies. The design of oscillators using negative resistance is outside the scope of this book.

Positive Feedback Oscillators

The oscillator consists of an amplifier and a Frequency Selective Network. The amplifier output is applied to the frequency selective network, the output of which is applied to the amplifier input. For the analysis, a switch can be imagined to open the closed loop signal path. If V_2 is exactly the same as V_1 , both in amplitude and in phase then steady state oscillations result. If the magnitude of $V_2 > V_1$ and the phase is the same then the oscillations will grow. If $V_2 < V_1$, then the oscillations will decay.

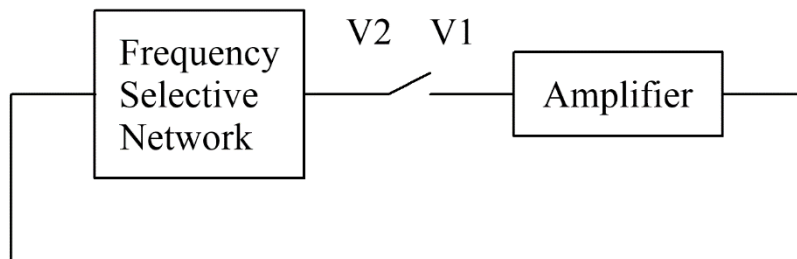


Figure. 6.1. Feedback oscillator block diagram.

Oscillator Design Process

- 1: Design the Feedback network to have the correct frequency selective behaviour at the required operating frequency. A high Q network will have a rapid change of phase with frequency resulting in a lower phase noise of the resulting oscillator.
- 2: Select or design the amplifier to have the required gain at the operating frequency. The input and output impedances should match the expected loads to be seen by the frequency selective network.
- 3: Simulate the amplifier and ensure the biasing is correct to provide the required gain and phase shift at the operating frequency.
- 4: Connect the frequency selective network and amplifier and do a linear analysis to ensure that the required gain (>1) and phase (V_2 in-phase with V_1) conditions are satisfied. In MWO the OSCTEST element is specially designed to perform this function and is used in place of the switch shown in the above diagram. It is important that the secondary parameter FC of OSCTEST be set to be above the expected fundamental frequency and below the second harmonic frequency.

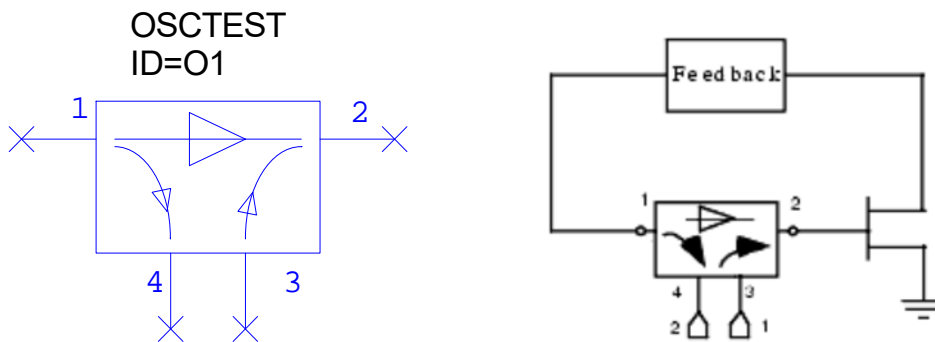


Figure 6.2. The use of OSCTEST for linear analysis of oscillators.

- 5: Once the circuit has been adjusted to have the correct gain and phase for oscillation, modify the linear circuit by replacing the OSCTEST probe with the OSCAPROBE. The OSCAPROBE is connected to ground at the point where the switch was, as shown below.

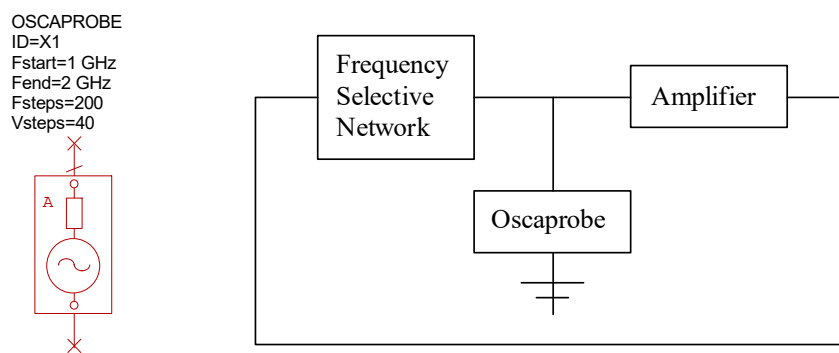


Figure 6.3. The use of OSCAPROBE for nonlinear analysis of oscillators.

The OSCAPROBE is a network that is a short circuit at the specified frequency of oscillation and an open circuit at all other frequencies, the voltage amplitude and phase is adjusted until no current flows through the probe, under which conditions the correct oscillating amplitude is determined. This amplitude is then used in a non-linear Harmonic

Balance simulation of the oscillator circuit. This then allows output waveforms, harmonics and the phase noise of the oscillator to be determined. The accompanying NI AWR DE project files for the oscillator designs presented in this chapter are very useful to investigate changes in phase noise performance, output power and harmonic levels that can be obtained by varying different parameters in the oscillators. It is important that the secondary parameter F0 be set to the expected oscillating frequency and that VPMax be set to be slightly larger than the saturated voltage at that node in the circuit.

Frequency Selective Networks

For typical RF and Microwave oscillators, the following oscillator types are commonly used:

Wien Bridge Oscillator, using an RC network with a $Q=1/3$. This is a low Q resulting in a high phase noise for the oscillator. The oscillator is however easy to construct and tune and as a result this oscillator is often used for audio frequencies, where the inductors required by other configurations would be too large to be used in oscillators.

Colpitts Oscillator, using a tapped capacitor LC network, and the similarly related,

Hartley Oscillator, which also uses a tapped Inductor LC network. Both the Colpitts and Hartley oscillators are similar, in their frequency range of operation, output voltage and phase noise. The LC resonators used in both the Colpitts and Hartley oscillators will have a typical maximum Q of 250. In practice, unloaded Q values of 100 are more common.

Voltage Controlled Oscillator. One of the capacitors in the LC network for a Colpitts or Hartley oscillator is replaced with a varactor diode, allowing the capacitance of the LC network to be varied by applying a DC bias. Voltage controlled oscillators are used in many applications.

Crystal Oscillator. A quartz crystal is used as part of the frequency selective network, resulting in a very high Q resonator. Fundamental mode crystal oscillators are available for frequencies between 32 kHz and 100MHz. Crystal oscillators have very low phase noise. Quartz Crystal resonators will be discussed in more details later.

Stripline or Microstrip transmission line resonator. At VHF and microwave frequencies, such resonators are a reasonable size and have typical unloaded Q values of 200.

Coaxial cavity oscillator. The resonators can be made from coaxial resonators with a centre length of one-quarter wavelength. These resonators can have unloaded Q values of several thousand. The resonators are large, restricting the applications.

Dielectric resonator oscillator. By filling the coaxial resonator with a material with a high dielectric constant, the linear dimension is reduced by the square root of the dielectric constant. Having a dielectric constant of 25 will thus reduce the volume of the resonator to 1/125 of the air filled resonator volume. Dielectric resonators are used frequently at microwave frequencies. The resonators can be based on the coaxial resonator and have a centre conductive resonator and conductive walls, or they can simply be a high dielectric material, relying on the dielectric-air interface to keep the electric fields inside the resonator.

A plot of the Q values of different resonators and their corresponding volume is shown in figure 6.4.

The phase noise of an oscillator is primarily determined by the Q of the resonator used in the oscillator, and the way that the amplifier loads the resonator. The higher the Q of the resonator, the lower the phase noise and in general, the lower the frequency variation that can be obtained by tuning the resonator. The choice of the resonator and its Q is thus the primary factor affecting the oscillator properties [1].

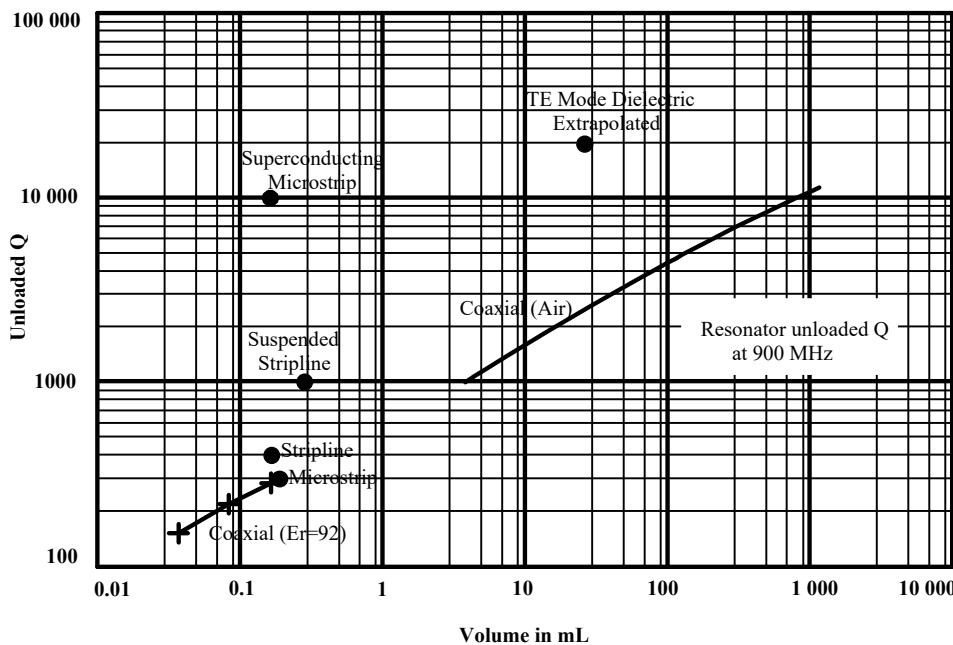


Figure 6.4. Q values and volume of different resonators at 900 MHz.

Oscillator Design Procedure

A 100 MHz oscillator is required, to operate from a 7V supply. The oscillator in this chapter can easily operate at > 100 MHz. Simply change F_0 in the Global Definitions of the project file for figures 6.8 to 6.19, to select the desired operating frequency.

Step 1: Select an Amplifier Type

The active device used in an oscillator is very important, factors for consideration are; Output power, oscillating frequency, supply voltage and cost. The low frequency phase noise of the oscillator does depend on the flicker noise of the amplifier, so that the noise figure of the amplifier is important for low noise oscillators.

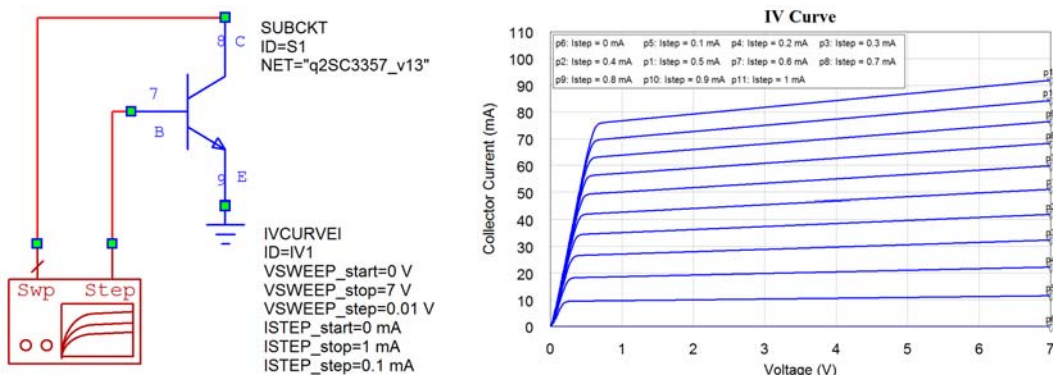


Figure 6.5. Circuit for determining the I-V characteristic of a transistor.

The most important design parameter is the biasing of the transistor. The IV curve is very useful in determining the correct biasing conditions. It should be realised that some of the critical transistor parameters like β can vary over a 5:1 ratio between transistors. The transistor parameters used in the models of the computer simulation software, include typical values. The design must be such that the oscillator will work under all permissible variations of transistor parameters. The I-V curve can easily be obtained in MWO as shown in figure 6.5:

For linear biasing, a 7V supply and quiescent collector current of between 40 and 5 mA is required. 15 mA is a good compromise to minimise the power dissipation in the transistor and still have sufficient output power.

Step 2: Design an Amplifier

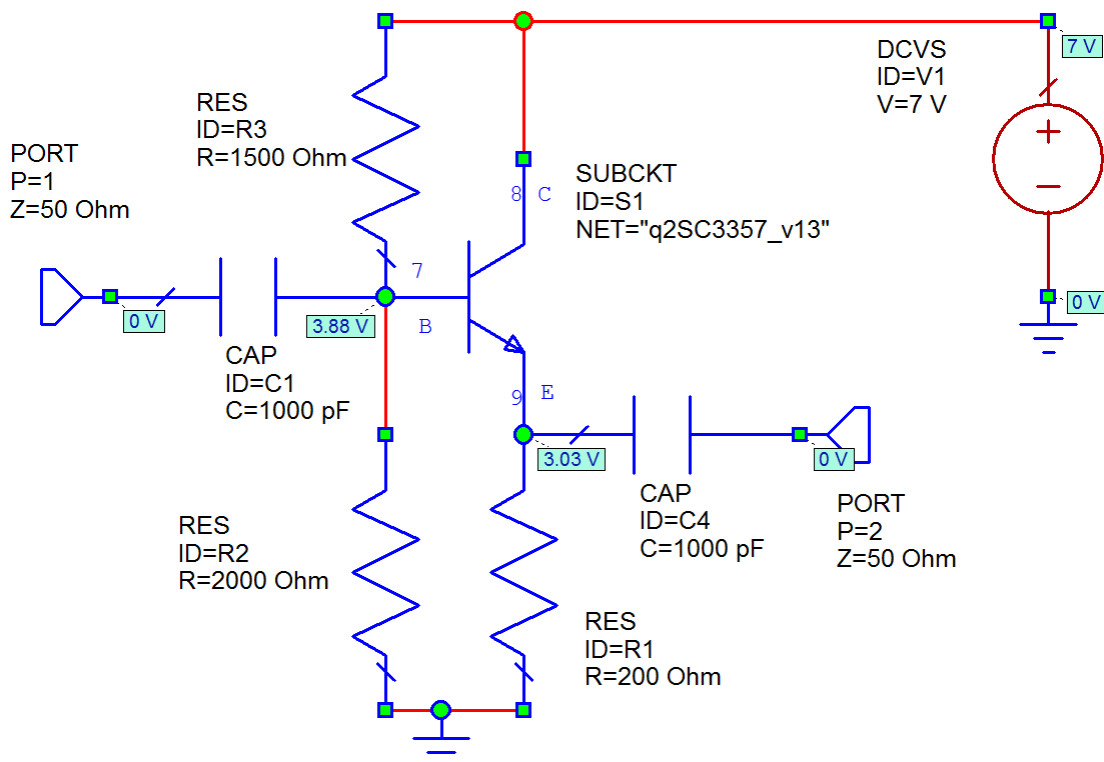


Figure 6.6. Amplifier for the Colpitts oscillator

A typical amplifier configuration and one that is used for this design is shown figure 6.6. The first step is to select the bias voltages. For a 7 Volt supply, and having an emitter follower configuration for the amplifier, the emitter voltage should be close to half of the supply voltage, minus one volt. This results in a large swing without the transistor saturating. For a quiescent current of 15 mA, the current through the biasing chain should be of the order of 1.5 mA to 3 mA, for good quiescent current stability with temperature. For an emitter voltage of 3 Volt, a base voltage of 3.5 Volt is desired, so that a biasing resistor, between 2.4 k Ω and 1.2 k Ω is required for R_3 , when the values are rounded to the nearest available resistor values. Since a relatively high input impedance is required, a 2 k Ω resistor is used. A 1.5 k Ω resistor is required to then obtain the 3.5 V at the base of the transistor using a 7 V supply. The annotation setting allows the circuit voltages to be indicated on the circuit diagram in Microwave Office, and allow the biasing and voltages to be checked.

Note: The gain of 4dB is the power gain taking the different input and output impedances into account. Input Impedance 638Ω and the output impedance is 17Ω , with a significant reactive component that will affect the resonance of the Colpitts oscillator if it is not allowed for in the design process.

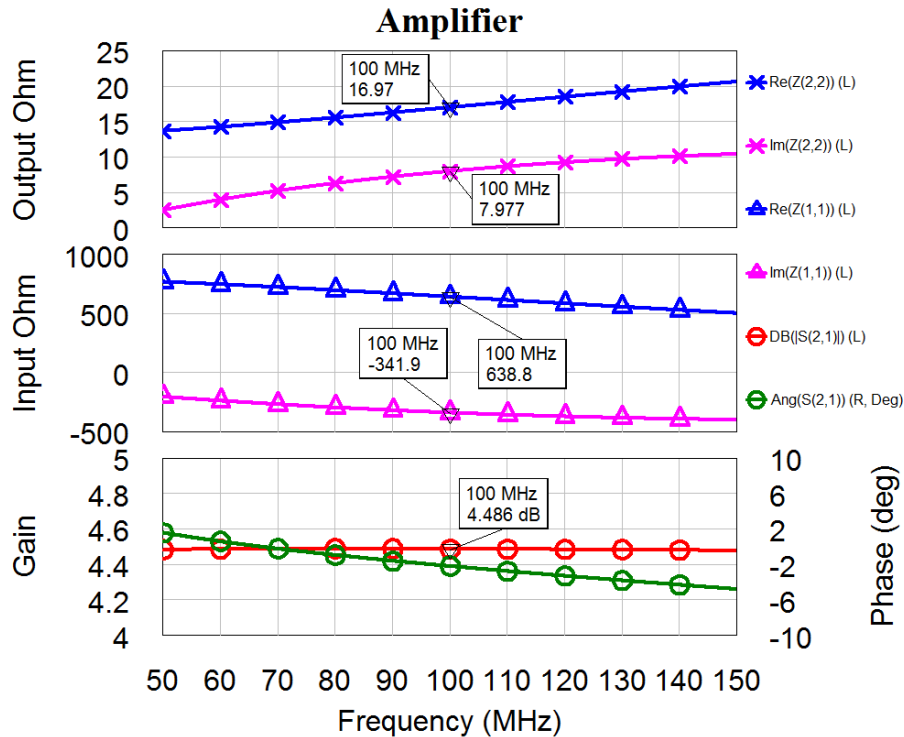


Figure 6.7. Amplifier Performance.

Step 3: Design a Resonator

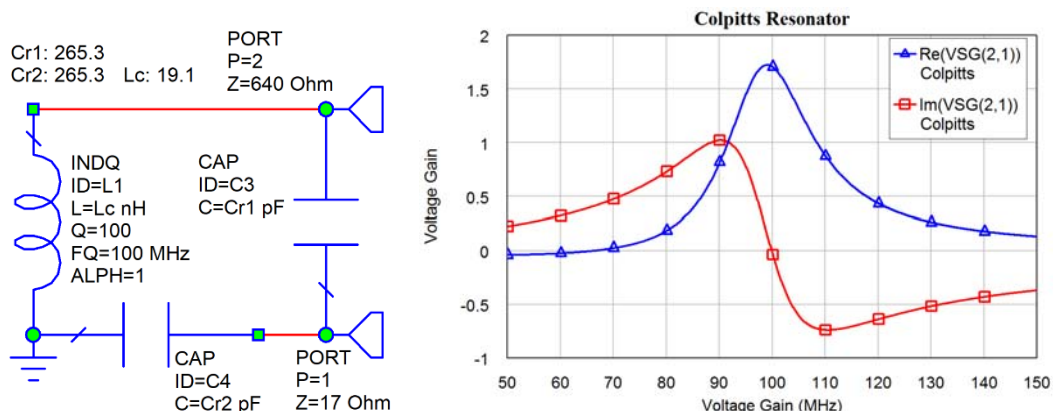


Figure 6.8. Colpitts resonator network

The resonator must be a frequency selective network, to ensure that the conditions for oscillation only apply at one frequency. In addition, the network must be matched to the input impedance and output impedance of the amplifier and have a high Q. The components can be tuned to ensure a 0° (or 180° if needed) phase shift at the required operating frequency. In figure 6.8, the imaginary part of the transfer function is not exactly zero, since the network shown is corresponds to the one actually used in the oscillator and allows for phase changes produced by the amplifier.

Step 4: Linear Oscillator Analysis

The resonator and amplifier are now combined into the one circuit. The element OSCTEST is used to determine the loop gain and phase shift. Set the secondary parameter FC to 160 MHz, which is just above the largest frequency of figure 6.9 and is below the expected 200 MHz second harmonic frequency. The resonator network is now tuned to give a phase shift of zero degrees between port 1 and 2, at the required operating frequency. If needed, the loop gain is changed to ensure that it is just slightly above one at the operating frequency. That then corresponds to the correct conditions for oscillations. To minimise the loading on the amplifier, and that load affecting the Q of the resonator circuit, port 3 is terminated in a 1 kΩ load.

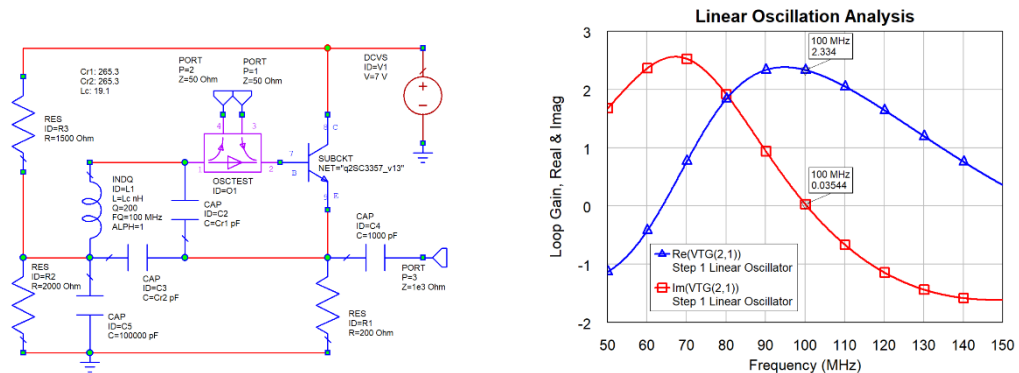


Figure 6.9. Linear analysis using OCSTEST

Step 5: Nonlinear Oscillator Analysis

Replace OSCTEST with OSCPROBE as shown in figure 6.10, to do a harmonic balance analysis. Set the secondary parameter F0, to 100 MHz, to make that the initial guess for the oscillation frequency and set the secondary parameter VpMax to 4V, since the oscillating waveform at the base of the transistor will be less than 4Vpp. This edition, the APLAC HB (Harmonic Balance) simulator, rather than the older Harmonic Balance simulator is used. This allows the oscillation frequency, output power, output waveforms, and output spectrum to be determined. The circuit parameters can now be tuned, to ensure the circuit oscillates correctly and produces a low phase noise. Equations are used in the *Global Definitions* block, to ensure that both the linear and non-linear circuit keep identical circuit elements. These equations are shown in figure 6.10. Useful parameters to tune are the resonator frequency Fo, Kc relating to the split of Cr1 and Cr2, the biasing resistors Rb1, Rb2 and the emitter resistor Rec.

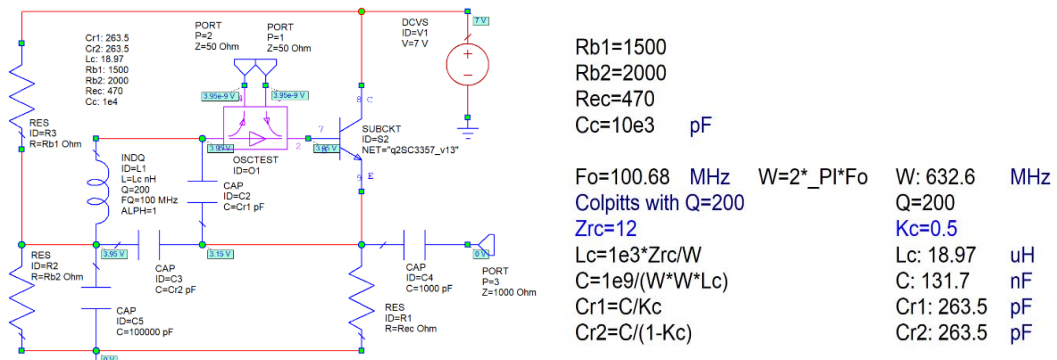


Figure 6.10. Circuit for non-linear analysis and corresponding circuit elements.

F_o is tuned to set the oscillation frequency to 100 MHz. Z_{rc} has a significant effect on the phase noise. At this stage, Z_{rc} is kept at 12Ω to give realistic component values. The effect of the output load at port 1 on the noise figure and output waveform can also be determined. The resulting circuit giving a good output voltage and noise figure is shown in figure 6.10. The output spectrum is shown in figure 6.11. The corresponding output waveform is shown in figure 6.12. The output waveform is large enough, ± 2.5 Volt and has harmonics that are more than 35 dB below the fundamental.

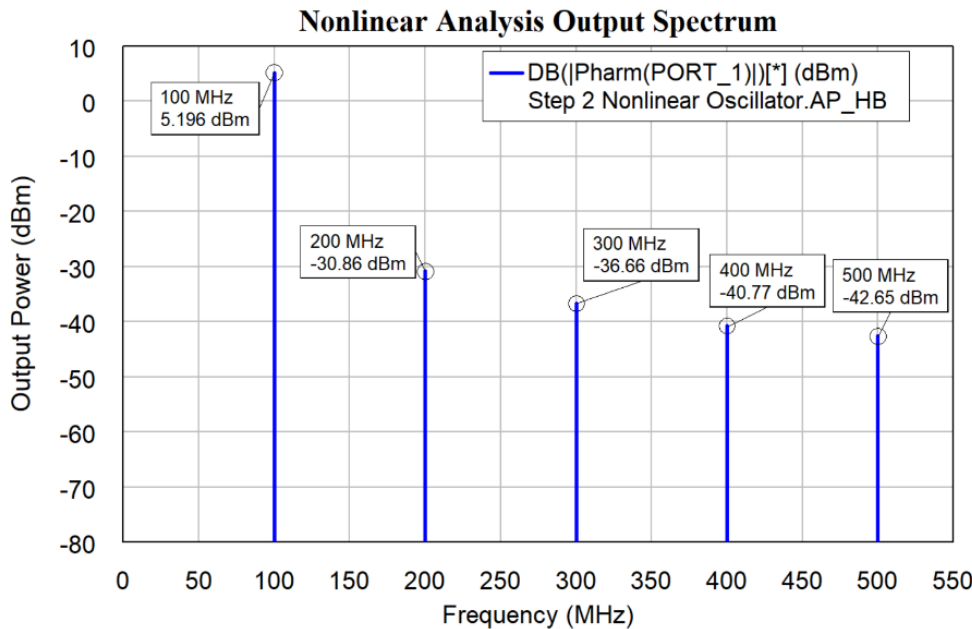


Figure 6.11. Output spectrum determined by non-linear analysis.

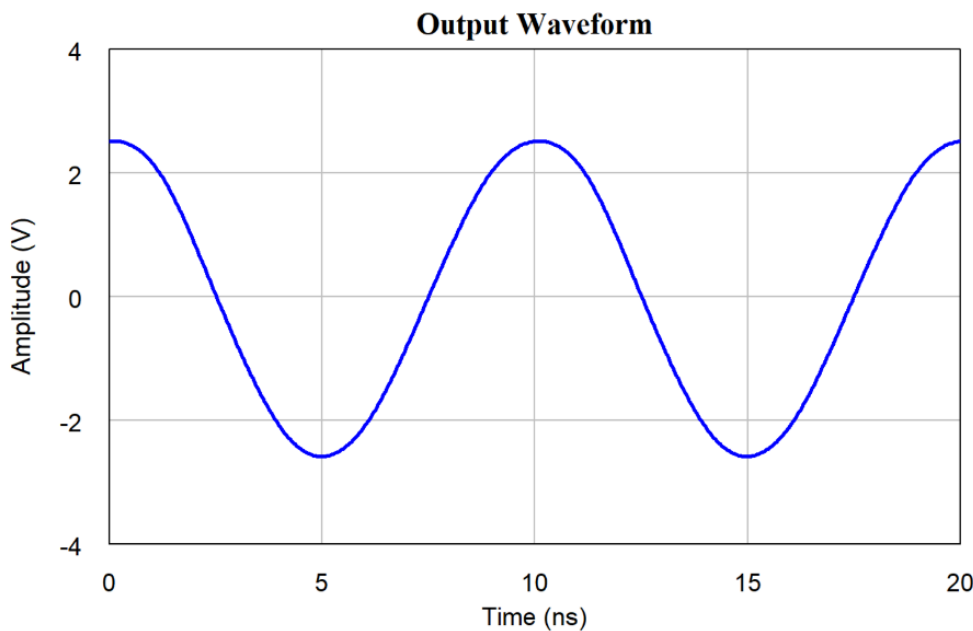


Figure 6.12. Output waveform determined by non-linear analysis.

The SWPVAR simulation control (*Element* \Rightarrow *Simulation Control* \Rightarrow *SWPVAR*) shown in the schematic of figure 6.10 allows the plotting of the sweep of inductor values and their corresponding oscillating frequency. The resulting plot is shown in figure 6.13.

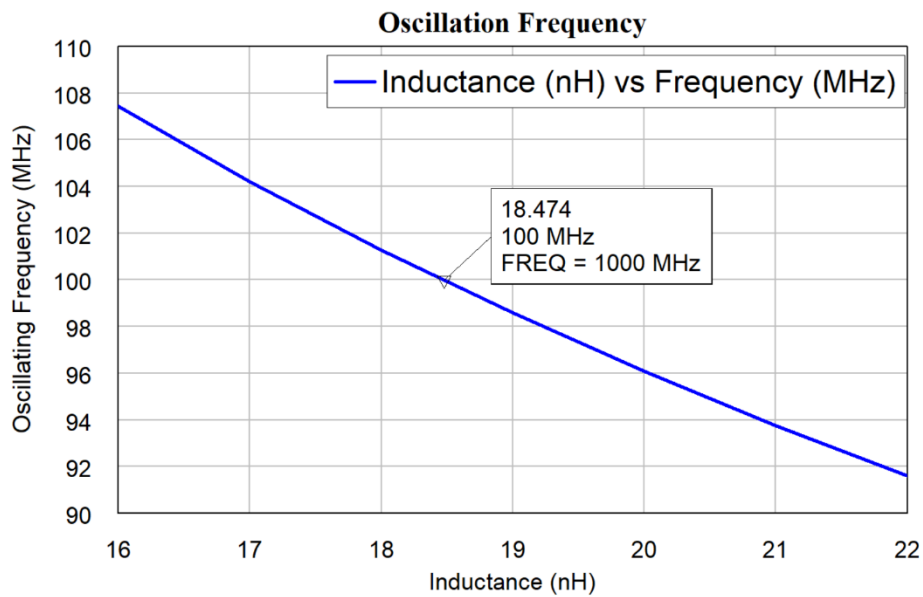


Figure 6.13. Change in oscillating frequency as the resonator inductor varies.

The non-linear analysis can also be used to determine the Phase Noise of the oscillator. The OSCNOISE measurement (*Element* \Rightarrow *MeasDevice* \Rightarrow *Controls* \Rightarrow *OSCNOISE*) allows the phase noise of the oscillator to be measured as shown in figure 6.14. The phase noise will depend on the Q of the resonant network as well as other parameters, such as the noise figure of the amplifier and the amplifier power level and the loading that the amplifier places on the resonant network. Being able to change the circuit elements in figure 6.10 and observe the effect of that change on the phase noise is a great advantage in designing good oscillators. In general, the higher the oscillating frequency, the higher the phase noise as a percentage deviation of the centre frequency.

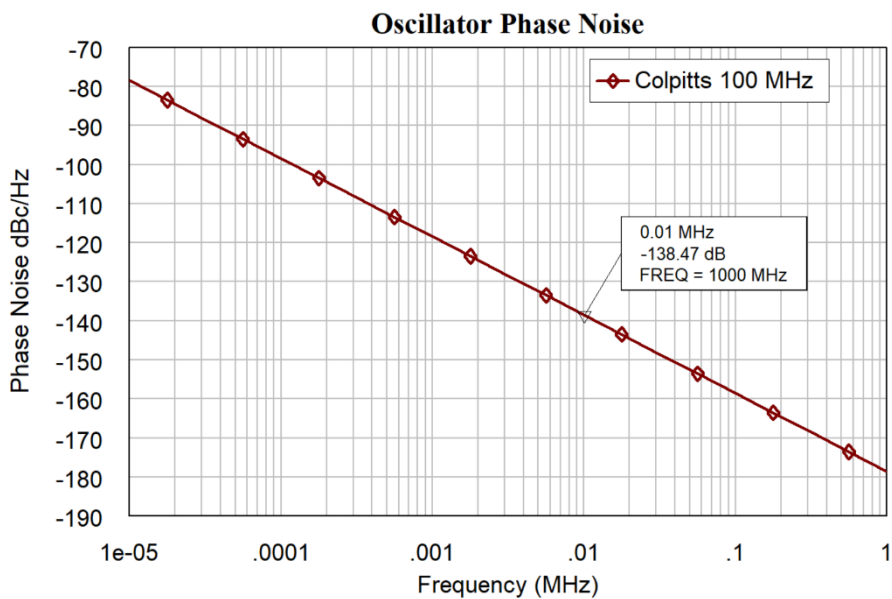


Figure 6.14. Phase noise of the oscillator using non-linear (harmonic balance) analysis.

The above design procedure allows the performance of an oscillator to be accurately determined prior to the hardware being produced. This greatly reduced the cost of designing oscillators. The non-linear analysis can only be produced when a full Spice

model of the active device is available. Many transistor manufacturers provide the required models for their transistors. Unfortunately, the SPICE models are not available for many commercially available Microwave Monolithic Integrated Circuits (MMIC). As shown in chapter 10, the same design process can be used for oscillators using Operational Amplifiers.

Example 6.1: Low Phase Noise Design

This example illustrates the importance of minimising the loading on the resonator in order to obtain the lowest phase noise. To give a fair comparison between the different oscillators alone, no buffer amplifiers are included at the output and the loading of the oscillator is minimised by making the impedance of the output port $10\text{ k}\Omega$. A Hartley oscillator uses a tapped inductor, while the Colpitts oscillator uses a tapped capacitor. A Hartley oscillator can be made using a common emitter transistor, driving the resonator as shown in figure 6.15. This circuit is typical of Hartley circuits presented on the web. The tapped inductor for the Hartley oscillator is normally made using one coil wound on a former, with a tapping point at the appropriate point on the coil. As a result, there will be some mutual coupling between those coils and in MWO. The mutual coupling changes the inductances. To facilitate the resonator calculations, the mutual coupling has been ignored and the tapped inductor is realised using 2 separate inductors. The designs presented are for a 100 MHz low phase noise oscillator. The resonator elements are calculated using equations in NI-AWR DE, so that the oscillation frequency can simply be changed by changing one variable.

Since the waveform amplitude across the OSCAPROBE element may be larger than the secondary parameter $V_{p\text{Max}}$, that value should be increased to 8V. It is also important to set the value of FC in the OSCTEST element to 160MHz, which is greater than the frequency sweep used for the linear gain test and less than the expected 200 MHz second harmonic of the oscillating frequency.

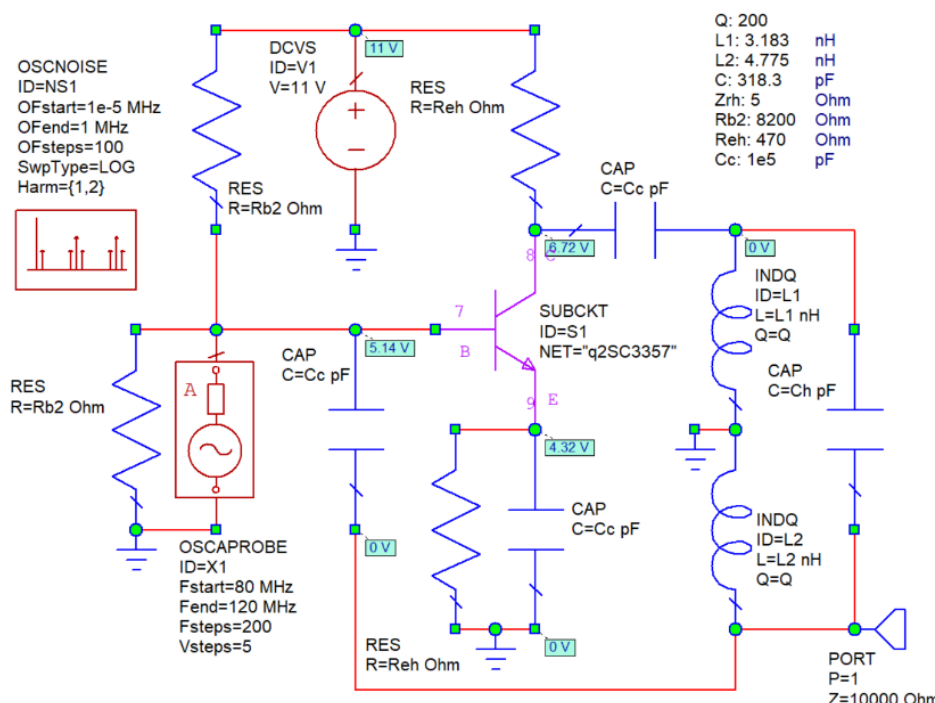


Figure 6.15 Common emitter amplifier Hartley 1 oscillator.

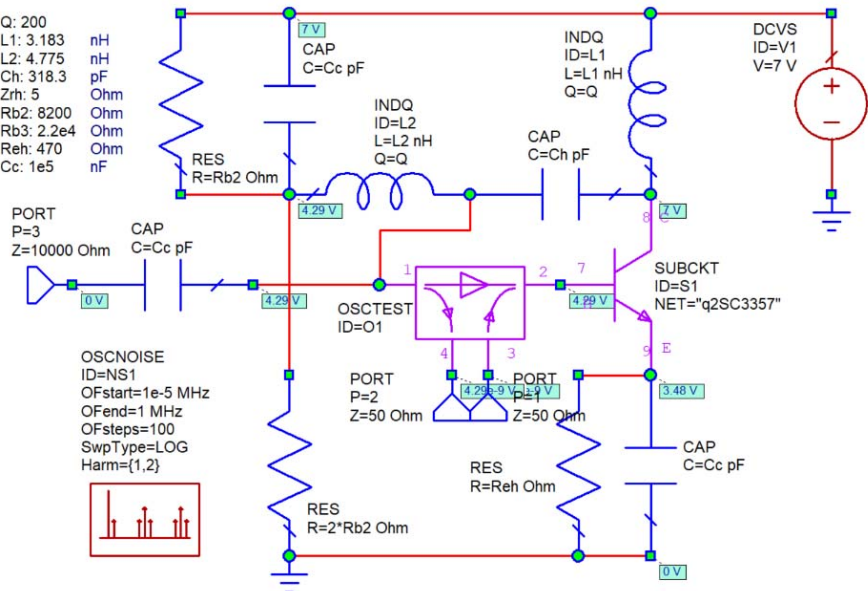


Figure 6.16 Lower phase noise Hartley 2 oscillator.

The problem with the circuit in figure 6.15 is that the collector resistor Reh and the load at Port 1 are loading the resonant network and will thus lower the Q of the resonator network and increase the phase noise. Rearranging the circuit and replacing collector resistor with the resonator, as shown in figure 6.16, removes the loading of the resonator and reduces the phase noise. The inductance of the resonator provides the DC path for the collector current and the base current for the transistor biasing. Having a high input impedance, external amplifier stage, reduces the resonator loading even more and minimises “load pulling”, which is the frequency change of the oscillator, due to variations in the load impedance at the output.

To ensure that a fair comparison can be made between the phase noise of the oscillators in figure 6.15 and 6.16, the same transistor, the same collector current and the same resonator total inductance and capacitance values are used. Figure 6.17 shows a comparison of the output spectra of these oscillators. The oscillator “Hartley2”, corresponding to figure 6.16 has a slightly larger output, and lower harmonics than the output of oscillator “Hartley1”, corresponding to figure 6.15. For these figure 6.17, the Q of the inductor used for the resonator, is $Q = 200$. Normally the Q of the capacitors used in the resonator is much higher than the Q of the inductors, so that the Q of the resonator is determined by the Q of the inductor. A Q of 200 can be achieved by careful construction of the inductor used for the resonator.

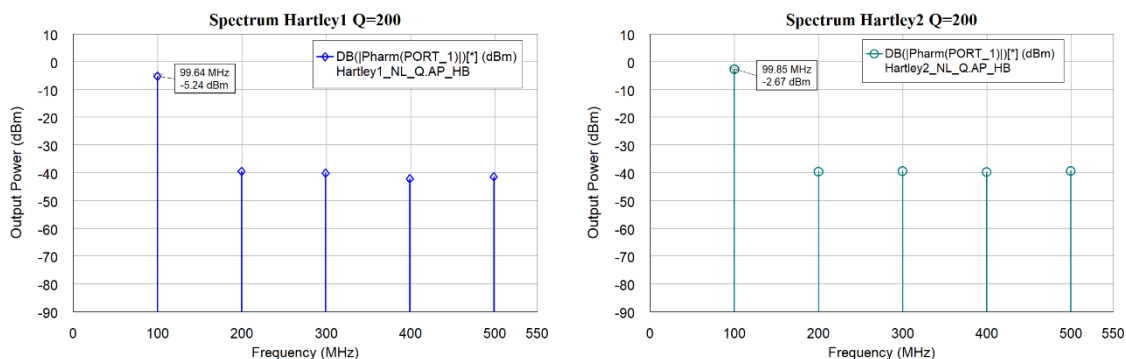


Figure 6.17 Hartley oscillator spectra. Left oscillator of figure 6.15, Right oscillator of figure 6.16

For the Colpitts Oscillator of figure 6.9 and 6.10, it is more difficult to minimise the loading of the resonator. By adding a buffer amplifier as shown in figure 6.18, the loading caused by the output can be reduced.

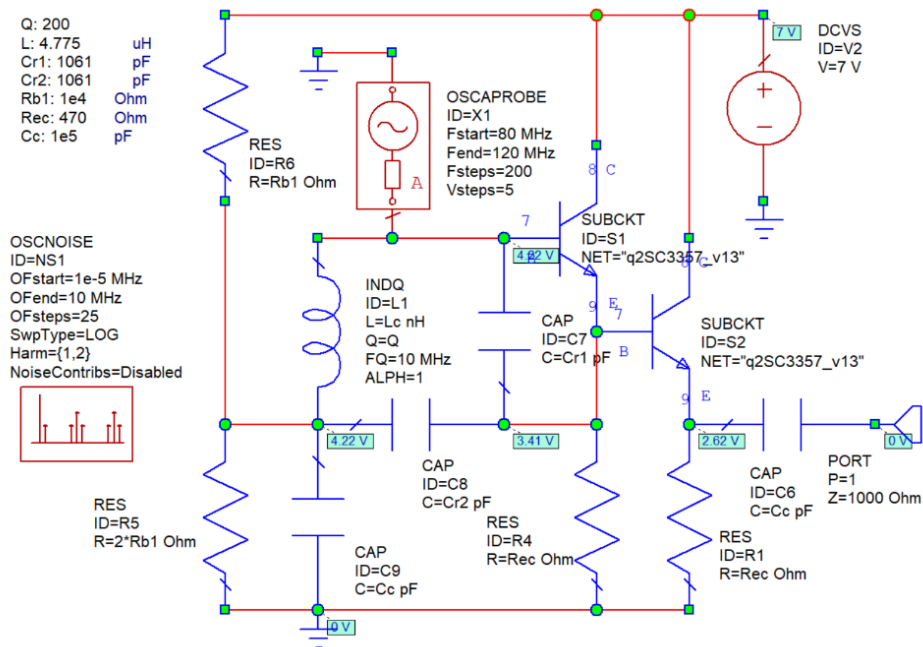


Figure 6.18 Colpitts oscillator with reduced output loading.

For the circuits shown in 6.15, 6.16 and 6.18, reducing the inductors and increasing the capacitors, reduces the impedance of the resonator and the loading effects due to the output. The optimum impedance required can be determined by observing the phase noise of the oscillator as circuit parameters are changed. The lowest phase noise is obtained with the lowest resonator impedance Z_{rh} (Hartley) or Z_{rc} (Colpitts). Very low resonator impedance result in very small inductances. As a result, the smallest resonator impedance used for figures 6.15 to 6.19 is 5Ω , corresponding to an 8 nH inductance. Figure 6.19 shows the phase noise of the oscillators of figure 6.15, 6.16, and the oscillator shown in 6.18, excluding the buffer amplifier, to ensure a fair comparison. All the circuit values are tuned to provide a low phase noise. The plots labelled “Q=200” use a resonator with a $Q=200$ and the plots labelled “ideal”, use resonators with $Q=10000$. The exact equations and values used are contained in the accompanying project files.

Figure 6.19 shows that changing the Hartley oscillator circuit of figure 6.15 to 6.16 reduces the phase noise from -144 dBc/Hz to -147.8 dBc/Hz . Using a resonator with a $Q=10000$ results in a phase noise of -159.2 dBc/Hz . That is a 15.2 dB improvement over the design of figure 6.15. This shows that the resonator Q and the loading of the resonator is the prime factor in determining the phase noise that can be obtained from an oscillator. To enable a comparison of the phase noise for different oscillators to be made, the markers in figure 6.14, 6.19 and 6.22 are all at a 0.01% deviation from the carrier. Figure 6.19 shows that circuit impedances that are not part of the resonator, limit the phase noise. The phase noise of the ideal Hartley oscillator is smaller than the phase noise of the ideal Colpitts oscillator, since the Hartley oscillator has less loading of the resonator due to other circuit components. A high resonator Q value is critical in obtaining a low phase noise. Changing the oscillation frequency to 10 MHz , results in nearly the same noise performance for the ideal Hartley and Colpitts oscillators.

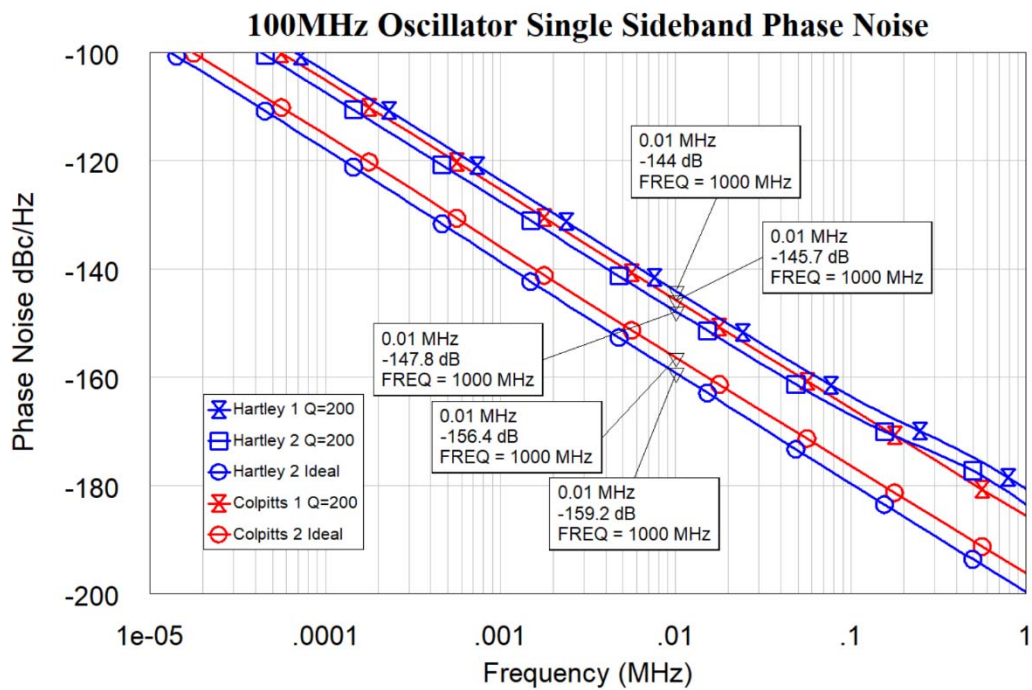


Figure 6.19 Hartley and Colpitts 100 MHz oscillator phase noise.

Crystal Oscillators

Crystal have very high Q values, so that crystal oscillators have much lower phase noise than oscillators with LC resonators.

Quartz Crystals

For details of Quartz Crystals see "Quartz Crystal Resonators and Oscillators for Frequency Control and Timing Applications - A Tutorial" [2] by the 2009 IEEE president John Vig. He has graciously given permission for those PowerPoint slides to be available as a resource for this book. As a result, they are included in the "Resources".

Example 6.2: Crystal Oscillator Design

The design of a crystal oscillator is similar to that of any other oscillator. For most fundamental mode crystal oscillators, the crystal is inductive at the operating frequency and the inductor in any LC oscillator is replaced with the crystal. In figure 6.20, the inductance of a phase shift oscillator is replaced with a quartz crystal. The inductance is calculated from the crystal's frequency F_s and capacitance C_1 . A minor frequency change for F_s is made for the resonance shown in figure 6.23 to be exactly at 25 MHz.

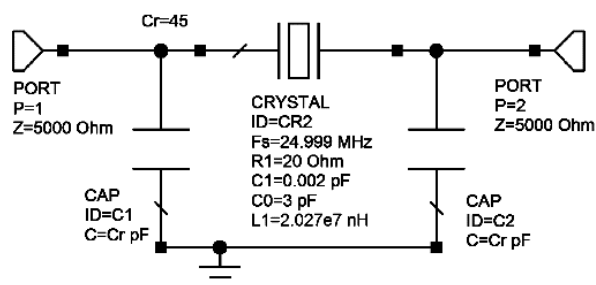


Figure 6.20. Phase shift network using a quartz crystal.

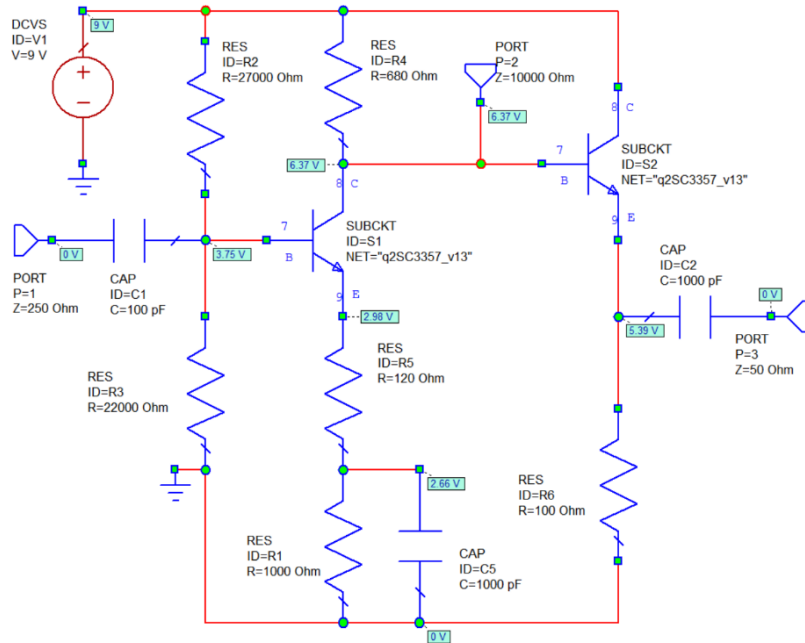


Figure 6.21. Amplifier for a 25 MHz crystal oscillator.

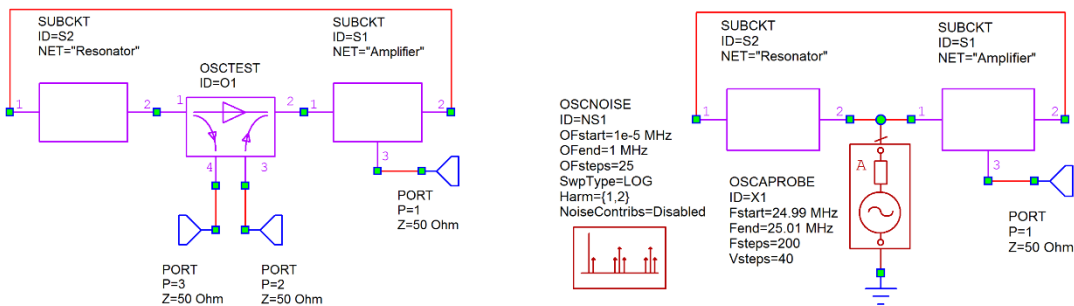


Figure 6.22. Linear and non-linear oscillator circuits

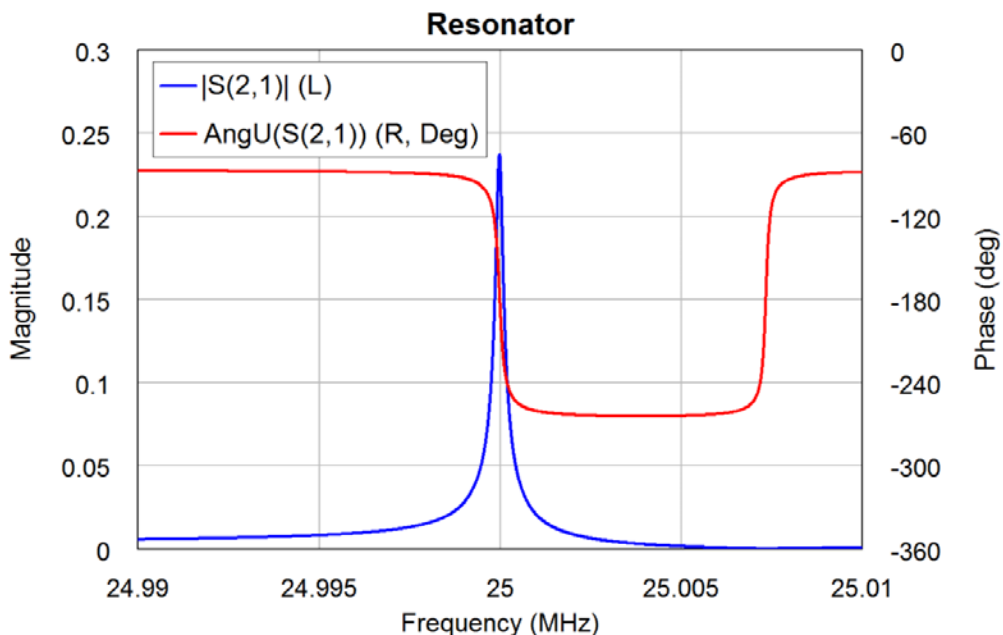


Figure 6.23. Frequency response of the resonator of figure 6.20.

The amplifier shown in figure 6.21 has a gain of 25 dB from the input port 1 to the output port 3. The gain from the input to port 2 is enough to cause oscillations. The gain of the amplifier can be controlled by changing $R4$, the resistor connected to the emitter, without affecting many other parameters. The resonant network and the amplifier are connected together to form a Crystal oscillator as shown in figure 6.22. Using OSCTEST, the gain around the amplifier and resonator loop is now determined using a linear oscillator analysis as shown in figures 6.23 and 6.24.

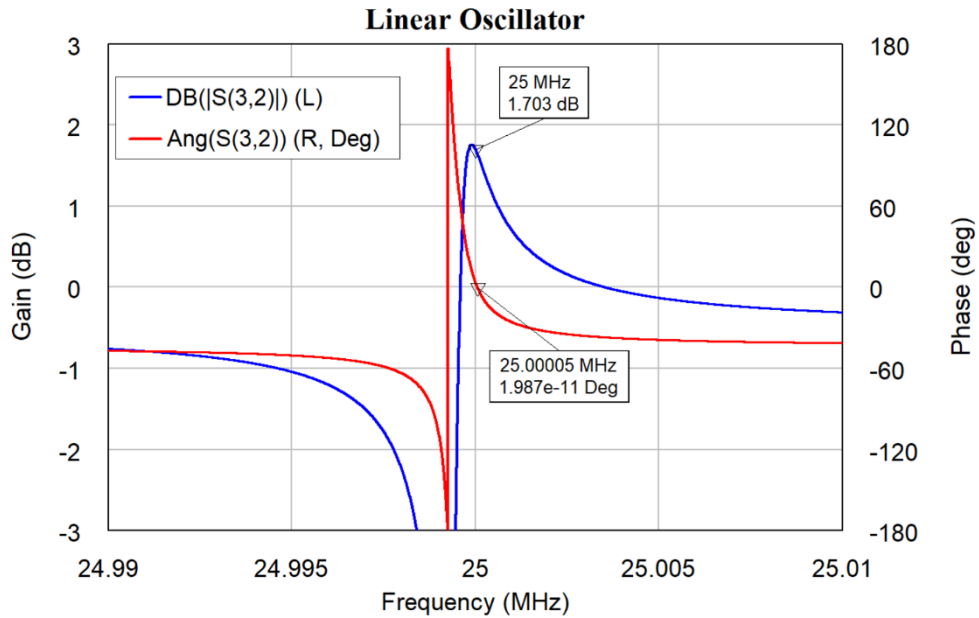


Figure 6.24. Frequency response for the oscillator using linear oscillator analysis (OSCTEST).

Replacing the OSCTEST element with the OSCAPROBE element as shown in figure 6.22, allows a harmonic balance analysis to be performed. Figure 6.25 shows the output spectrum, figure 6.26 shows the corresponding waveforms, and the phase noise is shown in figure 6.27

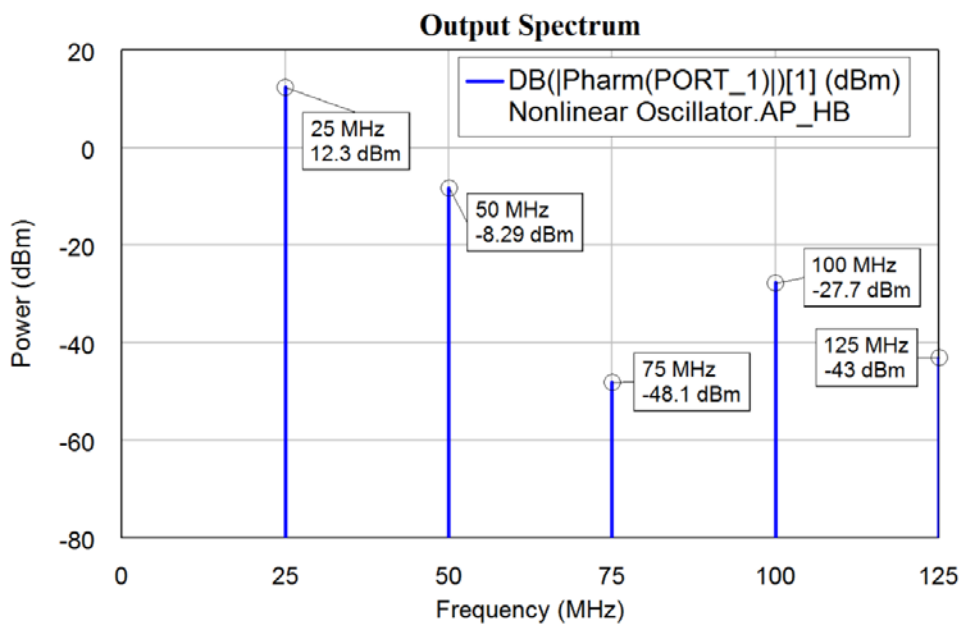


Figure 6.25. Output spectrum obtained using harmonic balance analysis. (OSCAPROBE)

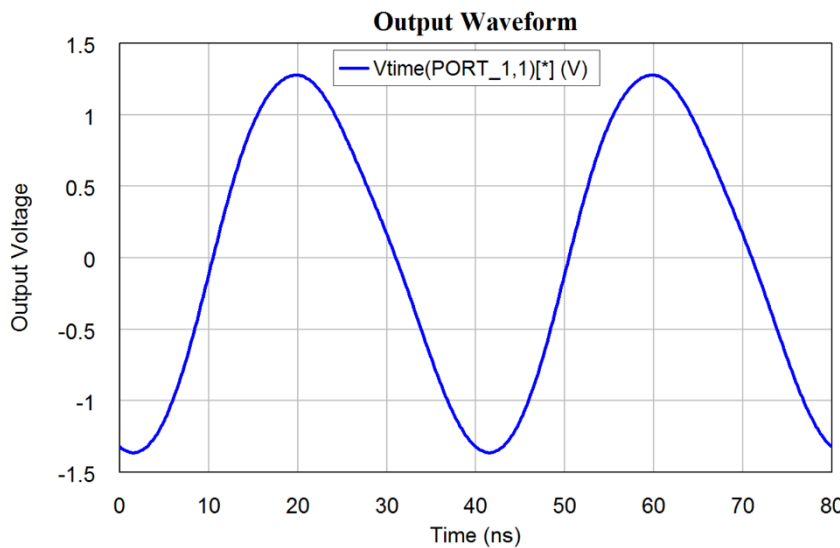


Figure 6.26. Output waveform obtained using nonlinear (harmonic balance) analysis.

By comparing figures 6.14 and 6.19 with figure 6.27, it can be seen that the crystal oscillator has a much lower phase noise, due to the Q of the resonator being much higher. The phase noise at 25 kHz in figure 6.27 is determined by the resistor and transistor noise rather than the resonator. For low noise crystal oscillators, the output amplifier should impose a negligible load on the resonator and should use low noise transistors and low resistor values. For best comparison the same transistors and the same APLAC-HB simulator is used in all the simulations of figures 6.14 to 6.27.

Using a varactor diode permits the electronic control of the frequency or frequency modulation of the oscillator of figure 6.6 to 6.14 and the oscillators of figure 6.15, 6.16 and 6.18. A 2:1 frequency range is possible. The frequency of crystal oscillators can however only be varied by several parts per million, and is used to obtain the precise frequency setting required for radio transmitters.

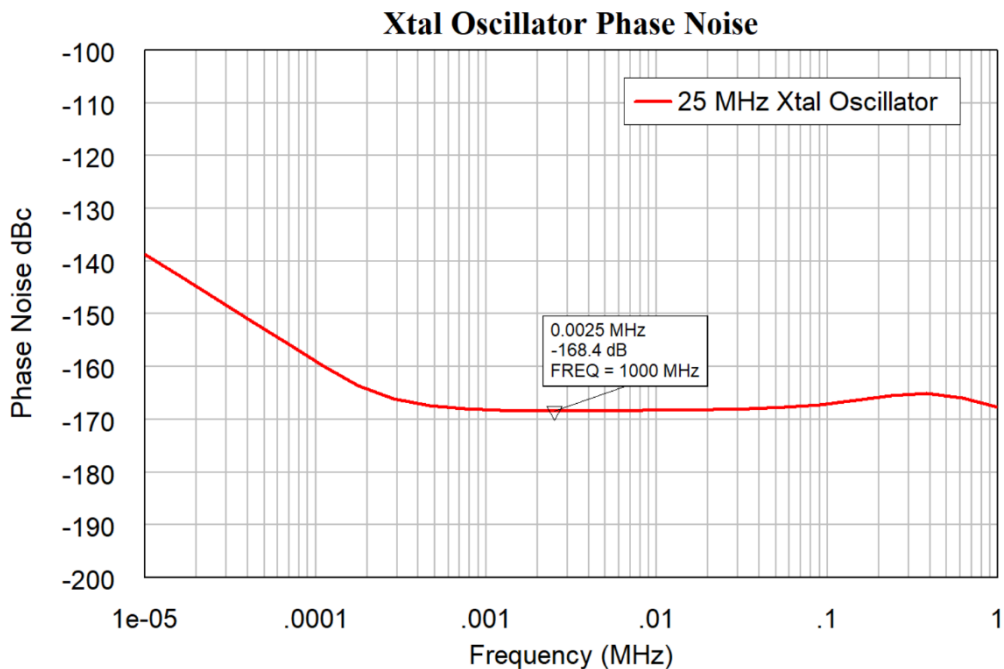


Figure 6.27. Phase noise of the oscillator.

RF and Microwave Oscillators

At RF and Microwave frequencies (above 1GHz), transmission lines are often used as circuit elements. The MAR6 amplifier, used here, is a typical MMIC costing less than \$10. These devices are very simple to use, are convenient, and can be used as low power amplifier blocks in many applications. The S parameters for these devices can be obtained from the Mini-Circuits web site as follows:

!MAR-6 (TA = 25°C, Id = 16mA)									
!FREQ.		S11		S21		S12		S22	
!MHz		dB	Ang	dB	Ang	dB	Ang	dB	Ang
# MHZ S DB R 50									
100	-27.96	171	20.1	171	-22.50	5	-27.96	-30	
500	-26.02	-105	18.7	138	-21.30	21	-20.00	-104	
1000	-17.72	-118	16.4	107	-18.80	28	-17.08	-150	
1500	-13.56	-140	14.1	84	-17.10	28	-16.48	180	
2000	-10.75	-163	12.0	65	-15.80	26	-15.92	157	
2500	-9.37	-176	10.3	55	-15.20	28	-15.92	150	
3000	-7.74	169	8.7	42	-14.80	25	-16.48	143	
3500	-6.74	157	7.2	30	-14.20	22	-17.72	144	
4000	-6.20	146	6.1	18	-13.80	20	-20.00	156	

Table 1. S parameter file from Mini-Circuits with added line in blue.

This file can be imported into Microwave Office so that those S parameters for the device can be used in a simulation. Theo import the s parameter file, it needs to be in the “Touchstone” file format [3]. The only change that needs to be made to the S parameter file as obtained from Mini-Circuits, is the addition of the line shown in blue:

MHZ S DB R 50

That line indicates to Microwave Office that the file has frequencies in MHz, contains S parameters, which must be in the order S11(Real, Imag), S21(Real, Imag), S12(Real, Imag) and S22(Real, Imag). The real part is in DB and the reference impedance is 50 ohm. Any line beginning with “!” is a comment line and is ignored in the data file import.

For other formats for data-files see the Microwave Office help files on “Adding Data Files to a project”, which includes details on the Touchstone Import files format. That data file is then used as a sub-circuit in the circuit diagram.

Example 6.3: 1 GHz Microstrip Oscillator Design

This data file is now used to design a 1 GHz oscillator using this MAR6 amplifier and using Microstrip circuits on a Rogers RO4003 substrate. The oscillator consists of three parts: The MAR6 amplifier, A Microstrip resonator (*TL1*) with tap coupling in order to obtain the correct impedance levels for the coupling into and out of the resonator and thirdly transmission lines *TL2* to *TL11*, which are required to connect the output back to the input and thus provide feedback. The path length around the loop must have the appropriate phase shift to ensure that oscillations will result. In addition, two coupling

capacitors are used to provide the correct DC levels at the input to the MAR6 and prevent the output from being shorted at DC.

The impedance of the resonator should be as low as possible to provide a reasonable Q, with low radiation losses and a good frequency stability. This is achieved by making the width of the resonator 5 mm, which corresponds to a characteristic impedance of 24.8Ω . A program TXLine, which is part of MWO is used for the calculations of the required length of the resonator. A screenshot of the resulting line parameters from TXLine is shown in figure 6.28.

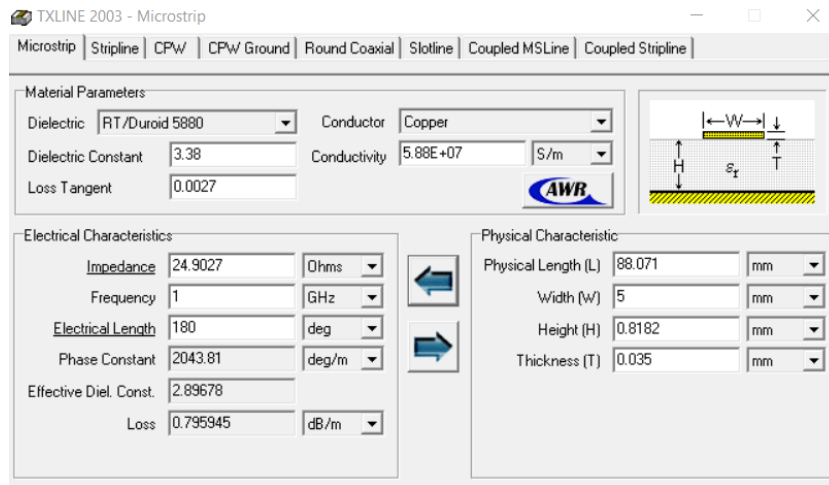
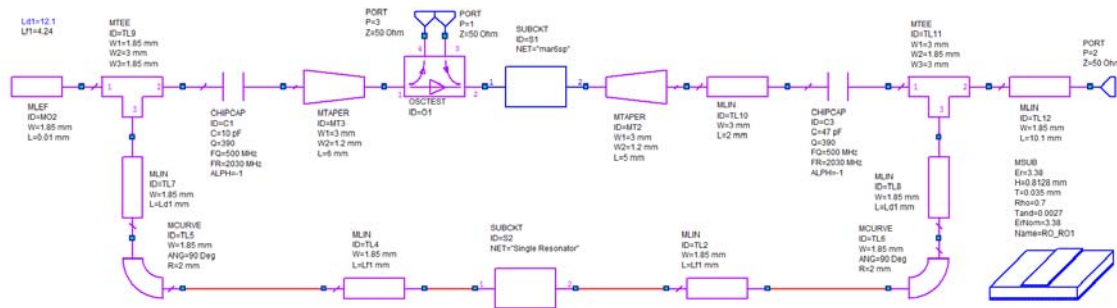


Figure 6.28. Resonator Width and Length Calculation

Since a full SPICE model is not available for the MAR6, only a linear analysis of the oscillator can be carried out. The circuit schematic for the oscillator is shown in figure 6.29. This design was produced in early 2005 and presented at [4]. At that time the more advanced X models were just becoming available and as a result MTEE, MCROSS and MLEF elements were used. For current designs, the more advanced EM based MTEEX, MCROSSX and MLEFX elements should be used. In addition Rogers had not yet suggested that $\epsilon_r = 3.55$ should be used for simulation of RO4003 substrates, so the value $\epsilon_r = 3.38$ was used in this design. To enable a comparison between the simulations and measurements to be made, the results in figures 6.32 to 6.36 are obtained from the original design.



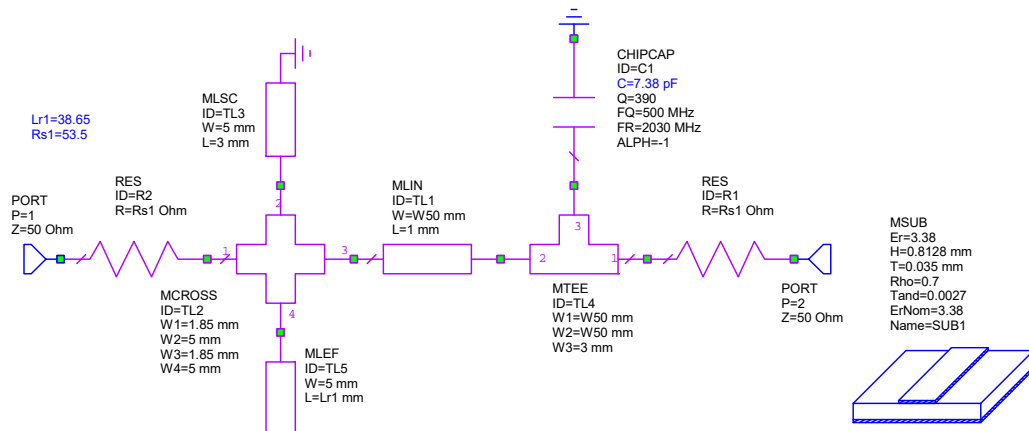


Figure 6.30. Circuit Schematic for 1GHz Microstrip resonator.



Figure 6.31. Layout for 1GHz Microstrip resonator.

The length of $TL3$ is made small as is practicable to minimise the loading of the resonator due to the rest of the circuit. The length of $TL3$ should be several times larger than the width of the connecting tracks, to ensure a uniform current distribution on the input and output connectors. The 50Ω track width of $TL1$ is 1.84 mm. As a result, the smallest length of $TL3$ is about 3 mm. Resistors $R1$ and $R2$ are placed at the input and output, to firstly provide a reasonable termination impedance to the amplifier at frequencies other than the resonant frequency and secondly to provide some fine tuning for the resonator loading, and thus the loop-gain of the oscillator. Figure 6.31 shows the layout for the resonator and the coupling capacitors. The left end of the circuit is grounded.

Figure 6.32 shows the amplitude and phase of the resonator of figure 5.29, as a function of frequency.

Tuning Step 1: Tune the length of the resonator $Lr1$, to ensure that the resonator has a maximum gain from port 1 to port 2 at the desired oscillating frequency in figure 6.32. The gain at other frequencies should be low, to ensure that the oscillator does not oscillate at another frequency.

The resonator has a well-behaved response at 1 GHz, but the amplifier gain is too high, so that there is a possibility of oscillation at the secondary response of 1.34 GHz. The loop gain of the amplifier and resonator must thus be carefully controlled to ensure that only oscillation at 1 GHz is possible.

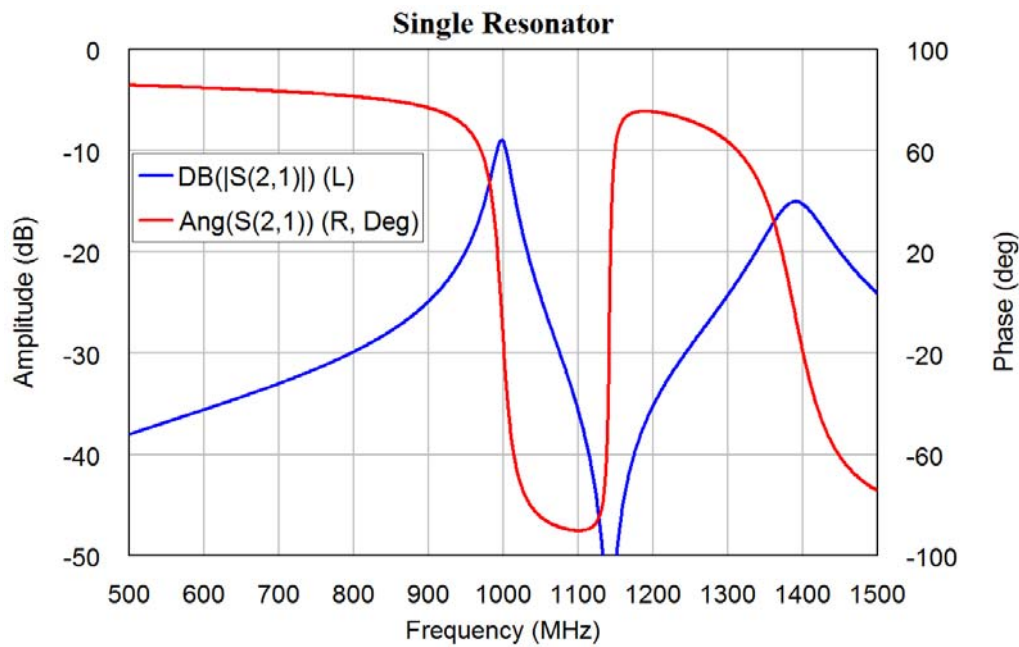


Figure 6.32. Resonator transfer function, amplitude and phase.

The element OSCTEST is used to check if the oscillator has the correct gain and phase in the feedback path. The phase shift around the loop should be exactly 0 degrees and the gain should be greater than one. An excess gain of 3 dB ensures that the loop gain is greater than one, even when different MAR 6 devices are used.

Tuning Step 2: The length of $TL7$ and $TL8$, which form part of the feedback signal path, are both adjusted in order to obtain the correct phase shift of 0° at 1 GHz. Having a loop gain greater than 1 and a 0° phase shift is a sufficient condition for oscillation.

Note that tuning capacitor $C1$ of figure 6.30 shows that this resonance at 1.3 GHz is due to that capacitor, so that it is desirable to keep this capacitor as small as possible.

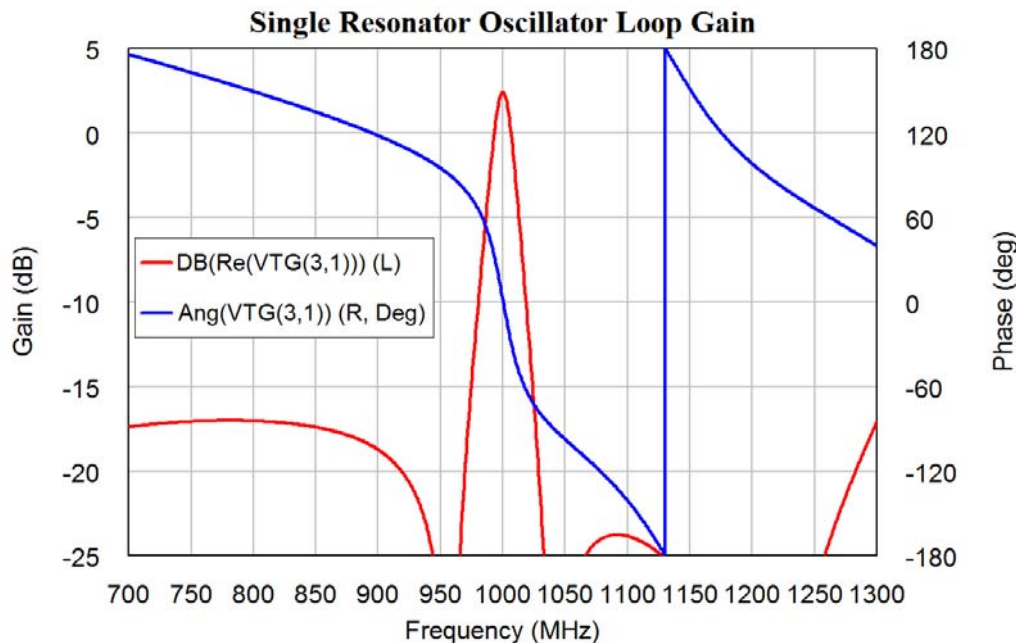


Figure 6.33. Single resonator oscillator open loop gain (OSCTEST) output.

Tuning Step 3: The design must now be arranged so that it fits on a PCB with all the track ends joining in the correct manner. The lengths of all the tracks and the phase shift produced by the MMIC must be kept exactly the correct length to satisfy the zero degree open loop phase shift from OSCTEST and a gain slightly greater than one as shown in figure 6.33.

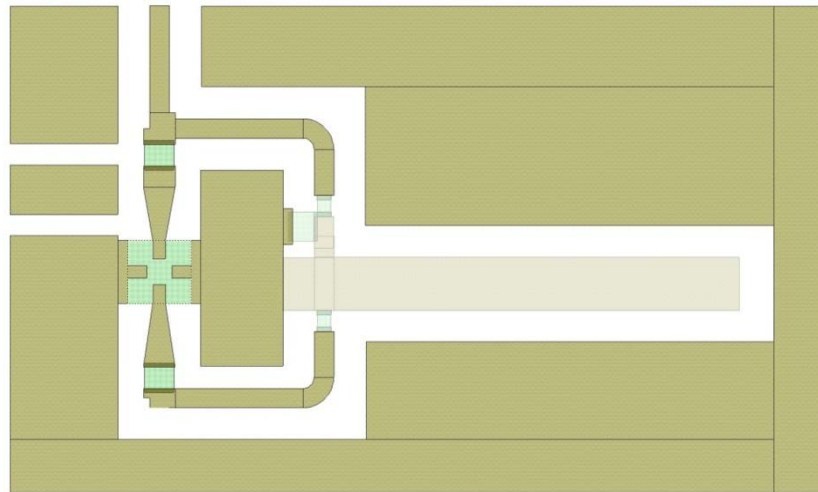


Figure 6.34. PCB layout for the 1GHz oscillator.

The resulting Microstrip layout is shown in figure 6.34, with the oscillator output at the top, the supply voltage pad at the left and the largest element being the resonator. The resonator is shown slightly lighter, since that is a separate element in the layout. The only elements not shown on this layout are the power supply biasing and vias connecting the ground pins of the MAR to the ground-plane. Figure 6.35 shows the corresponding hardware.

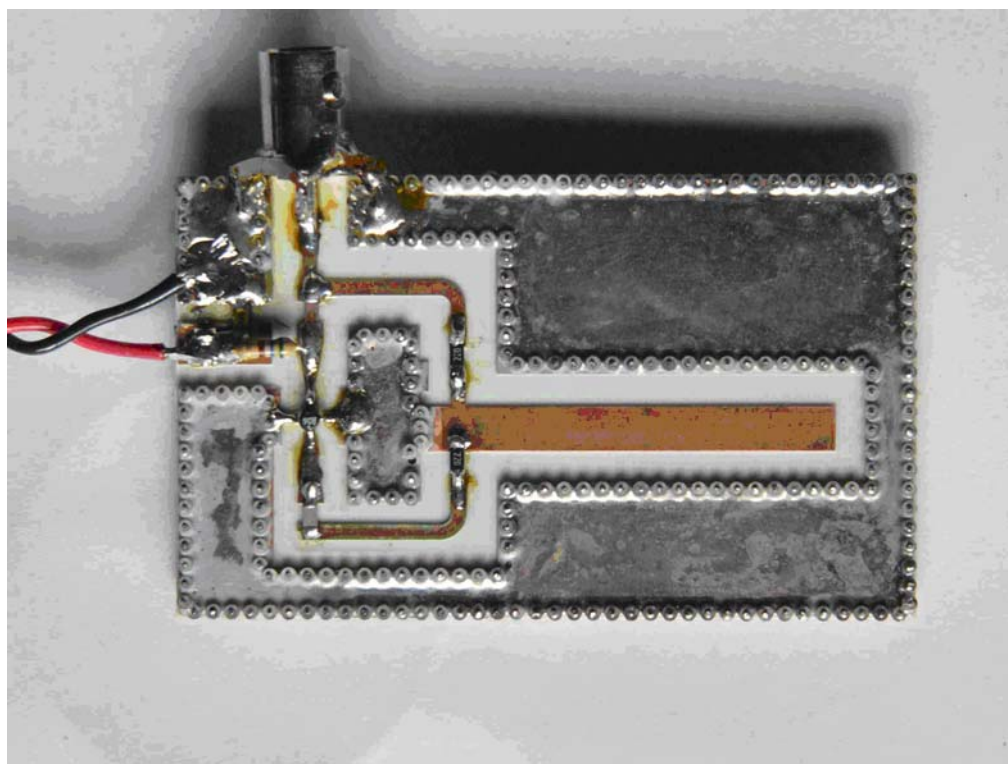


Figure 6.35. Photograph of the 1 GHz oscillator.

Figure 6.36 shows the spectrum obtained from the oscillator. The oscillator has a clean output signal and an acceptable phase noise performance. The output frequency is 990 MHz, which is within 1% of the design value. The output power is +5 dBm.

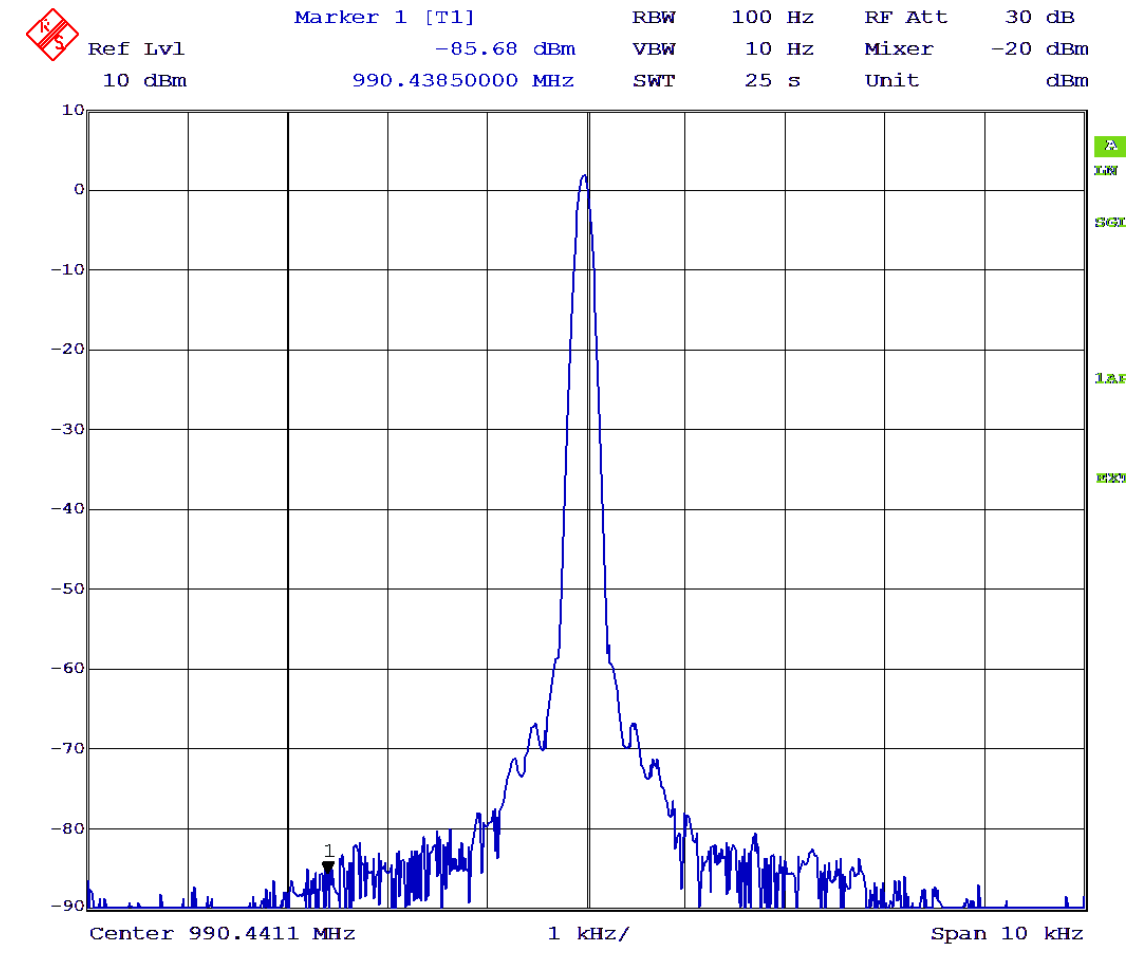


Figure 6.36. Measured output spectrum for the 1 GHz oscillator.

Dual Resonator Oscillator

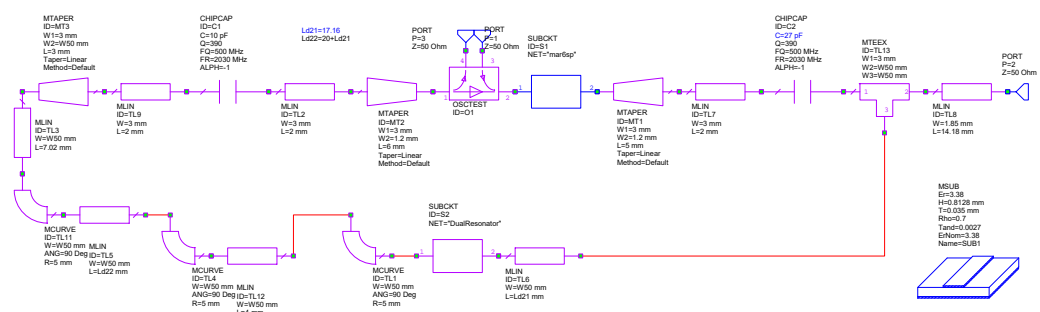


Figure 6.37. Circuit schematic for 1GHz dual resonator oscillator.

It is desirable to design oscillators, which produce the least amount of phase noise for a given frequency and tuning range. The primary factors determining the phase noise of the

oscillator are the Q of the resonant network, the noise figure of the amplifier and its output power [5]. Leeson's [5, 6] simplified model for phase noise shows the phase noise is inversely proportional to the square of the Q of the resonator. The higher the Q, the more rapid the resonator's change of phase with frequency at the resonance.

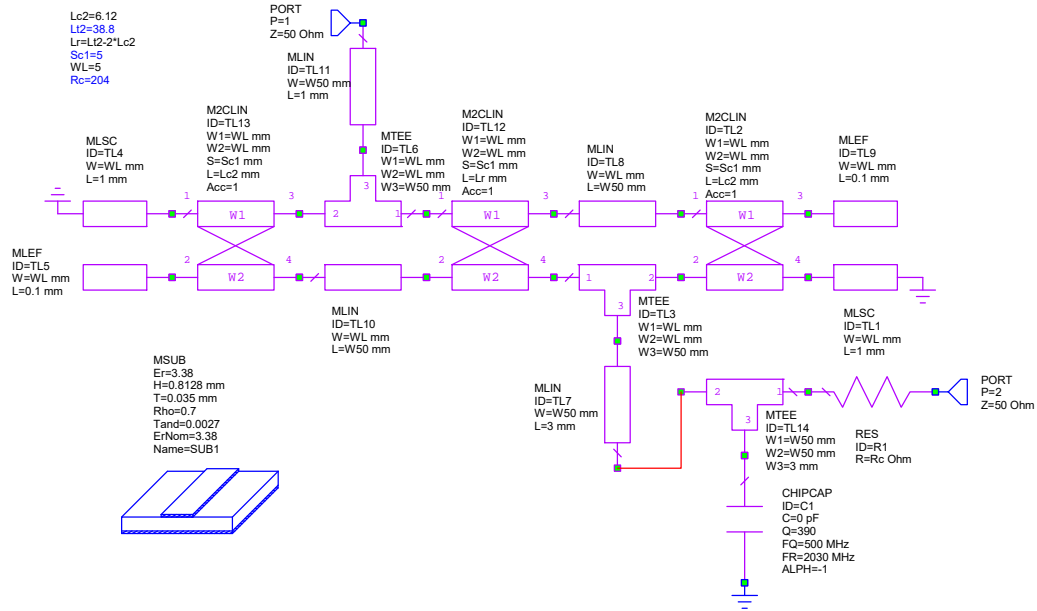


Figure 6.38. Simplified Circuit Schematic for 1GHz Microstrip coupled dual resonator.

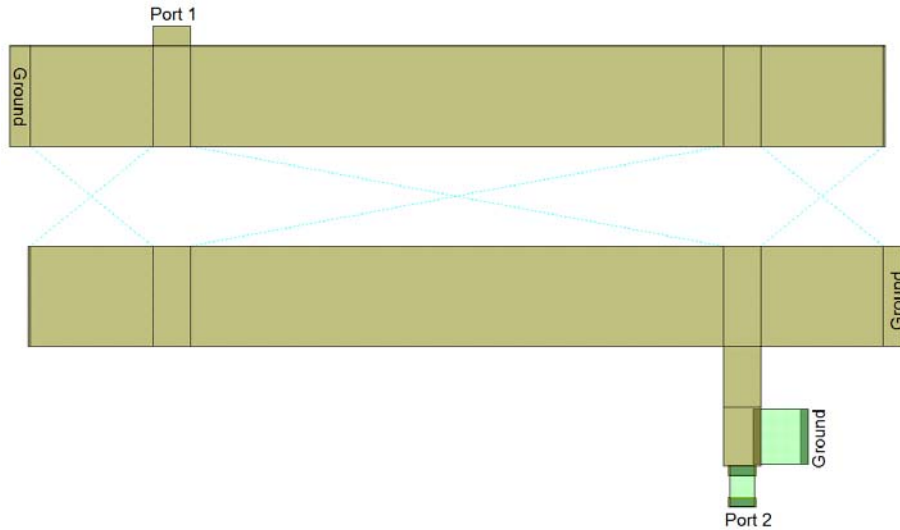


Figure 6.39. PCB layout of for the dual resonator of figure 6.38.

By using two resonators that are coupled, a faster change of phase at the resonance can be obtained, thus reducing the phase noise. Figures 6.30 and 6.31 show a single resonator. Figures 6.38 and 6.39 show the corresponding coupled dual resonator. As described above, this design was done early in 2005 [4] and the more advanced EM based Microstrip elements were not used. Like the tuning carried out on the single resonator shown in figure 6.30, the lengths of TL2 and TL13 of the double resonator are adjusted to minimise the loading on the resonator by the amplifier, while still giving the correct

open loop gain, corresponding to the switch in figure 6.1 being open. Thus producing a result similar to figure 6.33 for the single resonator design using OSCTEST.

An oscillator using a MAR6 amplifier, similar to figure 6.34 and 6.35, is designed and the lengths of $TL2$ and $TL13$ and the value of Rc are adjusted to ensure an open loop gain slightly greater than 0 dB and the length of the transmission lines making up the feedback loop are adjusted to give a 0° phase shift.

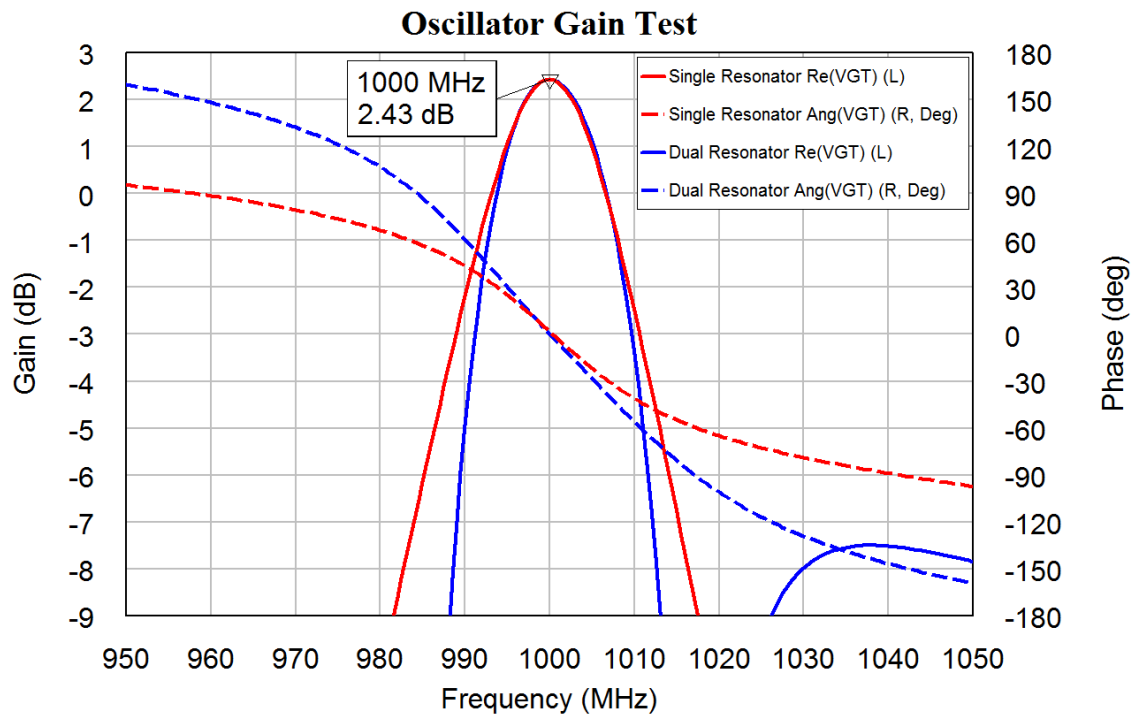


Figure 6.40. Comparison of single and dual resonator open loop gain and phase.

Figure 6.40 shows a comparison of the oscillator open loop gain for the single and dual resonator oscillator open loop gain. The rate of change of phase for the dual resonator is greater and since the same amplifier is used, the phase noise of the dual resonator oscillator should be less. The open loop gain has been adjusted to be the same for both circuits. Both circuits were also designed to have a 0° phase shift at 1 GHz. Both circuits should thus have the same oscillating frequency.

Figure 6.41 shows the resulting hardware and figure 6.42 shows the corresponding measured output spectrum. The oscillators of figures 6.35 and 6.41 use the same PCB material, the same amplifier and supply voltage and the same measurement technique. The only difference is the type of resonator used. Comparing figures 6.36 and 6.42 clearly shows the improved phase noise of the dual resonator design.

Since the non-linear models of the MAR amplifier are not available, it was not possible to do a phase noise measurement using NI AWR DE as was done for in figures 6.14, 6.19 and 6.27. A paper by the author [4] includes the design of a transistor amplifier, which is used with both the single resonator of figure 6.30 and the dual resonator of figure 6.38, and thus allows the phase noise for single and dual resonator designs to be compared. For those designs, the dual resonator oscillator gives a 3 dB phase noise improvement.

It is possible to extend this technique to more resonators, however an N resonator design can produce $N \times 180$ degree phase shift, making it progressively more difficult to ensure that only one oscillating frequency is possible.

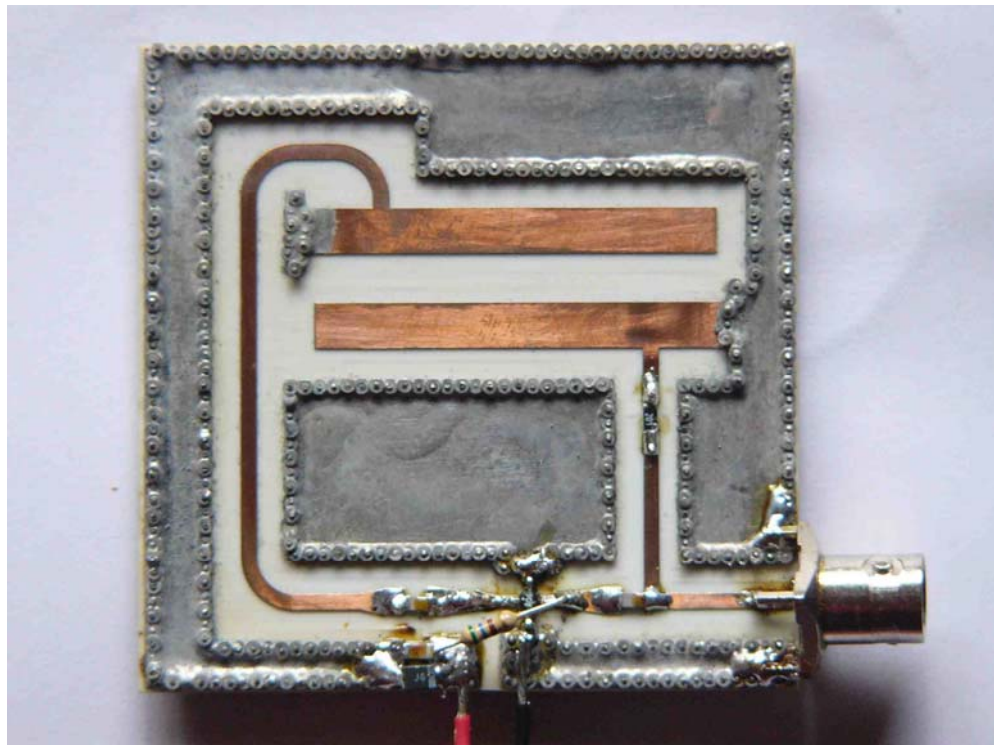


Figure 6.41. Photograph of the 1GHz dual resonator oscillator.

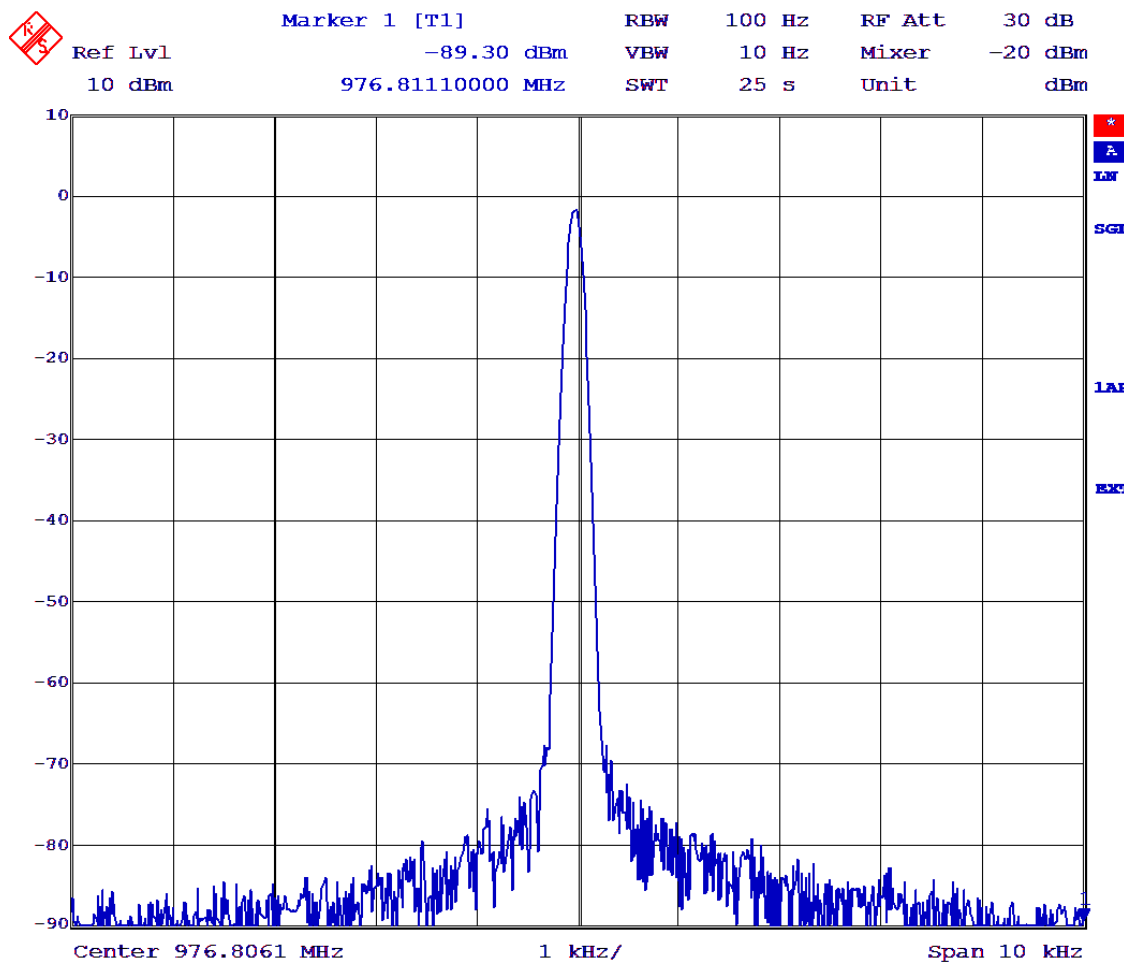


Figure 6.42. Measured output spectrum for the 1 GHz oscillator.

Design Improvements

The group delay of the open loop circuit gain as obtained from OSCTEST is directly related to the Q of a single resonator network. For a dual resonator, Q is not defined, so that the group delay is a good measure of the expected phase noise of the oscillator. For the single resonator design of figures 6.29 and 6.30, the group delay is 13.6 ns at 1 GHz. For the dual resonator design of figures 6.37 and 6.38, it is 16.17 ns at 1 GHz.

It is possible to improve the designs of figures 6.35 and 6.41, by reducing the loading on the resonators. To achieve the best accuracy for the simulation, the EM based MTEEX, MCROSSX and MLEFX elements are used and the Rogers recommended $\epsilon_r = 3.55$ is used for the simulation of the RO4003 substrate.

For the single resonator oscillator, capacitor $C1$ in figure 6.30, significantly reduces the loop gain as it is increased from 0 to 10 pF. Tuning without resonator gain variations can however be achieved by having a very small capacitor coupled at the top of the resonator, like the tuning screws in the interdigital filters as shown in figure 7.50. For the PCB layout, this can simply be done by soldering a nut to the ground-plane at the top of the resonator and using a screw parallel and above the top of the resonator to provide an adjustable small capacitance. That significantly increases the Q of the resonator and results in an OSCTEST loop-gain group delay of 23.09 ns.

For the dual resonator, resistors are included at the input and output of the resonator, like was used for the single resonator. For the dual resonator, the resonator cannot be tuned effectively by tuning one of the resonators as can be done for the single resonator. However, since the line lengths of the required tracks need to be much longer, as can be seen by comparing figures 6.35 and 6.41, it is possible to obtain good tuning control by placing a small capacitor at a strategic location along the feedback path. Then the lengths of $TL13$ and $TL2$, the resonator spacing $Sc1$ and the values of the terminating resistors $R1$ and $R2$ in figure 6.37 are tuned, to obtain the correct resonator frequency, the correct phase for OSCTEST and a high group delay.

For both the oscillators, the effect of external loads was reduced by inserting a 150Ω resistor in series with the oscillator output. The resulting reduction in output signal can easily be made up using an additional MMIC.

Figures 6.43 shows the OSCTEST loop gain and phase for both the improved single and dual resonator oscillators. Comparing this with figure 6.40 shows a narrower bandwidth, corresponding to a higher effective Q and a lower expected phase noise. The group delay of the single resonator oscillator is now 23.09 ns at 1 GHz and that of the dual resonator is 40.69 ns, a ratio of 1.76. This should give a 4.9 dB better phase noise [4] for the dual resonator oscillator compared with the single resonator oscillator.

Figures 6.44 and 6.45 show the corresponding layouts of the oscillators. Comparing figure 6.34 with 6.44 shows only minor differences in the layout. The capacitor at the top of the resonator is the 0-1 pF tuning capacitance used for setting the centre frequency. Comparing figure 6.41 with figure 6.45 shows significant differences. The spacing between the coupled resonators has increased significantly. To be able to produce the correct length of the feedback path, the feedback track had to be run in-between the resonators. It is not possible to obtain the correct length if the feedback was run outside the resonator, as was done in figure 6.41. The frequency tuning capacitor is the capacitor to ground at the top middle-right of the layout. Isolating that part of the ground-plane allows a varactor diode to be used for electronic frequency tuning.

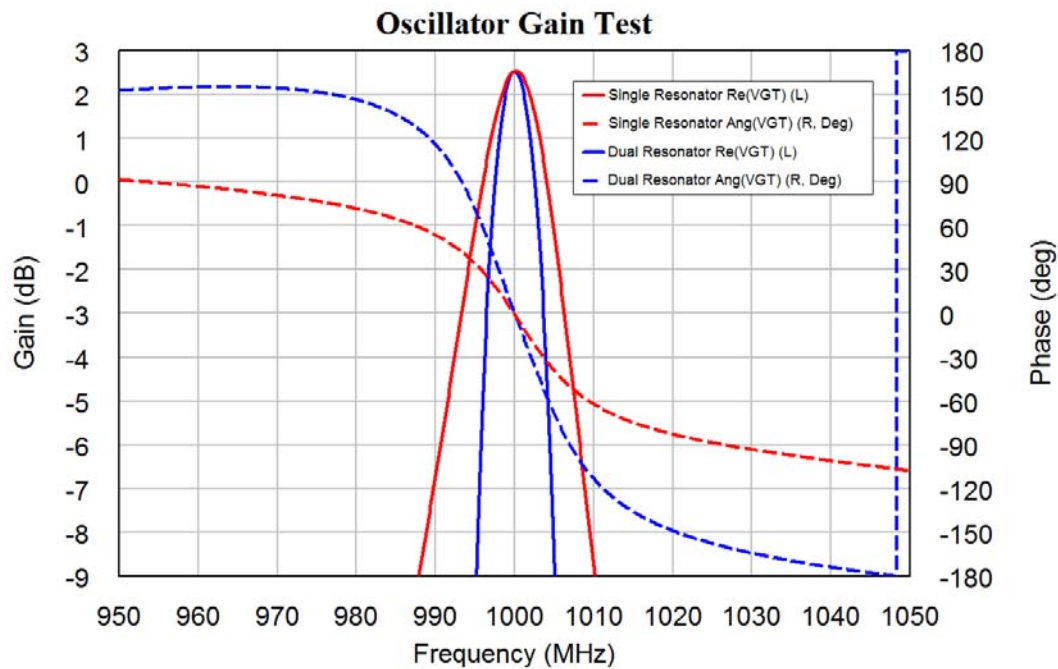


Figure 6.43. Comparison of improved single and dual resonator oscillator OSCTEST results.

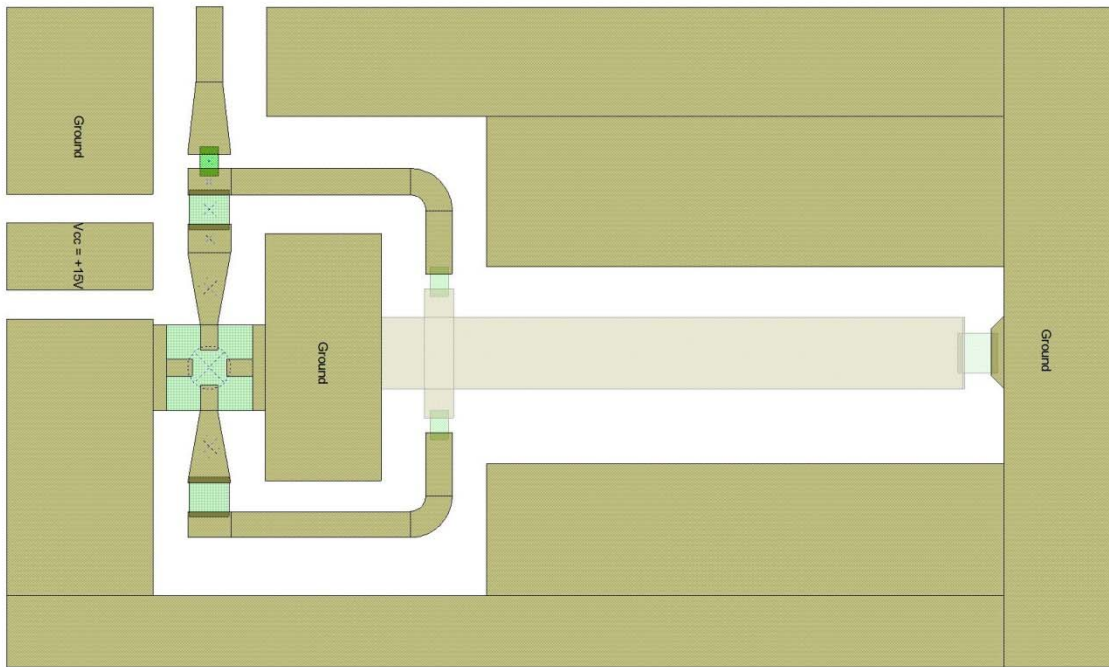


Figure 6.44. PCB layout for the improved 1GHz single resonator oscillator.

The distance between the resonators is larger than the distance between a resonator and the ground-plane. As a result, the ground-plane should have some effect on the oscillator performance. That should be evaluated using an EM simulator like AXIEM prior to construction of the circuit. The EM simulation process is described in the section “EM Simulation” in chapter 7 of this book and will not be dealt with here. The design techniques presented in this chapter will allow low noise RF and microwave oscillators to be designed. For a low phase noise, it is important to minimise the external loading on the resonator. Measuring the group delay as part of the OSCTEST gain and phase adjustment gives a good indication of the phase noise performance.

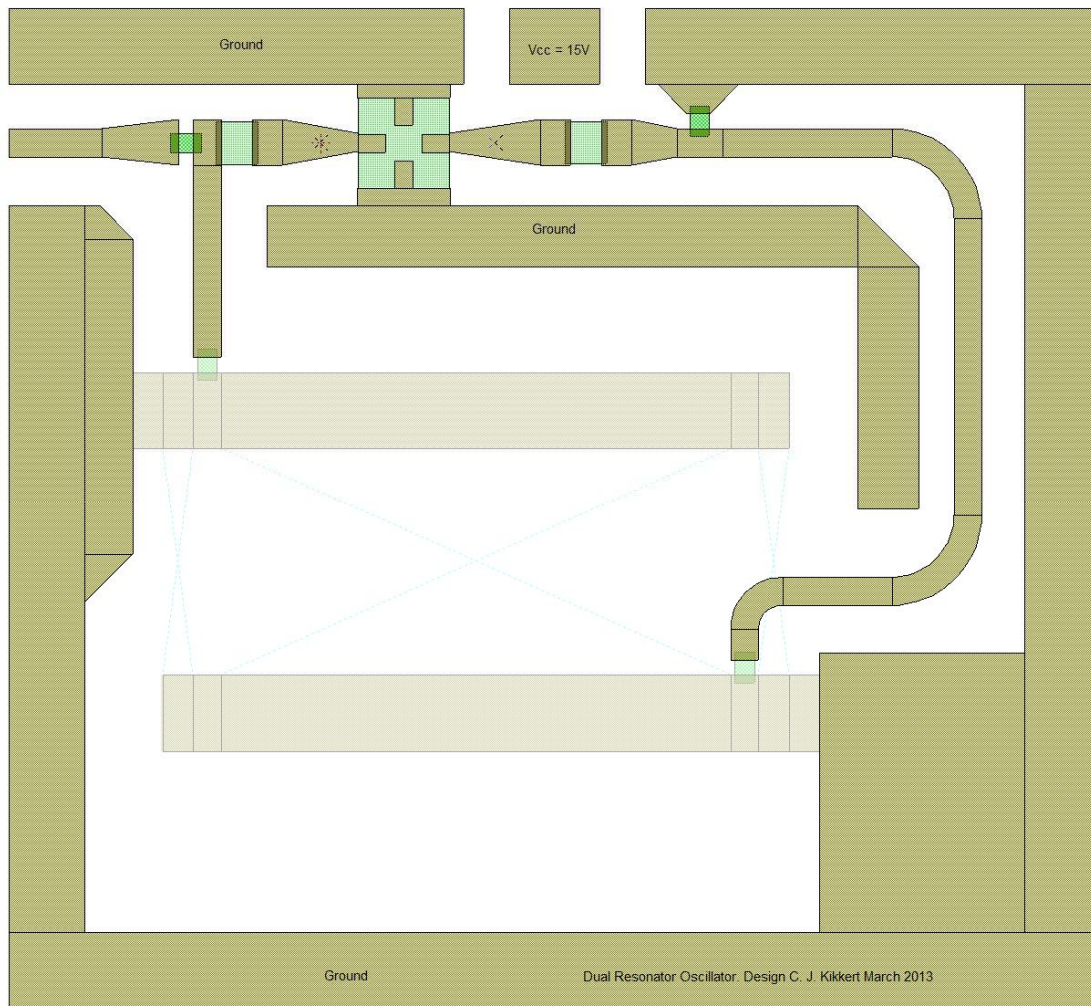


Figure 6.45. PCB layout for the improved 1GHz dual resonator oscillator.

References

- [1] J P Silver "Oscillator Resonator Design Tutorial", Oscillator Resonators, http://www.odyseus.nildram.co.uk/RFMicrowave_Theory_Page.htm,
- [2] John Vig "Quartz Crystal Resonators and Oscillators for Frequency Control and Timing Applications - A Tutorial", tf.nist.gov/sim/2010_Seminar/vig3.ppt. Nov 2008.
- [3] Touchstone File format, NI AWR DE Help: AWRDE User Guide, Chapter 3: Data Files (section 3.2.10).
- [4] Kikkert, C. J. "Dual Coupled Resonator Local Oscillator", IEEE Tencon '05, Melbourne, Australia, 21-24 November 2005, paper 1568965076.
- [5] www.rfic.co.uk "Phase Noise Tutorial Sheet", available from: http://www.odyseus.nildram.co.uk/Systems_And_Devices_Files/PhaseNoise.pdf.
- [6] D.B. Leeson, "A Simplified Model of Feedback Oscillator Noise Spectrum", Proceedings of the IEEE, Vol. 42, February 1965, pp. 329-330.

Chapter 7

RF Filters

Introduction

Filters used for RF signals are nearly always Bandpass filters using coupled resonator design techniques. The basic properties of the most common types of filters are:

Electrical Filters

LC Bandpass Filters. Typical unloaded Q values are 60-150, resulting in a large % Bandwidth filter with a high insertion loss. Frequency range 455 kHz to 2 GHz.

Helical Filters. Typical unloaded Q values > 1000. The Q value can be increased, by increasing the size of the resonator cavity. Frequency range 30 MHz – 1 GHz.

Coaxial Filters. Typical unloaded Q value > 5000. Frequency range 80 MHz – 2 GHz. Using a Ceramic dielectric results in a small size, for mobile radio use. Air dielectric coaxial filters are used for high power diplexers in Radio and TV transmitters.

Microstrip and stripline filters. Made using lines on PCB. Typical unloaded Q value 250. Wide % bandwidth.

Transmission Line Filters. Designs based on short or open circuited stubs. Wide Bandwidth.

Interdigital Filters. High Q and < 10% bandwidth.

Acoustic filters

Ceramic filters. Commonly used frequencies only. 455 kHz, 10.7 MHz IF filters, 800 MHz and 1.9 GHz diplexers for cellular phones.

Crystal Filters. Very High Q values and very low bandwidths. Typical 6 kHz Bandwidth at 10.7 MHz. Used for SSB filters. High cost compared to other filters.

SAW filters. Frequencies from 40MHz to 3 GHz. Relatively high insertion loss. The amplitude response and group delay can be controlled independently.

Several of the above filter types are discussed in detail in these notes.

Filter Design Revision

For this chapter, it is assumed that the reader knows about basic filter requirements and the resulting specifications of filtering characteristics if required, please refer to filter design texts, such as Zverev[1]. Most RF filter designs start with a normalised lowpass filter design and that filter has the required specifications in terms of filter order required, amplitude and group delay performance. This normalised lowpass filter is then transformed into the appropriate bandpass filter. There are two starting points:

- 1 Normalised LC filter tables or equations
- 2 K and Q filter tables.

These two are related and one can be derived from the other. For some filter types, like Butterworth filters, simple equations can be used for the normalised lowpass filter prototype.

Filter Tables

For RF designs K and Q tables are better than the LC filter tables or equations, since they include the effect of finite Q values in the resonators used. A good book for filter tables is “Handbook of Filter Synthesis” by A. I. Zverev, Wiley, 1967 [1] and more recently from Artech House. This together with Matthaei, Young, and Jones, “Microwave Filters, Impedance-Matching Networks, and Coupling Structures” [2] these are RF filter design classics and are still in print. Chapter 8 of Pozar [3] also describes microwave filters.

n	q0	I. L.	q 1	q n	k 12	k 23	k 34	k 45
2	INF.	0.000	1.4142	1.4142	0.7071			
	14.142	0.915	1.4142	1.4142	0.7071			
	7.071	1.938	1.4142	1.4142	0.7071			
	4.714	3.098	1.4142	1.4142	0.7071			
	3.536	4.437	1.4142	1.4142	0.7071			
	2.829	6.021	1.4142	1.4142	0.7071			
	2.357	7.959	1.4142	1.4142	0.7071			
	2.020	10.459	1.4142	1.4142	0.7071			
3	INF.	0.000	1.0000	1.0000	0.7071	0.7071		
	20.000	0.958	0.8041	1.4156	0.7687	0.6582		
	10.000	2.052	0.8007	1.5359	0.7388	0.6716		
	6.667	3.300	0.9097	1.6301	0.7005	0.6879		
	5.000	4.742	0.8226	1.7115	0.6567	0.7060		
	4.000	6.443	0.8406	1.7844	0.6077	0.7256		
	3.333	8.512	0.8625	1.8497	0.5524	0.7470		
	2.857	11.157	0.8884	1.9068	0.4883	0.7706		
4	INF.	0.000	0.7654	0.7654	0.8409	0.5412	0.8409	
	26.131	1.002	0.5376	1.4782	1.0927	0.5668	0.6670	
	13.066	2.162	0.5355	1.6875	1.0745	0.5546	0.6805	
	8.710	3.489	0.5417	1.8605	1.0411	0.5373	0.6992	
	6.533	5.020	0.5521	2.0170	1.0004	0.5161	0.7207	
	5.226	6.822	0.5656	2.1621	0.9547	0.4906	0.7444	
	4.355	9.003	0.5819	2.2961	0.9051	0.4592	0.7706	
	3.733	11.772	0.6012	2.4159	0.8518	0.4192	0.7998	

Table 7.1a. Butterworth Response, K And Q Value filter table, From Zverev[1], pp 341.

n	q0	I. L.	q 1	q n	k 12	k 23	k 34	k 45
5	INF.	0.000	0.6180	0.6180	1.0000	0.5559	0.5559	1.0000
	32.361	1.045	0.4001	1.5527	1.4542	0.6946	0.5285	0.6750
	32.361	1.045	0.5662	0.7261	1.0947	0.5636	0.5800	0.8106
	16.180	2.263	0.3990	1.8372	1.4414	0.6886	0.5200	0.6874
	16.180	2.263	0.5777	0.7577	1.0711	0.5408	0.6160	0.7452
	10.787	3.657	0.4036	2.0825	1.4088	0.6750	0.5080	0.7066
	10.787	3.657	0.5927	0.7869	1.0408	0.5144	0.6520	0.6860
	8.090	5.265	0.4111	2.3118	1.3670	0.6576	0.4927	0.7290
	8.090	5.265	0.6100	0.8157	1.0075	0.4844	0.6887	0.6278
	6.472	7.151	0.4206	2.5307	1.3195	0.6374	0.4732	0.7542
	6.472	7.151	0.6293	0.8449	0.9722	0.4501	0.7267	0.5681
	5.393	9.425	0.4321	2.7375	1.2675	0.6149	0.4479	0.7821
	5.393	9.425	0.6508	0.8748	0.9355	0.4103	0.7663	0.5048

Table 7.1b. Butterworth Response, K And Q Value filter table, From Zverev[1], pp 341.

Butterworth Filters

Butterworth filters have a maximally flat amplitude response. That means all the derivatives of the amplitude with respect to frequency are zero at DC. The Butterworth response is a good compromise between attenuation characteristic and group delay. The characteristics of the other filter types described in this chapter will be compared with the Butterworth filter to highlight the advantages and disadvantages of each filter type.

For a Butterworth Lowpass filter of n^{th} order, with a cut off frequency of f_c and a source and load resistance of R , the filter component values are given by:

$$C_i = \frac{1}{\pi f_c R} \sin \frac{(2i-1)\pi}{2n} \quad i=1,3,5,\dots \quad \text{Eqn. 7.1}$$

$$L_i = \frac{R}{\pi f_c} \sin \frac{(2i-1)\pi}{2n} \quad i=2,4,6,\dots \quad \text{Eqn. 7.2}$$

The first component ($i=1$) is a shunt capacitor, the second ($i=2$) component is a series inductor etc. The normalised q values and coupling coefficients are related to the normalised lowpass impedances for a filter, using the following equations:

$$q_0 = Z_1 \quad q_n = Z_n \quad k_{ij} = \frac{1}{\sqrt{Z_i Z_j}} \quad \text{Eqn. 7.3}$$

Where Z_i is the normalised impedance as obtained from LC filter tables or from equations 7.1 and 7.2. Applying equation 7.3 to equations 7.1 and 7.2 gives:

$$q_0 = q_n = 2 \sin \frac{(2-1)\pi}{2n} = 2 \sin \frac{\pi}{2n} \quad \text{Eqn. 7.4}$$

$$k_{ij} = \frac{1}{2 \sqrt{\sin \frac{(2i-1)\pi}{2n} \sin \frac{(2i+1)\pi}{2n}}} \quad i=1,3,5,\dots \quad \text{Eqn. 7.5}$$

These equations will then allow the k and q values for $IL = 0$ and $q_0 = \infty$ as shown in table 7.1 to be calculated.

Figure 7.1 shows the resulting circuit for a 7th order Lowpass filter with a 500 MHz cut-off frequency. For the Butterworth filter, equations 7.1 and 7.2 are used to calculate the required component values in the schematic. For the other filters, the component values are calculated using a spreadsheet and the filter tables in Zverev.

Seventh order Butterworth Low Pass Filter

For the Butterworth filter, the component values are calculated using the following equations:

$$Fc = 500 \quad Fc \text{ in MHz} \quad \pi = 3.142$$

$R = 50 \quad \text{Terminating Impedance in ohm}$

$$C1 = 1e6 * \text{Sin}(\pi/14) / (\pi * Fc * R) \quad C1: 2.833 \quad C \text{ in pf}$$

$$C3 = 1e6 * \text{Sin}(5\pi/14) / (\pi * Fc * R) \quad C3: 11.47$$

$$C5 = 1e6 * \text{Sin}(9\pi/14) / (\pi * Fc * R) \quad C5: 11.47$$

$$C7 = 1e6 * \text{Sin}(13\pi/14) / (\pi * Fc * R) \quad C7: 2.833$$

$$L2 = 1e3 * R * \text{Sin}(3\pi/14) / (\pi * Fc) \quad L2: 19.85 \quad L \text{ in nH}$$

$$L4 = 1e3 * R * \text{Sin}(7\pi/14) / (\pi * Fc) \quad L4: 31.83$$

$$L6 = 1e3 * R * \text{Sin}(11\pi/14) / (\pi * Fc) \quad L6: 19.85$$

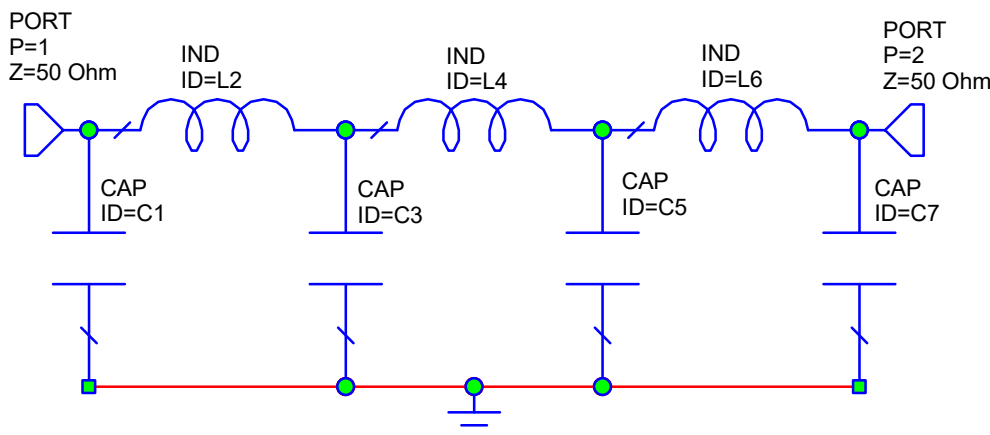


Figure 7.1. Butterworth Lowpass Filter.

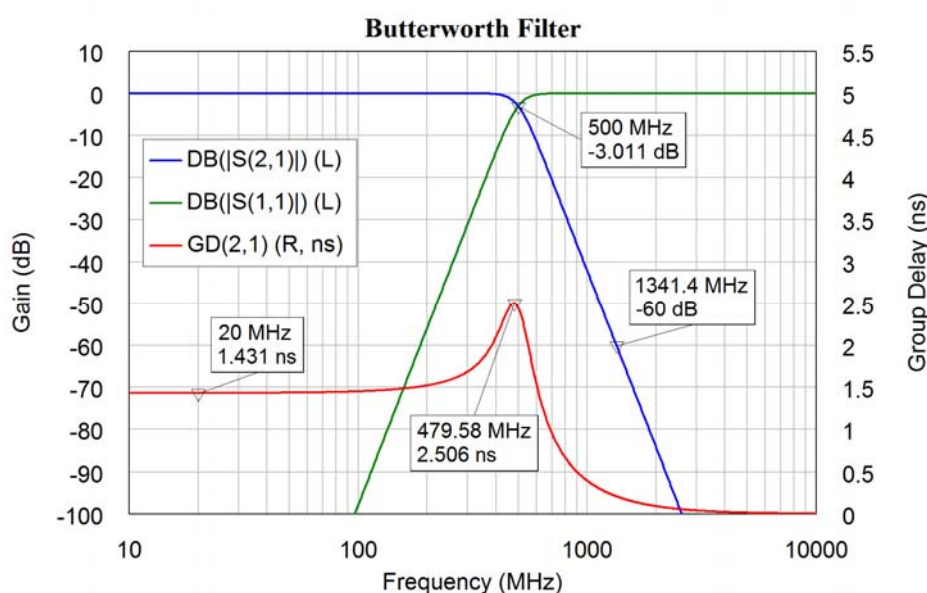


Figure 7.2. Butterworth Frequency Response.

The frequency response for the Butterworth filter is shown in figure 7.2. The group delay of Butterworth filters is reasonably flat but has a rise near the cut off frequency. The step response of these filters exhibits some ringing, which degrades its use for data communications.

Bessel Filters

The bigger the difference between the group delay at low frequency and the maximum group delay, normally occurring near the filter cut-off frequency of the filter, the bigger the ringing and overshoot in the step response. The Bessel filter has a maximally flat group delay and does not have any ringing or overshoot in its step response. As a result, the Bessel filter type is very suitable for data communication systems. Simple equations like equations 7.1 and 7.2 do not exist for Bessel filters, so that normalised filter element values have to be obtained from filter tables. Many filter tables for Bessel filters are normalised for a group delay of one second, rather than a 3 dB cut-off frequency. The Bessel filter in figure 7.3 has a cut-off frequency of 500 MHz so that accurate comparisons between the filter types can be made.

The Bessel filter has a less sharp roll-off of the attenuation characteristic but a flatter group delay than the Butterworth filter, as can be seen by comparing figure 7.2 and 7.4. For the Butterworth filter, the 60 dB attenuation level occurs at 1.3 GHz while for the Bessel filter it occurs at 2.4 GHz.

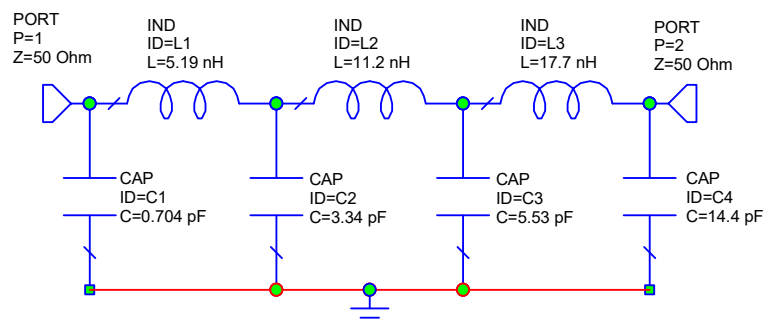


Figure 7.3. Bessel Lowpass Filter.

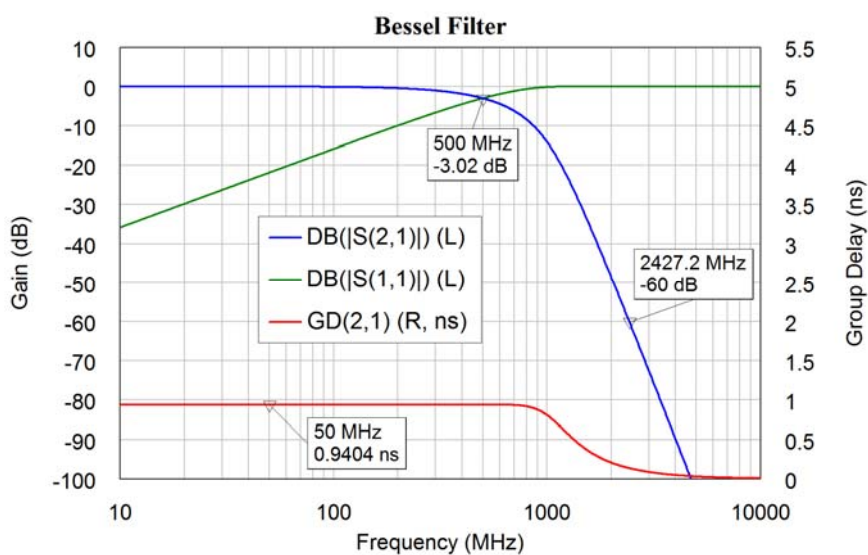


Figure 7.4. Bessel Lowpass Filter Frequency Response.

Chebyshev Filters

The Chebyshev filter has ripples in the passband and the value of the ripples is a parameter that is selected as part of the filter design. The filter of figure 7.5 has a 0.1 dB passband ripple as shown on figure 7.6. The inductors and capacitors for the Chebyshev filter are larger than those used in Bessel or Butterworth filters. The Chebyshev filter has a very sharp attenuation response in the stop band, with a -60 dB attenuation at 967 MHz, compared with 1.3 GHz for the same attenuation for the Butterworth filter. Increasing the passband ripple will increase the passband attenuation. The group delay for the Chebyshev filter is larger than that of the Bessel and Butterworth filters. As a result, the Scale on figure 7.6 is different from figure 7.2 and 7.4.

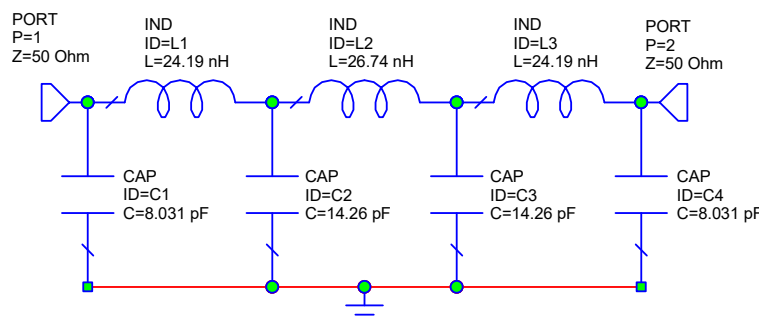


Figure 7.5. Chebyshev Lowpass Filter.

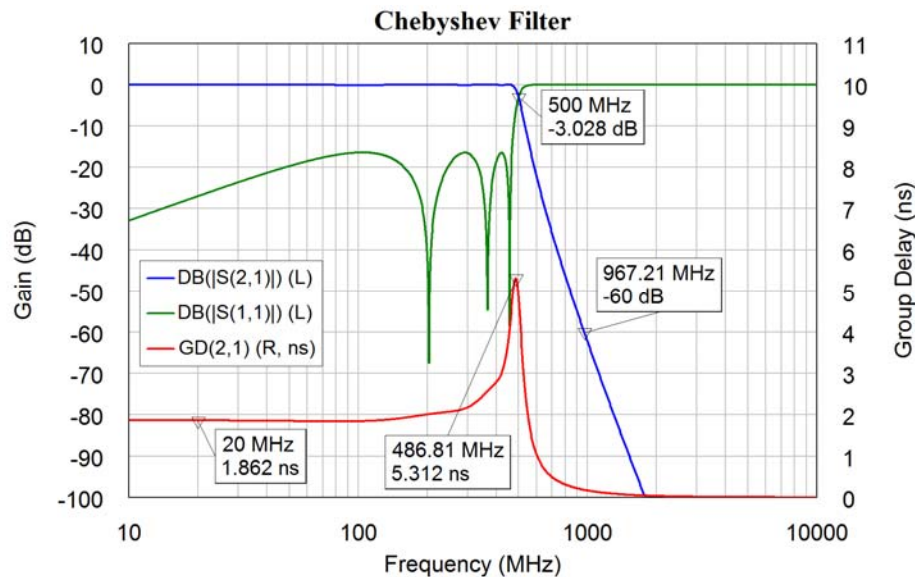


Figure 7.6. Chebyshev Lowpass Filter Frequency Response.

Cauer-Chebyshev Filters

A Cauer-Chebyshev filter is a derivative of the Chebyshev filter and has capacitors in parallel with the inductors to cause zeros in the stopband as shown in figure 7.7. The zeros are placed, such that the minimum stopband attenuation values are the same as shown in figure 7.8. This gives an even higher stopband attenuation, with a 60 dB attenuation at 628 MHz compared with 1.3 GHz for the Butterworth filter. The Cauer-Chebyshev filter has an even bigger variation in the group delay than the Chebyshev filter and will thus have very poor transient response. The group delay of the Chebyshev and Cauer-

Chebyshev filters are poor and these filters should not be used for data communications or applications where the group delay is important.

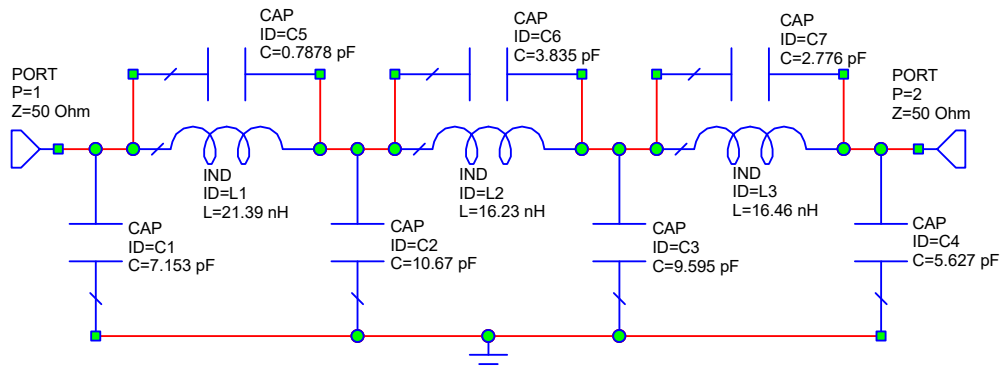


Figure 7.7. Cauer-Chebyshev Lowpass Filter.

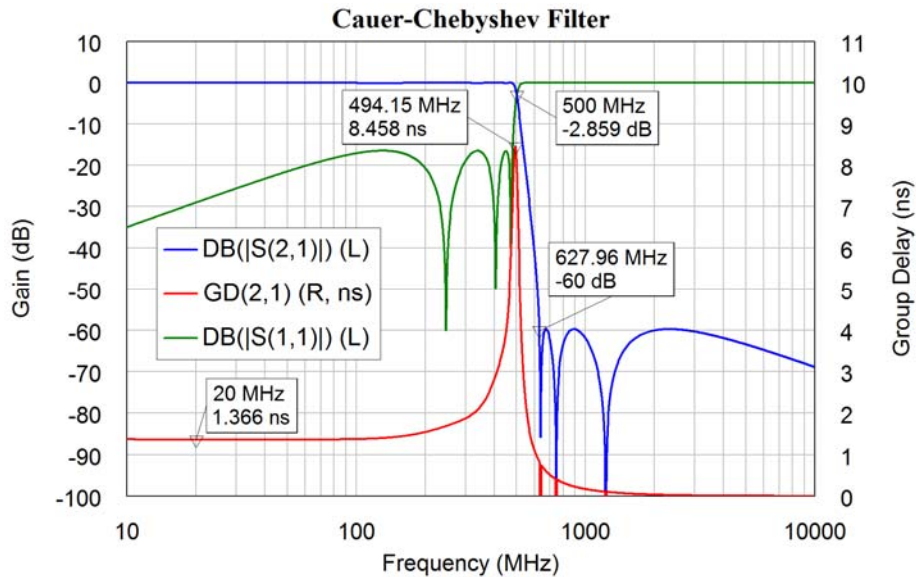


Figure 7.8. Cauer-Chebyshev Filter Frequency Response.

Figure 7.9 shows the passband response of the four different filter types. The 0.1 dB passband ripple of the Cauer-Chebyshev and Chebyshev filters can clearly be seen. The Bessel filter has a significant attenuation for frequencies above 100 MHz.

Both the Chebyshev and Cauer-Chebyshev filters have poles on an ellipse and are elliptical filters. As a result, it is better not to specify a filter as an elliptic filter since it does not fully specify the filter type.

From filter tables, which include losses due to the finite Q values of the filter elements, it can be determined that for a given Q value for the components, the Chebyshev filter has a higher passband insertion loss than a Butterworth filter and a Bessel filter has a lower insertion loss than a Butterworth filter. The same applies for Bandpass filters, so that for the same unloaded Q of the resonators used in coupled resonator RF filters, the Bessel filter will have the lowest insertion loss and the Chebyshev filter will have the highest insertion loss.

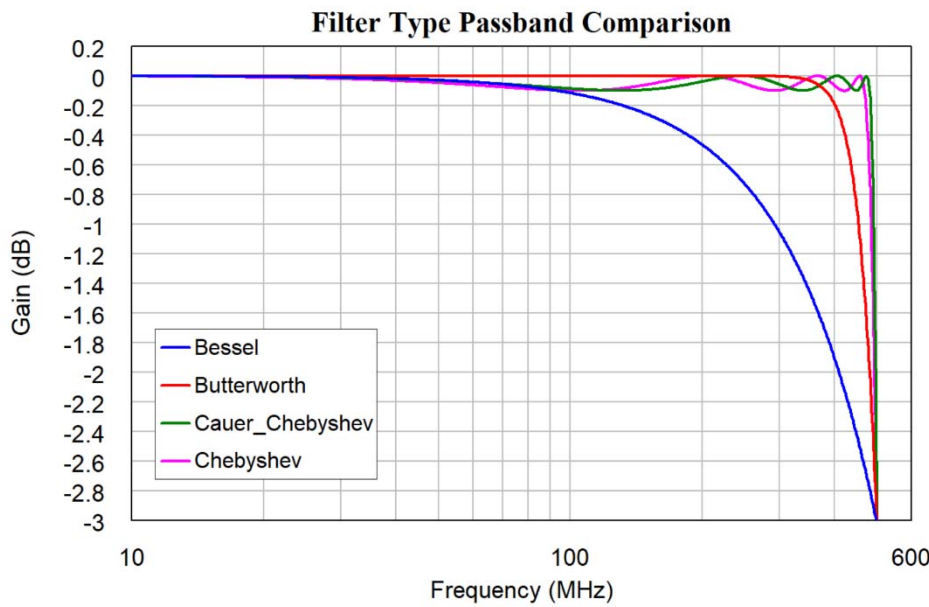


Figure 7.9. Passband Frequency Response of the filters of Figures 7.2, 7.4, 7.6 and 7.8.

The selection of the correct filter type is critical to ensure that the filter used satisfies both the transient response requirements and the passband insertion loss and stopband attenuation requirements for the filter. In digital communication applications, the Bit Error Rate (BER) after demodulating is the critical parameter. To reject signals in an adjacent channel intuition suggests the use of a Chebyshev filter. However, computer simulations carried out by the author [4] for a 3rd Generation Mobile Radio system, have shown that when there is a large unwanted signal in an adjacent channel, the lowest demodulated BER is obtained with a Bessel type filter response for the Channel filters.

Reflectionless Filters

The filters shown above have a low return loss in the pass band, but attenuate the signal by reflecting the signal and having a high return loss in the stop band. The hybrids discussed in chapters 3 and 4 all require a resistive termination at all ports, to provide the required performance. In some applications, such as RF amplifiers, as discussed in chapters 8 and 9, the high return loss can lead to instability of amplifiers. It is possible to design filters to have a low return loss, so that the filter absorbs rather than reflects the signals to be filtered out. These filters are called reflectionless filters. Minicircuits [5] now make a range of reflectionless low pass and bandpass filters. Having the IF port of a mixer terminated in a reflectionless low pass filter, results in a much cleaner output spectrum as described in [6].

The diplexer shown in figure 2.9 and 2.13 is in fact a reflectionless filter for the combined port (port 1), having a very low reflection coefficient at all frequencies. When used as a high pass filter, the below cut-off frequency signals appear at port 2. When used as a low pass filter, the above cut-off frequency signals appear at port 3. Port 1 will thus have a low reflection coefficient, but ports 2 and 3 do not. The frequency dependent signal steering principle of the diplexer can be used to design a filter to have low reflections at both input and output terminals. Since the design principles are different from the reflectionless filter of [5-8] and figure 7.14, these filters are called “low reflection filters” here. A low reflection low pass filter must thus include two high pass filters, one to absorb all the unwanted signals at the input and another to absorb them at the output. Similarly,

a low reflection high pass filter must include two low pass filters and a low reflection bandpass filters must include two bandstop filters.

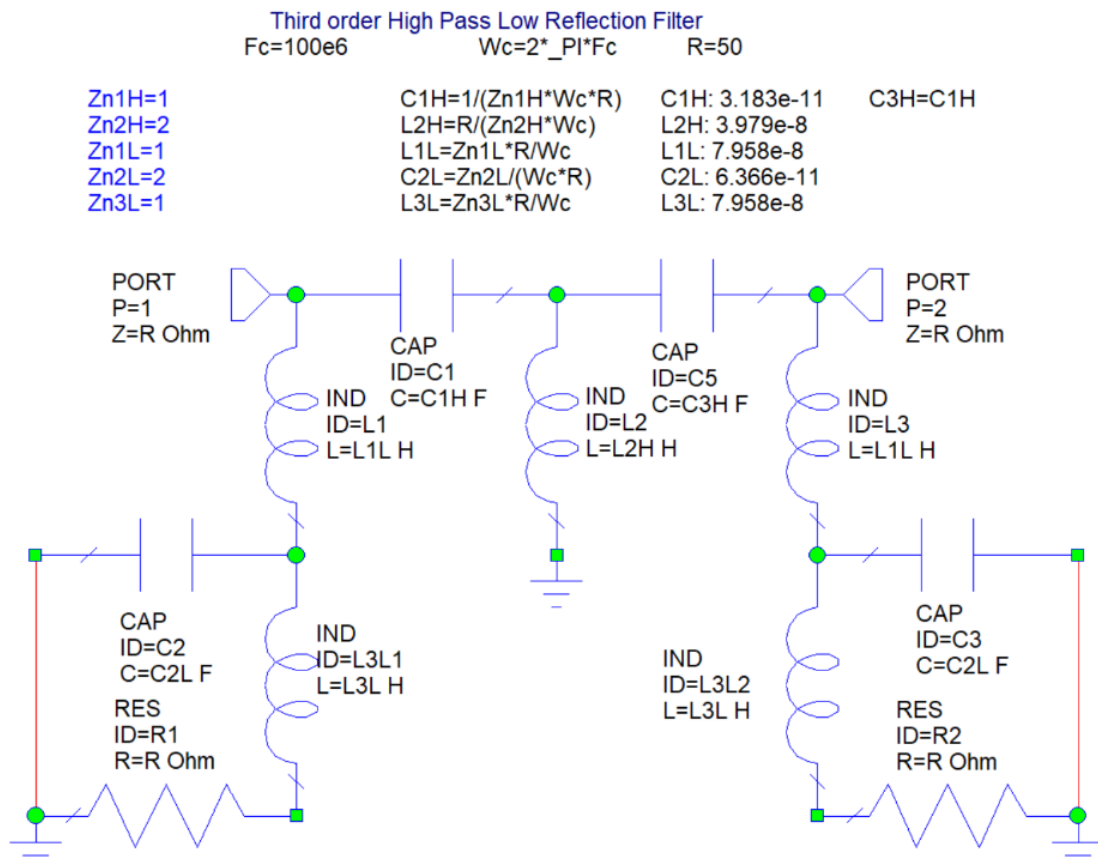


Figure 7.10. Low reflection 3rd order high pass filter, starting circuit.

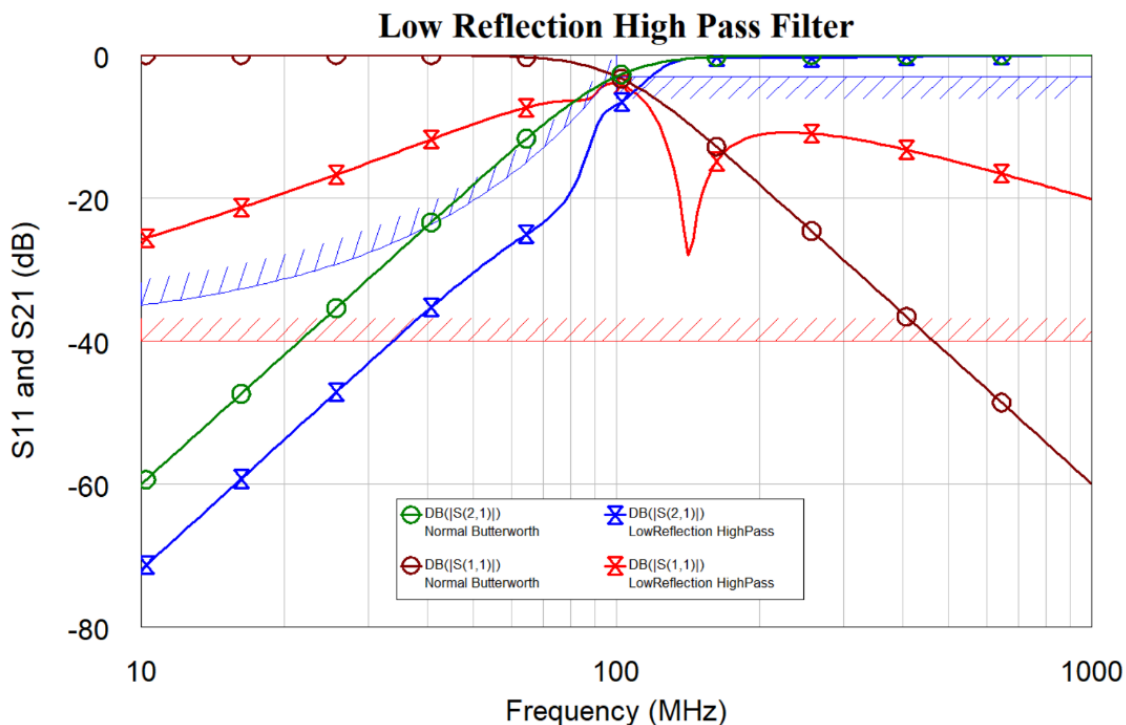


Figure 7.11. Low reflection 3rd order high pass filter, starting frequency response.

The design principles are outlined by designing a 3th order low reflection high pass filter with a cut-off frequency of 100 MHz and a 50 Ω impedance. Similar to figures 2.7 and 2.8, the input terminal of both the highpass and lowpass filters making up the low reflection filter must have a high impedance for the unwanted frequencies. Figure 7.10 shows the starting schematic. The ZnXX values are optimised, with the starting values being the normalised Butterworth filter impedance values obtained from equations 7.1 and 7.2 with $R = 1$ and $\omega_c = 1$. As a result, the highpass filter is symmetrical, with $C3H = C1H$. To obtain the best return loss, the symmetry restriction on the lowpass filters is removed, to allow $L1L$ and $L3L$ to become different during the optimisation.

Third order High Pass Low Reflection Filter		
$F_c=100e6$	$W_c=2\pi F_c$	$R=50$
$Zn1H=1.44040790172559$	$C1H=1/(Zn1H*W_c*R)$	$C1H: 2.21e-11$
$Zn2H=1.7393807396616$	$L2H=R/(Zn2H*W_c)$	$L2H: 4.575e-8$
$Zn1L=1.6400227606175$	$L1L=Zn1L*R/W_c$	$L1L: 1.305e-7$
$Zn2L=1.66758429969081$	$C2L=Zn2L/(W_c*R)$	$C2L: 5.308e-11$
$Zn3L=0.818190540664024$	$L3L=Zn3L*R/W_c$	$L3L: 6.511e-8$

Figure 7.12. Low reflection 3rd order high pass filter, optimised values.

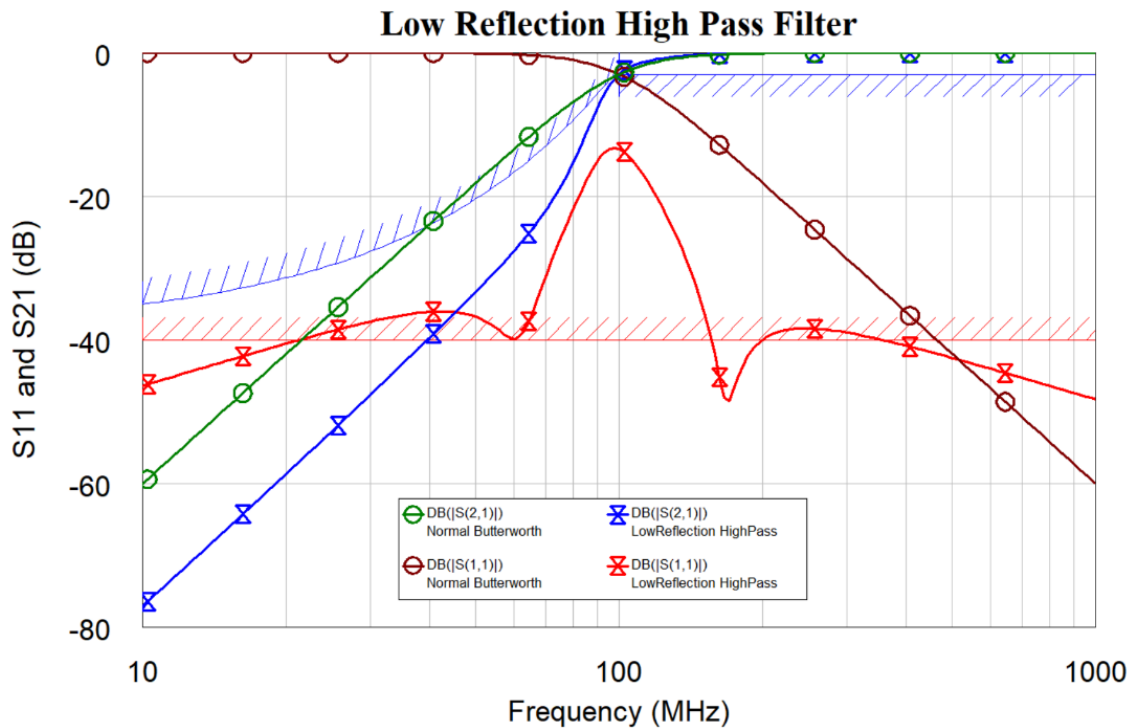


Figure 7.13. Optimised low reflection 3rd order high pass filter, frequency response.

The optimisation constraints are the passband and stopband attenuation, specified so that the corner frequency does not change during the optimisation, and the return loss. Figure 7.12, shows the component values after optimisation and figure 7.13 shows the resulting transfer function and return loss. The blue curve in figure 7.13 shows that this circuit has more attenuation in the stop band than the basic 3rd order Butterworth filter, corresponding to the green curve. At the cut off frequency, the red curve shows it has 10 dB more return loss than the return loss of the 3rd order Butterworth filter shown as the brown curve. Below 70 MHz, the low reflection filter has a return loss more than 30 dB, compared to close to 0 dB, for the conventional filter. That is thus a big improvement, but the low reflection filter requires 3 times the reactive components of a conventional low pass filter in addition to the two resistors to absorb the unwanted signals.

The design of the low reflection filter above has been based on a diplexer design. Microwaves101 [8] and Minicircuits [5] use a reflectionless filter design technique based on even and odd mode impedances [7]. This includes some cross-coupling between the output and the input. Figure 7.14 shows the circuit diagram similar to that used by [5] and figure 7.15 shows the frequency response and return loss after optimisation. The return loss of figure 7.15 is much better than that shown in [8] and shows the advantages of being able to optimise circuits using NI-AWRDE. Figure 7.15 shows that the return loss is ideal (<-300 dB), but the stopband attenuation is poorer than that of figure 7.13.

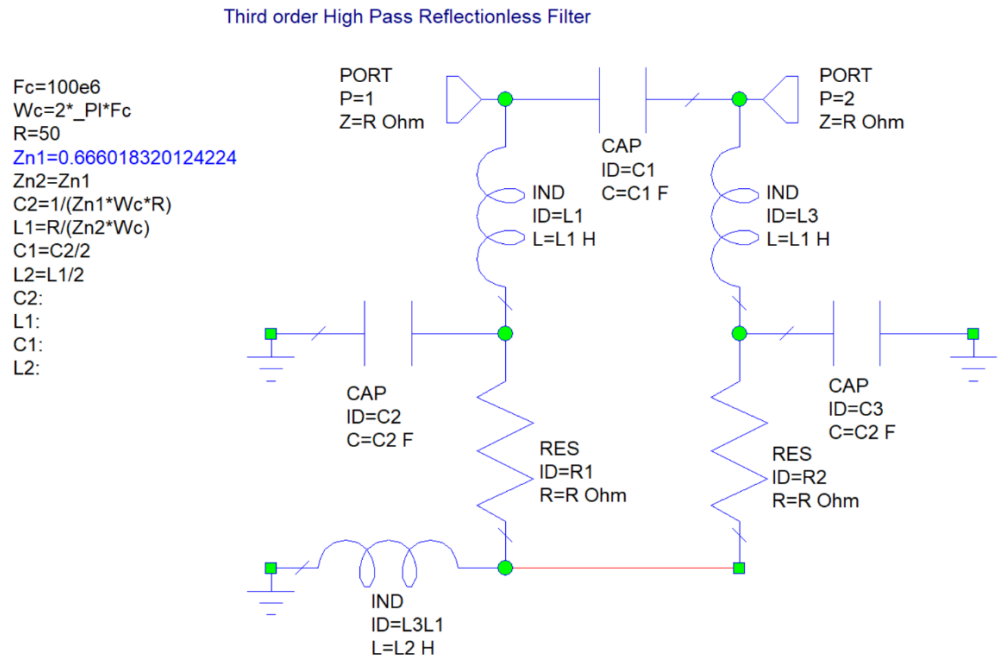


Figure 7.14. Even & Odd mode, impedance reflectionless filter circuit.

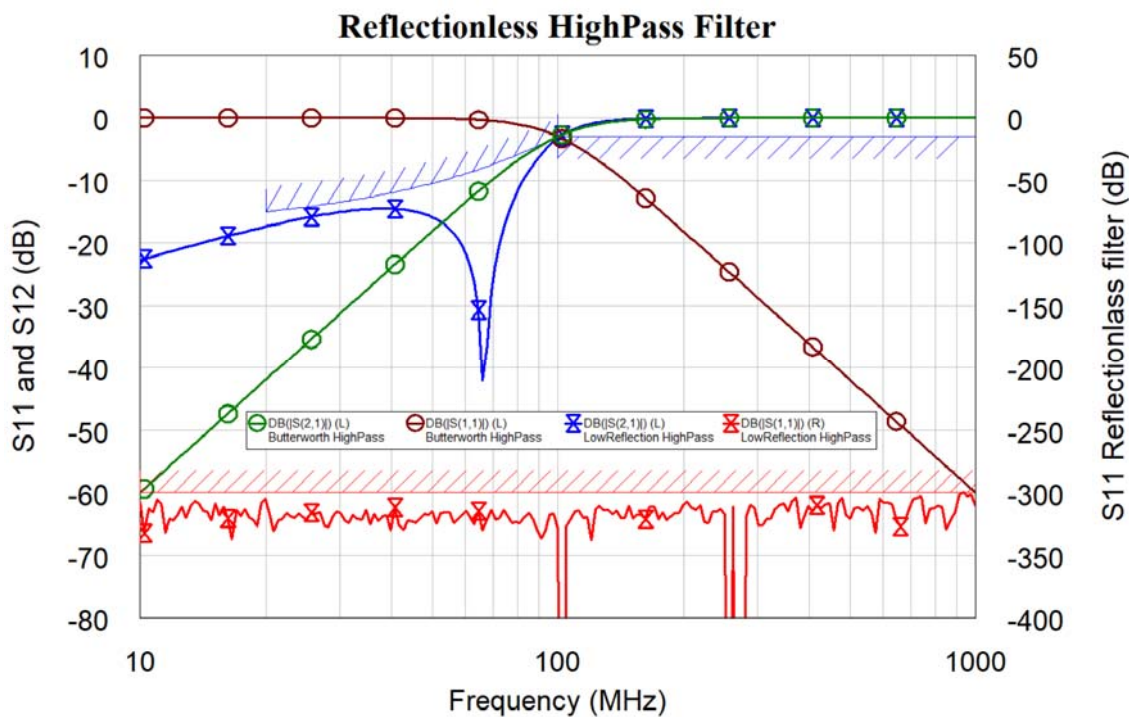


Figure 7.15. Even & Odd mode, impedance reflectionless filter frequency response.

Cascading these filters preserves the low return loss and increases the stopband attenuation. However, including a conventional high pass filter as part of such a cascaded filter, results in a passband return loss similar to that of the conventional high pass filter.

Low reflection and reflectionless lowpass, bandpass and bandstop filters can be made by using the relevant low-pass to highpass, low-pass to band-pass, low-pass to band-stop transformations described later in this chapter. These filters require close to twice the number of reactive components, compared to conventional filters.

Reflectionless filters are also very useful for ensuring stability of amplifiers described in chapter 8, by reducing the gain to signals outside the required bandwidth, whilst maintaining near ideal termination for the amplifier.

Higher order low reflection and reflectionless filters can be designed using the principles outlined in [7] for reflectionless filters and using the optimisation outlined in figures 7.10 to 7.14 for low reflection filters. In practice, both designs techniques will result in reflections less than -20 dB.

RF Lowpass Filter design

Lowpass filters at RF and microwave frequencies, can be designed and constructed using conventional LC filter design principles. However, care should be taken to ensure that:

- 1 The impedance of the leads is kept as small as possible. In particular, the impedance of the leads on capacitors connecting the capacitors to ground, or the length of any PCB layout track connecting the components to the ground-plane must be kept as small as possible, since its inductance will affect the frequency response of the filter.
- 2 Components must be used that have self-resonant frequencies well above the cut off frequency of the filter if a lowpass filter is used and well above any useable frequency if a high pass filter is used. Most commonly used capacitors have self-resonant frequencies well below 1 GHz.

It is feasible to design conventional LC lowpass filters with cut off frequencies in excess of 1 GHz. Surface-mount components generally have a higher cut-off frequency than leaded components. When the frequency becomes too high for either of them to be used, inductors can be replaced with thin transmission lines of the length required to give the desired inductance and capacitors can be replaced by wide transmission lines.

As an example, consider the design of a 7th order Butterworth lowpass filter with a cut off frequency of 2 GHz. From the equations 7.1 and 7.2 for Butterworth filters or from tables, by de-normalising and using a cut off of 2 GHz and input impedance of 50 Ω, the component values shown in table 7.2 are obtained for the filter.

L C	Value Required	Line Length	Line Width
L1	1.771 nH	3.54 mm	0.5 mm
C2	1.985 pF	4.2 mm	10 mm
L3	7.170 nH	13.5 mm	0.5 mm
C4	3.183 pF	6.6 mm	10 mm
L5	7.170 nH	13.5 mm	0.5 mm
C6	1.985 pF	4.2 mm	10 mm
L7	1.771 nH	3.54 mm	0.5 mm

Table 7.2. LC filter values and corresponding Microstrip line size.

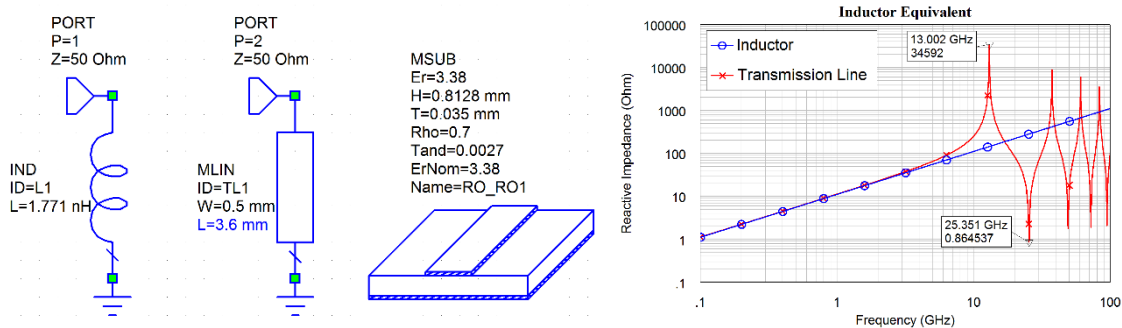


Figure 7.16. Replacement of inductors using Microstrip transmission lines

For Rogers RO4003 substrate with $H = 0.83$ mm and $T = 35$ μ m, the width for a 50Ω transmission line is 1.843 mm. the thinnest line that is desirable is 0.5 mm and the thickest is 10 mm. That corresponds to impedances of 96.5Ω and 14.3Ω respectively. One needs to find out what length of transmission lines corresponds to the inductance required for the filter. In NI AWR DE it is easy to compare the impedance of an inductor with one of a transmission line, as shown in figure 7.16. The circuit of figure 7.16, together with the line width restrictions results in the line widths and line lengths shown in table 7.2. The length of the transmission line is tuned to ensure that at low frequency both have the same impedance. It can be seen that the short section of transmission line accurately represents the inductor for frequencies up to 10 GHz. This process is repeated for all the inductances. Note for larger inductances, at higher frequencies the transmission line will be a quarter wavelength resulting in an infinite impedance or half a wavelength, resulting in a very small impedance. For lowpass filters, the length of the transmission line should be less than one-quarter wavelength for all frequencies of interest.

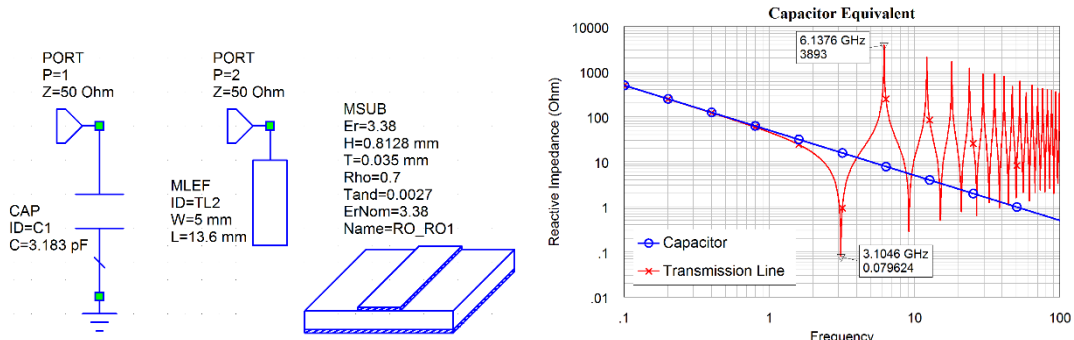


Figure 7.17. Replacement of capacitors using series Microstrip transmission lines.

The Capacitors can be replaced with open circuited transmission lines as shown in figure 7.17. The resulting line sections have been placed in table 7.2 and it can be seen that some line sections are wider than they are long, which will cause some errors in the simulation as the actual fields will be different from what is assumed in the simulation of the transmission lines.

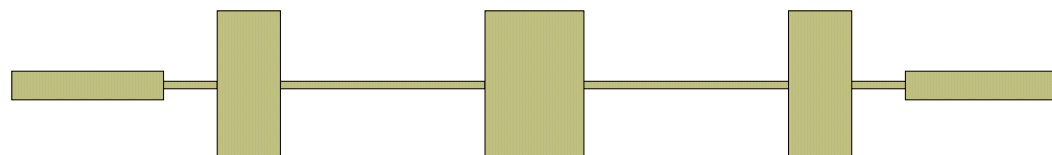


Figure 7.18. PCB Layout of the 2 GHz Lowpass filter.

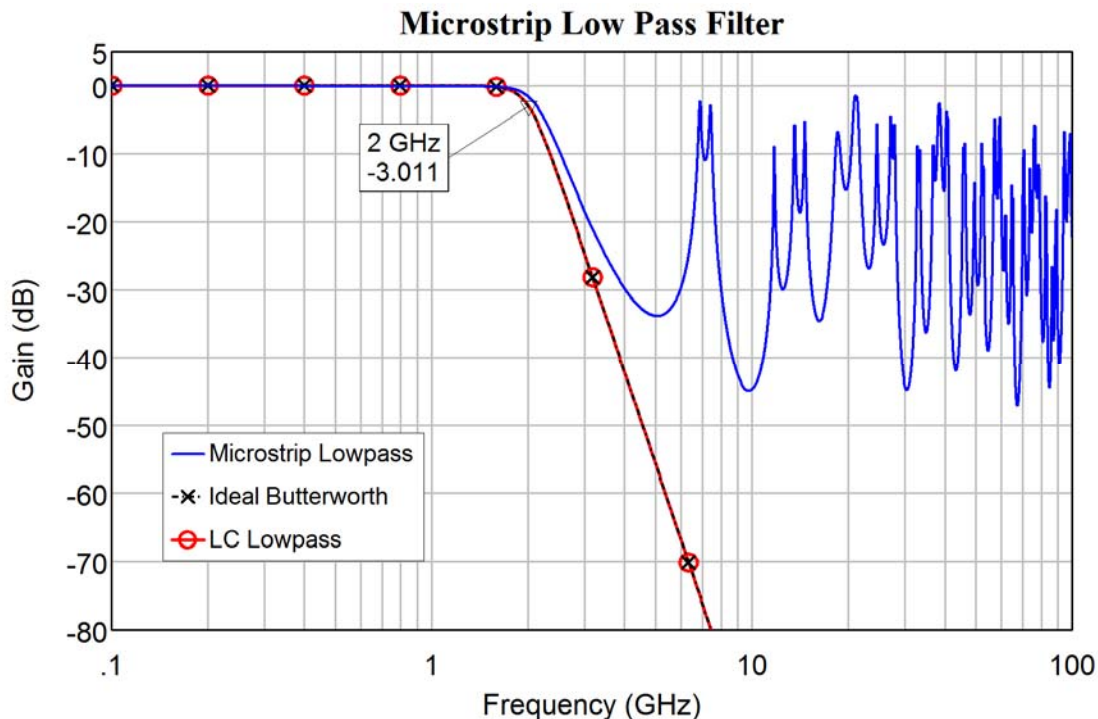


Figure 7.19. Frequency response of the LC filter and the corresponding Microstrip design.

Figure 7.19 compares the frequency response of the ideal LC filter (red) with the PCB filter of figure 7.19 (blue) and it shows that the PCB filter behaves well in the passband, but that the stopband performance is not very good. That is due to the elements becoming comparable to a quarter or half wavelength long at certain frequencies.

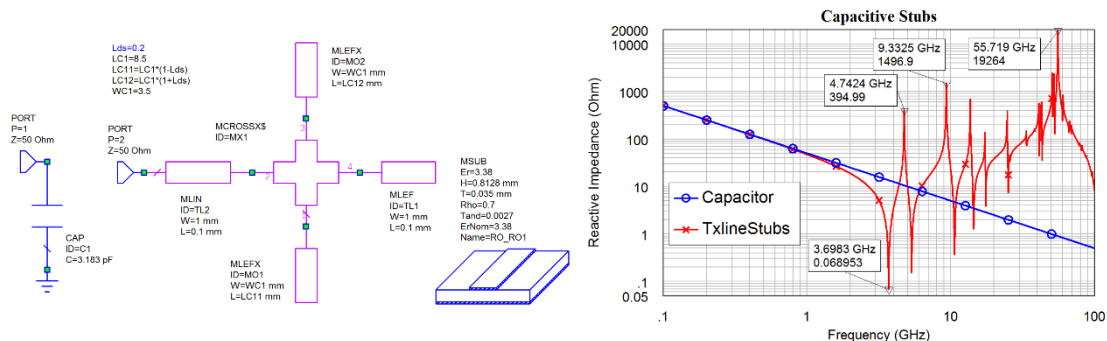


Figure 7.20. Replacement of capacitors using shunt Microstrip transmission lines.

By replacing the capacitors with open circuited shunt transmission lines as shown in figure 7.20, it is possible to obtain a better stopband performance. By making the lengths of the stubs connected at each cross-point slightly different, the effect of the transmission lines being one quarter or one-half wavelength is minimised. In figure 7.20, the transmission line has a high impedance of $2.48 \text{ k}\Omega$ at 2.48 GHz. For figure 7.20, by using stubs, the impedance is $1.82 \text{ k}\Omega$ at 9.2 GHz. By using radial stubs as shown in figure 7.21, the resonance can be extended even further to give a peak impedance of $1.59 \text{ k}\Omega$ at a frequency of 12.5 GHz. The shape of the radial stub is shown in figure 7.21. The angle for that stub is set to 60 degrees. A wider-angle stub will push the high impedance frequency even further. It is possible in a filter to vary the radii and angles to ensure that the resonances do not coincide.

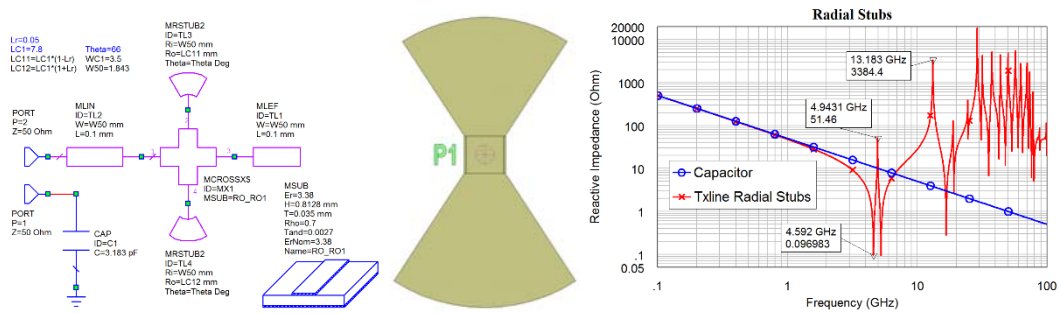


Figure 7.21. Replacement of capacitors using shunt radial stub Microstrip transmission lines.

Once the circuit schematic for the whole filter is complete, the lengths and width of the stubs and the lengths of the inductive sections are optimised, to ensure the filter meets the passband and the stopband specifications. As part of this, the width to length ratio of the stubs can be changed, to increase the attenuation at particular frequencies in the stopband. Starting with the line elements shown in table 7.1, the resulting circuit diagram of the filter, obtained after this optimisation, is shown in figure 7.22.

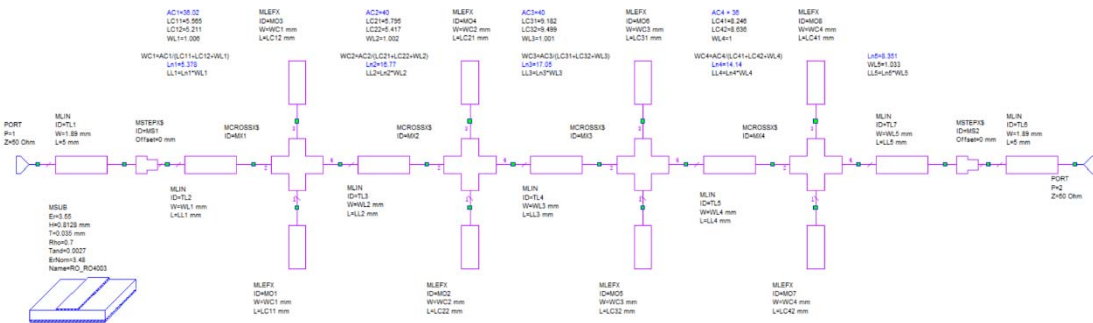


Figure 7.22. Circuit schematic for the 2 GHz lowpass filter.

EM VS Circuit Simulation

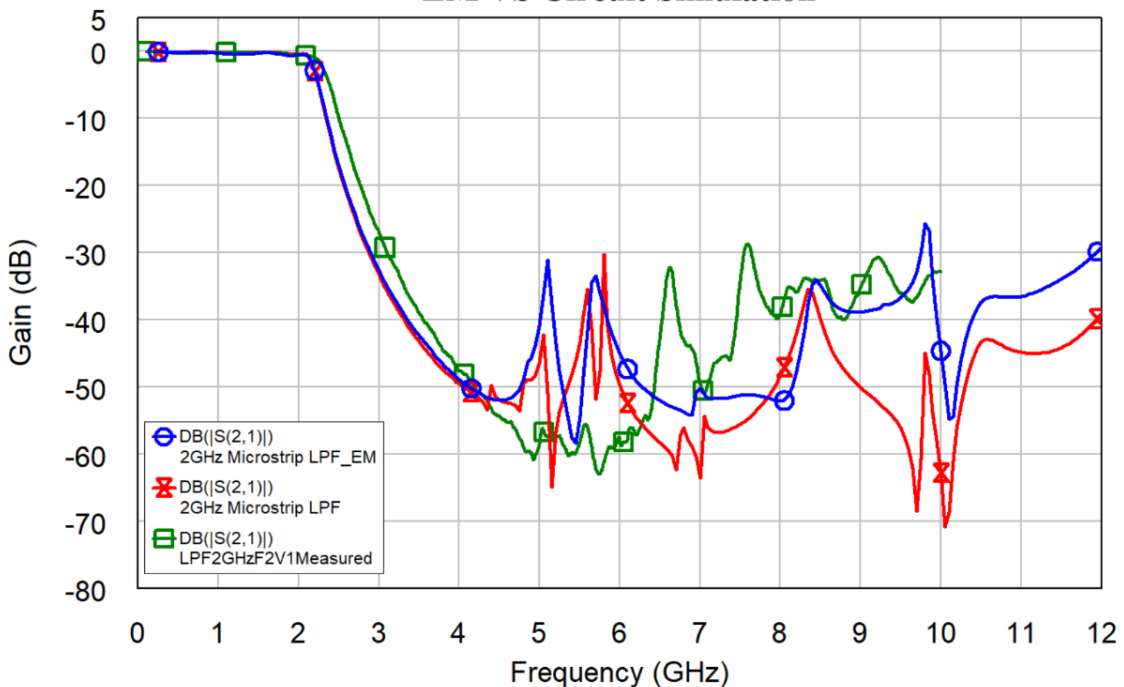


Figure 7.23. Frequency response of the 2 GHz lowpass filter.

The behaviour of the resulting filter is also calculated using a full electromagnetic (EM) simulation of the capacitive stub lines. The process of EM simulation using AXIEM is described in the section *EM simulation* in this chapter. The frequency response obtained from the circuit simulation, the EM simulation and the measured performance is shown in figure 7.23. It can be seen that there is a good agreement for frequencies below 4 GHz but that the stopband behaviour is still not adequate. The filter hardware realisation is shown in figure 7.24.

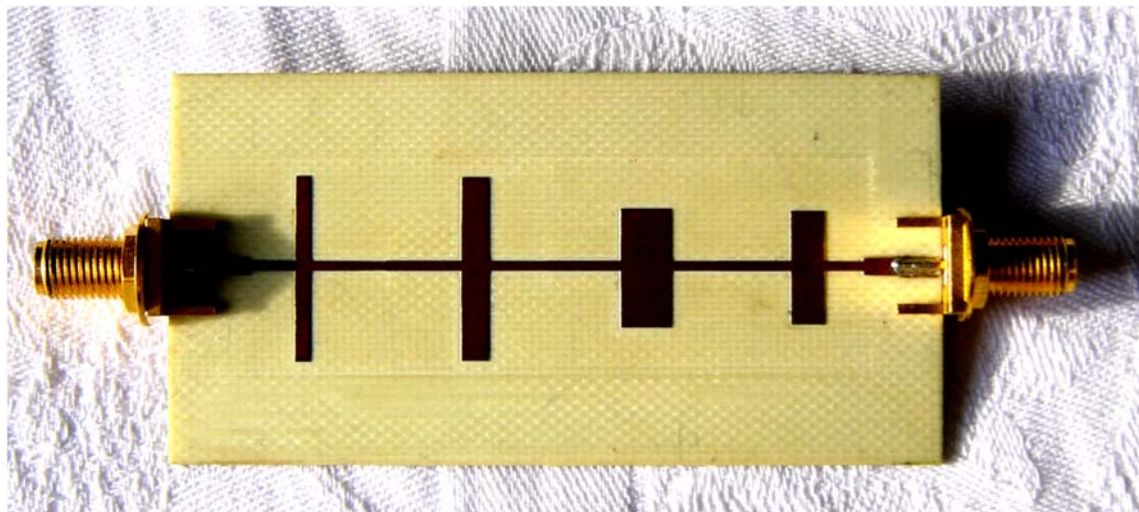


Figure 7.24. 2 GHz Lowpass filter hardware.

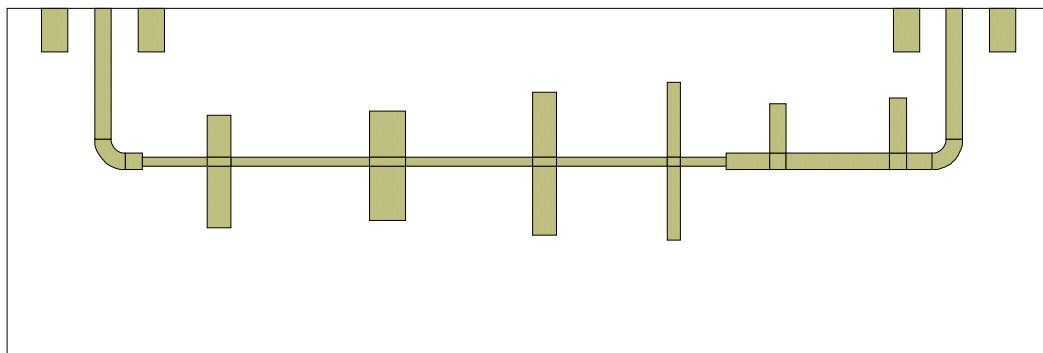


Figure 7.25. 2 GHz lowpass filter with stubs added.

The attenuation in the stopband can be improved by adding open circuited stubs, which create a transmission zero in the stopband at the frequencies where the filter without the stubs has an inadequate attenuation. In this application, a good stopband performance to up to 6 GHz was required. The stubs will affect the passband performance and the circuit elements need to be re-tuned and optimised to restore the passband performance to match that of figure 7.23. The resulting PCB layout is shown in figure 7.25. The end of each stub should be a minimum of 3 substrate thicknesses and preferably 5 substrate thicknesses (4 mm) away from the nearest metal structure to minimise coupling. This design satisfies that requirement. If needed the right most stub can be placed on the other side of the transmission line to reduce the distances to other structures.

This filter was constructed and figure 7.26 shows the simulated and measured performance. The simulated performance has a very good stopband performance. The

measured performance has a significant amount of coupling between the input and output, which is due to electromagnetic coupling between the input and output tracks and leads connecting the filter. The stopband performance was improved by enclosing the filter and placing microwave absorber on the ground-plane on the back of the filter and on the inside lid of the enclosure. The EM simulation in the stopband is sensitive to cell size. Figure 7.26 uses a cell size of 0.1 mm, using a cell size of 0.25 mm does not show a peak of -44 dB at 5.5 GHz and shows a larger peak at 6.5 GHz.

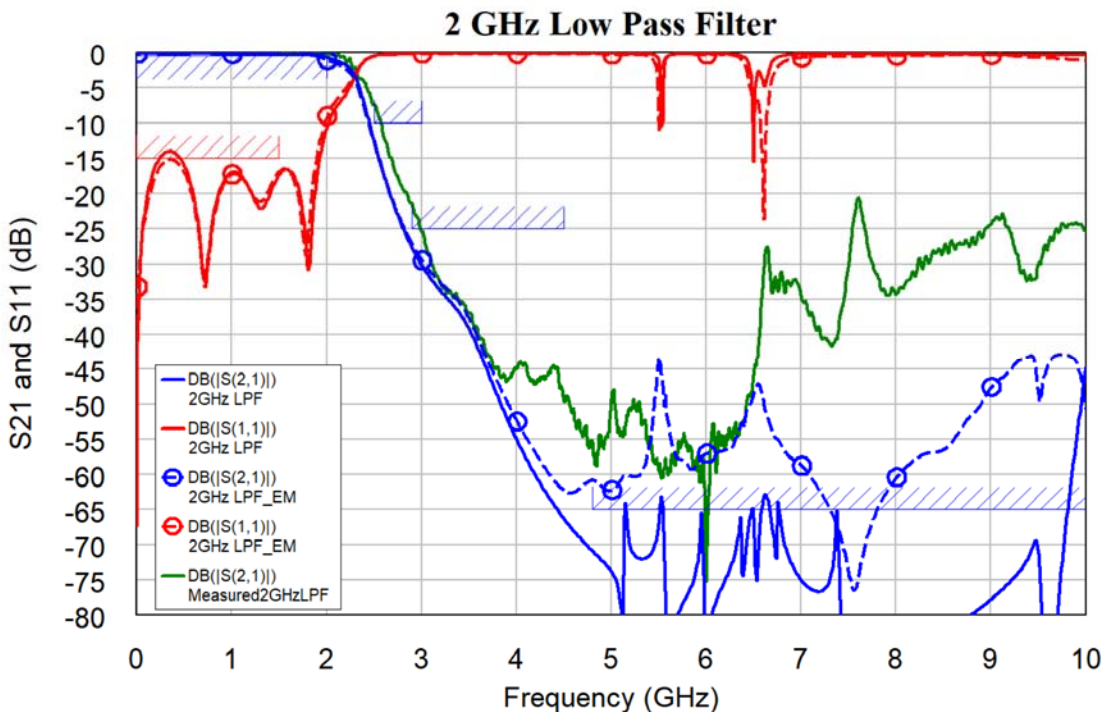


Figure 7.26. Simulated and measured performance of 2 GHz lowpass filter with stubs.

Bandpass Filter Design

LC Bandpass Filters

To illustrate the design principles, a filter with a centre frequency of 18.48 MHz and a bandwidth of 2 MHz is designed, using different techniques. This particular filter was required for a weather satellite data receiver, designed at JCU, to filter the IF data signal prior to demodulation. Since the transmitted signal is a Binary Phase Shift Keyed (BPSK) modulated RF signal containing digital data, a Bessel filter results in the lowest BER after demodulation.

Low-Pass to Band-Pass Transformation

A simple way of designing bandpass LC filters is to use the low-pass to band-pass transformation, described in most filter books. The low-pass to band-pass transformation will often give impractical component values for the bandwidths required for most RF filters. As a result, the low-pass to band-pass transformation is not suitable for most bandpass filter designs.

More practical component values are obtained using coupled resonator designs. The filter resulting from the low-pass to band-pass transformation is shown in figure 7.27. A

2.0 mH and a 4.4 mH inductor is required. These are very large inductors and will be difficult to make with acceptable Q values. Figure 7.28 shows the frequency response of this filter. The low-pass to band-pass transformation has transformed the amplitude response correctly, but the group delay is no longer flat.

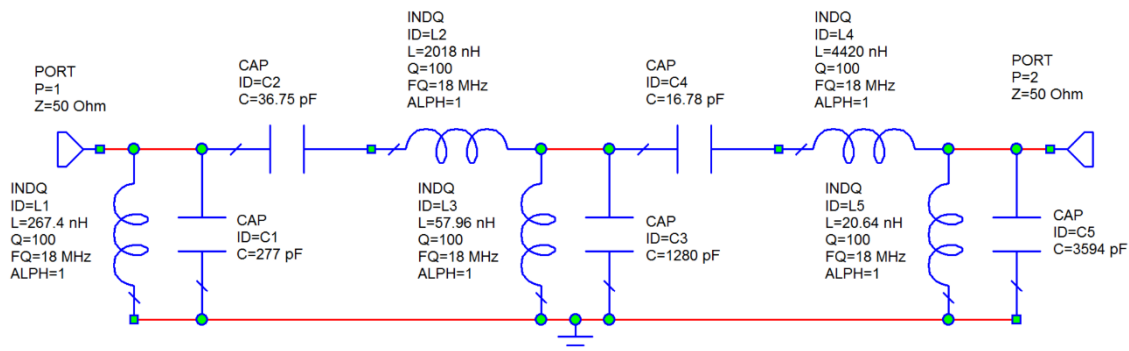


Figure 7.27. Filter from lowpass to bandpass transformation.

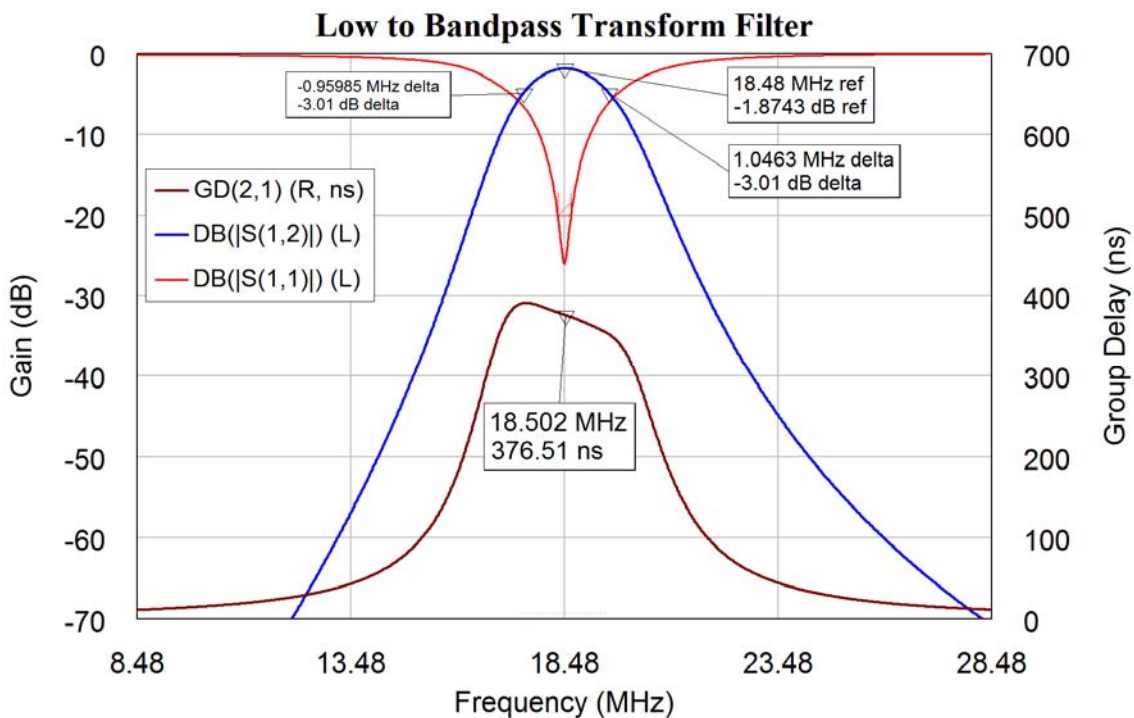


Figure 7.28. Frequency response of filter of figure 7.25.

LC Coupled Resonator Filter

In coupled resonator filters, the filter consists of a series of resonators, which are coupled using capacitive or inductive impedances, coupling loops, as shown connected to the BNC connectors in figure 7.58, or coupling apertures, as shown by the gap between the resonators in figures 7.57 and the slots cut between the resonators in figure 7.101. For many Microstrip filters like the one shown in example 7.1, the coupling between the resonators are achieved by varying the spacing between the MCFIL lines making up the filter. Example 7.3 shows how the correct coupling between resonators can be determined.

The centre frequency of the filter is determined by the frequency of the resonator and the bandwidth of the filter is determined by the coupling between the resonators. The input

impedance of the filter is determined by the coupling into the first resonator and conversely the output impedance is determined by the coupling out of the last resonator. For LC coupled resonator filters, the resonators consist of parallel LC circuits. The coupling between LC resonators can be done by connecting capacitors between the resonators, this is called capacitive coupling. The coupling can also be done by connecting inductors between the resonators, this is called inductive coupling. Capacitive coupling is the cheapest as standard capacitors can be used, while the inductors often need to be wound individually. Equation 7.3 together with normalised impedance values from Filter tables, or equations 7.5 for Butterworth filters, give the required coupling factors (K) for the desired filter.

The loading required to achieve the desired first and last resonator Q values, can be obtained from the Q values of the filter tables, from equation 7.3 or for Butterworth filters, equation 7.4. In many cases, filters with $50\ \Omega$ input and output impedances are required, while the desired loaded Q values of the resonators require very different impedances. A capacitive impedance transformer can be used to obtain the required impedance transformations.

Equations 7.3 and 7.4 only apply for lossless resonators. The K and Q filter tables in Zverev allow the filter to be designed to accommodate the finite Q values of the LC resonators, which result in the filter having an insertion loss. Table 1 shows the K and Q value table from Zverev for Butterworth filters. De-normalising the filter coefficients:

$$K_{ij} = k_{ij} \frac{BW}{F_c} \quad Q_n = q_n \frac{F_c}{BW} \quad \text{Eqn. 7.6}$$

Zverev shows that the coupling capacitor is given by:

$$C_{ij} = K_{ij} \sqrt{C_i C_j} = k_{ij} \frac{BW}{F_c} \sqrt{C_i C_j} \quad \text{Eqn. 7.7}$$

where C_i and C_j are the resonator capacitors for the i^{th} and j^{th} resonator and K_{ij} is the de-normalised coupling coefficient, k_{ij} is the normalised coupling coefficient from the tables, F_c is the centre frequency and BW is the filter bandwidth. Note the coupling capacitors are to be included in the total capacitance of the resonator so that for the resonator j the resonating capacitance is given by:

$$C_j = C_{res} - C_{ij} - C_{jk} \quad \text{Eqn. 7.8}$$

where C_{res} is the total resonating capacitance as determined from the resonant frequency and inductance for the resonator. Using coupling inductors results in:

$$L_{ij} = \frac{\sqrt{L_i L_j}}{K_{ij}} = \frac{F_c}{k_{ij} \times BW} \sqrt{L_i L_j} \quad \text{Eqn. 7.9}$$

Where L_i and L_j are the resonator inductors. In a similar manner, the coupling inductors must be considered part of the inductance of the resonator, so that the total resonator inductance is made up the inductance of the resonator in parallel with the coupling inductors on either side.

$$\frac{1}{L_j} = \frac{1}{L_{res}} - \frac{1}{L_{ij}} - \frac{1}{L_{jk}} \quad \text{Eqn. 7.10}$$

where L_{res} is the total resonating inductance as determined from the resonant frequency and capacitance for the resonator. To facilitate the design of these filters, Figure 7.29

shows the equations, which can be incorporated into a NI AWR DE project, to allow the component values for the filter shown in figure 7.30 to be calculated.

The design process is illustrated using the Bessel filter with an 18.48 MHz centre frequency and 2 MHz bandwidth filter, in the previous design. The filter design requires 4 resonators. Inductors with an inductance of 200 nH and an unloaded Q_0 of 100 are available. In LC resonators, the Q of the capacitors used is generally much higher than the Q of the inductors, so that by using equation 7.6, the resonator has a normalised q of:

$$q_0 = \frac{BW}{F_c} Q_0 = \frac{2}{18.48} 100 = 10.8 . \text{ From the Bessel filter tables in Zverev, the nearest value}$$

corresponds to a q_0 of 10.048 and results in an insertion loss of 1.85 dB. Since the actual Q is slightly higher, one should obtain an actual insertion loss that is slightly less as is evident from figures 31, 32 and 35. The corresponding K and Q values from this filter table for this value of q_0 are: $q_1 = 0.3891$, $q_4 = 0.5098$, $k_{12} = 1.7120$, $k_{23} = 0.6794$ and $k_{34} = 0.8512$. Entering those values in the LC Bandpass Filter design equations on the global definitions page of the accompanying NI AWR DE project file for figures 7.29 - 7.31 program gives the filter values as shown in figure 7.29.

AWRDE Global Definition folder. Design equations for any 4th order bandpass filter using LC components and capacitive coupling
Author C. J. Kikkert, James Cook University, 2015

```

pi=2*acos(0)          pi: 3.142
Fc=18.48              Centre Frequency in MHz
BW=2                  Bandwidth in MHz
n=4                  n - number of resonators
Zin=50                Zout=50
q1=2*sin(pi/twon)    q1: 0.7654
qn=q1                qn: 0.7654
k12=1/(2*sqrt(sin(pi/twon)*sin(3*pi/twon)))  Equations for Q and K for Butterworth filters with no loss
k23=1/(2*sqrt(sin(3*pi/twon)*sin(5*pi/twon)))  Included here for ease of use when designing Butterworth filters.
k34=1/(2*sqrt(sin(5*pi/twon)*sin(7*pi/twon)))  k12: 0.8409
                                                k23: 0.5412
                                                k34: 0.8409

NBW=BW/Fc            NBW: 0.1082
Lr=200                Lr -Resonator Inductance in nH
Qcoil=100              Qcoil - Q value of Lr
Cr=1e9/(Wc*Wc*Lr)    Cr -Resonator Capacitance in pF  Lra: 2e-7
                                                Cr: 370.9

In this example values from tables (Zverev) for inductor Q value of 100 are used.
q1a=0.3891            q1a - actual q1, from tables if allow for losses or from equations if ideal
qna=0.5098             qna - actual qn, from tables if allow for losses or from equations if ideal
k12a=1.7120            k12a - actual k12, from tables if allow for losses or from equations if ideal
k23a=0.6794            k23a - actual k23, from tables if allow for losses or from equations if ideal
k34a=0.8512            k34a - actual k34, from tables if allow for losses or from equations if ideal

Now calculate the component values
C12=k12a*NBW*Cr      C12: 68.71      Coupling Capacitances
C23=k23a*NBW*Cr      C23: 27.27
C34=k34a*NBW*Cr      C34: 34.16
Cr1=Cr-C12            Cr1: 302.1      Resonator Capacitances
Cr2=Cr-C12-C23       Cr2: 274.9
Cr3=Cr-C23-C34       Cr3: 309.4
Cr4=Cr-C34            Cr4: 336.7

Rt1=1e6*Wc*Lra*q1a/NBW  Rt1: 83.49      Input total resistance, Load and Coil
Rtn=1e6*Wc*Lra*qna/NBW  Rtn: 109.4      Output total resistance, Load and Coil
Rcoil=1e6*Wc*Lra*Qcoil  Rcoil: 2322
Rl1=Rt1*Rcoil/(Rcoil-Rt1)  Rl1: 86.61  Load resistance required at input
Rln=Rtn*Rcoil/(Rcoil-Rtn)  Rln: 114.8  Load resistance required at output

Now do a capacitive impedance transformation to obtain the required load and source impedances
C1s=Cr1*sqrt(Rl1/Zin)  Input      C1s: 397.7  Input shunt capacitance after load impedance transformation
C1t=C1s/(sqrt(Rl1/Zin)-1)  Output    C1t: 1258  Input top capacitance after load impedance transformation
Cns=Cr4*sqrt(Rln/Zout)  Input      Cns: 510.2  Output shunt capacitance after load impedance transformation
Cnt=Cns/(sqrt(Rln/Zout)-1)  Output    Cnt: 990.1  Output top capacitance after load impedance transformation

```

Figure 7.29. Global definitions LC bandpass filter design equations for a Bessel filter.

As can be seen, using equations in NI AWR DE in this way is very powerful. Just changing some input variables in these equations will calculate and simulate any 4 resonator bandpass filter. The equations can easily be modified for different numbers of resonators. The equations in figure 7.29 also include capacitive impedance transformation equations, to allow any desired input and output impedances to be

obtained. In addition, the K and Q equations for Butterworth filters have been included in these equations, so that if a Butterworth filter is required, those values can easily be linked to the actual K and Q values used for the filter (q_{1a} , q_{na} , k_{12a} , k_{23a} , k_{34a}).

Using those variables in the filter schematic gives the filter shown in figure 7.30. Since the values are calculated in the Global Definitions folder, the resulting variables have been displayed in figure 7.30 for convenience.

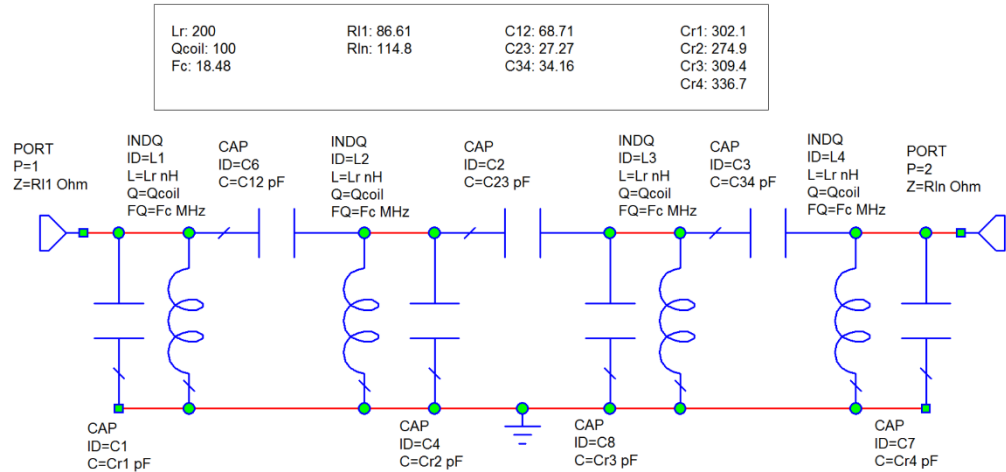


Figure 7.30. Capacitive coupled Bessel LC coupled resonator filter.

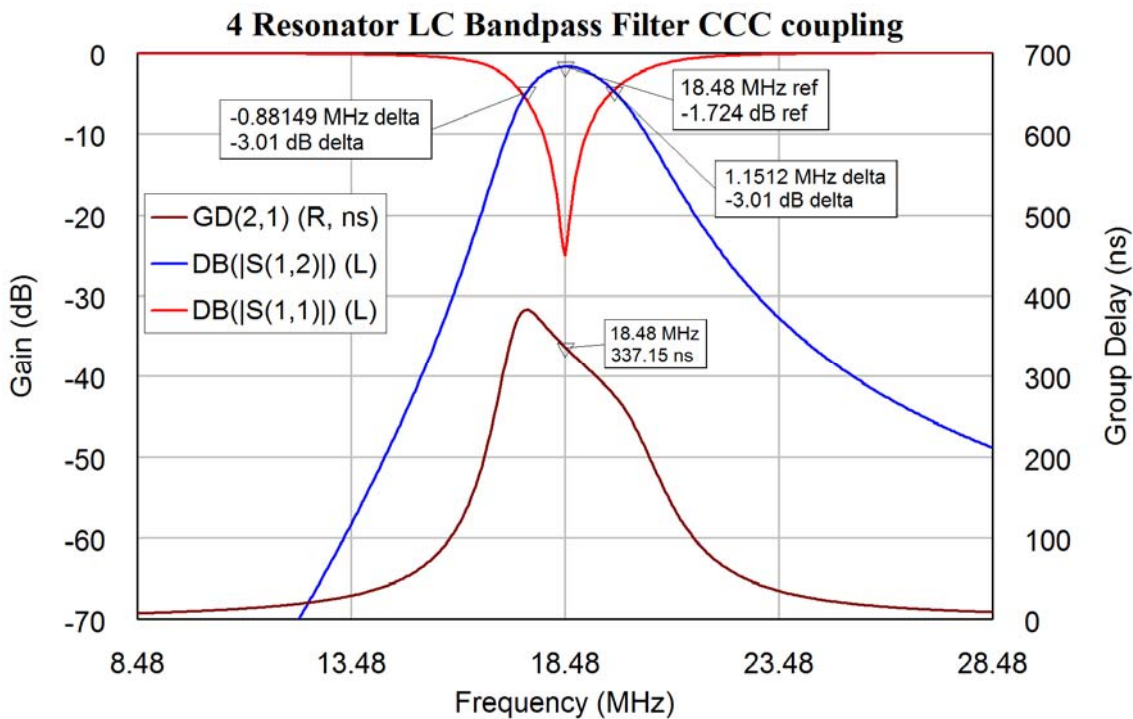


Figure 7.31. Frequency response of the filter of figure 7.30.

By comparing figure 7.28 and figure 7.31, it can be seen that capacitive coupling reduces the attenuation at high frequencies and increases the attenuation at low frequencies. In addition, the group delay is less flat than for the lowpass to bandpass transformation.

Instead of using capacitive coupling, inductive coupling can be used. For capacitive coupling, the total resonating capacitance is made up of the capacitor of a resonator plus the adjacent coupling capacitors according to equation 7.8, which is incorporated in the

LC Bandpass filter design program of figure 7.29. For inductive coupling the capacitance of the resonators are simply the resonant capacitance (371 pF in the design example) and the inductance of the resonator is adjusted to account for the coupling inductors. For this, the equations for the coupling capacitors in figure 7.29 are replaced with the equations shown in figure 7.32, which also shows the circuit of the filter. Figure 7.33 shows the frequency response of the filter. The group delay for inductive coupling has an opposite slope to the one for capacitive coupling.

Now calculate the component values required

$L_{12}=L_r/(k_{12a} \cdot NBW)$	$L_{12}: 1079$	Coupling Inductances
$L_{23}=L_r/(k_{23a} \cdot NBW)$	$L_{23}: 2720$	
$L_{34}=L_r/(k_{34a} \cdot NBW)$	$L_{34}: 2171$	
$L_{r1}=1/(1/L_{r1}/L_{12})$	$L_{r1}: 245.5$	Resonator Inductances
$L_{r2}=1/(1/L_{r1}/L_{12}-1/L_{23})$	$L_{r2}: 269.8$	
$L_{r3}=1/(1/L_{r1}/L_{23}-1/L_{34})$	$L_{r3}: 239.7$	
$L_{r4}=1/(1/L_{r1}/L_{34})$	$L_{r4}: 220.3$	

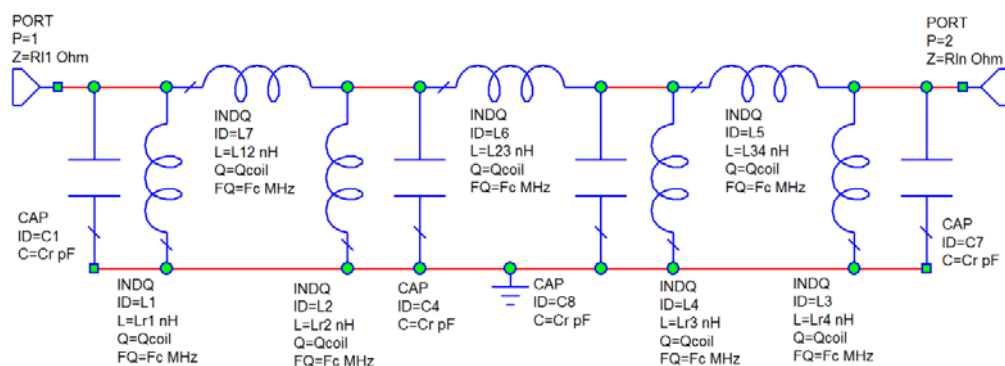


Figure 7.32. Inductively coupled LC resonator filter.

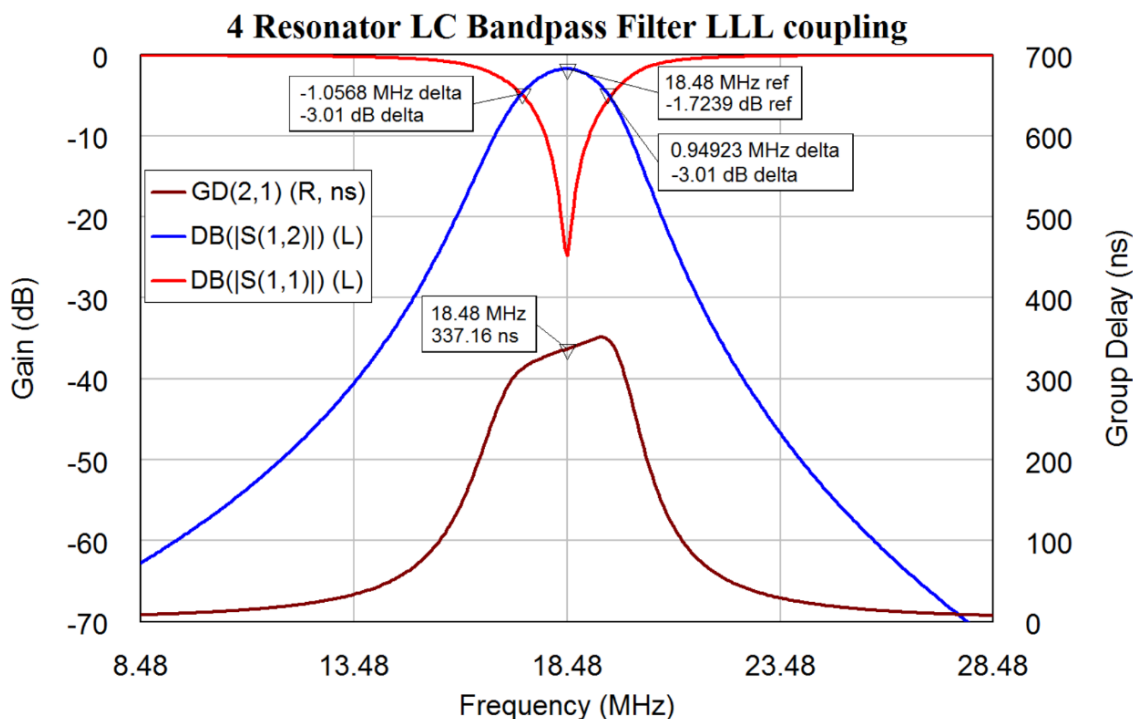


Figure 7.33. Frequency response of the filter of figure 7.32.

By using a combination of capacitive and inductive coupling, as shown in figure 7.34, a flatter group delay is obtained, as shown in figure 7.35. The equations from the Global

Definitions folder of the NI AWR DE project for figures 7.34 and 7.35 are shown in figure 7.34. If a filter with a flat group delay is to be designed and the extra cost of inductors over capacitors is a serious problem, then a filter with two coupling capacitors and one inductor can easily be obtained using these equations. The group delay of such a filter can still be made sufficiently flat over the passband using optimisation.

Now calculate the component values required

$L_{12}=L_r/(k_{12a} \cdot NBW)$	$L_{12}: 1079$	Coupling Inductance
$C_{23}=k_{23a} \cdot NBW \cdot C_r$	$C_{23}: 27.27$	Coupling Capacitance
$L_{34}=L_r/(k_{34a} \cdot NBW)$	$L_{34}: 2171$	Coupling Inductance
$L_{r1}=1/(1/L_r-1/L_{12})$	$L_{r1}: 245.5$	Resonator 1 Inductance
$C_{r1}=C_r$	$C_{r1}: 370.9$	Resonator 1 Capacitance
$L_{r2}=1/(1/L_r-1/L_{12})$	$L_{r2}: 245.5$	Resonator 2 Inductance
$C_{r2}=C_r-C_{23}$	$C_{r2}: 343.6$	Resonator 2 Capacitance
$L_{r3}=1/(1/L_r-1/L_{34})$	$L_{r3}: 220.3$	Resonator 3 Inductance
$C_{r3}=C_r-C_{23}$	$C_{r3}: 343.6$	Resonator 3 Capacitance
$L_{r4}=1/(1/L_r-1/L_{34})$	$L_{r4}: 220.3$	Resonator 4 Inductance
$C_{r4}=C_r$	$C_{r4}: 370.9$	Resonator 4 Capacitance

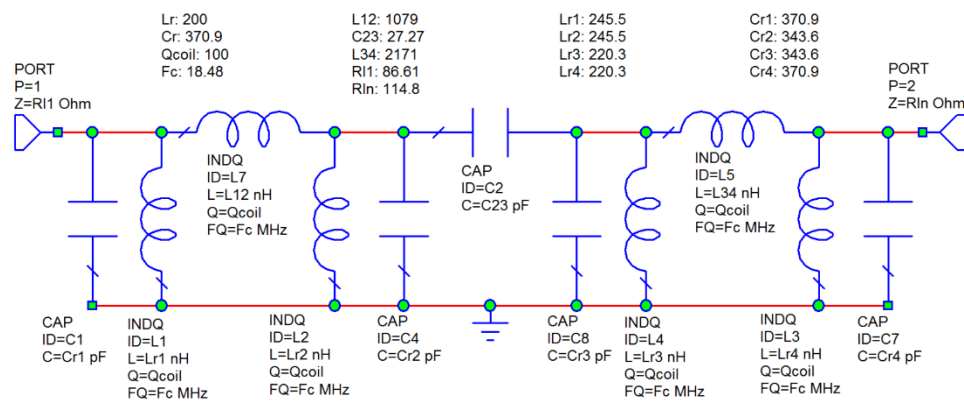


Figure 7.34. Filter with both capacitive and inductive coupling.

4 Resonator LC Bandpass Filter LCL coupling

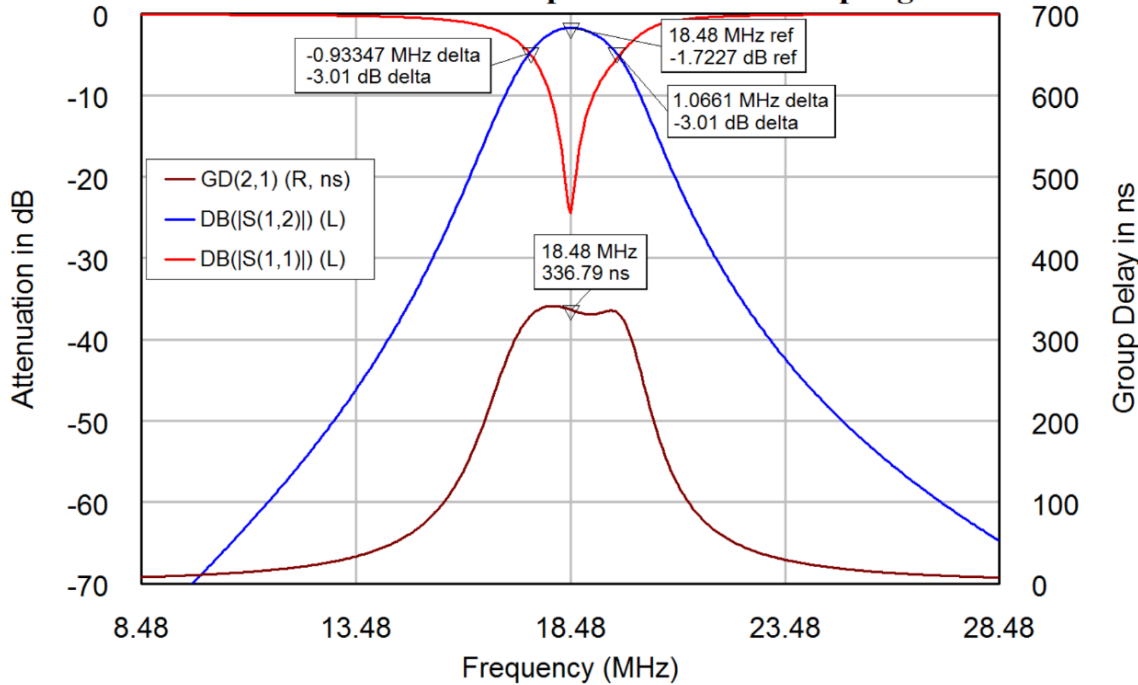


Figure 7.35. Frequency response of the filter of figure 7.34.

The input and output impedances of the filter can be changed to 50Ω , by replacing $C1$ and $C7$ with capacitive transformers as shown in figure 7.36. The equations for the value of $C1$ is calculated by the equation for $C1s$ ($C1$ shunt) and $C3$ is calculated as $C1t$ ($C1$ top). The impedance transformation for the output is done in a similar manner. This will slightly change the frequency response and the group delay. To achieve the best input and output match and a flat group delay, the component values linked to variables, calculated using the equations in the Global Definitions folder on the *Project* palette are replaced with the fixed values, which can be optimised. The filter is optimised to provide a flat group delay and meet the bandwidth specification. To achieve the lowest insertion loss at the centre frequency, S_{11} and S_{22} are optimised to be better than -30 dB at 18.48 MHz. The group delay is optimised to be as close to 325 nS as possible. Having a constant group delay results in a Bessel type filter and the filter bandwidth is determined by the group delay. The 325 nS group delay results in a 2 MHz bandwidth. The component values after optimisation are shown in figure 7.36. Figure 7.37 shows the corresponding frequency response. The resulting filter has a very flat group delay.

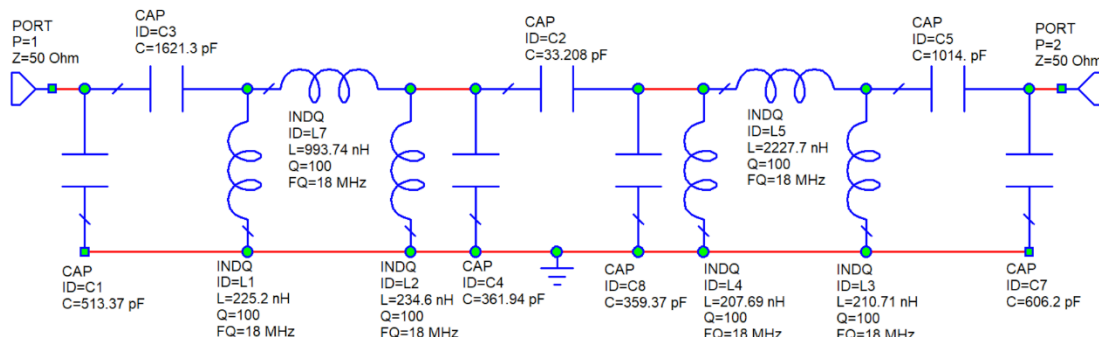


Figure 7.36. Optimised coupled resonator LC filter.

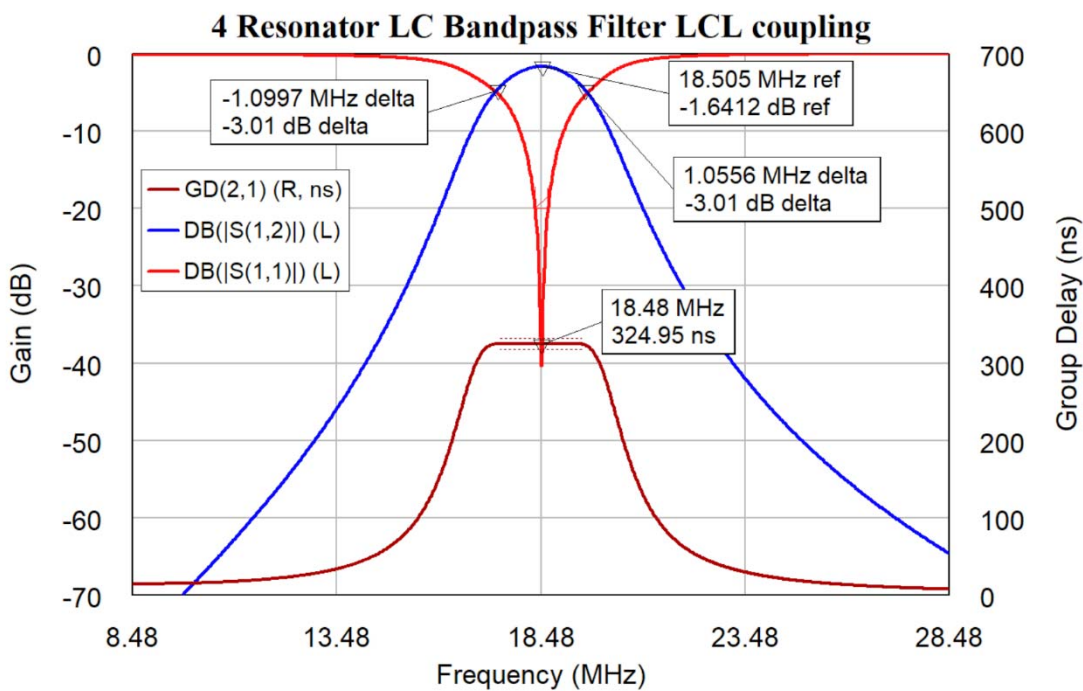


Figure 7.37. Frequency response of the filter of figure 7.36.

HF Filters

At higher frequencies, tuneable inductors become difficult to make and the inductors can be replaced by Microstrip inductors as shown in figure 7.38. This is a capacitive coupled LC resonator filter with a 160 MHz centre frequency and a 27 MHz bandwidth. The vertical transmission lines form the inductors. The parallel plates at the end of the transmission lines are pads for capacitors. Sufficient space is allowed to fit 2 capacitors in parallel to permit the capacitors to be realised with a high precision. The first and last inductors are tapped transmission lines, to allow the input and output to be coupled to the filter at the correct impedances.

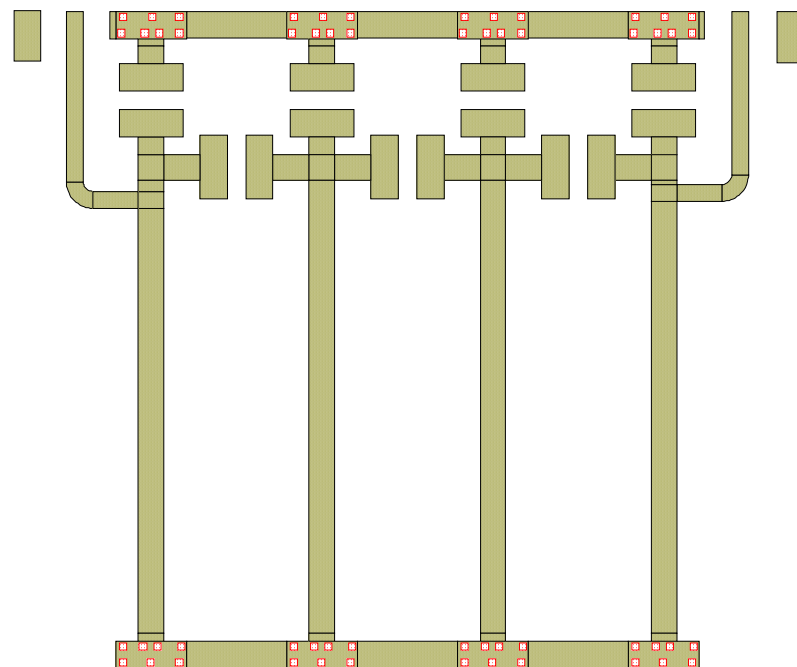


Figure 7.38. Coupled resonator filter using Microstrip inductors.

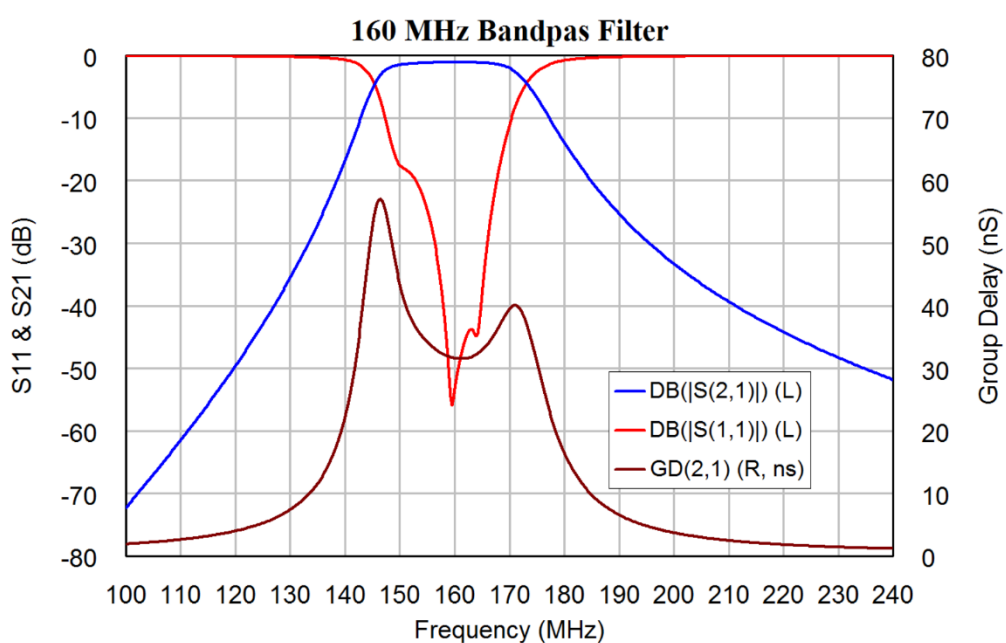


Figure 7.39. Frequency response of the filter of figure 7.38.

Figure 7.39 shows the frequency response of the filter. This filter had to satisfy passband insertion-loss constraints and as a result it corresponds to a Butterworth type frequency response and the group delay has peaks at the passband edges, similar to figure 7.2. Like the Bessel type filter of figure 7.31, the group delay is bigger at the lower corner frequency than the upper corner frequency. Like the other capacitive coupled filters, the attenuation at higher frequencies (220 MHz) is far less than the attenuation at lower frequencies (100 MHz). The measured frequency response of the filter is close to the calculated response shown in figure 7.39.

Cauer-Chebyshev Bandpass filters

Cauer-Chebyshev filters have zeros in the stopband resulting in equal ripples in the stopband as well as having ripples in the passband. It is more difficult to include zeros in the stopband of coupled resonator RF filters, as this requires coupling between adjacent resonators. It is also possible to include zeros of transmission by including open circuited stubs of one-quarter wavelength at the appropriate frequency. Such stubs are normally used to suppress the unwanted passbands occurring at the second and third harmonic of the passband frequency. In other RF filters, transmission zeros are placed at frequencies that must be rejected, such as the transmission frequency in the receive input of a diplexer. In these cases an equal stopband ripple design as specified by the Cauer-Chebyshev filters is not implemented.

Parallel Coupled-Line Filters

This filter type is also known as a stripline filter. For this filter, the design equations 7.11 to 7.14 can be used. However, one can also use the generalised coupled resonator filter equations shown in equations 29 and 30 and applied to the interdigital filter design example on page 170.

The filter parameters $a(i)$ and the resulting even and odd mode characteristic impedances are given as:

$$a(0) = \sqrt{\frac{\pi BW}{2q_1 F_c}} \quad \text{Eqn. 7.11}$$

$$a(i) = \frac{\pi BW}{2F_c} k_{i,i+1} \quad \text{Eqn. 7.12}$$

$$Z_{oo} = Z_{in} (1 - a(i) + a(i)^2) \quad \text{Eqn. 7.13}$$

$$Z_{oe} = Z_{in} (1 + a(i) + a(i)^2) \quad \text{Eqn. 7.14}$$

In these expressions BW is the bandwidth of the filter, F_c is the centre frequency, q_1, q_n are the normalised input and output loaded Q values and $k_{i,i+1}$ is the coupling coefficient between the i^{th} and the $(i+1)^{\text{th}}$ resonator as obtained from filter tables.

Example 7.1: 1 GHz, 70 MHz Bandwidth Filter

Design a 4-resonator filter with a bandwidth of 70 MHz and a centre frequency of 1 GHz. The attenuation should be as low as possible in the passband. The input and output impedances should be 50Ω . The filter is made using 0.82 mm thick RO4003 substrate with 35 micron copper. A Butterworth filter type is selected for the initial design.

Equations 7.4 and 7.5 can thus be used for obtaining the K and Q values, or they can be taken from table 7.1 to give:

Normalised

$$q_1 = q_n = 0.7654$$

$$k_{12} = k_{34} = 0.8409$$

$$k_{23} = 0.5412$$

De-normalised

$$Q_1 = Q_n = 0.7654 * 1000 / 70 = 10.93$$

$$K_{12} = K_{34} = 0.8409 * 70 / 1000 = 0.05886$$

$$K_{23} = 0.5412 * 70 / 1000 = 0.03788$$

Substituting this into equations 7.13 and 7.14 and substituting the resulting $a(0)$ and $a(i)$ into equations 7.11 and 7.12 gives the values for Z_{oe} and Z_{oo} shown below. Those values are then entered into the TxLine program as shown in figure 7.40.

Line	a	Z_{oe}	Z_{oo}	Width	Space	Length
0	0.3902	76.13	38.23	1.26 mm	0.12 mm	47.3 mm
1	0.09246	55.05	45.80	1.71 mm	1.08 mm	46.2 mm
2	0.05951	53.15	47.20	1.74 mm	1.57 mm	46.0 mm
3	0.09246	55.05	45.80	1.73 mm	1.2 mm	46.2 mm
4	0.3902	76.13	38.23	1.26 mm	0.12 mm	47.3 mm

Table 7.3 Parallel coupled-line filter parameters.

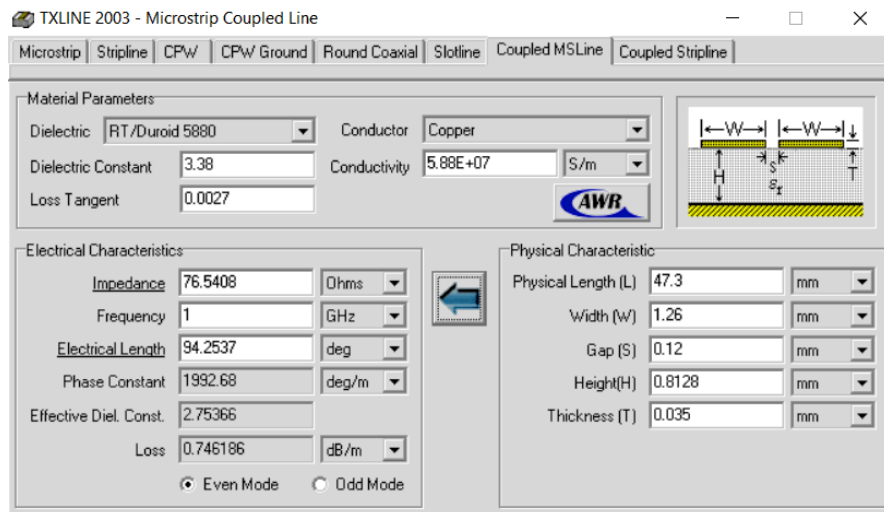


Figure 7.40. Calculating line widths and coupling gaps.

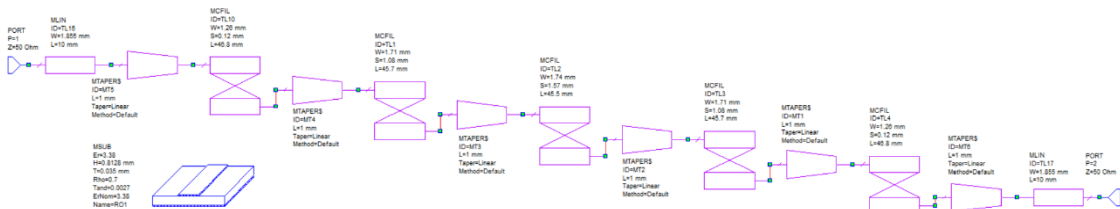


Figure 7.41. NI AWR DE schematic for the 1 GHz filter

Those line geometries are then entered in a circuit schematic to give the circuit shown in figure 7.41. End effects have been included by using the Microstrip filter element "MCFIL". A 1 mm long taper has been added between each coupled section to ensure that the coupled lines do not produce a short circuit at the transition in width. As a result, all resonators are shortened by 0.5mm to keep the total resonator length the same. The computer simulation software will produce a layout from the schematic as shown in figure 7.42. This layout can be plotted and produced as a PCB.

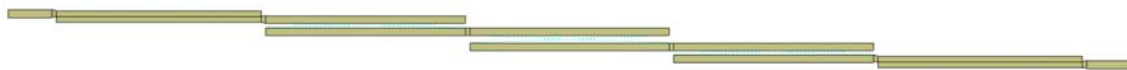


Figure 7.42. PCB layout for this filter produced by NI AWR DE.

Figure 7.43 shows a close-up of the centre of the first resonator, and shows *TL10*, *MT4* and *TL1* of figure 7.41. It can be seen that without the tapered transition a short circuit would be produced. The filter from figure 7.41 as designed using the above procedure has a centre frequency of 981 MHz, and is 1.9% low. The bandwidth is 62 MHz and is 12 % low. The resonator lengths and coupling gaps are optimised, using the optimisation routines in NI-AWR DE, to achieve the correct centre frequency and bandwidth. Since the design procedure gives a result very close to the specifications, the optimisation procedure is quick. The resulting frequency response is shown in figure 7.44. The insertion loss of the filter is 1.9 dB. The return loss can be improved if needed by setting optimisation goals on S_{11} and using the optimiser to automatically fine tune the elements.

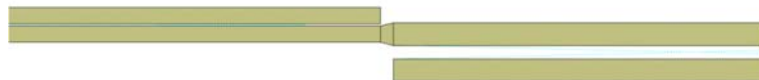


Figure 7.43. Close-up of part of figure 7.42, showing *TL10*, *MT4* and *TL1*.

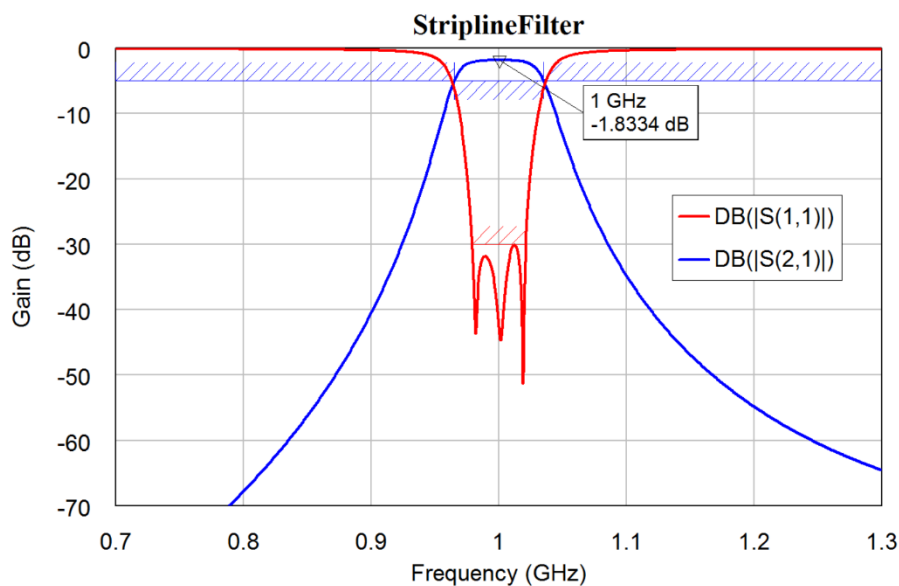


Figure 7.44. Frequency response of the filter from figure 7.41 after optimisation.

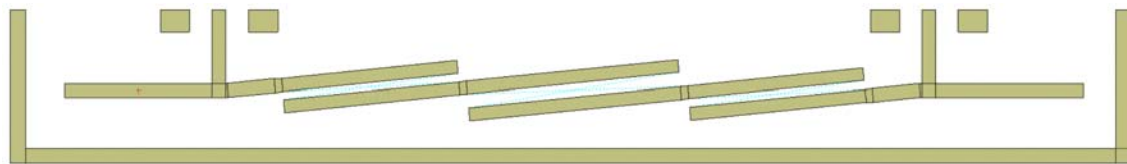


Figure 7.45. PCB layout for coupled-line filter with tap coupling into and out of the filter.

For the filter in figures 7.41 to 7.43, the input coupling gap is 0.14 mm. This gap is close to the limit of reliable manufacturing capability. To avoid this limitation, tap coupling is used to connect to the input and output resonators, as shown for the 100 MHz bandwidth at a 1.7 GHz centre frequency filter shown in figure 7.45. For wider bandwidth filters, the

input and output coupling gaps are very small and tap coupling is best. For very narrow bandwidth filters, the connection point for tap coupling becomes too close to the effective ground point of the first resonator, so that line coupling as shown in figure 7.41 is more practical.

The actual filter, when produced, will have a centre frequency and bandwidth that will be slightly different from the simulated results. These differences are due to; the computer simulation not being completely accurate, variations in PCB substrate materials, etching, or milling errors in producing the PCB and so on. In many instances, the filter performance will be good enough. When the filter specifications are critical, a second iteration of the filter can be produced, where the simulation is biased to correct for the discrepancy between the measured and simulated results.

Hairpin Filters

The filters of figure 7.42 and 7.45 are long and skinny and are difficult to mount securely. To obtain a better form factor for the filter, the resonators can be folded as shown in figure 7.46. Coupled resonator filters where the resonators are made up from quarter wavelength transmission lines will have additional passbands when the wavelength of the resonators are three quarter of a wavelength long, five quarter of a wavelength long and so on. These harmonic resonances are normally undesirable. To avoid these harmonic stubs can be added.

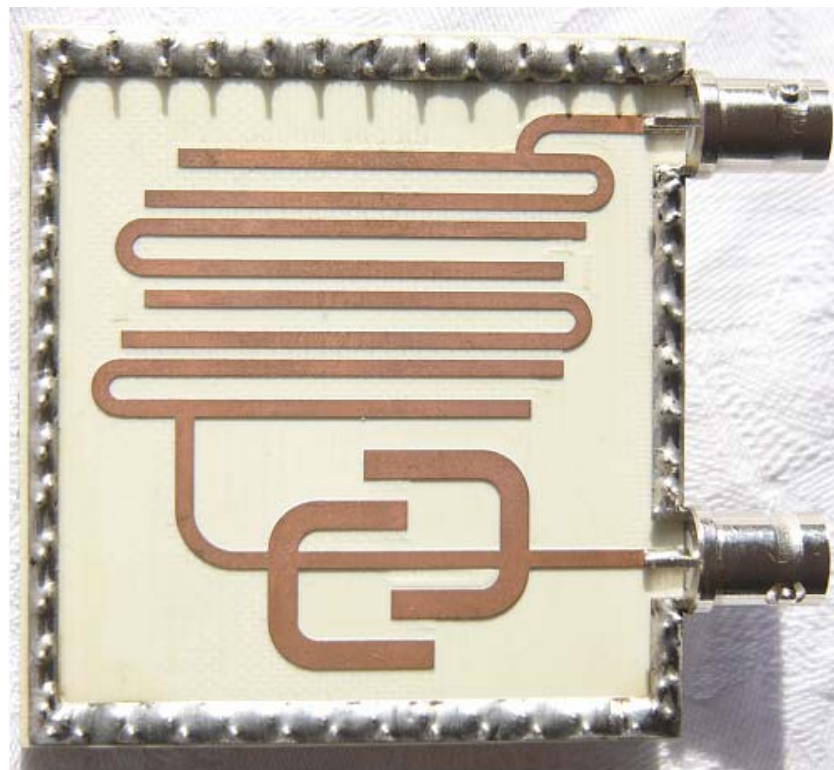


Figure 7.46. Hairpin filter with harmonic stubs.

The hairpin filter in figure 7.46 has two second and third harmonic suppression stubs incorporated as part of the design. The design procedure consists of firstly designing and optimising a basic hairpin filter as outlined in the previous example. Second and Third harmonic suppression stubs are then designed as a separate circuit, as shown in figure 7.47. The second harmonic stubs are one-quarter wavelength long at the second harmonic

and the third harmonic stubs are one-quarter wavelength long at the third harmonic. The spacing between the stubs is then adjusted such that the return loss of the circuit is large at the centre frequency of the filter, so that the harmonic stub circuit has the least effect on the filter performance. The stubs are folded to minimise the space used by the whole filter. Note this filter was designed and build before EM based X models were readily available. At present one would use MTEEX, MCROSSX\$ and MLEFX elements for better accuracy.

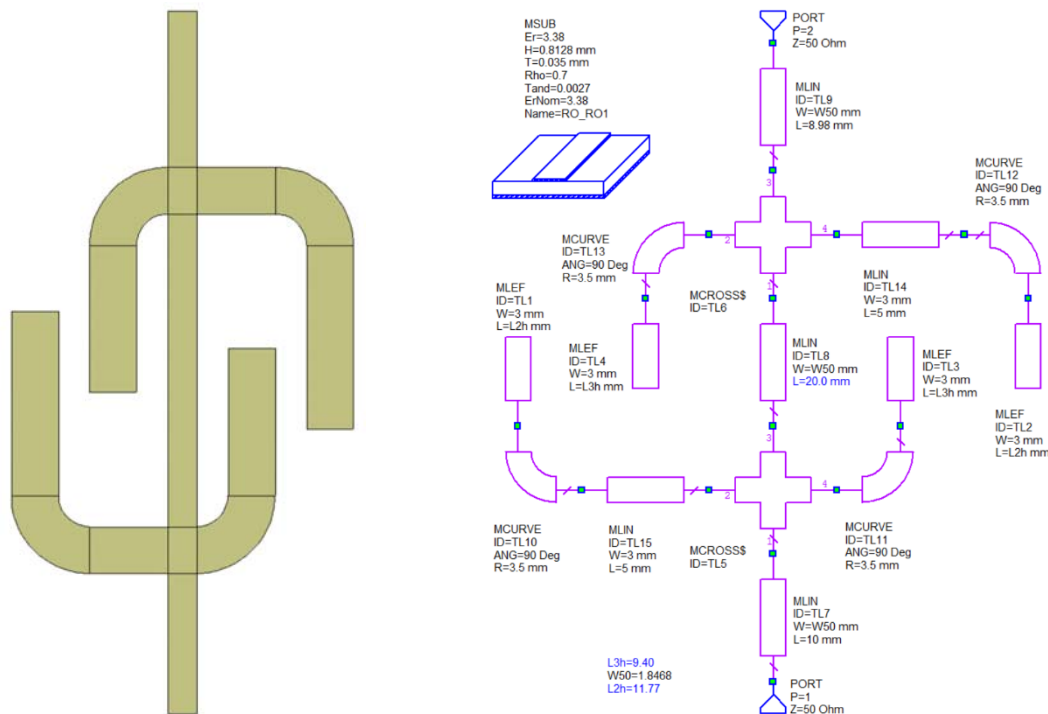


Figure 7.47. Folded harmonic stubs.

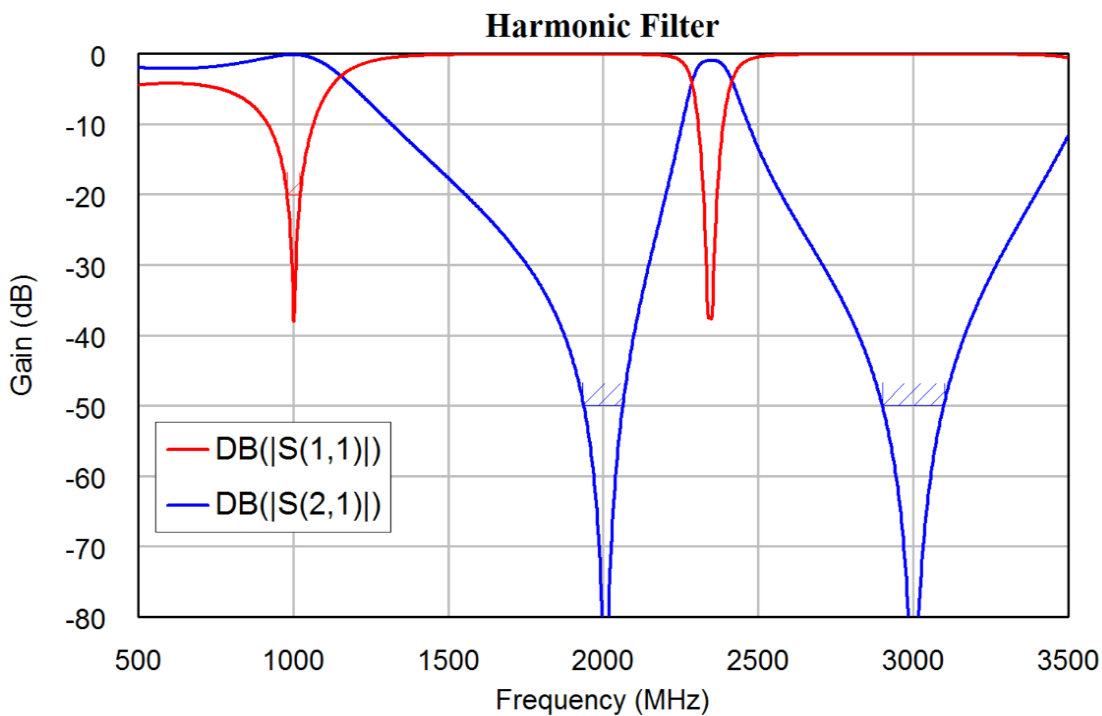


Figure 7.48. Frequency response of harmonic stubs.

Figure 7.48 shows the frequency response of the harmonic stub circuit. It can be seen that there is some effect on the passband of the filter, so that further optimisation to the design of the hairpin filter must be carried out in order to ensure that the combination of the hairpin filter and the harmonic stubs have the required passband response. Figures 7.51 and 7.52 show the frequency response of the actual filter of figure 7.46 and compares this with the frequency response of the simulation.

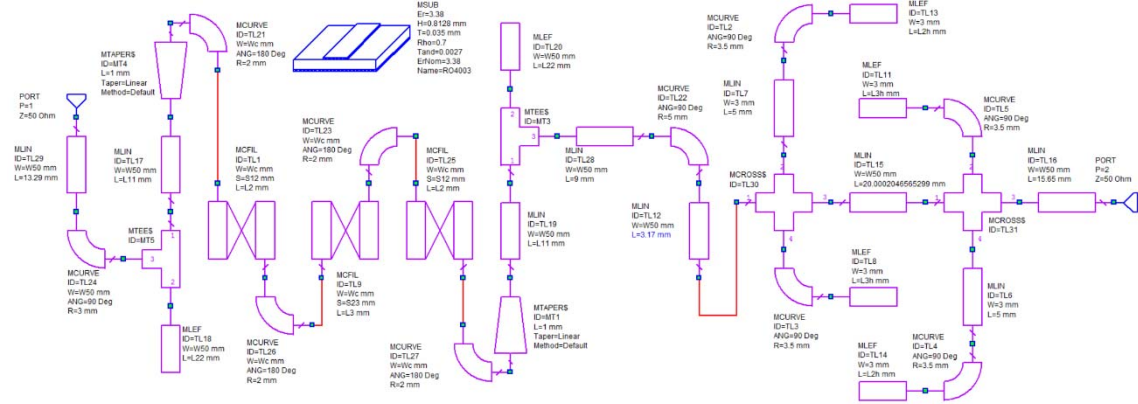


Figure 7.49. Circuit schematic of hairpin filter as built.

The filter hardware was realised from the circuit schematic using the “MCFIL” elements as shown in figure 7.49. To compare the different ways this circuit can be simulated, The MCFIL elements can be replaced with the coupled line element “MCLIN” with “MLEF” elements compensating for the end effect of the open circuited ends of the coupled line elements, as shown in figure 7.50. An AXIEM EM simulation is carried out on the circuit of figure 7.49, as described in the *EM Simulation* section later in this chapter. Finally the MTEES\$, MCROSS\$ and MLEF elements in 7.49 are replaced with the EM based elements MTEEX\$, MCROSSX\$ and MLEFX.

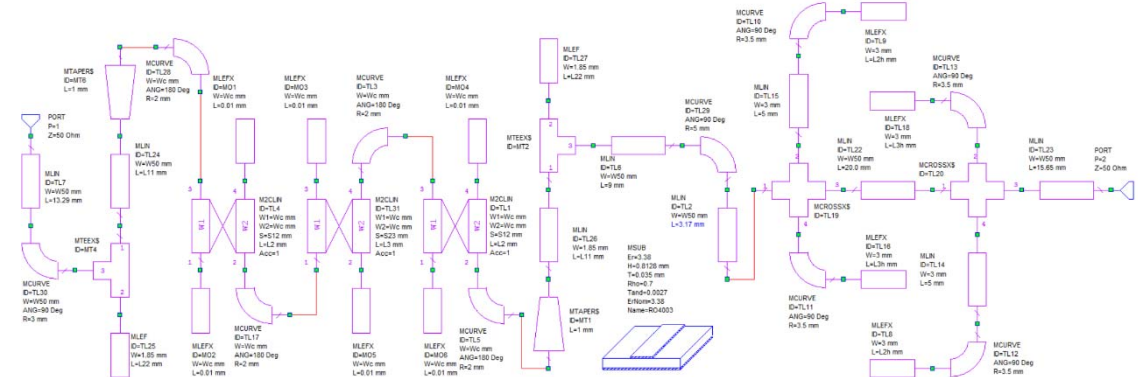


Figure 7.50. Circuit schematic of hairpin filter using MCLIN elements.

The value of $E_r = 3.38$ was specified by the manufacturer and is used for the simulation and optimisation of this filter prior to its manufacture. Figures 7.51 and 7.52 show a comparison between the simulated and measured performance. The EM simulation, using AXIEM and EM EXTRACTION, gives a better agreement for the passband centre frequency and bandwidth, than the circuit simulations. Using EM based elements MTEEX\$, MCROSSX\$ and MLEFX makes no noticeable difference below 2 GHz.

Figure 7.52 shows the stopband performance of the filter for both the measured performance and the computer simulation. The most significant difference is the reduction in attenuation in the stopband. This is due to EM coupling between parts of the

circuit and the input and output leads. The stopband attenuation can be optimised by mounting the filter in a conductive (aluminium) enclosure and applying microwave-absorbing material in the appropriate places, to be determined experimentally. In many cases, applying the absorber to the back ground-plane of the filter improves the stopband performance sufficiently. Both EM simulations give a good agreement between the measured and simulated results at 2 GHz, but the circuit simulations give a poor agreement there.

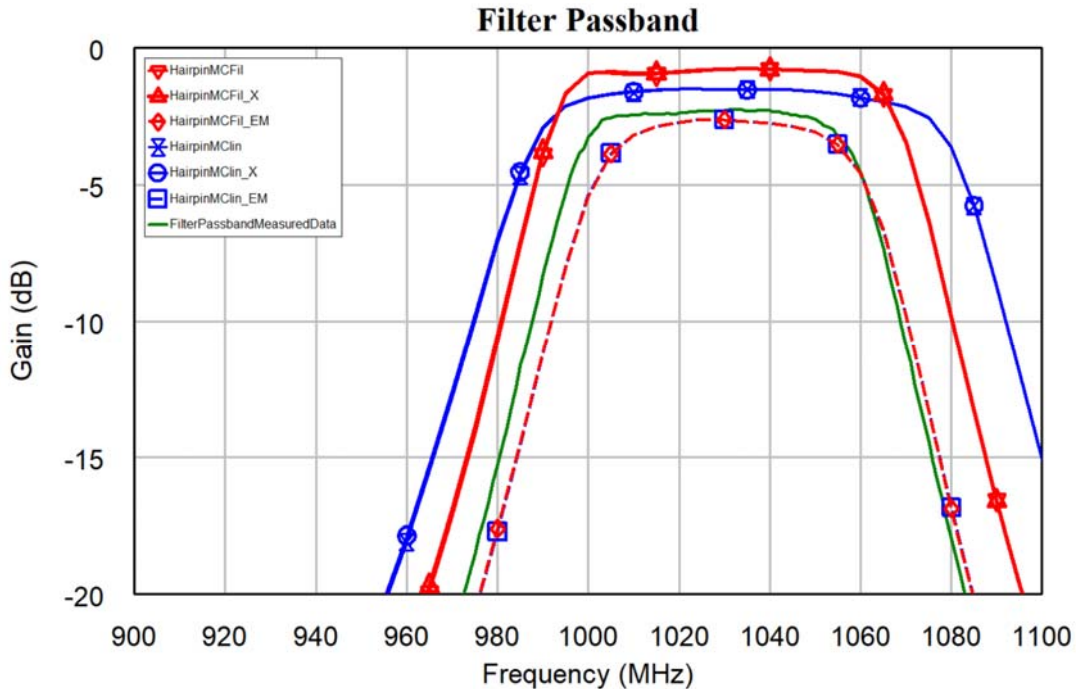


Figure 7.51. Passband response of hairpin filter of figures 7.46 and 7.49.

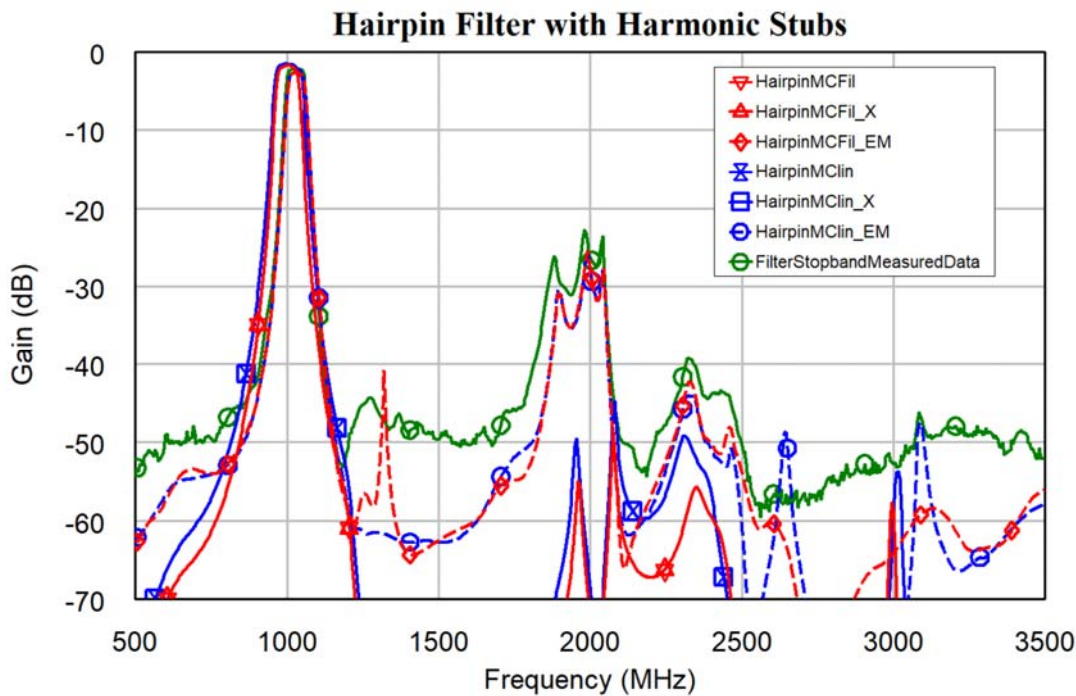


Figure 7.52. Frequency response of hairpin filter of figures 7.46 and 7.49.

Helical Filters

For high Q value resonators at UHF frequencies, a cylindrical rod of one-quarter wavelength long is placed inside a cavity. This cavity can be cylindrical but in many cases, the cavity is rectangular for ease of construction. Such cylindrical structures are called coaxial filters, as the cross-section of the filter is a coaxial transmission line.

At VHF frequencies, the size of the coaxial filter becomes too large for many applications. To reduce the length of the resonator, the centre quarter-wave resonator is wound as a helix. Often the helix is wound on a former or bobbin, as shown in figure 9.29 of Zverev [1]. One has to ensure that the material for the former is not lossy at the operating frequency. Polyethylene is suitable for low loss formers.

The resonators have shields between them to confine the fields for the resonators. The resonators are coupled by having the appropriate shield height, so that some of the field of a resonator couples to the next resonator. The coupling is controlled by adjusting the difference between the height of the shield and the top of the helix as shown by dimension "h" in figure 7.53. Alternately, the coupling can be achieved by having a coupling hole in the centre of a full-height shield or by having a slot at the bottom of the shield. The choice of coupling aperture depends on the construction of the cavity.

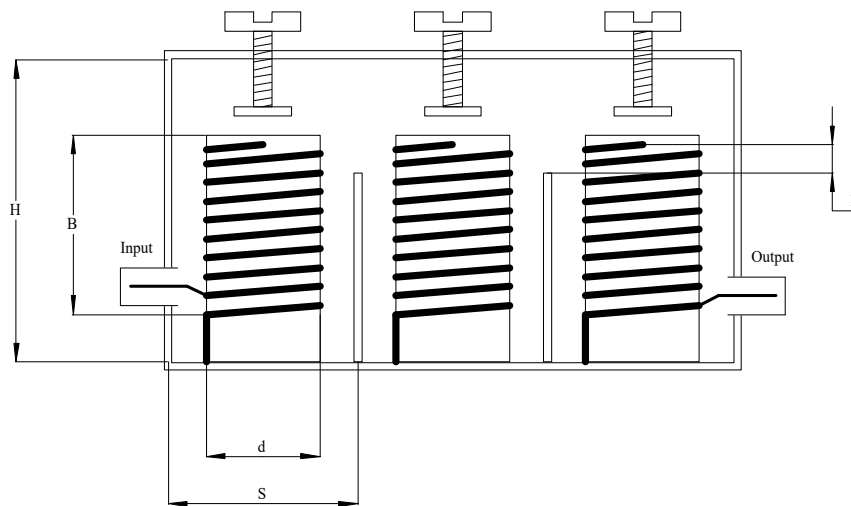


Figure 7.53. Drawing of a helical filter showing the sizes used in the formulae.

Formula for Helical Filters (from Zverev [1])

f is the centre frequency of the helical resonator in MHz

S is the width of the rectangular resonator cavity. (units m)

H is the height of the resonator cavity (units m)

B is the height of the helix (units m)

d is the diameter of the helix (units m)

N is the number of turns of the helix

Z_0 is the characteristic impedance of the helical transmission line in the cavity.

δ is the skin depth. The wire diameter should be > 5 times the skin depth.

Q_0 is the unloaded Q of the resonator cavity.

If instead of a rectangular cavity, a cylindrical cavity is used, the diameter D of the cavity is $D = 1.2 S$.

For the cavity:

$$d = 0.66S \quad \text{Eqn. 7.15}$$

$$B = S \quad \text{Eqn. 7.16}$$

$$H = 1.6S \quad \text{Eqn. 7.17}$$

$$Q_0 = 2363 \times S \sqrt{f} \quad \text{Eqn. 7.18}$$

For the highest Q value, the wire diameter of the helix is selected to be half the pitch of the helix. The gap between the wires is thus the same as the wire diameter.

For the helix:

$$N = \frac{40.6}{S \times f} \quad \text{Eqn. 7.19}$$

$$\delta = \frac{6.6 \times 10^{-5}}{\sqrt{f}} \quad \text{Eqn. 7.20}$$

$$Z_0 = \frac{2070}{S \times f} \quad \text{Eqn. 7.21}$$

$$\frac{R_b}{Z_0} = \frac{\pi}{4} \left(\frac{1}{Q_d} - \frac{1}{Q_0} \right) \quad \text{Eqn. 7.22}$$

The doubly loaded input Q_d , is defined as $\frac{1}{2} Q_1$ for the input tapping point calculation and $\frac{1}{2} Q_n$ for the output tapping point calculation, and represents the total load seen by the resonator if there is a very small insertion loss as is normally the case. The electrical length θ from the bottom of the helix to the point where the input or output connects to the helix is given by:

$$\sin(\theta) = \sqrt{\frac{R_b R_{tap}}{2Z_0^2}} \quad \text{Eqn. 7.23}$$

The gap between the shield and the top of the helix is given by:

$$K = 0.071 \left(\frac{h}{d} \right)^{1.91} \quad \text{Eqn. 7.24}$$

When the bandwidth increases, the gap between the top of the shield and the top of the coil increases. For wideband filters, no shield is required, thus reducing the cost of construction. In that instance, it is also possible to vary the coupling by varying the spacing between the resonators.

Example 7.2: 100 MHz, 1 MHz Bandwidth Filter

Design a helical filter to have a 1 MHz bandwidth at 100 MHz. A diecast box of 112 mm width and 50 mm depth and 90 mm height is available. This can be split into two cavities 56 x 50 x 90 mm. The average side S is 53 mm. The H/S ratio is $90/53 = 1.7$, which is close enough to the $H = 1.6S$ value from equation 7.17.

The K and Q values required can be obtained from table 1. Since for two resonators and Butterworth filters the K and Q values are independent of the insertion loss, equations 7.4 and 7.5 can be used to calculate the required K and Q values.

For Butterworth filters, equation 7.4 and 7.5 are:

$$q_0 = q_n = 2 \sin \frac{(2-1)\pi}{2n} = 2 \sin \frac{\pi}{2n} \quad \text{Eqn. 7.4}$$

$$k_{ij} = \frac{1}{2 \sqrt{\sin \frac{(2i-1)\pi}{2n} \sin \frac{(2i+1)\pi}{2n}}} \quad \text{Eqn. 7.5}$$

For a two-resonator filter $n = 2$, this gives $q = 1.4142$ and $k = 0.7071$

The reader is reminded that the small letters k and q denote the normalised values as would be obtained from table 7.1 and the capital letters K and Q are the de-normalised values, which relate to the normalised values by equations 7.6 and 7.7.

Since $S = 53$ mm and $f = 100$, equation 7.18 gives the unloaded Q of the cavity as: $Q_0 = 2363 * 0.053 * 10.0 = 1252$. The normalised unloaded Q is $q = 1259 * 1/100 = 12.52$. From the filter table 7.1, the resulting filter will thus have close to 1 dB insertion loss.

Since $S = 53$ mm, applying equation 7.15 gives the coil diameter as: $d = 35$ mm. From equation 7.17, the coil height is 53 mm and equation 7.19 indicates it requires 7.6 turns. The optimum wire diameter is thus $53/(2*7.6) = 3.49$ mm. A one-eighth of an inch copper tube is 3.2 mm and is used for winding the coil. The minimum wire diameter of five times the skin depth (equation 7.20) is 0.033 mm. For practical windings, the minimum skin depth requirement is normally satisfied.

From the filter tables the normalised values for Q and K are: $q_1 = q_n = 1.4142$ and $K_{12} = 0.7071$. De-normalising this gives $Q_1 = Q_n = 1.4142 * 100/1 = 141.42$ and $K_{12} = 0.7071 * 1/100 = 0.007071$. Q_1 and Q_n are the loaded Q values, which are due to the input and output load impedance being coupled into the resonators and thus appearing as a load to the resonators. The doubly loaded input Q is defined as $\frac{1}{2} Q_1$. This represents the total load seen by the resonator, if there is a very small insertion loss, as is the case here. The doubly loaded output Q is defined as $\frac{1}{2} Q_n$. Q_d is thus 70.71 for both the input and output. Putting this in the expression for R_b/Z_0 gives: $R_b/Z_0 = 0.0105$. Since we want the filter to be have 50Ω input and output impedance, $R_{\text{tap}} = 50 \Omega$ resulting in $\theta = 1.48$ degrees. Since the coil wire length is $7.6 * 35 * \pi = 842$ mm and corresponds to a quarter wavelength at the centre frequency, or 90 degrees, the tapping point should be $1.48 * 842 / 90 = 13.9$ mm from the bottom of the helix. In practice, the tapping point needs to be fine-tuned, to match the actual conditions after construction and include losses of the former used for winding the helix on.

For this Butterworth filter, the tapping points for the input and output are the same. For Chebyshev or Bessel filters, or for lossy higher order Butterworth filters, the input and output tapping points will be different, and the above calculation needs to be performed for Q_1 and for Q_n .

The filter was constructed and performed exactly as expected. The measured bandwidth for the helical filter was 1 MHz and the insertion loss was 0.8 dB. A photograph of the filter is shown in figure 7.54 and the measured response is shown on figure 7.55.

The tuning procedure for adjusting the tapping point for the input and output, and for verifying and if needed adjusting the coupling, is described on page 518 and figure 7.9.23 in Zverev [1]. This same procedure is used, to determine the coupling factors for interdigital filters as shown in figures 7.57, 7.58 and equations 7.29 and 7.30.

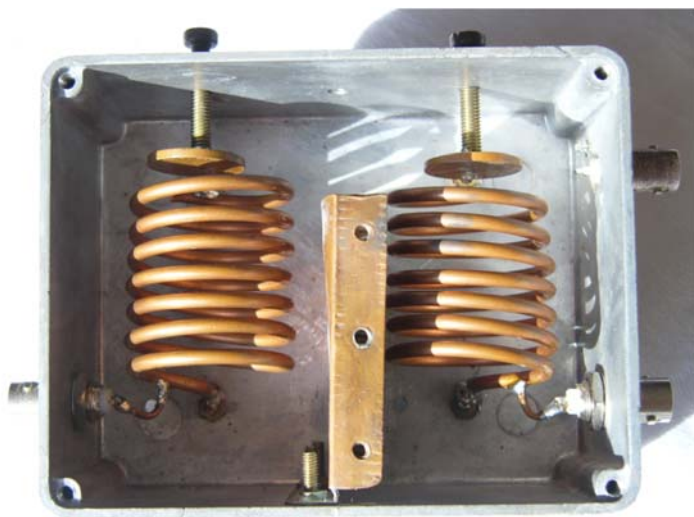


Figure 7.54. 101 MHz helical filter 1 MHz bandwidth

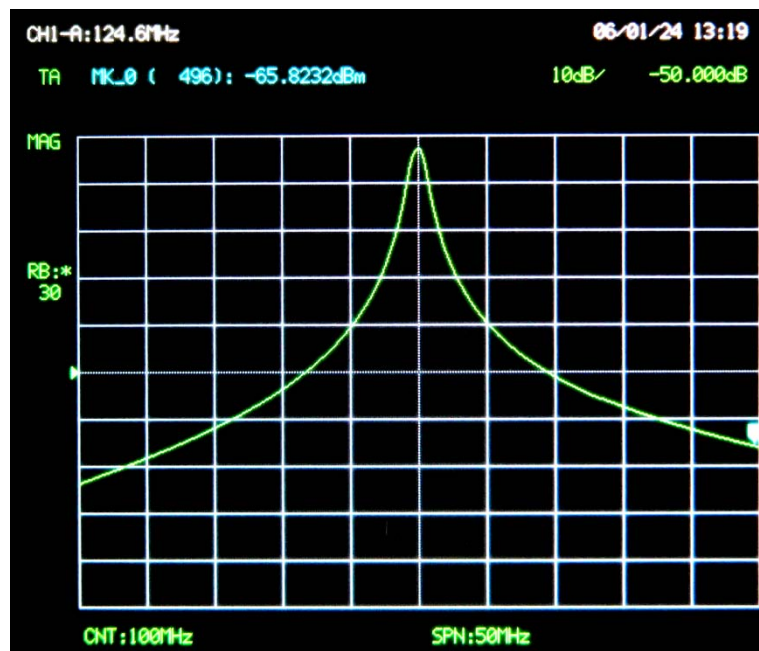


Figure 7.55. Frequency response of 101 MHz helical filter, vertical 10 dB/div.



Figure 7.56. Commercial Helical Filters. Temwell [9] Left, Toko [10] Right.

The left filter in figure 7.54 shows a 3-resonator 142 MHz helical filter with a bandwidth of 6 MHz from Temwell [9]. Each resonator is 8mm wide and 12mm high. Temwell specialise in helical filters and make commercial filters from 45 MHz to 2.6 GHz. The right filter in figure 7.54 is an older, 3-resonator, 137 MHz helical filter with a bandwidth of 2 MHz originally made by Toko [10]. The resonators are 12mm wide and 18mm high. Toko now only make dielectric filters. Temwell [9] now supply both filters in figure 7.56. The measured dimensions of these filters are the outside dimensions of the cavities. The ratio of the internal dimensions thus satisfies equation 7.17.

Interdigital Filters

With interdigital filters, the resonators are grounded at alternate ends. This reduces the coupling between the resonators and as a result, a compact filter can be constructed that has no walls between the individual resonators. A drawing of an interdigital filter is shown in figure 7.57a.

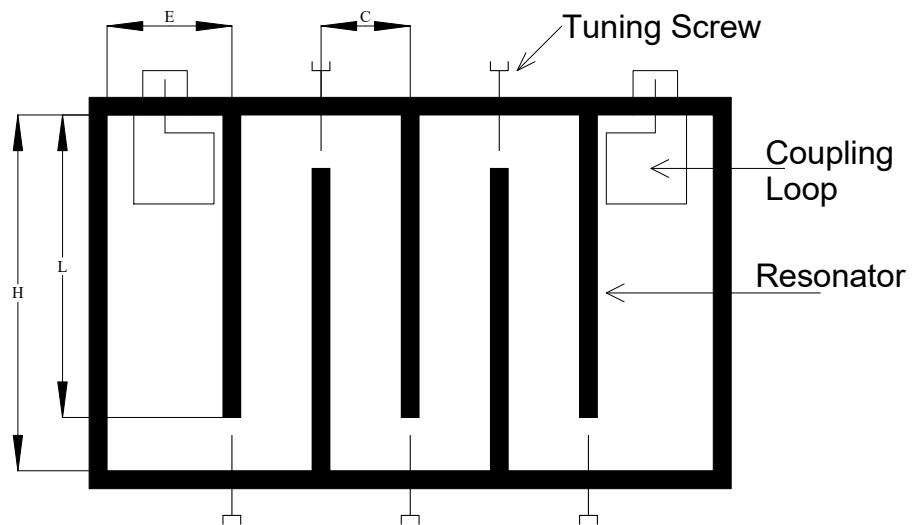


Figure 7.57a. Interdigital filter dimensions, top view.

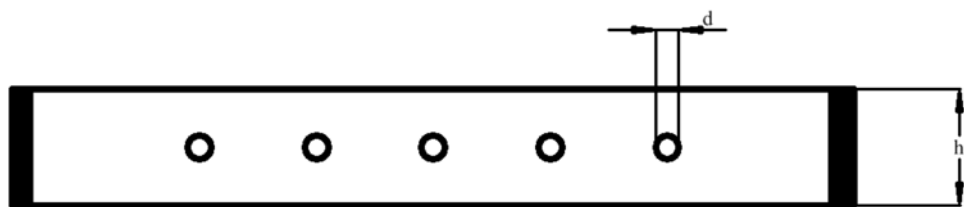


Figure 7.57b. Interdigital filter dimensions, side view.

For a small bandwidth (<10%) M. Dishal [11] provided the following equations for designing interdigital filters:

$$\frac{E}{h} = 0.6 \quad \text{Eqn. 7.25}$$

$$\text{Log}K = \left[-1.37 \frac{C}{h} + 0.91 \frac{d}{h} - 0.048 \right] \quad \text{Eqn. 7.26}$$

Where h (figure 7.57b) is the spacing between the walls and d is the rod diameter. Knowing K from the filter tables and d and h from the design specifications, allows the spacing C between the resonators to be calculated.

In addition, the impedance of the resonator is given by:

$$Z_0 = 138 \log \left[\frac{4h}{\pi d} \right] \tanh \left(\frac{\pi E}{h} \right) \quad \text{Eqn. 7.27}$$

The singly loaded Q for the input (Q_1) and output (Q_n) resonators are:

$$Q_1 = \frac{\pi R}{4Z_0} \frac{1}{\sin^2 \left(\frac{\pi \ell_1}{2L} \right)} \quad \text{Eqn. 7.28a}$$

$$Q_n = \frac{\pi R}{4Z_0} \frac{1}{\sin^2 \left(\frac{\pi \ell_n}{2L} \right)} \quad \text{Eqn. 7.28b}$$

Since Q_1 and Q_n can be obtained by de-normalising q_1 and q_n from filter tables, R is the desired termination impedance, (usually 50Ω) and Z_0 is the characteristic impedance of the resonator as obtained from equation 7.27, that the tapping points l_1 and l_n can be determined using equation 7.28.

Several companies produce commercial interdigital filters, K&L Microwave [12] is one of them. Interdigital filters have two forms:

Round Rod Interdigital Filters

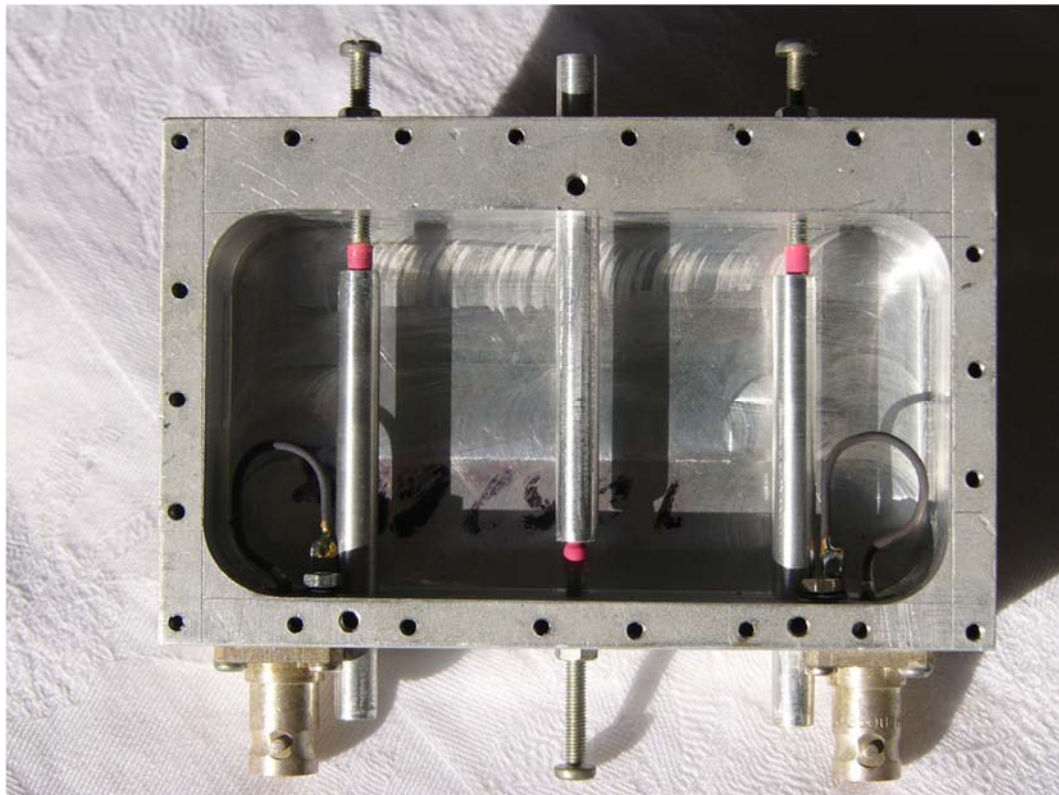


Figure 7.58. Interdigital filter for operation at 940 MHz, with top plate removed (Kikkert).

Similar to the Helical filter, the larger the filter cavity, the lower the insertion loss of the filter and the bigger the power handling capability of the filter. The Round Rod Interdigital filters are reasonably large and as a result have a low insertion loss and a high power handling capability, permitting them to be used at the output of transmitters. These filters normally have bandwidths less than 10%. The filters become very large for frequencies below 300 MHz. The coupling into the filter can be achieved by coupling loops as shown in figure 7.58, or by direct tapping to the resonator rod. In most instances the resonator rods length can be adjusted. This provides a coarse tuning adjustment. In the figure 7.58, the Allen key locking screws for the resonator rods can be seen at the base of each of the resonators allow the coarse adjustment to be performed. A small variable capacitor, in the form of an insulated screw that slides inside the hollow resonator rod, as shown in figure 7.58, result in filters that can easily be fine-tuned to the correct frequency.

The filter in figure 7.58 was designed using equations 25 to 28. Applying the coarse-tuning and fine-tuning and adjusting the coupling loops enabled a filter to be obtained, which satisfied the design specifications exactly.

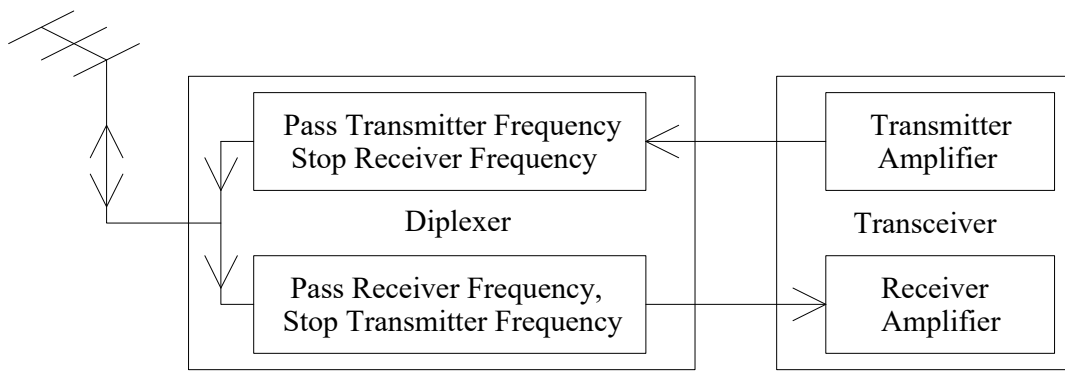


Figure 7.59. The use of a diplexer to provide full duplex operation.

Round rod interdigital filters are often used as a diplexer in mobile radio transceivers, as shown in figure 7.59. The filter connected to the receiver has a very high, typically greater than 60 dB, attenuation at the transmitter frequency. This ensures that the transmitter output, which is typically 25 W, does not damage the receiver input, which is typically designed to accurately demodulate signals of 1 nW. The use of the diplexer will thus permit full duplex operation, simultaneous transmission and reception, of the transceiver.

Mobile phones have similar diplexers. Some older phones use diplexers made using a ceramic material with a typical dielectric constant of 30, allowing a $\sqrt{30}$ reduction in each dimension of the filter as shown on the left of figure 10.2. The resulting filter will thus have 0.6% of the volume of the air-filled filter and have a fraction of the weight. More recent phones, use surface acoustic wave (SAW) or bulk acoustic wave (BAW) filters to obtain an even smaller size and weight, whilst keeping the same functionality shown in figure 7.59.

PCB Interdigital Filters

With circuit miniaturisation, and improved Microstrip simulation tools, interdigital filters are often designed using Stripline or Microstrip circuits for the resonating elements. The power handling capacity of these filters is small, so that they can only be used as filters

in receivers or low power parts of communication equipment. The design procedure is illustrated with the following example.

Example 7.3: 1 GHz, 70 MHz Bandpass Filter

Design a 5-resonator filter with a 70 MHz bandwidth centred at 1 GHz, using a RO4003 substrate for the PCB. The required k and q values can be obtained from table 1, the relevant part of which is shown in table 4. The design procedure used here is also described in [13, 14].

n	q0	I. L.	q 1	q n	k 12	k 23	k 34	k 45
5	INF.	0.000	0.6180	0.6180	1.0000	0.5559	0.5559	1.0000
	32.361	1.045	0.4001	1.5527	1.4542	0.6946	0.5285	0.6750
	32.361	1.045	0.5662	0.7261	1.0947	0.5636	0.5800	0.8106
	16.180	2.263	0.3990	1.8372	1.4414	0.6886	0.5200	0.6874
	16.180	2.263	0.5777	0.7577	1.0711	0.5408	0.6160	0.7452
	10.787	3.657	0.4036	2.0825	1.4088	0.6750	0.5080	0.7066
	10.787	3.657	0.5927	0.7869	1.0408	0.5144	0.6520	0.6860
	8.090	5.265	0.4111	2.3118	1.3670	0.6576	0.4927	0.7290
	8.090	5.265	0.6100	0.8157	1.0075	0.4844	0.6887	0.6278

Table 4. Butterworth response, K and Q value filter table, from Zverev [1], pp 341.

Notice that the k and q values vary depending on the losses. One could guess the losses to be about 2 dB and use the corresponding k and q values. Note that for each value of insertion loss, there are two sets of k and q values. Since the tap coupling is normally used and the tapping points only cover a limited range, it is desirable to select the table values where the difference between the q values is small.

Alternately, the design is done assuming no losses, so that equations 4 and 5 can be used. After the design is completed, any variations in k and q values required to accommodate the losses can be achieved by optimisation. That process is implemented here. The lossless q values are thus $q_1 = q_n = 0.6180$, resulting in $Q_1 = Q_n = 0.6180*1e9/70e6 = 8.828$.

The bandwidth, without loading due to adjacent resonators is given by equation 9.4.1 in Zverev [1] for the first and last resonator respectively as:

$$\text{Resonator 1 } \Delta_{3dB} = \frac{\text{FilterBW}_{3dB}}{q_1} \quad \text{Eqn. 7.29a}$$

$$\text{Resonator } n \Delta_{3dB} = \frac{\text{FilterBW}_{3dB}}{q_n} \quad \text{Eqn. 7.29b}$$

In our design the filter BW_{3dB} is 70 MHz, Δ_{3dB} is thus $70/0.618$ MHz = 113.2 MHz. For this filter, $q_1 = q_n$ and the input and output tapping points are the same.

The tapping point can be determined using NI AWR DE and the two-resonator circuit of figure 7.60. To prevent the second resonator from influencing the tuning of the tapping point, a very large coupling gap is used and the resonance of the coupled resonator is placed far away from the centre frequency by disabling all the possible elements as shown

in figure 7.60. To measure the voltage of the input resonator, a high impedance ($1 \text{ M}\Omega$) port (port 2) is connected to the resonator. The signal at port 2 is then the voltage at the top of resonator and has the correct frequency response for determining the loading of the resonator, as shown in the graph of figure 7.60. After tuning the tapping point for the correct bandwidth, the correct q_1 and q_n for the filter has been determined.

The tapping point in the circuit of figure 7.60 of 3.125 mm (+5 mm for TL7) results in the required 113.2 MHz bandwidth. The total resonator length of $L_{tot} = 46.46$ mm places the maximum response of the loaded resonator at 1 GHz.

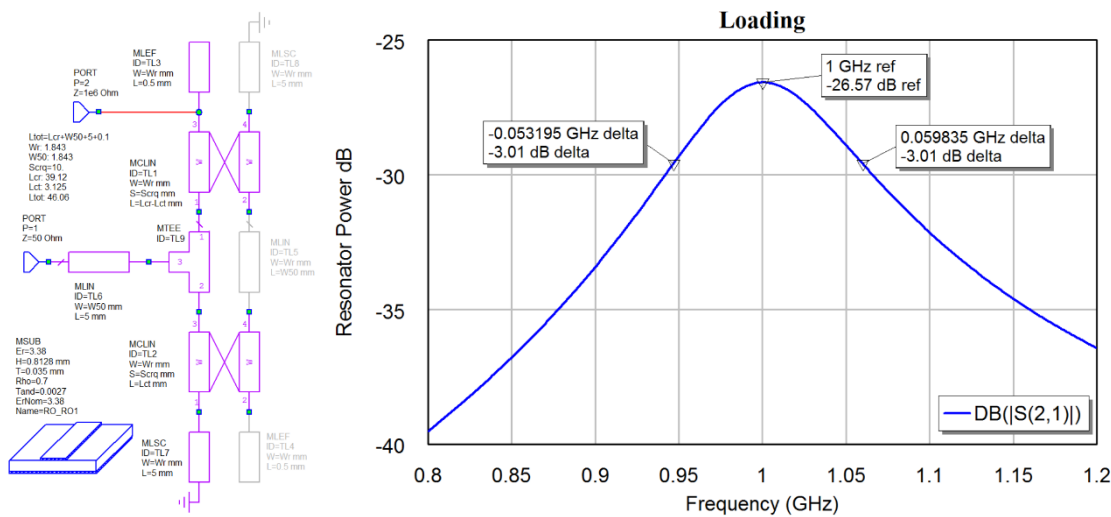


Figure 7.60. Left: circuit for input tap determination, right: frequency response.

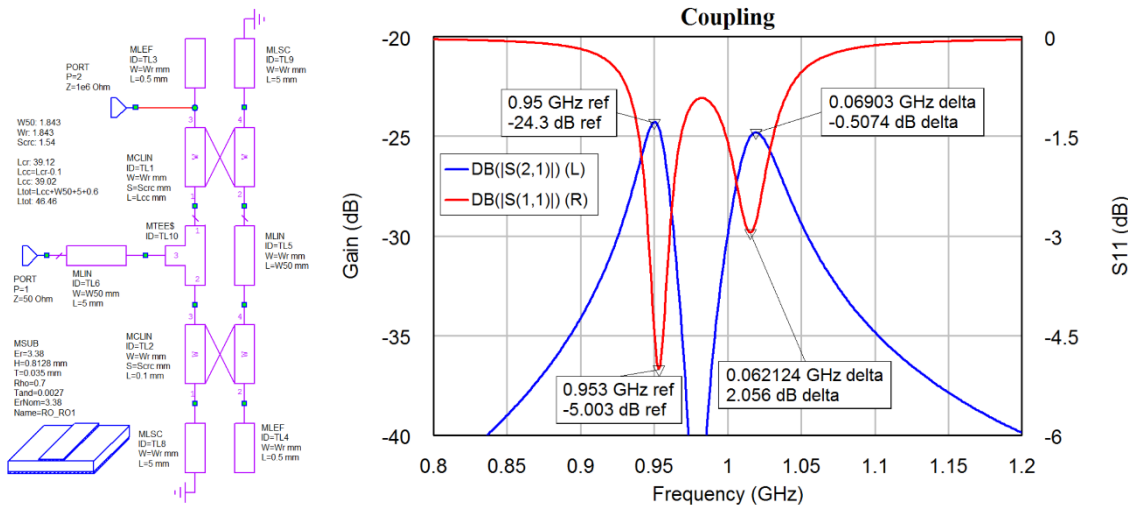


Figure 7.61. Left: circuit for coupling determination, right: frequency response.

The coupling gap is tuned to obtain the correct coupling between resonators. To reduce the effect of loading, the tapping length Lct is made as small as possible, while keeping the total resonator length the same as before, resulting in the test circuit shown in figure 7.61. When the second resonator is tuned and brought close to the first resonator, a double peak response will result as shown in figure 7.61. The frequency difference between the peaks is given by equation 9.4.3 in Zverev [1] as:

$$\Delta_{fp} = k_{12} BW_{3dB} \quad \text{Eqn. 7.30}$$

For this filter $k_{12} = 1$, so that $\Delta_{fp} = 70$ MHz for the peaks in frequency response of the test circuit, coupling between the first and second resonator as shown in figure 7.61. This corresponds to a coupling gap of 1.54 mm. The same test circuit is used to determine the coupling gaps for the other resonators. For the coupling between the second and the third resonator $\Delta_{fp} = 0.5559 * 70$ MHz = 38.9 MHz. The coupling gap is re-tuned to obtain a difference of 38.9 MHz between the peaks. This corresponds to a coupling gap of 2.5 mm. This procedure is then repeated for all the remaining coupling gaps for the filter using the respective coupling coefficients from tables or equations 4 and 5.

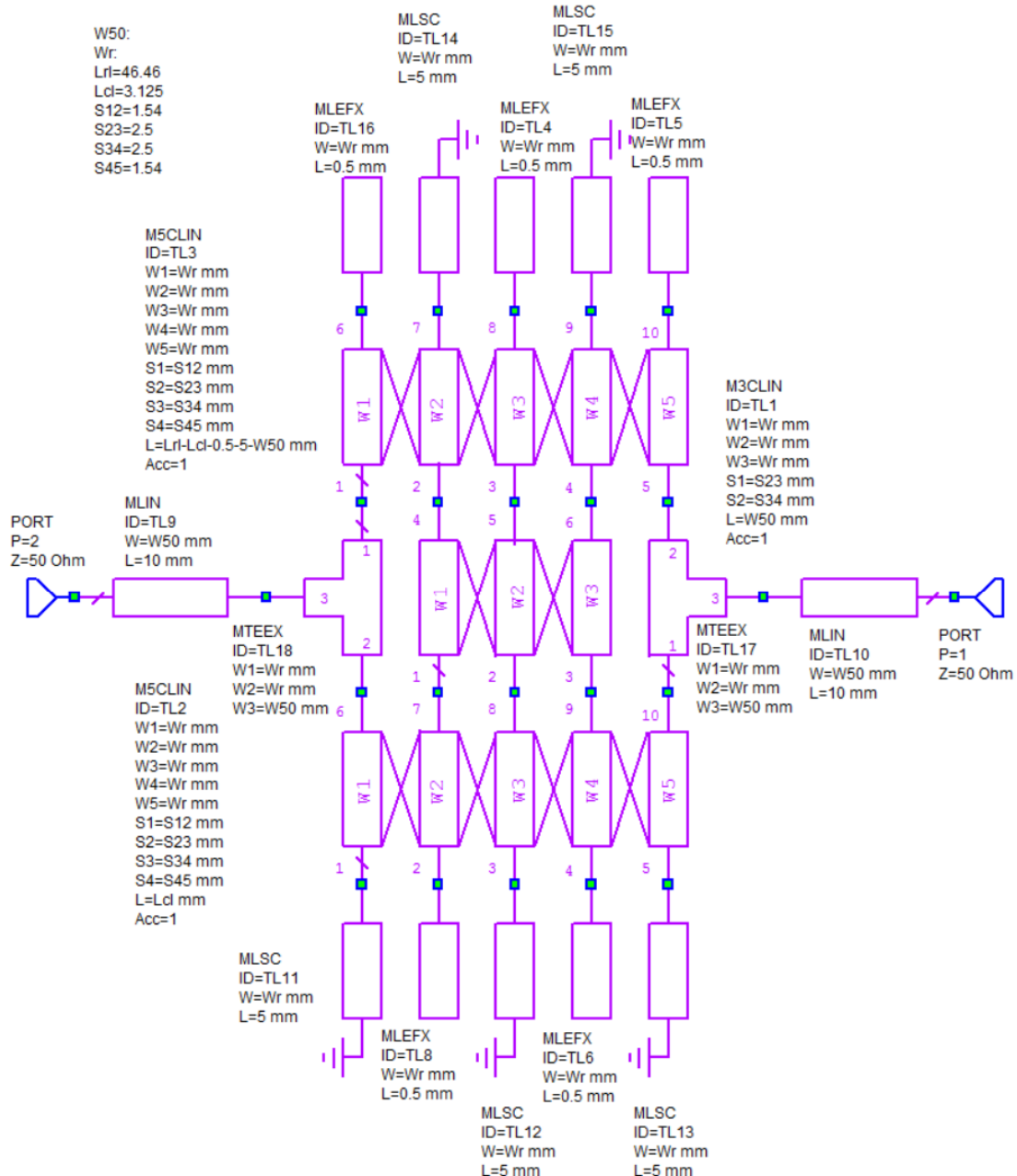


Figure 7.62. Circuit for the interdigital filter using calculated loading and coupling values.

Simulating this circuit of figure 7.62 gives a filter with a response close to the desired value, as shown in figure 7.63. To obtain the precise desired specification, the filter needs to be optimised. For a lossless Butterworth filter, the coupling gaps are symmetrical. However, for lossy filters or different filter types, asymmetrical coupling gaps result. For a practical Butterworth Bandpass filter, the design procedure can assume a lossless filter.

Subsequent optimisation for the desired filter performance, accommodates the losses by; allowing changes in resonator lengths, coupling points and coupling gaps. Note that after optimisation, the resonators in this design are not of equal length and the filter is no longer symmetrical from the input and output. This asymmetry is expected from k and q filter table for the 1.5 dB insertion loss that this filter has, as shown in table 4 of this chapter.

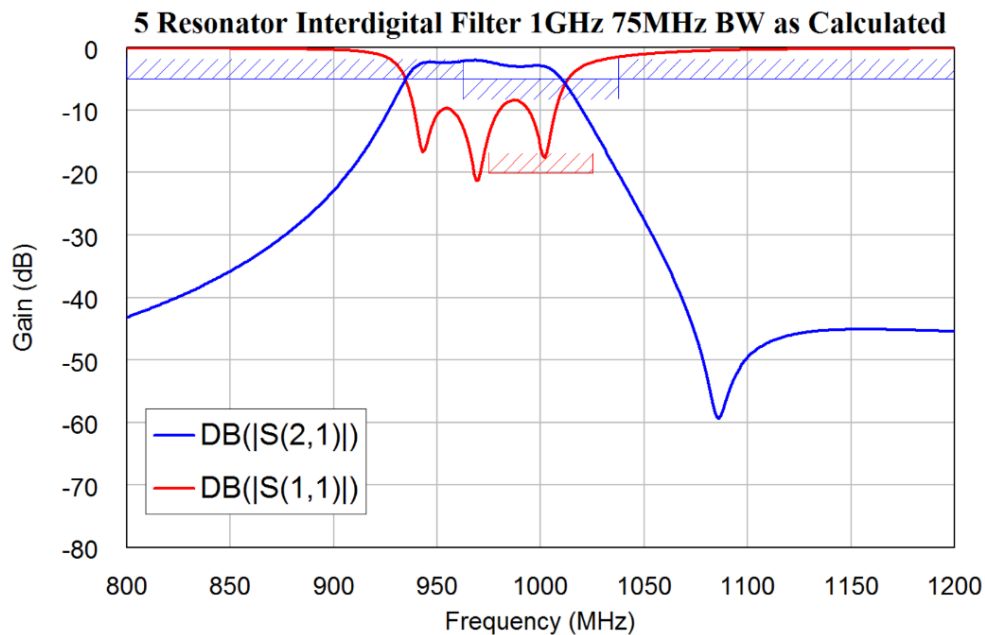


Figure 7.63. Frequency response of the filter of figure 7.62, as calculated.

The filter of figures 7.62 and 63 was optimised to give a 70 MHz bandwidth at a 1 GHz centre frequency, as shown in figure 7.64.

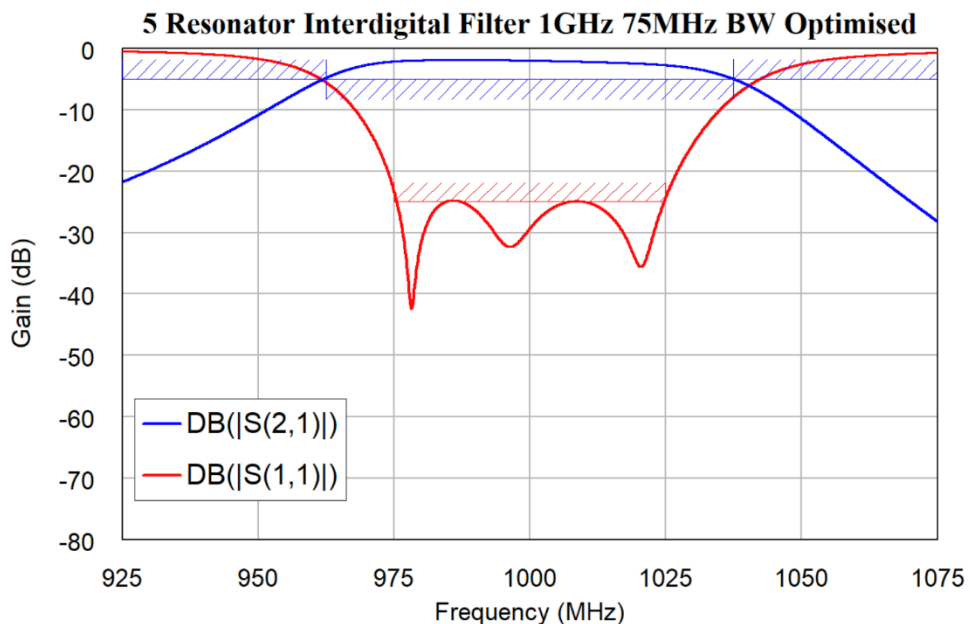


Figure 7.64. Frequency response of the filter of figure 7.62, after optimisation.

When the prototype filter was produced, it was found to be 20 MHz (2%) low in centre frequency, have a passband amplitude response that is slightly sloping and a bandwidth that was too small. To compensate the centre frequency of the designed filter, was shifted

to 1.02 GHz and the bandwidth was increased. By optimising for a low return loss in the passband one can ensure that the insertion loss is minimised. The passband attenuation slope is thus due to the changing transmission line losses of the resonators with frequency. It is possible to specify a sloping passband attenuation to compensate for this, but this will result in a higher insertion loss and a worse return loss. The measured performance of the second filter is shown in blue in figure 7.65 and it has a centre frequency of 984 MHz compared to the 1 GHz specification. The measured bandwidth is 92 MHz compared to the 70 MHz specification. This may be sufficiently close to satisfy the required specifications. If this is inadequate, then another filter needs to be designed.

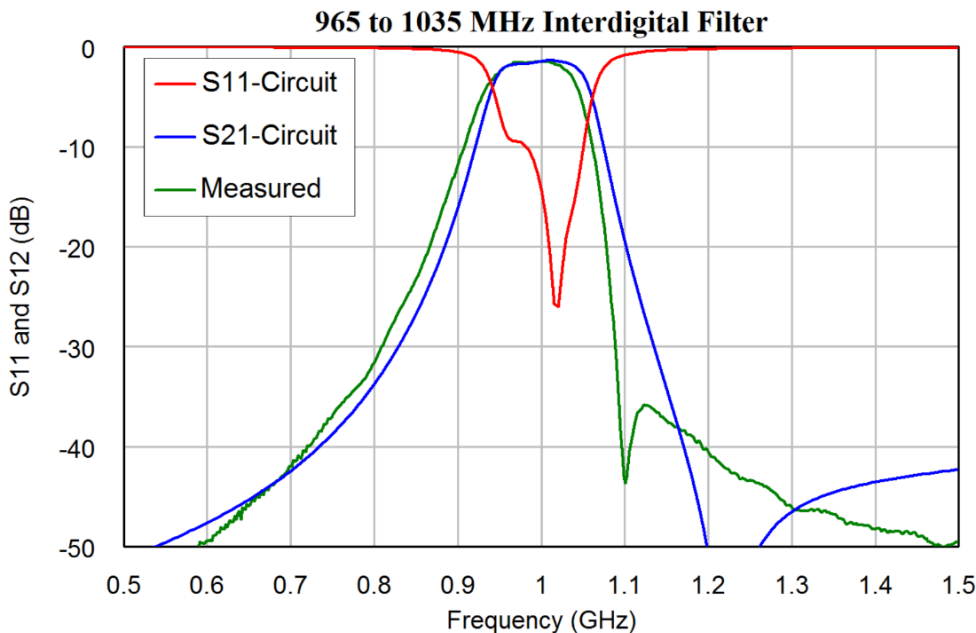


Figure 7.65. Measured and designed frequency response of the interdigital filter.

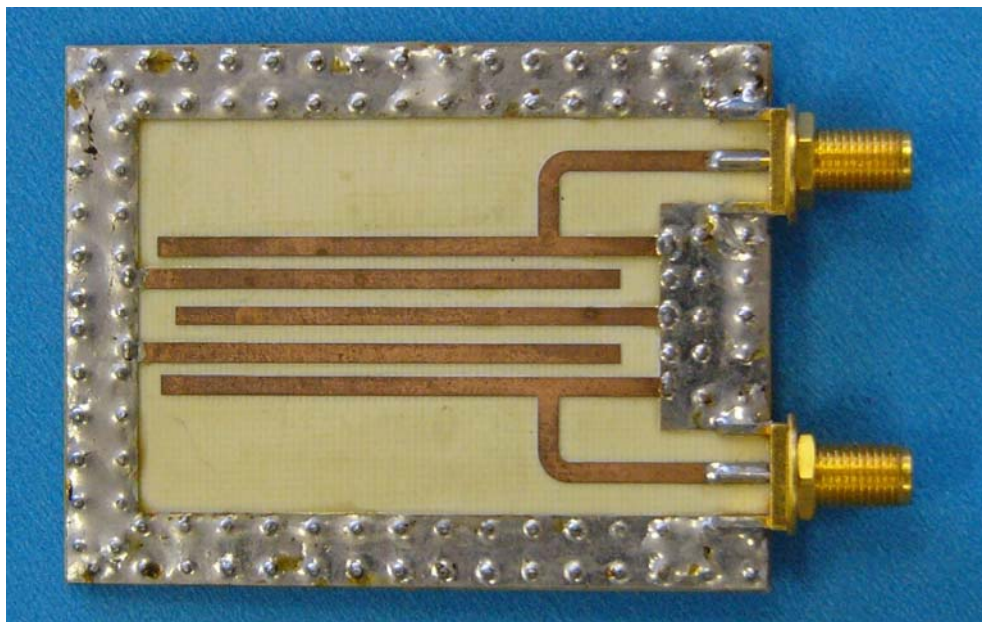


Figure 7.66. Microstrip interdigital filter, 70 MHz bandwidth at 1 GHz.

Figure 7.66 shows the resulting filter realisation. For this realisation, bends are incorporated in the input and output transmission lines, so that the input and output

connectors can be mounted on the same panel. Interdigital filters are often used in commercial designs as can be seen in figure 7.67, which is part of a microwave layout produced by Codan in Adelaide, South Australia. Comparing figures 7.66 and 7.67, shows that the procedure for earthing the grounded end of the resonator to the bottom layer ground-plane is slightly different. The positioning of the vias in figure 7.66 is the most likely cause of the centre frequency being 2% low.

As the number of resonators increases, the stopband attenuation does not significantly increase. As a result, hairpin or direct-coupled filters are a better choice when a very high close-in stopband attenuation is required. Interdigital filters are however smaller than hairpin or direct-coupled filters and they are thus the best filter to use when PCB space is at a premium.

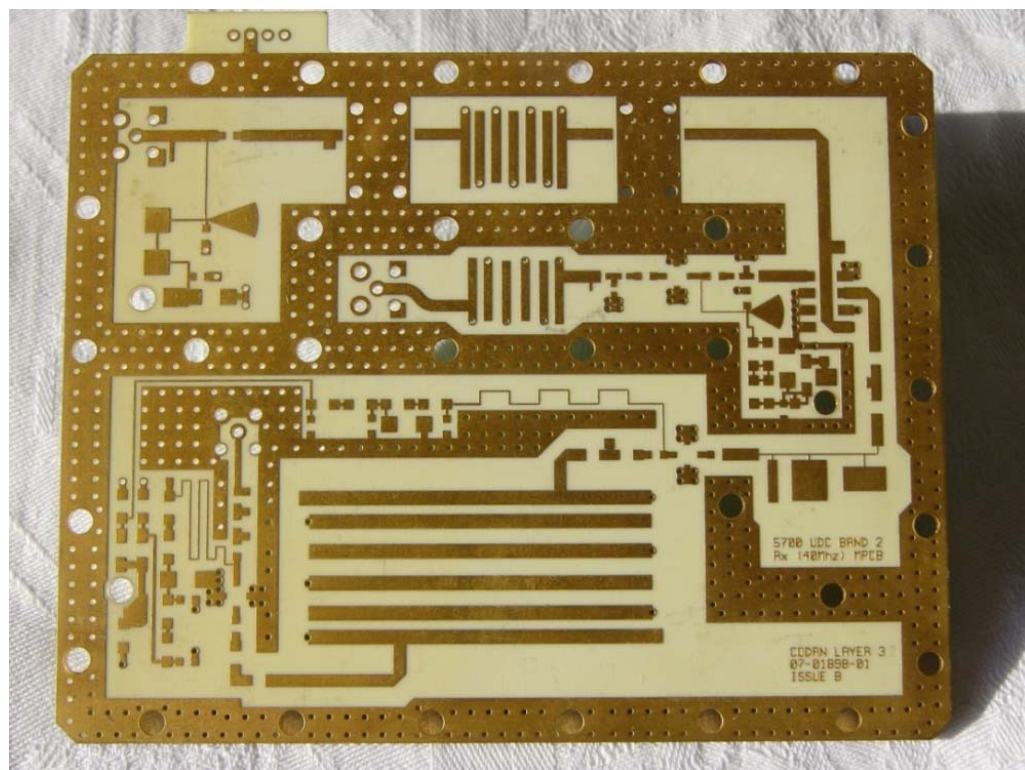


Figure 7.67. PCB showing three interdigital filters. (Codan [15]).

Direct-Coupled Resonator Filters

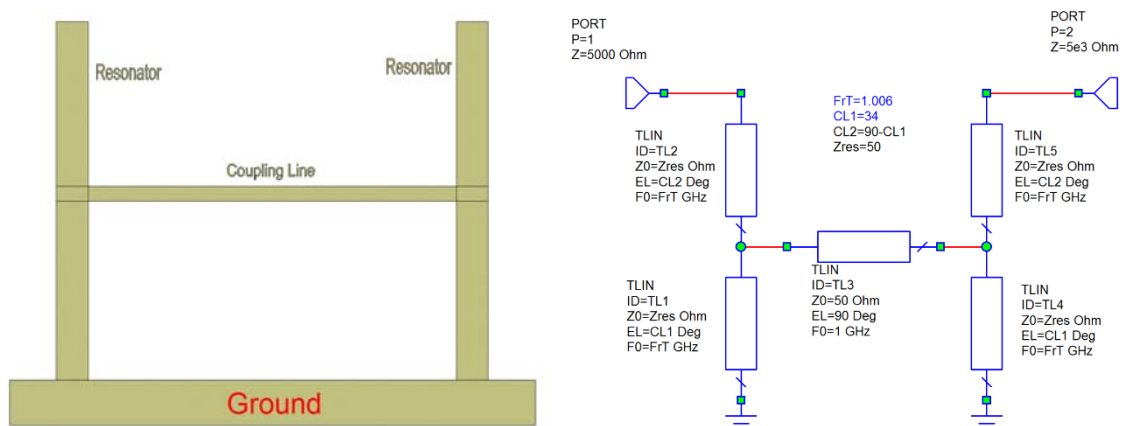


Figure 7.68. Transmission line coupled resonators.

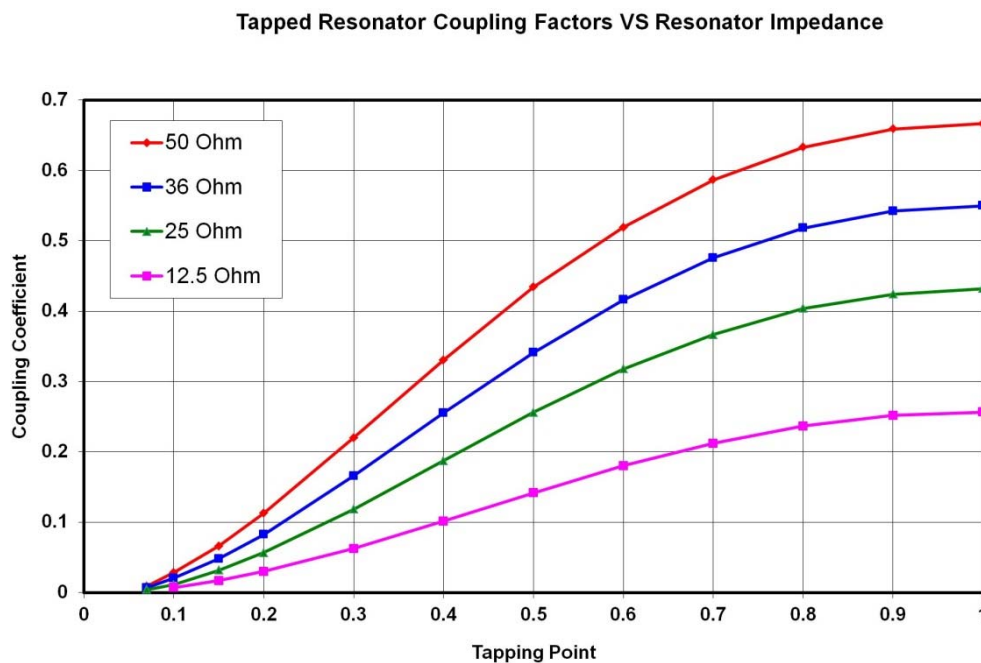


Figure 7.69. Coupling coefficient versus tapping point for different line impedances.

This design technique is also described by the author in [13]. When the percentage bandwidth of the filter becomes greater than 20%, the coupling gaps for interdigital filters become too small to be produced using readily available technology. As a result, a different coupling technique is required. It is possible to couple two resonators using a quarter-wavelength long transmission line as shown in figure 7.70. The coupling can be varied by changing the tapping point. When this is done, graphs similar to figure 7.61 are produced by the circuit of figure 7.68 and from equation 7.30 the coupling coefficient can be determined as a function of tapping point as shown in figure 7.69, since the spacing between the peaks and the bandwidth are known.

Example 7.4: 1 GHz, 500 MHz Bandwidth Filter

The coupling coefficients shown in figure 7.69 can now be applied to the design of a wideband filter. As an example, the design of a 5-resonator Butterworth bandpass filter with a lower 3 dB cut-off frequency of 750 MHz and an upper cut off frequency of 1250 MHz is chosen the filter will thus have a 50% bandwidth.

Equations 4 and 5 give the normalized Q values and coupling coefficients as:

$$\begin{aligned} \text{Normalised} \\ q_1 = q_n &= 0.618 \\ k_{12} = k_{45} &= 1 \\ k_{23} = k_{34} &= 0.5559 \end{aligned}$$

$$\begin{aligned} \text{De-normalised for 50\% Bandwidth} \\ Q_1 = Q_n &= 1.236 \\ K_{12} = K_{45} &= 0.5 \\ K_{23} = K_{34} &= 0.278 \end{aligned}$$

Figure 7.69 shows that different transmission line impedances should be used for different coupling coefficients in order to obtain realistic tapping points. For the filter, 50 Ω transmission lines are used for the input and output resonators, which require the highest coupling coefficients of 0.5. For the other resonators, 36 Ω transmission lines, which have lower losses, are used. Interpolating the tapping points from figure 7.69, results in the following normalized tapping points, TXLine results in the following resonator line lengths:

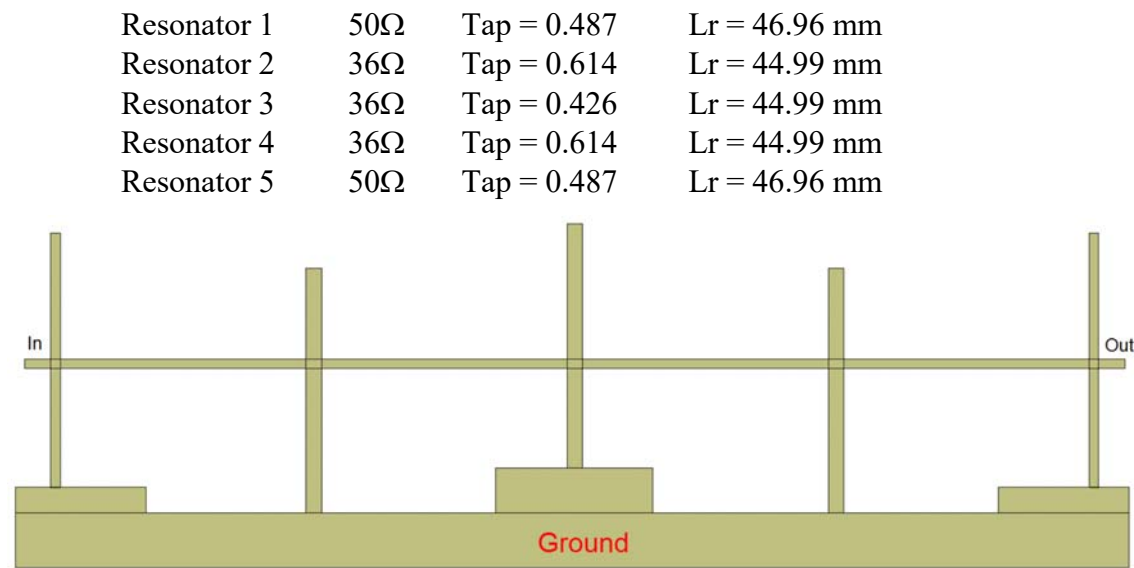


Figure 7.70. Filter layout for initial tap values.

Entering those values in the NI AWR DE circuit schematic of the filter, results in the initial filter layout shown in figure 7.70, with the corresponding frequency response shown in figure 7.71. To highlight differences between the 750 MHz and 1250 MHz, corner frequency specifications and frequency-response obtained from the computer simulation, an optimisation mask is superimposed on figure 7.71. In addition, an optimisation mask for a -1 dB attenuation from 780 MHz to 1220 MHz is shown. It can be seen that the design procedure results in a filter that has a bandwidth that closely matches the design specifications, but whose centre frequency is 3.5% low. This difference is due to the end effect of the open circuit resonators not being taken into account in the above calculations.

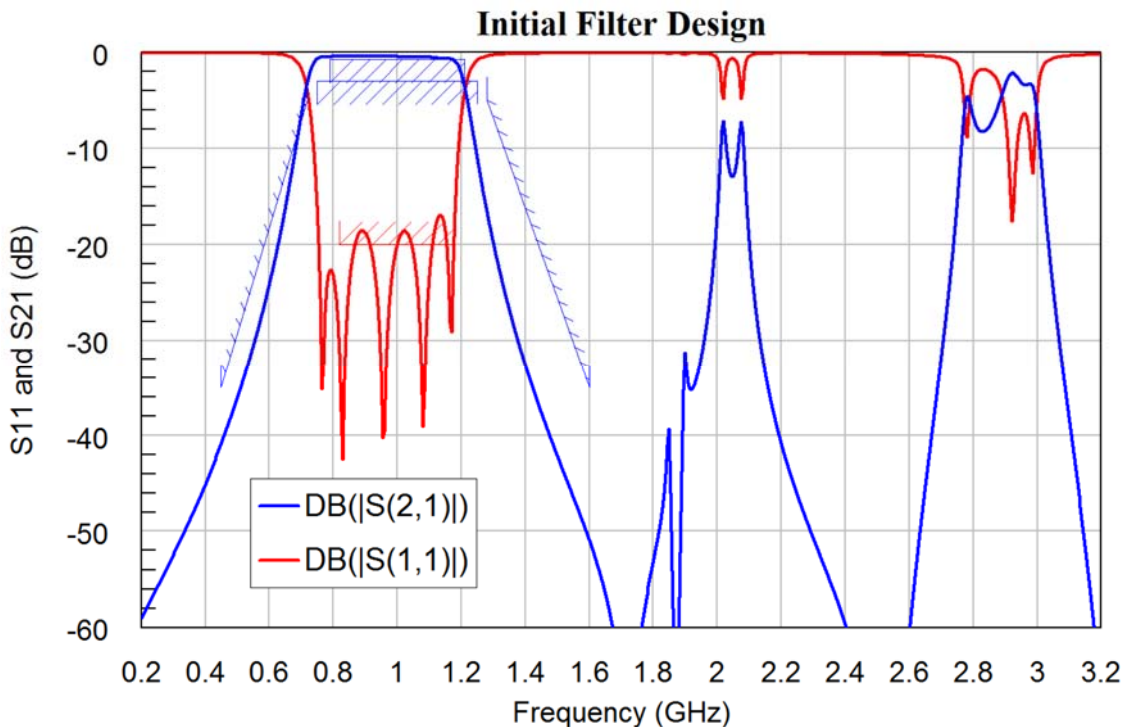


Figure 7.71. Frequency response for initial wideband filter.

Fine Tuning the Filter

To shift the centre frequency, the length of all the resonators is changed slightly using the ‘tuning simulation’ capability of NI AWR DE. In addition, it is desirable to fine-tune the filter to obtain the lowest insertion loss. This is best achieved by ensuring that the filter has a low return loss. Setting the optimiser constraints on S_{11} to be less than -20 dB and carrying out the first stage of the optimisation process of the filter to meet this return loss as well as the passband specifications results in the following tapping points:

Resonator 1	50Ω	Tap = 0.5147
Resonator 2	36Ω	Tap = 0.5969
Resonator 3	36Ω	Tap = 0.4304
Resonator 4	36Ω	Tap = 0.5969
Resonator 5	50Ω	Tap = 0.5147

Figure 7.72 shows the resulting frequency response of the filter after this first stage of optimisation. For a wideband filter implementation like this, the spurious response at the harmonics, particularly that at 2 GHz is unacceptable. To provide better attenuation at those frequencies, stubs need to be added to the filter. Those stubs will distort the frequency response of the filter. In order to minimise the effect of the stubs on the centre frequency of the filter, it is desirable to use two sets of stubs and vary the spacing between the two sets of stubs to provide a low return loss at the centre frequency of the filter. In addition, it is desirable to make the harmonic stubs slightly different lengths, to widen the bandwidth over which good harmonic attenuation is obtained.

In addition, some change in the harmonic response is obtained by changing the length of the coupling lines. Comparing figures 7.71 and 72, for a filter with a quarter wavelength coupling line, with that of figures 7.82 and 85, for a filter with a one-eighth wavelength transmission line for the coupling illustrates this effect.

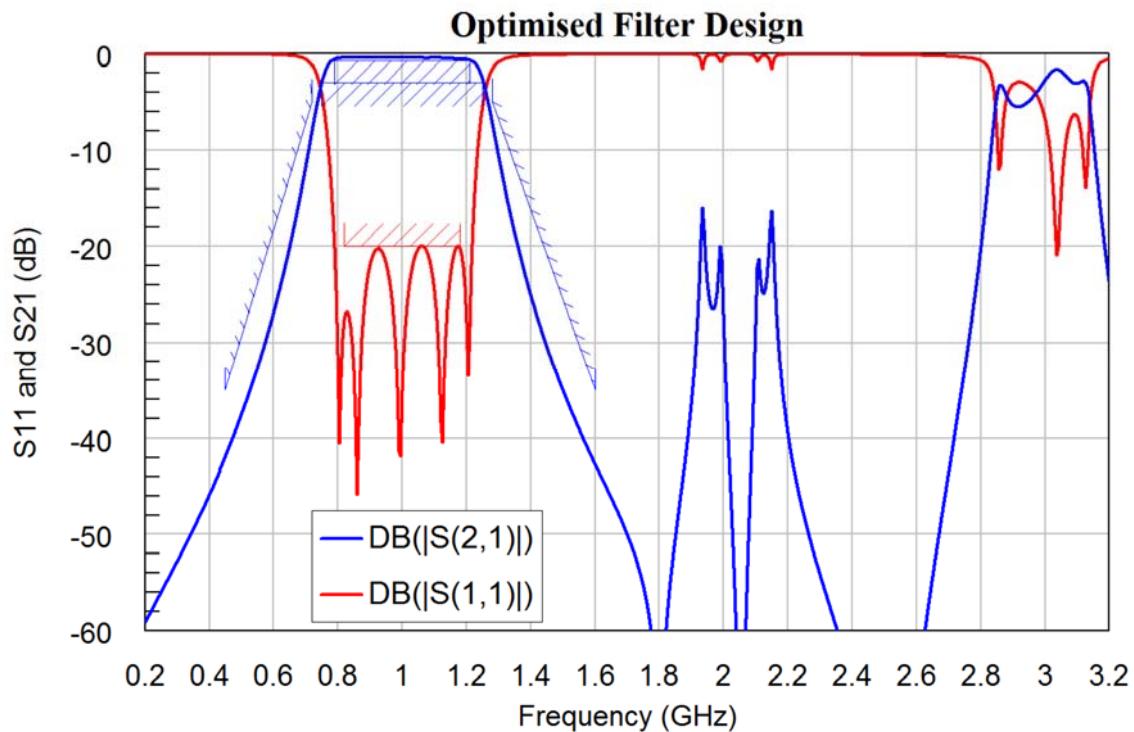


Figure 7.72. Frequency response of the filter after stage 1 optimisation.

The final step in the filter design is to change the layout from a simple design as shown in figure 7.70, to a more compact and easier to manufacture design. To achieve this, the three tiered ground level shown in figure 7.70 is made one level and the coupling transmission lines are folded and bent in order to take up as little space as possible, while connecting to the resonators at the correct tapping points. The harmonic stubs may be folded, as shown in figures 7.46 and 47. The final layout should also ensure that the input and output connectors are in the correct location for mounting the filter. Figure 7.73 is a photograph of the final filter.

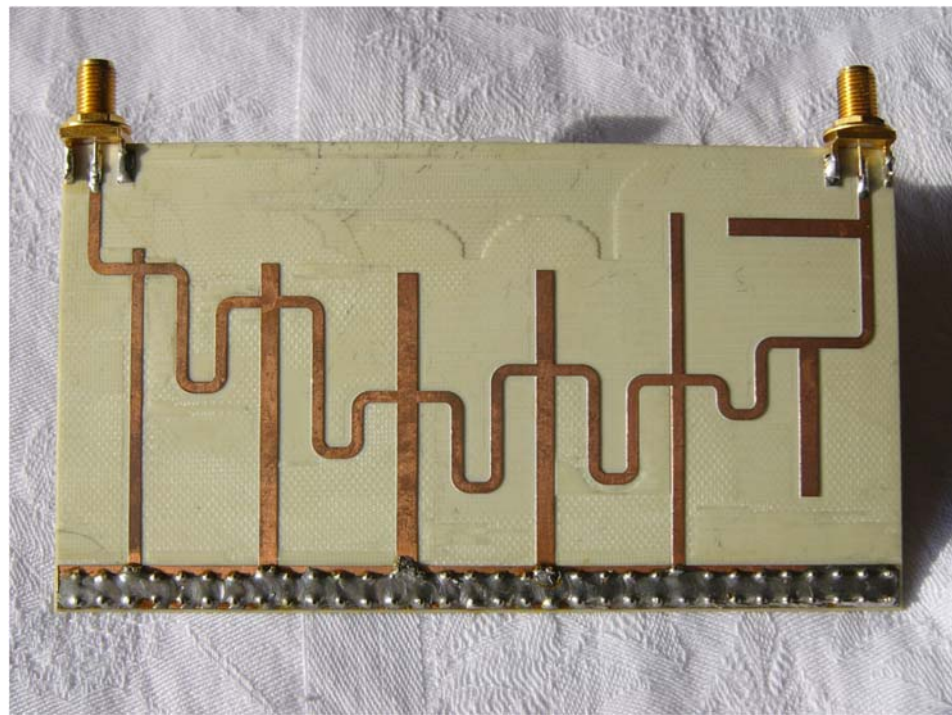


Figure 7.73. 750 MHz to 1250 MHz filter hardware.

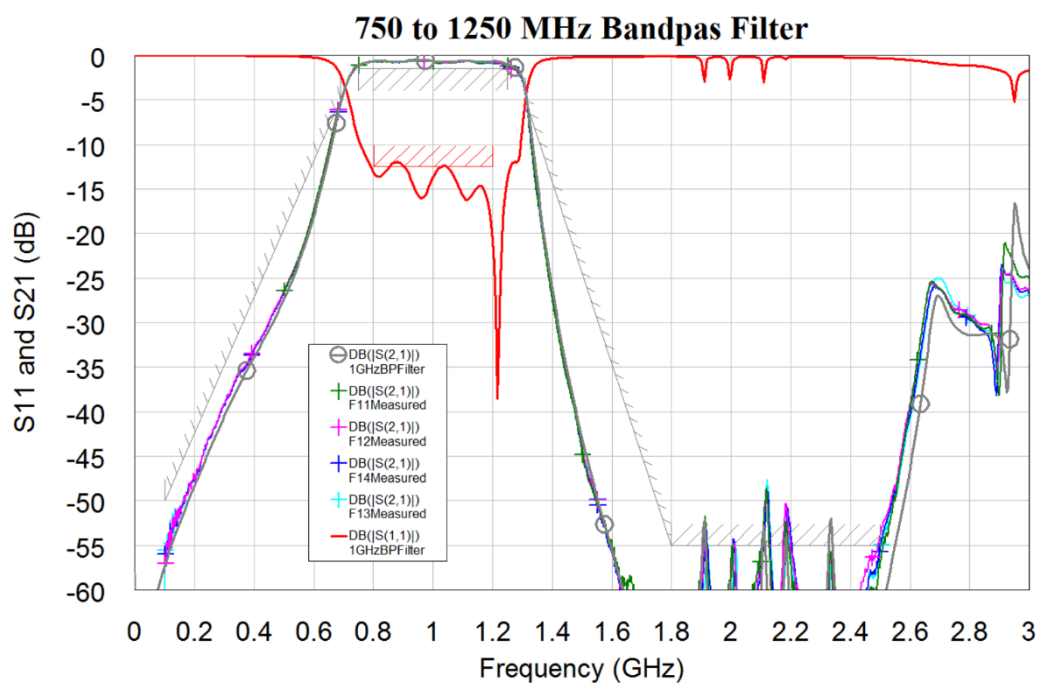


Figure 7.74. Frequency response of the filter of figure 7.73.

Figure 7.74 shows the frequency response of the final filter after optimisation, it also shows the final optimisation limits used. To determine the reliability of the design technique, four filters were constructed. The measured frequency response of those filters is also shown in figure 7.74. It can be seen that the design technique results in highly repeatable filters, whose measured performance agrees remarkably with the results from computer simulation. The agreement between the measured and simulated results for these filters is much better than those for the hairpin filter of figure 7.46, or the interdigital filter of figure 7.65 and 7.66. It should be noted that the right most resonator is significantly larger than the other resonators. This is required to compensate for the effects of the harmonic stubs on the passband response.

Microstrip Filter Comparison

When designing a Microstrip Bandpass filter, it can be designed as: an interdigital filter, a Comline Filter, a hairpin filter or a direct-coupled resonator filter [14]. Each of these filters have advantages and disadvantages. To highlight the comparative performance of these filters, a 5-resonator filter with a centre frequency of 1 GHz and a 70 MHz bandwidth was designed as using each of these four filter types. The filters were optimised using the same optimisation limits. Each filter has 10 mm tracks connecting to the tapping point to allow a connector to be soldered to that track. The same RO4003 substrate was used and all resonators are 3 mm wide. For each of the filter types, a simple test circuit like those shown in figures 7.60, 7.61 or 7.68 is used. The tapping and coupling test circuit for the Comline filter, is shown in figure 7.75 and that for the hairpin filter is shown in figure 7.76.

The input tapping for all these four circuits is adjusted to obtain frequency responses like figures 58 and 59, but with the bandwidths as per equations 29 and 30 for the relevant filter. Since the centre frequency, bandwidth and the number of resonators for these filters is the same as those of figures 58 and 59, exactly the same responses should be obtained. The coupling tuning, can be done most accurately when the end resonator loading is reduced as done in figures 7.75 and 7.76.

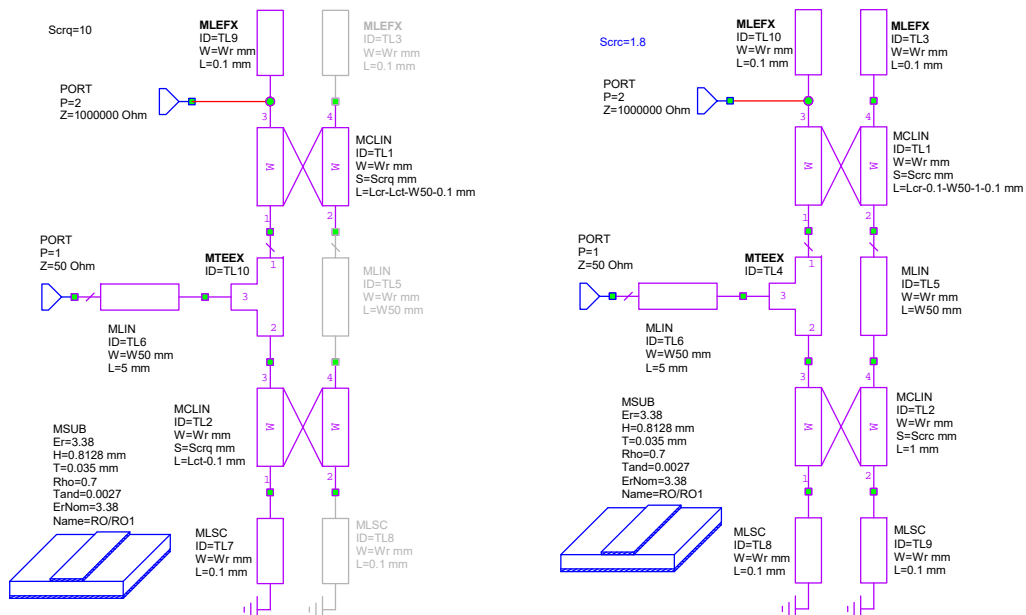


Figure 7.75. Resonator loading and coupling test circuit for Comline filters.

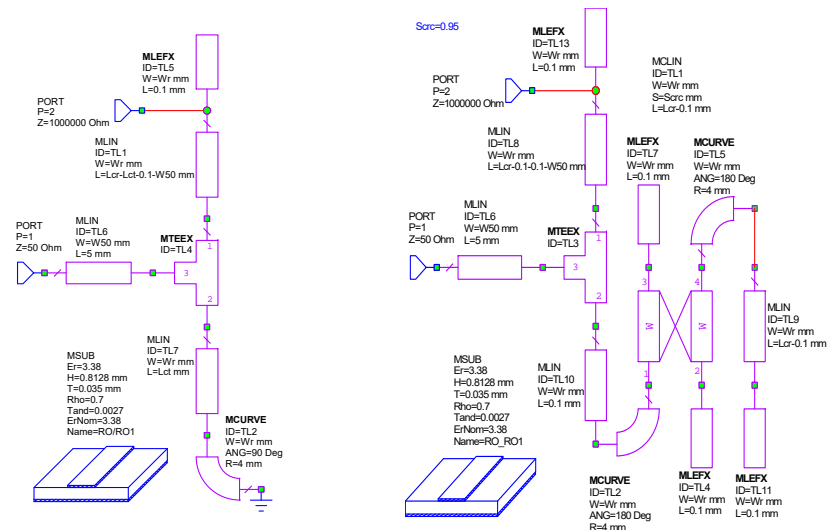


Figure 7.76. Resonator loading and coupling test circuit for hairpin filters.

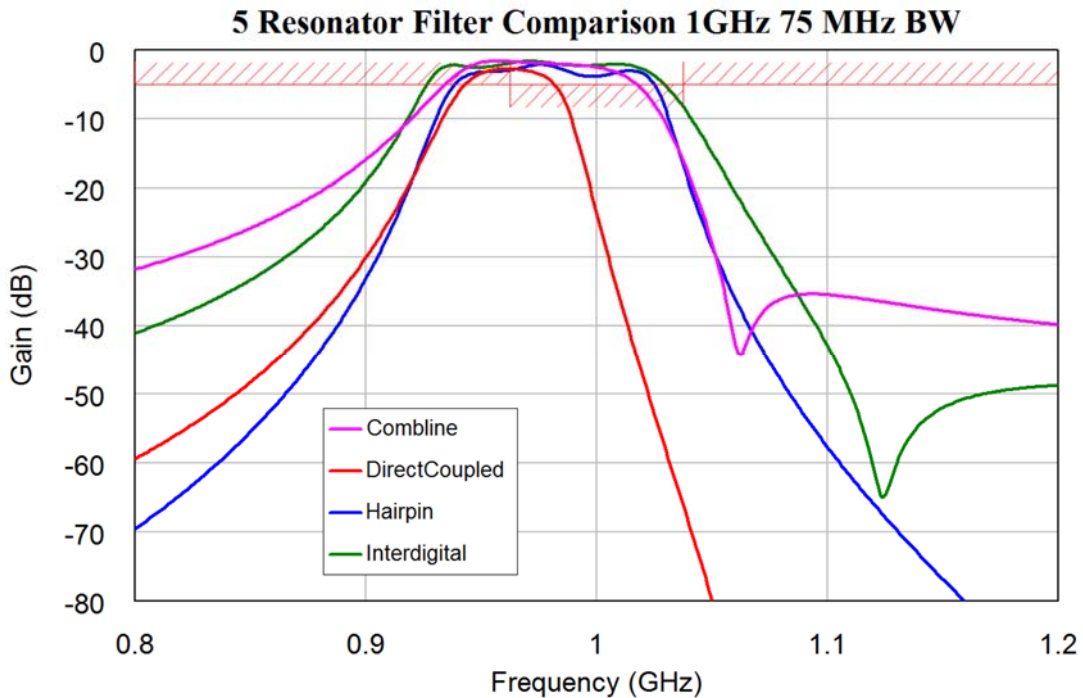


Figure 7.77. Filter performance with parameters as calculated.

Figure 7.77 shows the initial frequency response of the four 5-resonator filters, when the tapping and coupling gaps are set to those calculated using the test circuits.

The performance of all these filters is close enough that the specifications can be met using some simple optimisation. The tuning and optimisation is best done in three stages: Firstly adjust the resonator length using manual tuning, to give the correct centre frequency. The second step is to fine-tune the coupling gaps and tapping points using optimisation, to get as close to the requirements as possible. The final step is to allow the individual resonator lengths to be optimised as well as further minor optimisation of the coupling gaps and resonators. Since there is a significant interaction between the parameters to be optimised, the local random optimisation is most likely to result in the best optimisation. If the optimisation gets stuck, changing the weight of the worst error may get the optimisation out of the local minima and thus result in lower error costs.

Figure 7.78 shows the final performance of the filters after optimisation. The hairpin filter has a good symmetrical filter response and has good stopband attenuation. The direct-coupled resonator filter has a better higher frequency attenuation, but a poorer lower frequency attenuation. The interdigital filter has a poorer attenuation characteristic, compared with the other filters. In particular, the attenuation near 1 GHz is only 50 dB. The Combline filter has the worst close-in stopband attenuation of these filters. Combline filters are used less often than interdigital filters.

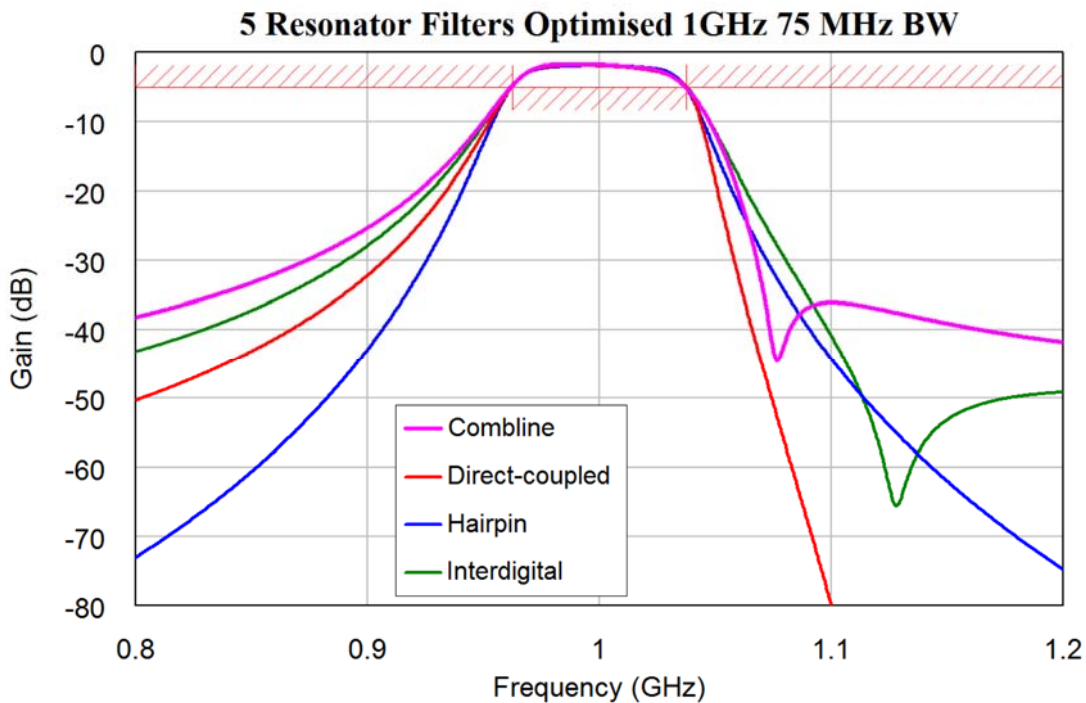


Figure 7.78. Frequency response of three 5-resonator filters.

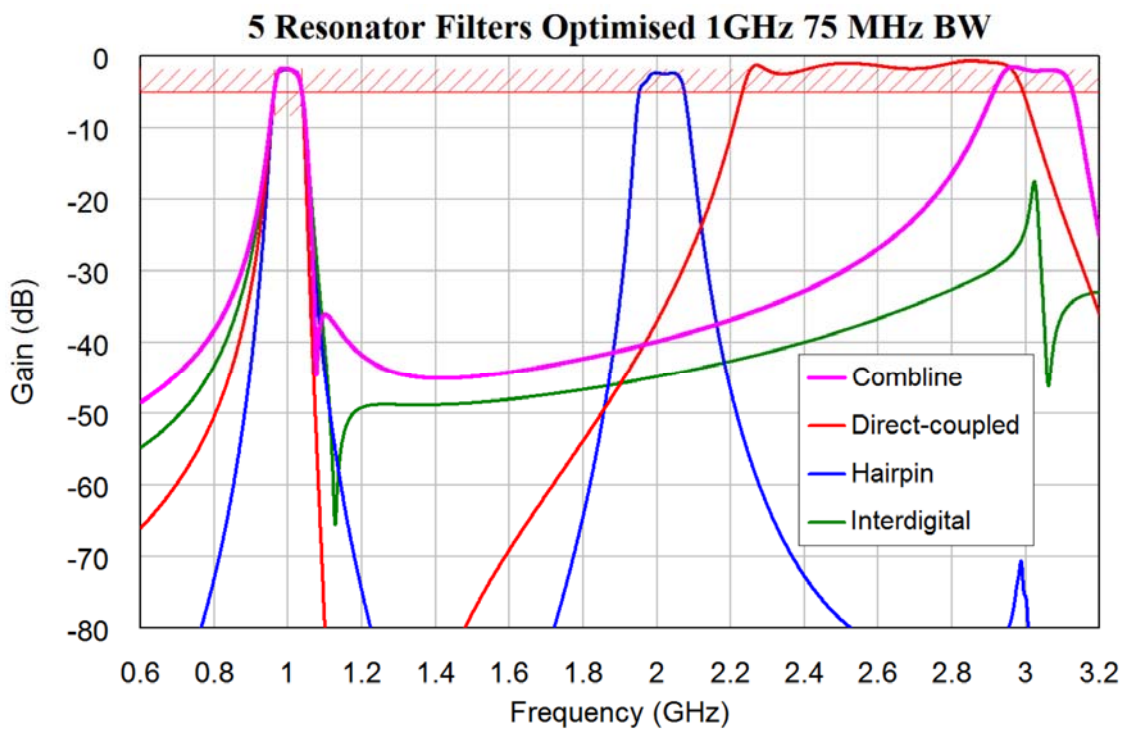


Figure 7.79. Harmonic response of the filters of figure 7.73.

Figure 7.79 shows the frequency response of the four filters at the harmonics of the 1 GHz passband. For the direct-coupled resonator filter the lengths of the coupling lines was 12.5% of a wavelength, which is half of the length of the coupling lines used for the filter in figure 7.73. This resulted in a lower harmonic attenuation. The direct-coupled filter has the best close-in stopband attenuation, but the worst stopband attenuation above 2 times the centre frequency. The second harmonic response from the hairpin filter is significant, but can be removed using harmonic stubs. The interdigital filter does not have a significant harmonic response, but it does not have a very good stopband attenuation either. The stopband attenuation for interdigital filters does not significantly improve with filter order. The Comline filter is the smallest, occupying 41 x 60 mm. The interdigital filter is slightly larger occupying 42 x 60 mm. The direct-coupled resonator filter, occupies 75 x 60 mm and the hairpin filter is the largest, occupying 78 x 68 mm.

Figures 7.80 to 7.81 show the hardware of the four filters, approximately to the same scale. The Comline filter is slightly smaller than the interdigital filter, but in most instances, there is not enough space saving to warrant the worse stopband attenuation.



Figure 7.80. Interdigital filter hardware.

(42x60mm)

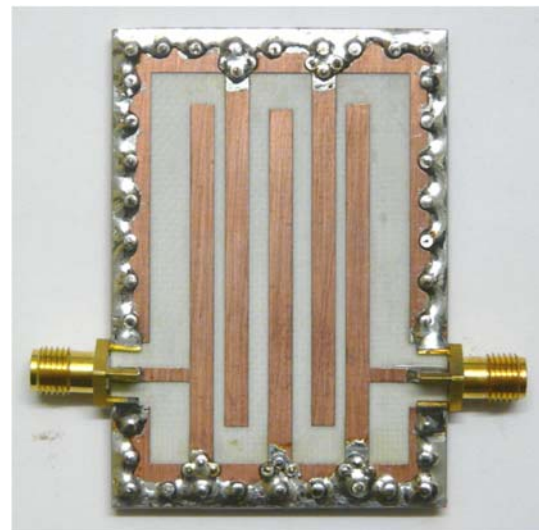


Figure 7.81. Comline filter hardware.

(41x60mm)

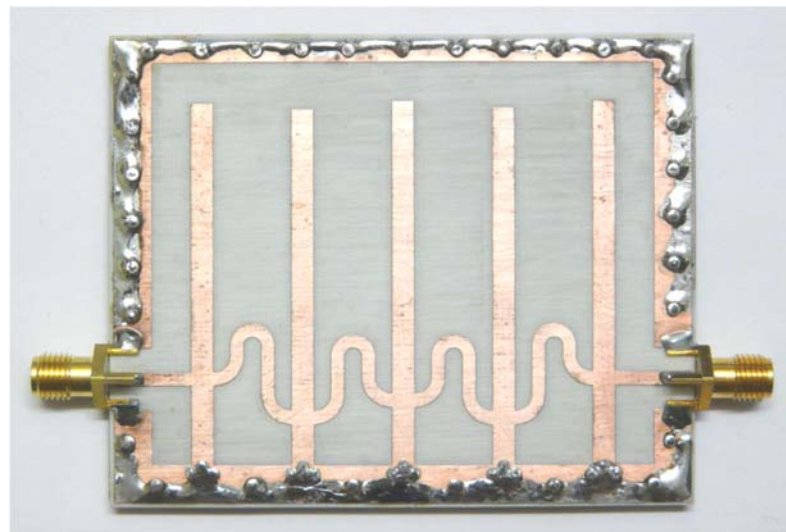


Figure 7.82. Direct-coupled filter hardware. (75x60mm).

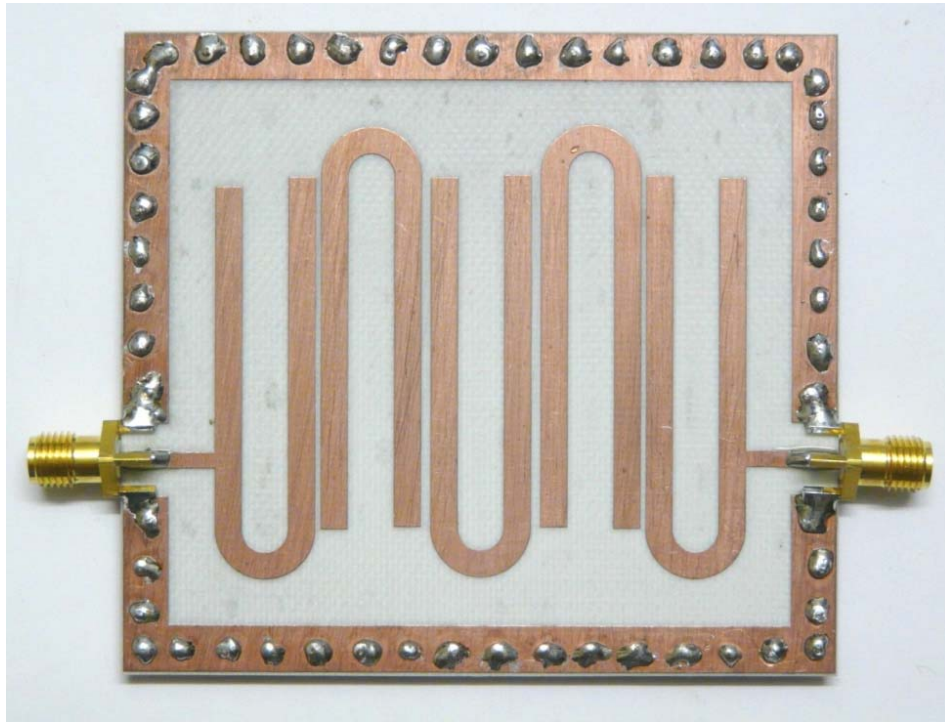


Figure 7.83. Hairpin filter hardware. (78x68mm).

Figures 7.84 to 7.87 show the measured frequency responses of the filters. Comparing these with figures 7.78 and 7.79, shows the remarkable agreement between the calculated and measured results. The passband of the interdigital, combline, and direct-coupled filters are a few percent lower than calculated. The difference matches the length of the pins used in connecting the grounded end of the resonators to the ground-plane on the bottom of the PCB. This can be taken into consideration in the second iteration of the filter designs if needed.

The hairpin filter has a measured centre frequency that is very close to the desired 1 GHz centre frequency. This is due to no ground connections being required, thus removing an uncertainty of pin or via placement from the design. From the measured passband responses, hairpin filters have a better close in stopband attenuation and a more accurate centre frequency are thus a good choice for one off designs, where the performance has to be correct first time. The frequency error between the measured and calculated centre frequency for the interdigital, combline and direct-coupled filters, closely responds to the resonator length equal to the thickness of the substrate.

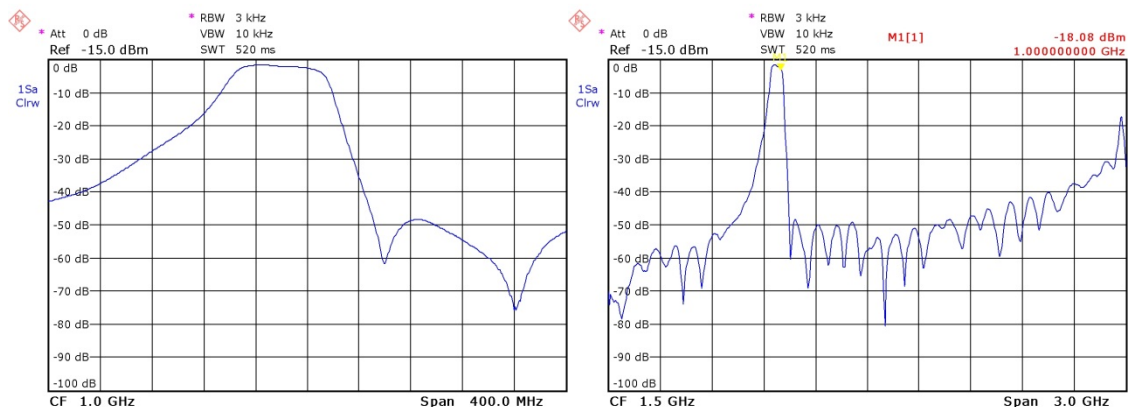


Figure 7.84. Measured frequency response of interdigital filter.

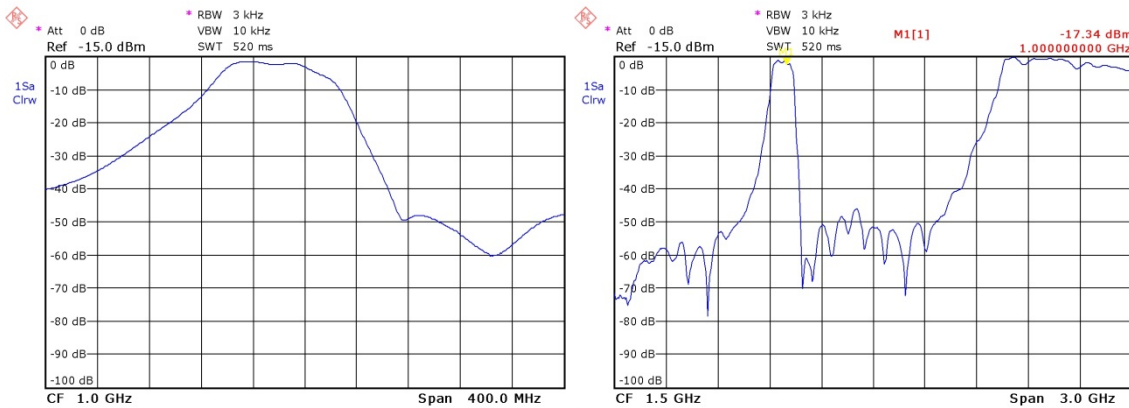


Figure 7.85. Measured frequency response of combline filter.

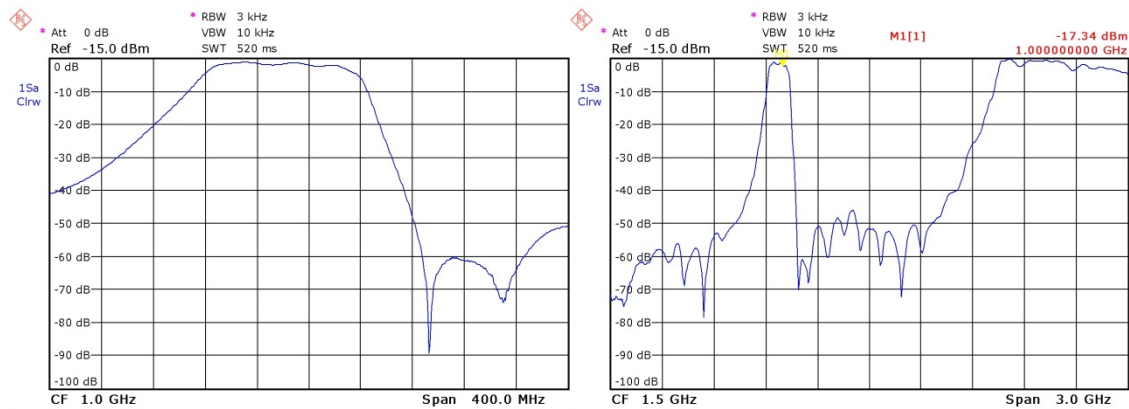


Figure 7.86. Measured frequency response of direct-coupled filter.

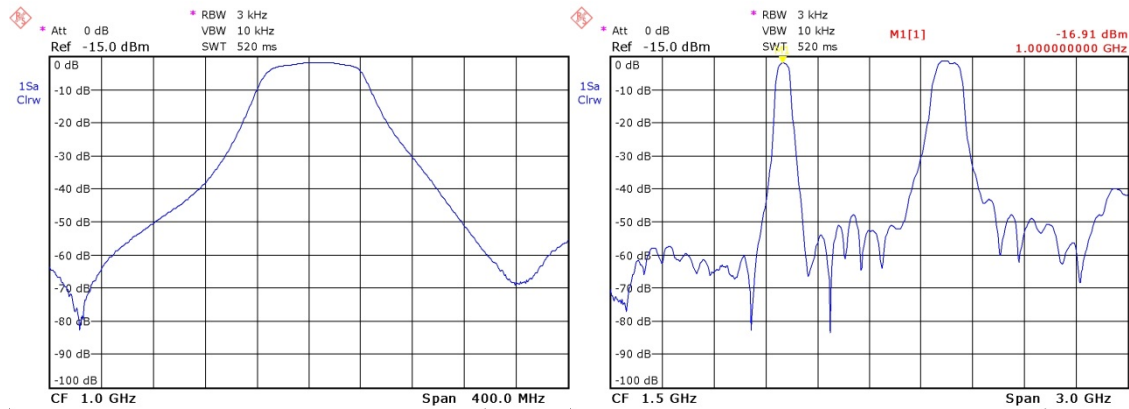


Figure 7.87. Measured frequency response of hairpin filter.

EM Simulation

Prior to NI AWR DE Version 10, it was very time consuming to prepare a circuit, like the hairpin filter in figure 7.83, for an EM simulation. In version 10, *circuit extraction* was introduced. That allows the simple conversion of the circuit to an EM model for EM simulation to be carried out. The EM simulation speed improved significantly in version 13, making it now practical to use EM simulations as part of the design process.

The hairpin filter of figure 7.83, was designed and optimised using circuit simulation only. To minimise the effect of frequency response changes when this circuit is mounted

in an enclosure, a grounded track, connected with vias to the ground-plane was included in the PCB layout as shown in figure 7.83. EM simulation allows the designer to ensure that the grounded ring around the circuit does not cause any unwanted changes to the circuit's performance, by including an analysis of the coupling between the filter and the grounded ring. To illustrate the process, an EM simulation of the hairpin filter of figure 7.83 is now described.

The first step is to ensure that all circuit elements can be EM extracted. Select each element in turn and select *Properties* \Rightarrow *Model Options* and ensure a “ \checkmark ” is placed in the *Enable* checkbox of the *EM EXTRACT Options* window. Add the *EXTRACT* element to the circuit diagram, by selection *Draw* \Rightarrow *More Elements* \Rightarrow *Extraction Control Block*, or *CNTRL-L* and place the Extract element on the circuit schematic, as shown in figure 7.88.

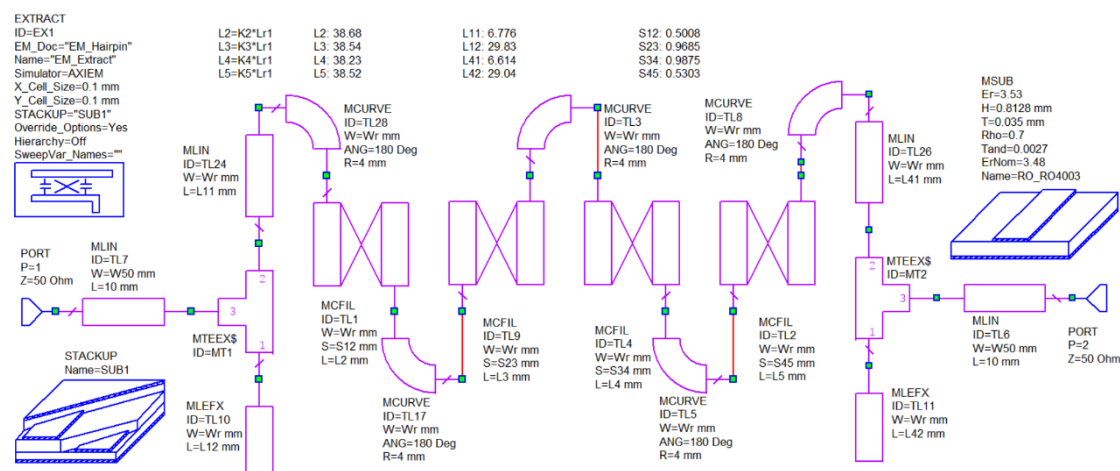


Figure 7.88. Hairpin filter circuit with EM control elements added.

There are several different EM simulators available, as can be seen from the drop-down selection for the simulator in the *EXTRACT* element. Analyst allows arbitrary 3-dimensional components to be simulated. In this case, a much simpler 3D planar EM analysis is required. The hairpin circuit is fairly complex, as a result AXIEM is used in this example. It gives good results and is much faster than EMSight. Select AXIEM in the Simulator dropdown box of the *EXTRACT* control element. Right clicking on *EXTRACT* shows which circuit elements are included in the extraction, by highlighting them in red. Ensure that all circuit elements are included.

From the circuit element catalogue select *Substrates* \Rightarrow *STACKUP* and add the Stackup element to the circuit diagram and give that a suitable name if required. Add the Stackup circuit element name to *EXTRACT* using the *STACKUP* dropdown box in the *EXTRACT* element. Left click on the *STACKUP* element and set E_r and other the material definitions and other properties to match the substrate and conductors to be used. For the *Line Type* property, select *Initialise* to match the *Line Type* used to the circuit diagram layers. The Line Type of *Top Copper* and the Material Name *Copper*, is used in the circuit of figure 7.88. Repeat this process for any other circuits to be simulated at the same time. Initially use the default settings for the *EXTRACT* element. Since the EM simulation can take a reasonable time, for the initial EM simulation, set the X and Y cell sizes to 1 mm, until the simulation completes without errors after which the cell sizes can be reduced. Reducing cell sizes will increase the accuracy and the time required to complete the simulation. For example, simulation of one of the enclosures used in the NI

AWR DE files for figures 7.88 to 7.94, on a modern laptop, takes about 9 minutes using a 1 mm cell size, 25 minutes using a 0.1 mm cell size and more than 5 days using a 0.01 mm cell size. Before starting an EM simulation, make sure that all the elements in the layout are snapped together. The first time the simulation is run, the EM structures corresponding to the STACKUP element are created. Check that there are no errors, which could affect the accuracy of the simulation. After the first simulation, right click on the enclosures in the *EM Structures* and ensure that the materials are defined correctly and that the layers are set up correctly, if not correct those in the STACKUP element.

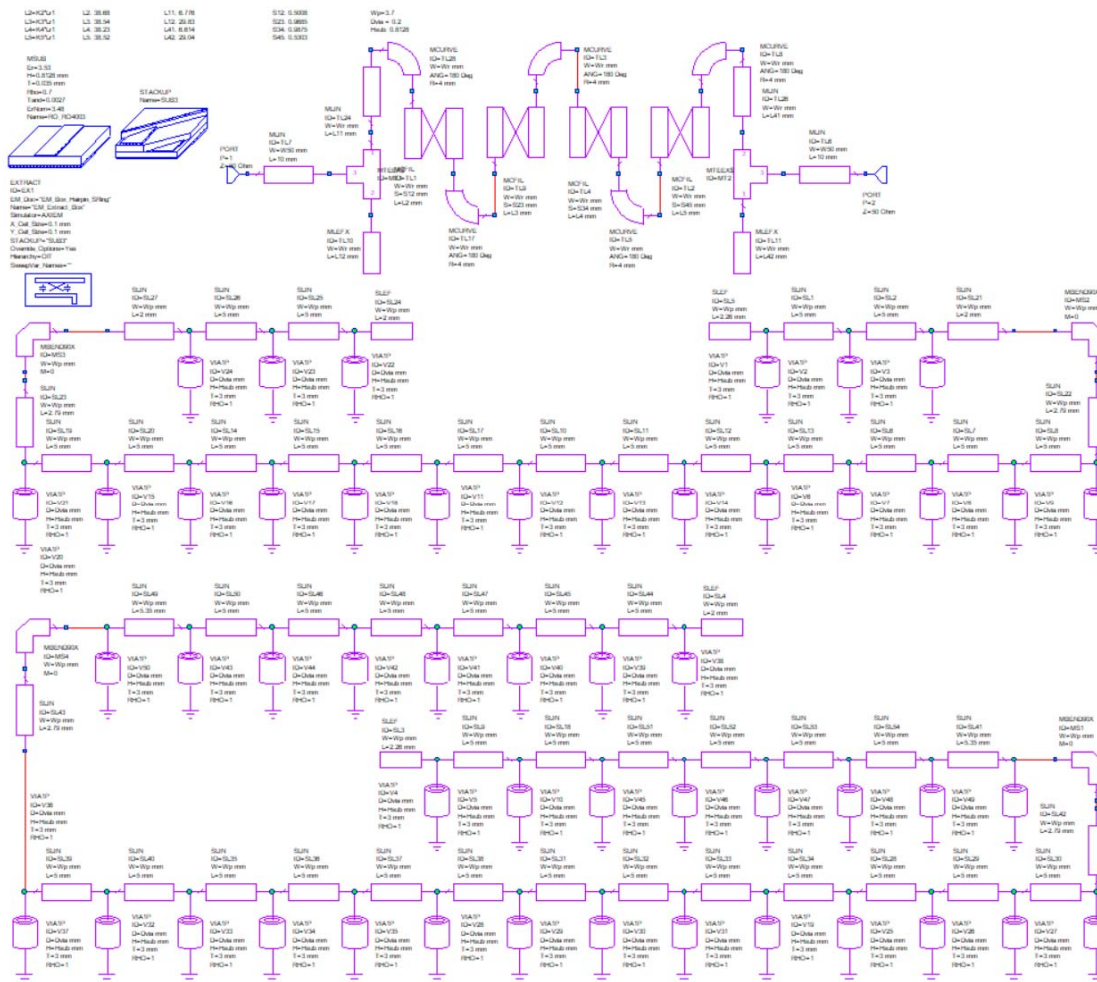


Figure 7.89. Hairpin filter circuit with EM control elements and shielding ring added.

The NI AWR DE project file for the comparison between the circuit and EM simulation of the hairpin filter, as presented in figures 7.88 - 7.94 has 5 circuits in it. The numbers in the labels in figures 7.94 and 7.95 correspond to the numbers for the circuits in the following descriptions. The first circuit (1_Hairpin Circuit) is the hairpin circuit schematic used to produce figure 7.83, including the grounded ring, which surrounds the PCB, made using the MCFIL element for the coupling of the resonators. The second circuit (2_Hairpin EM) is an EM simulation of the filter circuit only, without the PCB border.

The third circuit (3_Hairpin EM PCBRing) is the same as the first circuit, but with the grounded PCB border ring made up from transmission lines with vias spaced approximately 5 mm apart, added, as shown in figure 7.89. The EM simulation of

figure 7.89 includes the coupling between the hairpin filter and the grounded PCB border ring. Comparing the EM simulation of the hairpin only circuit with the EM simulation of the hairpin with the PCB border, allows the effect of the PCB border to be evaluated.

The fourth circuit (4_Hairpin EM Box_PCBRing) is the same as the third circuit, except that copper walls are used for the EM structure in STACKUP and a copper top boundary is used 25 mm above the circuit board. That matches a typical mounting of the circuit board in a metal box enclosure. Varying the height of the top boundary above the circuit board will allow the smallest enclosure size to be determined. Note that AXIEM ignores the sidewall boundary conditions, however the PCB border shown on figure 7.83 minimises any fields at the side boundaries, so that there is no practical difference between having no sidewall or a copper sidewall.

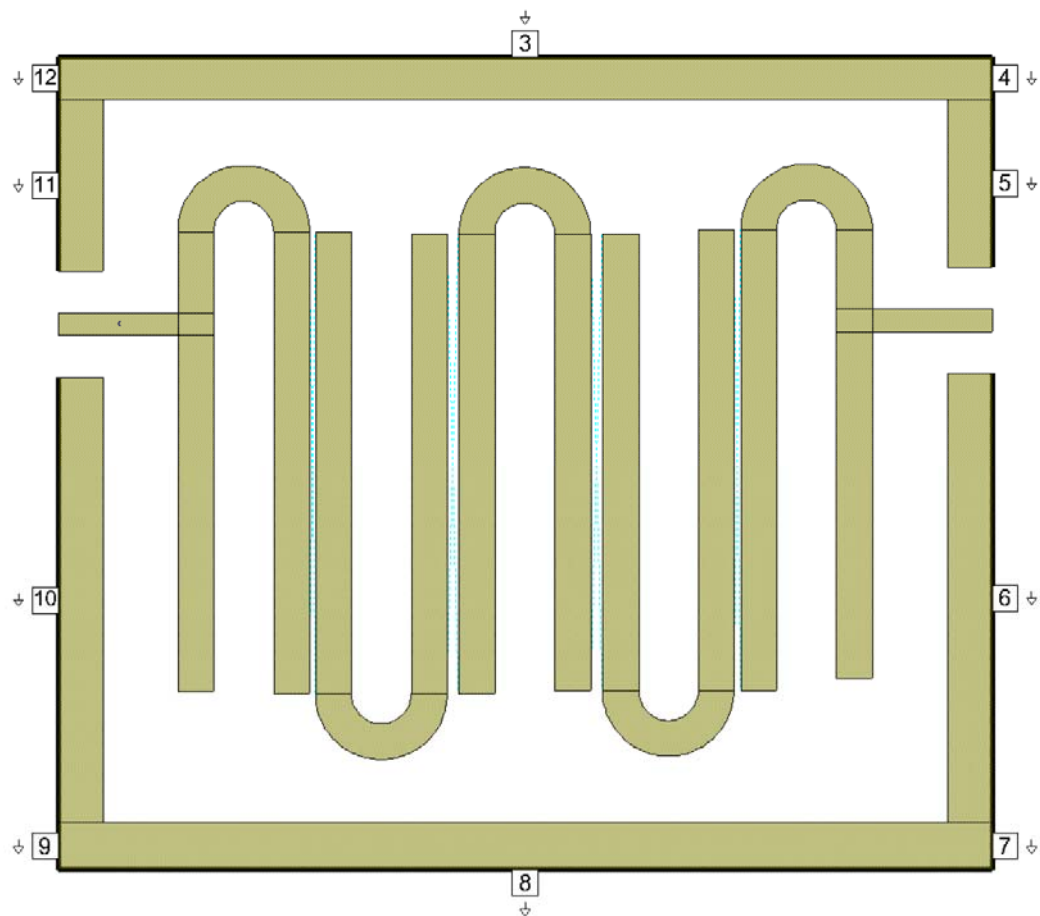


Figure 7.90. PCB border simulation using grounded extraction ports.

The fifth circuit (5_Hairpin EM EPort_PCBRing) uses the layout of the first circuit and places Extraction Ports on the outer edges of the shapes making up the PCB border. This is done by selecting one of the shapes, *Selecting Draw* \Rightarrow *Extraction Port* and placing the port on the outside edge of the board. Then select the properties of the extraction port by double clicking on it. Use the *Explicit Ground Reference* dropdown window to set the port to “*Connect to lower*”. That will then earth the shape and show a ground symbol on the layout. Right-click on the shape and select *Shape Properties*. Enable EM extraction and set the group name to the name of the EM Extraction element on the circuit schematic. This process is repeated for all the shapes. The resulting layout is shown in figure 7.90. It should be noted that circuit 1, 3, 4 and 5 all have exactly the same layout, but that the PCB border is treated different in their simulation.

This technique of using extraction ports on the PCB border was used for including the PCB border shown in figure 7.46 in the EM simulations shown in figures 7.51 and 7.52.

Since the layouts for each of the EM simulations are different, a different extraction name needs to be used for each of the EM simulations. To produce the circuit schematic for circuit 4, the schematic for circuit 3 (3_Hairpin EM PCBRing) was duplicated and renamed “hairpin EM Box_PCBRing”. The extraction *Group Name* of each of the elements then needs to be changed from: *EM_Extract* to *EM_Extract_Box*. This is done by viewing the layout of circuit 5, selecting all and then selecting Element Properties and in the *Model Options*, change the *Group Name* to *EM_Extract_Box*. That will change all the elements at once.

Before any EM simulation is carried out check that all the elements are linked to the EXTRACT element in the schematic, by left clicking on it. All the linked elements show up in red. While keeping the EXTRACT element selected, select *View* \Rightarrow *View Layout*. All the elements to be included in the EM simulation, should be shown in red and should all be joined correctly.

All the 5 circuits can then be simulated. If the EM simulation fails, some Extraction Control Block Properties may need to be changed. Firstly ensure the values are set to their default values, as V13 has different simulation settings to earlier versions. This is done by right clicking on the “extract element”. Then selecting properties and in the *Extraction Control Block Properties* window, select *AXIEM* and click *reset defaults*. If this fails to resolve the problem, change the parameters that caused the simulation failure as shown in the status window.

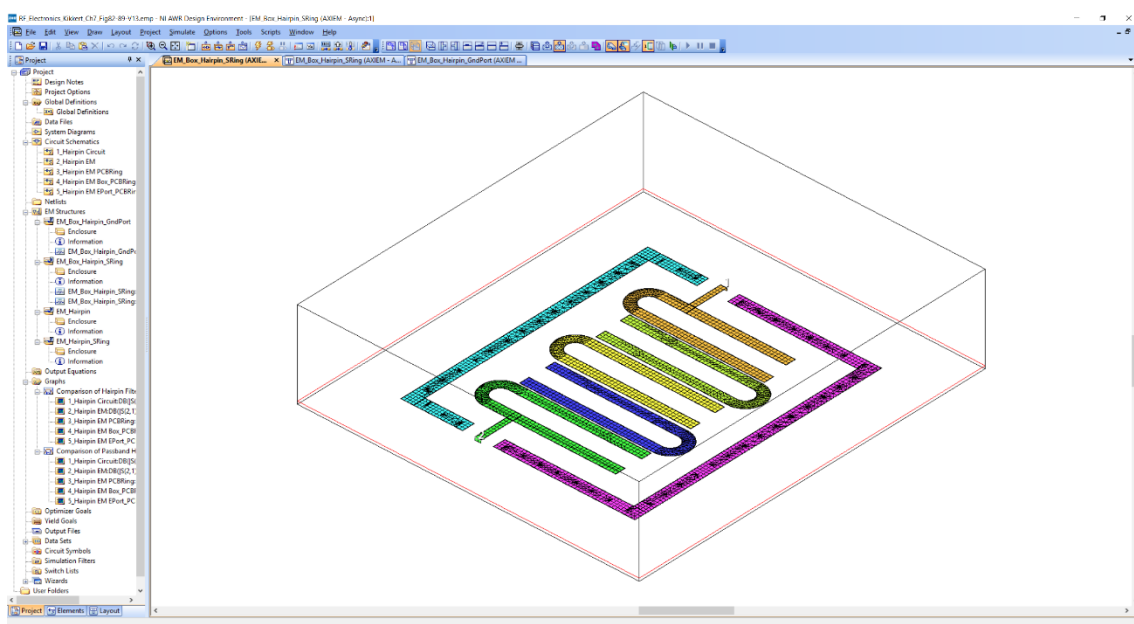


Figure 7.91. 3D Layout of hairpin filter of figure 7.89 with mesh shown.

AXIEM produces a mesh for the circuit layouts and uses those meshed elements to perform the EM analysis. To see the mesh, select the relevant structure in *EM Structures* such as: *EM_Box_Hairpin_SRing* of figure 7.91, right click on that structure and select *Mesh*. Selecting *View* and *View EM Layout*, will show the 2D mesh, as shown in figure 7.92. Note the way that the meshing is performed in the bends of the hairpin filter. Figure 7.93 shows a close-up of the meshing applied to the bends of the hairpin filters for the AXIEM simulation (left) and the EMSight simulation (right). It can be seen that

AXIEM uses less mesh elements and models the shape of the bend more accurately than EMSight. Requiring more mesh elements results in a slower simulation. Using a cell size of 0.1 mm and a typical computer, both circuits of figure 7.88 and 7.89 take 25 minutes to complete using AXIEM, but the circuit of figure 7.88 alone took more than 2 days to complete using EMSight and gave several warnings about convergence, thus producing an incorrect result. EMSight will be more accurate than AXIEM to use on simple couplers, like the one shown in figures 4.39 to 4.45.

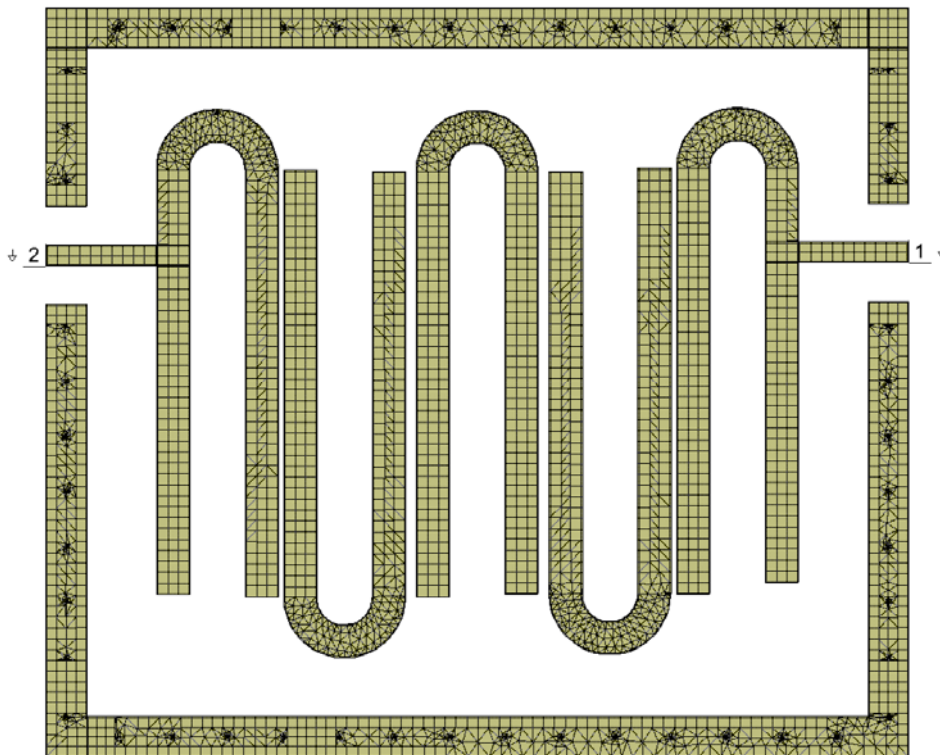


Figure 7.92. 2D Layout of hairpin filter of figure 7.89 with mesh shown.

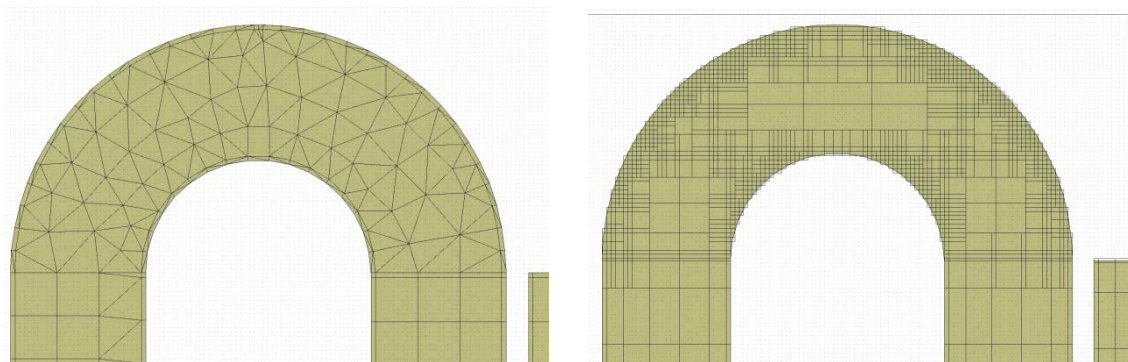


Figure 7.93. Close up of meshing applied by AXIEM (Left) and EMSight (Right).

For the filter design and optimisation, circuit simulation with $E_r=3.38$ and $E_{r\text{Nom}}=3.38$ was used. Rogers in their datasheet [16] for R04003 specify $E_r=3.38$ and suggest that $E_r=3.55$ is used for simulation. The circuit and EM simulation shown in figures 7.51 and 7.52 used $E_r=3.38$ for all simulations and the EM simulations are very close to the measured results. For the filter of figure 7.83, the circuit simulation shown in figures 7.94 and 7.95 with $E_r=3.38$ gives the desired 1 GHz centre frequency and $E_r=3.53$ gives the desired 1 GHz centre frequency for the EM simulation.

A Change of E_r from 3.38 to 3.53 gives a 2% change in centre frequency. The circuit and EM simulations centre frequencies will thus differ by 2%, as shown in figure 7.51 (for same E_r) and figure 7.94 (different E_r). The difference between the desired and measured centre frequency of the circuit in figure 7.46 is 30 MHz (3%), as shown in figure 7.51. For the filter in figure 7.83, it is 5 MHz (0.5%), as shown in figure 7.87. The filter in figure 7.46 uses 1.75mm wide resonators and the filter in figure 7.83 uses 3mm wide resonators. The wider resonators result in a lower insertion loss and less impedance errors due to inaccuracies in milling or etching of the PCB.

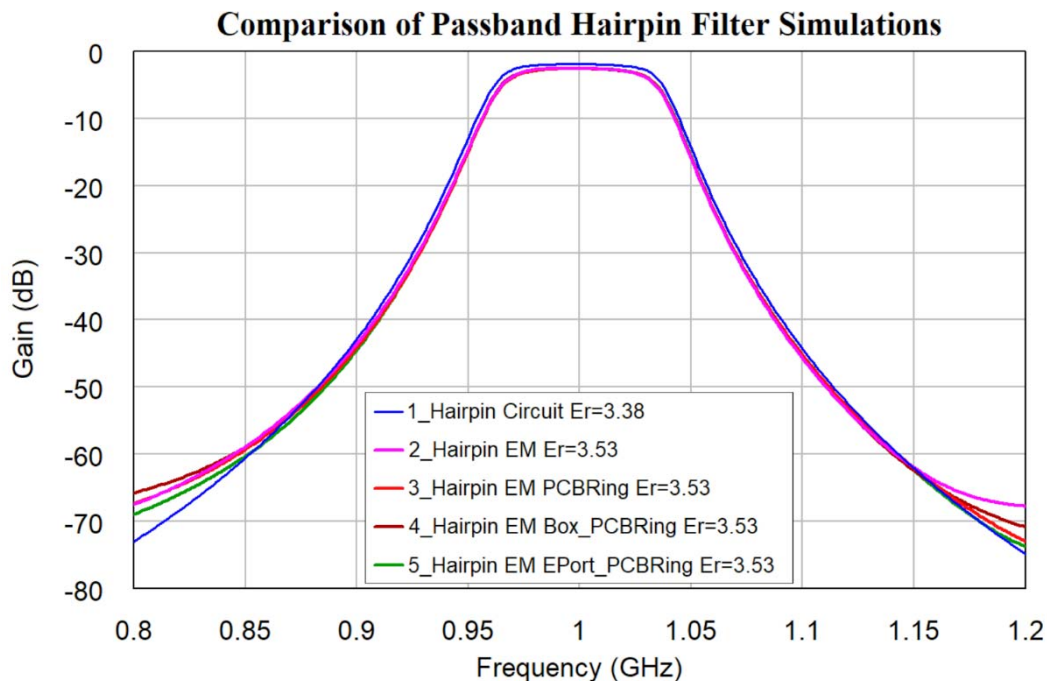


Figure 7.94. Passband Frequency response of Circuit and EM simulations of the hairpin filter.

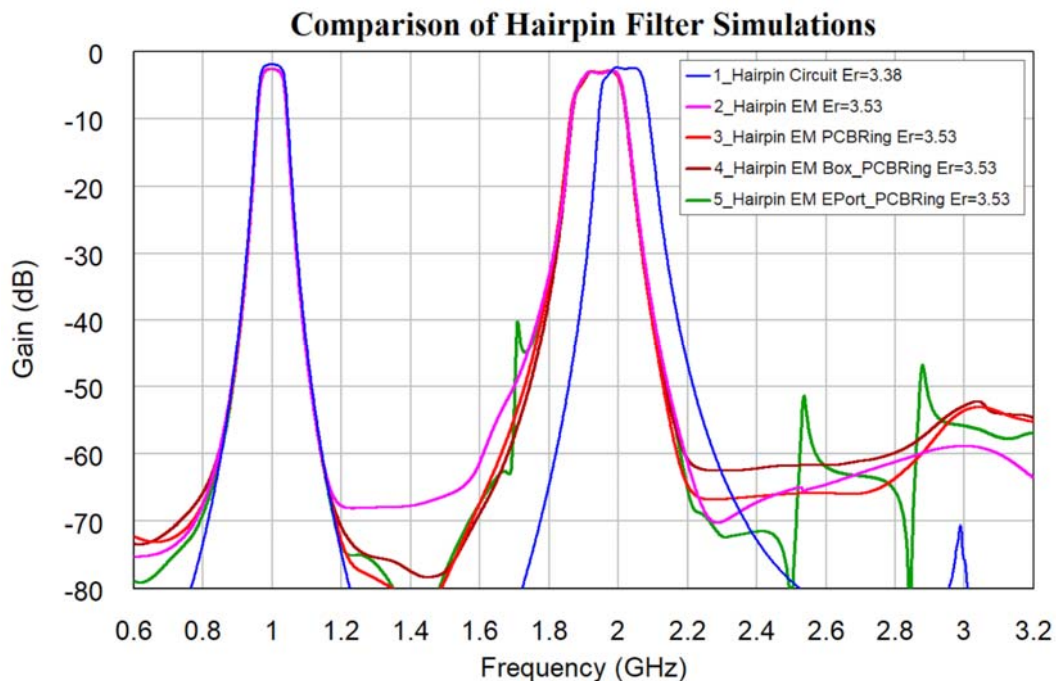


Figure 7.95. Passband Frequency response of Circuit and EM simulations of the hairpin filter.

Figure 7.94 shows a very good agreement in the passband for the 4 different EM filter simulations. That also shows that the screening ring or the top boundary conductor does not affect the passband response.

Figure 7.95 shows the harmonic response of the 5 filter simulations. The EM simulation of circuits 3, 4 and 5, those with the boundary ring, show a lower attenuation in the 500 MHz to 750 MHz frequency regions.

The second harmonic response of the filter is shifted in the EM simulation compared to the circuit simulation. The measured frequency of the second harmonic response on figure 7.87 exactly matches the second harmonic response from the EM simulation in figure 7.95. This shows that EM simulation is required, to determine the frequency response of a filter accurately. As expected figure 7.87, shows less stopband attenuation, due to leakage between cables used in the measurement setup

Since NI AWR DE V10, the ability to use the Extraction control block with AXIEM has made it feasible to obtain accurate EM simulations of RF designs, including the effect of any screening ground-planes on the top layer. Prior to the Extraction being available, EM simulation required a significant effort without a guaranteed useful result.

Coaxial Filters



Figure 7.96. Coaxial cavity dimensions. Figure 7.97. Coaxial cavity diplexer for 80 MHz (UM).



Coaxial filters are similar in principle to helical filters, except that the resonator is a straight rod, rather than a wound helix as shown in figure 7.96. The length of the centre rod is a quarter wavelength. For the highest Q values, the ratio of the centre rod diameter to the inner diameter of the cavity is such that the characteristic impedance of the coaxial line forming the resonator is 77Ω . The equation for the characteristic impedance of a coaxial transmission line is:

$$Z_c = \frac{1}{2\pi} \sqrt{\left(\frac{\mu_0}{\epsilon_0}\right) \ln\left(\frac{B}{A}\right)} = \frac{60}{\sqrt{\epsilon_r}} \ln\left(\frac{B}{A}\right) \quad \text{Eqn. 7.30}$$

So that the maximum Q is obtained when $B/A = 3.6$.

Typical Q values are in the range of 2000 to 10000. Because cavity filters have such a high Q, they are used in many applications requiring a low insertion loss. Air filled coaxial filters have a high power handling capability and are typically used for filters and combiners for radio and TV transmitters and in mobile radio and mobile phone base stations.

Figure 7.97 shows a typical coaxial filter used in a mobile radio talk-through repeater operating at 80 MHz. The total height of the filter is 1.2 m and the cavities are 200 mm in diameter. The cavities used in this filter have a Q of 5000. The round cylinders at the top of the cavities are isolators, which ensure that the input impedance to the filter is perfectly matched over the entire bandwidth of the transmitter.

Some coaxial cavities are much smaller. Older mobile (cell) phones contain diplexers with ceramic filled coaxial resonators. Figure 7.98 shows a surface mount, ceramic 3-resonator coaxial filter for such applications. Using a high dielectric constant material for the cavity gives a significant reduction in filter size. The centre frequency of this filter is 881 MHz. The filter is 14 mm long.

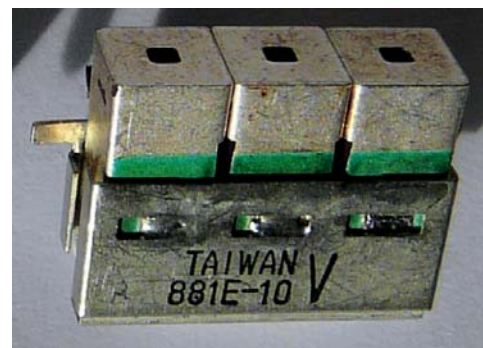


Figure 7.98. Coaxial cavity filter (UM).



Figure 7.99. Cavity filter diplexer for mobile radio applications [17].

For mobile radios, used by trucks or taxis to talk to their base, a coaxial diplexer is often used to provide isolation between the transmitter and the receiver in their mobile radio. Figure 7.99 shows a typical coaxial diplexer. The receive frequency is 450.625 MHz and the transmit frequency is 460.125 MHz. These radios typically have a transmission power level of 25 W (43.98 dBm). The receiver typically has signals of -60 dBm applied to it, so that the difference between the transmitted and received signal is more than 100 dB. Connecting the transmitter directly to the receiver will result in severe damage to the input circuitry, but the diplexer prevents this.

As shown in Figure 7.100, at the receiver frequency of 450.625 MHz, the diplexer of figure 7.99 causes a less than 1 dB loss between the antenna and the receiver ports and more than 60 dB isolation between the antenna and the transmitter ports, thus protecting the input from any spurious signals generated by the transmitter at the receiver frequency.

At the transmitter frequency of 460.125 MHz, the diplexer provides less than 1 dB loss between the transmitter port and the antenna port, so that virtually all the 25W output signal is transmitted. At this frequency, there is more than 60 dB isolation between the antenna and receiver ports, thus protecting the input from the high power levels generated by the transmitter.

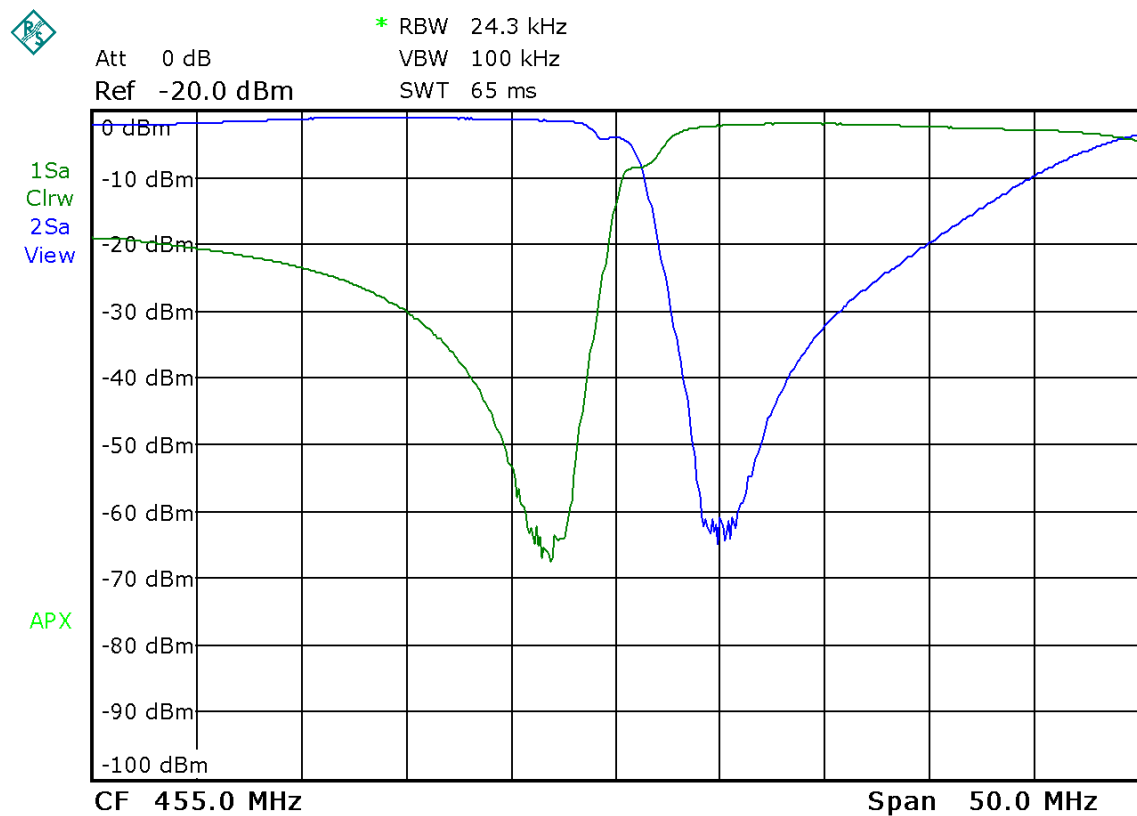


Figure 7.100. Frequency response of the diplexer of figure 7.99.

For low loss, high power microwave filters; it is often convenient to mill the whole filter out of a solid block of aluminium, as shown in figure 7.101. Martin [18] provides design tools for this. By including coupling between non-adjacent cavities, zeros of transmission can be included. In the filter of figure 7.101, non-adjacent cavity coupling has been applied to the first and last resonator.

These filters are tuned by capacitive top loading on each resonator. Each of the resonators is thus a fraction shorter than a quarter wavelength, with the required top-loading capacitance making up this shortfall.

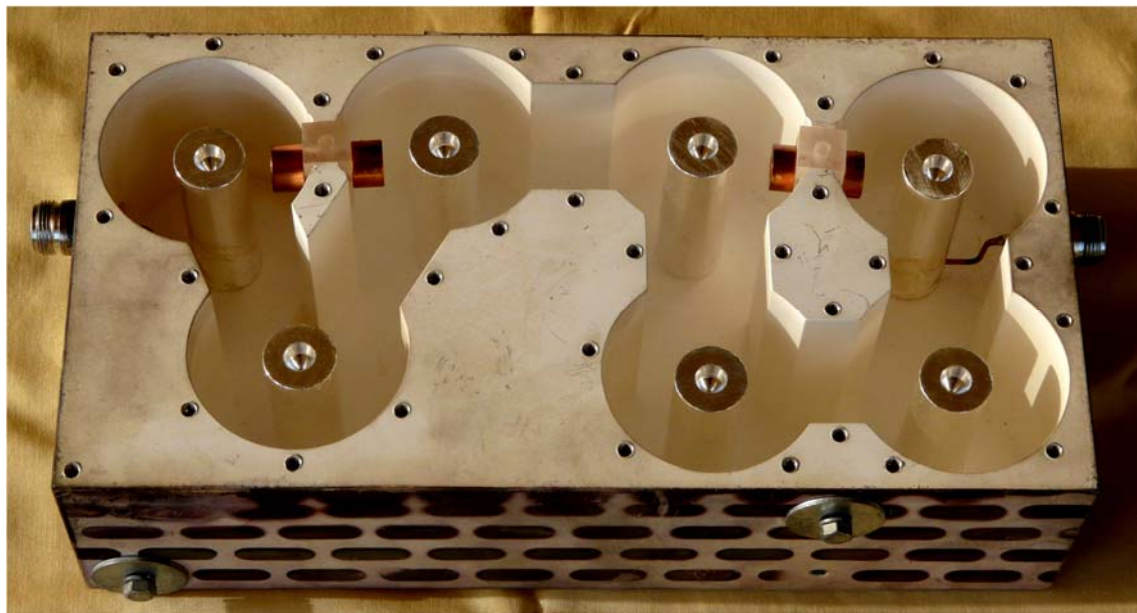


Figure 7.101. 1.8 GHz Coaxial Cavity Filter.

Ceramic Filters

For many consumer applications IF filters are required at only a few specific frequencies. For example, all FM radios have an IF of 10.7 MHz. All AM radios use a 455 kHz IF. As a result, commercial filter manufacturers like Murata have a wide variety of low cost filters available for those frequencies. To achieve small size, low cost and freedom from microphony, ceramic materials are used for the resonators. Two typical 10.7 MHz ceramic IF filters are shown in figure 7.102. Many of the latest versions are surface mount instead of the through-hole filters shown in figure 7.102. The right hand filter contains two filters like the left hand one, inside the one casing and is used to provide more filtering of unwanted signals. Most of the FM IF filters are designed to provide a flat group delay over the passband. This minimised the distortion caused by the IF filter to the demodulated audio signals.



Figure 7.102. 10.7MHz ceramic IF filters [19].

In addition there are many filters available for specific IF applications, such as 5.5 MHz and 6 MHz for analogue TV sound IF, 38.9 MHz for Digital Audio Broadcasting (DAB), 44 MHz for digital TV receivers etc.

Ceramic resonator filters are also used for RF filtering. The Murata Gigafil range for instance contains many different RF filters covering the 800 to 950 MHz mobile phone band and the 1.4 to 2.4 GHz mobile phone and WLAN bands.

Since these ceramic filters are mass-produced, their cost is very low and it may be worthwhile to modify one's design to be able to incorporate these filters.

SAW Filters

The resonators considered so far have electromagnetic or acoustic resonances with the resonator being a quarter wavelength. Voltages across an input transducer on the surface of a piezo-electric substrate, causes an acoustic wave to travel along the surface of the substrate. These travelling waves then induce voltages on a second transducer, which is used as an output transducer. By correctly designing the shape of these transducers, filtering can be achieved, with independent control over both the amplitude and group delay. Surface Acoustic Wave (SAW) filters are thus normally used for TV IF filters, IF filters for radars and other applications where sharp filtering is required and where the group delay must be absolutely flat.

Since the input transducer generates a travelling wave in the direction of the output transducer as well as one in the opposite direction, which must be absorbed, SAW filters have a high insertion loss, typically 12 dB for devices with a centre frequency of 70 MHz and 4 dB for devices operating at 2 GHz [20]. Because of their low cost, small size and good performance, SAW filters are used in many consumer devices. The design of SAW filters is outside the scope of this book.

References

1. A. I. Zverev, *Handbook of Filter Synthesis*, Wiley, 1967, Helical Filters pp 499-521, k and q Filter Tables, p 341, Eqn. 9.4.3 pp 517.
2. G G. Matthaei, L. Young, and E. M. T. Jones, *Microwave Filters, Impedance-Matching Networks, and Coupling Structures*. Boston, MA: Artech House, 1980. pp.583-650.
3. D. Pozar, *Microwave Engineering*, Third Edition, Wiley, 2005. pp. 416-438.
4. Kikkert C. J, "The Effect of Amplifier Distortion and Filter Type on BER of WCDMA-UMTS Mobile Radio Systems", 2nd International Conference on Signal Processing and Communication Systems (ICSPCS 2008), Gold Coast, Australia, 15-17 December 2008, ISBN: 978-0-9756934-6-9.
5. Minicircuits, Reflectionless Filters. <https://www.minicircuits.com/pdfs/XHF-23+.pdf>
6. Pairing Mixers with Reflectionless Filters to Improve System performance, Minicircuits AN-75-007, <https://www.minicircuits.com/app/AN75-007.pdf>
7. Morgan M. A. and T. A. Boyd, Synthesis of a New Class of Reflectionless Filter Prototypes, National Radio Astronomy Observatory. <https://arxiv.org/ftp/arxiv/papers/1008/1008.3502.pdf>
8. Microwaves 101, Reflectionless filters. <https://www.microwaves101.com/encycopedias/reflectionless-filters>
9. Temwell Corporation, <http://www.temwell.com.tw/>

10. Toko, <http://www.toko.co.jp/top/en/index.html>
11. M. Dishal, "A Simple Design Procedure for Small Percentage Bandwidth Round Rod Interdigital Filters" MTT, Vol 13, No5, Sep 1965, pp 696 – 698.
12. K&L Microwave, <http://www.klmicrowave.com/products.php>, 9IR20-7500/X2000-O/O Wide Band Interdigital Filter Datasheet, http://www.klmicrowave.com/product_attach/plk50_1_9IR20.pdf
13. Kikkert, C. J. "Designing Low Cost Wideband Microstrip Bandpass Filters", IEEE Tencon '05, Melbourne, Australia, 21-24 November 2005.
14. Kikkert, C. J. "A Design Technique for Microstrip Filters" ICECS 2008, St Julians, Malta, 31 Aug.-3 Sep. 2008.
15. Codan, <http://www.codan.com.au/>
16. Rogers, R04000 Data. <http://www.rogerscorp.com/documents/726/acm/RO4000-Laminates---Data-sheet.pdf>
17. Hills Communications, part of Hills Ltd, <http://www.hills.com.au>
18. P. Martin, "Designing Microwave Band Pass Filters", 19 Mar 2011. Available: https://awrcorp.com/download/kb.aspx?file=EC_Mstrip_BPFilter.pdf
19. Murata Manufacturing Co, Ceramic Filters <http://www.murata.com/en-global/products/filter/cerafil>
20. Murata Manufacturing Co, SAW Based Components <http://wireless.murata.com/eng/products/saw-based-components.html>

Chapter 8

Amplifiers: Stability, Noise and Gain

Introduction

A few years ago, if one had to use an RF or IF amplifier, one had to design it using individual transistors and associated passive components. Now for many commercial RF frequency bands there are low cost IC's available, which perform as well or better than discrete transistor designs. For example, Analog Devices HMC8410 low noise amplifier has a 10 MHz to 10 GHz bandwidth and a noise typical figure of 1.1 dB. The Minicircuits CMA-5043+ is an LTCC amplifier with a 50 MHz to 4 GHz bandwidth and a 0.75 dB noise figure. Many other manufacturers have similar devices.

For IF amplifiers at HF frequencies it is now also possible to use high speed operational amplifiers, resulting in IF strips that have an excellent linearity and very low intermodulation distortion. VHF cable TV repeaters can be used for medium power amplifiers. There are also many amplifier modules available with a very high linearity, particularly for the frequency bands used by mobile phones, wireless LAN, Bluetooth and other high volume consumer frequencies.

The principles for obtaining stability and low noise, outlined in this chapter, also apply to the latest Microwave Monolithic ICs (MMIC) and individual BJT and FET devices, such as High Electron Mobility Transistors (HEMT).

MMIC

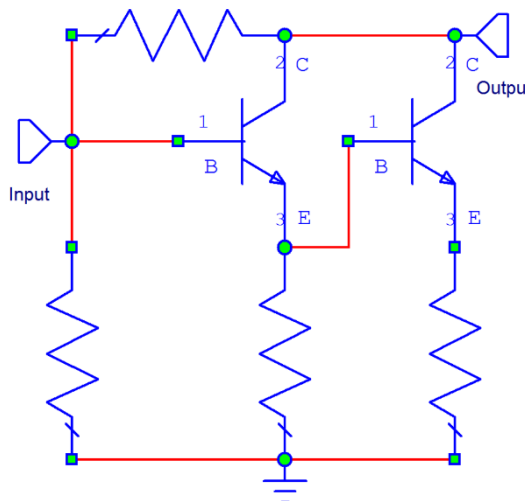


Figure 8.1. Typical Mini-Circuits MMIC circuit diagram.

Several IC manufacturers like Agilent, Mini-Circuits and Freescale (Motorola) produce general purpose Microwave Monolithic Integrated Circuits (MMIC): These can be used as general-purpose amplifier blocks and can be used at frequencies from DC up to 10 GHz. Several devices also have low noise figures, for example, the Mini-Circuits [1] MAR6+ amplifier has a bandwidth of DC to 2 GHz and a noise figure of 3 dB and the GALI S66+ [2] amplifier has a bandwidth of DC to 2 GHz and a noise figure of 2.7 dB. These devices have sufficient low noise figures to result in economical commercial solutions.

There are two types of general purpose MMIC's: 1) Fixed voltage and 2) Constant current. The fixed voltage MMIC's are designed to operate at a supply voltage of typically 5 or 3.6 Volt.

Mini-Circuit's MAR, ERA, Gali and Lee series of amplifiers all require a constant current source and have a typical circuit diagram as shown in figure 8.1. Many of the MMIC's are made using InGaP HBTs (indium gallium phosphide Heterojunction Bipolar Transistors). Others are made using GaAs PHEMTs (Gallium Arsenide Enhancement Mode Pseudomorphic High Electron Mobility Transistors).

A suitable constant supply is obtained, by using a resistor to set the current supplied to the MMIC as shown in figure 8.2. The RF loading of that resistor is minimised by having a large inductor in series with the resistor. Since the resistor is typically $600\ \Omega$ for a 12 Volt supply voltage, in many applications a slightly reduced gain can be tolerated and the inductor can be removed. This series resistor, together with the DC feedback resistor, between the collector and base of the transistor in figure 8.1, result in a stable quiescent current as the temperature changes.

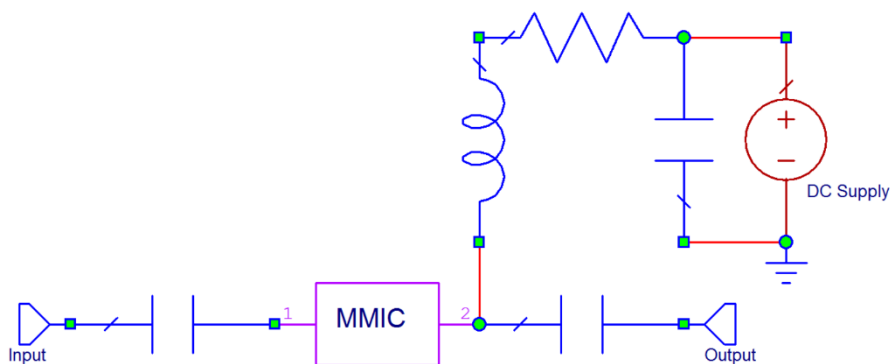


Figure 8.2 Typical connection requirement for an MMIC.

Most MMIC devices are unconditionally stable. However, since these devices have very wide bandwidths, microwave layout techniques must be used to ensure that the devices remain stable. As a typical example it is essential that the inductance of the ground pin connections of the MMIC are kept as low as possible. This is achieved by ensuring that the earth pins of the MMIC are soldered to a large ground plane and that a via connecting the top ground-plane to the bottom ground-plane is very close to the earth pin of the MMIC in the Microstrip PCB layout.

These amplifier modules and MMIC's can now be used for the majority of RF and microwave designs. There are applications, such as ultra-low noise amplifiers, microwave amplifiers and high power amplifiers, where amplifier modules and MMIC's cannot be used. For such designs, a knowledge of amplifier stability, noise figure and gain circles, which are described in this chapter is essential.

Requirement for Stability

For power amplifier design, a single power transistor, or several combined in parallel, are used to provide the required amplification at the required frequency, with the required linearity. The amplifier should be stable and not oscillate at any frequency under normal operating conditions. Amplifier stability and matching of input and output, ensuring that the highest power output is obtained, are the most critical parameters in a power amplifier design.

Smith Chart Revision

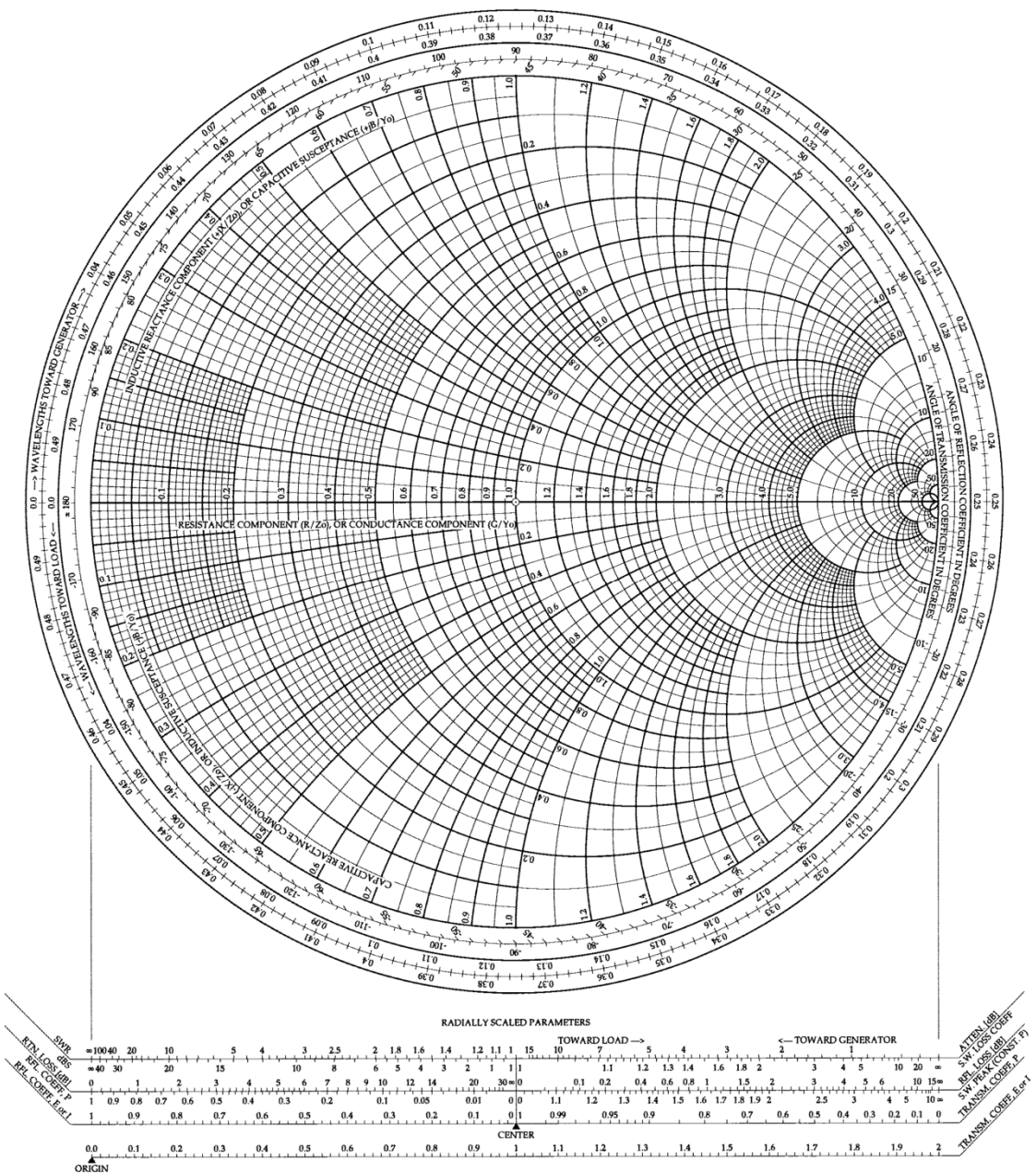


Figure 8.3. Smith Chart; a plot of the normalised reflection coefficient Γ .

To ensure that the amplifier is matched at the input and output, normally the return loss S_{11} at the input and S_{22} at the output of the amplifier is measured. In order to be able to adjust these reflection coefficients correctly, it is desirable to know both their magnitude and phase at different frequencies. The Smith Chart is a polar plot of reflection coefficient and allows both the magnitude and phase of the reflection coefficient to be plotted versus frequency. Such plots are very useful in visualising the behaviour of the reflection coefficient, and what action is required to improve the matching of the devices. As shown later in this chapter, the Smith Chart is very useful in visualising the stability of amplifiers.

The Smith Chart was developed by P. Smith [3, 4] in 1939. It is a polar plot of the reflection coefficient superimposed with circles for real and reactive normalised

impedances. It allows a good visualisation of the impedance of RF networks as the frequency changes. Some prior knowledge of the Smith Chart is presumed here and only the equations 8.1 and 8.2 governing the Smith chart are stated here, for a more detailed discussion on the Smith chart please refer to D. M. Pozar [5] or similar books. The copyright of the Smith Chart has been released into the public domain by the copyright holder. The normalised reflection coefficient Γ is and the normalised impedance Z_L of a network are related by:

$$\Gamma = \frac{Z_L - 1}{Z_L + 1} = |\Gamma| \angle e^{j\theta} = \Gamma_r + j\Gamma_j \quad \text{or} \quad Z_L = \frac{1 + \Gamma}{1 - \Gamma} = R_L + jX_L \quad \text{Eqn. 8.1}$$

The Smith chart is a plot of $|\Gamma| \angle e^{j\theta}$ and this also represents Z_L and we can plot contours of $Z_L = R_L + jX_L$. Solving for R_L and X_L gives:

$$R_L = \frac{1 - \Gamma_r^2 - \Gamma_j^2}{(1 - \Gamma_r)^2 + \Gamma_j^2} \quad \text{and} \quad X_L = \frac{2\Gamma_j}{(1 - \Gamma_r)^2 + \Gamma_j^2} \quad \text{Eqn. 8.2}$$

R_L and X_L form a family of circles, which are also plotted on the Smith Chart. $\Gamma = 0$ is the centre of the Smith Chart. The Smith chart is a very useful tool for showing impedance values versus frequency.

Paper versions of the Smith Chart are now seldom used for design calculations, but the Smith chart is an integral part of modern computer based design tools. NI AWR DE allows the results of the RF network simulation to be plotted on a Smith Chart, as well as rectangular and polar charts. In NI AWR DE, the centre part of the Smith chart can be expanded or compressed, by right clicking on the smith chart of figure 9.41 and selecting *Grid* and setting the *Size* to *Expanded* or *Compressed*. *Compressed* shows more of the area outside the outside the $\Gamma = 1$ region on the Smith Chart and is useful for plotting stability circles. *Expanded* provides a close up of the centre of the Smith Chart and is useful for visualising impedance matching.

Scattering Parameters Revision

Pozar [5] provides a more detailed description of S parameters than is presented here.

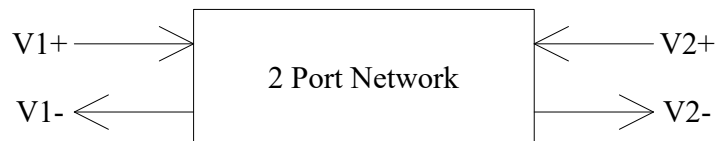


Figure 8.4. S parameter definitions.

$$\begin{bmatrix} V_1^- \\ V_2^- \end{bmatrix} = \begin{bmatrix} S_{11} & S_{12} \\ S_{21} & S_{22} \end{bmatrix} \begin{bmatrix} V_1^+ \\ V_2^+ \end{bmatrix} \quad \text{Eqn. 8.3}$$

$$S_{11} = \left. \frac{V_1^-}{V_1^+} \right|_{V_2^+ = 0} \quad \text{i.e. reflection coefficient at port 1, with port 2 matched.}$$

$$S_{22} = \left. \frac{V_2^-}{V_2^+} \right|_{V_1^+ = 0} \quad \text{i.e. reflection coefficient at port 2, with port 1 matched.}$$

$$S_{21} = \frac{V_2^-}{V_1^+} \Big|_{V_2^+ = 0} \quad \text{i.e forward gain, with port 2 matched.}$$

$$S_{12} = \frac{V_1^-}{V_2^+} \Big|_{V_1^+ = 0} \quad \text{i.e reverse gain, with port 1 matched.}$$

An amplifier is unilateral if $S_{12} = 0$, i.e. the reverse gain is zero. That applies to many amplifiers, particularly operational amplifiers and other ICs where the output is well separated from the input.

The input reflection coefficient is:

$$\Gamma_{in} = S_{11} + \frac{S_{12}S_{21}\Gamma_{load}}{1 - S_{22}\Gamma_{load}} \quad \text{For a unilateral amplifier } \Gamma_{in} = S_{11} \quad \text{Eqn. 8.4}$$

$$\Gamma_{out} = S_{22} + \frac{S_{21}S_{12}\Gamma_{source}}{1 - S_{11}\Gamma_{source}} \quad \text{For a unilateral amplifier } \Gamma_{out} = S_{22} \quad \text{Eqn. 8.5}$$

The Available Power Gain (G_A) is the ratio of the maximum available power at the load to the maximum available power at the source. It is the amplifier gain under ideal conditions as it assumes conjugate input and output matching. G_A is defined as:

$$G_A = \frac{\text{Power available from network}}{\text{Power available from source}} = \frac{|S_{21}|^2(1 - |\Gamma_{source}|^2)}{|1 - S_{11}\Gamma_{source}|^2(1 - |\Gamma_{out}|^2)} \quad \text{Eqn. 8.6}$$

The Transducer Power Gain (G_T) is the ratio of the actual power at the load to the maximum available power at the source. It is the amplifier gain under actual load conditions. It assumes a conjugate input match, but uses the actual output match. G_T is defined as:

$$G_T = \frac{\text{Power delivered to the load}}{\text{Power available from source}} = \frac{|S_{21}|^2(1 - |\Gamma_{source}|^2)(1 - |\Gamma_{load}|^2)}{|1 - \Gamma_{source}\Gamma_{in}|^2|1 - S_{22}\Gamma_{load}|^2} \quad \text{Eqn. 8.7}$$

There are measurement functions for G_A and G_T in NI AWR DE.

Under ideal conditions, $\Gamma_{source} = 0$ and $\Gamma_{load} = 0$ so that

$$G_A = G_T = |S_{21}|^2 \quad \text{Eqn. 8.8}$$

An amplifier includes input and output matching circuits as shown

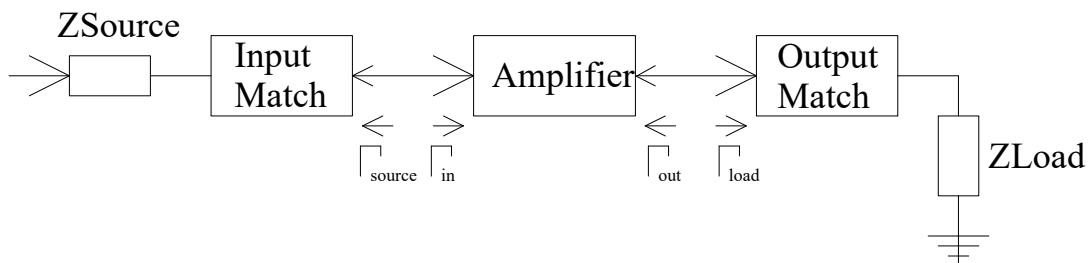


Figure 8.5. Amplifier block diagram.

The input match provides maximum power when $\Gamma_{in} = \Gamma_{source}^*$ so that the gain of the input matching network is $G_S = 1$. Similar when the output has a conjugate match so that $\Gamma_{out} = \Gamma_{load}^*$, then $G_L = 1$. In general:

$$G_S = \frac{1 - |\Gamma_{source}|^2}{1 - \Gamma_{in} \Gamma_{source}} \quad \text{Eqn. 8.9}$$

$$G_0 = |S_{21}|^2 \quad \text{Eqn. 8.10}$$

$$G_L = \frac{1 - |\Gamma_{load}|^2}{1 - \Gamma_{out} \Gamma_{load}} \quad \text{Eqn. 8.11}$$

The gain of the whole amplifier is:

$$G_T = G_s * G_0 * G_L \quad \text{Eqn. 8.12}$$

Under ideally matched conditions $G_S = 1$ and $G_L = 1$ so that the gain is thus:

$$G_T = |S_{21}|^2, \text{ as was obtained before in equation 8.8}$$

Stability

Oscillations will occur if $G_S \rightarrow \infty$ or $G_L \rightarrow \infty$

For oscillations due to the input, $G_S \rightarrow \infty$ so that from equation 8.9, $\Gamma_{in} * \Gamma_{source} = 1$.

Oscillators often are designed by deliberately making $\Gamma_{in} * \Gamma_{source} = 1$. Equation 8.4 shows how Γ_{in} depends on other parameters, which together with Γ_{source} can be manipulated to ensure that $\Gamma_{in} * \Gamma_{source} = 1$ is only satisfied at one frequency, thus ensuring stable oscillations. The amplifier is stable if $\Gamma_{in} < 1$ for all values of Γ_{load} .

Similarly, for oscillations due to the output, $G_L \rightarrow \infty$ so that from equation 8.11, $\Gamma_{out} * \Gamma_{load} = 1$. For oscillator design, equation 8.5 shows how Γ_{out} depends on other parameters, which together with Γ_{load} can be manipulated to ensure that $\Gamma_{out} * \Gamma_{load} = 1$ is only satisfied at one frequency, thus ensuring stable oscillations. The amplifier is stable if $\Gamma_{out} < 1$ for all values of Γ_{source} .

For unilateral amplifiers $S_{12} = 0$, so that $\Gamma_{in} = S_{11}$ and $\Gamma_{out} = S_{22}$. This makes it relatively easy to ensure that the amplifier is stable. However many amplifiers are not unilateral, making it more difficult to determine the load and source conditions where the amplifier is stable.

Stability Circles

Setting $|\Gamma_{in}| = 1$ in equation 8.4, allows it to be solved for the values Γ_{load} that form the border between stable and unstable regions of the amplifier operation. When plotted on the Smith Chart, this border forms a circle, which shows the input impedances that cause the instability. This is called the Input Stability Circle [5, 6]. Similarly, Setting $|\Gamma_{out}| = 1$ in equation 8.5 allows it to be solved for the values Γ_{source} that form the border between stable and unstable regions of the amplifier operation. When plotted on the Smith Chart, this is a circle and is called the Output Stability Circle [5, 6].

These stability circles show the border between stable and unstable regions. Depending on the values of the s parameters, the centre of these stability circles can be inside or outside the unit circle. For the input Stability Circle, if $S_{22} > 1$, then the inside of the Stability Circle is stable and if $S_{22} < 1$, then the outside of the Stability Circle is stable. Similarly, for the output Stability Circle, if $S_{11} > 1$, then the inside of the Stability Circle is stable and if $S_{11} < 1$, then the outside of the Stability Circle is stable.

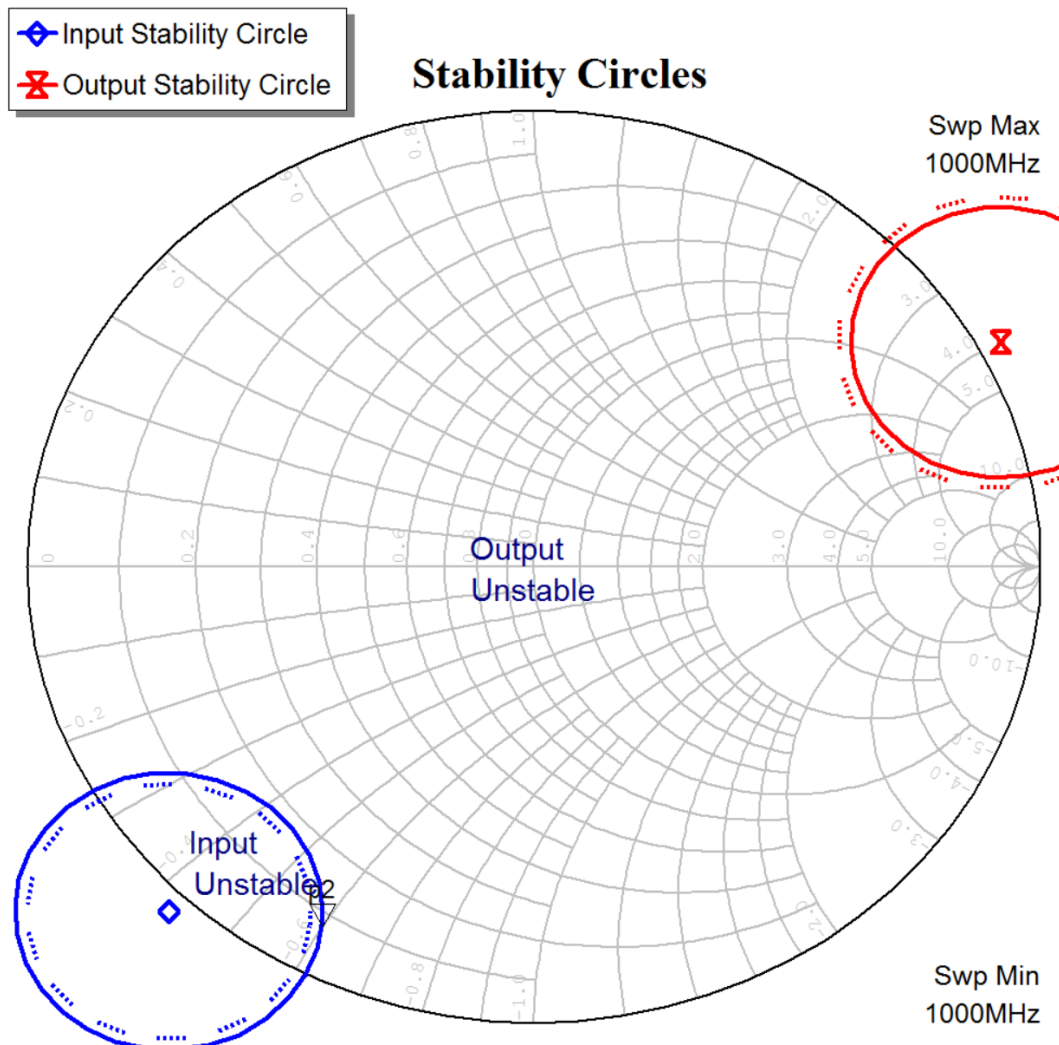


Figure 8.6. Input and output stability circles.

NI AWR DE allows stability circles to be plotted. Figure 8.6 shows the input and output stability circles for the following S parameter values: $S_{11} = 1.0300 \angle 150^\circ$, $S_{21} = 1.2 \angle 0^\circ$, $S_{12} = 0.015 \angle 10^\circ$ and $S_{22} = 0.97 \angle -45^\circ$. The blue circle is the Input Stability Circle and the Red circle is the Output Stability Circle. For the Input Stability Circle plotted in figure 8.6, $|S_{22}| < 1$ and the unstable region is inside the junction of the Smith Chart, with $|\Gamma| < 1$ and the inside of the Input Stability Circle. The area is labelled “*Input Unstable*” on figure 8.6, covers only a small area of the Smith Chart. For the Output Stability Circle plotted in figure 8.6, $|S_{11}| > 1$ and the unstable region is inside the junction of the Smith Chart, with $|\Gamma| < 1$ and the outside of the Input Stability Circle. That unstable area, is labelled “*Output Unstable*” on figure 8.6 and covers most of the Smith Chart.

Stability circles will thus allow the input and output matching to be arranged to ensure that an amplifier is stable under normal operation.

Unconditional Stability

An amplifier is unconditionally stable if $|\Gamma_{in}| < 1$ and $|\Gamma_{out}| < 1$, for all passive load and source impedances. As an example, the first version of the MAR6 amplifier was unconditionally stable. For this to occur, both the input and output stability circles lie outside the normal Smith Chart. The second version, the MAR6A amplifier is conditionally stable.

Conditional Stability

An amplifier is conditionally stable if $|\Gamma_{in}| < 1$ and $|\Gamma_{out}| < 1$, only for certain load and source impedances. As an example, the early version of the MAR8 amplifier was only conditionally stable and both input and output reflection coefficients had to be less than 0.5. For conditional stability, either or both the input and output stability circles partially lie inside the normal Smith Chart.

Stability Factors: Measures of Stability

The **Rollet's stability factor**, K is defined as:

$$K = \frac{1 - |S_{11}|^2 - |S_{22}|^2 - |\Delta|^2}{2|S_{12}S_{21}|} \quad \text{Where } |\Delta| = |S_{11}S_{22} - S_{12}S_{21}| \quad \text{Eqn. 8.13}$$

In addition, the auxiliary stability factor is defined as:

$$B = 1 + |S_{11}|^2 - |S_{22}|^2 - |\Delta|^2 \quad \text{Eqn. 8.14}$$

For unconditional stability $K > 1$ and $B > 0$.

The **Geometric Stability Factor**, μ is defined as:

$$\mu = \frac{1 - |S_{22}|^2}{|S_{22} - \Delta S_{11}^*| + |S_{12}S_{21}|} \quad \text{Eqn. 8.15}$$

This stability factor measures the distance from the centre of the Smith Chart to the nearest unstable region. For unconditional stability, $\mu > 1$. In addition, the larger the value of μ , the more stable the amplifier.

The Rollet's stability factors K and B and the Geometric Stability Factors for both the input and output of an amplifier are available as measurements in NI AWR DE, so that an amplifier's stability can easily be determined at any frequency. It is important that the stability of an amplifier is determined at all possible frequencies, since if the device is unstable it will likely oscillate. If the designer only measures the performance of the amplifier in the operating band and it is oscillating at a frequency far removed from the operating frequency, the designer will be at a loss to explain the very poor amplifier performance, until a spectrum analyser is used to check for oscillations over a wide frequency range. Note that the possibility of oscillations of an amplifier determined by these stability factors are not the only ones that cause oscillations. The lack of power supply decoupling, poor circuit layout and ground-plane integrity and EM coupling between the output and input circuits and leads are common causes of oscillation. Sometimes these oscillations can be cured by using shielding and microwave absorbers

[7] in strategic places. Figure 7.59 shows a good layout to avoid coupling between different parts of the hardware.

If the amplifier is not unconditionally stable, then the source and load must be carefully controlled to ensure that the amplifier is stable under normal operating conditions.

Design for Maximum Gain

To design an amplifier for maximum gain, the input matching network and the output matching network are both designed to provide a conjugate impedance match at the operating frequencies, thus making $G_S = 1$ and $G_L = 1$, as outlined above. Since the power gain depends on the impedance match at the input, one can plot constant gain circles on the Smith Chart, to show how the gain varies with the matching impedance. Designing an amplifier for maximum power gain may result in unstable operation.

Amplifier Noise Figure

Often an amplifier must be designed for a low noise figure. The input matching conditions for the lowest noise figure are different from those for a high power gain, so that a reduced gain is obtained from the amplifier when one designs it for low noise performance. In addition, the match for best noise may make the amplifier only conditionally stable.

This section gives a brief overview of noise figure, noise power and equivalent temperature. Pozar [5] gives a detailed description of these concepts. The noise figure (F) of a circuit block or amplifier is defined as the ratio of the actual noise at the output of the circuit, over the noise that will be obtained if the circuit is noiseless. If N_a is the noise at the amplifier output, and N_i is the noise at the input and G is the power gain of the amplifier. Often the noise is referred to the input. N_e is the noise of the amplifier output, referred to the input of the amplifier. The noise figure is thus:

$$F = \frac{N_a}{GN_i} = \frac{GN_e}{GN_i} = \frac{N_e}{N_i} \quad \text{Eqn. 8.16}$$

For an resistor of $R \Omega$, at an absolute temperature (K) of T_0 , the thermal noise (N_0) produced is:

$$N_0 = kT_0B \quad \text{Eqn. 8.17}$$

The noise figure can thus also be written as:

$$F = \frac{T_0 + T_e}{T_0} \quad \text{Eqn. 8.18}$$

where T_e is the equivalent noise temperature of the amplifier and is the additional noise temperature, referred to the input, that is caused by the amplifier and T_0 is the ambient temperature of the input of the amplifier. The noise performance of an amplifier is either; specified as a noise figure or as an equivalent noise temperature. Equation 8.18 allows the conversion from one to the other.

Often amplifiers are used in cascade, with the output of one amplifier driving another. If the first amplifier has a noise figure F_1 and a gain of G_1 and for the amplifier that follows it is F_2 , and G_2 and so on. Then for that system, the total noise figure and noise temperature can be shown to be:

$$F_{total} = F_1 + \frac{F_2 - 1}{G_1} + \frac{F_3 - 1}{G_1 G_2} + \frac{F_4 - 1}{G_1 G_2 G_3} + \dots \quad \text{Eqn. 8.19}$$

$$F_{total} = T_1 + \frac{T_2}{G_1} + \frac{T_3}{G_1 G_2} + \frac{T_4}{G_1 G_2 G_3} + \dots \quad \text{Eqn. 8.20}$$

These are known as Friis formulas for noise factor and noise temperature, after Harald T Friis [8]. They show that the noise figure of the first amplifier in a chain is the most critical. The noise figure of a Low Noise Block (LNB), such as shown in figure 10.4, which are mounted at the focal points of satellite dishes and convert the satellite signal to signals around 1 GHz with a gain of more than 60 dB, is typically 0.6 to 0.9 dB [9]. The noise figure of the LNB is the most critical parameter for these devices. It is difficult to design an amplifier, which has such low noise figures and are stable.

The interaction between stability factors, noise factors and gain are illustrated using the design of a low noise amplifier for the region of 950 to 1000 MHz using a 2SC3357/NE85634 low noise transistor. The specifications of that transistor are: NF = 1.1 dB TYP., Ga = 7.5 dB TYP. @ VCE = 10 V, IC = 7 mA, f = 1 GHz. The model for the NE85634 transistor is available from the *Libraries* \Rightarrow *Parts by Vendor* \Rightarrow *Renesas* \Rightarrow *Nonlinear* \Rightarrow *Discrete* \Rightarrow *Low Noise_Bip_Tr* \Rightarrow *2_LowNoise_Bip_Tr_(JEITA)*. That device is no longer made by Renesas, but is made by others and is still readily available. It is used in this chapter, since it nicely illustrates the problems one can encounter in the design of low noise and stable amplifiers.

The noise figure will vary with frequency. At $< 1\text{MHz}$ the noise rises due to $1/f$ noise at a rate of 20 dB per decade. This $1/f$ noise is not normally included in the model for the transistor, since external components such as coupling capacitors are likely to dominate the noise figure at those frequencies. At high frequencies the noise rises because of changes in the transistor parameters. The noise figure in these the regions rises at 40 dB per decade. In addition the noise voltage changes with collector current and voltage across the transistor. The noise figure for the transistor is shown in figure 8.7. Coleman [10] shows how the noise figure relates to different transistor parameters.

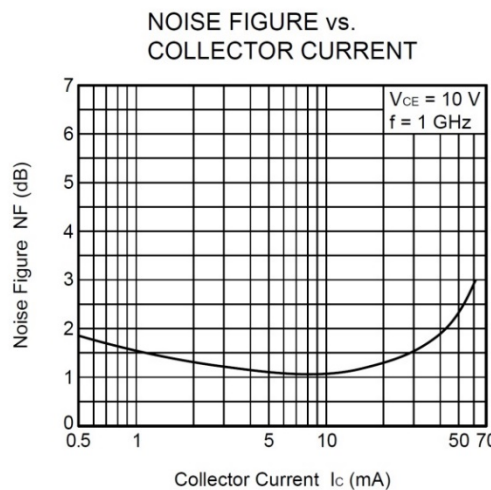


Figure 8.7. Noise figure versus collector current [11].

To start the design, a basic amplifier as shown in figure 8.8 is used. The biasing resistors are chosen to cause a 7 mA collector current, corresponding to the minimum noise figure. Note that the resulting noise figure is worse at 1 GHz than claimed in [11].

The noise figure and gain can now be calculated using computer simulation and they are shown in figure 8.9. The rise in noise figure at low frequency is due to the input coupling capacitor causing an impedance mismatch at low frequency. The rise in noise figure at

high frequency is due to changes in transistor parameters and corresponds to a drop in gain. The supply voltage, emitter resistor and bias resistor values are tuned, to obtain the best noise figure. The values shown in figure 8.8 correspond to the lowest noise figure consistent with a high power gain.

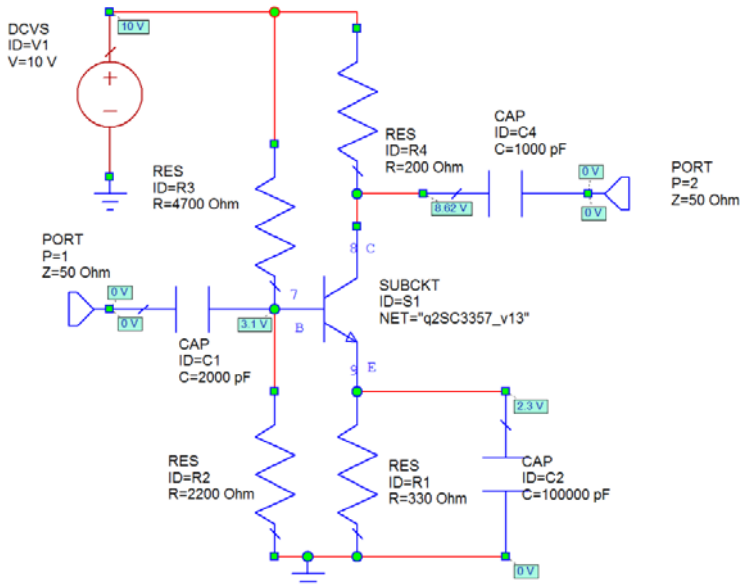


Figure 8.8. Basic low noise amplifier.

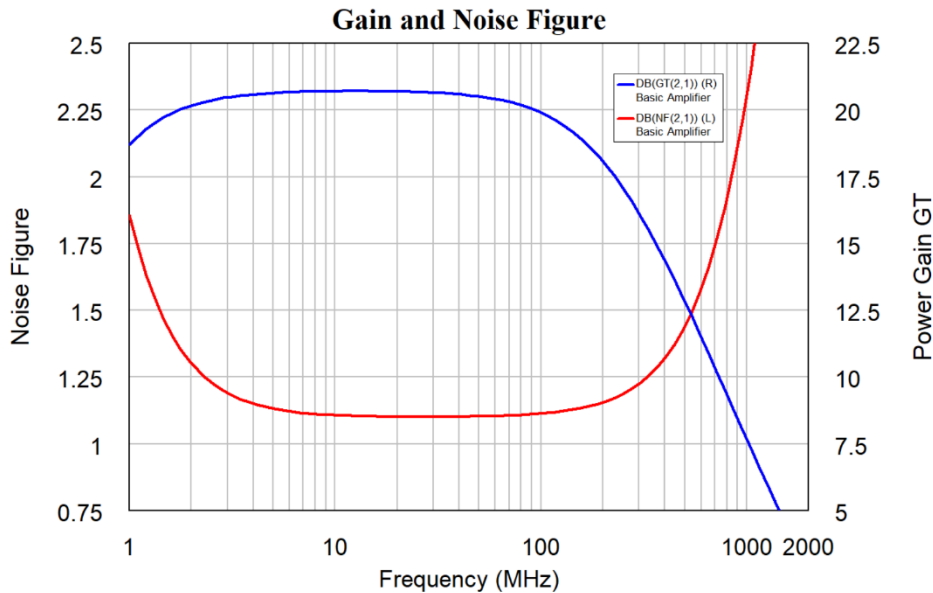


Figure 8.9. Noise figure and gain of the basic amplifier.

Figure 8.10 shows a plot of K, B and Input μ and Output μ stability factors. It can be seen that in the region of 25 MHz to 300 MHz, the amplifier is only conditionally stable. The amplifier is stable with a 50 Ω source and load impedance as shown in the gain plot of figure 8.9. Figure 8.11 shows the input and output stability circles plotted at 100 MHz, confirming that the amplifier is only conditionally stable. The Input Stability Circle is shown in pink and the Output Stability Circle is shown in blue. It can be seen that the Output Stability Circle causes the biggest problem. Figure 8.12 shows the input and output stability circles over a 50 to 1500 MHz sweep. For an unconditionally stable amplifier, the entire inside of the Smith Chart will be clear of any stability circles.

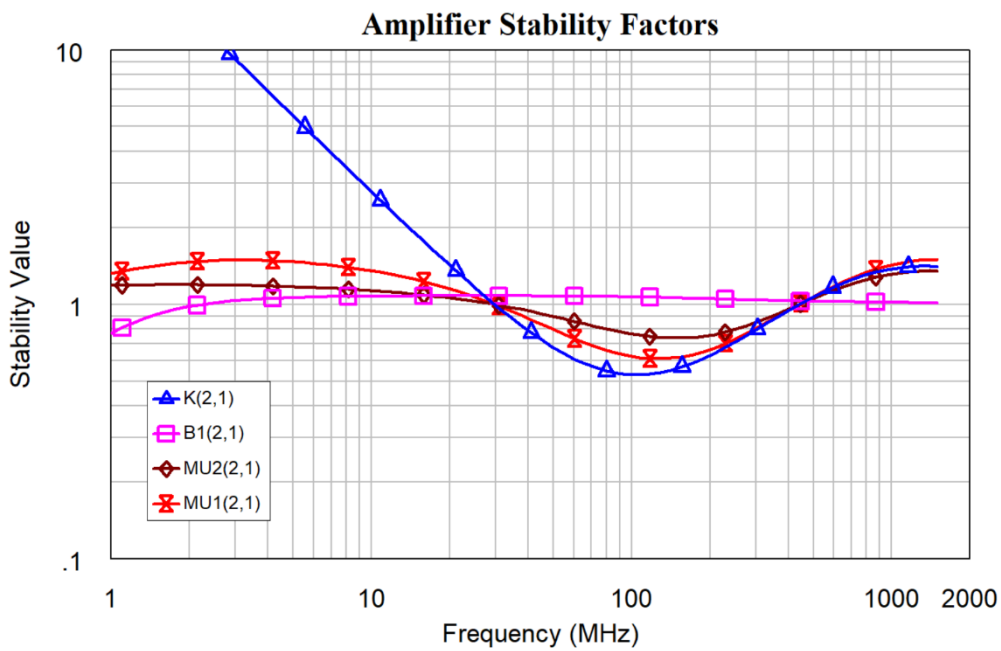


Figure 8.10. Stability factors for the basic amplifier.

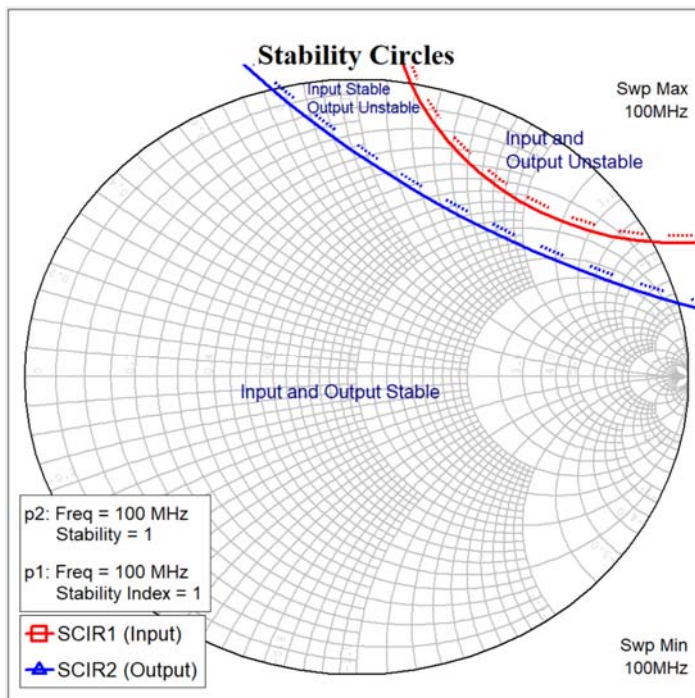


Figure 8.11. Stability input and output circles at 100MHz.

Figure 8.13 shows the constant Noise figure circles and the constant gain circles at 100 MHz. Matching the amplifier input to the centre of the constant noise circles, results in the lowest noise figure. Note that the centre of the constant noise circles lie close the origin of the Smith Chart, so that the existing $50\ \Omega$ match is good for the best noise figure. Matching the amplifier input to the centre of the constant gain circles, results in the highest gain. The centres for the circles for available power are nowhere near the centre of the Smith Chart, so that a match for noise figure will not result in the highest power gain. Normally the first stage of a low noise amplifier is matched for the lowest noise figure and the second stage is matched for the highest power gain, since equations 8.19

and 8.20 show that the noise figure of the first stage is critical, but the noise figure of later amplifier stages have much less effect.

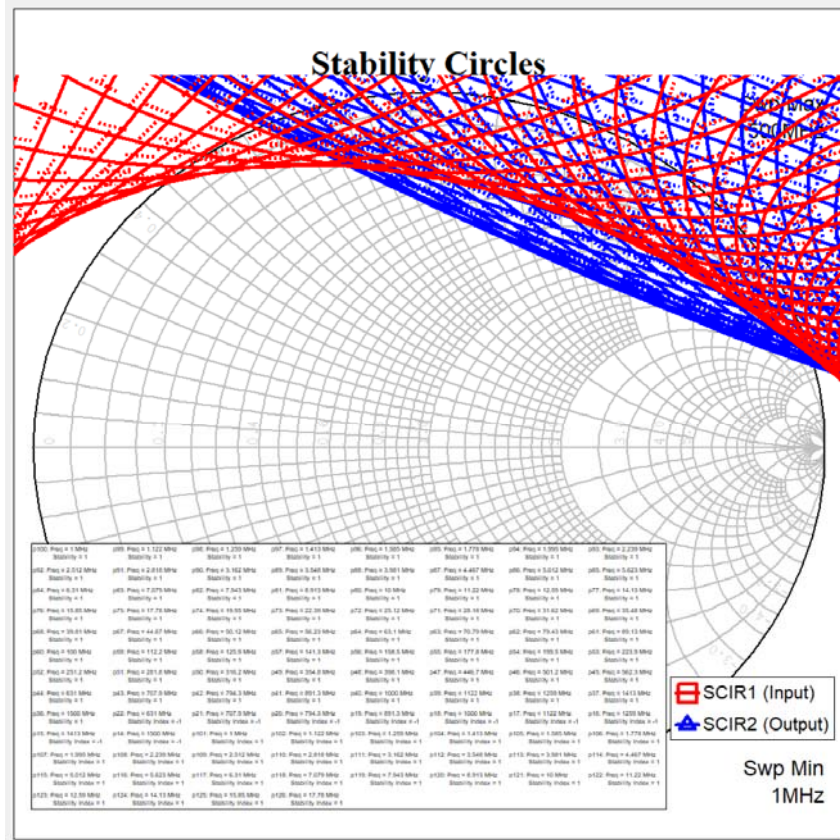


Figure 8.12. Stability input and output circles over 50-1500MHz.

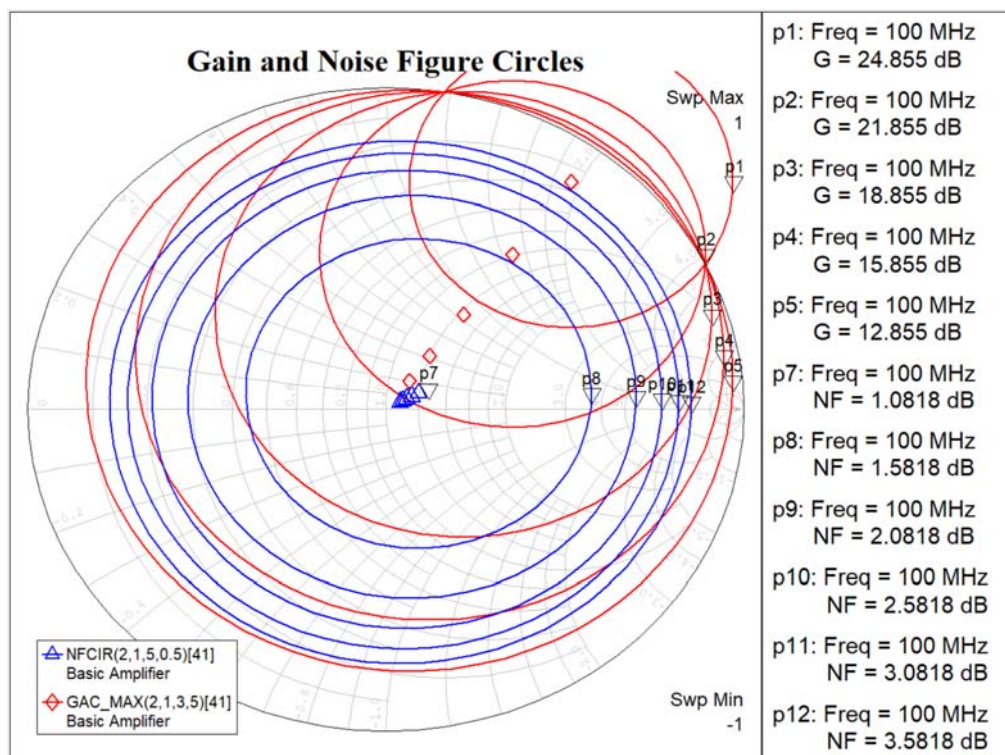


Figure 8.13. Constant gain and noise figure circles at 100 MHz.

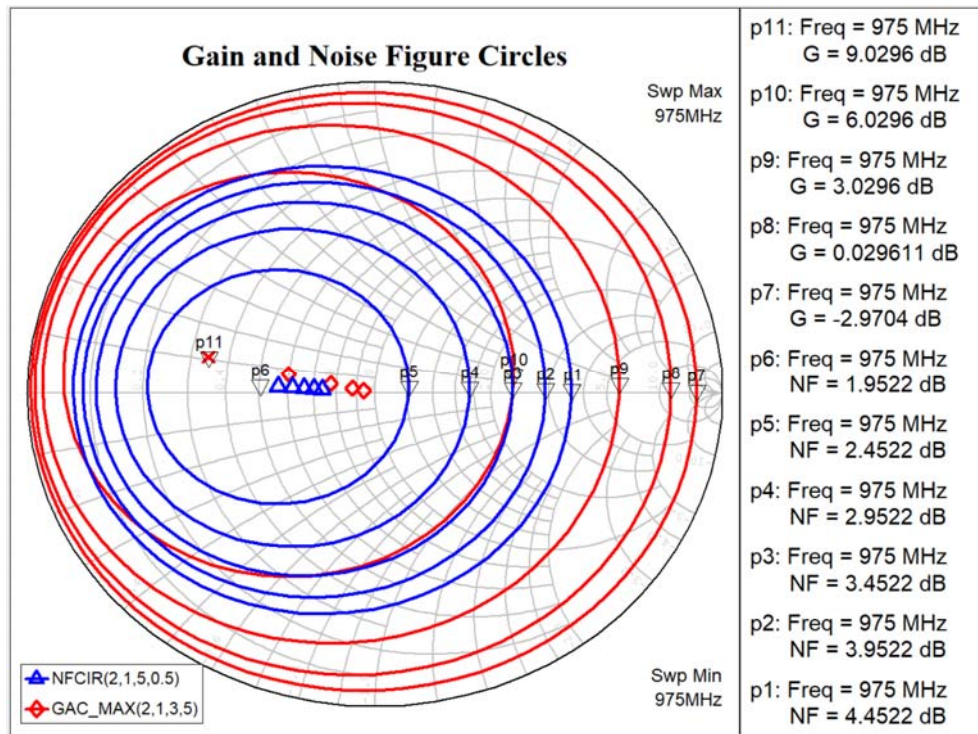


Figure 8.14. Constant gain and noise figure circles at 975 MHz.

In the region of 950 to 1000 MHz the locations of the constant gain and noise circles are very different, as shown in figure 8.14, so that the input matching needs to be changed to obtain the best noise figure. Again, the centres of constant noise figure and those of constant available power, do not coincide, so that one must either match for the best noise figure or the best power gain. From figure 8.12 and figure 8.14, it can be seen that the matching for the lowest noise at 1 GHz, will result in a worse stability, since the operating point is closer to the stability circles.

Improving the Noise Figure

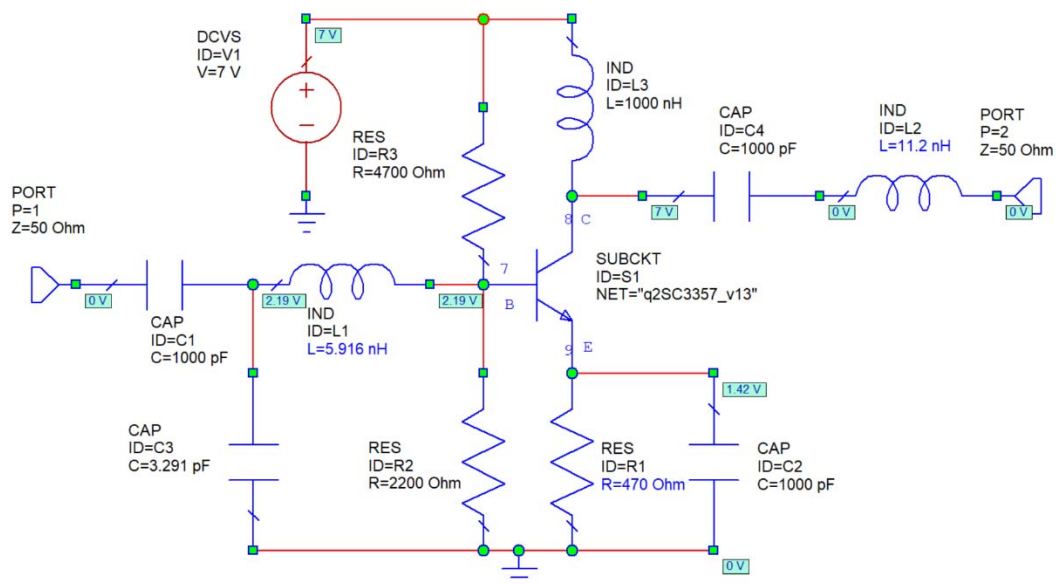


Figure 8.15. Low noise amplifier for 950-1000 MHz.

To improve the noise figure at 975 MHz, LC tuning elements C3, L1 and L2 are added and the noise figure was tuned to give the lowest noise figure. As part of that optimisation process, the value of the coupling capacitors were reduced, to prevent oscillations at low frequency. This results in the circuit shown in figure 8.15.

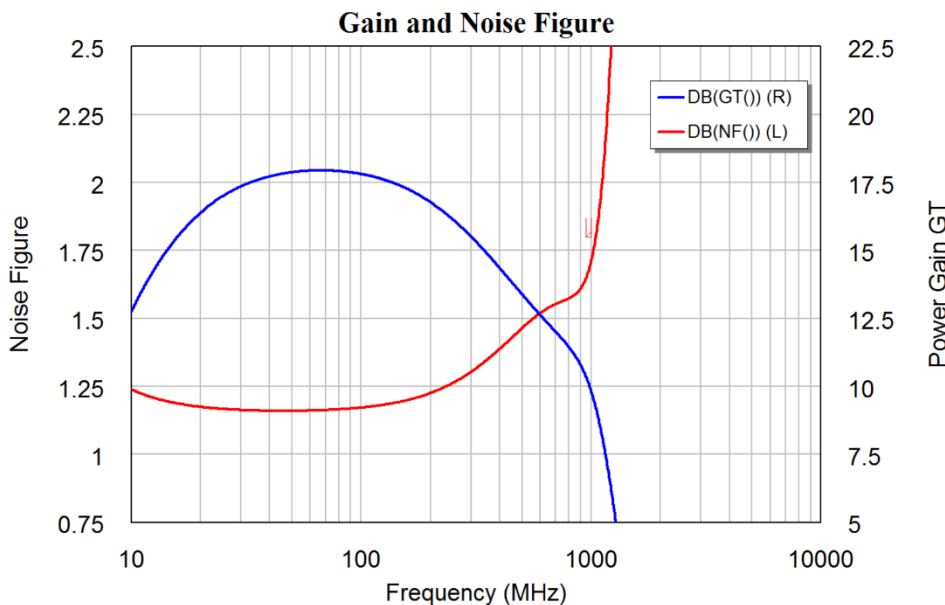


Figure 8.16. Noise figure and gain of the 950-1000 MHz amplifier.

By comparing figure 8.9 and figure 8.16, it can be seen that the only a slight improvement in the noise figure at 950-1000 MHz has been obtained. The operating frequency of the amplifier is very close to the maximum useable frequency for the transistor and it is much better to use a higher frequency transistor, such as the NESG3031, so that the noise figure and gain are flatter at the operating frequency. The NESG3031 can easily have a gain greater than 20 dB and a noise figure less than 0.75 dB at a frequency of 1 GHz. Such transistors are however likely to be more expensive. The use of the 2SC3357 transistor allows stability problems and their solutions to be demonstrated.

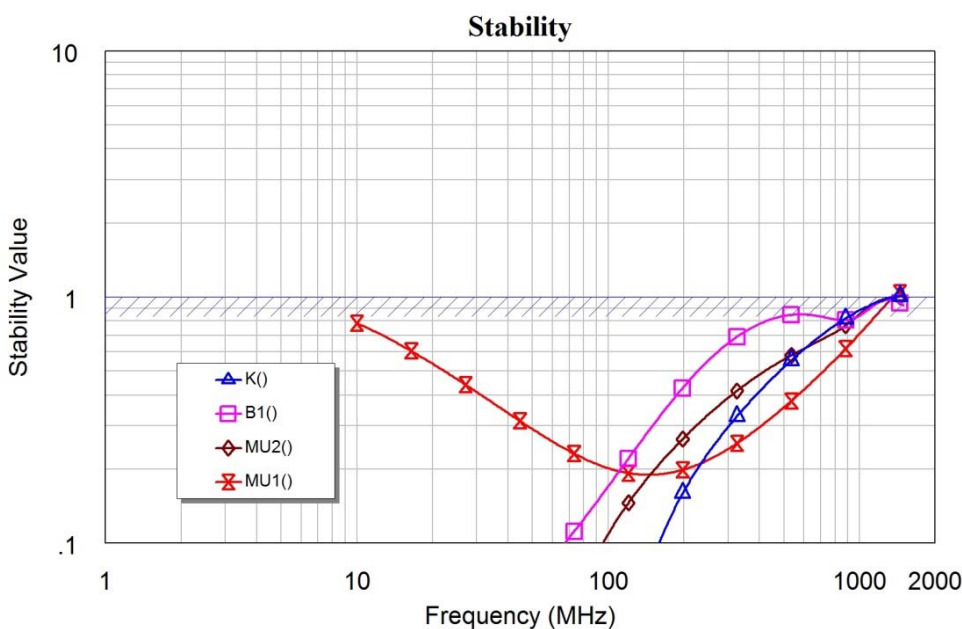


Figure 8.17. Stability factors for the amplifier of figure 8.15.

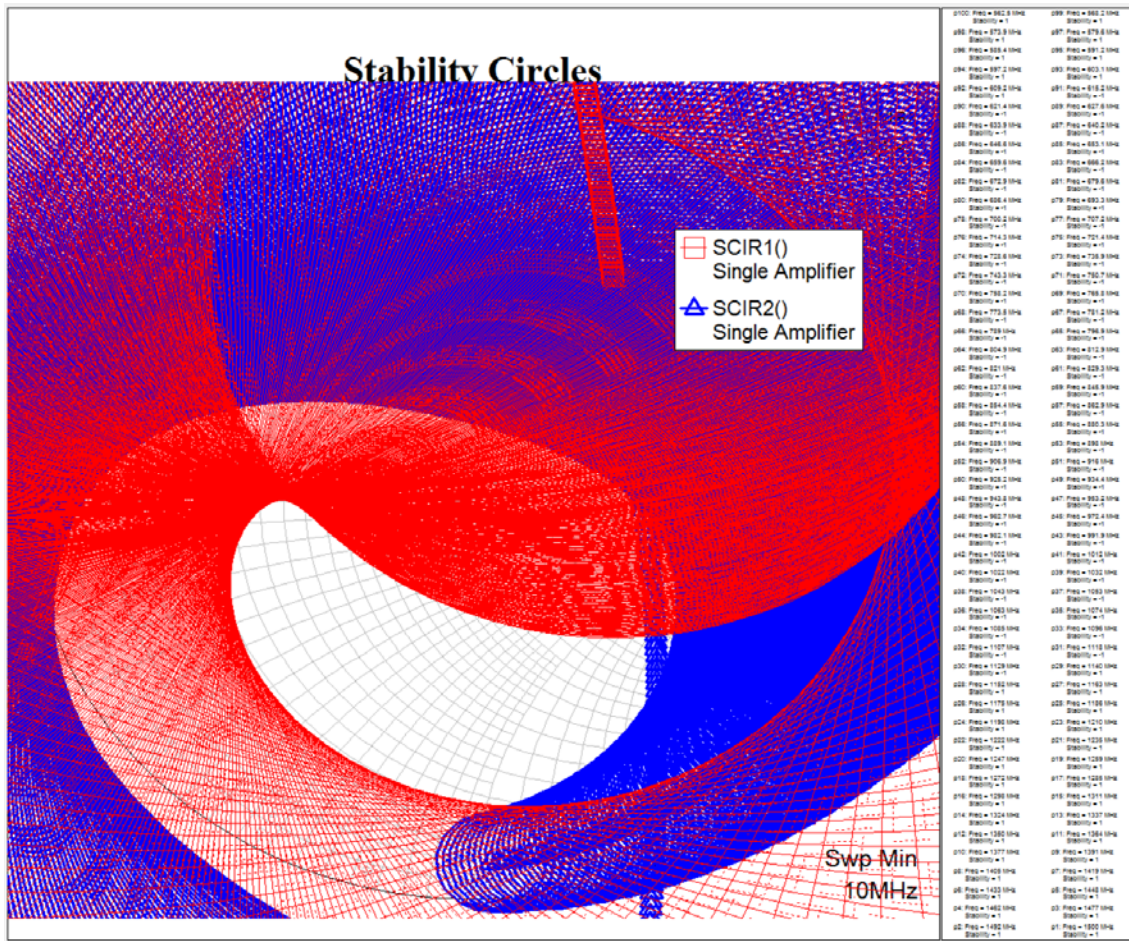


Figure 8.18. Stability input and output circles, 50 - 1500MHz, for the amplifier of figure 8.15.

Comparing figure 8.17 with figure 8.10 shows that the amplifier is far less stable than the basic amplifier. The amplifier is unconditionally stable in the 950 - 1000 MHz frequency region. However, it is close to instability in the 30 to 300 MHz frequency region. Comparing figure 8.18 with figure 8.12, shows that the clear area of the Smith Chart, corresponding to stable operation in figure 8.12 than in figure 8.18. Figure 18 also shows that one must have an impedance mismatch for the amplifier to be stable since the centre of the smith chart is covered by the input stability circles. For clarity, a narrow line thickness has been used of the front, red input stability circles and a wide line thickness has been used for the behind, blue output circles.

Figure 8.19 shows the gain and noise figure circles of the amplifier at 975 MHz. Note that the centre of the noise figure circles has been shifted to the origin due to the input tuning. The output tuning has little effect on the noise figure. The best noise figure that can be obtained is 1.68 dB. The output matching is adjusted, to increase the output power at 975 MHz as much as possible.

In many practical situations, particularly with power amplifiers, the transistors used will have a falling gain at 20 dB per decade over the operating range. As shown in the above example, that can lead to instability at frequencies far removed from the operating region. Any simulation for a practical design must include a stability analysis over a very wide frequency range.

It is not possible to improve the stability by changing the output L3, of figure 8.15, to a tuned network and thus reducing the bandwidth of the amplifier, since that result in

impedances close to the edge of the Smith Chart for some frequencies, thus worsening the stability. It is in general very difficult to ensure unconditional stability and a low noise figure. In some instances, the exact source impedance, from say an Antenna, and load impedance, from following amplifiers is known and the amplifier can be kept stable. In other instances, the source and load impedances are not well known or well controlled and the amplifier design must then ensure that the amplifier is unconditionally stable.

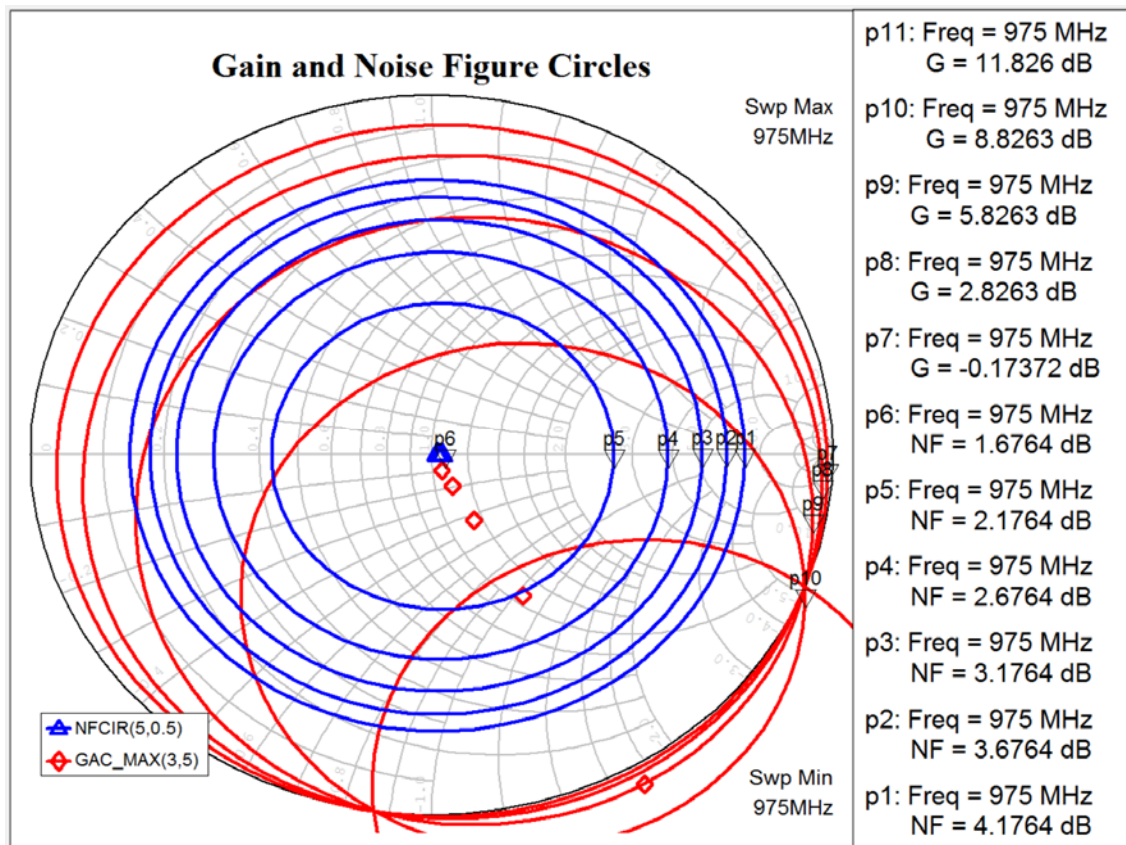


Figure 8.19. Gain and noise figure circles for the 950-1000 MHz amplifier.

Improving Amplifier Stability

Couplers at Input and Output

If the amplifier is conditionally stable in the required operating frequency region, then the stability may be improved by using a branch line coupler or other 90° hybrid and have two identical low noise amplifiers connected to them, as shown in figure 8.20.

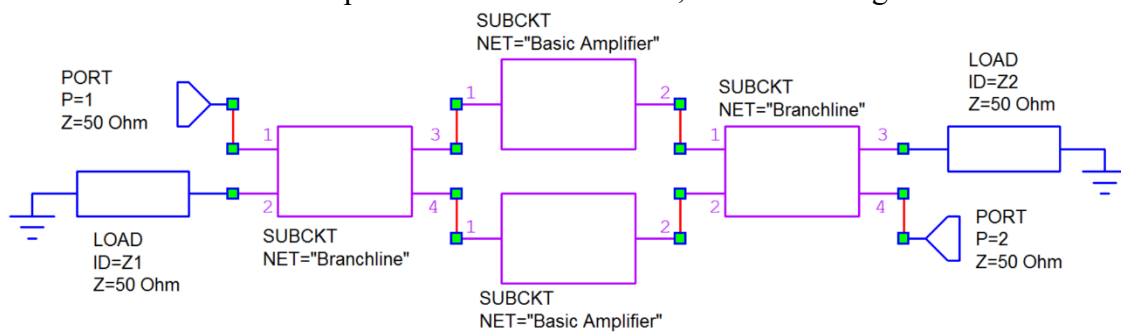


Figure 8.20. Dual low noise amplifier.

The use of 90° hybrids causes each of the amplifiers to see a VSWR of better than 2:1 in all instances and any reflections from the inputs of the amplifiers will end up in the load resistor connected to the port. That will improve the stability close to the operating frequency but may make the stability away from the operating frequency worse. In the circuit of figure 8.15, the amplifier is unconditionally stable in the 950 MHz to 1 GHz region, so this technique will not have any effect. The bandwidth of this amplifier is too wide for Branchline couplers to be used to improve the stability, as these are narrowband devices. However, other 90° hybrids, like the backward-coupled transmission-line hybrid can be used effectively.

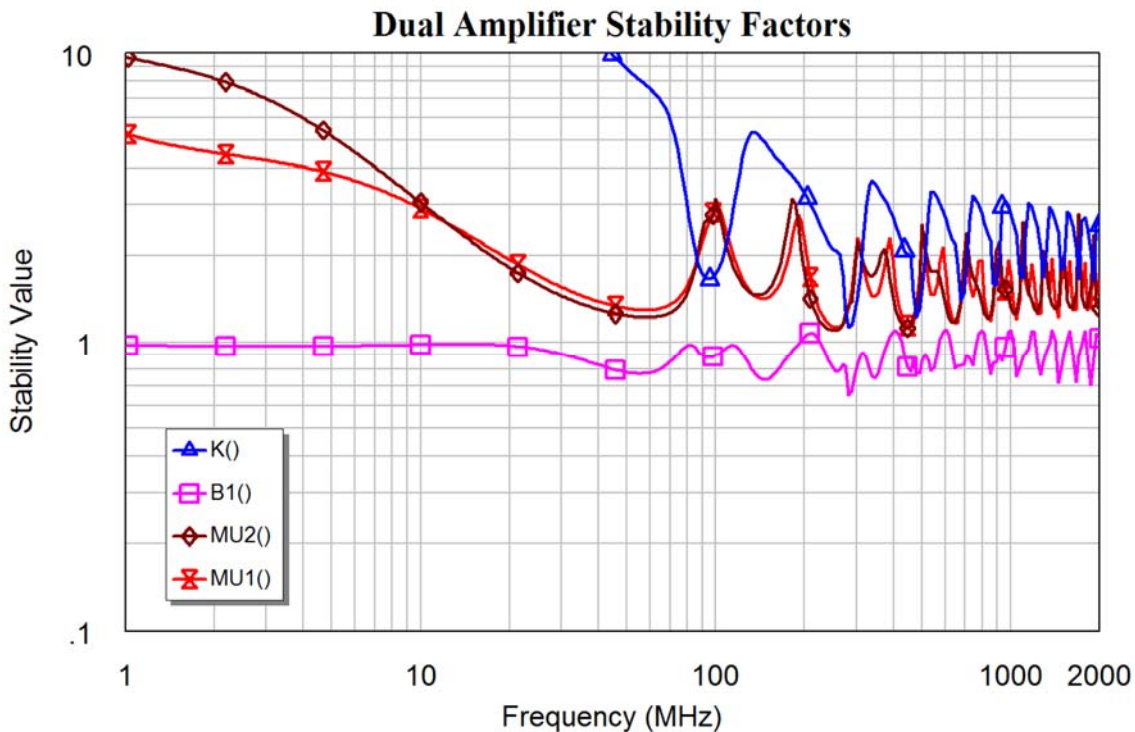


Figure 8.21. Stability factors for the dual amplifier.

To illustrate the changes in amplifier stability, the amplifier of figure 8.8 is used in the configuration of figure 8.20. Figure 8.10 shows that at 100 MHz this amplifier is only marginally stable. Figure 8.21 shows the stability factors for this dual amplifier using two Branchline couplers with a centre frequency of 100 MHz. This amplifier is unconditionally stable.

The amplifier will however only give a low noise figure in the region where the Branchline coupler operates as a proper power divider. That is only a 20% bandwidth around 100 MHz. In many instances a 20% bandwidth is sufficient. Having an unconditionally stable amplifier will then allow the input matching to be changed, to the location on the Smith chart that provides the lowest noise figure, regardless of stability considerations.

This technique will provide a worst case VSWR of 2:1 for each individual amplifier. If that results in unconditional stability, then the dual amplifier will also be unconditionally stable. If the individual amplifiers are not stable with a VSWR less than 2, then the dual amplifier may also not be stable. For example applying Branchline couplers centred at 975 MHz to the amplifier of figure 8.15, results in an amplifier that oscillates.

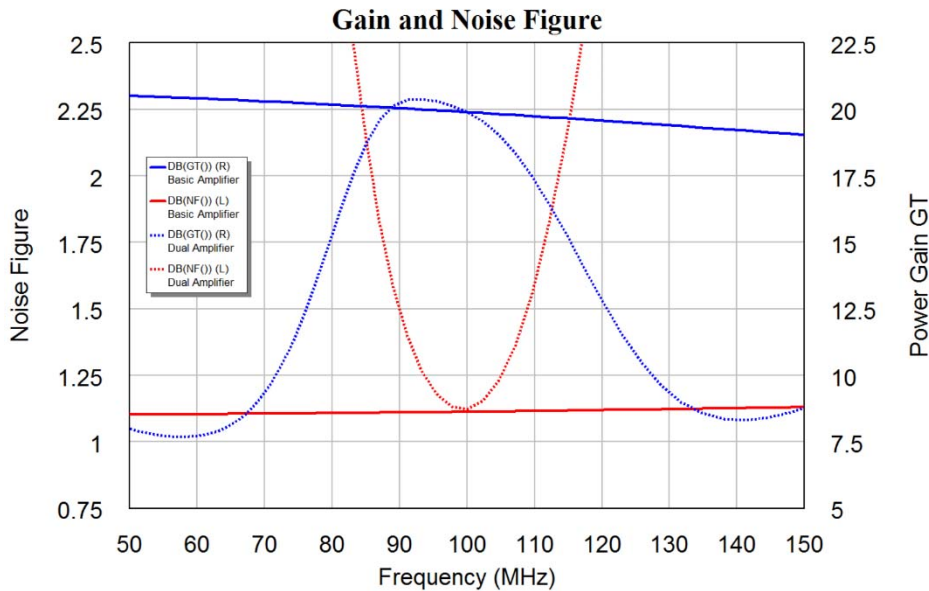
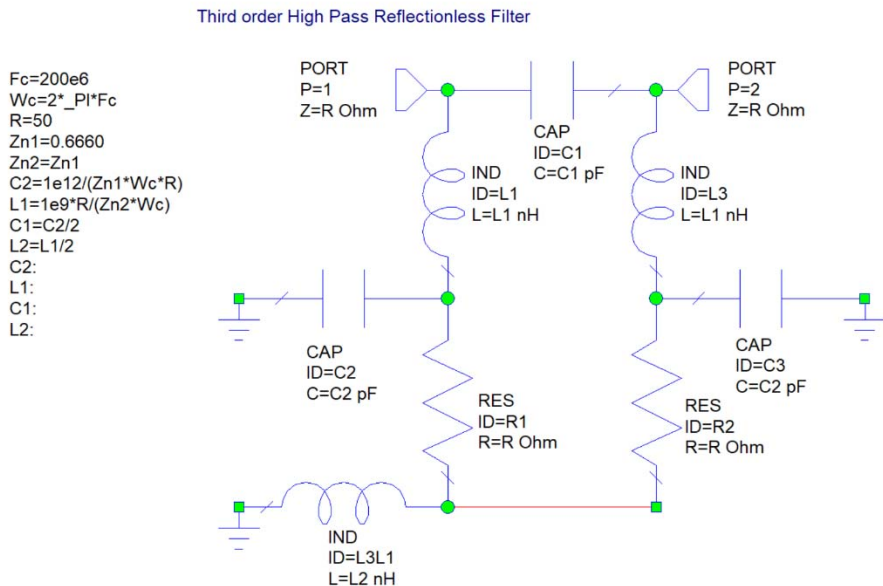


Figure 8.22. Stability factors for the dual amplifier.

Alternately adding a circulator at the input, and output will make the amplifier stable. Circulators are however, narrowband devices and the stability outside their bandwidth needs to be carefully investigated as part of the design procedure.

Bandwidth Limiting using Reflectionless filters

Figure 8.23. Reflectionless high pass filter with $F_c = 200$ MHz.

In many cases, the amplifier may be conditionally stable outside the operational frequency range. If the low noise amplifier is used at the input of a receiver, filters may be required to prevent unwanted input signals from passing through the filter. Using conventional filters is likely to make the amplifier less stable. However using reflectionless filters, as described in chapter 7, to the input and/or output may make the amplifier more stable. If this amplifier is to be used above 300 MHz, then a reflectionless

high pass filter with a 200 MHz cut off frequency will ensure signals above 300 MHz are passed amplified without loss. Figure 8.23 shows the circuit of the reflectionless filter used. It is similar to the filter in figure 7.14, but with a 200 kHz cut off frequency. Those filters can be applied at the input or the output of the amplifier. The best stability is obtained when the reflectionless filters are included at both the input and the output of the amplifier. The amplifier is the same as is shown in figure 8.8. Comparing figures 8.24 and 8.10 shows that the amplifier stability is improved significantly.

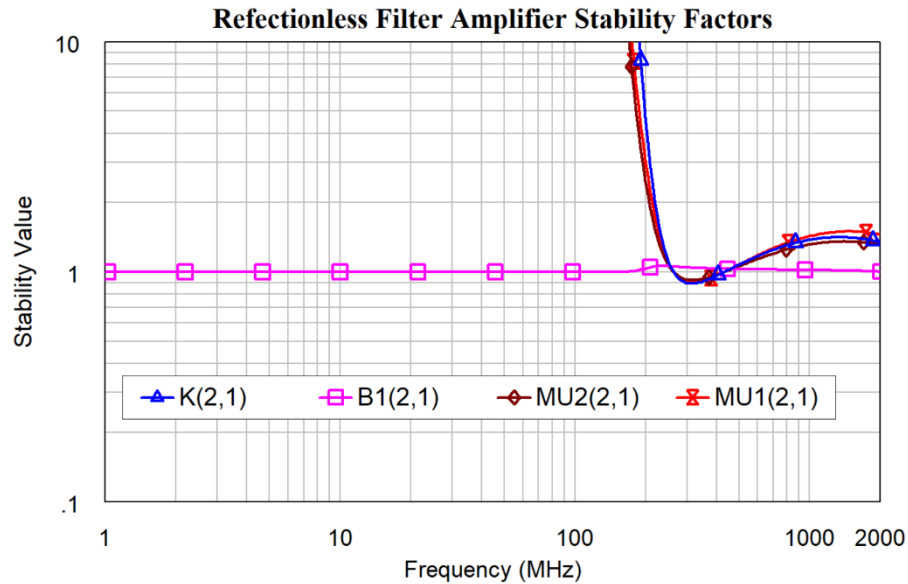


Figure 8.24. Stability factors for amplifier with reflectionless filters.

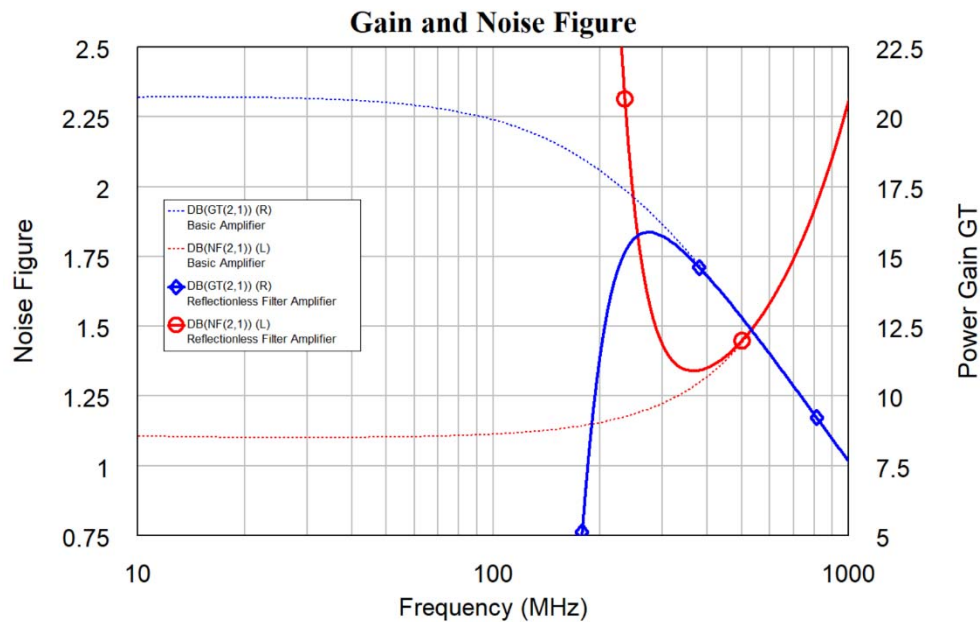


Figure 8.25. Gain and Noise figure of amplifier with reflectionless filters.

Figure 8.25 shows the resulting gain and noise figure of the amplifier, with and without the reflectionless filters. Above 300 MHz the filters have little effect on the amplifier performance. Reflectionless filters can thus be used to stabilise low noise amplifiers and prevent them being overloaded by out of band signals, without affecting the noise figure and gain of the amplifier in the desired frequency band.

Resistors at Output

Generally, if one adds resistors at the input, then the noise figure of an amplifier will increase, however the stability can be improved. Adding resistors at the output will reduce the gain but can make the amplifier unconditionally stable. There are three possible ways to add resistances to the output:

- 1) In series with the output, thus increasing the impedance that the amplifier sees.
- 2) As a shunt across the output, thus decreasing the impedance that the amplifier sees.
- 3) As a T or Pi Pad, thus keeping the impedance that the amplifier sees constant.

For the amplifier of figure 8.8, inserting a $110\ \Omega$ resistor in series with the output, reduces the amplifier gain at 10 MHz to 17.5 dB and at 100 MHz to 16 dB. It makes the amplifier unconditionally stable without significantly affecting the noise figure in the 10-100 MHz region, making the minimum noise figure 1.11dB, compared to 1.10 dB in figure 8.9. However, the noise figure at 1 GHz rises from 2.31 dB in figure 8.9 to 3.09 dB with this $110\ \Omega$ series resistance.

For the amplifier of figure 8.8, inserting a $120\ \Omega$ resistor as a shunt across the output, reduces the amplifier gain at 10 MHz to 18.2 dB and at 100 MHz to 17.5 dB. It makes the amplifier unconditionally stable without significantly affecting the noise figure in the 10-100 MHz region, making the minimum noise figure 1.13dB, compared to 1.10 dB in figure 8.9. However, the noise figure at 1 GHz rises from 2.31 dB in figure 8.9 to 2.5 dB with this $120\ \Omega$ shunt resistance. The amplifier will this have a higher gain and a better noise figure at 1 GHz than using the series resistance.

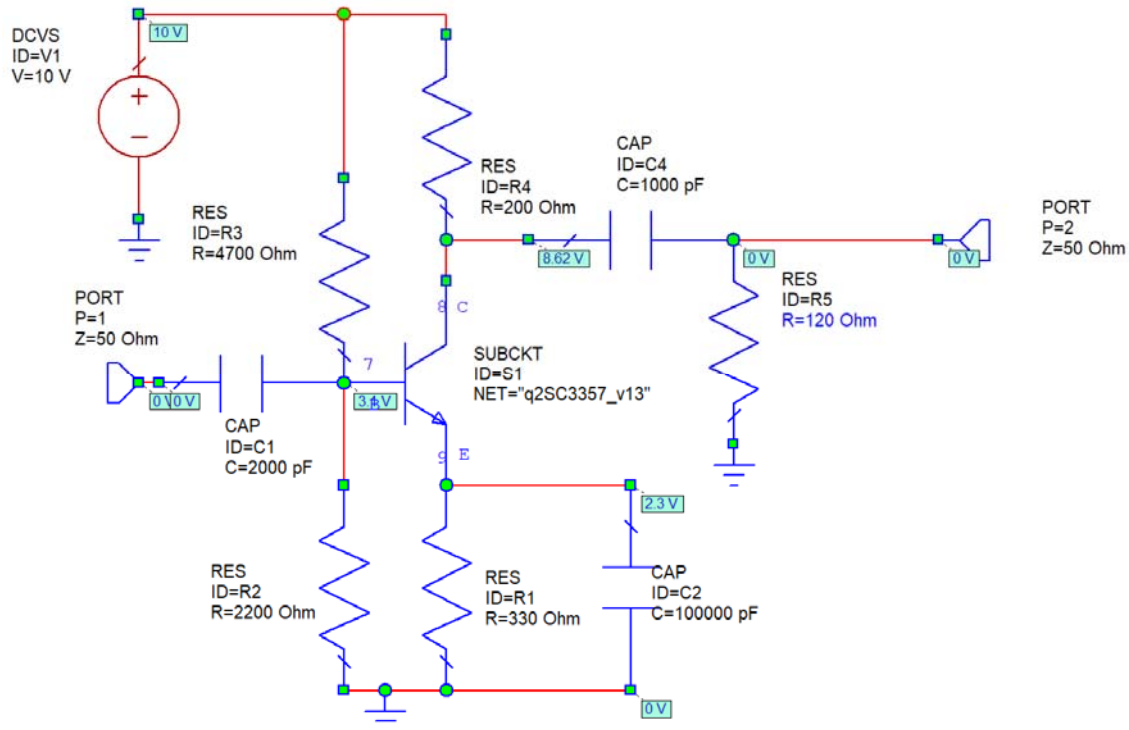


Figure 8.26. Stable low noise amplifier.

For the amplifier of figure 8.8, inserting a 2.3 dB $50\ \Omega$ Pi resistor pad at the output, reduces the amplifier gain at 10 MHz to 18.4 dB and at 100 MHz to 17.6 dB. It makes the amplifier unconditionally stable without significantly affecting the noise figure in the 10-100 MHz region, making the minimum noise figure 1.135 dB, compared to 1.10 dB in figure 8.9. However, the noise figure at 1 GHz rises from 2.25 dB in figure 8.9 to 2.6 dB with this 2.3 dB pad. The amplifier will this have a higher gain but a worse noise figure at 1 GHz than using the shunt resistance.

In this situation, the shunt resistance provides the better performance of the three options. That is not always the case. Figure 8.26 shows the resulting circuit.

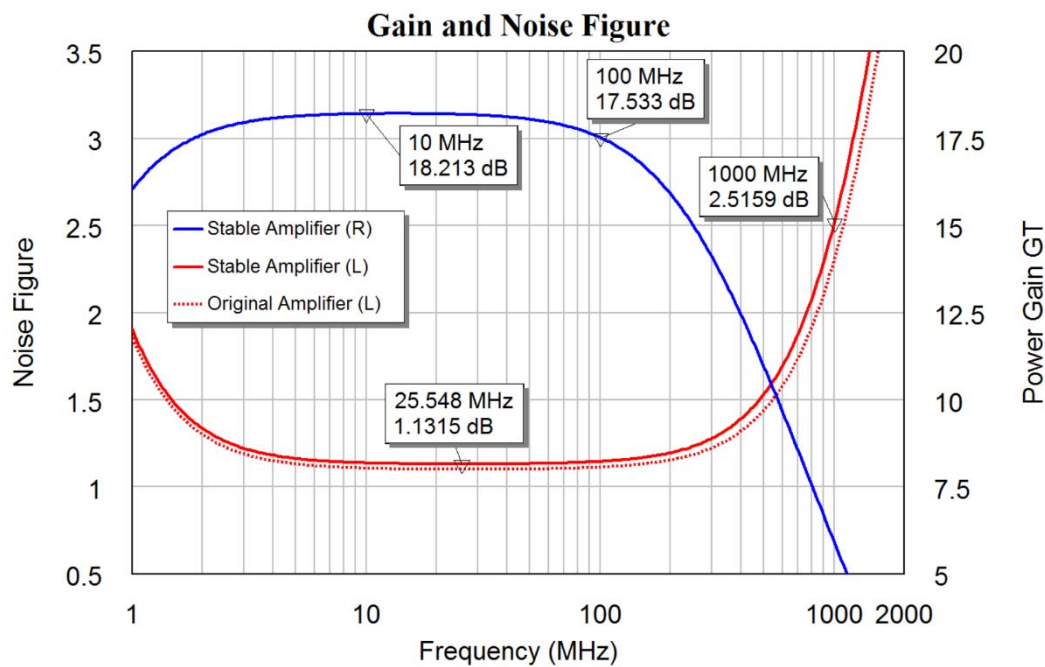


Figure 8.27. Noise figure and gain of the amplifier of figure 8.26.

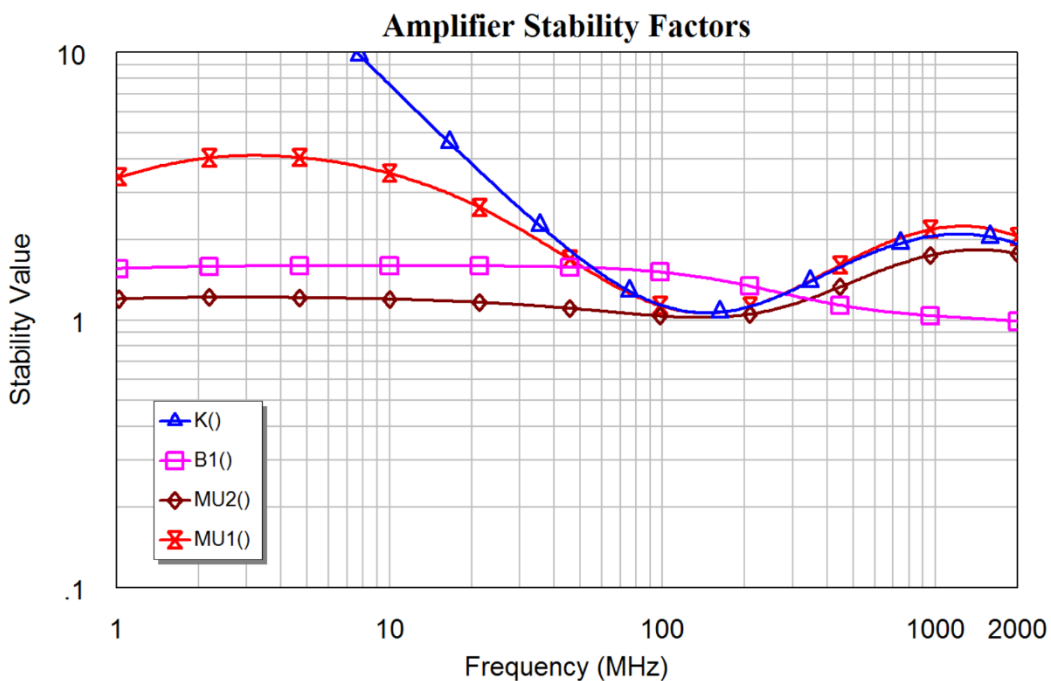


Figure 8.28. Stability factors of the amplifier of figure 8.26.

Figure 8.27 shows the Gain of the amplifier. Comparing this with figure 8.9 shows that the gain has been reduced by 2.5 dB in order to make the amplifier unconditionally stable. This loss of gain can be compensated for in subsequent amplifier stages, without affecting the noise figure. Figure 8.27 also plots the noise figure of the stable amplifier of figure 8.26 as the solid red line and the conditionally stable amplifier of figure 8.8 as the dotted red line. It can be seen that making the amplifier stable has only had a slight effect on the noise figure.

Adding resistors at the output will make the amplifier more stable whilst providing a low noise figure over a wide bandwidth. It is however not possible to make the amplifier of figure 8.15 stable, whilst maintaining a better noise figure at 1 GHz than the amplifier of figure 8.8.

Because of the frequency limitations of this 2SC3357 [7] transistor, if it is to be specially used as a low noise amplifier in the 950 MHz to 1 GHz frequency band, then it would be better to use a different transistor, which has a wider frequency response. The datasheet for the 2SC3357, as shown in figure 8.7 claims a noise figure of 1.1 dB at 1 GHz. However no test circuit is provided and that noise figure could not be obtained using the model for the 2SC3357 transistor available from the χ Libraries \Rightarrow Parts by Vendor \Rightarrow Renesas \Rightarrow Nonlinear \Rightarrow Discrete \Rightarrow Low Noise _Bip_Tr \Rightarrow 2_LowNoise_Bip_Tr_(JEITA).

References

Note: all web addresses were checked in May 2018.

1. MiniCircuits, MAR6+ data sheet, <http://www.minicircuits.com/pdfs/MAR-6+.pdf>
2. MiniCircuits, Gali S66+ data sheet, <http://www.minicircuits.com/pdfs/GALI-S66.pdf>
3. Smith, P. H. “*Transmission Line Calculator*”, Electronics, Vol. 12, No. 1, pp 29-31, January 1939.
4. Smith, P. H. “*An Improved Transmission Line Calculator*”, Electronics, Vol. 17, No. 1, p 130, January 1944
5. D. M. Pozar, “*Microwave Engineering*” 3rd Edition, Wiley, 2005, Section 4.3 and Chapter 11. ISBN 0 471 44878 8
6. R. Gilmore, “*Practical RF Circuit Design for Modern Wireless Systems*”, Artech House, 2003.
7. Ecosorb Microwave absorber. <http://www.eccosorb.com/products-eccosorb-high-loss-absorbers.htm>
8. Harald T Friis Biography http://ethw.org/Harald_T._Friis
9. C. Coleman; *An introduction to Radio Frequency Engineering*, Cambridge University Press, 2004. ISBN 0 521 83481 3.
10. NORSAT LNB, <http://www.norsat.com/solutions/microwave-products/lnb-ku-band/>
11. Renesas Electronic Corporation (NEC): 2SC3357 Low Noise transistor Data sheet <https://www.renesas.com/en-n/doc/YOUSYS/document/003/PU10211EJ01V0DS.pdf>

Chapter 9

Impedance Matching of Power Amplifiers

Introduction

In order to obtain the most power from a bipolar or field effect transistor, the input and output impedances of the device must be matched to that of the circuit in which it is placed. Similarly, if an antenna is to be driven effectively, the antenna needs to be matched. For the maximum power transfer, the source impedance and the load impedance must be a conjugate match, that is the resistive parts must be the same and the imaginary parts must be the same magnitude but opposite polarity.

Large Signal Parameters

For power transistors, the large signal input and output impedances and the large signal S parameters are very different from the small signal impedances and small signal S parameters. For a given transistor, small signal parameters should be used for input signals such that are small, so that the device behaves in a linear manner, i.e. the superposition and scaling of signals is valid. The large signal parameters should be used in designs for the same device, if the magnitude of the input signals are such that, the device no longer behaves in a linear manner.

Types of Matching

Transformer Matching: RF Transformers can be used for wideband impedance-matching. The main limitations are the restricted range of available impedances (due to the turns-ratios being limited) and the frequency limitations on transformers.

LC Matching: Inductors and capacitors are used to provide the impedance transformation. LC matching results in a relatively narrow bandwidth match. LC matching is very practical at frequencies up to 1 GHz. Above 1 GHz, transmission-line matching is more economical. LC matching permits easy tuning of the match to allow for device variations.

Transmission-Line Matching: A transmission-line of a required length and Characteristic Impedance is used to obtain the required composite match. Such a match tends to be of a broader frequency range than LC matching and can be applied at frequencies above 100 MHz. Below 100 MHz the transmission-lines required tend to be too long to be practical. It is difficult to tune the length and characteristic impedance of a transmission-line once constructed.

For each application, each of the above matching techniques must be evaluated against the design criteria and the most appropriate technique selected.

Choice of Components and Q Value

It is very important that the value of capacitors and inductors used be measured at the operating frequency. Many capacitors are not suitable for RF applications, as their self-resonance frequency is below the required operating frequency. For power applications, inductors need to be selected for the required current carrying capability and inductors with ferrite cores may not be suitable as their losses may be too high.

For a simple parallel tuned network, like the Pi network, the circulating current in a resonator is approximately Q times the external load current. For a 50 Watt amplifier, driving a 50Ω load, the load current is 1 Amp. For $Q = 10$, the current circulating in the Pi network is thus of the order of 10 Amps. This can cause significant heating and failure of the components. For some networks like both the T networks and the Bandpass L network, very high voltages can be experienced at some nodes and this can lead to voltage breakdown of components. The higher the Q , the higher the stress on the components. A high Q value can also cause the matching network to drift out of match as the components change due to temperature. In general a Q value as low as possible is desirable, as this will give the widest bandwidth match and the lowest component stress. If the network is to be used as an output-matching network of an amplifier and harmonics are to be filtered as well, a higher Q value can be considered, since the higher the Q , the higher the attenuation at the amplifier harmonics. For amplifier output networks, where harmonic filtering is required, cascaded matching networks preferred as a means to achieve the required harmonic attenuation. To obtain a wide bandwidth and use a low Q , successive impedance transformations are normally used, as described in this chapter, in the section on broadband matching.

Since the current and voltage limits in the output-matching networks are very important, a trade-off between the Q value and the order of the filter will need to be considered sections, in order to achieve the required harmonic attenuation and bandwidth.

LC Matching

In LC matching, inductors and capacitors are used to obtain the required conjugate impedance match. The equations for calculating the components required are contained in Motorola Application Note AN267 [1]. LC matching is very practical for power amplifiers up to 1 GHz. A good indication of the suitability of LC matching for a transistor can be obtained by noting the type of matching used for test circuits in the manufacturer's data sheet for the transistor.

Because it is easy to tune the matching network using variable capacitors, these LC matching networks are normally used by the manufacturers to determine the input and output impedance of the devices. The device is placed in a test jig and the matching network is adjusted to obtain the required output power at a good efficiency and with a low input return loss. The values of the resulting LC matching components are then used to determine the input and output impedance of the device.

Motorola AN267 [1] describes 4 types of matching networks. In all the equations used in this chapter, the device impedance is R_d+jX_d and the load impedance is R_L . That notation is different from AN267, where R_1 and R_L can readily be confused, particularly if a lowercase L is used. In the equations presented here, it is not assumed that the device is capacitive, so that X_d is used for the reactive part of the device impedance, instead of $-X_{cout}$, as in AN267. For the Pi Network, in AN267, the reactive part of the device impedance must manually be included in the matching network capacitance. The reactive part is included in equation 9.1.

In AN267 [1], different expressions for A and B are used for the bandpass T and the lowpass T networks. In this book, consistent expression for A and B are used. In AN267 the term A for the bandpass T network is wrong. The LC matching equations 9.1 to 9.16 presented in this book are consistent and correct.

In the designs presented here, the equations for the matching networks are evaluated inside AWRDE. This allows design parameters to be changed or optimised and allows the effect of such design parameters changes to be observed.

Pi Network

The Pi matching network is very useful for matching high impedance sources to $50\ \Omega$ loads. Pi matching is normally used in valve, or tube, amplifiers. For high power solid-state devices, the impedance values become impractical with very large capacitors and very small inductors being required. Figure 9.1 shows the Pi network used for matching.

To obtain the component values, firstly decide on a Q value for the matching network. The Q value will affect the bandwidth, harmonic attenuation and component stress. For the Pi network, the input impedance needs to be a parallel network, so that a series to parallel transformation may need to be applied before the network evaluation as shown in equation 9.1, which transforms the device impedance of R_D+jX_D into R_P in parallel with X_P . The equations for the Pi network in AN267 assume that the device is resistive and that any reactive impedances are compensated for after the Pi network is designed.

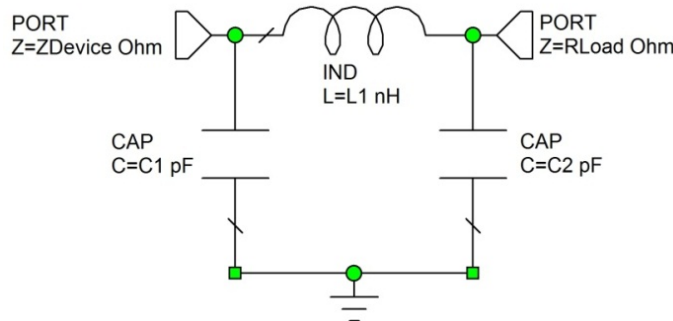


Figure 9.1. Pi matching network.

The equations in the included MWO files handle reactive parts correctly. The complete equations for the Pi matching network are as follows:

Type equation here.

$$R_p = \frac{R_D^2 + X_D^2}{R_D} \quad X_p = \frac{R_D^2 + X_D^2}{X_D} \quad \text{Eqn. 9.1}$$

$$Y_{C1} = \frac{1}{X_{C1}} = \frac{Q}{R_p} + \frac{1}{X_p} \quad \text{Eqn. 9.2}$$

$$X_{C2} = R_L \sqrt{\frac{\frac{R_p}{R_L}}{(Q^2 + 1) - \frac{R_p}{R_L}}} \quad \text{Eqn. 9.3}$$

$$X_L = \frac{QR_p + \frac{R_p R_L}{X_{C2}}}{Q^2 + 1} \quad \text{Eqn. 9.4}$$

Note that $Q^2 + 1$ must be larger than R_P/R_L for X_{C2} to be valid, so that there is a minimum Q value for a given impedance transformation ratio.

Low Pass T Network

The low pass T network is very good for use as an output-matching network for a power amplifier stage, where the amplifier is to be connected to an antenna. Having a series inductor (L_1) as the element connected to the device results in an open circuit to the second harmonic currents, resulting in a reduced current flow through the transistor and resulting in a higher efficiency. However, since the output voltage is more distorted a higher inter-modulation distortion may result. For more severe filtering of harmonics, a cascaded set of low pass matching networks is desirable.

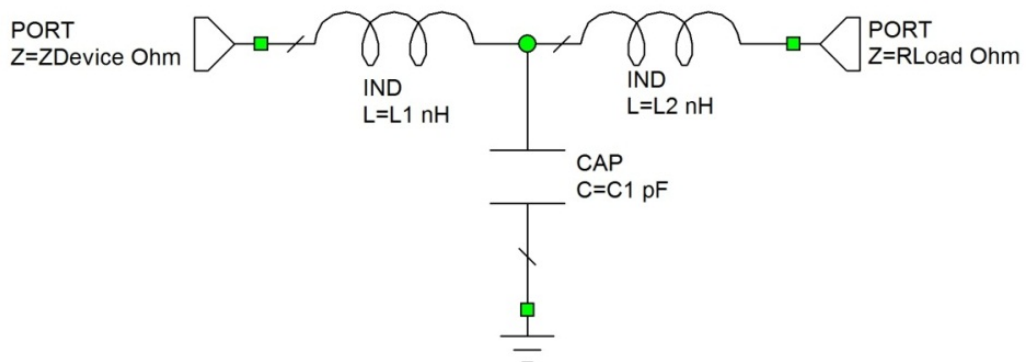


Figure 9.2. T matching network.

The equations for the low pass T network are as follows:

$$X_{L1} = QR_D - X_D \quad \text{where } R_D + jX_D \text{ is the device impedance} \quad \text{Eqn. 9.5}$$

$$X_{L2} = R_L A \quad \text{Eqn. 9.6}$$

$$X_{C1} = \frac{B}{Q + A} \quad \text{Eqn. 9.7}$$

where

$$A = \sqrt{\left[\frac{R_D(1+Q^2)}{R_L} \right] - 1} = \sqrt{\left[\frac{B}{R_L} \right] - 1} \quad \text{Eqn. 9.8}$$

$$B = R_D(1+Q^2) \quad \text{Eqn. 9.9}$$

Note this network clearly shows that the Q used in the matching network relates to the impedance transformation ratio. The minimum Q occurs when $A_1=0$, so that

$$Q_{\min} = \sqrt{\frac{R_L}{R_D} - 1} \quad \text{Eqn. 9.10}$$

Bandpass L Network

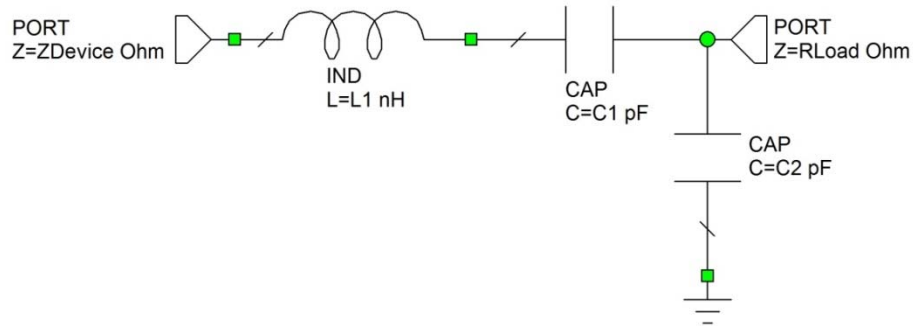


Figure 9.3. Bandpass L matching network.

The bandpass L network is often used as test circuit by semiconductor manufacturers. It incorporates a DC block (C_1), to allow biasing to be set up for the input of transistors and to prevent any DC supply from appearing on the output of an amplifier stage. Normally C_1 and C_2 are adjustable, making it very easy to tune the amplifier for either a peak of output for an output-matching network or for the best input match for an input matching network.

The equations for the band pass L network are as follows:

$$X_{C1} = QR_d \quad \text{where } R_d + jX_d \text{ is the device impedance} \quad \text{Eqn. 9.11}$$

$$X_{C2} = R_i \sqrt{\frac{R_d}{R_i - R_d}} \quad \text{Eqn. 9.12}$$

$$X_{L2} = X_{C1} + \left(\frac{R_d R_L}{X_{C2}} \right) \quad \text{Eqn. 9.13}$$

The device reactance X_d is incorporated in either C_2 for capacitive device impedances or into L_2 for inductive device impedances. In the equations of figures 9.7 and 9.8, this is incorporated by having $X_{pd} = X_d$ and $X_{md} = 0$ if $X_d > 0$ and having $X_{pd} = 0$ and $X_{md} = X_d$ if $X_d < 0$. This will ensure the lowest Q of the network and thus the widest bandwidth. This network can only be used if $R_d < R_L$, since the parts under the square root sign

Bandpass T Network

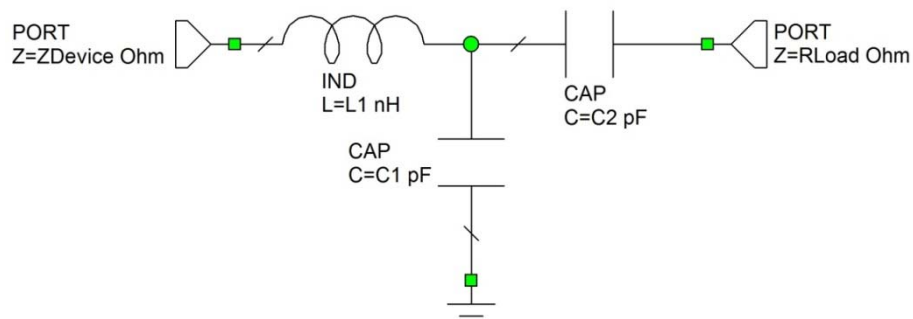


Figure 9.4. Bandpass T matching network.

The equations for the band pass T network are as follows:

$$X_{L1} = QR_D - X_D \quad \text{where } R_D + jX_D \text{ is the device impedance} \quad \text{Eqn. 9.14}$$

$$X_{C2} = A R_L \quad \text{Eqn. 9.15}$$

$$X_{C1} = \frac{B}{Q - A} \quad \text{Eqn. 9.16}$$

Where A and B and the minimum Q are as before:

This network can only be used if $R_D < R_L$, since otherwise negative values for C_1 result.

Important notes:

- 1 Some of the equations for the Pi network are different since the reactive parts of the device are handled in the equations presented here and in the global variables panel of the AWRDE files for figures 9.9 to 9.19, while they are not included in AN267 [1].
- 2 In these notes A and B are kept the same in these notes, while A and B are swapped and changed in AN267.
- 3 In AN267 the term A for the Bandpass T is wrong. AN267 uses:

$$A_{267} = \sqrt{\left[\frac{R_D(1+Q^2)}{R_L} \right]} - 1 = \sqrt{\left[\frac{B}{R_L} \right]} - 1 \quad \text{Eqn. 9.18}$$

That will not give a correct match, as can be verified by using AWRDE. The square root should be extended to cover the -1 term as in the expression for A in equation 9.17.

Capacitive Impedance Transformer

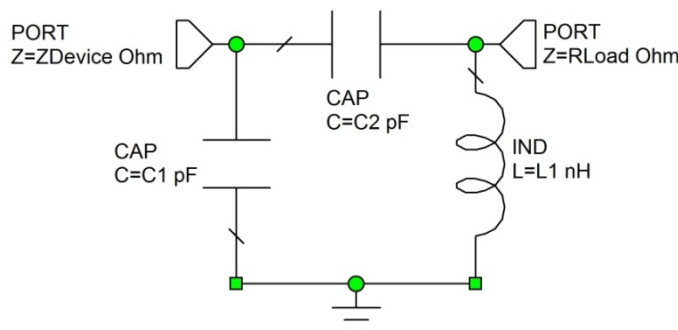


Figure 9.5. Capacitive Impedance Transformer matching network.

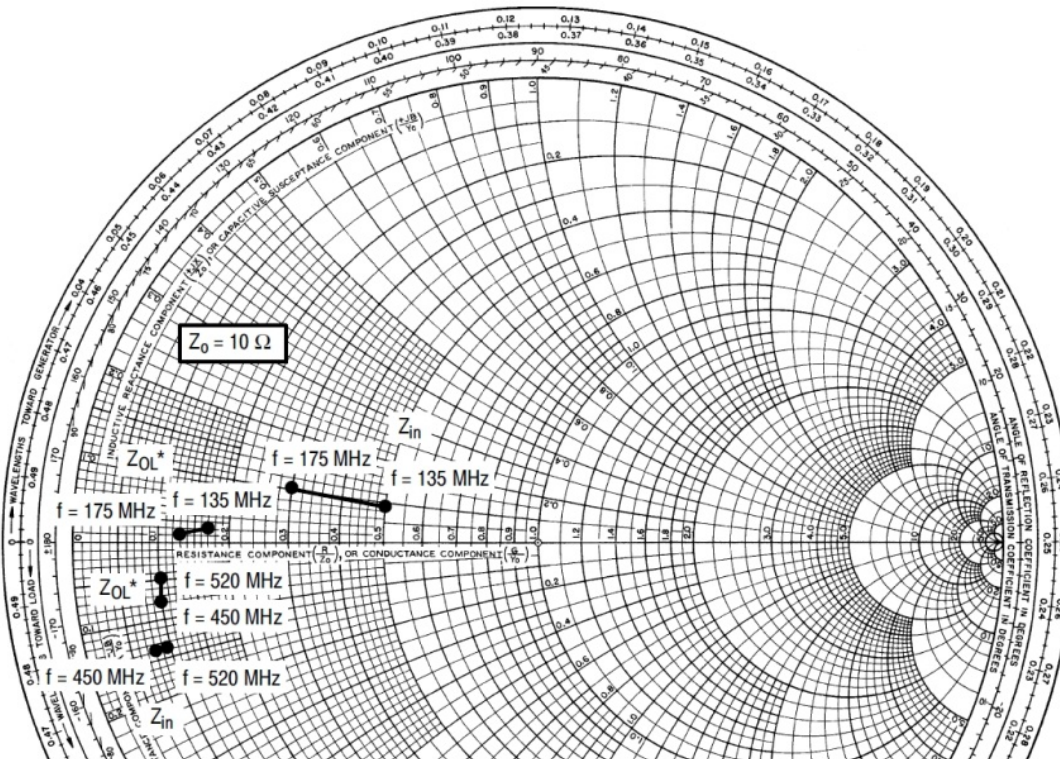
The capacitive transformer is not included in AN267, but this network can be quite useful and give very realisable components in inter-stage matching networks. The network is thus used to match the output impedance of one transistor to the input impedance of another transistor. The circuit is related to the lowpass Pi network, except the ground and the input port are changed. For this network, the output impedance at port 2 is always larger than that at port 1.

For a non-reactive device, the equations for the component values are the same as those for the Pi network, with the input impedance being the same (at port 1), but the reference impedance 50Ω now being the same as $(R_L - R_{device})$ used in the Pi network. So instead

of R_L I, the value $R_L - R_{device}$ is used in the equations. The calculations for the capacitive transformer in the included the equations of figure 9.7 and 9.8. These equations handle the reactive part by using the equations for a resistive device and then tuning C_2 and L_1 to obtain a correct match and frequency, using variables K_r and K_f , in figures 9.7 and 9.8, for the impedance ratio and the frequency tuning respectively. These variables can be tuned manually, or they can be tuned by optimisation.

Example 9.1: 150 MHz, 35 W Amplifier

To illustrate the design process, the above equations are applied to an MRF1535NT1 [2], 12.5V, 35 W, lateral N-Channel MOS FET to obtain a suitable match. This FET is suitable for operation from 135 MHz to 520 MHz and can thus be used for mobile radio applications. An amplifier at 150 MHz is required.



$$V_{DD} = 12.5 \text{ V}, I_{DQ} = 250 \text{ mA}, P_{out} = 35 \text{ W}$$

f MHz	Z_{in} Ω	Z_{OL^*} Ω
135	$5.0 + j0.9$	$1.7 + j0.2$
155	$5.0 + j0.9$	$1.7 + j0.2$
175	$3.0 + j1.0$	$1.3 + j0.1$

$$V_{DD} = 12.5 \text{ V}, I_{DQ} = 500 \text{ mA}, P_{out} = 35 \text{ W}$$

f MHz	Z_{in} Ω	Z_{OL^*} Ω
450	$0.8 - j1.4$	$1.0 - j0.8$
470	$0.9 - j1.4$	$1.1 - j0.6$
500	$1.0 - j1.4$	$1.1 - j0.6$
520	$0.9 - j1.4$	$1.1 - j0.5$

Figure 9.6. Part of datasheet showing large signal input and output impedances [2].

Using the manufacturer's data, shown in figure 9.6, the input impedance at the required frequency is determined. It should be noted that these values do depend on individual device and the quiescent current, so that in practice the actual values may be slightly

different. For this device the input impedance is the same at 137 MHz and 155 MHz, and is $5 + j0.9 \Omega$. The $j0.9 \Omega$ reactance corresponds to a 955 pH inductor at 150 MHz.

To calculate the required matching network components, equations 9.1 to 9.18 must be evaluated. For a Pi network, AN267 does not include the device reactance as part of C1. Equation 9.2 includes any device reactance as part of C1. Including any device reactance as part of C1 results in a lower effective Q and thus gives a wider bandwidth for the matching network. For the AWRDE project files for figures 9.9 to 9.20, equations 9.1 to 9.18 are included as part of the "Global Variables". Those equations are shown in figures 9.7 and 9.8.

The Q value to be selected for the matching network is a compromise. For a wide bandwidth, a low Q is required. However, the desired matching may not be possible at low Q values. For this FET only the bandpass L and Pi network are possible for matching with Q values below Q = 3. If a Q value of 2.5 is used as shown in figure 9.7, the values for L_{lt2} and C_{lt} for the Low Pass T network are shown as complex values. For example $L_{lt2} = 1.703E-24 + j2.782E-8$. This is not a realisable inductor. The lowpass T and the bandpass T matching networks are thus not realisable. Even with a network having real valued components, does not mean that it is a practical network. For instance, the Pi network requires a 8.17 nH inductor, which is too small to produce reliably as a wound inductor.

Figure 9.8 shows the same equations for the MRF1535NT1 with a Q = 3.5. It can be seen from the values in the right column that all the network parameters are real and all networks can be used.

Matching Network Equations.
 Fm Matching Frequency in MHz, Rd real part of device impedance, Xpd positive device reactance
 Xmd negative device reactance, use either Xpd or Xmd. If Xd = -5 then Xpd=0 and Xmd = -5
 Change Fm or Q and simulate to view their effect

Fm=150	Kp=1.944	Kt=1.857	Set Kp and Kt for correct bandwidth
Q=2.5	Qp=Q/Kp	Qt=Kt*Q	
Rl=50		TwoPi=4*Acos(0)	Qp: 1.286
Rd=5	Xpd=0.9	Xd=Xpd+Xmd	Qt: 4.643
Wm=TwoPi*Fm*1e6		Zin=complex(Rd,Xd)	Xd: 0.9
			Zin: (5,0.9)

Pi Matching

$R_p = (R_d * R_d + X_d * X_d) / R_d$	$C_{p1} = 1/(W_m * X_{cp1})$	Cp1: 3.013e-10
$X_p = (R_d * R_d + X_d * X_d) / X_d$	$C_{p2} = 1/(W_m * X_{cp2})$	Cp2: 1.055e-10
$Y_p = 1/X_p$	$L_{lp} = X_{lp} / W_m$	Lp: 1.291e-8
$X_{cp1} = (Q_p / R_p + Y_p)$		
$X_{cp2} = R_l^2 * (sqrt((R_p / R_l) / ((Q_p * Q_p + 1) - (R_p / R_l))))$		
$X_{lp} = (Q_p * R_p + (R_p * R_l / X_{cp2})) / (Q_p * Q_p + 1)$		

Low Pass T

$X_{lt1} = (R_d * Q_t - X_d)$	$L_{lt1} = X_{lt1} / W_m$	Llt1: 2.367e-8
$A_2 = ((R_d^2 * (1 + Q_t * Q_t) / R_l) - 1)$	$A = Sqrt(A_2)$	A: 1.12
$B = R_d * (1 + Q_t * Q_t)$		B: 112.8
$Q_{min} = sqrt(R_l / R_d)$		Qmin: 3
$X_{lt2} = R_l * A$	$L_{lt2} = X_{lt2} / W_m$	Llt2: 5.944e-8
$X_{clt} = B / (Q_t + A)$	$C_{lt} = 1 / (W_m * X_{clt})$	Clt: 5.422e-11

Band Pass L

$X_{cb1} = R_d * Q + X_{md}$	$C_{b1} = 1 / (W_m * X_{cb1})$	Cb1: 8.488e-11
$X_{cb2} = R_l * sqrt(R_d / (R_l - R_d))$	$C_{b2} = 1 / (W_m * X_{cb2})$	Cb2: 6.366e-11
$X_{lb1} = X_{cb1} - X_d + (R_d * R_l / X_{cb2})$	$L_{lb1} = X_{lb1} / W_m$	Lb1: 2.822e-8

Band Pass T

$X_{bt} = (R_d * Q_t - X_d)$	$L_{bt} = X_{bt} / W_m$	Lbt: 2.367e-8
$X_{bt2} = R_l * A$	$C_{bt2} = 1 / (W_m * X_{bt2})$	Cbt2: 1.894e-11
$X_{cbt1} = B / (Q_t - A)$	$C_{bt1} = 1 / (W_m * X_{cbt1})$	Cbt1: 3.314e-11

Capacitive Transformer

Kr=0.578	Kf=1.065	Set Kr and Kf for correct match at required centre frequency
$R_o = Kr * R_l - R_p$		Cp1: 3.013e-10
$X_{cct} = R_o * (sqrt((R_p / R_o) / ((Q_p * Q_p + 1) - (R_p / R_o))))$	$C_{cct} = 1 / (W_m * X_{cct})$	Cct: 1.496e-10
$X_{lct} = K_f * (Q_p * R_p + (R_p * R_o / X_{cct})) / (Q_p * Q_p + 1)$	$L_{ct} = X_{lct} / W_m$	Lct: 1.018e-8

Figure 9.7. Input matching component values for a MRF1532 MOSFET, Q=2.5.

Matching Network Equations.

Fm Matching Frequency in MHz, Rd real part of device impedance, Xpd positive device reactance
Xmd negative device reactance. use either Xpd or Xmd. If Xd = -5 then Xpd=0 and Xmd = -5

Change Fm or Q and simulate to view their effect

Fm=150	Kp=1.944	Kt=1.857	Set Kp and Kt for correct bandwidth
Q=3.5	Qp=Q/Kp	Qt=Kt*Q	
RI=50			Qp: 1.8
Rd=5	Xpd=0.9	Xmd=-0.0	Qt: 6.5
Wm=TwoPi*Fm*1e6			Xd: 0.9
			Zin=complex(Rd,Xd)
			Zin: (5,0.9)

Pi Matching

Rp = (Rd * Rd + Xd * Xd) / Rd		
Xp = (Rd * Rd + Xd * Xd) / Xd		
Yp=1/Xp		
Ycp1= (Qp/Rp +Yp)		
Xcp1= (1/Ycp1)	Cp1= 1/(Wm*Xcp1)	Cp1: 4.071e-10
Xcp2=RI*(sqrt((Rp/RI)/((Qp*Qp+1)-(Rp/RI))))	Cp2=1/(Wm*Xcp2)	Cp2: 1.344e-10
Xlp=(Qp*Rp+(Rp*RI/Xcp2))/(Qp*Qp+1)	Lp=Xlp/Wm	Lp: 1.05e-8

Low Pass T

Xl1t1= (Rd*Qt - Xd)	L1t1=Xl1t1/Wm	L1t1: 3.353e-8
A2=((Rd*(1+Qt*Qt)/RI) -1)	A=Sqr(A2)	A: 1.823
B=Rd*(1+Qt*Qt)		B: 216.2
Qmin=sqr(RI/Rd-1)		Qmin: 3
Xl1t2=RI*A	L1t2=Xl1t2/Wm	L1t2: 9.673e-8
Xclt=B/(Qt+A)	Clt= 1/(Wm*Xclt)	Clt: 4.084e-11

Band Pass L

Xcbl1= Rd*Q + Xmd	Cbl1= 1/(Wm*Xcbl1)	Cbl1: 6.063e-11
Xcbl2=RI*sqrt(Rd/(RI-Rd))	Cbl2= 1/(Wm*Xcbl2)	Cbl2: 6.366e-11
Xlbl=Xcbl1 - Xd+ (Rd*RI/Xcbl2)	Lbl=Xlbl/Wm	Lbl: 3.353e-8

Band Pass T

Xlbt= (Rd*Qt - Xd)	Lbt=Xlbt/Wm	Lbt: 3.353e-8
Xcbt2=RI*A	Cbt2= 1/(Wm*Xcbt2)	Cbt2: 1.164e-11
Xcbt1=B/(Qt-A)	Cbt1= 1/(Wm*Xcbt1)	Cbt1: 2.295e-11

Capacitive Transformer

Kr=0.578	Kf=1.065	Set Kr and Kf for correct match at required centre frequency
Ro=Kr*RI-Rp		Cp1: 4.071e-10
Xcct=Ro*(sqrt((Rp/Ro)/((Qp*Qp+1)-(Rp/Ro))))	Cct=1/(Wm*Xcct)	Cct: 1.923e-10
Xlct=Kf*(Qp*Rp+(Rp*Ro/Xcct))/(Qp*Qp+1)	Lct=Xlct/Wm	Lct: 8.392e-9

Figure 9.8. Input matching component values for a MRF1532 MOSFET, Q=3.5

The choice of network to be selected then depends on the frequency response and the component values for the different networks. The Q is normally selected to be as low as possible, as this will provide the widest bandwidth possible.

When comparing the frequency response of the matching networks, the Pi network has a lower bandwidth if the same Q value is used. A closer frequency response is obtained when Qp, the Q for the Pi network or the Capacitive Transformer, is half the Q of the bandpass L network and when the Q of the lowpass T and bandpass T are twice that of the bandpass L network. In figure 9.7, the same Q values are used for all the networks, to show that the Pi network does not have a minimum Q, and can be realised at low Q values.

In order to have an exact source impedance of $5 + j0.9 \Omega$, it is convenient to make a complex input variable Z_{in} , using $Z_{in} = \text{complex}(R_d, X_d)$. Note that for a signal applied to the device port (Port 1), the network will have a voltage gain, since there is an impedance transformation. A passive network cannot have a power gain. Figures 9.9 to 9.20 show that the bandwidth over which a good match is obtained is smaller than the bandwidth obtained with transformer matching and transmission-line matching, which are described later in this chapter. The impedance match and insertion loss versus frequency for the different types of matching network and matching to the large signal input impedance of the MRF1535NT1 MOSFET is shown in figures 9.9 to 9.20.

Pi Network

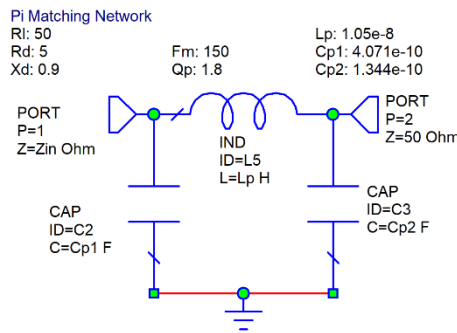


Figure 9.9. Values for the Pi matching network.

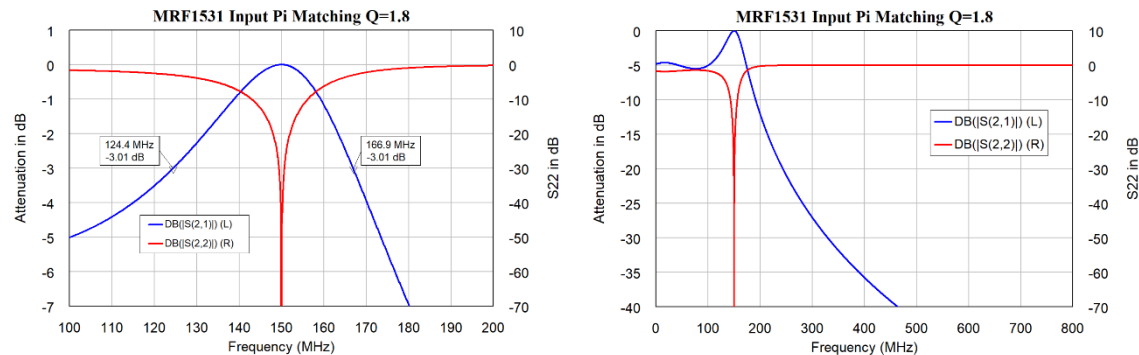


Figure 9.10. Frequency response of the Pi matching network.

Lowpass T Network

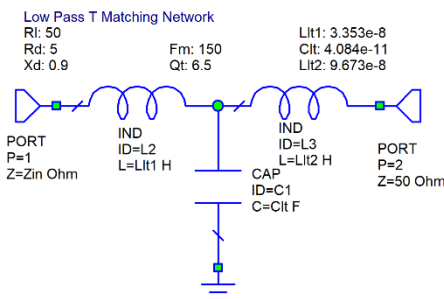


Figure 9.11. Values for the lowpass T matching network.

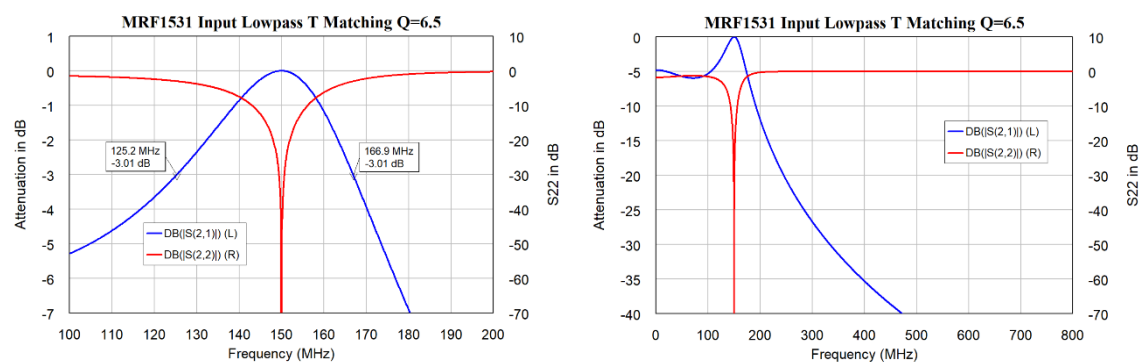


Figure 9.12. Frequency response of the lowpass T matching network.

Bandpass L Network

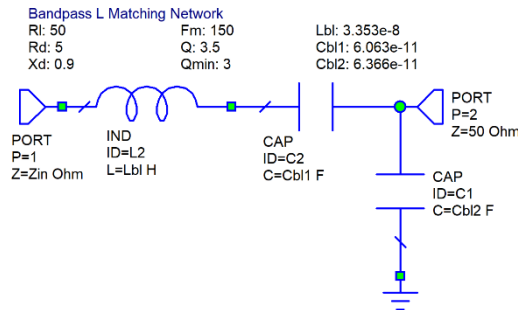


Figure 9.13. Values for the bandpass L matching network.

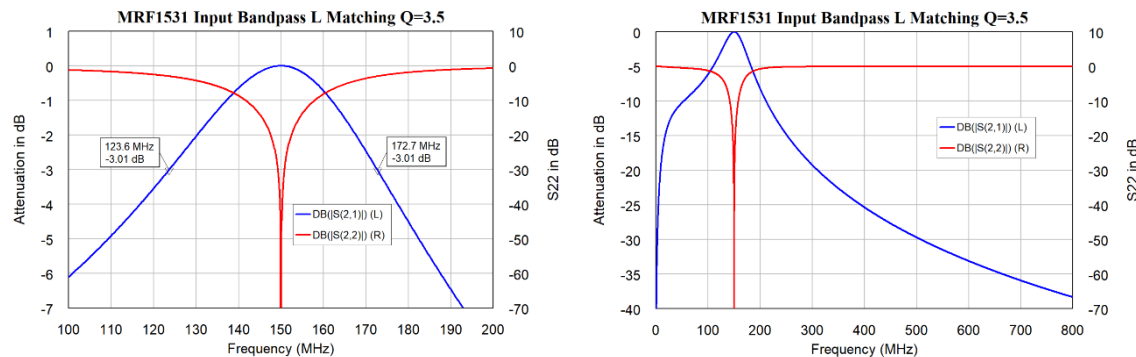


Figure 9.14. Frequency response of the Bandpass L matching network.

Bandpass T Network

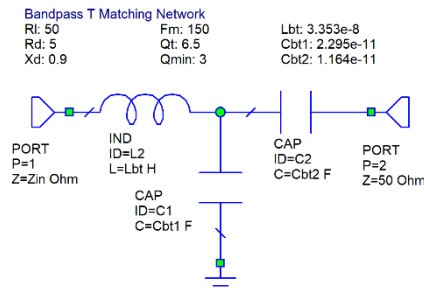


Figure 9.15. Values for the bandpass T matching network.

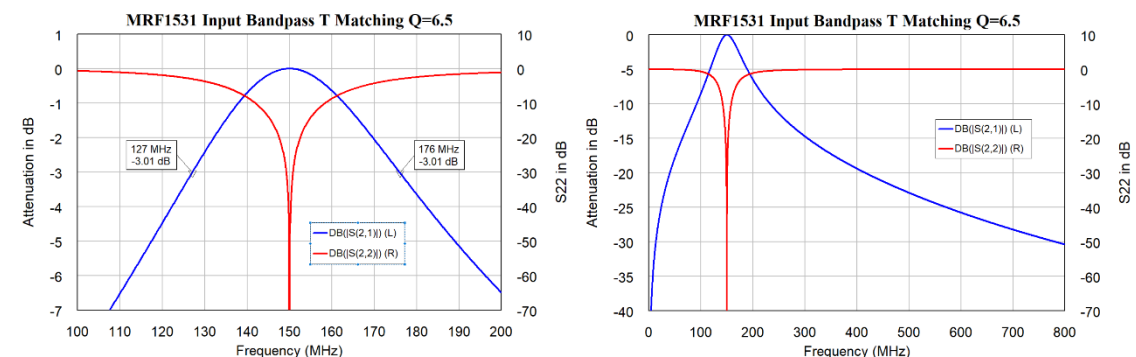


Figure 9.16. Frequency response of the bandpass T matching network.

Capacitive Transformer Network

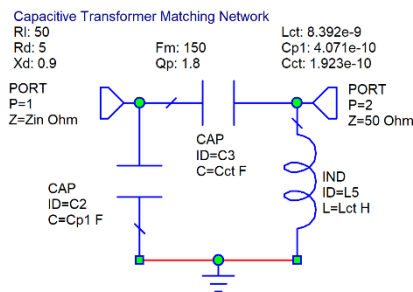


Figure 17. Values for the Capacitive Transformer matching network.

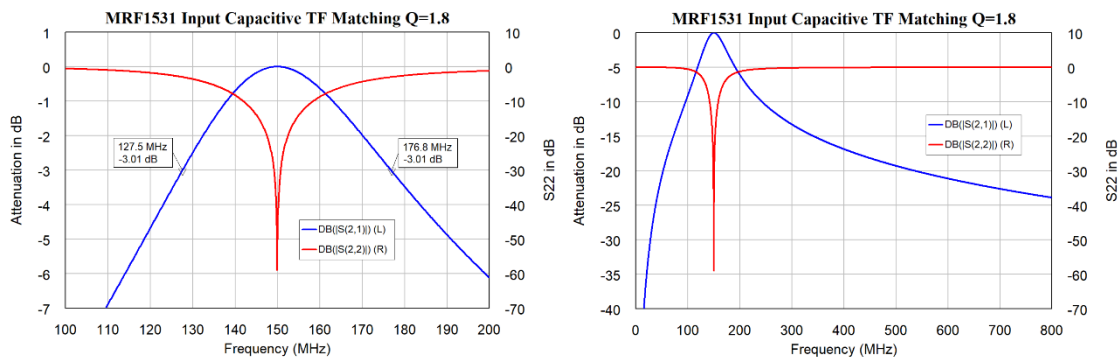


Figure 9.18. Frequency response of the capacitive transformer-matching network.

Comparing the attenuation of the networks in figures 9.10, 9.12, 9.14, 9.16 and 9.18 at 800 MHz, shows a progressive reduction in attenuation. The Pi network and Lowpass T are thus the best networks to be used if harmonics of the source are to be filtered out.

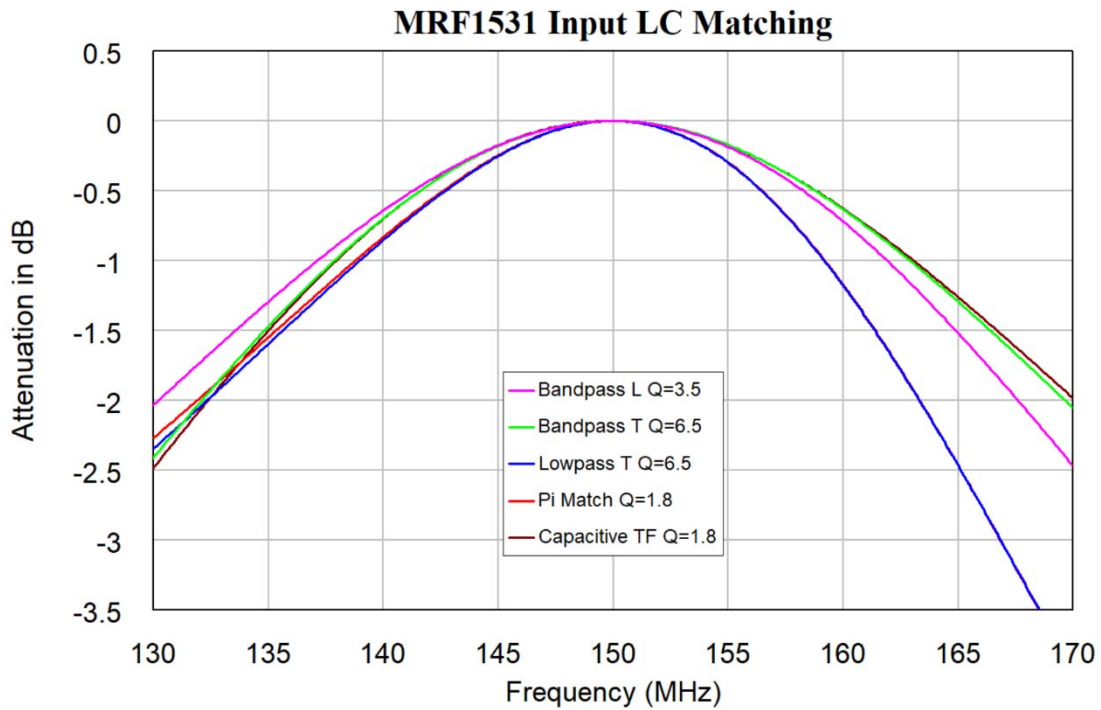


Figure 9.19. Comparison of LC matching networks.

Figures 9.19 and 9.20 show a comparison of the impedance matching performance of the LC networks of figures 9 to 18. The Pi matching network has the lowest bandwidth, but it does not have a minimum Q and its Q can be adjusted to make the bandwidth comparable to the other networks if needed.

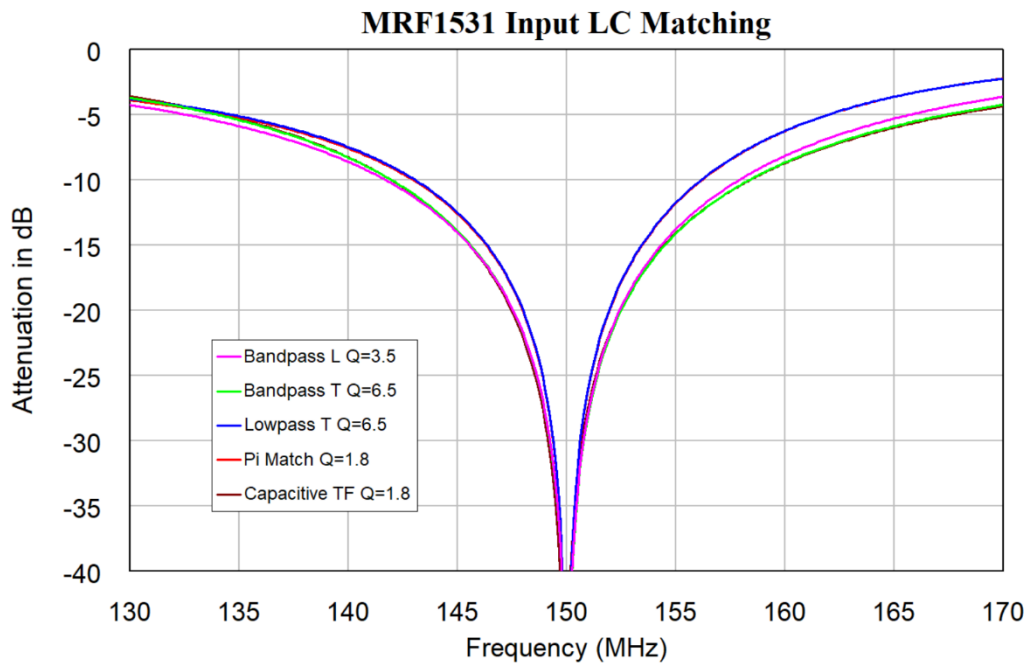


Figure 9.20. Comparison of LC matching networks, Q=3.5 for all networks.

The lowpass T, the bandpass T and the bandpass L networks, all present a high impedance at the second harmonic of the input frequency. This results in smaller second harmonic currents to flow in the bipolar transistor or FET and this slightly increases its efficiency. These networks will however result in higher peak voltages, due to the device impedance at the second harmonic being close to an open-circuit. This may then exceed the voltage breakdown ratings of the device or the components used in the matching network. The low pass networks are also good for filtering out harmonics produced by the amplifier. Bandpass T, bandpass L and the capacitive transformer networks all have a capacitance in series with the input to output path. This avoids the need for an additional coupling capacitor to set the bias level correctly.

If the required bandwidth or the required harmonic attenuation cannot be obtained, several matching networks can be cascaded, allowing the impedance transformation ratios to be reduced, thus increasing the bandwidth. Cascading several low pass networks significantly increases the harmonic attenuation.

Transformer Matching

In transformer matching, an RF transformer, as described in Chapter 3 of his book is used to provide the impedance transformation required. Since the number of turns used must be an integer and the impedance transformation is the turns-ratio squared, the impedance transformation ratios are limited to the square of simple fractions. For the matching of the MOSFET in this example, a $5 + j0.9 \Omega$ impedance is required. This can best be approximated by a 3:1 turns-ratio transformer, giving a 9:1 impedance transformation, so that a 50Ω source is transformed into a 5.55Ω impedance, which is sufficiently close to $5 + j0.9 \Omega$ for most of the power to be transferred effectively.

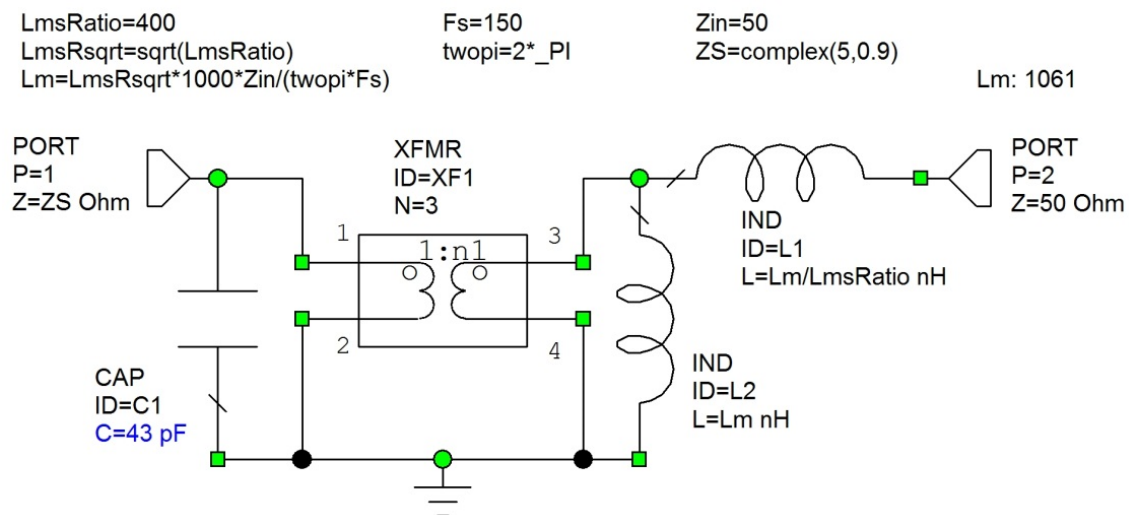


Figure 9.21. Values for the Transformer matching network.

A practical RF transformer can be represented by an ideal transformer, with a magnetising inductance in parallel with it and a leakage inductance in series with it, as shown in figure 9.21. The magnetising and leakage inductances are chosen to give a centre frequency of 150 MHz. The 400:1 ratio between L_m and L_s is on the low side of the typical range, so that the bandwidth typically will be larger than what is shown here.

In this example, the impedance to be matched is assumed to be constant at $5 + j0.9 \Omega$. In practice the device impedance changes significantly over such the several decades of bandwidth of the RF transformer, thus limiting the frequency range over which the device is properly matched. FET amplifiers that are well matched up to 100 MHz can easily be designed, as is evident from many power FET manufacturers' application notes. The performance obtained by the transformer-matching network is shown on figure 9.22.

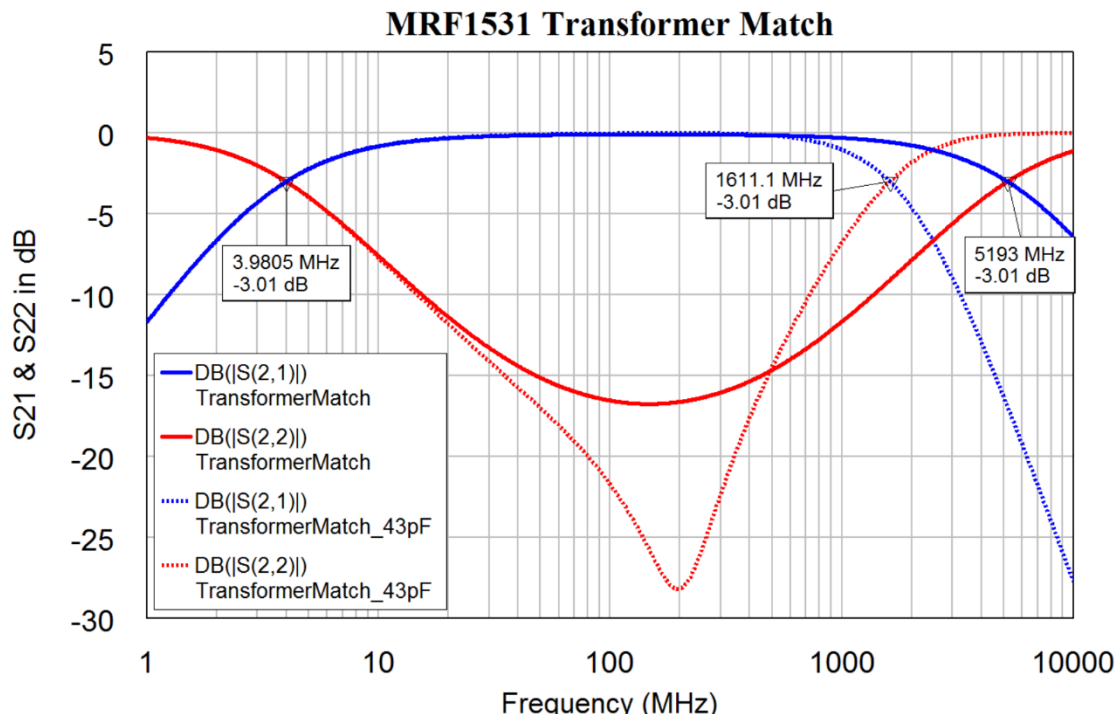


Figure 9.22. Frequency response of transformer matching network with and without reactive tuning capacitor.

If needed, the reactive part can be resonated out, using a 43 pF capacitance across pin 1 and 2 of the transformer as shown in figure 9.21. This capacitor can be tuned to provide an optimum match at 150 MHz, as shown in figure 9.22. Note that adding the capacitance will reduce the upper corner frequency of the transformer-matching network. Due to the turns-ratio of the transformer being limited to integer values, the impedance match is not as good as that of the LC networks or that of the transmission-line networks described later. The model of figure 9.21 does not contain all the parasitic elements encountered in a practical transformer circuit, and the actual FET characteristics may be slightly different from the values given in the data sheet. The value of the tuning capacitance required is thus best determined experimentally, using the value obtained by the computer simulation of figures 9.21 and 9.22, as a starting point.

Transmission-Line Matching

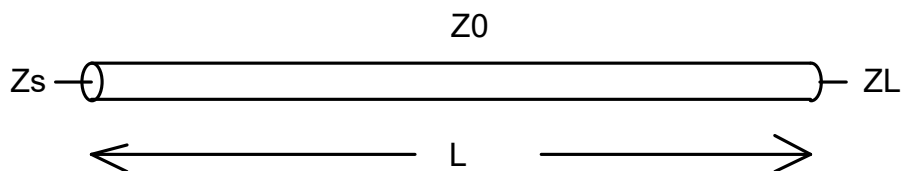


Figure 9.23. Transmission-line sending and load impedances.

For a transmission-line of characteristic impedance Z_0 and length L , shown in figure 9.23, the impedance looking into a transmission-line that is terminated in a load Z_L is:

$$Z_s = Z_0 \frac{Z_L + jZ_0 \tan(\beta l)}{Z_0 + jZ_L \tan(\beta l)} \quad \text{Eqn. 9.18}$$

By substituting $Z_s = R_s + jX_s$ and $Z_L = R_L + jX_L$ and then solving for Z_0 and the transmission-line length $\theta = \beta l$ as an electrical length, one obtains the following equations:

$$Z_0 = \sqrt{\frac{R_s |Z_L|^2 - R_L |Z_s|^2}{R_L - R_s}} \quad \text{Eqn. 9.19}$$

$$\theta = \text{Arc tan} \left(\frac{Z_0 (R_s - R_L)}{R_s X_L + R_L X_s} \right) \quad \text{Eqn. 9.20}$$

This assumes that Z_0 is real and $\tan(\beta l)$ is real. These equations do not always give a match, but if no match is possible, shifting the impedance by using a short length of transmission-line will always result in a match. Equations 9.19 and 9.20 are included in the AWRDE project file for the transmission-line matching network. For matching a $5 + j0.9 \Omega$ impedance, being the same impedance match as is used in figures 9.9 to 9.20, these equations give $Z_0 = 15.78$ and $\theta = 86.37$ degrees and this can be included in the AWRDE circuit diagram as the variables shown in figures 9.23 and 9.24.

Figure 9.25, shows the frequency range of the resulting impedance match. It can be seen that transmission-line matching gives a broadband impedance match. The only limitations are that firstly, it is difficult to tune the matching impedances to allow for device

variations and secondly the line lengths can physically become too large. This is why this technique is predominantly used above 100 MHz. Transmission-lines can replace the inductors used in the LC matching. This will then allow for some tuning of the matching network by changing the values and locations of capacitors. The replacement of the inductors used in Low pass T matching networks of figure 9.11, with transmission-lines is often done in commercial applications above 100 MHz.

```

RS=5      XS=0.9      MZS2=RS*RS+XS*XS
ZS=complex(RS,XS)
RL=50      XL=0       MZL2=RL*RL+XL*XL
Z0=sqrt((RS*MZL2-RL*MZS2)/(RL-RS))      Z0: 15.78
ELen=deg(atan((Z0*(RL-RS))/(RS*XL+RL*XS)))  ELen: 86.37

```

Figure 9.23. Transmission-line matching equations in the Global Equations panel.



Figure 9.24. Values for the transmission-line matching network.

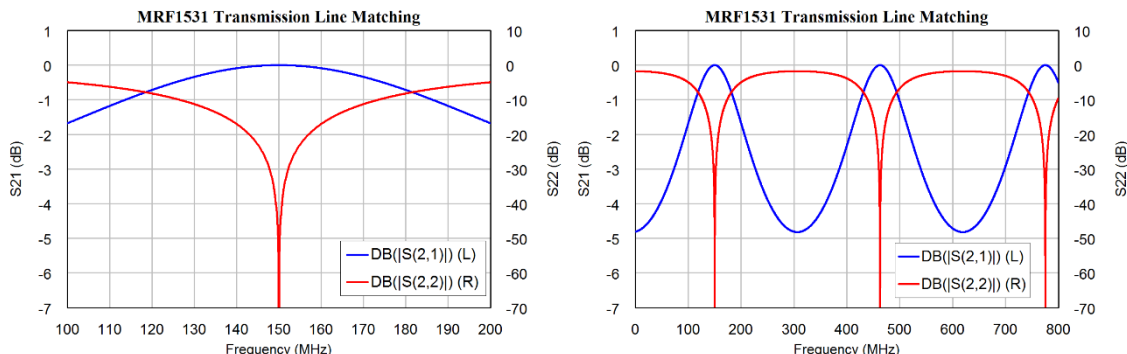


Figure 9.25. Frequency response of the transmission-line matching network.

Broadband Matching

Sometimes a wideband match is required. This can either be a wideband match into an active device, or a simple impedance transformation. If a wideband match into an active device is required, then the either the device impedance must be able to be accurately represented by a simple circuit, i.e. a resistor and capacitor or inductor. Or one must use the small or large signal S parameter data, as the case may be, for a data table in NI AWR DE and use that for the complex impedance vector variable in the global definitions panel of AWRDE. If the amplifier operates as a non-linear device and creates multiple harmonics, then the device needs to be characterized by a nonlinear model, which would require models like X-parameters, S-functions or a time-domain waveform to model the device. The use of those is beyond the scope of this book.

Since AWRDE is good at optimising networks, it is easiest to design a first-guess of the matching network by cascading a succession of simple matching networks and then improve the performance by optimisation. As an example, consider an impedance transformation from 50 ohm to 1.85 ohm. The impedance transformation ratio is 27 to one and this is achieved by cascading three pi networks with impedance transformations of 3 to one. The impedance levels are thus 50Ω , 16.67Ω , 5.55Ω and 1.85Ω . The match

is required for the 250MHz to 500MHz range and provide a return loss of less than -15 dB. The individual impedance match calculations are done at a centre frequency of 353 MHz, being the geometric mean of 250MHz and 500MHz. Figure 9.26 shows the circuit of the matching network, with the element values linked to the equations of figure 9.27.

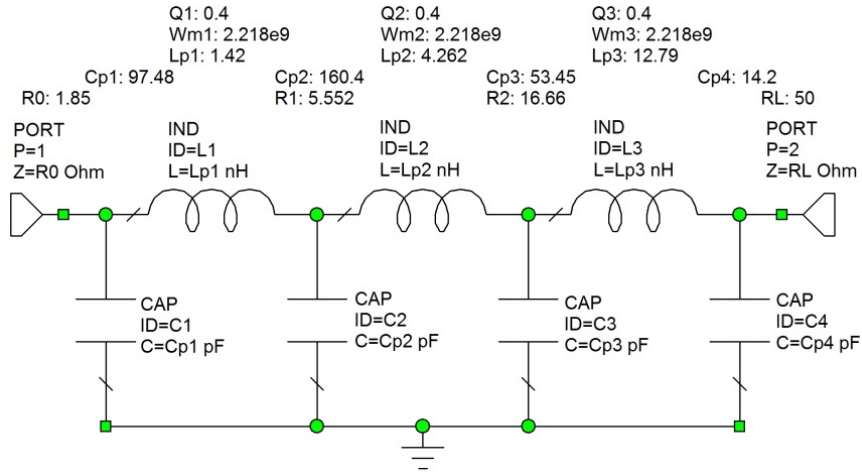


Figure 9.26. Starting broadband match schematic.

$R0=1.85$	$X0=0$	$R0: 1.85$
$RL=50$		$RL: 50$
$R=\text{pow}((RL/R0),(1/3))$	$KR1=R$	$R: 3.001$
$R1=KR1*R0$		$R1: 5.552$
$R2=KR2*R0$		$R2: 16.66$
$R3=RL$		$KR2: 9.006$
$Fm=353$	$Wm=2* \text{Pi} * Fm * 1e6$	$Wm: 2.218e9$
$Q1=0.4$	$Wm1=2.218e9$	
$Q2=Q1$	$Wm2=Wm$	
$Q3=Q1$	$Wm3=Wm$	
Pi Match 1		
If nonzero $X0$ then enable:		
$Rp = (R0 * R0 + X0 * X0) / R0$		$Rp: 1.85$
$Yp = X0 / (R0 * R0 + X0 * X0)$		$Yp: 0$
$Ycp11 = (Q1/Rp + Yp)$		
$Xcp11 = (1/Ycp11)$	$Cp11 = 1e12 / (Wm1 * Xcp11)$	$Cp11: 97.48$
$Xcp12 = R1 * (\sqrt{(Rp/R1) / ((Q1 * Q1 + 1) * (Rp/R1))})$	$Cp12 = 1e12 / (Wm1 * Xcp12)$	$Cp12: 127.9$
$Xlp1 = (Q1 * Rp + (Rp * R1 / Xcp12)) / (Q1 * Q1 + 1)$	$Lp1 = Xlp1 * 1e9 / (Wm1)$	$Lp1: 1.42$
If $X0 = 0$ then enable:		
$Rp=R0$		
$Yp=0$		
Pi Match 2		
$Ycp21 = (Q2/R1)$	$Cp21 = 1e12 / (Wm2 * Xcp21)$	$Cp21: 32.48$
$Xcp21 = (1/Ycp21)$		
$Xcp22 = R2 * (\sqrt{(R1/R2) / ((Q2 * Q2 + 1) * (R1/R2))})$	$Cp22 = 1e12 / (Wm2 * Xcp22)$	$Cp22: 42.63$
$Xlp2 = (Q2 * R1 + (R1 * R2 / Xcp22)) / (Q2 * Q2 + 1)$	$Lp2 = Xlp2 * 1e9 / (Wm2)$	$Lp2: 4.262$
Pi Match 3		
$Ycp31 = (Q3/R2)$	$Cp31 = 1e12 / (Wm3 * Xcp31)$	$Cp31: 10.82$
$Xcp31 = (1/Ycp31)$		
$Xcp32 = R3 * (\sqrt{(R2/R3) / ((Q3 * Q3 + 1) * (R2/R3))})$	$Cp32 = 1e12 / (Wm3 * Xcp32)$	$Cp32: 14.2$
$Xlp3 = (Q3 * R2 + (R2 * R3 / Xcp32)) / (Q3 * Q3 + 1)$	$Lp3 = Xlp3 * 1e9 / (Wm3)$	$Lp3: 12.79$
Combine C's		
$Cp1=Cp11$		$Cp1: 97.48$
$Cp2=Cp12+Cp21$		$Cp2: 160.4$
$Cp3=Cp22+Cp31$		$Cp3: 53.45$
$Cp4=Cp32$		$Cp4: 14.2$

Figure 9.27. Global definition equations for the broadband matching network.

For the broadest possible match, a low Q is used. A Q of 0.4 will give realisable components for the Pi networks. To facilitate the inclusion of a reactive part of the low impedance load, the required equations are included in figure 9.27, but are disabled (and shown in green) as they are not required for this example. The equations in figure 9.27 can accommodate any impedance level. They can also be extended to include more sections.

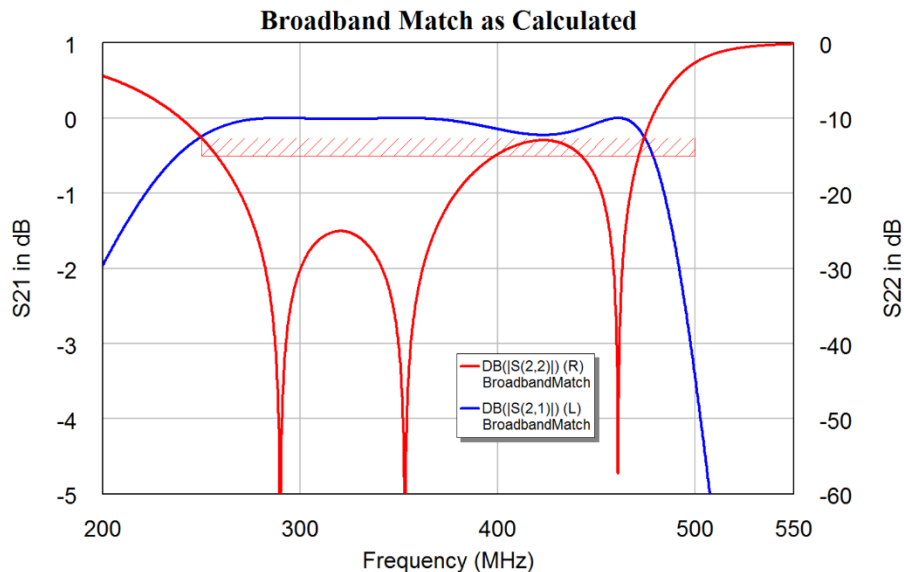


Figure 9.28. Starting broadband match S_{21} and S_{22} .

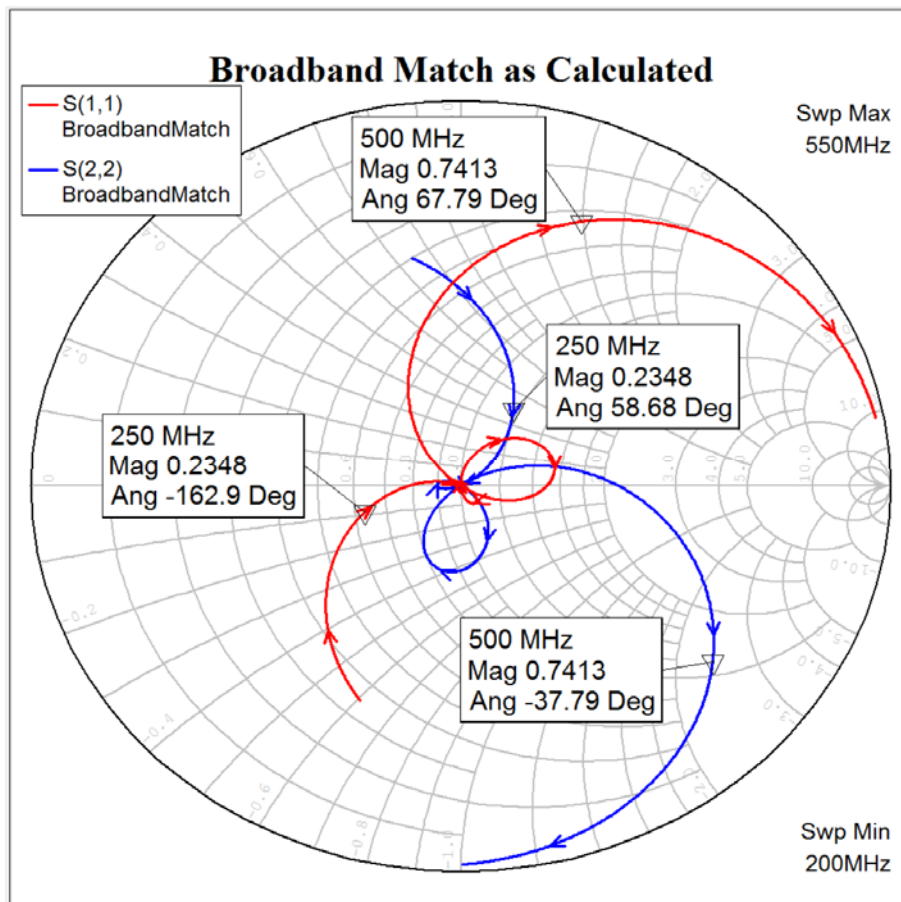


Figure 9.29. Starting broadband match S_{11} and S_{22} on a Smith Chart.

Figures 9.28 and 9.29 shows the frequency response and return loss of the initial design, obtained from the equations in figure 9.27. It can be seen that simply using 3 Pi matching sections is a good starting point for the design. For output-matching, a lowpass T section provides better efficiency, so that one or more a lowpass T section followed by sat one or more lowpass Pi sections couple be used. A bandpass section can also be included to provide DC coupling as part of a broadband matching network.

The impedance match does not quite meet the requirement of having S_{11} or S_{22} to be less than -15 dB over the 250 MHz to 500 MHz bandwidth, so the network is optimised to meet the specification of having, as shown by the optimisation limits of figure 9.28.

There are different ways of optimising this circuit. Firstly, the individual elements can be optimised, by simply replacing the variables for the component values figure 9.26 with the calculated values that can be optimised. The calculated component values are used as the starting values for the element values of the matching network. Alternately one can keep calculating the component values using the equations in figure 9.27, but have different Q values, centre frequencies and impedance transformation ratios for each of the three matching sections. The initial values for Q1, Q2 and Q3 are the design value $Q = 0.4$ used in figure 9.27 and the initial values for W_{m1} , W_{m2} and W_{m3} are the design value $W_m = 2\pi \times 353 \times 10^6 = 2.218 \times 10^9$. The initial impedance transformation ratio is 3.001, giving the intermediate impedances R_1 and R_2 shown in figures 9.26 and 9.27.

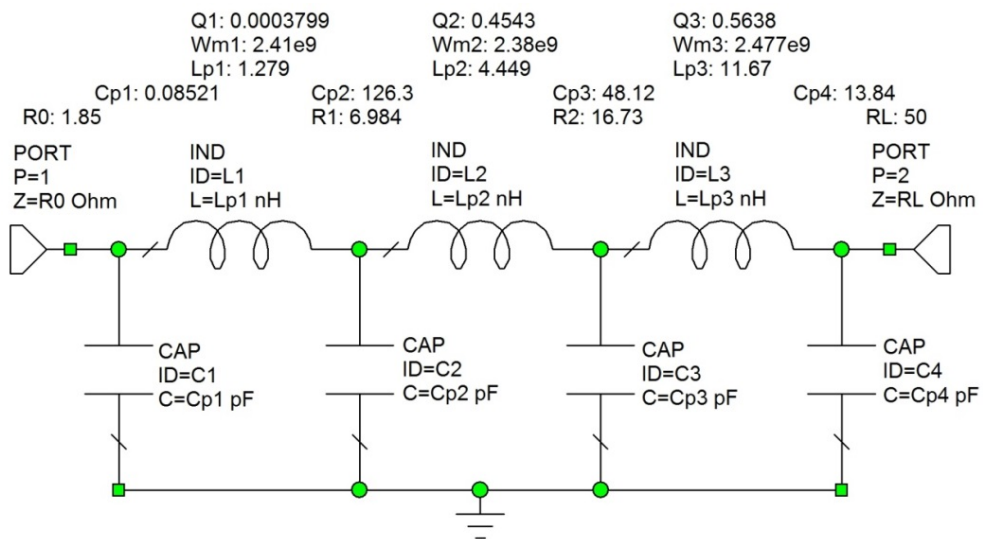


Figure 9.30. Final broadband match schematic.

Neither of the element or the Q, W_m and Impedance Ratio optimisations will achieve a perfect optimisation. However, the resulting final specification errors are very small. The Q, W_m and Impedance ratio optimisation results in a specification error and are used for the figures 9.30 to 9.32. For AWR 10, the quickest optimisation is obtained using the Simplex Optimiser, but most other optimisers will also give good results. There is no unique optimum match for the network of figure 9.30. Depending on the optimiser used and minor variations in the starting conditions, different final component values are obtained. Optimisations having impedance transformation ratios close to the initial values of figure 9.26, centre frequencies in the 250-500 MHz range and low Q values are suitable. For the circuit of figure 9.30, Q_1 is very small, resulting in a very small value of C_1 , which can be deleted in practice. As a result, the network can also be realised using a lowpass T network, followed by a Pi network.

It can be seen that $|S_{22}|$ is now less than -15 dB for virtually the entire 250 – 500 MHz frequency range. The curve for $|S_{11}|$ is identical to that for $|S_{22}|$. Figure 9.32 shows the Smith chart of the network after optimisation. It can be seen that a good match over the entire 250 MHz to 500 MHz bandwidth is obtained, with the magnitude of the reflection coefficient being less than 0.1874 from 250 MHz to 500 MHz.

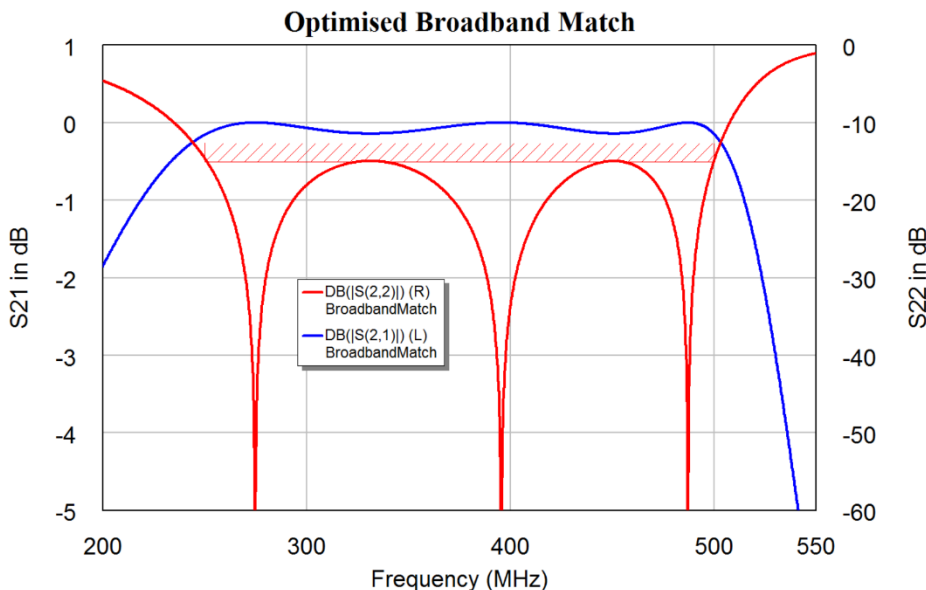


Figure 9.31. Final broadband match S_{21} and S_{22} .

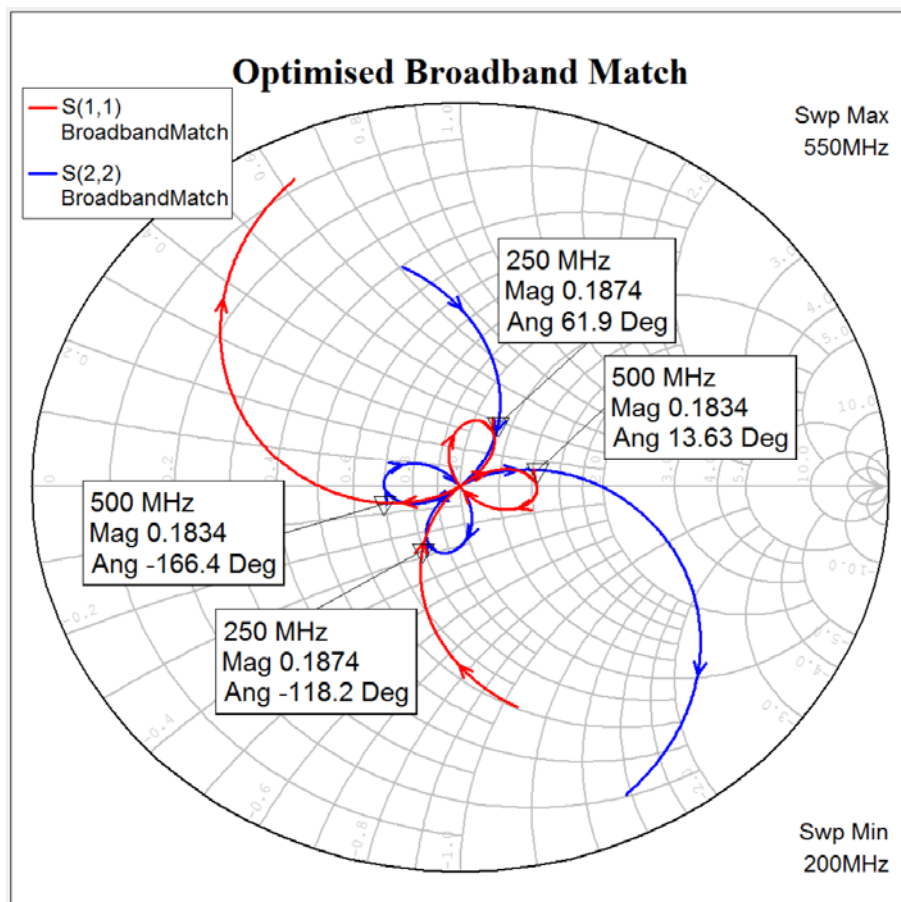


Figure 9.32. Final broadband match S_{11} and S_{22} on a Smith chart.

For impedance matches of the output of transistors or FET's, it is desirable to make the first section a lowpass T network. This is achieved by replacing the first Pi matching section with the equivalent lowpass T using equations 9.5 to 9.7.

Example 9.2: Broadband Amplifier

Applying broadband matching to a transistor or FET results in additional problems. Since the device is not normally unilateral, there is an interaction between the input and output matching. As an example consider the MRF1535NT1 MOSFET that we used before for the impedance matching. From the manufacturer's data sheet, the S parameters at a drain current of 2 Amp is in table 9.1:

!MRF1535NT1, 12.5V IDQ = 2.0 A, 35W MOS FET								
# MHZ S MA R 50								
!F	S11		S21		S12		S22	
!MHz	S11	Ang	S21	Ang	S12	Ang	S22	Ang
50	0.94	-176	9.42	88	0.005	-72	0.89	-177
100	0.94	-178	4.56	82	0.005	4	0.89	-177
150	0.94	-178	2.99	78	0.003	7	0.89	-177
200	0.94	-178	2.14	74	0.005	17	0.90	-176
250	0.95	-178	1.67	71	0.004	40	0.90	-175
300	0.95	-178	1.32	67	0.007	35	0.91	-175
350	0.95	-178	1.08	67	0.005	57	0.92	-174
400	0.96	-178	0.93	63	0.003	50	0.93	-173
450	0.96	-178	0.78	62	0.007	68	0.93	-173
500	0.96	-177	0.68	61	0.004	99	0.94	-173
550	0.97	-177	0.59	58	0.008	78	0.93	-175
600	0.97	-178	0.51	57	0.009	92	0.92	-174

Table 9.1. MRF1535NT1 small-signal parameter data [2].

The lines beginning with ! are comments and have been added for clarity. The line

MHZ S MA R 50

indicates that the frequency in the following file is in MHz, it is an S parameter file and the values are magnitude (rather than dB) and the reference impedance is 50 ohm.

This can now be used as a sub-circuit in NI AWR DE. For this example, a match from 250MHz to 450MHz is required. An input matching network will consist of a coupling capacitor followed by a Pi section and a lowpass T section. Having the lowpass T section at the input of the MOSFET provides a lower Q match for the input capacitance of the MOSFET than a Pi network. At the output, a lowpass T section is used to provide a high amplifier efficiency, by having an inductor in series with the output. This is followed by a Pi section in order to obtain good harmonic filtering. To determine the components of the matching networks the input and output impedances of the MOSFET is required. The centre of the 250 MHz to 450 MHz frequency band is 350 MHz, for which large signal S parameter data are given.

From equation 8.4, for an amplifier with a perfect output match, $\Gamma_{in} = S_{11}$ and from equation 8.5, for an amplifier with a perfect input match, $\Gamma_{out} = S_{22}$, so that from equation 8.1:

$$Z_{in} = Z_0 \frac{1 - S_{11}}{1 + S_{11}} \quad \text{Eqn. 9.21}$$

$$Z_{out} = Z_0 \frac{1 - S_{22}}{1 + S_{22}} \quad \text{Eqn. 9.22}$$

Using the values from table 9.1 in these equations results in:

$$Z_{in} = 1.282 - j0.8722 \Omega \quad \text{and} \quad Z_{out} = 2.089 - j2.616 \Omega \quad \text{Eqn. 9.23}$$

Freescale's AN721 [3] shows that the empirical load resistance for a power transistor is:

$$R_L = \frac{[V_{cc} - V_{CE(sat)}]^2}{2P_{out}} \quad \text{Eqn. 9.24}$$

Assuming a 12.5V supply, $V_{ce(sat)} = 1$ V and $R_L = 2.089$ as shown in equation 9.23, the output from the amplifier is 31.7 Watt. This agrees with figure 9.11 or the device data sheet [2]. With an $IDQ = 2A$ as per table 9.1, the quiescent power dissipation is 25W. Under the full load conditions, the amplifier will be supplying 32 W RF power and the amplifier will be highly nonlinear. In practice, this amplifier should give a linear output to about 10 W. The amplifier's linear output power can be increased by increasing IDQ to close to the maximum 6A. That will however require careful heat sinking to keep the transistor below its maximum operating temperature.

MRF1535NT1 Transistor
S parameters at 350MHz, $S11=0.95\text{Ang}-178$, $S21=1.08\text{Ang}67$, $S12=0.005\text{Ang}57$, $S22=0.92\text{Ang}-174$

$S11=\text{polar}(0.95, -178)$	$S11: (-0.9494, -0.03315)$		
$S21=\text{polar}(1.08, 67)$	$S21: (0.422, 0.9941)$		
$S12=\text{polar}(0.005, 57)$	$S12: (0.002723, 0.004193)$		
$S22=\text{polar}(0.92, -174)$	$S22: (-0.915, -0.09617)$		
$Zin=50*(1+S11)/(1-S11)$	$Rin=\text{real}(Zin)$	$Xin=\text{imag}(Zin)$	$Zin: (1.282, -0.8722)$
$Zout=50*(1+S22)/(1-S22)$	$Rout=\text{real}(Zout)$	$Xout=\text{imag}(Zout)$	$Zout: (2.089, -2.616)$
$Ri1=50$	$Rin: 1.282$	$Xin: -0.8722$	
$Ri2=\sqrt{Ri1*Rin}$			$Ri2: 8.008$
$Ro1=50$	$Rout: 2.089$	$Xout: -2.616$	
$Ro2=\sqrt{Ro1*Rout}$			$Ro2: 10.22$
$Freq=3.5e8$		$Wm=2*\pi*Freq$	$Wm: 2.199e9$
$Qi=2.5$			
$Qo=2.5$			
Pi Match input			
$Ycp1=(Qi/Ri1)$		$Qipmin=\sqrt{Ri1/Ri2}$	$Qipmin: 2.499$
$Xcp1=(1/Ycp1)$		$Cpi1=1e12/(Wm*Xcp1)$	$Cpi1: 22.74$
$Xcp2=Ro2^2*(\sqrt{(Ri1/Ri2)/((Qi*Qi+1)-(Ri1/Ri2))})$		$Cpi2=1e12/(Wm*Xcp2)$	$Cpi2: 22.79$
$Xlpi=(Qi*Ri1+(Ri1*Ro2*Xcp2))/(Qi*Qi+1)$		$Lpi=1e9*Xlpi/(Wm)$	$Lpi: 9.099$
LowPassT Match input			
$Xlit1=(Rin*Qi - Xin)$		$Lti1=1e9*Xlit1/Wm$	$Lti1: 1.855$
$Ai2=((Rin*(1+Qi*Qi)/Ri2) - 1)$		$Ai=\sqrt{Ai2}$	$Ai: 0.4014$
$Bi=Rin*(1+Qi*Qi)$			$Bi: 9.298$
$Qitmin=\sqrt{Ri2/Rin-1}$			$Qitmin: 2.29$
$Xlit2=Ro2^2*Ai$		$Lti2=1e9*Xlit2/Wm$	$Lti2: 1.462$
$Xcit=Bi/(Qi+Ai)$		$Cti=1e12/(Wm*Xcit)$	$Cti: 141.9$
Pi Match output			
$Ycp01=(Qo/Ro1)$		$Qopmin=\sqrt{Ro1/Ro2}$	$Qopmin: 2.212$
$Xcp01=(1/Ycp01)$		$Cpo1=1e12/(Wm*Xcp01)$	$Cpo1: 22.74$
$Xcp02=Ro2^2*(\sqrt{(Ro1/Ro2)/((Qo*Qo+1)-(Ro1/Ro2))})$		$Cpo2=1e12/(Wm*Xcp02)$	$Cpo2: 30.89$
$Xlpo=(Qo*Ro1+(Ro1*Ro2*Xcp02))/(Qo*Qo+1)$		$Lpo=Xlpo*1e9/(Wm)$	$Lpo: 10.02$
LowPassT Match output			
$Xlot1=(Rout*Qo - Xout)$		$Lto1=1e9*Xlot1/Wm$	$Lto1: 3.564$
$Ao2=((Rout*(1+Qo*Qo)/Ro2) - 1)$		$Ao=\sqrt{Ao2}$	$Ao: 0.6942$
$Bo=Rout*(1+Qo*Qo)$			$Bo: 15.15$
$Qotmin=\sqrt{Ro2/Rin-1}$			$Qotmin: 2.29$
$Xlot2=Ro2^2*Bo$		$Lto2=1e9*Xlot2/Wm$	$Lto2: 3.226$
$Xcot=Bo/(Qo+Ao)$		$Cto=1e12/(Wm*Xcot)$	$Cto: 95.9$

Figure 9.33. Equations for initial values of matching networks.

Since the input and output impedances are much smaller than 50Ω , having the coupling capacitors at the 50Ω sides of the matching networks result in smaller coupling capacitors. This does however place an extra DC voltage on the capacitors of the output-matching network and that may exceed the voltage ratings of those capacitors.

The initial component values for the input and output matching networks are calculated at 350 MHz, using a progressive impedance transformation and a lowpass T section at the amplifier terminals and a Pi section at the input and output terminals. Figure 9.33 shows the equations for AWRDE to calculate these matching circuit component values using the manufacturers S parameters as a starting point. These networks are then connected to the large signal S parameter model of the MOS FET as shown in figure 9.34.

The corresponding frequency response of the amplifier, together with S_{11} , S_{22} and the stability factors for the amplifier. It can be seen that this simple matching procedure provides a reasonable input and output match is obtained and that this results in a >15 dB gain up to 400 MHz. There are however some problems. For unconditional stability, K must be greater than one and $B1$ must be greater than zero or the input and output μ coefficients must be greater than one. This is the case in the 250 to 450 MHz frequency band, but is not the case outside this region, particularly in the 50 to 150MHz

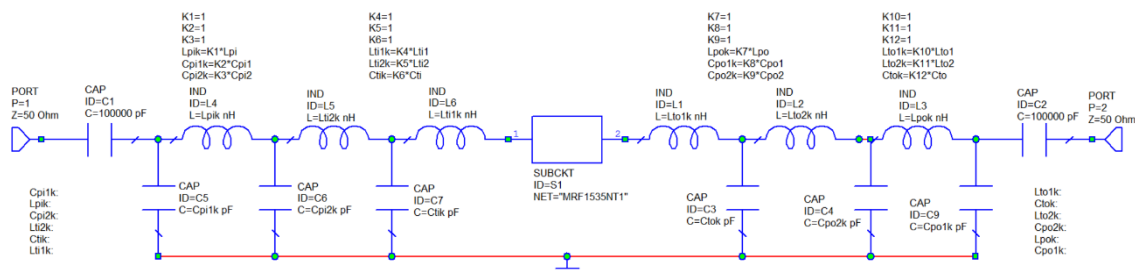


Figure 9.34. Broadband amplifier matching network as calculated.

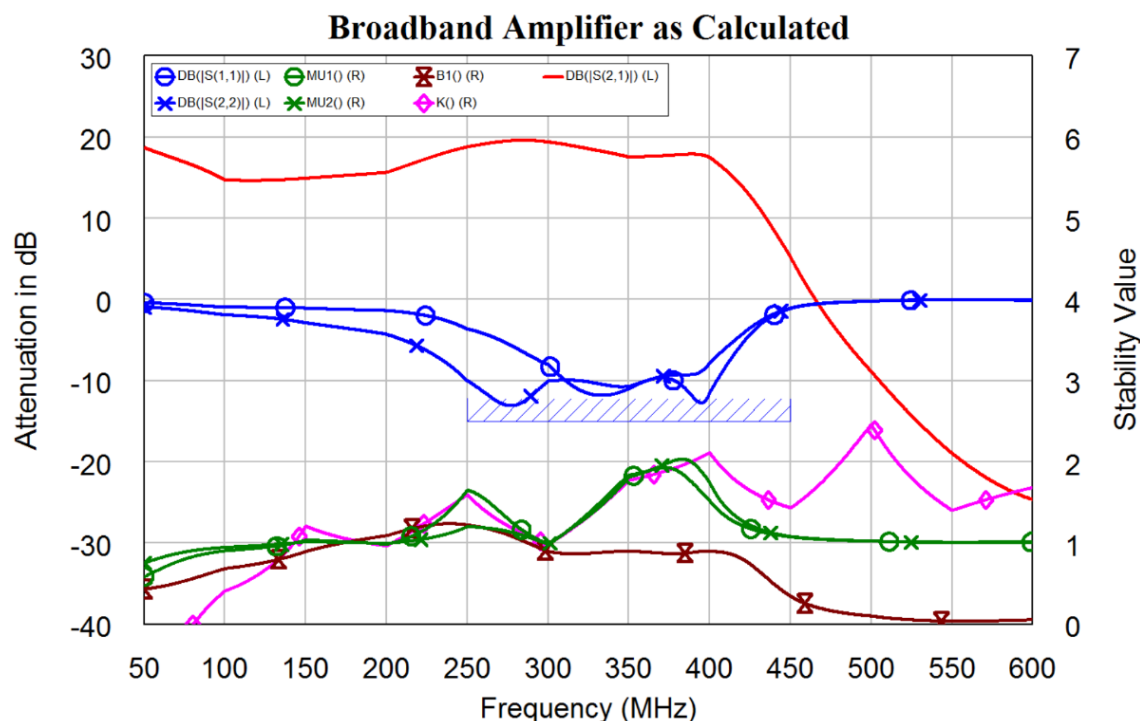


Figure 9.35. Performance of broadband amplifier as calculated.

The initial network is optimised to improve the input and output match over the 250 MHz to 450 MHz range. The circuit after optimisation is shown in figure 9.36. The gain has improved slightly in the 250 MHz to 450 MHz region due to the improved impedance matching. The stability has improved in the 250 MHz to 450 MHz bandwidth, but the circuit is still conditionally stable in the 50 MHz to 100 MHz frequency region.

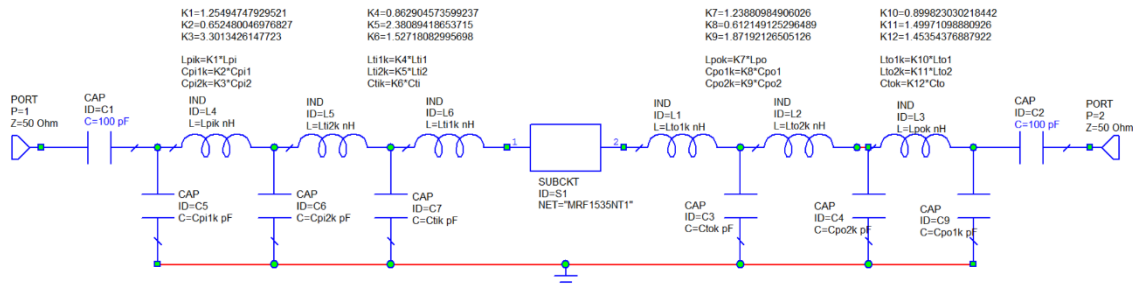


Figure 9.36. Broadband amplifier matching network after optimisation.

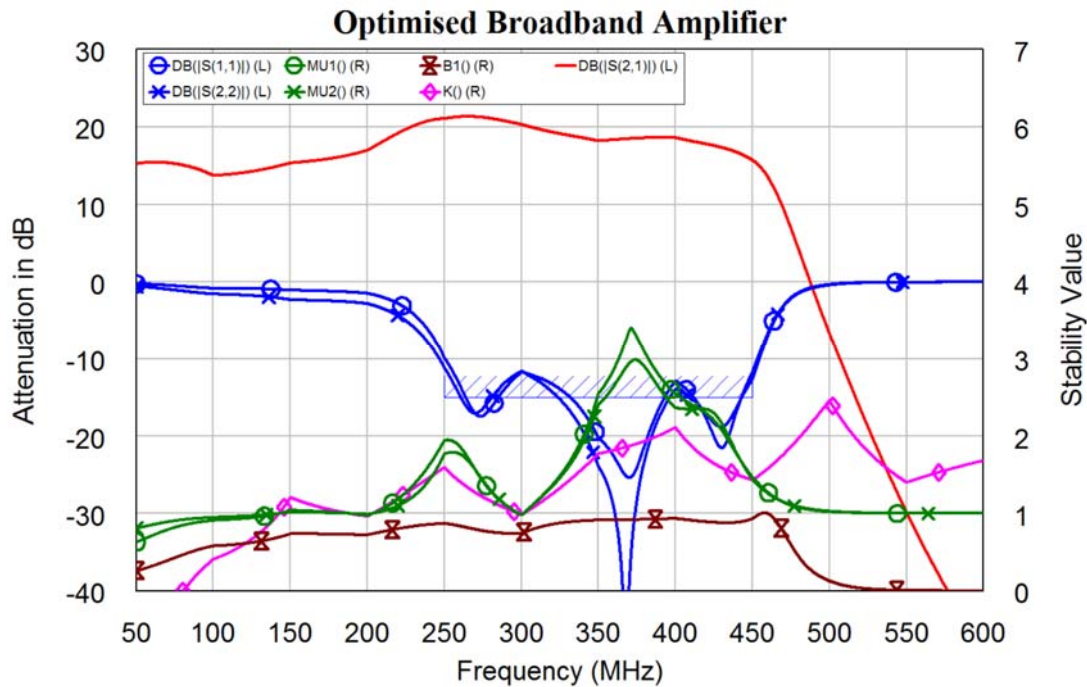
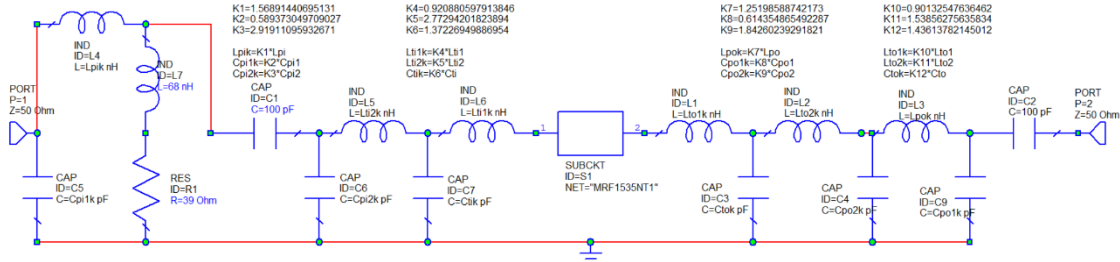


Figure 9.37. Performance of broadband amplifier after optimisation.

As can be seen from table 9.1, the FET has a very high gain at low frequency as a result; the amplifier will tend to oscillate at low frequencies. To reduce the gain at low frequencies and provide the required DC isolation at the input, input and output coupling capacitors (C_1 and C_2) are used. In figures 9.34 and 9.46, these capacitors were made large, to ensure that they did not affect the frequency response. Now these capacitors are tuned to reduce the gain at low frequency. This alone however does not improve the stability sufficiently and the amplifier remains conditionally stable in the 50 to 100 MHz frequency range. An unconditionally stable amplifier can be obtained by using resistors and ensuring that they are only effective at low frequencies, by using series inductors. Resistor R_1 and inductor L_7 in figure 9.38 perform this function. R_1 , L_7 and C_1 are tuned to ensure the amplifier is unconditionally stable. This changes the input and output match over the 250 MHz to 450 MHz range, so that the amplifier must be optimised again to ensure the best input and output match is obtained whilst maintaining stability. The stability is ensured by including $MU1()$ and $MU2()$ as optimisation parameters and setting

a very high penalty factor to ensure that they are >1 from 1 MHz to 600 MHz. The resulting circuit diagram is shown in figure 9.38 and the corresponding performance is shown in figure 9.39. It can be seen that the amplifier is well matched over the 250 MHz to 450 MHz range and is unconditionally stable, except for 200 MHz, where $MU1() = 0.977$ and $MU2() = 0.990$.



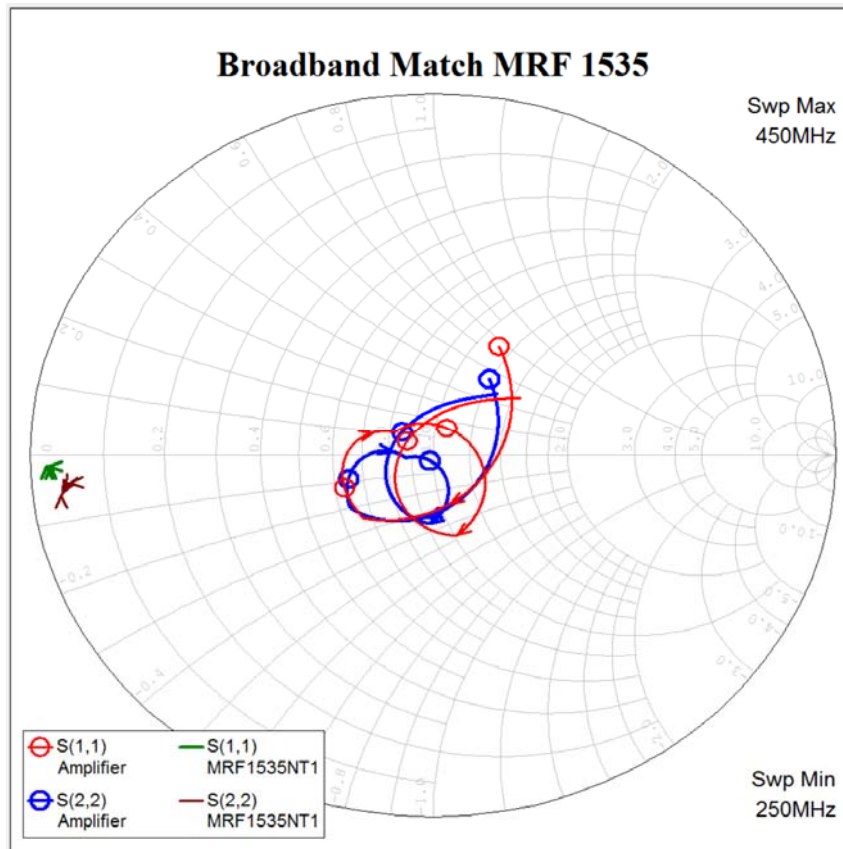


Figure 9.40. Impedance match of broadband amplifier.

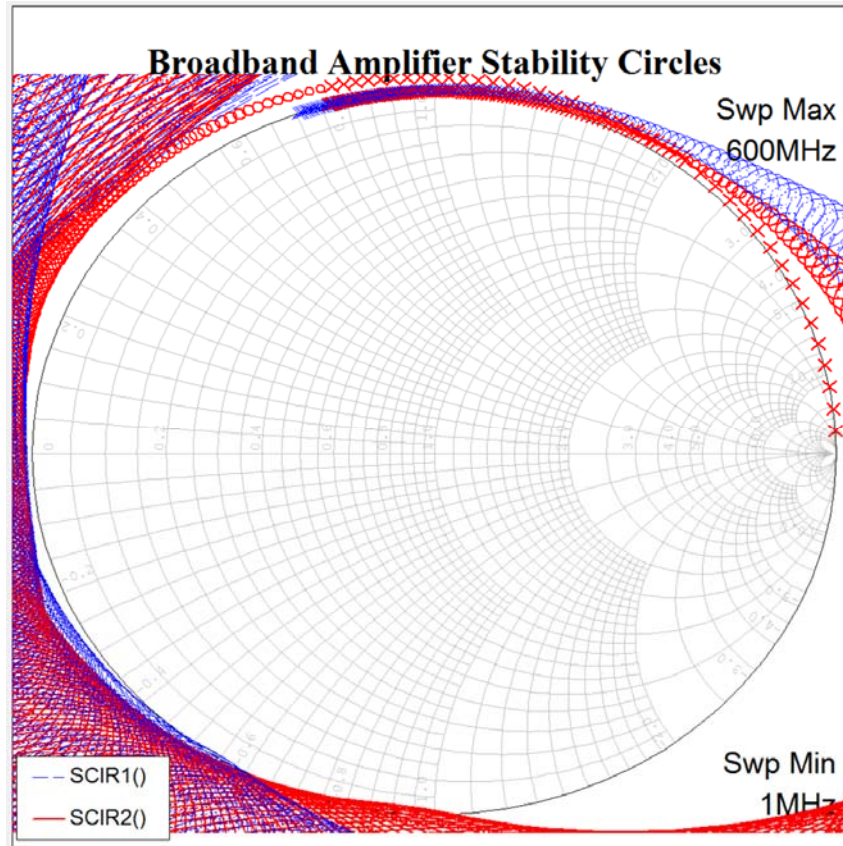
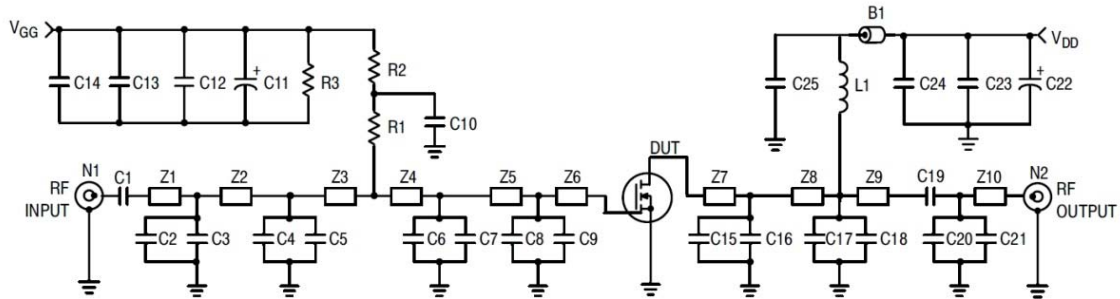


Figure 9.41. Stability circles of broadband amplifier.



B1	Ferroxcube VK200	C21	1.8 pF, 100 mil Chip Capacitor
C1	160 pF, 100 mil Chip Capacitor	L1	47.5 nH, 5 Turn, Coilcraft
C2	3 pF, 100 mil Chip Capacitor	N1, N2	Type N Flange Mounts
C3	3.6 pF, 100 mil Chip Capacitor	R1	500 Ω Chip Resistor (0805)
C4	2.2 pF, 100 mil Chip Capacitor	R2	1 k Ω Chip Resistor (0805)
C5	10 pF, 100 mil Chip Capacitor	R3	33 k Ω , 1/8 W Chip Resistor
C6, C7	16 pF, 100 mil Chip Capacitors	Z1	0.480" x 0.080" Microstrip
C8, C15, C16	27 pF, 100 mil Chip Capacitors	Z2	1.070" x 0.080" Microstrip
C9	43 pF, 100 mil Chip Capacitor	Z3	0.290" x 0.080" Microstrip
C10, C14, C25	160 pF, 100 mil Chip Capacitors	Z4	0.160" x 0.080" Microstrip
C11, C22	10 μ F, 50 V Electrolytic Capacitors	Z5, Z8	0.120" x 0.080" Microstrip
C12, C24	1,200 pF, 100 mil Chip Capacitors	Z6, Z7	0.120" x 0.223" Microstrip
C13, C23	0.1 μ F, 100 mil Chip Capacitors	Z9	1.380" x 0.080" Microstrip
C17, C18	24 pF, 100 mil Chip Capacitors	Z10	0.625" x 0.080" Microstrip
C19	160 pF, 100 mil Chip Capacitor	Board	Glass Teflon®, 31 mils
C20	8.2 pF, 100 mil Chip Capacitor		

Figure 10.450 - 520 MHz Broadband Test Circuit

Figure 9.42. Matching network from MRF1535NT1 from data sheet [2].

To lower production costs, the inductors in figure 9.38 can be replaced by Microstrip transmission lines, as shown in figure 7.10. That will change the input and output match slightly, so that further optimisation may be required. Figure 9.42 shows the 450-520 MHz broadband test circuit from the MRF1535NT1 data sheet [2]. That matching network is very similar to the one presented in this example. Notice that the tracks for Z_6 and Z_7 are very wide. For many devices, the manufacturers provide exact layout information for their devices. Unfortunately, that information is not provided in the datasheet [2].

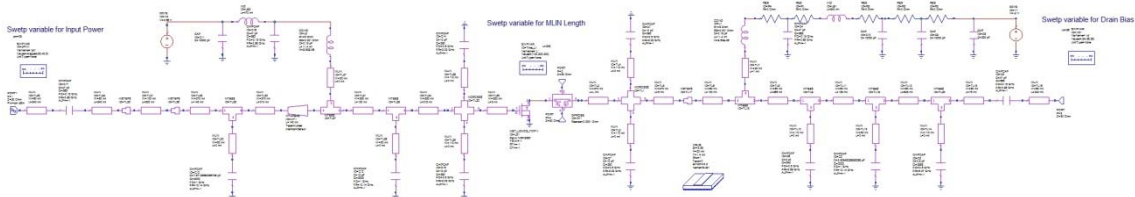


Figure 9.43. 60 W 900 MHz FET amplifier [5].

In many cases, the matching networks are more complex than what has been described here. As an example figure 9.43 shows the circuit for an MRF 9060 amplifier 60 Watt amplifier operating in the 900 to 1000 MHz frequency region, from the *Freescale LDMOS Swept Variables Example* from AWRDE. This is one of the examples from AWRDE and is similar to sample designs done by Freescale. Figure 9.44 gives the corresponding PCB layout. Notice how the low transmission-line impedances required for the input matching result in very wide PCB tracks. FET's in general are more linear than bipolar transistors and are thus preferred for applications requiring a low intermodulation distortion, as is required in mobile radio base-station amplifiers or DAB

and TV transmitters. FET's have very high gains at low frequencies and are thus more susceptible to instability.

During the last few years, the number of available RF devices has reduced significantly, particularly devices operating below 800 MHz. Many discrete RF devices have a relatively short availability life. For example the MRF 9060 devices used in the *Freescale LDMOS Swept Variables* Example from AWRDE, are no longer available. Possible replacement parts are the MRFE6S9045NR1 or MRFE6S9060NR1 devices. In many cases, such changes require a package change and thus require a completely new design.

That design example is very good, as it demonstrates how a design's performance can be investigated, when it is subject to variations of things like input power, source and drain voltage changes and tolerances on line lengths used in the PCB layout. This shows the types of computer simulation that should be undertaken to ensure that the design is likely to work properly when constructed.

Many of the RF device manufacturers [6], now have AWRDE models for their devices, as library parts, thus allowing more accurate simulations to be carried out. This website does not have models for the MRF1535NT1 or the MRFE9060 devices, however the AWRDE LDMOS model library that can be accessed inside AWRDE from *X Libraries* \Rightarrow **AWR web site* \Rightarrow *Parts by Type* \Rightarrow *Nonlinear* \Rightarrow *Freescale* \Rightarrow *LDMOS* \Rightarrow *Cancelled*, includes the MRFE9060. For locations outside the USA, and behind firewalls of many universities or companies, the web based *X Library* on the **AWR web site* library may be too slow or not work at all. In those instances, the relevant libraries should be installed locally. Appendix 1 gives detailed instructions on how to do this.

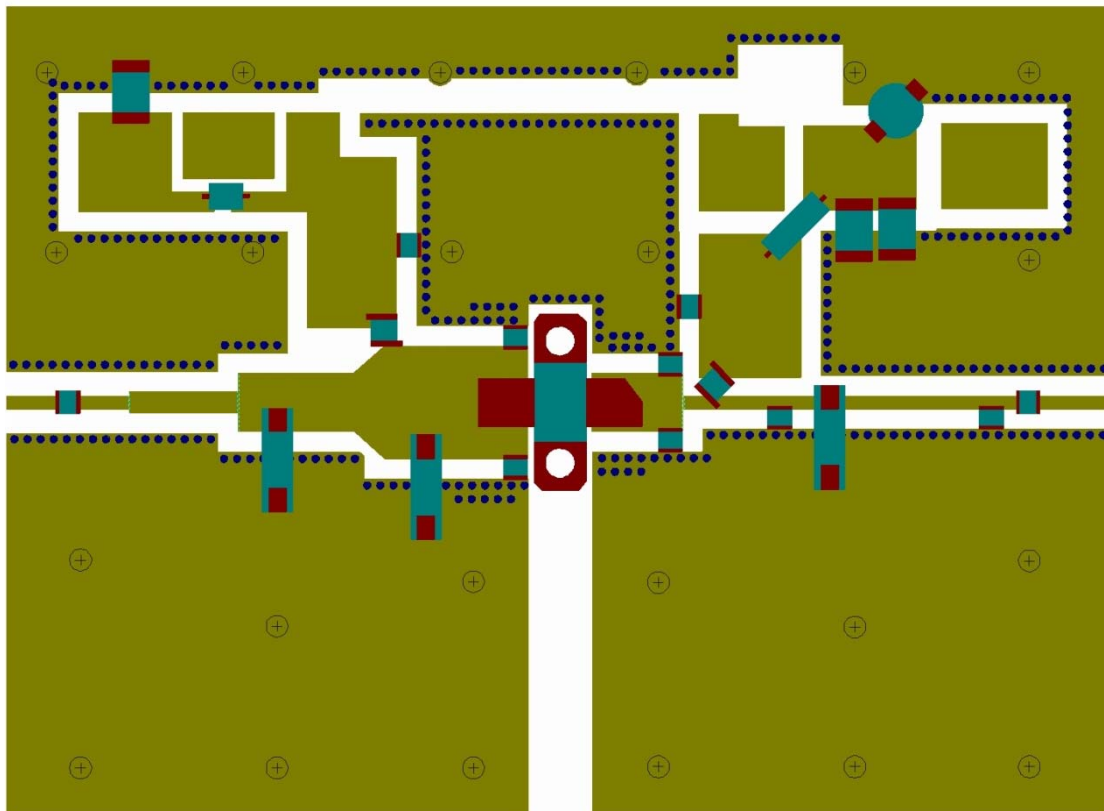


Figure 9.44. 60 W 900 MHz FET amplifier layout (AWR/Freescale Example [6]).

References

1. F. Davis, Motorola (Freescale, NXP) Semiconductor Application Note AN267, “Matching Network Designs with Computer Solutions.” 1993. http://cache.freescale.com/files/rf_if/doc/app_note/AN267.pdf
2. Freescale Semiconductor Technical Data, MRF1535NT1 data sheet Rev13, June 2009. <https://cache.nxp.com/docs/en/data-sheet/MRF1535N.pdf>
3. B. Becciolini, “Motorola (Freescale, NXP) Semiconductor Application Note AN721, “Impedance Matching applied to RF Power Transistors”, October, 2005. http://cache.freescale.com/files/rf_if/doc/app_note/AN721.pdf
4. A. Wood, B. Davidson, “Motorola (Freescale) Semiconductor Application Note AN1526, http://cache.freescale.com/files/rf_if/doc/app_note/AN1526.pdf
5. Freescale and AWR, Example “*Freescale LDMOS Swept Variables.emp*”, included in the AWRDE example files.
6. NXP Models for NI AWR Corporation Microwave Office®, https://www.nxp.com/products/rf/rf-high-power-models/models-for-ni-awr-corporation-microwave-office:RF_HIGH_POWER_MODELS_AWR

Chapter 10

Operational Amplifiers

Introduction

Operational amplifiers (OpAmps) with 3 dB bandwidths larger than 1.5 GHz are now available. Such operational amplifiers are used in consumer applications like hard disk drives, computer monitors, industrial and medical applications, such as CAT scanners. In addition one can use these operational amplifiers for IF amplifiers in many communication receiver applications.

These high-speed amplifiers fall into two categories [1, 2]:

Voltage Feedback Amplifiers

Current Feedback Amplifiers

The Voltage Feedback amplifiers have the same properties as common operational amplifiers, such as the LF356 or LM741, used at low frequencies. The Voltage feedback amplifiers have lower noise, better dc performance and more freedom in feedback impedance selection.

The Current Feedback [3] amplifiers on the other hand have faster slew rates and lower distortion, but have restrictions on feedback configurations.

Voltage Feedback Amplifier Theory

If an operational amplifier has input voltages V_1 and V_2 at the input terminals, then for a voltage feedback amplifier the output voltage is:

$$V_{out} = A(s) * (V_1 - V_2) \quad \text{Eqn. 10.1}$$

where $A(s)$ is the open loop gain, which is frequency dependent. Consider the non-inverting amplifier configuration:

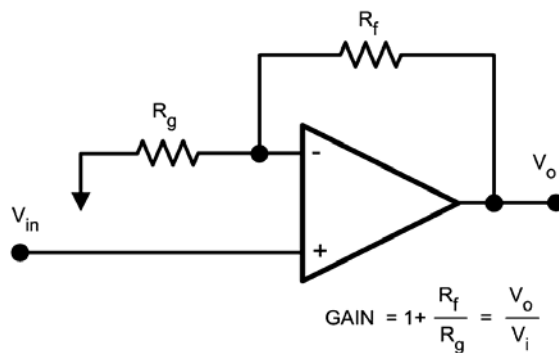


Figure 10.1. Non-inverting Amplifier [1]

$$\text{If } G = \frac{R_f + R_g}{R_g} \quad \text{Eqn. 10.2}$$

$$\text{Then } V_{out} = V_{in} \left(\frac{G}{1 + \frac{G}{A(s)}} \right) = V_{in} \left(\frac{G * A(s)}{A(s) + G} \right) \quad \text{Eqn. 10.3}$$

When $A(s)$ is very large, then the gain is approximately;

$$V_{out} = V_{in} * G \quad \text{Eqn. 10.4}$$

When $A(s) = G$ the gain will be 3 dB below the gain when $A(s)$ is very large. The frequency when $A(s) = G$ is thus the bandwidth of the amplifier. Since $A(s)$ decreases with frequency as shown in figure 2, the bandwidth of the amplifier will depend on the gain as is also shown in figure 2.

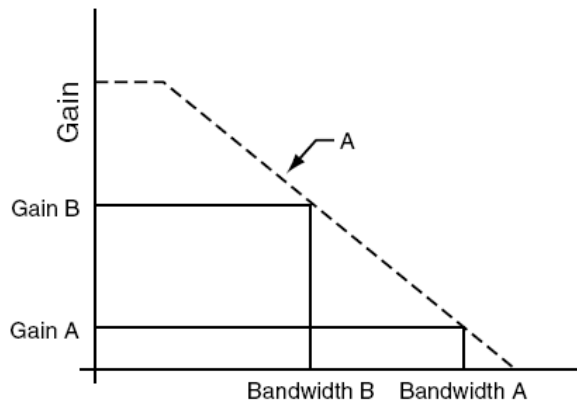


Figure 10.2. Open loop and Closed loop gain of Voltage Feedback Amplifier [1]

If the gain of the amplifier is

$$A(s) = A(s) * (1 + D) \quad \text{Eqn. 10.5}$$

Then the gain of the amplifier can be written as:

$$V_{out} = V_{in} \left(\frac{G}{1 + \frac{G}{A(s)*(1+D)}} \right) = V_{in} \left\{ G * \left(1 - \frac{G}{A(s)*(1+D)} \right) \right\} = V_{in} \left\{ G * \left(1 - \frac{G}{A(s)*(1+D)} \right) \right\} \quad \text{Eqn. 10.6}$$

Current Feedback Amplifier Theory

The Current feedback amplifier produces an output voltage proportional to an “Error current” I_{error} .

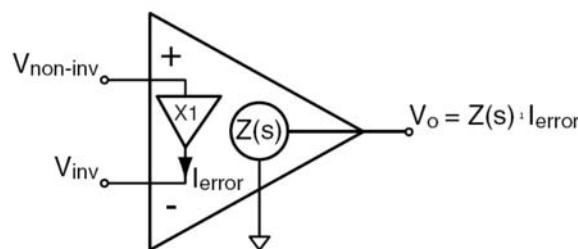


Figure 10.3 Current Feedback amplifier configuration [1]

For the inverting amplifier configuration, the equations for the amplifier are:

$$i_{error} = \frac{V_{in} - V_o}{R_f} + \frac{V_{in}}{R_g} \quad \text{Eqn. 10.7}$$

Since $V_o = Z(s)I_{error}$, substituting for I_{error} in the above equation after manipulation leads to:

$$V_o = \frac{R_g}{Z(s) + R_f} V_{in} \quad \text{Eqn. 10.8}$$

The current feedback amplifier will thus have a transfer function of:

$$V_o = \left[\frac{G}{1 + \frac{R_f}{Z(s)}} \right] \quad \text{Eqn. 10.9}$$

Compared with the transfer function of the voltage feedback amplifier of:

$$V_o = \left[\frac{G}{1 + \frac{G}{A(s)}} \right] \quad \text{Eqn. 10.10}$$

Where $G = \frac{R_f + R_g}{R_g}$ is the gain of an ideal amplifier Eqn. 10.11

The amplifier corner frequency is when $G/A(s) = 1$ or when $R_f/Z(s) = 1$. The way $G/A(s)$ and $R_f/Z(s)$ changes with frequency will thus result in a difference in the bandwidth of the amplifiers. Halving both R_f and R_g , keeps the gain the same for both amplifier configurations, and double the bandwidth of the current feedback amplifier, but not change the bandwidth for the voltage feedback amplifier. Halving R_g and keeping R_f the same, will increase the gain G , as per equation 10.10 for both amplifiers. According to figure 11.2, this will reduce the bandwidth of the voltage feedback amplifier by close to half. Changing R_g will not change the bandwidth of the current feedback amplifier. The feedback resistor R_f can only be varied over a small range. For example, the LMH6702 has been optimised for a 237Ω feedback resistor. Using a lower value can lead to excessive ringing in a pulse response and a higher value will limit the bandwidth.

Current and Voltage Feedback Amplifier Comparison

Voltage feedback (VFB) OpAmps, are normally used for teaching about OpAmps at universities and as a result, most engineers are very familiar with them. Voltage feedback OpAmps have high open loop gains, low offset voltage and low input bias currents. The +ve and -ve input circuit architectures are the same, so that input bias and noise currents for both inputs of VFB OpAmps are approximately equal. For FET input OpAmps the bias currents can be less than 1 pA. For low voltage power supplies, rail to rail inputs and outputs are required. The vast majority of rail to rail OpAmps are voltage feedback devices.

Current feedback OpAmps have a lower open loop gain and lower input impedances. That results in less gain accuracy. The +ve and -ve input circuit architectures are different, so that the input bias and noise currents are different. Current feedback amplifiers are thus not very suitable for integrators. Current feedback OpAmps, are optimised for a fixed feedback resistor and that makes it more difficult for them to be used for active filters. Current feedback amplifiers have larger bandwidths, higher slew rates and generally have a lower distortion than voltage feedback amplifiers, as can be seen in the table 10.1. The vast majority of high bandwidth, high output power OpAmps, such as those used for xDSL drivers are current feedback amplifiers. For a fair comparison, the fastest commercial grade operational amplifiers from the same manufacturer, capable of operating from $\pm 4V$ to $\pm 6V$ supplies, are used in table 10.1.

	Current Feedback	Voltage Feedback
Device	LMH 6702	THS4211
3dB Bandwidth (Gain = 2)	1.7 GHz	325 MHz
Slew rate	3100 V/ μ s	970 V/ μ s
Noise Voltage	1.83 nV/ $\sqrt{\text{Hz}}$	7 nV/ $\sqrt{\text{Hz}}$ (1 MHz)
Noise Current	3.0 pA/ $\sqrt{\text{Hz}}$	4 pA/ $\sqrt{\text{Hz}}$ (10 MHz)
Distortion (HD2)	-79 dBc (20 MHz, 2Vpp)	-68 dBc (30 MHz, 2Vpp)
Distortion (HD3)	-88 dBc (20 MHz, 2Vpp)	-80 dBc (30 MHz, 2Vpp)
Input Offset Voltage	1 mV	3 mV
Input Bias Current	8 μ A	7 μ A
Input Offset Current		0.3 μ A
Load Resistor test circuit	100 Ω	499 Ω
Feedback Resistor test circuit	237 Ω	392 Ω
Feedback Resistor range	Narrow	Very wide
Supply Voltage	± 4 V to ± 6 V	± 2.5 V to ± 7.5 V
Supply Current	12.5 mA	19 mA
Output Current	80 mA	170 mA
Output Voltage ± 5 Vs	± 3.5 V	± 5 V
Input Impedance	1.4 M Ω	6 G Ω
Input Capacitance	1.6 pF	0.3 pF

Table 10.1. Current and Voltage Feedback performance comparison.

Example 10.1: High Impedance 10 kHz-20 MHz Amplifier

As part of an On-Line Impedance Analyser [4], a voltage sensor is required, to measure Power Line Communication (PLC) signals, with frequencies from 10 kHz to 20 MHz, which are injected onto 240V, 50 Hz, mains voltage power lines. The input impedance of the circuit should be greater than 500 k Ω . The design of this voltage sensor shows how either current or voltage feedback amplifiers, best satisfy the requirements for different parts of the circuit. The PLC signals on the power line are about 1V, so that more than 60 dB mains voltage attenuation is required for a >12 dB signal to mains voltage ratio, to enable accurate signal detection. Filtering out the mains voltage and passing the PLC signals, requires a high pass filter with a 10 kHz cut off frequency. The whole circuit is to operate from ± 5 V supplies. OpAmps with a 12V total (± 6 V) supply voltage capability are used for reliability. AD8058 Dual OpAmps are used for the voltage feedback amplifiers and AD8017 Dual OpAmps are used for the current feedback amplifiers. Their .cir Spice models can readily be imported into NI AWR DE to permit simulation.

Figure 10.4 shows the circuit diagram of the complete voltage sensor. The operational amplifiers A1 and A2 are a high impedance high pass buffer amplifier. The 27 pF capacitor and the 56 k Ω resistor to ground, form a high pass filter, that is part of the

Butterworth high pass frequency response of the whole voltage sensor. That capacitor, together with the potential divider consisting of the $500\text{ k}\Omega$ and $56\text{ k}\Omega$ resistors ensure that the mains voltage does not cause any damage to the OpAmps A1 and A2. For these values, a 240V 50Hz mains voltage, results in 130 mV at the input terminal of the OpAmp, which is quite safe. The potentiometer has an 8.35 times voltage reduction at high frequency. This has to be made up using gain in the other part of the circuit.

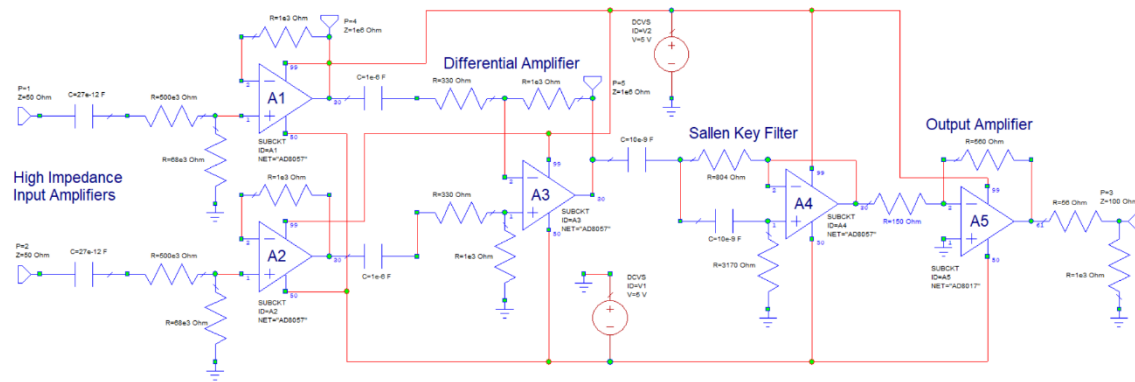


Figure 10.4. PLC Frequency Voltage Sensor.

The AD8057/8058 OpAmp has a 2 pF input capacitance (to ground) and that with the $68\text{ k}\Omega$ resistor at the input pin of the OpAmp causes a 1.33 MHz low pass corner frequency, which is far less than the 20 MHz required upper frequency. Reducing the $68\text{ k}\Omega$ resistor will increase the high frequency corner frequency, but reduces the output voltage of the circuit. The THS4211 Voltage amplifier of table 10.1, with an input capacitance of 0.3 pF will have a better high frequency response. However, the Texas Instruments Spice models do not at this stage import easily into NI AWR DE. For accurate differential input capability, it is important that both OpAmps A1 and A2 are matched as close as possible. Using a Dual OpAmp ensures that both A1 and A2 are well matched and operate at the same temperature. The THS4211 is only available as a single amplifier in each package, while the AD8058 is a Dual OpAmp.

High Impedance Input stage

The design options for the high impedance input amplifiers in figure 10.4 will now be considered. A suitable circuit is shown in figure 10.5.

Since 240V (679V_{pp}) mains voltages are present at the amplifier input, the mains voltage must be attenuated to be less than 1V_{pp} , to prevent the input amplifier clipping when measuring the PLC signals above 10 kHz as required. The input capacitors $CS1$ must have a voltage rating $>240\text{V}_{\text{ac}}$. For a first order high pass filter, with a 10 kHz cut off frequency, a mains voltage of 3.4V_{pp} results. Therefore, about 10 dB additional attenuation is required for this first amplifier stage. An input impedance $>500\text{ k}\Omega$ is required, so that the amplifier does not load the circuit to be measured. The 2 pF input capacitance of the OpAmp is an $8\text{ k}\Omega$ impedance at 10 MHz, so that the input impedance is primarily determined by $RS1$, which must be $500\text{ k}\Omega$ in order to satisfy the input impedance requirement.

Initially $RF2$ in figure 10.5 is removed, so that the amplifier gain is determined by $RS1$ and $RS2$ only. The resistor $RS2$ is required to firstly provide the more than 10 dB mains frequency attenuation, and secondly shift the corner frequency due to the 2 pF input capacitance to a higher frequency. When $RS1 = 500\text{ k}\Omega$, $RS2 = 220\text{ k}\Omega$ provides 10.3 dB

attenuation. That will however result in an upper corner frequency of 521 kHz. $RS2 = 56\text{ k}\Omega$ provides an attenuation of 20 dB and an upper corner frequency of 1.58 MHz while $RS2 = 8.2\text{ k}\Omega$ provides an attenuation of 35.8 dB and an upper corner frequency of 9.9 MHz. Figure 10.6 shows the corresponding frequency responses using a full Spice simulation of the circuit of figure 10.5.

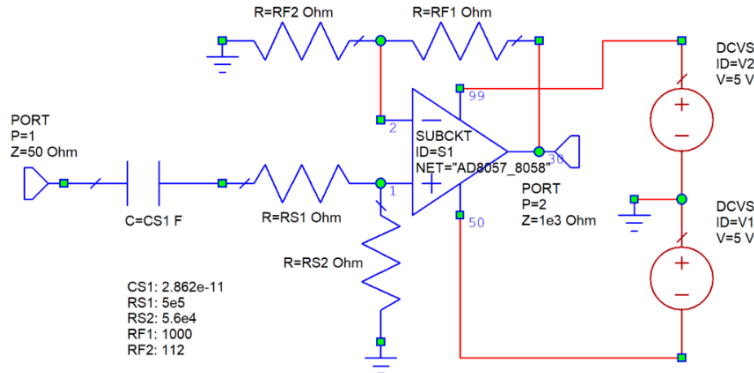


Figure 10.5. High impedance input amplifier.

Initially $RF2$ in figure 10.5 is removed, so that the amplifier gain is determined by $RS1$ and $RS2$ only. The resistor $RS2$ is required to firstly provide the more than 10 dB mains frequency attenuation, and secondly shift the corner frequency due to the 2 pF input capacitance to a higher frequency. When $RS1 = 500\text{ k}\Omega$, $RS2 = 220\text{ k}\Omega$ provides 10.3 dB attenuation. That will however result in an upper corner frequency of 521 kHz. $RS2 = 56\text{ k}\Omega$ provides an attenuation of 20 dB and an upper corner frequency of 1.58 MHz while $RS2 = 8.2\text{ k}\Omega$ provides an attenuation of 35.8 dB and an upper corner frequency of 9.9 MHz. Figure 10.6 shows the corresponding frequency responses using a full Spice simulation of the circuit of figure 10.5.

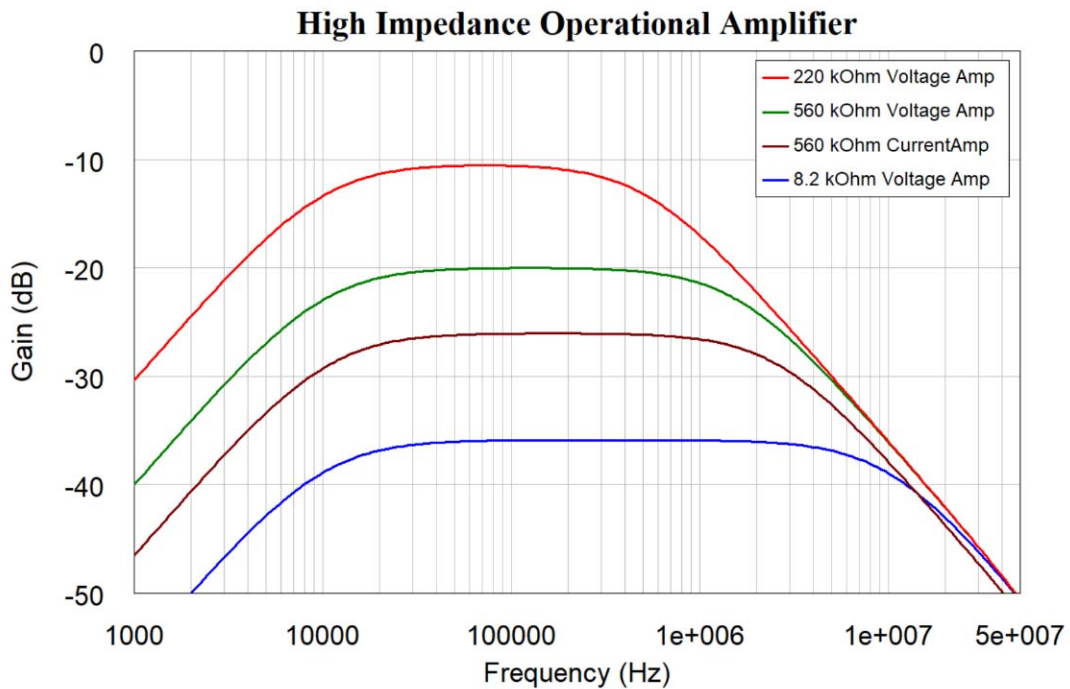


Figure 10.6. High input impedance operational amplifier frequency response.

Figure 10.6 shows that for this application, the current amplifier has 6 dB less gain than calculated and current feedback amplifiers are not suitable for having high value resistors connected to their inputs. Since the PLC signals to be detected are less than 1V at the input terminals, $RS2 = 8.2 \text{ k}\Omega$ with a 35.8 dB loss results in less than 16 mV signal and a poor SNR for detecting that signal at the OpAmp output.

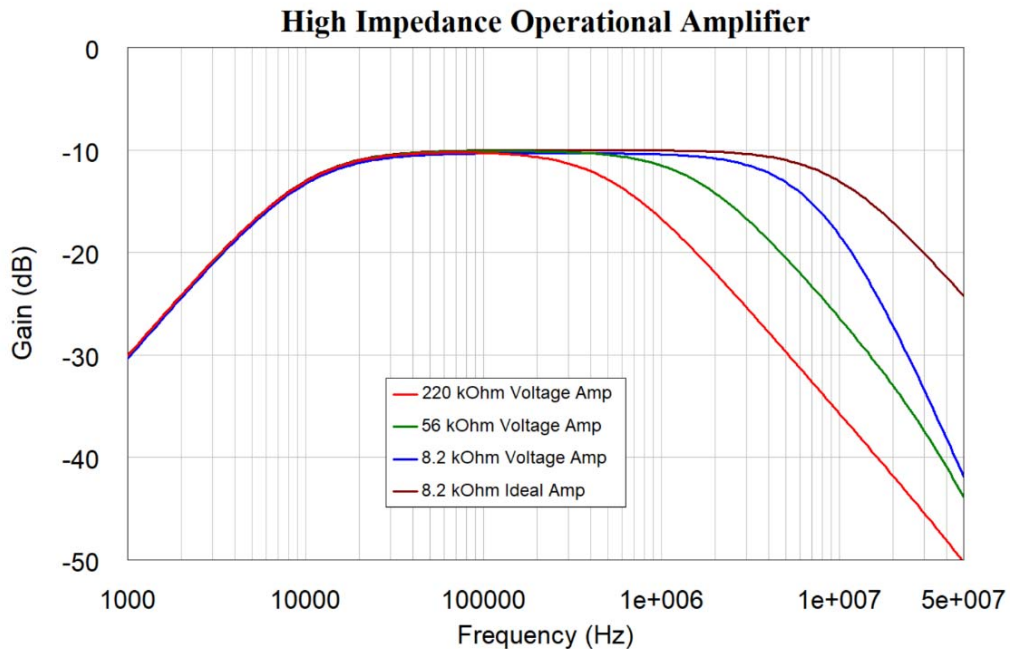


Figure 10.7. Amplifier circuits of figure 10.5 with same gain and $RS2$ varied.

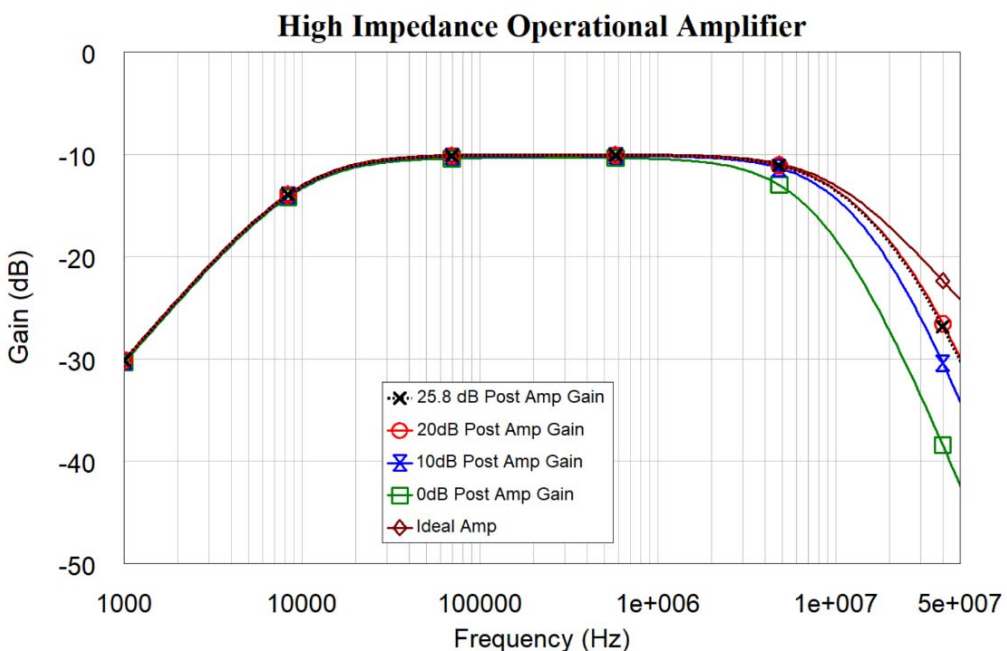


Figure 10.8. Amplifiers, with $RS2 = 8.2 \text{ k}\Omega$, varied $RF2$ and post amplifier gain.

The gain is now set to -10 dB for all the voltage-feedback amplifier configurations, by including $RF2$, as shown in figure 10.5, in the circuit. The resulting frequency responses are shown in figure 10.7. Applying the required 25.8 dB gain to the amplifier with

$RS = 8.2 \text{ k}\Omega$, results in a high frequency response that is limited by the OpAmp characteristics. To show this the frequency response obtained from an ideal amplifier, including the 2 pF input capacitance of the actual OpAmp is included in figure 10.7. To obtain a good high frequency response, the gain that can be obtained is thus limited. To show this in more detail, an AD8017 current feedback amplifier is placed at the output of the circuit of figure 10.5, and the gain of the high impedance amplifier with $RS2 = 8.2 \text{ k}\Omega$ is varied by changing both $RF2$ and the gain of the current feedback amplifier, so that the whole amplifier gain is -10 dB. The gain of this additional current feedback amplifier is shown as Post Amp Gain in figure 10.8.

Since $RS = 8.2 \text{ k}\Omega$ results in an attenuation of 35.8 dB, for the current feedback amplifier with 0dB gain, the voltage feedback amplifier of figure 10.5 needs a 25.8 dB gain due to $RF2$. Similarly, a 10dB post amplifier gain needs a 15.8 dB amplifier gain and 20 dB post amplifier gain needs a 5.8 dB amplifier gain. As a reference, the frequency response due to an ideal OpAmp is included in figure 10.8. This shows that the best performance is obtained when the gain due to $RF2$ is less than 6dB and 20 dB of amplifier gain is used for the current amplifier that follows the high impedance input stage. Since such a gain would cause overload due to mains voltages, this amplifier needs to be included after a further high pass filter stage.

These design simulations are only part of the story. An early version of this amplifier used $RS1 = 1 \text{ M}\Omega$ and $RS2 = 100 \text{ k}\Omega$, together with AD8045 OpAmps, which are single OpAmps with a 1.3 pF input capacitance. Figure 10.9 shows the measured frequency response of the same circuit when different size surface-mount resistors are used for $RS1$. The SMD resistors have a very small capacitance associated with them and that changes the high frequency response. These effects can only be measured using actual hardware.

When building the full circuit of figure 10.4, it was found that the common mode input performance, requiring a very good gain match of A1 and A2, was far superior using Dual OpAmps. As a result, the AD8058, Dual OpAmp shown in figure 10.4 were used. For the hardware of figure 10.4, the best frequency response and noise performance was obtained using $RS2 = 68 \text{ k}\Omega$.

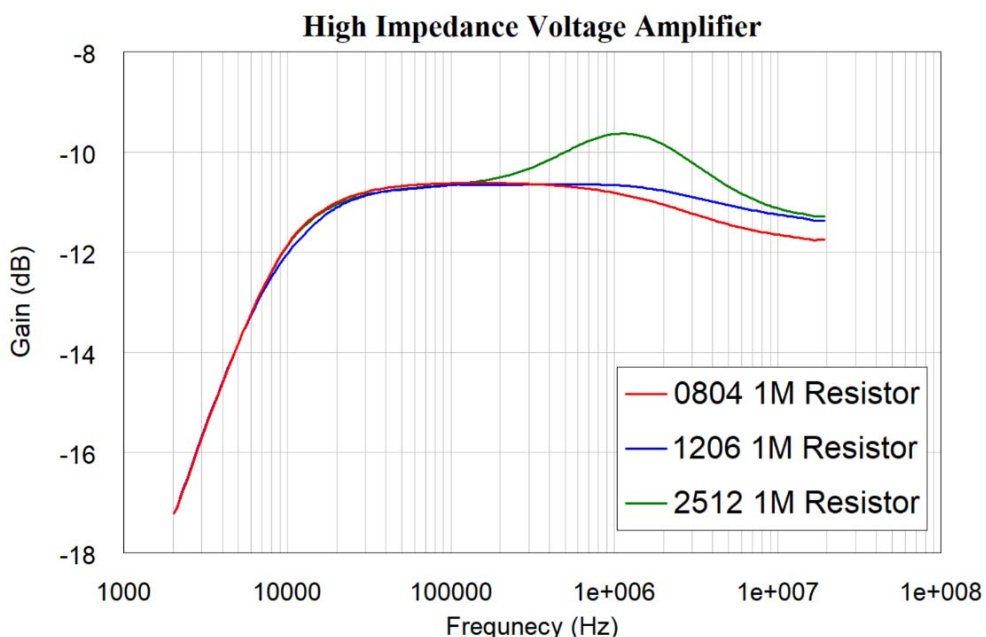


Figure 10.9. High input impedance operational amplifier measured frequency response.

This example shows that a high frequency OpAmp design involves compromises to ensure that the OpAmp characteristics cause the least degradation in system noise and bandwidth performance. In addition, component properties will significantly affect the performance of the amplifier in unpredictable ways, as shown in figure 10.9.

Other OpAmp Stages

The design of the high input impedance amplifier of figure 10.5 is the most difficult part of the design of the circuit in figure 10.4. The final value used for $RS2 = 68 \text{ k}\Omega$, results in a signal loss of 18.4 dB.

We now consider the remainder of that circuit. The gain for the differential amplifier A3 is chosen to be 3 (9.6 dB), which then produces total gain of -8.9 dB, which is close to the -10 dB gain to prevent mains voltage overload. The 330Ω and $1 \text{ k}\Omega$ resistors used allow either voltage feedback or a current feedback OpAmps to be used.

The 10 kHz high pass filter used to remove the mains voltages, consists of a first order high pass filter at the high input impedance amplifiers A1 and A2, together with a second order Sallen-Key high Pass filter for A4, to result in a third order Butterworth high pass frequency response. The required resistor values are 804Ω and $3.17 \text{ k}\Omega$, together with 10 nF capacitors. Those resistor values are more suitable for voltage feedback amplifiers. However the impedances can be changed, so that the feedback resistor required matches the optimised value to the current feedback amplifiers are to be used. The AD8058 is a relatively low cost Dual OpAmp, one package can be used for both the differential amplifier and the Sallen-Key high Pass filter. The decision on whether to use voltage or current feedback amplifiers is thus mainly determined by cost and PCB area used, as well as the limitations outlined above and in [1-3].

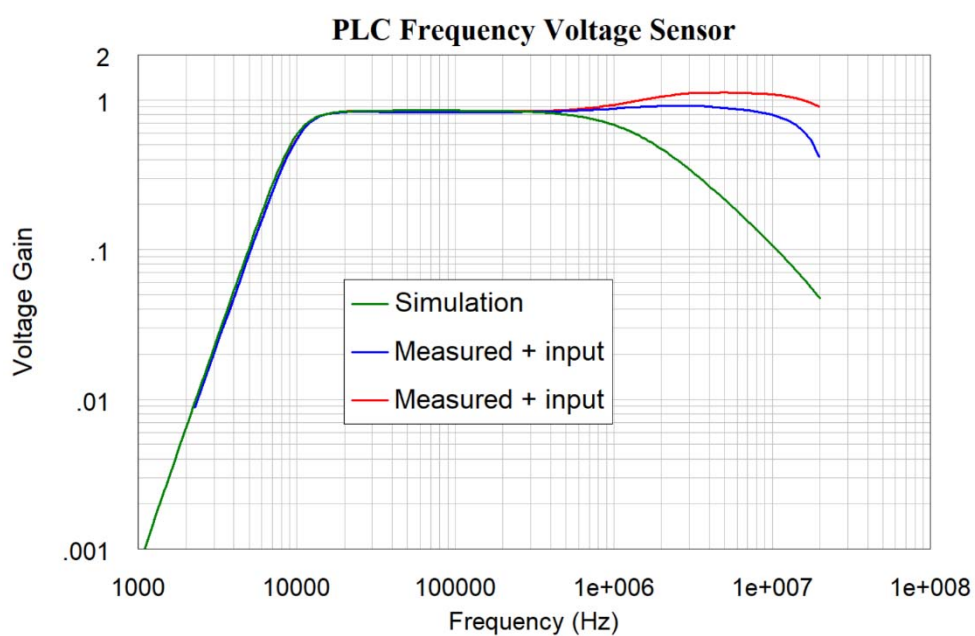


Figure 10.10. Measured and simulated frequency response of circuit of figure 10.4.

The output amplifier must be able to drive 50Ω coaxial cable used to connect the BNC output terminals to a digital oscilloscope or PicoScope used to digitise the measured voltages. Oscilloscopes typically have a 30 pF input capacitance and RG58 coaxial cable typically has a capacitance of 100 pF/m . The output operational amplifier must thus be

able to drive low impedances. The AD8017 is a low cost, high output current, 160 MHz bandwidth, current feedback OpAmp, suitable for line drivers in xDSL modems. The AD8017 is used for the output amplifier. A gain of 11.4 dB is used to provide a gain close to 1 for the whole circuit of figure 10.4. A $56\ \Omega$ resistor is included in series with the AD8017 output, to firstly provide a close to $50\ \Omega$ output impedance and secondly provide protection for the AD8017 in case a short circuit is applied at the output.

Figure 10.10 shows the measured and simulated frequency response of the whole circuit. Even though both A1 and A2 are in the same package, the layout is made as symmetrical as possible and the matched resistors from the same batches are used, the frequency response of the +ve input (A1) and the -ve input (A2) are different. The prototype made with AD8045 amplifiers had bigger differences between the inputs.

Figure 10.11 shows the second version of the prototype hardware for the high impedance voltage sensor of figure 10.4. As part of the measurements, it was found that an AD8039 Dual OpAmp has a slightly better common mode performance, i.e. less difference between amplifier A1 and A2 in figure 10.4, than the same circuit with an AD8058 Dual OpAmp. Unfortunately, the Spice model for the AD8038/8039 OpAmp cannot be imported directly into NI AWR DE as the AD8038 has a “disable” input, which prevents the import. The specified performance of the AD8039 and AD8057 OpAmps is very similar, however the quiescent current for the Dual AD8039 is 2 mA compared to 14 mA for the Dual AD8058, so that the hardware can run longer from a 12V battery.

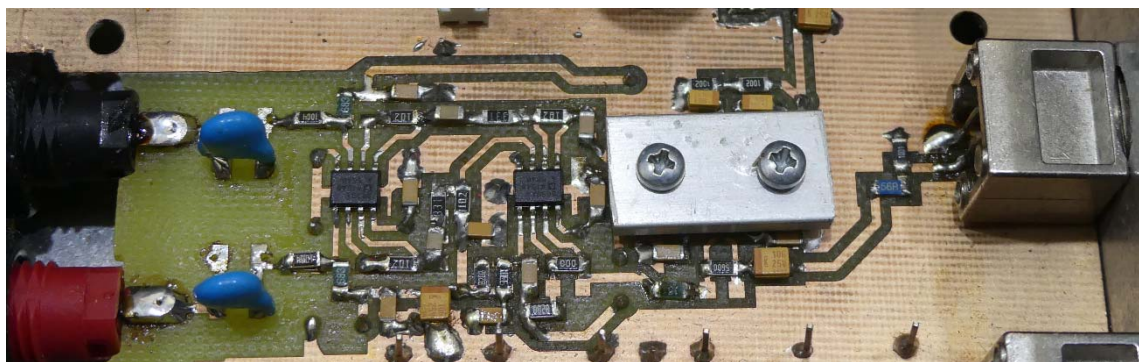


Figure 10.11. Hardware of circuit of figure 10.4.

Low Noise Designs using Operational Amplifiers

The noise voltage associated with a resistor is;

$$E_{NR} = \sqrt{4kTBR} \quad \text{Eqn. 10.12}$$

Where:

K = Boltzman's constant $1.38064852 \times 10^{-23}$ Joules/Kelvin

T = Absolute temperature Kelvin

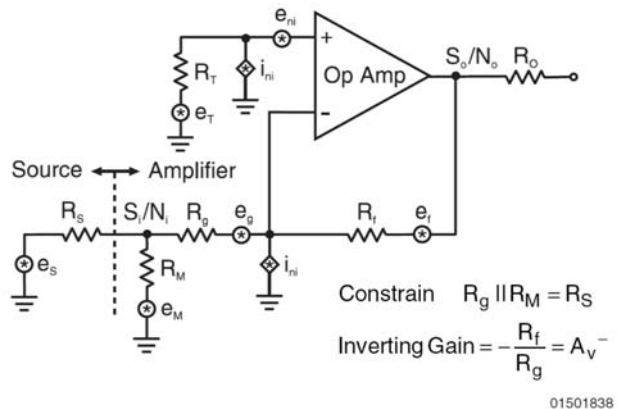
B = Bandwidth in Hz

R = Resistance in Ω

In a circuit each resistor is then associated with its own noise source which has a random noise voltage of E_{NR} . In addition the operational amplifier produces noise which can most accurately be represented as voltage (e_{ni}) and current noise sources (i_{ni+} and i_{ni-}) at the inputs, as shown in figure 10.12.

The values for e_{ni} , i_{ni+} and i_{ni-} are normally obtained from manufacturer's data sheets. Table 10.2 shows the noise performance of some low noise amplifiers from different

manufacturers. The noise of operational amplifiers will rise at low frequency, as shown in figures 10.13, 10.14 and 10.17, and is inversely proportional to frequency at low frequencies, due to flicker noise or 1/f noise. The corner frequency of that 1/f noise may be important in a design. For example if a microphone amplifier is required, the noise performance at less than 1 kHz is important and the ADA4898 has a better noise performance at those frequencies than the LMH6629, which has a better noise performance at higher frequencies.



01501838

Figure 10.12 Noise sources in an operational amplifier configuration (Fig 29 of [5])

Manufacturer	Part	Type	nV/\sqrt{Hz}	pA/\sqrt{Hz}	1/f Hz	GBWP MHz
Texas Instruments	LMH6629	VFB	0.69	2.6	5 kHz	900
Texas Instruments	OPA847	VFB	0.85	2.7	1 kHz	3500
Texas Instruments	TH4031	VFB	1.6	1.3	1 kHz	100
Analog Devices	AD8000	CFB	4.3	26-,3.4+	300 Hz	1500
Analog Devices	AD8099	VFB	0.950	2.6	10 kHz	510
Analog Devices	ADA4898	VFB	0.9	2.4	20 Hz	65

Table 10.2. Low Noise Operational Amplifiers.

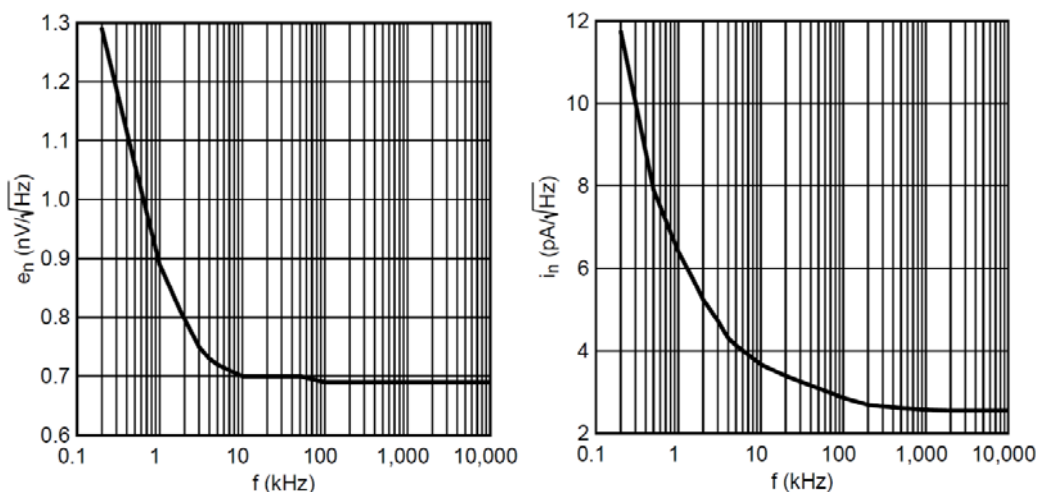


Figure 10.13. Noise of LMH6629 versus frequency

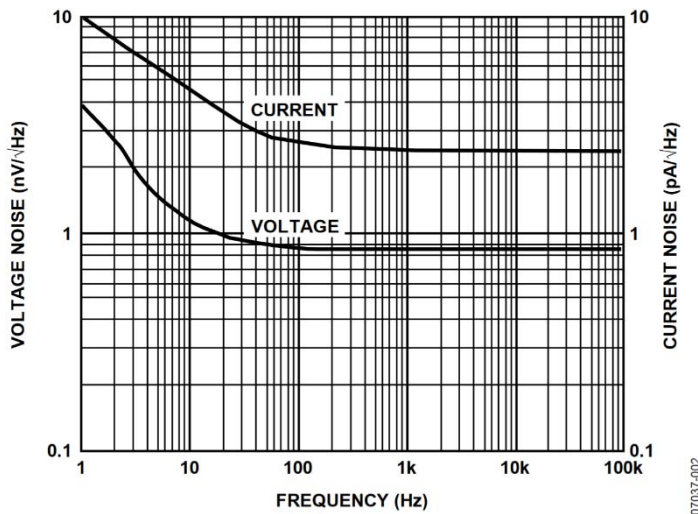


Figure 10.14. Noise and Distortion of ADA4898

Since the noise sources in the circuit are un-correlated, the total noise from the amplifier is obtained by adding the noise powers of those sources.

The amplifier configuration and the value of impedances used significantly affect the resulting noise performance of an amplifier as shown in the following example.

Example 10.2: Amplifier Design for Noise Performance.

A microphone has a source impedance $R_s = 600 \Omega$ and requires a load resistance larger than $1 \text{ k}\Omega$ for the microphone to operate correctly. The normal output from the microphone is 1mV. An amplifier with a voltage gain of close to 1000 is required. Figure 10.15 shows the circuit diagram of the non-inverting amplifier circuit. In practice, coupling capacitors are used at the input and output, to ensure that the amplifier output clips symmetrically and that no DC offset voltage occurs at the output. R_g should be such that it is much larger than the resistance of tracks used in the PCB or the resistance between the grounded side of R_g and the common ground point of the amplifier. R_g should be small to minimise the thermal noise of the resistor, which is amplified by the amplifier gain.

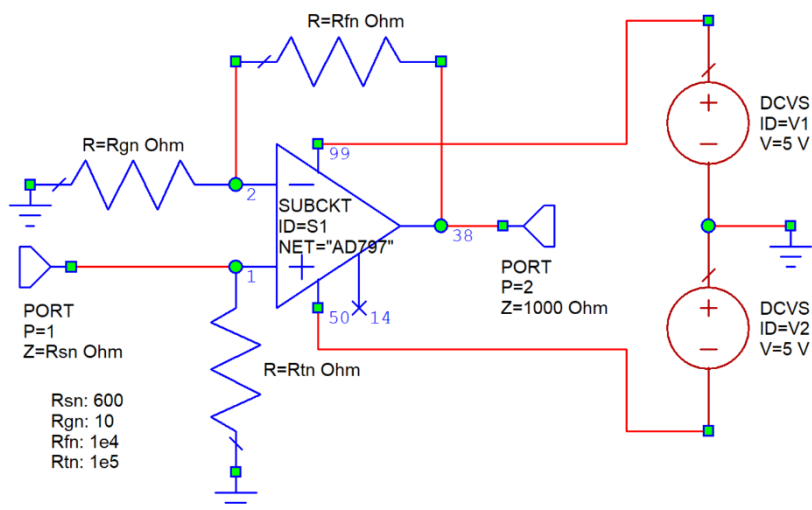


Figure 10.15. Non-inverting amplifier.

For the non-inverting amplifier, the noise power at the output of the OpAmp due to each component is evaluated using equations 10.13 to 10.20, [7, 8]:

$$\text{OpAmp noise voltage} \quad P_{e_n} = e_n^2 B \left(\frac{R_f + R_g}{R_g} \right)^2 \quad \text{Eqn. 10.13}$$

$$\text{OpAmp noise current +in} \quad P_{i_{np}} = (i_{np} \frac{R_s R_t}{R_s + R_t})^2 B \left(\frac{R_f + R_g}{R_g} \right)^2 \quad \text{Eqn. 10.14}$$

$$\text{OpAmp noise current -in} \quad P_{i_{nn}} = (i_{nn} \frac{R_g R_f}{R_g + R_f})^2 B \left(\frac{R_f}{R_g} \right)^2 \quad \text{Eqn. 10.15}$$

$$\text{Resistor } R_s \text{ noise} \quad PR_s = 4kTBR_s \left(\frac{R_t}{R_s + R_t} \frac{R_f + R_g}{R_g} \right)^2 \quad \text{Eqn. 10.16}$$

$$\text{Resistor } R_t \text{ noise} \quad PR_t = 4kTBR_t \left(\frac{R_s}{R_s + R_t} \frac{R_f + R_g}{R_g} \right)^2 \quad \text{Eqn. 10.17}$$

$$\text{Resistor } R_g \text{ noise} \quad PR_g = 4kTBR_g \left(\frac{R_f}{R_g} \right)^2 \quad \text{Eqn. 10.18}$$

$$\text{Resistor } R_f \text{ noise} \quad PR_f = 4kTBR_f \quad \text{Eqn. 10.19}$$

$$\text{OpAmp Voltage Gain} \quad \text{Gain}_v = \frac{R_s}{R_s + R_t} \frac{R_f + R_g}{R_g} \quad \text{Eqn. 10.20}$$

For the non-inverting amplifier, $R_g = 10 \Omega$ is a good compromise. R_f sets the gain and $R_f = 10 \text{ k}\Omega$ results in a gain of $G = (R_f + R_g)/R_g = 1001$. Some bias current needs to flow into the non-inverting OpAmp input, so that a resistor R_t is required. R_t should be large enough, not to load the input and small enough not to cause any DC offset voltage at the output due to the OpAmp bias current. R_t should be $> 1 \text{ k}\Omega$ to prevent loading the microphone and small enough to ensure that the input bias current does not cause an offset voltage. The source impedance R_s and R_t form a potentiometer, which reduces the input signal. $R_t = 100 \text{ k}\Omega$ results in a 0.6% voltage drop across this potentiometer and a total amplifier gain of 995, which is close enough to the desired gain. Equation 10.17 shows that the value of R_t has little effect on the amplifier noise output since $R_s/(R_s + R_t)$ is very small.

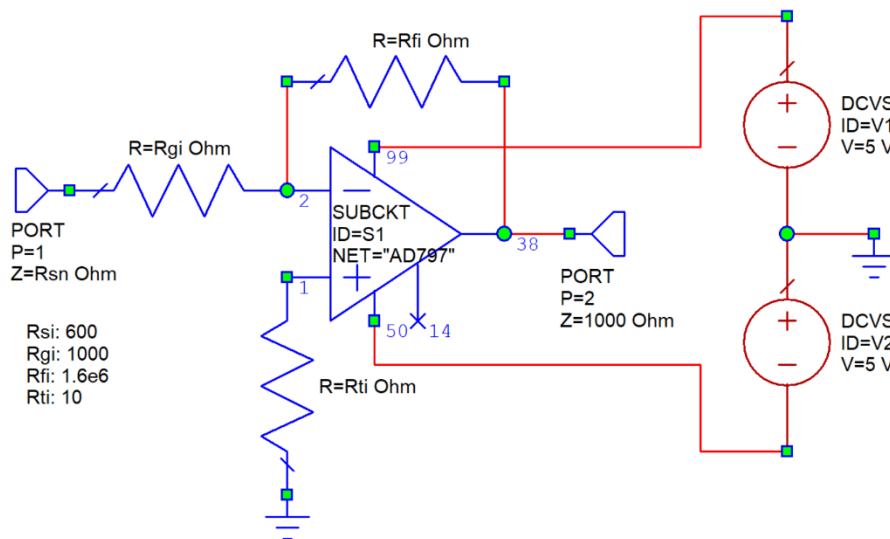


Figure 10.16. Inverting amplifier.

For the inverting amplifier, a minimum value of $R_g = 1 \text{ k}\Omega$, is required to prevent loading the microphone. Since $R_s = 600 \Omega$ and $R_g = 1\text{k}\Omega$, for a gain $G = R_f / (R_s + R_g) = 1000$, a value of $R_f = 1.6 \text{ M}\Omega$ is required. Resistor R_t must now be small to not affect the noise at the output. $R_t = 10 \Omega$ is suitable. Figure 10.16 shows the resulting circuit. Equations 0.19 and 10.21 to 10.27 determine the noise contributions of each of the noise sources in the inverting amplifier. For the inverting amplifier, the noise power at the output of the OpAmp due to each component is as follows:

$$\text{OpAmp noise voltage} \quad P_{e_n} = e_n^2 B \left(\frac{R_f + R_g + R_s}{R_g} \right)^2 \quad \text{Eqn. 10.21}$$

$$\text{OpAmp noise current +in} \quad P_{i_{np}} = (i_{np} R_t)^2 B \left(\frac{R_f + R_g + R_s}{R_g} \right)^2 \quad \text{Eqn. 10.22}$$

$$\text{OpAmp noise current -in} \quad P_{i_{nn}} = (i_{nn} \frac{(R_g + R_s) R_f}{R_g + R_s + R_f})^2 B \left(\frac{R_f}{R_g} \right)^2 \quad \text{Eqn. 10.23}$$

$$\text{Resistor } R_s \text{ noise} \quad P_{R_s} = 4kT B R_s \left(\frac{R_f}{R_g + R_s} \right)^2 \quad \text{Eqn. 10.24}$$

$$\text{Resistor } R_t \text{ noise} \quad P_{R_t} = 4kT B R_t \left(\frac{R_f + R_g + R_s}{R_g + R_s} \right)^2 \quad \text{Eqn. 10.25}$$

$$\text{Resistor } R_g \text{ noise} \quad P_{R_g} = 4kT B R_g \left(\frac{R_f}{R_g + R_s} \right)^2 \quad \text{Eqn. 10.26}$$

$$\text{Resistor } R_f \text{ noise} \quad P_{R_f} = 4kT B R_f \quad \text{Eqn. 10.19}$$

$$\text{OpAmp Voltage Gain} \quad \text{Gain}_v = -\frac{R_f}{R_g + R_s} \quad \text{Eqn. 10.27}$$

These equations are included in the project files for figures 10.15 and 10.16. This allows the noise contribution of each noise source to be determined and component values to be tuned to minimise the noise, whilst maintaining practical component values. To compare the noise performance, these equations are also entered in a spreadsheet, the results of which are presented in table 3. For this example $T = 290$ Kelvin and the bandwidth $B = 20$ kHz. For Voltage feedback amplifiers, the +ve input noise current (i_{np}) is normally the same as the -ve input noise current (i_{nn}), however for current feedback amplifiers, they are normally different since the +ve and -ve input circuit architectures are different. Table 10.2 shows that for the AD8000, the -ve input current noise is $26 \text{ pA}/\sqrt{\text{Hz}}$ and the +ve input current noise is $3.4 \text{ pA}/\sqrt{\text{Hz}}$. In figure 10.12, the +ve and -ve input current noise is assumed to be the same, (i_{ni}).

The ADA4898 includes a power down switch, which causes simulation errors in NI AWR DE. So for the calculations in table 10.3 and simulation in figure 10.17, an AD 797 OpAmp is used, since it is suitable and its Spice model include input voltage and current noise models. The Analog Devices AD797.cir can be directly imported as a netlist into NI AWR DE. At 1 kHz, that amplifier has an input noise voltage of $0.9 \text{ nV}/\sqrt{\text{Hz}}$ and an input current noise of $2.0 \text{ pA}/\sqrt{\text{Hz}}$. Since this is a voltage feedback amplifier, this input current noise value applies to both the +ve and the -ve input terminals.

Table 10.3 shows that for the non-inverting amplifier, the dominant noise contribution is from the microphone source resistance R_s , and the second largest is due to the input current noise at the +ve input terminal. That current, flows through R_s in parallel with R_t and the resulting noise is thus directly related to R_s . All the other noise contributions are

more than 10 times smaller than the noise power due to R_s . That is close to the best that can be achieved.

Operational amplifier Noise calculation	
Temperature	290
4kT	1.60E-20
Bandwidth (Hz)	20000
Rs	Source resistance
Rt	Resistance to ground at non-inverting input
Rg	Input resistance series with inverting input
Rf	Feedback resistor

Op Amp	AD 797			
	Non Inverting Op Amp		Inverting Amp	
	Value	Output Noise	Value	Output Noise
en nV	0.9	1.623E-08	0.9	1.620E-08
in+ pA	2.0	2.851E-08	2.0	8.000E-12
in- pA	2.0	8.000E-12	2.0	2.044E-07
Rs	600	1.903E-07	600	1.922E-07
Rt	1.00E+05	1.142E-09	1.00E+01	3.210E-09
Rg	10	3.203E-09	1.00E+03	3.203E-07
Rf	10000	3.203E-12	1.60E+06	5.125E-10
Gain (FB)	995		1000	
RInp	5.96E+02			
Ripp	9.99001		1.598E+03	
Total Power/Hz		1.20E-11		3.68E-11
Total Noise				
Power		2.39E-07		7.37E-07
Noise Voltage				
mV		4.89E-01		8.58E-01

Signal In, Out				
mV	1	995	1	1000
SNR		66.17		61.33
Noise figure dB		1.00		5.84
Noise figure		1.26		3.83

Table 10.3. Noise for inverting and non-inverting amplifier configurations.

For the inverting amplifier, the noise caused by the 1 k Ω resistor R_g is the largest noise contributor. That resistor value is the lowest that can be used to load the microphone output. The input current noise at the -ve input terminal is the second largest noise contribution and this is mainly due to the value of R_f , which is limited by the gain required. The third largest noise contribution is due to R_s . The noise produced by R_s is thus not the dominant noise contribution. The non-inverting amplifier configuration is thus always preferred for low noise designs and it has a significantly higher signal to noise ratio and much lower noise figure than an inverting amplifier configuration. These calculations are for a microphone amplifier at audio frequencies, however the same principles apply for low noise operational amplifiers used in say MRI applications.

Figure 10.17 shows the Spice simulation of the amplifier. The 1.00 dB noise figure in table 3 for the non-inverting amplifier agrees closely with the 1.009 dB noise figure

obtained for the simulation in figure 10.17. From table 10.2, using an ADA8099, OPA847 or LMH6620, OpAmp will achieve a much wider bandwidth and similar to the noise performance to the transistor amplifier design in figure 8.9, so that low noise OpAmps can be used for receiver front end designs provided the required frequency is in the operational frequency range of the OpAmp.

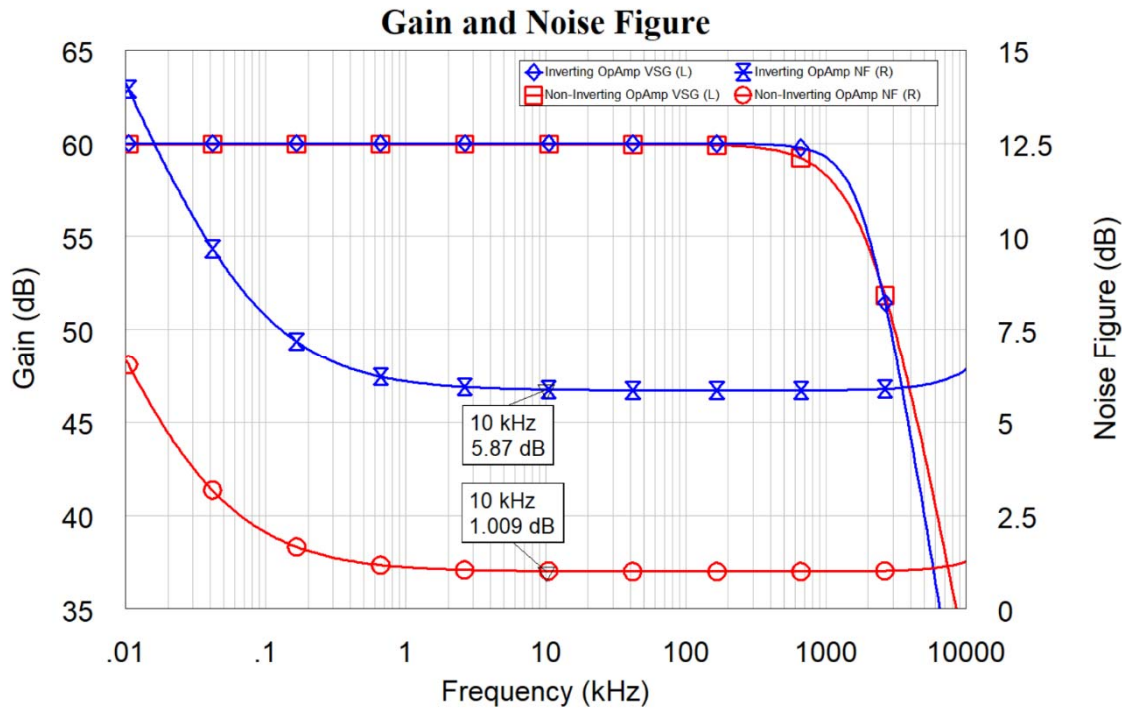


Figure 10.17. Gain and noise figure of amplifiers of fig. 10.15 and 10.16.

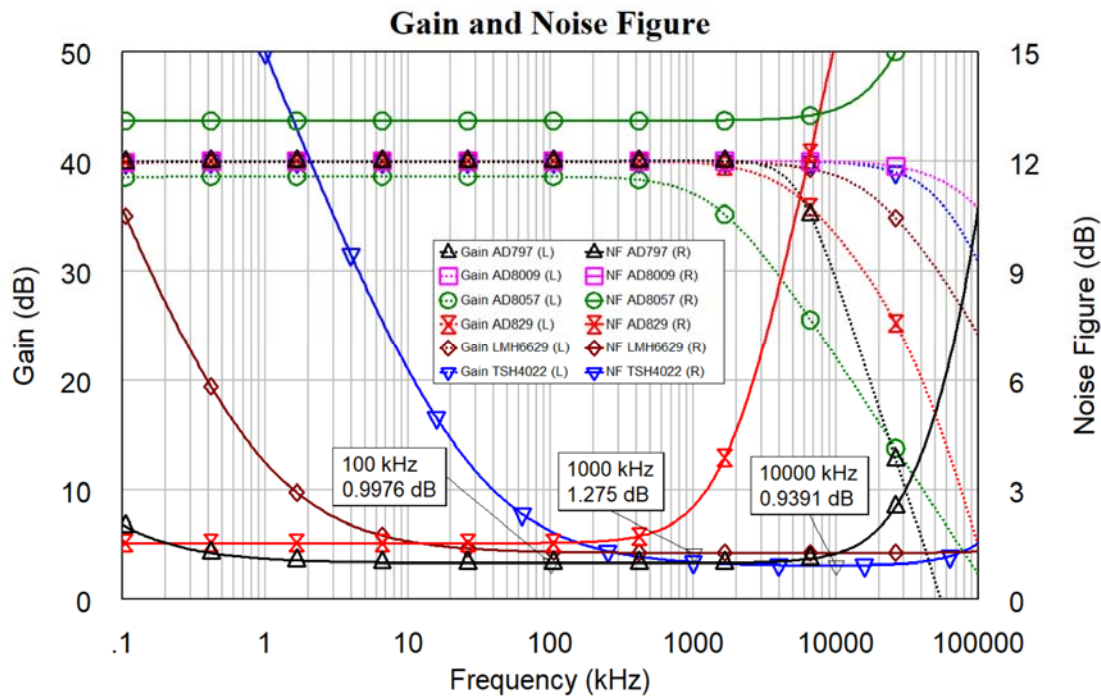


Figure 10.18. Gain and noise figure of different OpAmps.

Figure 10.18 shows the gain and noise figure performance for several high frequency low noise OpAmps from different manufacturers. The circuit used are the same as figure 10.16, but with $R_{gn} = 10 \Omega$ and $R_{fn} = 1 \text{ k}\Omega$, resulting in a 40 dB voltage gain, so that 3dB bandwidths in excess of 30 MHz can be obtained. In addition, the supply voltages are changed to match those used for the test circuits in the OpAmp data sheets. Figure 10.18 shows that noise figures of less than 1.5 dB can be obtained from 1 kHz to 100 MHz. In many cases, the Spice files will import directly. In some cases, the file extensions need to be renamed to `.cir` to allow NI AWR DE to convert the PSpice files. Several high frequency low noise amplifiers, like the AD8099, have power-down pins, which at this stage cause problems in importing the PSpice files into NI AWR DE.

Oscillator using Operational Amplifiers

Since OpAmps can be used to frequencies above 100 MHz, Op Amps can be used for oscillators. Chapter 6 describes the design procedure for oscillators. A Colpitts resonator is slightly cheaper since only one inductor is used. In both one capacitor in the resonator can be replaced with a varactor diode, to produce a Voltage Controlled Oscillator (VCO). The correct DC biasing on the OpAmp pins is required and it is desirable not to have a short circuit path at DC between the output and ground, since any DC offset on the output will then cause current limiting or failure in the OpAmp. As shown in figure 6.19, for a Hartley oscillator, this requires one less resistor and has reduced loading on the resonator.

To gain some understanding of the fundamental limitations, a linear OpAmp model (OPAMP) is used and output limiting is applied by using back to back diodes to clip the output. A Spice model SDIOODE, which includes noise, is used. Figure 10.19 shows the circuits for a 10 MHz Hartley oscillator using this ideal OpAmp with output limiting. A Hartley oscillator is shown on the left and a Colpitts oscillator is shown on the right. The left circuit is used for the linear oscillator analysis to verify that the correct gain and phase shift occurs. The right circuit is used for the non-linear oscillator analysis to determine the oscillating frequency, output spectrum, phase noise, and waveforms, as described in chapter 6.

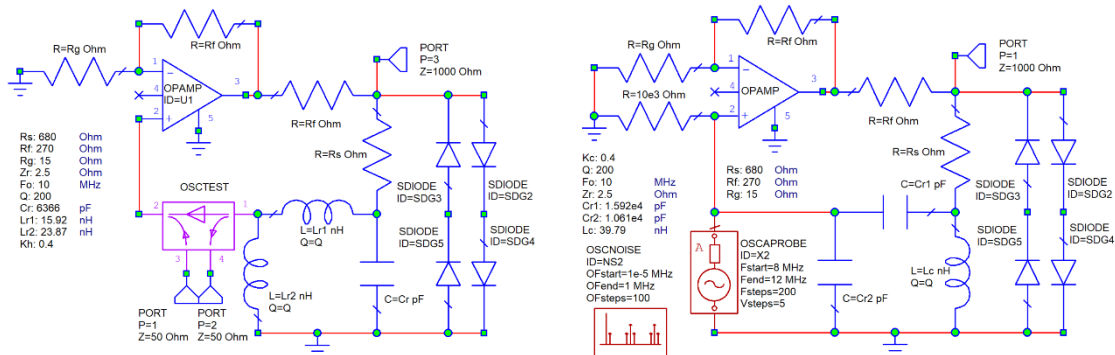


Figure 10.19. Circuits for 10 MHz oscillator, with ideal OpAmps.

The changes in performance can be investigated by changing the circuit gain (R_g), the resonator impedance (Z_r), the ratio $Kh = L_{r1}/L_{r2}$ and the current limiting resistor (R_s). In some cases, the best performance is obtained with values that are limited by other constraints. For example reducing the resonator impedance Z_r , reduces the phase noise. Reducing Kh also reduces the phase noise. However it is difficult to make inductors reliably when $L_{r1} \leq 16 \text{ nH}$. Increasing the gain by reducing R_g , increases the output voltage and decreases the phase noise. In a practical OpAmp, that also decreases the bandwidth and may prevent oscillation. Optimising Z_r , Kh , R_g and R_s to minimise the

phase noise, while keeping $LrI \leq 16$ nH, results in $Zr = 2.5$, $Kh = 0.4$, $Rg = 15 \Omega$, $Rs = 680 \Omega$, and results in a OSCTEST loop gain of 1.66, which is close to the minimum value of 1 required for oscillation. The same values, $Zr = 2.5$, $Kc = 0.4$, $Rg = 15 \Omega$ and $Rs = 680 \Omega$ are also used for the Hartley oscillator. The circuit values shown in figure 10.19 correspond to these values.

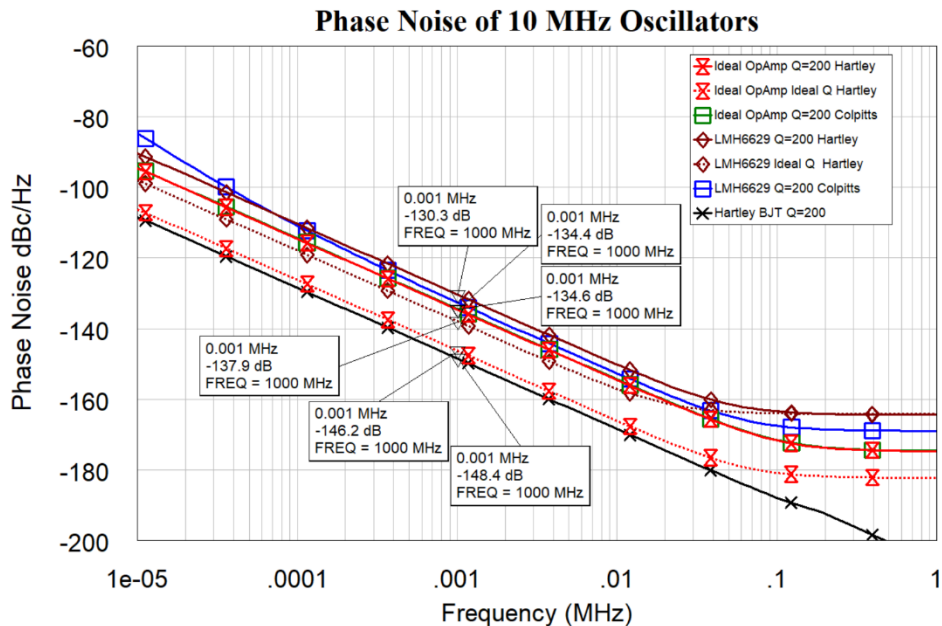


Figure 10.20. Phase noise for 10 MHz Hartley and Colpitts oscillators using OpAmps.

Figure 10.20 shows the phase noise for the ideal OpAmp oscillators of figure 10.19, together with a 10 MHz frequency version of the Hartley oscillator shown in figures 6.16 and 6.19 and Spice simulations of LMH6629 OpAmps, using the circuit shown in figure 10.21 but with the resistor, inductor and capacitor values shown in figure 10.19. It can be seen that the ideal OpAmps with a $Q = 200$ perform $(134.6-148.4) = 13.8$ dB worse than the BJT based oscillator of figure 6.16 and the phase noise for the LMH6629 OpAmp circuits is 18.1 dB worse. The phase noise with $Q = 200$, for the Hartley and Colpitts oscillators is nearly the same for both the ideal OpAmps and the LMH6629 OpAmps.

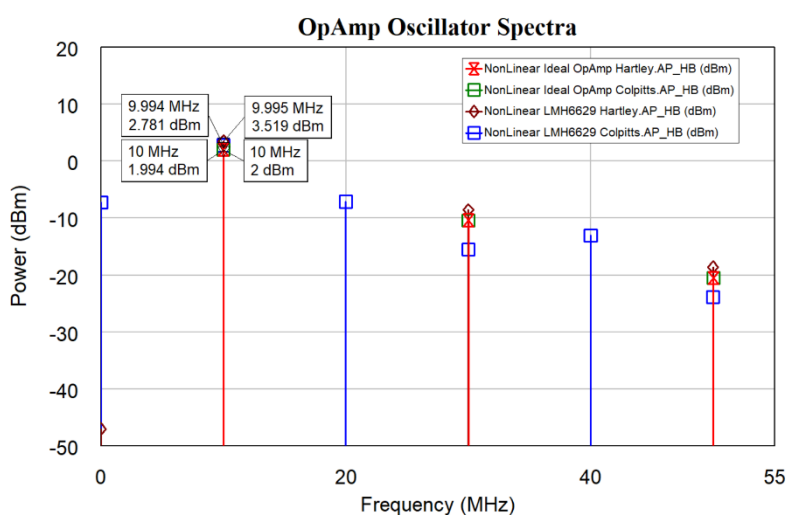


Figure 10.21. Spectra for 10 MHz Hartley and Colpitts oscillators using OpAmps.

In figure 10.20, using an ideal resonator Q for the Hartley oscillator with ideal OpAmps, lowers the phase noise from -134.6 dB to -148.4 dB in, and for the simulation of the LMH6629, it only lowers the phase noise from -130.3 dB to -137.9 dB, showing that the OpAmp is a major factor in determining the phase noise.

Figure 10.21 shows the spectra for the Hartley and Colpitts oscillators with ideal OpAmps and LMH6629 OpAmps and using the same component values as shown in figure 10.19. For the ideal OpAmp and the LMH6629 OpAmp circuits, the fundamental output is nearly the same for the respective Colpitts and Hartley oscillators. Figure 10.22 shows the corresponding waveforms, as well as the output waveform of the BJT oscillator of figure 6.16. The diodes with the ideal OpAmp provide a similar output to the LMH6629. The limiting produced by the BJT is larger and asymmetrical.

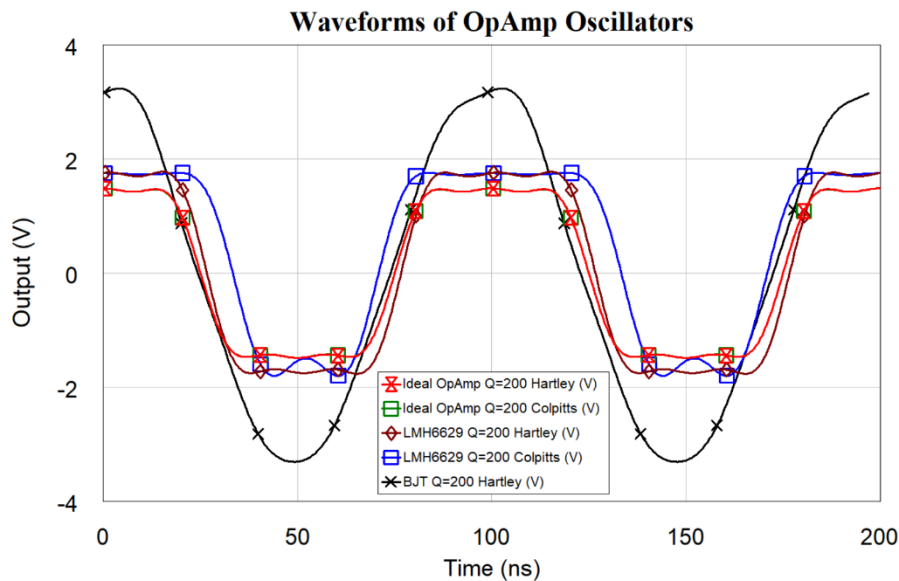


Figure 10.22. Waveforms of Hartley and Colpitts oscillators.

To compare the phase noise from oscillators using different OpAmps, the circuit of figure 10.23 is used, with the same component values but different OpAmps and supply voltages to match those required by the OpAmp. That circuit is the similar to figure 10.19.

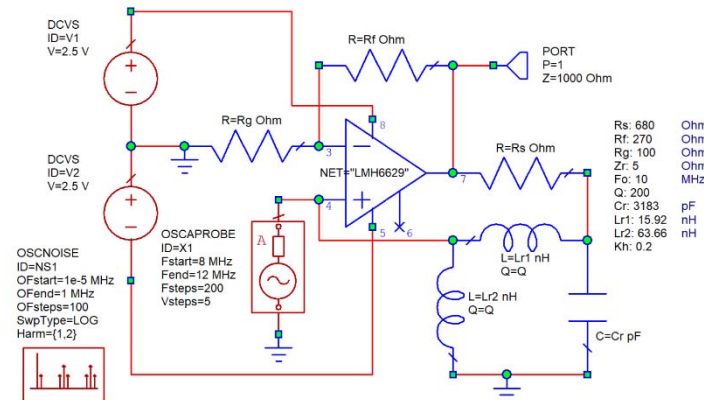


Figure 10.23. Circuits for 10 MHz oscillator, with LMH6629 OpAmp shown.

For the circuits running from $\pm 15V$ supplies, the secondary parameter `VpMax` of OSCAPROBE must be set to 15V for the simulation to converge. The resistor R_s prevents

the low output impedance of the OpAmp from loading the resonator. While keeping $Lr1 \leq 16 \text{ nH}$, Zr , Kh , Rg and Rs were again optimised to minimise the phase noise, and resulted in $Zr = 5$, $Kh = 0.2$, $Rg = 100 \Omega$ and $Rs = 680 \Omega$. Kh and Rg are slightly different from the values for the ideal OpAmp oscillators in figure 10.19.

Figure 10.24 shows the phase noise of these oscillators and as a reference a 10 MHz frequency version of the Hartley oscillator shown in figures 6.16 is again included.

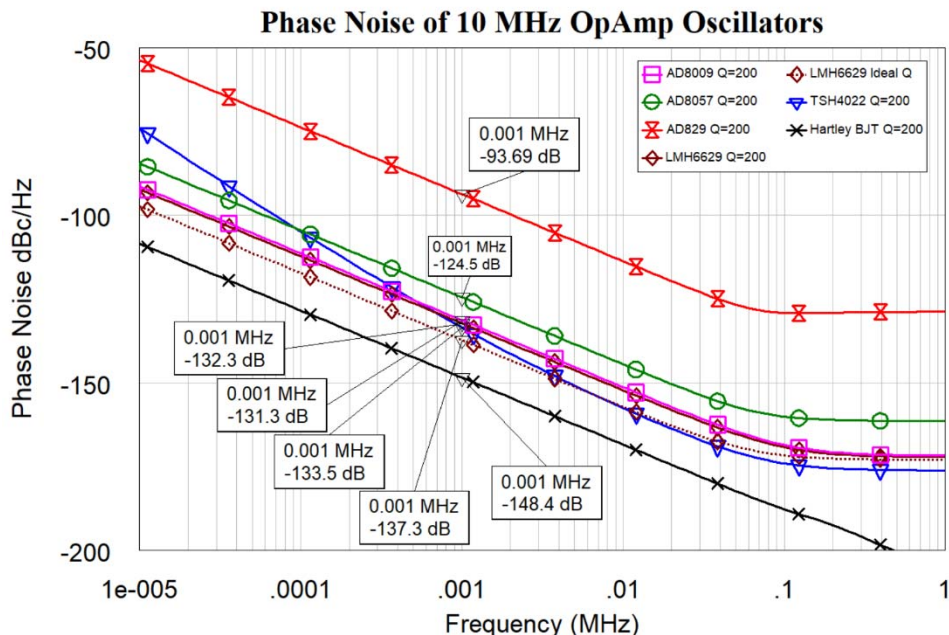


Figure 10.24. Phase noise for a 10 MHz oscillator using different OpAmps.

Comparing figures 10.20 and 10.24, show that for $Q = 200$, the ideal OpAmp model of figure 19, produces a slightly lower phase noise (-134.6 dB) compared with the best phase noise for the Spice models of actual OpAmps (-133.5 dB). For the LM6629 and $Q=200$, the phase noise in figure 10.20, is $134.6 - 132.3 = 2.3$ dB worse than in figure 10.24. The phase noise performance of the AD829 OpAmp circuit is much worse than that of the other oscillators. The BJT Hartley oscillator of figure 6.16 has a lower phase noise than can be achieved by low noise OpAmps.

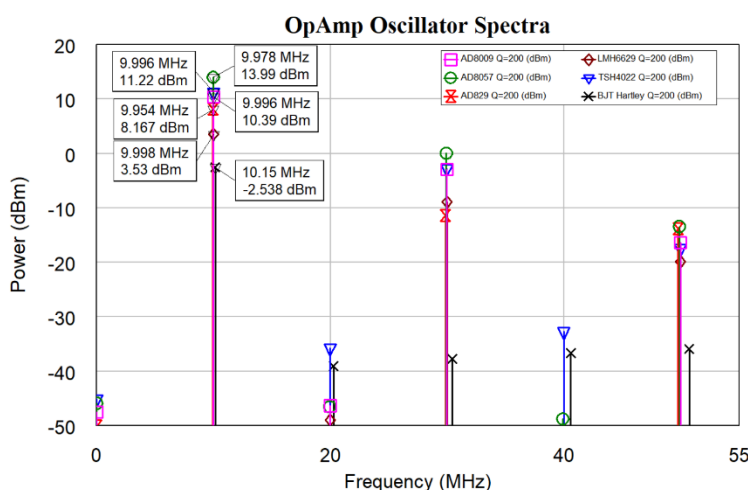


Figure 10.25. Output spectra for the oscillators of figure 10.23.

Figure 10.25 shows the output spectra of the different OpAmp circuits and compares that with the BJT Hartley oscillator of figure 6.16, operating at 10 MHz. The BJT oscillator has a $10\text{ k}\Omega$ load, while the OpAmp circuits have a $1\text{ k}\Omega$ load and much bigger outputs. Even though all the resonator components are identical, the oscillating frequency is slightly different due to differences in the input impedance and phase shifts of the active devices.

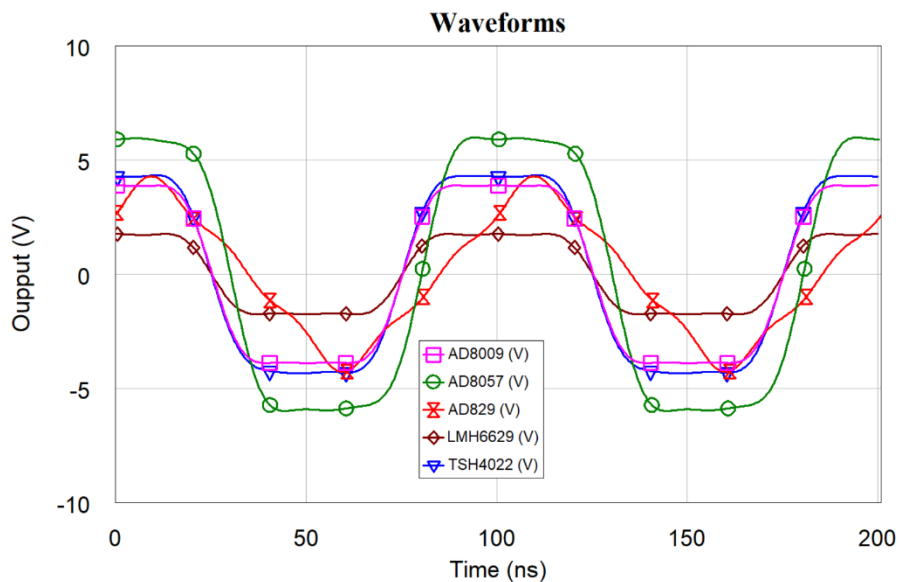


Figure 10.26. Waveforms of the oscillators of figure 10.23.

Figure 10.26 shows the output waveforms of the oscillators. The AD829 has $\pm 15\text{V}$ power supplies, the AD8009, AD8057 and the TSH4022 have $\pm 5\text{V}$ power supplies and the LMH6629 $\pm 2.5\text{V}$ power supplies. The AD829 circuit exhibits slew rate limiting. That is an explanation for the poor phase noise performance of the AD829 in figure 10.24. Compared with the BJT Hartley oscillator output waveform shown in figure 10.22, the OpAmp waveforms show severe clipping.

Limitation of Simulations

Simulation can give a good indication of the expected performance of a circuit. However as indicated in figure 10.9, series inductance and parallel capacitance associated with many resistors can result in a measured hardware performance that is different from the simulation results.

It is also important to critically evaluate the simulated results. For example, figure 10.26 shows a peak output voltage of $\pm 5.98\text{V}$ for the AD8057 OpAmp oscillator. That voltage is larger than the $\pm 5\text{V}$ power supplies, and is thus not possible.

Sometimes the simulations raise questions that can only be answered by constructing the hardware and measuring the performance. For instance, in figure 10.18, the AD8057 has a lower bandwidth and poorer noise figure than the AD829. In figure 10.24 it is the other way around. In the light of the AD8057 simulation giving unrealistic output voltages, which one is right?

The simulated phase noise for the TSH4022 OpAmp with component values corresponding to figure 10.23, with an ideal resonator is worse than that with a Q of 200.

That is not what one would expect. The phase noise of the TSH4022 oscillator in figure 10.24 has a different slope compared to the other oscillators. Are these correct results?

The nonlinear simulation using the AD797 OpAmp would not converge, even though the linear simulation shows a suitable gain and phase shift for oscillation and figure 10.18 shows that the bandwidth of the AD797 is larger than the AD8057. Will this AD797 circuit oscillate or is the expected 10 MHz output frequency beyond its capabilities?

The PSpice simulation models are very complex and may not necessarily accurately include all the parameters needed for a particular simulation. The simulation accuracy should improve over time. One should remember that a model will always only be an approximation of the actual hardware, and can help us understand the operating principles of the circuit to be designed, so that the best performance can be obtained from a design.

References

1. Brandenburg D “Current vs. Voltage Feedback Amplifiers” National Semiconductor Application Note OA-30, Jan 1998, <http://cas.ee.ic.ac.uk/people/dario/files/E416/OA-30.pdf>
2. Analog Devices “Choosing between Voltage Feedback (VFB) and Current Feedback (CFB) Op Amps”, Tutorial MT-60, www.analog.com/media/en/training-seminars/tutorials/MT-060.pdf
3. Texas Instruments, OA Current Feedback Op Amp Applications Circuit Guide, April 2013, <http://www.ti.com/lit/an/snoa365c/snoa365c.pdf>
4. Kikkert, C. J. and S Zhu, Resistive Shunt Impedance Analyzer, 2016 International Symposium on Power Line Communications and its Applications, Bottrop, Germany, 20-23 March 2016. pp 150-155 ISBN 978-1-4673-6642-7
5. Texas Instruments OA11 “A Tutorial on Applying OpAmps to RF Applications”, <http://www.ti.com/lit/an/snoa390b/snoa390b.pdf>
6. Texas Instruments, LM6626 Data sheet: “LMH6624/LMH6626 Single/Dual Ultra Low Noise Wideband Operational Amplifier”, <http://www.ti.com/product/LMH6626>
7. Texas Instruments, Noise Analysis in Operational Amplifier Circuits, 2007, <http://www.ti.com/lit/an/slva043b/slva043b.pdf>
8. Analog Devices, MT-40 Tutorial, Op Amp Tutorial Output Noise Calculations for Single –Pole System, 2009, <http://www.analog.com/media/en/training-seminars/tutorials/MT-049.pdf>

Chapter 11

Circuit Manufacture

Introduction

Once the design of the electronic circuit is complete, the circuit has to be fabricated. The method used will depend on: 1) The frequency at which the circuit operates, 2) Whether it is a prototype or a full production design and 3) What market the circuit is designed for. Low cost consumer circuits require very different manufacturing techniques compared with military or space electronics, to achieve the required electrical, mechanical, thermal and reliability performance. The most common technique for manufacturing a circuit is to use a printed circuit board. A Printed Circuits Board (PCB) consists of an insulating material forming the PCB substrate onto which conductive tracks are placed. Components forming the circuit are connected to those tracks. There are two basic ways of producing PCBs:

Subtractive Process: Conductive Layer Removal

A conductive layer, like copper, covers one or both side of the PCB substrate and the conductive layer is removed where there are to be no tracks. The metal can be removed using chemical etching, milling or laser ablation.

For conventional PCB manufacture, chemical etching of copper clad printed circuit boards is the most common PCB manufacturing technique. For medium to large production runs, thick film screen printing techniques, described later in this chapter, are used to screen print etch resistant inks to protect the copper foil, where the tracks are to be placed. For prototype boards or for smaller production runs, the whole board is covered with a photosensitive material, which hardens when exposed to light. A photographic transparency, with dark areas where the track is to be removed from and clear areas where the track is to be, is placed on the PCB and exposed to light. Alternately, a laser exposes the areas where tracks need to be to light, avoiding the use of negatives and providing a better resolution photoresist image.

The unexposed areas of photoresist are washed away and the resulting exposed board is then etched to remove the unwanted copper. These chemical techniques are the dominant means of producing commercial PCBs. For prototypes, as described later in this chapter, PCB milling and Laser ablation is often used as the setup cost for producing a PCB is reduced.

Additive Process: Depositing Tracks and Vias

In this method, the conductive tracks are deposited onto the substrate. For thick and LTCC circuits, the conductive or dielectric tracks are screen printed on a bare substrate material and then fired to make them permanent. Such tracks have a higher resistance and in many cases, a layer of copper of the required thickness needs to be plated onto those tracks to obtain the required conductivity. Electro-plating is commonly used for this. To ensure that all tracks have the same copper or gold thickness plated on them, all tracks must be electrically connected during the electroplating process.

This PCB manufacturing process which ensures this, is called the **semi additive process**, where a seed layer, of approximately 1 to 2 μm of conductive material, often copper or gold, is used to cover the entire substrate. The most common way of achieving this is to use a series of chemical baths, to deposit this seed layer on the substrate. For thin film circuits, the seed layer can be produced, by placing the ceramic substrates in a vacuum chamber and sputtering gold onto them. The seed layer ensures that all the tracks on the circuit board are connected.

The areas where no tracks are required are covered with a protective coating, using screen-printing or photoresist. Electroplating is used to build up the tracks to the required thickness. The protective coating or photoresist is then removed, followed by a light etch to remove the seed layer.

The additive process minimises the amount of copper that is to be etched away and thus results in less copper and etching waste that needs to be recycled. Additive processes are required to produce the vias in double and multi layered printed circuit boards. As a result, the additive process is favoured for the production of multilayered PCBs.

Printed Circuit Board Materials

- Most PCBs are made by having thin copper sheets glued to an insulating substrate material, called a laminate. The copper thickness depends on the applications. Typical thicknesses are 2, 1, $\frac{1}{2}$ and $\frac{1}{4}$ oz. copper per square foot, which corresponds to a copper thickness of 70 μm , 35 μm , 17 μm or 9 μm respectively. The copper thickness together with the track width must satisfy the current carrying capability and resistive loss requirements of the tracks. Subtractive processes are used to produce the required circuit boards.

Conventional PCB laminates consist of a filler or reinforcing material and a thermoset resin. These sheets are cured at high temperature and pressure. The mechanical and dielectric properties of the laminates depend on the composition of the laminate.

For very low cost and low frequency applications, paper pulp or cotton and epoxy resins are used. FR2 and FR3 boards are examples of this. For higher mechanical strength, woven fibreglass mats are used as reinforcement for the thermoset resins. The temperature range over which the board can be used, and the dielectric properties are governed by the type of resin used. By using resins containing Polytetrafluoroethylene (PTFE or Teflon®) and/or ceramics such as Alumina, PCBs with low losses at microwave frequencies can be obtained. In some applications, the fire retardant properties of the laminates must also be considered in the laminate selection process. The AWRDE *Libraries* \Rightarrow *AWR Web site* \Rightarrow *Parts by Type* \Rightarrow *Substrates* contain details of PCB substrates. The number manufacturers has reduced during the last few years. The manufacture of RF PCB substrates is now dominated by the Isola Group [1], Rogers [2] and Taconic [3].

Conventional PCB Substrates

Paper and Resin Substrates; FR2 and FR3

These substrates consisting of a mixture of paper pulp and a resin. Phenolic resin for FR2 and epoxy for FR3. They are mainly used in low cost consumer products, and are not normally used for multilayer boards. FR3 has a dielectric constant of approximately 2.3 but this is not controlled and the loss tangent is not specified. An advantage of FR2/3 and

similar, paper based laminated are that holes and slots can be punched. This laminate is not recommended for RF designs. FR3 has a poor heat tolerance and scorches easily. FR3 is normally light brown with a smooth texture.

Figure 10.1 shows a typical low cost AM/FM radio manufactures using FR3 circuit board. The advantage of being able to punch out a particular shape can be seen.

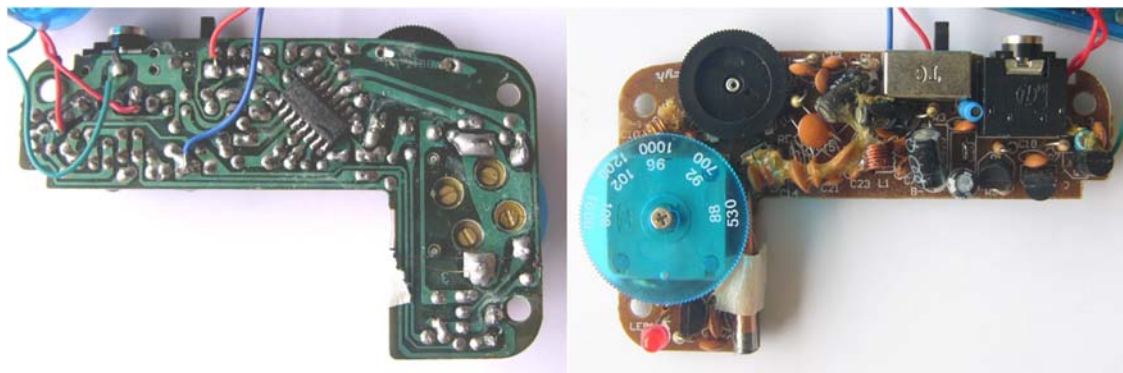


Figure 10.1 FR2/3 Printed Circuit Board for a low cost AM / FM radio. (Unknown manufacturer).

Fibreglass and Epoxy Substrates; FR4, FR408, IS400

This is a substrate consisting of a mixture of fibreglass and epoxy. It is suitable for professional quality PCBs and has the following properties:

Dielectric Constant	4.7 at DC decreasing to 4.4 at 10 GHz.
Dissipation factor (Tan(δ))	0.014
Q at 50 MHz	95
Max Temperature	130 °C

Table 10.1. FR4 Properties.



Figure 10.2. FR4 Multilayer Printed Circuit Board. (Nokia Mobile Phone).

At James Cook University, our prototype boards are milled and as a result, we have been using FR3 for prototype PCBs since the fibreglass used in FR4 and many other PCBs is carcinogenic. Special precautions are required to ensure that the fine fibreglass particles produced by the PCB milling process are not inhaled. FR3 is safer in that respect, however

FR4 is a much better circuit board in that it has a better heat tolerance, is stronger and the dielectric constant is specified to 10 GHz.

FR4 PCB's can be made with many layers. Simpler PCBs have 4 layers, with one layer being earth, one layer being the supply voltage and the outer layers containing the tracks that are connected to the IC's and passive components. FR4 is normally green and semi-translucent, often this can be seen at the left edge of the board as in figure 10.2. The green colour is due to the solder resist and not due to the laminate. The large component at the left edge of the board is a ceramic diplexer. Normally many printed circuits are etched together, on one sheet, or panel, as shown in figure 10.3. Cut-outs are provided to enable the individual circuits to be removed easily.

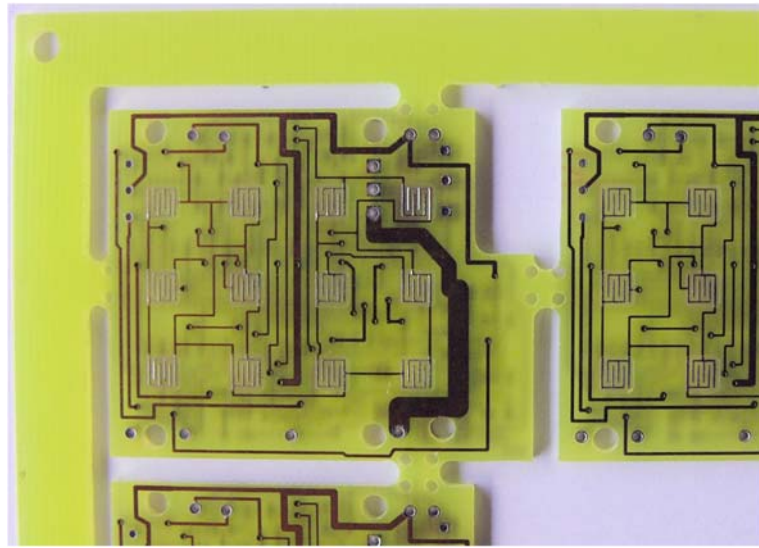


Figure 10.3. FR4 PCB showing cut-outs. (Layout by JCU).

FR3 and FR4 are ANSI terms, manufacturers such as Isola have fibreglass and epoxy products under names like FR408, IS400, IS410, and IS 420. Different resins used have different dielectric constants, typically ranging from 4.7 shown in table 10.1 to 3.67 for FR408.

Microwave and RF Printed Circuit Board Materials

FR3 and FR4 can be used for PCBs to 1 GHz, however above these frequencies the losses may become significant. To avoid reflections, at microwave frequencies many of the connections are made using transmission lines of a specified impedance. For FR3 and FR4, the dielectric constant and thickness varies from one batch to the next, so that the characteristic impedance of transmission lines on the PCB also varies. This is not suitable for many RF designs.

The major laminate manufacturers make many different PCB laminates, especially for the RF and microwave frequency range. As an example several different laminates from Rogers Corporation, are described here, to illustrate that different applications require RF laminates with different properties.

RT/duroid 58X0

RT/duroid 58X0 is a glass microfiber reinforced PTFE (Teflon) composite. The two products in this family are RT/duroid 5870 ($\epsilon_r = 2.33$) and 5880 ($\epsilon_r = 2.2$). These were

developed in the 1960's and are the oldest Rogers products. The low dielectric constant and the low dielectric loss of typically 0.0005 make these materials best suited for high frequency broadband applications where dispersion and losses need to be minimized.

A high dielectric constant reduces the size of the circuit. For frequencies above 20 GHz, circuits with a high dielectric constant become too small so that at these frequencies a low dielectric constant has to be used. Because of their low water absorption characteristics, RT/duroid 58X0 is good for applications in high moisture environments. The LNC of figure 10.4 is located at the focal point of antenna, which is sometimes very hot, sometimes very cold, and sometimes very wet. RT/duroid is thus a good choice for the PCB material. RT/duroid is flexible and thin laminates require care in mounting them securely. RT/duroid is normally brown and the woven glass mat can clearly be seen in figure 10.4. If the dielectric constant of the PTFE composite filling and the glass microfibers are slightly different then small local variations in dielectric constant will occur. Having a random orientation of the microfibers minimises that variation. The glass reinforcing provides an excellent strength and prevents tracks from cracking.

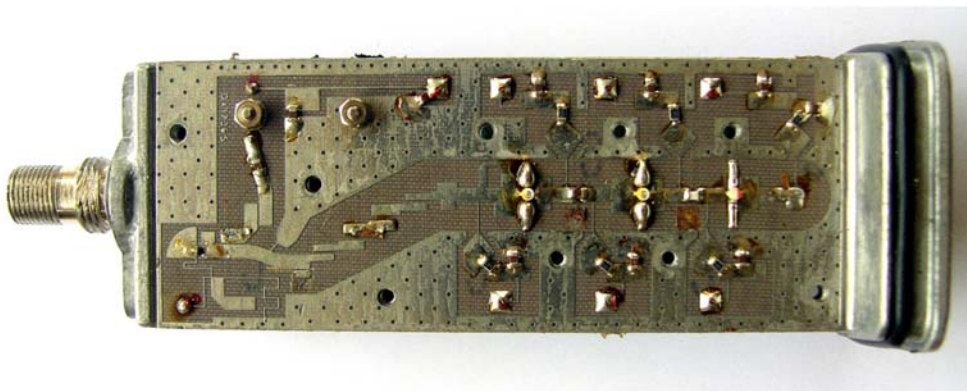


Figure 10.4. Ku band (12 GHz) low noise converter (LNC) using RT/duroid (Norsat).

RT/duroid 6000 (PTFE/Ceramic Laminates)

There are three laminates in this family; RT/duroid 6002 ($\epsilon_r = 2.94$), RT/duroid 6006 ($\epsilon_r = 6.15$) and 6010LM ($\epsilon_r = 10.2$). The thermal coefficient of the laminate matches that of copper. The laminates are more rigid and thus easier to mount. This product is ideal for applications in thermal changing environments such as space. Multilayer boards are possible with this laminate. RT/duroid 6000 is a military specified substrate and thus very expensive.

RO3000 and RO3200 (PTFE/Ceramic Laminates)

The RO3000® materials family consists of four grades, RO3003™ ($\epsilon_r = 3.0$), RO3035 ($\epsilon_r = 3.50$), RO3006 ($\epsilon_r = 6.15$) and RO3010 ($\epsilon_r = 10.2$). These laminates are aimed at a commercial market and are a lot cheaper than the corresponding RT/duroid 6000 laminates. The temperature coefficient of expansion matches that of copper and FR4 in the X-Y plane, so that multilayer RO3000/FR4 boards can easily be made.

RO4000

The RO4000 series is a woven glass/ ceramic loaded thermoset plastic resin laminate. This is a low cost commercial laminate, which is especially suited for multilayer boards

using RO4000 and FR4. The boards have a glass transition temperature (T_g) $> 280^\circ\text{C}$ and can thus be used with conventional PCB processing techniques, such as wave soldering and surface mount techniques. Unlike PTFE based microwave materials, no special through-hole treatments or handling procedures are required. Therefore, RO4000 material circuit processing and assembly costs are comparable to FR4 epoxy/glass laminates. RO4003C has an ϵ_r of 3.38 and RO4350B has an ϵ_r of 3.48.

The Microstrip filters if figures 7.58, 7.65 and 7.72 to 7.75 have all been made using RO4003.

Other Laminates

Other manufacturers have a similar range of RF and Microwave laminates to the Rogers products described above. For example, Isola have several RF and Microwave laminates. I-Tera and IS-680 are two examples, however Isola's web sites [1,2] do not specify the details of the laminates. Taconic's also has several RF and Microwave laminates. RF-35 is a fibreglass and PTFE/Ceramic laminate, similar to RO3035. It also has a dielectric constant of 3.5. Taconic's TLY uses a fibreglass/PTFE laminate and is similar to RT-duroid 58X0. TLY has dielectric constants from 2.17 to 2.40 and a loss tangent of 0.0009. Park Electrochemical Corp [4] produces both conventional PCB type materials and RF and microwave type laminates. Their Nelco N4000-13 EP substrate is similar to the RO4003 substrates used for the filters in chapter 7, apart from the dissipation factor being 3 times higher for the NELCO boards.

Multilayer Boards

There are many applications where RF circuits require multilayer boards. One example is a Stripline RF circuit. Another is a multilayer board with an RF/Microwave substrate for an RF layout and an FR4 type substrate for power supply, control, and digital signal processing. A Prepreg sheet is a thin uncured sheet, containing fibreglass, thermoset resins, and fillers. The laminates are normally produced by gluing copper sheets to one or more Prepreg sheets, and curing them using pressure and heat.

For multilayer boards, jigs with locating pins are used to ensure that each of the boards making up the multilayer board are in perfect alignment. For a multilayer board, the inner layers are etched. The boards are stacked with Prepreg sheets between the multilayer boards, to form the multilayer board. In many cases, the same Prepreg sheets that are used to make the double-sided boards are used. That will space all the copper layers evenly, as shown in figure 10.5.

The vias in the boards are drilled and electro plated. At this stage, the outer layers have not yet been etched, so that all vias are connected to the outer copper, so that electroplating of the vias is possible. The outer layers are then etched to produce the required tracks on them. The solder pads and solder mask are then applied, completing the PCB. It is possible to have vias on inner layers only. These are called blind or buried vias and are produced on a 2 or 4 layer board and then the location of these vias are not drilled in the outer copper layers. Buried vias offer space savings and provide some intellectual property protection by making it a little bit more difficult to trace the design, but they also make it more difficult to fault-find.

Several types of adhesives can be used depending on the laminates to be bonded. Figure 10.5 shows a typical construction requiring an RO4003 Stripline circuit bonded to an FR4 multilayer construction. For constructing the Stripline circuit, a high frequency bond-film

like the RO4450 “Prepreg” sheet from Rogers is required. The bonding sheets are close to 0.1 mm thick and have dielectric constants from 3.3 to 3.54 at 10 GHz, matching the dielectric constants of the RO4000® series laminates. The loss tangent of the Prepreg bonding sheets of 0.004 at 10 GHz is close to the 0.0037 and 0.0037 for the RO4000® laminates, so that no sudden changes in dielectric occur in the multilayer board. Each manufacturer has Prepreg sheets and bond sheets with properties that match their microwave laminates.

For a combination of microwave and FR4 boards, the inner layer of the microwave board should be a ground plane so that the dielectric properties of the Prepreg sheet joining the microwave and FR4 are not so important. A good low cost option is to use the standard bond films used for FR4 for making multilayer PCBs.

For bonding the laminates and Prepreg or bonding sheets are clamped at a pressure of typically 2.8 MPa and a temperature of typically 225°C for more than one hour. That temperature varies with the properties of the Prepreg sheets. Since air has an $\epsilon_r = 1$, it is important to prevent air bubbles, particularly when high dielectric substrates or Striplines are used, since air-bubbles change the characteristic impedance of the Stripline at the point of the air-bubble and cause a discontinuity.

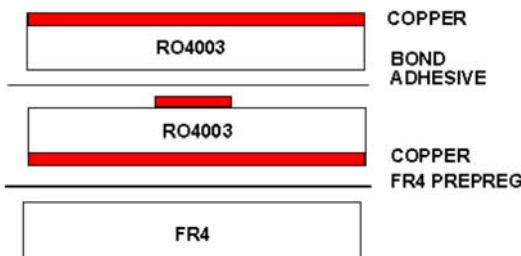


Figure 10.5. Bonding laminates to form a multilayer board [3].

Non-Clad Substrates

During the 1980's the microwave PCB substrates were not sufficiently developed and many of the microwave circuits had to be produced on Alumina substrates using thin film techniques. These non-clad substrates are now only used for precision microwave circuits using thin film techniques and for low cost thick film circuits at both RF and low frequencies.

Companies such as Coors Ceramics [5] and Morgan Technical Ceramics [6] produce dielectric materials that can be used for such RF substrates. Ceramic substrates are also used in many packaging applications. A paper by F. Bechtold [7] gives a good overview on this.

Alumina Substrates

Alumina is the dominant substrate material for thick and thin film applications. The dielectric constant is close to 10, with both the dielectric constant and cost increasing with the purity of the substrate. For lower cost applications, Thick film substrate materials with 85% to 95% purity are used. In many cases these substrates are used “as fired” for low frequency applications or ground flat for low cost microwave applications. For precision, low-loss microwave applications 99.5% to 99.8% purity substrates are used and these may be ground and polished in order to remove any surface irregularities and ensure a

constant thickness of the entire substrate. Alumina is ideal for demanding low loss applications, such as substrates for thin film circuits.

Other Substrates

Ceramic materials with higher dielectric constants are used to reduce the size and thus weight of resonators used for oscillators and filters. Dielectric resonator oscillators (DRO) [8, 9] are used in LNCs for satellite receivers. The LNC in figure 10.4 has a dielectric resonator oscillator mounted on the other side of the PCB shown in figure 10.4. The diplexer shown in the left of figure 10.2 and the coaxial cavity filter in figure 7.82 are examples.

Manufacturing

RF printed circuit boards can be designed in a similar way to conventional PCBs, so that programs like Altium (formerly known as Protel) [10] or Autodesk's (formerly CadSoft) Eagle [11] can be used to produce the circuit board layout. For circuits like Stripline filters, and other RF circuits, where the characteristics and lengths of transmission lines are critical, then software like AWRDE or ADS is required. All of these programs can produce Gerber plot files, which are used to produce prototype RF boards, either by commercial PCB manufacturers, or by the milling machines used by many universities for prototypes. The Gerber plot files can also be imported into Altium or Eagle to produce a combined RF and conventional PCB. Such technology is required for the multilayer boards shown in figure 10.5.

Normal PCBs are protected using a solder-mask. Unless the thickness and the properties of the dielectric of the solder-mask is taken into account in designing the RF circuit, solder-masks should not be used for RF boards. Instead, to prevent corrosion, Gold plating is normally used on the RF circuits as shown in figure 7.59.

Manufacturing using a PCB Milling Machine

Many universities use a special PCB milling machine [12] to produce the prototype PCB's produced by students. The ceramic filler used in RF substrates like RO4003 are much more abrasive than the epoxy, paper, and fibreglass used in FR3 and FR4 type substrates. As a result, the cost of milling bits is a major cost in the production of those boards. For milling the more flexible PTFE boards, like RT/Duroid, the substrate needs to be thick enough to be able to be held flat as part of the milling process, so that the more rigid RO4003 substrates are the best to use in PCB milling machines. Since the milling process can disperse copper and PCB substrate materials in the air, the appropriate workplace health and safety considerations must be considered.

Manufacturing using Laser Ablation

In recent years PCB cutters have become available that use UV laser to remove the copper from PCB laminates by Laser ablation [13]. Minimum track widths of 50 μm and gaps between tracks of 25 μm are possible (ProtoLaser S). The plotting accuracy is 2 μm . These sizes are smaller than can be achieved reliably with conventional etching. The larger machines are fast enough for commercial production. Since no hazardous chemicals are used, apart from the high power required by the laser, this is an environmentally friendly means of producing PCBs. However, since the ablation process

vaporises copper and PCB substrate materials, the appropriate workplace health and safety considerations must be considered.

Layout Hints

Many PCB manufacturers can etch to a specified accuracy. Typical values for the thinnest track widths and spacing can be made are 0.1 mm (0.04") and larger values are desirable [14]. Ensure the tracks can handle the required current. Note 0.001" is called *thou* in the UK, and *mil* in the USA. In Europe *mil* is an abbreviation of a millimetre and it is also a measurement of angle. To avoid this confusion *mil* is not used in this book. Many of the modern ICs have 0.5 mm pitch of the leads on the IC. The 0.5 mm track pitch can easily be achieved using present day PCB manufacture.

The minimum drill size that should be used is typically 0.2 mm diameter. The smallest pad size for vias or leaded components, which should be used is the drill size plus 0.5 mm, however small pads will lift off easily when components are soldered to them. For through-hole components use a drill size that is approximately 0.1 mm larger than the lead size and use a pad that is approximately 1 mm larger than the drill size. The recommended hole size for a standard leaded resistor or capacitor is 0.9 mm with a pad size of 2 mm. To ensure that the circuit can be changed if needed, for prototyping boards a bigger pad size is advisable.

For milling of PCBs, the tolerances are slightly different. For a typical milling machine [13], the tool alignment has a $\pm 2 \mu\text{m}$ tolerance. A minimum recommended track size is 0.5 mm, with a 0.2 mm minimum spacing. (0.2 mm wide milling bits are the smallest milling commonly used). Having a 0.25 mm spacing ensures that 2 milling cuts are made, thus reducing the chance of short circuits. For short track lengths, track widths of 0.2 mm are possible, however such thin tracks should be avoided for long tracks since tracks may lift due to the mechanical friction of the milling bits. When milling circuit boards, as much ground-plane as possible should be left on the board, to minimise the amount of milling that has to be done and minimise the milling time and cost. In addition, the extra ground-plane provides some rigidity for thin boards to prevent them from curling. The ground plane can be used to provide a heat sink to remove heat from the circuit.

For RF boards the bottom conductor should be a high integrity ground-plane underneath any RF transmission lines to provide the correct Microstrip circuit configuration. Vias connected to tracks and leaded components affect the integrity of that ground-plane. As a result, surface mount components should be used in any RF design. If needed leaded components can be soldered onto pads on the top layer. To prevent performance changes as the RF circuit is mounted in an enclosure and to provide suitable mounting locations, it is desirable to provide an earthed strip around the RF board as shown in figures 7.60, 7.61 and 7.74 to 7.77. In figure 7.61, the big holes are used for mounting the board and the many small holes are vias, connecting the earthed area to the ground-plane. Note that this grounded area is also used to minimise EM coupling between the different parts of the circuit.

Thin Film

The polished Alumina used for the thin film substrates has a very low dielectric loss. Thin film circuits can be made to better accuracies and smaller sizes than etched PCB's.

Thin film circuits can be produced using semi additive processes, where a 1 to 2 μm seed-layer of gold is applied to an Alumina substrate. A photographic mask is then applied to

the places where no track is required and the tracks are then electroplated to the correct thickness of several tens of μm . The photo-resist is then removed and a quick etch removes the seed-layer, where no tracks should be, but does not completely remove the tracks. The required solder-pads are then added, together with dielectric dams to prevent the lead from solder leaching into the gold.

Microfab [15] specialise in the design and production of thin film circuits, predominantly for space and military applications and use a subtractive process where the whole substrate is covered with copper or gold and then ion beam etching [16] is used to remove the conductive layer as required. This process achieves etching tolerances of 0.2 μm , compared to 2 μm for PCB based technology.

The designer may have to adjust the track widths in the design, to compensate for the changes in track width caused by the production processes. For a 35 μm conductor thickness, corresponding to 1 oz. copper per square foot, then the additive process of depositing tracks will expand the tracks by tens of μm as plating will also occur on the sides of the tracks, where they are not confined by the photoresist. If subtractive processes are used then some etching on the sides will occur and the tracks will reduce in width by tens of μm in addition to the other manufacturing tolerances. Ion beam etching or laser ablation does not under-etch and will thus result in more accurate track widths. Once the amount of over-etching or under-etching is known, then the track widths can be adjusted to compensate for this. If the line widths are made as variables, then this correction factor can be set to zero for simulation and set for the required correction when the layout is exported to the plotter.

Thin film circuits are much more expensive than RF and microwave PCB, circuits, so that thin film circuits are only used where the accuracy and reliability requirements demand its use. At present thin film techniques are used firstly for very high frequency applications, such as 30 GHz filters [15]. Secondly, Alumina has a very good thermal conductivity. As a result, thin film techniques are often used for power applications, where the Alumina substrate is in contact with a heat-sink. A typical example is the 20 W Class C 800-900 MHz amplifier hybrid, shown in figure 10.6. The whole circuit including heat sink is 56 mm long. The bond-wires for the large output transistor on the right can clearly be seen.

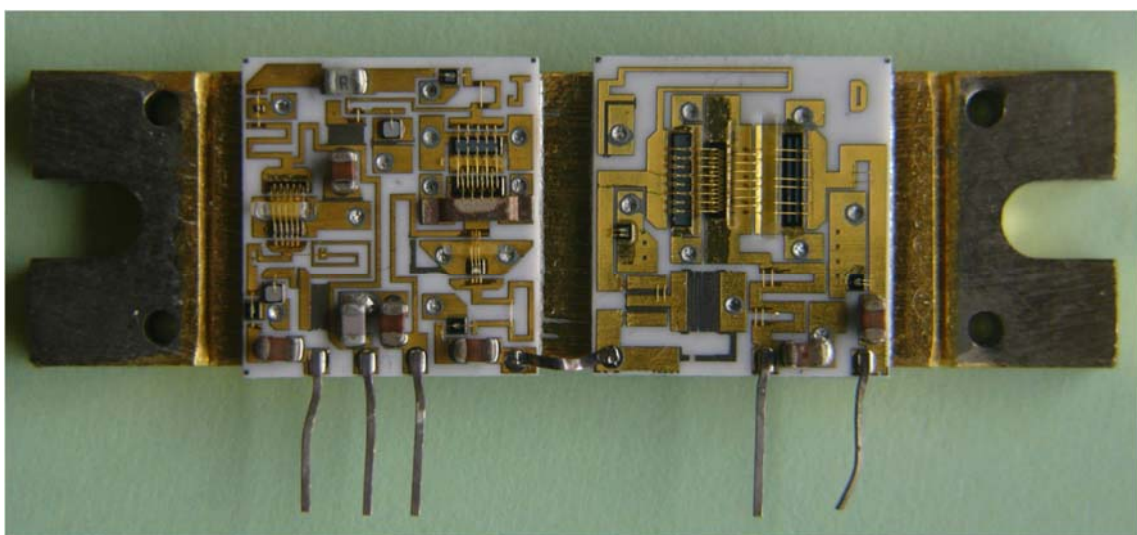


Figure 10.6. 20 W Class C amplifier hybrid MHW820 (Motorola).

Thick Film

Thick film techniques have a slightly higher circuit set up cost as several screen masks need to be made, but they have a lower increment cost as no etching or milling of the PCB's are required. In thick film techniques, a substrate, which normally is an Alumina substrate, has conductive, resistive or insulating inks applied to them using precision screen-printing technology. The substrate is then fired at typically 850 °C to harden the tracks and thus provide the correct circuit connections. Dielectric layers can be made, so that tracks can cross each other. For a multilayer track circuit, several separate firings may need to be made. Similarly, capacitors can be made by firstly using a conductive ink to form the one electrode and firing that. Then a dielectric layer is applied and fired, followed by another conductive layer for the other electrode. Resistors can be made using resistive inks and inductors can be made by printing conductive spirals. This results in a high-density circuit board of low cost. The low thermal coefficient of expansion (TCE) of ceramic materials guarantees mechanical stability and is closely matched to that of ICs for bare chip assembly.

The printing screen has a photographically produced mask applied to it, with the screen being open where the tracks need to go and being blocked everywhere else. The printing screen is placed in contact with the substrate and the ink pastes are applied with a squeegee to the screen. The inks can also be applied using other techniques, such as spraying, dipping using the appropriate screening techniques to ensure that the inks are only deposited where they are supposed to be.

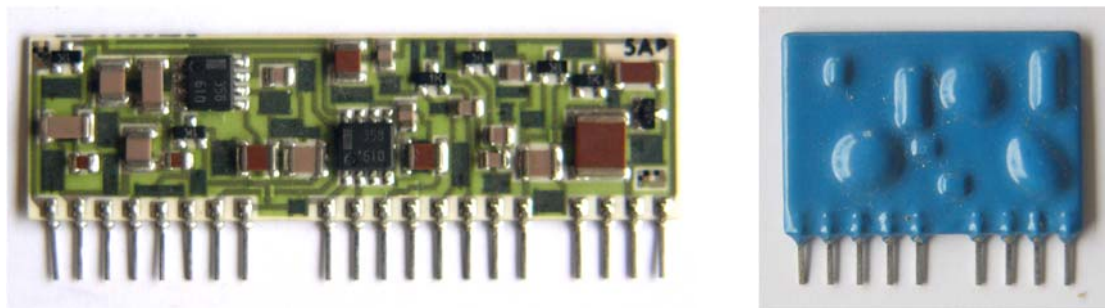


Figure 10.7. Thick film circuits before and after a protective coating has been applied.

Figure 10.7 shows some typical thick film circuits. The circuit on the left shows, that thick film circuits can have a high component density. After the circuit is tested, the whole circuit is protected with a protective coating as shown on the right of figure 10.7. This makes thick film circuits very suitable for hazardous or wet environmental conditions.

Many companies like Hybrid Electronics [17] and DuPont [18], specialise in the design and production of thick film circuits.

Printing Screens

The ink is normally applied using a squeegee. When the ink is applied, the thickness of the ink is close to the thickness of the screen. By varying the thickness of the screen, the thickness of the tracks can be varied.

The screens used for the printing can be made from stainless steel, with a typical fibre diameter between 30 and 100 µm, a 50 to 224 µm mesh aperture and 65 to 220 µm mesh thickness with an aperture of 39 to 47%. Stainless steel screens are used for large production runs.

Screens can also be made from polyester. Polyester screens have a shorter life but are cheaper, and are thus used for smaller production runs. The screens have a typical fibre diameter between 35 and 110 μm , a 43 to 185 μm mesh aperture and 60 to 160 μm mesh thickness with an aperture of 30 to 40%.

Pastes (Inks)

Conductivity: The conductivity of the pastes is given in terms of milliohm/square. The resistance of a printed conductor of 10 mm x 10 mm, is the same as the resistance of a conductor of 100 mm x 100 mm, as long as the thickness is the same.

Thick film inks [19] contain precious metals, glass, and/or ceramic powders dispersed in an organic medium. Specialized compositions create conductors, resistors, and dielectrics for a variety of applications and operating environments. Table 2 shows the typical conductivity of various conductive inks. Copper inks are difficult to use since they require an oxygen free atmosphere in the ovens, to prevent oxidisation. The palladium inks are used for solder pads.

Conductor Material	Sheet resistance (m Ω /square)
Copper	1.5
Silver platinum	2.0
Gold	3.0
Silver palladium	30
Gold palladium	30

Table 2. Comparison of sheet resistance of conductive pastes.

RF Applications of Thick Film Circuits

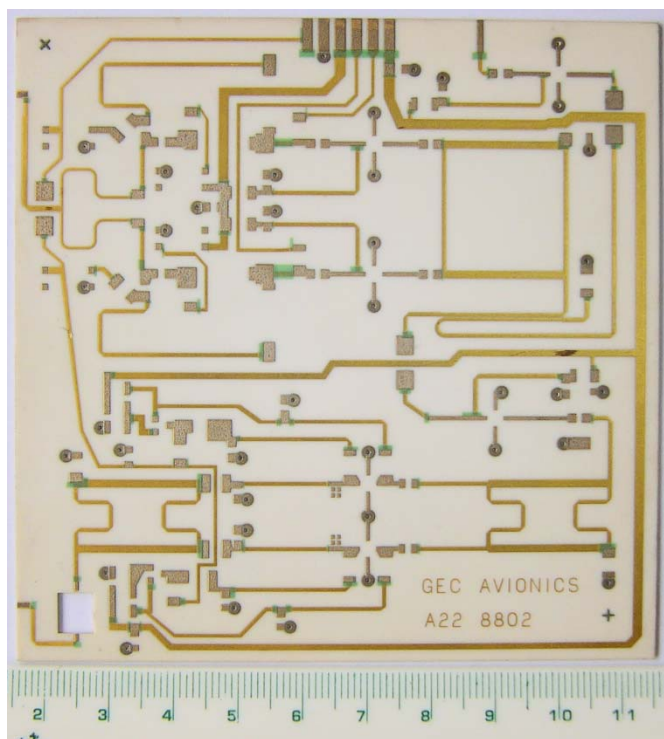


Figure 10.8. Thick film RF circuit on Alumina. (GEC Avionics, designer Kikkert).

The Alumina substrate has a very low loss, and that is why it is used for thin film circuits. The application of the required tracks using thick film techniques is a lot cheaper than doing the same using thin film techniques. For accurate transmission line widths, fine screens need to be used and allowances need to be made for spreading of the inks. Figure 10.8 shows a circuit for a low noise amplifier and I-Q gain control circuit for a receiver beam steering application at 1.6 GHz. The circuit is 100 mm x 100 mm in size.

Thick film techniques are also used to produce patch antennae for mobile radio systems. In many cases, the antenna needs to be shaped to conform to the contours of the mobile phone. Thick film techniques are also used to coat the ceramic blocks of the dielectric filters used as a diplexer shown on the left of the mobile phone in figure 10.2.

Manufacturing using 3D printing

Recently 3D printers capable of printing printed circuit boards have become available. [20, 21, 22]. The printer prints dielectric ink, or conductive ink in the location required in order to make the required printed circuit board. The dielectric ink from Nano Dimension [21] has a dielectric constant of 2.2 to 3.7 at 1 MHz. and a loss tangent of 0.02 to 0.04 at 1 MHz. Having such a wide range of dielectric constant makes it difficult to produce accurate transmission lines or accurate Stripline or Microstrip RF filters. The AgCite conductive ink uses silver nanoparticles and has a conductivity up to 35 MS/m. Silver has a conductivity of 63 MS/m, Copper 59.6 MS/m, Gold 41 MS/m and Aluminium 35 MS/m. The inks thus have a similar conductivity to Aluminium. No ink is deposited where a hole is required and a pad is made by surrounding the hole with conductive ink. The inks use UV curing. A 200 x 200 mm printing area with a 3 mm thickness can be deposited. The smallest print trace width and pitch is 90 μ m. Conventional thickness PCB's can be made and may contain many connector layers, so that very dense boards can be made. However, it is not possible to print on ceramic substrates, so the Nano Dimension's PCB printer has limited RF application.

The Voltera PCB printer [21] is much lower in cost and can process a conventional 4" x 5.3" or 101 x 134mm FR4 substrate. It deposits silver nanoparticle inks to print tracks. No dielectric inks are available, so only 2 layer boards can be built. The inks use heat curing. The minimum track width is 0.2 mm. The datasheet gives no accuracy of the track widths and this may limit the accuracy of Stripline impedances. The cost of the inks is high, but since very little conductive ink is required for a typical board, this technology may soon be economical for RF circuit prototyping.

The Optomec company [22], uses aerosol jet technology to spray conductive, resistive or dielectric inks from a variety of suppliers onto a surface. Having an aerosol jet, removes the tight milling/printing head to PCB distance constraints and thus allows the inks to be deposited on curved surfaces. In one mass-production example, microwave 3D antennas are printed onto odd shaped surfaces for use inside smart phones. A minimum line thickness of 10 μ m and a line spacing of 20 μ m is possible, though a larger spacing is preferred. That is a 9 times thinner line width, than is possible for etched PCB's [12-14]. It is also possible to print semiconductors, so that advanced microwave electronic circuits can be fully printed on virtually any substrate. This may also lead to new sensors, which include the sensor, electronics, transmitter and antenna, as well as a battery and photovoltaic devices, all made using 3D printed technology. Electronic circuits, their antenna, as well as the leads connecting them can all be printed onto a contoured substrate.

Some of these printers are suitable for University prototyping and others are capable of producing 30 000 circuits per week and are used for consumer devices. Typical examples

of applications and their resulting circuits are shown in “*Top 10 Industrial Applications for Additive Manufacturing*” [23]. Due to the ability of being able to make the circuits in any shape, the 3D circuit board printing is also used for military and aeronautical applications. This technique will become more common in future. Figure 10.9 shows a 4 layer 3D demonstration printed circuit board.

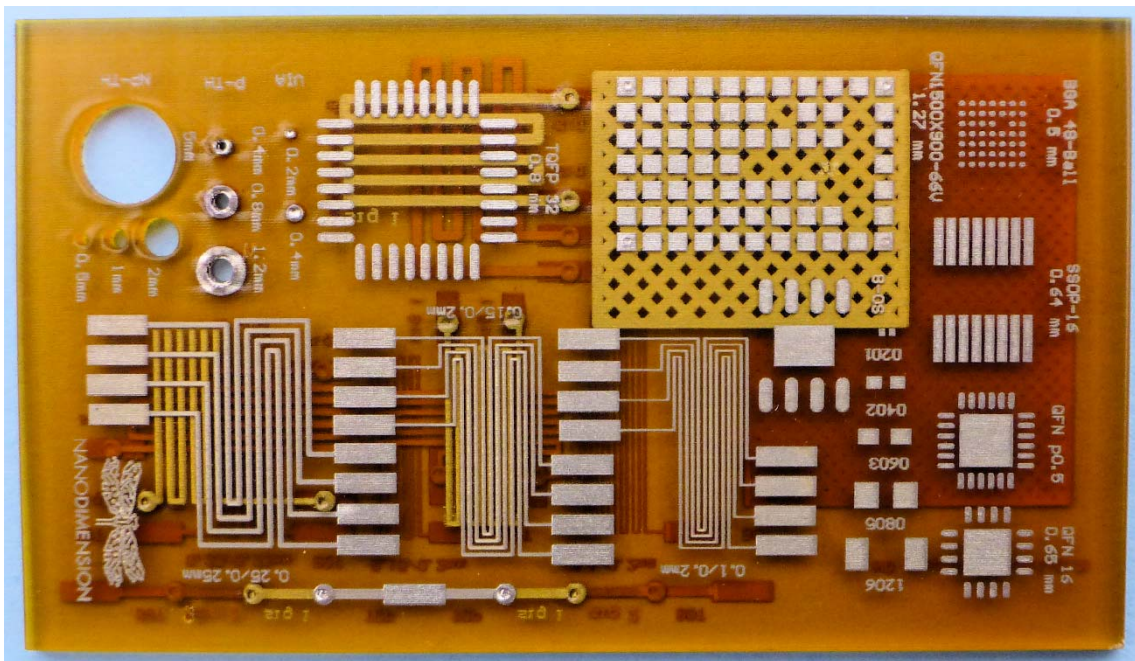


Figure 10.9. Multilayer 3D printed circuit board. [20]

Low Temperature Cofired Ceramic (LTCC)

The Low Temperature Cofired Ceramic (LTCC) technology [24, 25] is a means of producing small 3D and multilayer circuits at a relatively low cost. The technique is similar to thick film techniques, except many layers of ceramic are used, each of which has conductive, dielectric, and / or resistive pastes applied to them. The pastes are applied to ceramic sheets that have not yet been fired. These are called a green-sheets and are normally supplied on a tape. The printed sheets are then laminated together and fired in one process. By means of vias, connections can be made from one layer to another, as shown in figure 10.10.

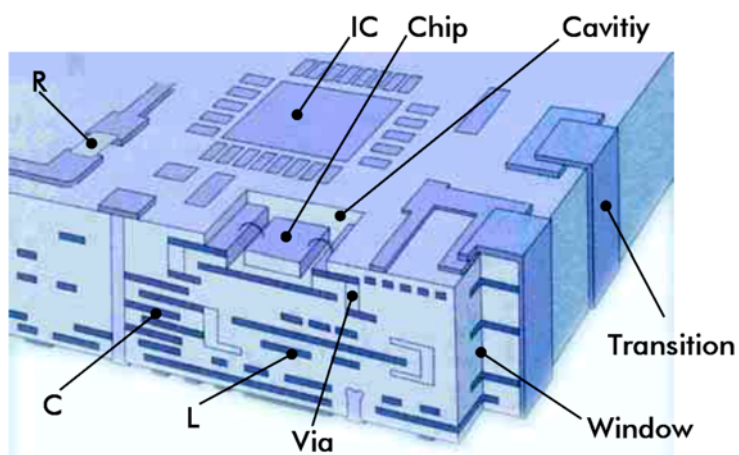


Figure 10.10. Typical LTCC circuit [20].

The low firing temperature for the ceramic green sheets allow low resistivity conductors like silver, gold, copper and alloys with palladium and platinum to be used. The pastes are printed on the green-sheet using conventional thick film techniques. Special thick-film pastes must be used since the ceramic shrinks 10 to 15 percent in x/y-axis and about 10 to 45 percent in z-axis.

It is also possible to integrate passive elements like resistors, capacitors, inductors, and transformers into the substrate. Resistors are processed with the help of special pastes, which have to be printed on the tape just like conductor lines and are cofired. Capacitors and inductors can be made by forming the conductive lines into plates or coils respectively. LTCC technology permits the construction of Stripline as opposed to Microstrip circuits, thus reducing radiation and permitting the construction of couplers with broadside rather than edge coupling, resulting in a high amount of coupling. Combining that with the ability to include active devices on the same small circuit opens up great possibilities.

Many mixers [25], filters [26] and directional couplers [27] produced by Mini-Circuits [25-27], Murata [28] and other manufacturers now use LTCC technology. The filters and couplers use the same principles as outlined in chapters 7 and 4 respectively of this book. However, LTCC allows 3 dimensional layouts, so that broadside coupled lines can easily be made. The high dielectric constant of the ceramic material used also results in small circuits. LTCC technology is also good for low cost reliable hardware required for the automotive industry [29].

References

1. Isola Group, <http://www.isola-group.com/>
2. Rogers Corporation <http://www.rogerscorporation.com/>
3. Taconic Advanced Dielectric Division, <http://www.taconic-add.com>
4. Park Electrochemical Corp. <https://parkelectro.com/rfmicrowave-printed-circuit-materials/>
5. CoorsTek products: Ceramic Substrates, http://www.coorstek.com/resource-library/library/8510-1083_polished_substrates.pdf
6. Morgan Technical Ceramics, Technical Ceramics Products <http://www.morgantechicalceramics.com>
7. Bechtold, F. "A Comprehensive Overview on Today's Ceramic Substrate Technologies", European Microelectronics and Packaging Conference, 2009. EMPC 2009. Rimini, Italy, 15-18 June 2009.
8. Miteq, Dielectric Resonator Oscillators. <https://nardamiteq.com/docs/D210B.PDF>
9. General Electronic Devices, Dielectric Resonator Oscillators, <http://www.gedlm.com/DRO/DRO.asp>
10. Altium <http://www.altium.com/>
11. Autodesk Eagle PCB Design Software, <https://www.autodesk.com/products/eagle/overview>
12. LPKF Circuit Board Plotters <http://www.lpkf.com/products/rapid-pcb-prototyping/circuit-board-plotter/index.htm>
13. LPKF PCB processing equipment. <http://www.lpkf.com/products/pcb-processing/microline-5000.htm>
14. PCB Design Guide and Manufacturing Input Requirement <https://wwwpcbpower.com/technology/design-guideline>
15. MicroFab http://www.microfabnh.com/bandpass_filters.php

16. Stauss W, T Lizotte Ion Beam Technology, MicroFab
http://www.microfabnh.com/ion_beam_etch_technology.php.
17. Hybrid Electronics, Thick Film custom circuits. <http://www.hybrid-electronics.com/>.
18. Dupont, Hybrids Circuit Materials <http://www.dupont.com/products-and-services/electronic-electrical-materials/hybrid-circuit-materials.html>
19. Koartan, Thick Film Conductor Pastes.
<http://www.inseto.co.uk/products/thickfilmconductors.htm>.
20. NanoDimension, <http://www.nano-di.com>.
21. Voltera Circuit printing, <https://www.voltera.io/product/print/>
22. Optomec Aerosol Jet Core applications, <https://www.optomec.com/printed-electronics/aerosol-jet-core-applications/>
23. Top 10 industrial applications for additive manufacturing, pdf available from <https://www.optomec.com/additive-manufacturing/>
24. IMST GmbH LTCC web site <http://www.ltcc.de/en/home.php>
25. Mini-Circuits, Low Cost Triple Balanced LTCC mixer
<http://www.minicircuits.com/pages/pdfs/tech4.pdf> and
<http://www.minicircuits.com/app/AN00-002.pdf>
26. Mini-Circuits, BFCN Series LTCC Band Pass Filters
<https://www.minicircuits.com/WebStore/Filters.html>
27. Mini-Circuits, Surface Mount LTCC Quadrature Splitters.
<http://www.minicircuits.com/pages/pdfs/tech2.pdf> and
<http://www.minicircuits.com/app/AN10-005.pdf>
28. Murata, <http://www.murata.com/en-global/products/substrate/ltcc>
29. Murata, Application examples of LTCC <http://www.murata.com/en-global/products/substrate/ltcc/application>

Appendix

Importing Local Vendor and Spice Files

Local Vendor Libraries

NI AWR DE contains MWO and VSS libraries that accessible from the AWR web site. It may be desirable to download and install those libraries locally, and access the elements locally, rather than having to rely on internet access. Local access is desirable in classroom teaching, since an additional delay is involved in accessing the AWR web site. To install the libraries locally, follow the procedures described below. This information can also be found on the AWR web site under knowledge base. The FAQ: How to Install a Local Copy of the Vendor Parts Library [1].

Download the Vendor Libraries from the AWR web site at: <http://web.awrcorp.com> and select *Support Resources* \Rightarrow *Download Site*. Then login, select Vendor Libraries and click on the Version 14 Vendor Library Installer to download the latest libraries (416.05 MB).

Run the installation program to install the library files. They will by default unzip to the directory: “*C:\ProgramData\AWR\Design Environment\14.0*”. After the extraction, that directory will contain a folder “*xml_local*”, which contains all the Vendor Local files.

For MWO library access, open that folder and locate the “*MWO_Vendor_Local.xml*” file.

Copy the “*MWO_Vendor_Local.xml*” file to the Circuits Elements folder of the xml library location (typically *C:\ProgramData\AWR\Design Environment\14.0\xml\Circuit Elements*). To find the location, open AWRDE and select “*Help* \Rightarrow *Show Files/Directories*” and double click on *XMLUser* to open the “*xml/Circuits Elements*” folder and then copy the “*MWO_Vendor_Local.xml*” file into that “*xml/Circuits Elements*” folder.

The “*MWO_Vendor_Local.xml*” file is a text file that contain the following line:

```
<FILE Name="MWO Vendor Local">C:\ProgramData\AWR\Design Environment\14.0\xml_local\top_v14_local_MWO.xml</FILE>
```

If you have used the default location for the extraction, the “*MWO_Vendor_Local.xml*” file does not need to be changed. However if a different directory is used, the above line in the “*MWO_Vendor_Local.xml*” needs to be edited to point to the correct directory. Before editing the file, it is desirable to make a copy first, so that any errors can be reversed.

After starting AWRDE, the *MWO_Vendor_Local* files will be shown in the *X libraries* section of the *Circuits Element* Browser.

For VSS library access, the same process is followed and the “*VSS_Vendor_Local.xml*” file is copied to the “*xml/System Blocks*” directory folder.

After starting AWRDE, the *VSS_Vendor_Local* files will be shown in the *X libraries* section of the *System Block* Browser.

Importing Spice Device Models

The process of importing Spice files is illustrated using some examples. Since chapter 10 uses Spice models of operational amplifiers (OpAmps), they are used to illustrate the process. Very useful information outlining this process is given in the help files, available

from inside AWRDE by selecting “*Help* \Rightarrow *Help on Selected item*” and in the NI AWR Design Environment Help, type Pspice in the searchtext box and click on the first item in the list “*User Guide* > *Netlists* > *5.3 Importing or Linking to a Netlist*”. The Spice files are text files, so one can use a standard text editor to inspect and edit the spice files if needed.

As an example of the process, the Spice model of an AD797 [2] operational amplifier is required. From the Analog Devices web site search for AD797, then select and download the spice model. That is a *.cir* file. In a NI AWR DE project, select *Netlist* \Rightarrow *Import Netlist* and select the *ad797.cir* file to import. In a circuit Schematic, the spice file can then be added by “*Draw* \Rightarrow *Add Subcircuit*” and then selecting the AD797 element. It is desirable to change the square box *SUBCKT* symbol to one commonly used for OpAmps, by selecting “*Properties* \Rightarrow *Symbol*” and then selecting *OpAmp6@APLAC.syf* as the symbol to be used. That then allows a schematic like figure 10.15 to be produced.

The simulation will show some warnings where resistors $R=0$ are replaced with small non-zero values. If it is desirable not to have errors, the netlist can be edited in a text editor to replace the zero ohm resistors with the suggested values, like $R2=1e-6$. That will then allow an easier identification of any other errors generated by the simulation.

The same process is used for importing Spice files for other devices such as transistors, or diodes.

Sometimes the file for netlist to be imported is not a *.cir*, *.sp* or *.inc* file. As an example the zip file for the Spice model for the OPA659 [3], contains the file *OPA_Pspice_Model.txt*. To import the netlist, select the file browser to show all files and then select *OPA_Pspice_Model.txt* since the file extension does not match one of the designated Spice extensions, a new window, requiring the selection of the type of import to be used. In this case, select Pspice and the file is imported. The circuit then simulates correctly, however with many warnings. Importing the circuit as a Hspice *.sp* circuit gives less warnings, but they may be more serious, since parameters for transistors inside the IC are not recognised. Both simulations appear to give the same results.

Sometimes the Spice files are in a format that cannot easily be imported. For example the zip file for the OPA691 [4] from the Texas Instruments web site contains *.dsn*, *.lib*, *.olb* and *.opj* files. None of those can be imported correctly into NI AWR DE. The *.lib* file will import. But since it is not a native APLAC file, it cannot be placed as a subcircuit. In addition, since this OpAmp has a disable pin, the associated switch may cause problems.

Many modern OpAmps incorporate an enable pin. At this stage that often does not import correctly. For example the ADA4895 [5]. Downloading the PSpice file from the Analog Devices web site and importing the *.cir* file results in ‘*S_Device*’ not found in conversion table and ‘*vswitch*’ not found in conversion table. As a result, the resulting netlist will not give correct results when used in a simulation.

It is possible to edit and correct the Spice files to eliminate errors and warnings that occur during importing of the spice files. For example the ‘*S_Device*’ and ‘*vswitch*’ descriptions in the ADA4895 Spice files can be modified, so that the enable pin is deleted and the OpAmp is always enabled. That will then overcome the errors during the importation of the files. In future NI AWR DE versions, these elements may import correctly and the switch may be able to be controlled using transistors or DC voltages.

References

1. FAQ: How to Install a Local Copy of the Vendor Parts Library.
<http://kb.awr.com/display/help/How+to+Install+a+Local+Copy+of+the+Vendor+Parts+Library>
2. Analog Devices, AD797, Ultralow Distortion, Ultralow Noise Op Amp.
<http://www.analog.com/en/products/amplifiers/operational-amplifiers/high-voltage-amplifiers-greaterthanequalto-12v/ad797.html>
3. Texas Instruments, OPA659, 650 MHz unity gain stable JFET Operational Amplifier. <http://www.ti.com/product/OPA659>
4. Texas Instruments, OPA691Wideband Current Feedback Operational Amplifier with Disable. <http://www.ti.com/product/OPA691>
5. Analog Devices, ADA4895-1, Low Power, 1 nV/ $\sqrt{\text{Hz}}$, $G \geq 10$ Stable, Rail to Rail Output Amplifier.
<http://www.analog.com/en/products/amplifiers/operational-amplifiers/low-noise-amplifiers-lessthanequalto-10nv/ada4895-1.html>